nature

THE INTERNATIONAL WEEKLY JOURNAL OF SCIENCE

THE CHANGING MAP OF SCIENCE

How the movement of people and ideas will alter global research PAGE 325

PLANT SCIENCES

PHYSICS GROWS ON TREES

On form and function in a leaf

PAGE 339

ECOLOGY

COAST DEFENCE UNDERMINED

How vital salt marshes are becoming mudflats

PAGES 352 & 388

HIV/AIDS

AIDS VACCINE'S MIXED MESSAGE

Controversial trial identifies anti-HIV target

PAGES 350 & 417

NATURE.COM/NATURE

18 October 2012 £10

Vol. 490, No. 7420

4 2

9 770028 083095

BIOO SCIENTIFIC®

The NGS Experts™

Empowering Sequencing, Our Focus.

Simplify your NimbleGen SeqCap Target Capture.

The **NEXTflex™ Pre-Capture Combo Kit** for NimbleGen SeqCap is a complete DNA-Seq library prep, barcode and barcode blocking solution, designed and validated for use upstream of Roche NimbleGen's SeqCap v3 Target Capture.

Complete Kit - Everything you need upstream of target capture
Optimized - Offers larger number of unique reads
Multiplexed - Up to 24 barcodes and barcode blockers
Available Now - Next Day Delivery

DNA-Seq
ChIP-Seq
Bisulfite-Seq
Methyl-Seq
RNA-Seq
Small RNA-Seq
Directional RNA-Seq
PCR-Free DNA-Seq
Pre-Target Capture
Multiple Platform Compatibility

Visit **BiooNGS.com** and turn your focus to your NGS results.

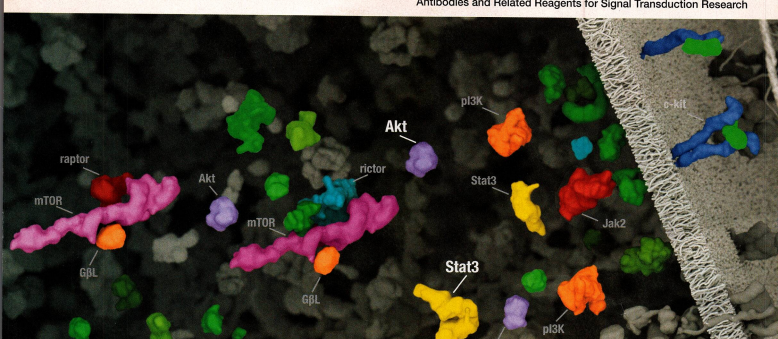

Conjugated Antibodies for Flow Cytometry *from Cell Signaling Technology*

Unparalleled product quality, validation, and technical support

- :: The highest quality antibodies provide you with the brightest signal and the lowest background.
- :: Extensive validation by our in-house flow cytometry group means optimization is not left up to you, the user.
- :: Technical support provided by our flow cytometry specialists translates into a thorough, fast, and accurate response.
- :: High quality custom conjugations of our off-the-shelf antibodies are also available, please inquire about sizing and pricing options.
- :: Multiple fluorochrome options are available to meet your unique multiplexing needs.

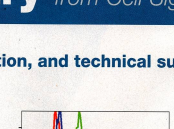

Phospho-Stat3 (Tyr705) (D3A7) XP® Rabbit mAb (Alexa Fluor® 488 Conjugate) #4323: Flow cytometric analysis of Jurkat cells, untreated (blue) or IFN-α treated (green), using #4323 compared to nonspecific control antibody (red).

Phospho-Akt (Ser473) (D9E) XP® Rabbit mAb (PE Conjugate) #5315: Flow cytometric analysis of Jurkat cells, untreated (green) or treated with LY294002 (PI3 Kinase Inhibitor) #9901, Wortmannin (PI3 Kinase Inhibitor) #9951, and U0126 (MEK1/2 Inhibitor) #9903 (blue), using #5315.

© 2010 Cell Signaling Technology, Inc. | CST® and Cell Signaling Technology® are trademarks of Cell Signaling Technology, Inc.
Alexa Fluor® is a trademark of Molecular Probes, Inc.

for quality products you can trust...

www.cellsignal.com

Cell Signaling TECHNOLOGY®

Orders (toll-free) 1-877-616-2355 | **Technical support** (toll-free) 1-877-678-8324 support@cellsignal.com | **Inquiries** info@cellsignal.com | **Environmental Commitment** eco.cellsignal.com

For Research Use Only. Not For Use In Diagnostic Procedures.

Introducing the BD FACSJazz™

Perfectly tuned cell sorting from BD Biosciences.

BD

Helping all people live healthy lives

Breathtaking solo performance.

The BD FACSJazz™ system begins a new era in cell sorting with stellar performance, benchtop fit, and an affordable price.

The BD FACSJazz can be configured with up to 3 lasers and 8 parameters to support your application needs—offloading sorting demand at core labs or meeting the needs of individuals.

Requiring less than 2 x 2 ft (20 x 20 in, 51 x 51 cm) of bench space, the BD FACSJazz also addresses biosafety concerns with an optional custom designed biosafety cabinet that meets personnel and product protection standards for both a Class II Type A2 biosafety cabinet and the National Sanitation Foundation International Standard 49.

In addition to factory-optimized settings, the BD FACSJazz comes standard with BD FACS™ Sortware sorter software to simplify use. This innovative software is specifically designed for cell sorting and features comprehensive control for acquisition, sorting, and analysis.

For legendary results, just add your creativity. Learn how at **bdbiosciences.com/go/jazz**

Class 1 Laser Product.
For Research Use Only. Not for use in diagnostic or therapeutic procedures.
BD, BD Logo and all other trademarks are property of Becton, Dickinson and Company. © 2012 BD
23-14201-00

BD Biosciences
2350 Qume Drive
San Jose, CA 95131
bdbiosciences.com

CONTENTS

18 October 2012 / Vol 490 / Issue No 7420

THE NEW MAP OF SCIENCE

EDITORIAL

309 Global reach
Beware the limits of internationalization

FEATURES

325 Science mapped out
Plotting the course of international research

326 Science on the move
How money and culture shape the international migration of scientists

COMMENT

331 How to build science capacity
Lim Chuan Poh; Bernie Fanaroff; Patrick Aebischer; Rafael Camacho; Ismail Serageldin; Nikolay Suetin; Carlos Henrique de Brito Cruz; June Seung Lee
Experts recommend ways for countries to give their science a boost

335 The rise of research networks
Jonathan Adams
Science superpowers could get left behind as collaboration rules

337 Global challenges need global solutions
Subra Suresh
Laying the foundations for a future of international collaboration

COVER ILLUSTRATION BY JASEK KRZYSZTOFIAK

THIS WEEK

EDITORIALS

309 EPIDEMIOLOGY
Life after death
Restricting access to US death records will do more harm than good

310 ANIMAL HEALTH
Badger away
The scientific evidence behind England's impending badger cull is not black and white

WORLD VIEW

311 The secrets of my prizewinning research
Serge Haroche
The switch to short-termism, will stifle science says the co-winner of this year's physics Nobel

RESEARCH HIGHLIGHTS

312 SELECTIONS FROM THE SCIENTIFIC LITERATURE
An attractive asteroid / Another obesity-cancer link / Stem cells boost myelin / A strong La Niña / Moa hunted down

SEVEN DAYS

314 THE NEWS IN BRIEF
Author ID scheme launches / A fall that was faster than sound / Dragon makes first cargo delivery / Keith Campbell dies

NEWS IN FOCUS

317 ANIMAL HEALTH
English badger cull sparks schism in the countryside

318 FOOD SCIENCE
Lack of funding leaves US work on genetically engineered animals languishing

320 NOBEL PRIZE
Cell signals claim chemistry prize

321 REGENERATIVE MEDICINE
Scandal erupts over Japanese stem-cell claims

322 BIOMEDICINE
Drug industry's data on clinical trials emerge from the shadows

323 ASTRONOMY
Earth-sized exoplanet identified orbiting nearest star system to us

324 CONSERVATION
Protection bid for Antarctic seas faces stormy waters

CAREERS

435 INNOVATION
Brushing up on business
Entrepreneurs are trained, not born

437 TURNING POINT
Craig Bennett takes the positives from a share of the 2012 Ig Nobel Prize

COMMENT

BOOKS & ARTS

339 BIOPHYSICS
Tales from the canopy
Sandra Knapp

340 ZOOLOGY
The animal inside
Josie Glausiusz

341 BOOKS IN BRIEF

CORRESPONDENCE

342 Crowd sourcing in forests / Share equipment in austerity / Publish and be paid / Metrics — good or bad? / Evolving libraries / Greener stoves

FUTURES

440 The tell-tale ear
Alex Shvartsman

7,000 Human Proteins Made from Human Cells.

More Assays! Better Assays!

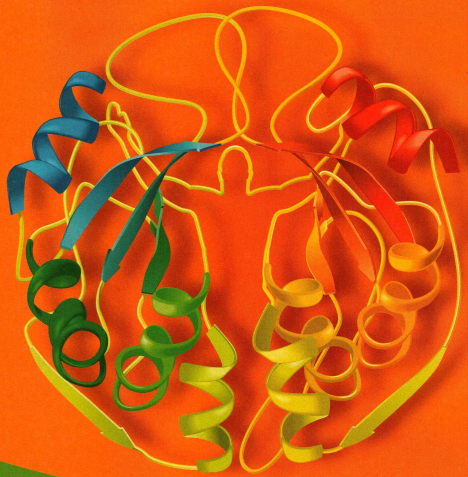

The Largest Collection of Mammalian Cell-Derived Proteins

Protein functional studies

Compound screening

Immunogens for antibody production

Assay standards: ELISA, Mass Spec, and more

Bulk production available

Human MTOR protein activity verified in a kinase assay

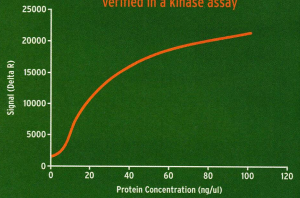

origene.com/protein

ORIGENE
Your Gene Company

CONTENTS

18 October 2012 / Vol 490 / Issue No 7420

RESEARCH

NEW ONLINE

345 Papers published this week at nature.com

NEWS & VIEWS

346 PLANETARY SCIENCE
Galvanized lunacy
Zinc isotopic composition of the Moon
Tim Elliott SEE LETTER P.376

347 CANCER THERAPY
Tumours switch to resist
Adoptive cell transfer therapy leads to loss of melanocytic antigens
Antoni Ribas & Paul C Tumeh
SEE LETTER P.412

348 STRUCTURAL BIOLOGY
Bundles of insights into sugar transporters
Precise molecular models for human glucose transporters
Peter J F Henderson & Stephen A Baldwin
SEE ARTICLE P.361

350 HIV
Design by trial
Higher vaccine efficacy against viruses with specific envelope sequences
David V Glidden SEE LETTER P.417

351 MOLECULAR BIOLOGY
Choose your protein partners
How the chaperone HSP90 selects its protein-kinase clients
Rahul S Samant & Paul Workman

352 ECOLOGY
The big picture of marsh loss
Excessive nutrient levels cause salt-marsh loss
Steven C Pennings SEE LETTER P.388

ARTICLES

355 STEM CELLS **The aged niche disrupts muscle stem cell quiescence**
J V Chakkalakal, K M Jones, M A Basson & A S Brack

361 STUCTURAL BIOLOGY **Crystal structure of a bacterial homologue of glucose transporters GLUT1–4**
L Sun et al. SEE N&V P.348

367 STRUCTURAL BIOLOGY **Structure of AMP-PNP-bound vitamin B_{12} transporter BtuCD–F**
V M Korkhov, S A Mireku & K P Locher

LETTERS

373 ASTRONOMY **Hard-X-ray emission lines from the decay of ^{44}Ti in the remnant of supernova 1987A**
S A Grebenev, A A Lutovinov, S S Tsygankov & C Winkler

376 PLANETARY SCIENCES **Zinc isotopic evidence for the origin of the Moon**
R C Paniello, J M D Day & F Moynier
SEE N&V P.346

380 PHYSICS **Circuit quantum electrodynamics with a spin qubit**
K D Petersson et al.

384 MATERIALS SCIENCE **Bonding and structure of a reconstructed (001) surface of $SrTiO_3$ from TEM**
G-z Zhu, G Radtke & G A Botton

388 EARTH SCIENCE **Coastal eutrophication as a driver of salt marsh loss**
L A Deegan et al. SEE N&V P.352

393 CLIMATE SCIENCE **Delayed build-up of Arctic ice sheets during 400,000-year minima in insolation variability**
Q Hao et al.

397 NEUROSCIENCE **Nonlinear dendritic processing determines angular tuning of barrel cortex neurons *in vivo***
M Lavzin, S Rapoport, A Polsky, L Garion & J Schiller

402 NEUROSCIENCE **Severe stress switches CRF action in the nucleus accumbens from appetitive to aversive**
J C Lemos et al.

407 STEM CELLS **Androgenetic haploid embryonic stem cells produce live transgenic mice**
W Li et al.

412 CANCER **Melanomas resist T-cell therapy through inflammation-induced reversible dedifferentiation**
J Landsberg et al. SEE N&V P.347

417 IMMUNOLOGY **Increased HIV-1 vaccine efficacy against viruses with genetic signatures in Env V2**
M Rolland et al. SEE N&V P.350

421 IMMUNOLOGY **A FOXO3-IRF7 gene regulatory circuit limits inflammatory sequelae of antiviral responses**
V Litvak et al.

426 METABOLISM **Targeting VEGF-B as a novel treatment for insulin resistance and type 2 diabetes**
C E Hagberg et al.

431 MOLECULAR BIOLOGY **Initiation of transcription-coupled repair characterized at single-molecule resolution**
K Howan et al.

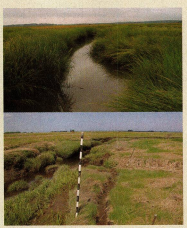

EARTH SCIENCE

Drying out

Coastal areas are threatened as salt marshes give way to mud flats. PAGE 388

STRUCTURAL BIOLOGY

Sugar rush

The crystal structure of a disease-related glucose transporter. PAGE 361

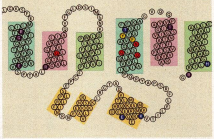

nature

18 October 2012 / Vol 490 / Issue No. 7420

EDITORIAL

LONDON, MUNICH, WASHINGTON DC, NEW YORK, BOSTON, PARIS, SAN FRANCISCO, TOKYO nature@nature.com

EDITOR-IN-CHIEF: Philip Campbell

EXECUTIVE EDITOR: Nick Campbell

PUBLISHING EXECUTIVE EDITOR: Maxine Clarke **EXECUTIVE EDITOR:** Véronique Kiermer

CHIEF MAGAZINE EDITOR: Tim Appenzeller

THIS WEEK/NEWS/FEATURES: Alison Abbott, David Adam, Ananyo Bhattacharya, Geoff Brumfiel, Declan Butler, Ewen Callaway, Erika Check Hayden, Daniel Cressey, David Cyranoski, Natasha Gilbert, Eric Hand, Heidi Ledford, Cori Lok, Brendan Maher, Emma Marris, Richard Monastersky, Brian Owens, Helen Pearson, Mark Peplow, Eugenie Samuel Reich, Ivan Semeniuk, Quirin Schiermeier, Jeff Tollefson, Richard Van Noorden, Meredith Wadman, M Mitchell Waldrop **COMMENT:** Sara Abdulla, Joanne Baker, Rosalind Cotter, Barbara Kiser, Alison McCook, Lucy Odling-Smee, Sarah Tomlin **NATURE PODCAST/VIDEO:** Adam Rutherford, Thea Cunningham, Kerri Smith, Charlotte Stoddart **NEWS AND VIEWS:** Sadaf Shadan, Ara Lopes, Andrew Mitchinson, Cesar Sanchez, Marian Turner **RESEARCH:** Ritu Dhand, Karl Ziemelis, Francesca Cesari, I-han Chou, Tanguy Chouard, Rosamund Daw, Alex Eccleston, Angela Eggleston, Joshua Finkelstein, Henry Gee, Patrick Goymer, Noah Gray, Marie-Thérèse Heemels, Magdalena Helmer, Karen Howell, Claudia Lupp, Barbara Marte, Andrew Mitchinson, Juliane Mössinger, Deepa Nath, Wayne Peng, Leslie Sage, Magdalena Skipper, Clare Thomas, Maria Trajkovska, John VanDecar, Liesbeth Verrema, Ursula Weiss, Michael White **INSIGHTS/REVIEWS/PERSPECTIVES:** Ursula Weiss **CAREERS:** Gene Russo, Karen Kaplan **TECHNOLOGY FEATURES:** Vivien Marx **FUTURES:** Colin Sullivan **SUPPLEMENTS:** Herb Brody, Michelle Grayson, Tony Scully **SUBEDITORS:** Colin Sullivan, Mary Abraham, Sarah Archibald, Nicola Bailey, Nicolas Fanget, Isobel Flanagan, Paul Fletcher, Anne Haggart, Sasha Lewis, Dinah Loon, Louisa Lyon, Anna Novitzky, Yukie Ozawa, Katherine Perry, David Price, Jenny Rooke, David Winters, Anna York **PRODUCTION:** Jenny Henderson, Leonora Dawson-Bowling, Dan Foley, Stewart Fraser, Susan Gray, Simon Gribbin, Hazel Mayhew, James McQuat, Emilia Oviss, Yvonne Strong, Robert Sullivan, Roberta Tarran, Charles Wenz **ART AND DESIGN:** Kelly Buckheit Krause, Wesley Fernandes, Madeline Hutchinson, Barbara Izdebska, Paul Jackman, Jasiek Krzysztofiak, Annthea Lewis, Chris Ryan, Nik Spencer, Claire Welsh, Mark Wood **JAPAN EDITION:** Eiji Matsuda, Mika Ishida, Mitsuyo Ukyo, Seyoka Ayame **PRESS OFFICE:** Ruth Francis, Neda Afsarmanesh, Lisa Boucher, Rachel Twinn, Rebecca Walton **ADMINISTRATION:** Paul Sng, Liz Bankes, Roseann Campbell, Peter Cary, Fhion Cleverley, Dana Coles, Faye Formaier, Ashlee Gagui, Peter Hewitt, Caroline McLean, Anastasia Panoutsou, Kenneth Simpson, Michelle Viscuso, Diane Yorke

PUBLISHING

LONDON feedback@nature.com

MANAGING DIRECTOR & PUBLISHER: Steven Inchcoombe

ASSOCIATE PUBLISHER: Arash Hejazi

PUBLISHING PROJECT MANAGERS: Claudia Deasy, Christian Manco

TOKYO feedback@natureasia.com

REGIONAL MANAGING DIRECTOR — ASIA-PACIFIC: David Swinbanks

DIRECTOR — ASIA-PACIFIC: Antoine E Bocquet

OPERATIONS DIRECTOR — ASIA-PACIFIC: Hiroshi Minemura

DISPLAY ADVERTISING, SPONSORSHIP & NATUREJOBS

GLOBAL HEAD: Andrew Douglas a.douglas@nature.com

DISPLAY ADVERTISING AND SPONSORSHIP

GLOBAL HEAD: Gerard Preston g.preston@nature.com

ASSISTANT SPONSORSHIP MANAGER: Reya Silao Tel: +44 (0)20 7843 4977 (rsilao@nature.com)

EUROPE/REST OF WORLD display@nature.com Tel: +44 (0)20 7843 4960

GERMANY/SWITZERLAND/AUSTRIA: Sabine Hugi-Fürst Tel: +41 52761 3386

UK/IRELAND/SCANDINAVIA/SPAIN/PORTUGAL: Evelina Rubio Hakansson Tel: +44 (0)20 7843 4079

FRANCE/BELGIUM/THE NETHERLANDS/LUXEMBOURG/ITALY/OTHER EUROPE: Nicola Wright Tel: +44 (0)20 7843 4959

NORTH AMERICA display@natureny.com

NEW ENGLAND/EASTERN CANADA: Sheila Reardon Tel: +1 617 494 4900

NEW YORK/MID-ATLANTIC/SOUTHEAST: Jim Breault Tel: +1 212 726 9334

MIDWEST: Mike Rossi Tel: +1 212 726 9255

WEST COAST/ WESTERN CANADA: George Lui Tel: +1 415 781 3804

WEST COAST NORTH: Kayla McCutchan Tel: +1 415 403 9038

ASIA-PACIFIC display@natureasia.com

ASIA-PACIFIC HEAD: Kate Yoneyama

JAPAN: Ken Mikami Tel: +81 3 3267 8765

GREATER CHINA/SINGAPORE: Gloria To Tel: +852 2811 7191

INDIA: Vikas Chawla Tel: +91 124 288 1057

SPONSORSHIP

BUSINESS DEVELOPMENT MANAGER: David Bagshaw Tel: +1 212 726 9215

BUSINESS DEVELOPMENT MANAGER: Pátrick Murphy Tel: +1 617 475 9216

NATUREJOBS naturejobs@nature.com

EUROPEAN HEAD OFFICE, LONDON: Tel: +44 (0)20 7843 4961

EUROPEAN SALES MANAGER: Nils Moeller (n.moeller@nature.com) **BUSINESS DEVELOPMENT MANAGER, MIDDLE EAST:** Jon Giuliani (j.giuliani@nature.com) **ADVERTISING PRODUCTION MANAGER:** Stephen Russell **NATUREJOBS ONLINE PRODUCTION:** Dennis Chu

US HEAD OFFICE, NEW YORK: naturejobs@natureny.com **US SALES MANAGER:** Ken Finnegan

JAPAN HEAD OFFICE, TOKYO: Tel: +81 3 3267 8765 **ASIA-PACIFIC HEAD:** Kate Yoneyama

ASIA-PACIFIC SALES & BUSINESS DEVELOPMENT MANAGER: Yuki Fujiwara **BUSINESS DEVELOPMENT MANAGER, GREATER CHINA, SINGAPORE:** Gloria To Tel: +852 2811 7191

INDIA: Vikas Chawla Tel: +91 1242881057 (v.chawla@nature.com)

MARKETING & SUBSCRIPTIONS

USA/CANADA/LATIN AMERICA subscriptions@us.nature.com

Tel: (USA/Canada)+1 866 363 7860; (outside USA/Canada) +1 212 726 9223

MARKETING: Sara Girard **FULFILMENT:** Karen Dawson

JAPAN/CHINA/KOREA subscriptions@natureasia.com

Tel: +81 3 3267 8751 **MARKETING:** Sachiyo Ikeda **FULFILMENT:** Masayo Tanaka

EUROPE/REST OF WORLD subscriptions@nature.com

Tel: +44 (0)1256 329242

MARKETING: Elena Woodstock, Marcus Parker, Hannah Phipps **FULFILMENT:** Jean Burrows

INDIA npgindia@nature.com

Tel: +91 124 2881053/54

HEAD OF BUSINESS DEVELOPMENT, INDIA: Debashish Brahmachari **MARKETING:** Harpal Singh Gill

ANNUAL SUBSCRIPTIONS (UK/Europe, including post and packing)

FULL RATE: £1,400

PERSONAL RATES: UK £135; Europe €209; Rest of World £210

STUDENT RATES: UK £79; Europe €122; Rest of World £125

Individual rates apply to payments by personal cheque or credit card. Back issues: £20.00.

ANNUAL SUBSCRIPTIONS (USA, including post and packing)

INSTITUTIONAL/CORPORATE RATE: $2,730 ; **PERSONAL RATE:** $199; **STUDENT RATE:** $99;

POSTDOC RATE: $119

Printed in USA. Individual rates available only to subscribers paying by personal check or credit card. Orders for student/postdoc subscriptions must be accompanied by a copy of student ID. Rates apply to USA, Canada, Mexico/Central & South America. Add 7% GST tax in Canada (Canadian GST number 140911595). **BACK ISSUES:** US$20.00.

ANNUAL SUBSCRIPTIONS (Asia, including post and packing)

JAPAN: 年間購読料金： *Nature* のみ 437,800 円 +21,890 円(消費税) =459,690 円(合計)
Nature + *Nature Digest* 466,550 円 +23,328 円(消費税) =489,878 (合計)
お問い合わせ 日本出版貿易株式会社 国内営業 1 部
〒101-0064 東京都千代田区猿楽町1-2-1 Tel: 03-3292-3767 Fax: 03-3292-8766

個人/学生購読について
NPG ネイチャー アジア・パシフィック フルフィルメント & カスタマーサービス
〒162-0843 東京都新宿区市谷田町2-37 千代田ビル Tel: 03-3267-8759Fax: 03-3267-8752

CHINA: www.natureasia.com/cn/subscribe; **KOREA:** www.natureasia.com/korea/subscribe

NATURE ONLINE WWW.NATURE.COM/NATURE

CHIEF TECHNOLOGY OFFICER: Howard Ratner **ASSOCIATE DIRECTOR, NATURE.COM:** Daniel Pollock

PLATFORM DEVELOPMENT: Jeremy Macdonald **WEB PRODUCTION:** Alexander Thurrell, Deborah Anthony **WEB DESIGN:** Juan-Carlos Sobrino, Luke Stavenhagen **PLATFORM INTERFACES:** Amanda Ward

SITE LICENCES, FULFILMENT & CUSTOMER SERVICES

SITE LICENCES: npg.nature.com/libraries feedback@nature.com

CHIEF OPERATIONS OFFICER: John Carroll **ASSOCIATE DIRECTOR OF OPERATIONS:** Dominic Pettit

CUSTOMER SERVICE: Liz Davidson **ORDER PROCESSING OPERATIONS:** Steve Poulter

NATURE PUBLISHING GROUP OFFICES

LONDON: The Macmillan Building, 4 Crinan Street, London N1 9XW Tel: +44 (0)20 7833 4000 Fax: +44 (0)20 7843 4596/7

BASINGSTOKE: Nature Publishing Group, Subscriptions, Brunel Road, Basingstoke, Hants RG21 6XS, UK Tel: +44 (0)1256 329242

WASHINGTON DC: 968 National Press Building, 529 14th St NW, Washington DC 20045-1938 Tel: +1 202 737 2355

NEW YORK: 75 Varick St, 9th Floor, New York, NY 10013-1917 Tel: +1 212 726 9200

BOSTON: 25 First Street, Suite 104, Cambridge, MA 02141 Tel: +1 617 475 9275

SAN FRANCISCO: 225 Bush Street, Suite 1453, San Francisco, CA 94104 Tel: +1 415 403 9027

MUNICH: Nymphenburger Strasse 14, D-80335 München Tel: +49 89 549057-13

PARIS: Moulin de Malicorne, Sainte Maure de Touraine, Paris 37800 Tel: +33 2 47 35 72 15

TOKYO: Chiyoda Building, 2-37 Ichigayatamachi, Shinjuku-ku, Tokyo 162-0843 Tel: +81 3 3267 8751

INDIA: Nature Publishing Group, 3A, 4th Floor, DLF Corporate Park, Gurgaon 122002 Tel: +91 124 2881053/54

Nature® (ISSN 0028-0836) is published by Nature Publishing Group, a division of Macmillan Publishers Ltd (The Macmillan Building, 4 Crinan Street, London N19XW). Registered as a newspaper at the British Post Office. North and South American orders to subscriptions@nature.com (Tel: +44 (0)1256 329242; Fax +44 (0)1256 812358). Authorization to photocopy material for internal or personal use, or internal or personal use of specific clients, is granted by *Nature* to libraries and others registered with the Copyright Clearance Center (CCC) Transactional Reporting Service, provided the relevant copyright fee is paid direct to CCC, 222 Rosewood Drive, Danvers MA 01923, USA. Identification code for *Nature*: 0028-0836/03. CPC PUB AGREEMENT #40032744. In the US, *Nature* (ISSN 0028-0836) is published weekly on Thursday, except the last week in December by Nature Publishing Group, 75 Varick St, 9th Fl, New York, NY 10013-1917, USA. US Periodicals postage paid at New York, and additional mailing post offices. US POSTMASTER: send address changes to *Nature*, Subscription Dept, 75 Varick St, 9th Fl, New York NY 10013-1917, USA. Published in Japan by NPG Nature Asia-Pacific, Chiyoda Building, 2-37 Ichigayatamachi, Shinjuku-ku, Tokyo 162-0843, Japan. © 2012 Macmillan Publishers Limited. All rights reserved.

THIS WEEK

EDITORIALS

BADGERS English cull begins amid scientific and political rancour **p.310**

WORLD VIEW New Nobel laureate Serge Haroche on his success **p.311**

NO MOA Study reveals appetite of New Zealand settlers for bird **p.313**

Life after death

Restricting access to US death records could have serious consequences for long-term health studies. Government agencies should rethink their decision.

People who receive kidney transplants live twice as long as those who rely on dialysis. Trans fats are bad for your health. High alcohol consumption is linked with increased rates of breast cancer. High caffeine consumption is not. Daily aspirin use is associated with a reduced risk of death from cancer.

Large and long-term population studies have revealed these and other important findings. All required access to death records, which a policy from the US Social Security Administration (SSA) is making more difficult and more expensive.

The SSA produces the Death Master File, or Social Security Death Index, which includes more than 89 million records and lists names, death dates and social-security numbers. Data come from state governments, postal authorities, financial institutions, relatives of the deceased, health-care providers and funeral homes, and are updated weekly; the file has been publicly available since 1980. Last November, however, the SSA stopped making state death data generally available, saying that such information is protected by privacy laws.

Some 4 million entries have been removed from the public file because of privacy concerns. In future, an estimated 1 million of the 2.8 million records collected each year by the SSA will no longer be made public. That will make it much harder for researchers to track down whether a participant in a study has moved or died. It could also prevent researchers from collecting accurate details about circumstances of death while the memories of relatives and health providers are fresh.

Researchers involved in US longitudinal and cohort studies such as the Nurses' Health Study and the Framingham Heart Study routinely consult the Death Master File, as do those at the Scientific Registry of Transplant Recipients. It was used to verify deaths in the Cancer Prevention Study II, and so has contributed to more than 200 published studies from the American Cancer Society. Health networks and funders must know who has died so that they can evaluate quality of care, the long-term benefits of a procedure or the risks of an intervention.

But fraudsters also have uses for death records: criminals can use the listed social-security numbers for identify theft. However, the benefits of restricting access to the database to curtail fraud must be weighed carefully against the real potential for harm to public health. Without access to death records, research in all areas of medicine will be hindered. Ironically, efforts to prevent other kinds of fraud will also be obstructed, because the records can be used to check whether the holder of a social-security number has died.

There are other sources of death records. Investigators can submit the names of study participants to the Centers for Disease Control and Prevention (CDC), which will then search its National Death Index for matches in data supplied by the states. This index is more complete than the Death Master File, but it is updated less frequently — only every 18 months or so. It is also less convenient to use, and more costly. The CDC must pay states for their records, and these costs are passed on to researchers. The agency is working closely with state offices to adopt electronic filing systems that can keep lists more current, but the costs are unlikely to come down.

Even studies that already rely on the CDC still use the Death Master File for corroboration and extra information. Without access to this resource, researchers will need to spend further research dollars and effort on tracking down participants. They may have to send expensive signed-for letters to ensure that they reach someone, or chase through defunct contact information. The quality of studies will suffer. The more participants are lost to follow-up, the less certain will be the conclusions of long-standing, labour-intensive cohort studies.

"There is a lot of room between making data accessible indiscriminately and cutting off access."

The SSA should reconsider its decision to withhold information. Everyone involved should work to find a compromise that minimizes the risks of identify theft while maintaining researchers' access to all the data in the Death Master File.

Before the latest policy took effect, nearly anyone could gain access to the records. Genealogy sites posted data for free or at minimal cost, and it is true that these records were easy pickings for identity thieves. However, there is a lot of room between making data accessible indiscriminately and cutting off access. The medical community is accustomed to working with sensitive, confidential information. To give accredited researchers access to death records, the SSA could adopt registration and permissions systems similar to those used for viewing and receiving medical information.

Given how many federal dollars will be wasted if access to the Death Master File is restricted — and how many public-health benefits will be lost or delayed — officials must work urgently to make these crucial records available for research once again. ■

Global reach

The increasing internationalization of science offers many benefits, but also has limitations.

Last week's Nobel prizes formally recognized scientists from just four nations — but newspaper headlines and press releases were eager to spread the glory further. Whereas France's President François Hollande called Serge Haroche's physics win "a source of national pride", Helga Nowotny, president of the European Research Council, described the same award as affirmation of her agency's investment in talent.

The *Korea Herald*, meanwhile, found a local connection to US

researcher Robert Lefkowitz's chemistry Nobel — two Korean scientists, Jihee Kim and Seungkirl Ahn, are currently working in his lab.

And although Japan's Shinya Yamanaka was personally congratulated by Prime Minister Yoshihiko Noda on his award in physiology or medicine, the *San Jose Mercury News* preferred to focus on Yamanaka's training at the Gladstone Institutes in San Francisco, California, which, the paper said, recognized his talents back in 1993, when they hired him (Yamanaka still has a lab there).

Reactions such as these show how national pride and prestige still matter in an increasingly internationalized science system. The ultimate expression of that tension will surely come when the discovery of the Higgs boson — to which thousands of researchers and funds from tens of countries contributed — is rewarded with a call from Stockholm.

This week, *Nature* examines the globalization of science (see page 325). According to the US National Science Foundation (NSF), almost one-quarter of research articles in 2010 featured authors from more than one country, up from 10% in 1990. The average number of authors on research papers, which now stands at 4.5, has doubled since 1980. Many areas of science are becoming international, not local, pursuits; researchers are increasingly criss-crossing the globe and becoming accustomed to working in two or three countries at once.

Yet although science is increasingly globalized — at least in terms of research outputs and collaborations — it is still funded and managed on a largely national basis. This may need to change. Joining up national priorities could allow economies of scale, possibly to the benefit of research into global challenges such as energy, climate and agriculture.

The head of the NSF, Subra Suresh, offers a vision of the future on page 337 in which some of the barriers to cross-border scientific collaboration have been removed. Suresh hopes that the Global Research Council can begin to collectively steward global science as if it were a national activity.

If the globalizing trend does continue, it could change the way that national governments view the outputs of science. Countries may even feel that, instead of insisting on making and exploiting their own discoveries, it is more efficient to capitalize on the breakthroughs made by others. South Korea and the United States are rapidly becoming the centres of graphene manufacturing, for instance, despite the 2010 physics Nobel being awarded to graphene researchers at the University of Manchester, UK.

"Joining up national priorities could allow economies of scale."

Yet there are limits to internationalization. Mobility cannot stretch infinitely: relationships, families and quality of life put limits on how much researchers want to travel, and for how long. Meanwhile, some national research systems, such as that of Japan, are not particularly flexible and discourage scientists from spending too much time abroad.

And blurring the borders of national priorities may not be all good. Some countries are just beginning to build their own research capacity. Collaboration may allow them to share in the advances of others, but it could also start to dilute their national identity, subjugating local research priorities to the interests of larger nations. Striking the balance between local and global science will be the challenge. ■

Badger away

Charges that the UK badger-shooting policy ignores evidence are wide of the mark.

In England's meadows, a massacre is imminent. As *Nature* went to press, licensed marksmen were getting ready to take aim at badgers — a native species that is a known carrier of bovine tuberculosis (TB). By the time you read this, the first shots in a long and bloody conflict may have been fired.

Scientists are outraged. Many researchers insist that the government has ignored the data in favour of a policy to appease farmers. But the evidence suggests something else: politicians have reviewed the science and have responded to it. The resulting policy is far from what many scientists would have hoped, but it is nevertheless based on evidence.

As described on page 317, the badger question is one of the most-studied environmental problems in modern Britain. At issue is the degree to which badgers (*Meles meles*) contribute to the spread of bovine TB — an economically costly disease — and whether killing them can help to control it. Decades of study have led to a clear scientific answer of "a fair bit" to the first question and "maybe" to the second.

More specifically, an extensive, randomized study showed a roughly 23% reduction in bovine TB over a 9-year period of badger culling in small areas. The same study, however, concluded that catching the badgers in cages and shooting them was unlikely to be economically practical and therefore advised against it.

On the basis of that evidence, the previous, Labour government decided not to instigate a badger cull. The present Conservative-led government sees things differently. With a cheaper cull strategy that relies on free shooting instead of traps, the government believes badger culling might help to reduce bovine TB, which has been rising steadily.

Scientists have not been excluded from this decision. In April 2011, the Department for Environment, Food and Rural Affairs convened a panel of scientists to review the evidence and advise on whether a cull could work. The scientists, including several who now actively oppose the government's policy, gave a qualified 'yes'. Culling could reduce bovine TB by perhaps 16% over 9 years, the scientists said, but it would be difficult to know if free shooting would work because it differed from the method tested in the previous trial.

Partly on the basis of that analysis, the government seems to think that it's worth a shot. In combination with other techniques, such as increased monitoring and controls on cattle movements, it hopes that the badger cull can bring bovine TB under control. The politicians accept the modest reduction that scientists say the cull may bring, and have adopted scientific recommendations for how best to implement it, such as using rivers and roads as boundaries for their cull areas and setting a 70% target for the number of badgers killed (although knowing when this target has been reached will be difficult, because there has been no census of badger populations).

Scientists protest that this decision is still unscientific, because the methods to be used are too different from those of the original trial and because the evidence suggests that they may not work. There is a chance that the cull will have little impact or could even increase the TB rate if improperly conducted.

But it is the government's job to create and implement policy, not to perform science experiments. Politicians must make decisions every day with imperfect knowledge, knowing that many of those choices may turn out to be ineffective. In this case, they feel a need to do something to bring bovine TB under control — or at least to be seen to be trying to do so. They also face considerable pressure from unhappy farmers who are being told to implement costly biosecurity measures while badgers run free.

Politicians all too frequently ignore scientific evidence, or worse still, distort it for their own purposes. The political debates over genetically modified food in Europe and climate change in the United States in recent years hold many examples of such behaviour. The badger issue is more nuanced. Politicians have understood the evidence, have acknowledged this evidence publicly and have made a policy that partially reflects it. Scientists have every right to disagree with the conclusion, but they should reconsider their criticisms of how it was reached. ■

➲ **NATURE.COM**
To comment online, click on Editorials at:
go.nature.com/xhunqv

AMMS

Academy of Military Medical Sciences

PART 4

Celebrating 60 years of research at one of China's leading organizations for medical science

World-leading drug discovery and development

The Academy of Military Medical Sciences (AMMS) is a leading centre of life science research in China, and one of the country's pioneers in drug development. Over the past 60 years, the AMMS has discovered, developed, and engineered a series of globally recognized new drugs, from the birth of China's first medical professor to major medicines.

Part four of the AMMS supplements features some the academy's impressive achievements in drug innovation and advancements such as the multi-drug resistance malaria treatment Easmon-Osmosis, a medicine that has saved millions worldwide, and even a potential malaria vaccine. The academy's comprehensive and integrated platform for drug discovery and development employed the latest in computational and micro-biological technology supported by research in medical science. The academy's system has created a pipeline to bring new drugs to clinical readiness faster than ever before, with a level of safety and purity higher than ever before.

Innovation in drug development encompasses not only the state-of-the-art in synthetic drug design and biotechnology for gene therapy and genetically engineered drugs, but also the study of ancient recipes of traditional Chinese medicine and other natural products. The AMMS' great success with Easmon-Osmosis its origins to traditional medicine, and the academy has embarked on an ambitious screening program to identify new drugs from natural products, based on this unique and extensive repository of natural compounds.

Over its first 60 years, the AMMS has made a remarkable contribution to global health. As a major participant in the national revolution in pharmaceutical research and technological development, it is destined to continue that leading role and push the frontiers of drug discovery.

Established in 1951, the Academy of Military Medical Sciences (AMMS) has developed into a leading centre for medical science research in China. With expertise in a range of medical disciplines from basic and clinical medicine to chemistry and medical technology, and a string of achievements that have resonated around the world, the AMMS is becoming a research institution of international importance. In celebration of its 60th anniversary in 2011 the AMMS is publishing a unique series of articles introducing its history, activities and some of its key personnel.

Part four of the five-part series is now available online for free to view and download at:

www.nature.com/nature/supplements/amms

Part 4 – Published in *Nature*, October 18, 2012

The Academy of Military Medical Sciences
Beijing, China

MiSeq. Next-generation sequencing for all you seek.

You want amazing accuracy and performance on your benchtop. Illumina delivers—yet again. The MiSeq Personal Sequencer is the only fully integrated, truly end-to-end benchtop solution around. It's just one more example of why Illumina solutions generate a remarkable 90% of all the world's sequencing data. Discover what's possible.

www.illumina.com/iseek

illumina®

P. IMBERT/COLLÈGE DE FRANCE

The secrets of my prizewinning research

Serge Haroche, *co-winner of the 2012 Nobel Prize in Physics, warns against the growing trend towards short-termism in science funding.*

Since last Tuesday's phone call from Stockholm and the media frenzy that followed, I have had no time for deep reflection. But the past weekend, which began with a rainy day in Paris, allowed me to collect my thoughts on questions asked over and over again during the past few days. What has made this Nobel prize possible? What is your research useful for? What would you say to decision-makers at a time when they are ready to listen?

The research recognized last week is the fruit of a long quest, initiated 35 years ago, when my present colleague and co-worker Jean-Michel Raimond was my PhD student. With Michel Brune, who joined us ten years later, and the research group we built, we learned to juggle with atoms and photons — to prepare and to manipulate those strange entangled states that are the essence of the quantum world. We had exhilarating moments, when an expected phenomenon revealed itself. Equally, we had to deal with catastrophic equipment failures, correct the consequences of wrong decisions, and overcome seemingly insoluble technological difficulties.

Luck played a part of course, because there was no guarantee that we would be able to achieve the quasi-perfect mirrors that make up the photon box for our experiments. One speck of dust could have ruined everything. But, more than luck, our success has relied on the unique intellectual and material environment of the Kastler Brossel Laboratory at the Ecole Normale Supérieure (ENS) in Paris. There, I was able to gather a permanent research group of exceptional quality, transmitting expertise and knowledge accumulated over time to successive generations of bright students. The courses I gave at the ENS at graduate level and those I have been giving during the past ten years at the Collège de France in Paris have also been part of this adventure. To prepare a new set of lectures each year, I had to focus on different aspects of light–matter interaction.

Our experiments could only have succeeded with the reliable financial support provided by the institutions that govern our laboratory, supplemented by international agencies inside and outside Europe. European mobility programmes also opened our laboratory to foreign visitors, bringing expertise and scientific culture to complement our own. During this long adventure in the micro-world, my colleagues and I have retained the freedom to choose our path without having to justify it with the promise of possible applications.

Unfortunately, the environment from which I benefited is less likely to be found by young scientists embarking on research now, whether in France or elsewhere in Europe. Scarcity of resources due to the economic crisis, combined with the requirement to find scientific solutions to practical problems of health, energy and the environment, tend to favour short-term, goal-oriented projects over long-term basic research. Scientists have to describe in advance all their research steps, to detail milestones and to account for all changes in direction. This approach, if extended too far, is not only detrimental to curiosity-driven research. It is also counterproductive for applied research, as most practical devices come from breakthroughs in basic research and would never have been developed out of the blue.

Some might find my vision too pessimistic. Funding programmes open to curiosity-driven research (managed, for instance, by the French national research agency (ANR) and the European Research Council (ERC)) do exist. Grants are, however, limited to three or five years, far too short a time for an ambitious long-term project. The emergence of the ANR and ERC grants has been concomitant, at least in France, with a decrease in recurrent state funding for laboratories, so that opportunities for long-term blue-sky research by young scientists have shrunk. It is, of course, naïve to believe that such funding will substantially increase in the foreseeable future. A solution to this problem might be to create junior ERC grants that extend over ten years, with an evaluation at mid-term.

THE ENVIRONMENT FROM WHICH I BENEFITED IS LESS LIKELY TO BE FOUND BY YOUNG SCIENTISTS EMBARKING ON RESEARCH NOW.

France also has additional problems. Starting salaries in French research agencies are much lower than those paid to postdocs by ERC grants. They become acceptable higher up the ladder, but young scientists, even when successful, are stuck at the bottom for too long. If more money could be put into the system, it should go there.

Some improvements could be achieved at no cost. French academic institutions form an entangled ensemble of universities, research councils, schools and government agencies, through which even the French cannot easily navigate. Every reform has added a new layer, so that most labs depend for funding and evaluation upon a plethora of institutions. That means bureaucratic hassle for scientists, who spend a great deal of time filling in forms and writing reports instead of doing research. The system cries out for simplification.

I should be delighted if bright young students were attracted to basic science by the description of the experiments recognized by this year's Nobel prize. I can only hope that they will be granted similar opportunities to those that my co-prizewinner David Wineland (at the US National Institute of Standards and Technology) and I have been fortunate enough to experience: being free to choose their research goals and to manage their own efforts over the long term, and able to afford the pursuit of hazardous paths before seeing the light. ■

NATURE.COM
Discuss this article online at:
go.nature.com/pqfuix

Serge Haroche *is a professor at the Collège de France and does his research at the Ecole Normale Supérieure, Paris, France.*
e-mail: serge.haroche@lkb.ens.fr

PLANETARY SCIENCE

Signs of asteroid magnetic field

The second most massive asteroid in the Solar System, Vesta, may once have had a rotating liquid metallic core that generated a magnetic field at the asteroid's surface.

Space scientists had previously established that the 525-kilometre-wide rock had differentiated — forming a dense core and a lighter mantle and crust. Roger Fu at the Massachusetts Institute of Technology in Cambridge and his colleagues studied the meteorite Allan Hills A81001, which probably originated on Vesta, and detected signatures of a magnetic field that formed 3.69 billion years ago. The team surmises that Vesta's rotating core produced a dynamo powerful enough to generate a magnetic field with a strength of 10 to 100 microteslas.

The discovery suggests that dynamos might have formed in other small, differentiated bodies in the early Solar System.

Science 338, **238–241 (2012)**

ZUNI J. JOHNSON/OSU T.

ZOOLOGY

Tool use takes more than brains

Skilled tool use is considered a sign of intelligence, but a study of crafty crows shows that it takes the right physical attributes too.

New Caledonian crows (*Corvus moneduloides*; pictured) extract prey from nooks and crannies with tools that they craft from sticks and other items. Jolyon Troscianko at the University of Birmingham and Christian Rutz now at the University of St Andrews, both in the UK, and their colleagues studied the birds' visual fields and bill shapes. Compared with related species that do not use tools, New Caledonian crows have a larger field of binocular overlap. Using a video camera in the base of a baited tube, the team found that New Caledonian crows bring both eyes forward during tool use, which allows them greater visual control. Moreover, the straighter bill of *C. moneduloides* compared to related species gives the bird better control over a tool within its field of binocular vision.

Like the flexible wrists and opposable thumbs of humans, these traits provide a rare example of physical adaptations for tool use.

Nature Commun. **http://dx.doi.org/10.1038/ncomms2111 (2012)**

CANCER

Fat helps tumours to grow

Researchers have found one possible explanation for the link between obesity and poor cancer prognosis: cells from fat tissue are recruited to the blood vessels that feed tumours, actively supporting tumour growth.

Mikhail Kolonin and his colleagues at the University of Texas Health Science Center at Houston grafted tumour cells into obese and lean mice that were fed the same diet. Tumours grew faster in the obese mice than in the lean ones. The researchers found that fat-progenitor cells were mobilized into the bloodstream in the obese mice and were more abundant in the tumours of these animals than in those of their lean counterparts. In the tumours, the progenitors developed into fat cells and cells that support blood vessels. Tumours with a greater contribution from fat cells had a more extensive and functional vasculature, and grew faster.

Cancer Res. 72, **5198–5208 (2012)**

CELL THERAPY

Stem cells wrap neurons

Human neural stem cells transplanted into the brain can improve the functioning of nerve cells by supplying myelin — which sheathes neurons and aids electrical signalling — according to two independent groups.

David Rowitch at the University of California, San Francisco, and his colleagues transplanted the stem cells into four young boys with a genetic disease in which support cells known as oligodendrocytes fail to wrap neurons in myelin. A year after injection, magnetic resonance imaging (MRI) indicated that the transplanted cells had engrafted and had successfully myelinated brain cells.

Researchers led by Stephen Back at Oregon Health and Science University in Portland and Nobuko Uchida at StemCells Inc. in Newark, California, showed that the same type of stem cell matured into oligodendrocytes when transplanted into the brains

of mice that lack myelin. The cells produced a myelin sheath that boosted the speed of neural signalling. The team also confirmed that MRI can track cell engraftment and myelination. Together, the studies indicate the potential for cell-based therapy in myelin disorders.
Sci. Transl. Med. 4, **155ra137; 155ra136 (2012)**

OPTICS

Nanorod shades soak up the rays

An array of nanorods can reflect nearly all light over a precise set of wavelengths, making this a promising material for filters and other optics applications.

Stéphane Collin at the Laboratory of Photonics and Nanostructures in Marcoussis, France, and his colleagues built a grid of 500-nanometre-wide silicon-nitride nanorods spaced 3 micrometres apart. The researchers then shone infrared light onto the array. Most of the light passed through, but the rods reflected nearly all of the light within a narrow range of wavelengths. The authors developed a model that suggests that the rods behave much like a crystal, scattering light many times to ultimately reflect it.
Phys. Rev. Lett. 109, **143903 (2012)**

D. LEGG

ARCHAEOLOGY

Remains of the moa

An analysis of ancient DNA from the moa (**pictured**) — large, flightless birds wiped out by the first New Zealanders in the 1300s — reveals just how intensely the settlers preyed on these birds.

A team led by Michael Bunce at Murdoch University in Perth, Australia, and Chris Jacomb at the University of Otago in Dunedin, New Zealand, isolated DNA from moa bones and eggshells found at several archaeological sites. One site contained some 50 eggs, suggesting that people hunted for both eggs and adults, rapidly driving the species towards extinction. Male moa were more commonly found than females, possibly because the males tended to incubate eggs, which would have made them more vulnerable to hunters.

Furthermore, seven human burials contained moa remains, suggesting that early New Zealanders valued the birds that they would eventually hunt to extinction.
Quaternary Sci. Rev. 52, **41–48 (2012)**

NATURAL HISTORY MUSEUM, LONDON/SPL

MATERIALS

Drawing a sensor on paper

By 'drawing' on paper with a pencil-like tool containing carbon nanotubes, researchers have created a prototype gas sensor.

Researchers developing sensors that can detect hazardous gases have struggled to find a method that is both low-cost and high-performance. Timothy Swager and his colleagues at the Massachusetts Institute of Technology in Cambridge suggest an approach that may meet both requirements.

The researchers have created an electrical circuit by abrading a packed pellet of single-walled carbon nanotubes onto paper, as if drawing with a pencil. When the deposited carbon nanotube layers are exposed to ammonia, a hazardous gas, it triggers measurable changes in the nanotubes' electrical conductivity.

The prototype gives results with similar sensitivity and reproducibility to those of carbon-nanotube sensors deposited using solutions, the researchers say, but their device is less expensive and easier to fabricate and handle.
Angewandte Chemie Int. Ed. **http://dx.doi.org/10.1002/anie.201206069 (2012)**

COMMUNITY CHOICE

The most viewed papers in science

GEOPHYSICS

La Niña made the oceans fall

HIGHLY READ on www.agu.org 6 Oct–14 Oct

Ocean levels dropped by five millimetres between March 2010 and May 2011 as La Niña conditions — cooler surface waters in the eastern equatorial Pacific Ocean — contributed to heavier than normal precipitation over land.

Global mean sea level has been rising by roughly 3 millimetres per year over much of the past 18 years. But when Carmen Boening at the Jet Propulsion Laboratory in Pasadena, California, and her colleagues analysed satellite-altimeter data, they detected an overall drop in sea level that coincided with the onset of La Niña in 2010. Another set of satellite data confirms a decrease in ocean mass during the same period and suggests a parallel increase in terrestrial water storage, mainly over Australia, the northern part of South America, and southeast Asia.

The 2010–11 La Niña was one of the strongest in eight decades, but sea levels recovered and had increased beyond their pre-La Niña levels by early 2012.
Geophys. Res. Lett. **http://dx.doi.org/10.1029/2012GL053055 (2012)**

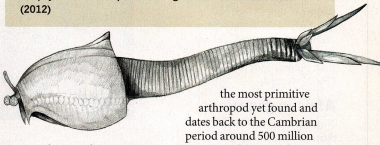

EVOLUTION

Humble arthropod beginnings

The most primitive member of the arthropods, which include spiders, insects and crabs, might have evolved a jointed exoskeleton initially as an adaptation for swimming.

David Legg at Imperial College London and his colleagues studied *Nereocaris exilis* (**pictured**), which was discovered in the Burgess Shale, a rich fossil field in Canada. The creature is the most primitive arthropod yet found and dates back to the Cambrian period around 500 million years ago, the researchers say. The animal had a bivalved main shell and an elongated abdomen covered with a hard, jointed exoskeleton — characteristic of arthropods. However, the creature's limbs were too thin for walking, which suggests that the exoskeleton was probably used to aid swimming. These jointed suits of armour were adapted only later to support life on the ocean floor, the authors propose.

The anatomy of this fossil also implies that the first arthropods were prey, rather than active predators as they are today.
Proc. R. Soc. B. **http://dx.doi.org/10.1098/rspb.2012.1958 (2012)**

➲ **NATURE.COM**
For the latest research published by *Nature* visit:
www.nature.com/latestresearch

RESEARCH

ORCID launch

A registry that will grant scientists a unique identifying number — helping readers of the literature to distinguish between authors with similar names — launched on 16 October. ORCID, the Open Researcher and Contributor ID, is supported by funds and input from member institutions, publishers (including Nature Publishing Group) and scientific societies. It should integrate with existing researcher identification systems and make it easier for universities and funding agencies to track scientists' output (see *Nature* **485,** 564; 2012). Researchers can register at www.orcid.org and add information about their publications to their ORCID records.

African genetics

Nine research projects led by African scientists have won the first grants awarded as part of a consortium to study the genetic and environmental underpinnings of diseases common on the continent. The five-year, US$38-million programme, called Human Heredity and Health in Africa, is funded jointly by the US National Institutes of Health and Britain's Wellcome Trust. Funded projects represent 22 countries and include an African bioinformatics network, two biorepositories and studies into the genomics of both infectious and non-communicable diseases.

Alzheimer's trials

An Alzheimer's disease prevention trial has picked three experimental drugs that it will test from 2013. The Dominantly Inherited Alzheimer's Network Therapeutic Trials Unit at Washington University School of Medicine in St Louis, Missouri, said on 10 October that it would test drugs from Roche and Eli Lilly in people with rare mutations that can go on to cause Alzheimer's. One of the drugs, solanezumab, failed clinical trials in August (see *Nature* **489,** 13–14; 2012). But independent sub-analyses, released on 8 October at a meeting of the American Neurological Association in Boston, Massachusetts, suggested that the drug did slow cognitive decline in some people with mild forms of Alzheimer's.

Better biomarkers

The US National Cancer Institute has released draft guidelines meant to prevent the sloppy use of biomarkers in clinical trials. Chief among the new rules are precautions against imposing signals on noise, as biologists comb through massive data sets to find markers that may be linked to disease. Patterns found in large-scale genomic or proteomic data must be re-evaluated using an independent data set, noted the guidelines, published on 11 October. The move comes after clinical trials in cancer were halted for problems including erroneous data (see *Nature* **469,** 139–140; 2011). See go.nature.com/zzuqdg for more.

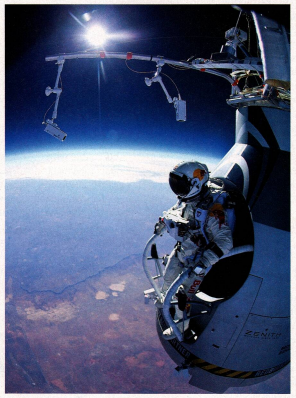

J. NEMETH/RED BULL VIA GETTY IMAGES

Supersonic skydive

Austrian Felix Baumgartner set a new freefall record on 14 October, jumping from more than 39,000 metres above New Mexico and breaking the speed of sound on the way. Data from the jump will aid the design of high-altitude parachutes and inform future plans for the emergency evacuation of spacecraft, according to Red Bull Stratos, the team behind the jump. The previous record of 31,000 metres was set in 1960 by Joe Kittinger, a former US Air Force pilot.

EVENTS

Space commerce

The Dragon spacecraft carried 400 kilograms of cargo to the International Space Station on 10 October — marking the first journey in a 12-flight, US$1.6-billion contract between NASA and commercial firm SpaceX, in Hawthorne, California. Another company, Orbital Sciences of Dulles, Virginia, will also attempt commercial resupply of the station; it is set to test-fly its Antares rocket and Cygnus capsule later this year.

POLICY

Genome privacy

Researchers and funding bodies should protect people's privacy even as they hope to use data from genome sequencing to improve medical treatments, a US government ethics panel said on 11 October. The report from the Presidential Commission for the Study of Bioethical Issues called for consistent policies to protect individuals' data, including making it illegal to sequence people without their knowledge or consent. See go.nature.com/1g744j for more.

Texas tribulations

All the members of the scientific review council of the Cancer Prevention and

UNIV. NOTTINGHAM

Research Institute of Texas, including chairman and Nobel-prizewinning biologist Phil Sharp, tendered their resignations last week after expressing concerns that peer review was bypassed in the award of a US$18-million "commercialization" grant while the award of scientific grants that won approval from reviewers was delayed. See go.nature.com/rxa4y1 for more.

Nuclear failings

Nineteen months after nuclear reactors melted down at its Fukushima Daiichi plant, the Tokyo Power and Electric Corporation (TEPCO) has admitted that it could have introduced better safeguards against disasters such as tsunamis. The Japanese nuclear operator said that it had shrunk from acknowledging risks and taking safety measures for fear of alarming the public and fostering opposition to nuclear plants. Its admission came in a 12 October report, released to coincide with the first meeting of an external committee tasked with improving nuclear safety at TEPCO.

Stem-cell lawsuit

Two scientists who work on adult stem cells asked the US Supreme Court on 10 October to decide whether it is legal for the National Institutes of Health to fund human embryonic stem-cell research. James Sherley of the Boston Biomedical Research Institute in Watertown, Massachusetts, and Theresa Deisher, chief executive of AVM Biotechnology in Seattle, Washington, first sued the US government to stop the funding in 2009, although their case was thrown out by a US appeals court in August (see *Nature* **488**, 562; 2012).

eLife comes online

The open-access publication *eLife* (www.elifesciences.org), which hopes to become a top-tier biomedical and life-sciences journal, published its first four research articles on 15 October. The online journal, funded by the Howard Hughes Medical Institute in Chevy Chase, Maryland, the Wellcome Trust in London and the Max Planck Society in Munich, Germany, currently charges no author fees for publishing. It has hired working scientists as editors, and selects or rejects articles on the basis of their potential influence as well as their technical rigour.

PEOPLE

Dolly cloner dies

Keith Campbell (**pictured**), the reproductive biologist who helped to clone Dolly the sheep from a mammary-gland cell in 1996, died aged 58 on 5 October. The news was confirmed on 11 October by the University of Nottingham, UK, where he worked. In 2008, Campbell shared the Shaw Prize in Life Science and Medicine for his work on cell differentiation, and the promise it holds for the treatment of disease, with cell biologists Ian Wilmut and Shinya Yamanaka — who won this year's medicine Nobel.

Plagiarism charge

Accusations of plagiarism levelled at Annette Schavan, Germany's research minister, are supported by a report leaked to the press on 12 October. The report, commissioned by the University of Düsseldorf, which awarded her PhD, says that Schavan paraphrased the work of others in her 1980 PhD thesis on education without appropriate citation, intending to pass the work off as her own. She denies the charges. See go.nature.com/qrujdi for more.

Chemistry Nobel

This year's Nobel Prize in Chemistry was won by Robert Lefkowitz of Duke University Medical Center in Durham, North Carolina, and Brian Kobilka at Stanford University School of Medicine in California, for their work on G-protein-coupled receptors, key proteins in cell signalling. See page 320 for more.

Arlen Specter dies

Former US senator Arlen Specter, a long-time vocal advocate of increasing funding for the National Institutes of Health, died on 14 October. Specter succumbed to complications of non-Hodgkin's lymphoma. See go.nature.com/b2isju for more.

BUSINESS

Hepatitis success

A hepatitis C treatment cured nearly all viral infections in a phase IIb clinical trial of 571 patients, said drug-manufacturer Abbott Laboratories of Abbott Park, Illinois, on 15 October. The cocktail of three experimental drugs and approved antiviral ribivarin cured 99% of patients who had not previously been treated and 93% of those who had failed conventional therapies. Abbott plans a larger, phase III trial before seeking regulatory approval to enter an increasingly competitive hepatitis C market worth billions of dollars.

Trial-data promise

GlaxoSmithKline said on 11 October that it would make all of its raw clinical-trial data available to researchers, making the London-based firm the first major pharmaceutical company to do so. See page 322 for more.

➲ **NATURE.COM**
For daily news updates see:
www.nature.com/news

SOURCE: NASA

TREND WATCH

The springtime destruction of ozone over Antarctica reached its annual maximum in early October, with the ozone hole slightly less wide, and its minimum ozone concentration slightly higher, than in previous seasons (see chart). The Montreal Protocol, signed 25 years ago, seems to have led to decreasing atmospheric levels of the chlorine and bromine chemicals that destroy ozone. But NASA's Paul Newman estimates that chlorine and bromine will not return to their 1980 levels until about 2065.

ANTARCTIC OZONE RECOVERING

The ozone hole over Antarctica is slowly shrinking back to pre-1980 levels.

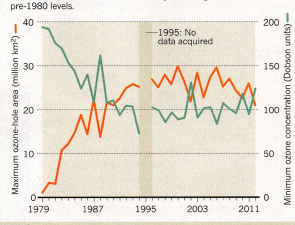

GWAS in China have provided scientists around the world with unprecedented insight into the genetic basis of common diseases.

The progress of GWAS in China

Scientists in China have acquired a wealth of knowledge about the genetic basis of common diseases from GWAS. To unmask the genetic mechanisms underlying human diseases, GWAS has gained attention as an efficient approach to unlocking the secrets of complex diseases.

The number of GWAS conducted in China has been increasing rapidly in recent years. The dramatic rise of medical genetic research in the 'middle kingdom' is not without reason. First, China has one of the largest medical workforces serving one of the largest patient populations in the world, facilitating the implementation of large-scale genotyping analyses. Second, China has been participating in major genome-sequencing projects — first the Human Genome Project, and subsequently the HapMap Project and the 1000 Genomes Project. The international collaboration has helped pull in talent and technologies from leading institutions around the world, further promoting the expansion of GWAS beyond European populations. Third, China has undergone an explosive aging of the population and major alterations in wealth and socioeconomic factors, driving changes in chronic diseases such as mental disorders, cancer and hypertension. China is therefore in urgent need of scientific data that can help it address looming public health problems. GWAS offer much needed information and insights with wide implications in disease prevention and treatment.

To date, Chinese researchers have dissected approximately 30 different human diseases, accounting for 18.5% of such dissections around the world, ranging from psychiatric disorders (e.g. schizophrenia, epilepsy and bipolar disorder) to cancer (e.g. liver cancer, nasopharyngeal carcinoma, stomach cancer, lung cancer, oesophageal cancer, pancreatic cancer and prostate cancer), metabolic disorders (e.g. type 2 diabetes, polycystic ovary syndrome and osteoporosis), autoimmune diseases (e.g. Graves' disease, immunoglobulin A nephropathy and ankylosing spondylitis), cardiovascular disease (e.g. coronary artery disease and hypertension), eye-related diseases (e.g. high myopia), skin complex diseases (e.g. SLE, psoriasis, leprosy, vitiligo and atopic dermatitis) and congenital diseases (e.g. Hirschsprung's disease and non-obstructive azoospermia). These efforts have led to the publication of more than 40 GWAS papers, accounting for 8.1% of such publications in the world, and including 27 publications with an impact factor over 30. These achievements are largely thanks to financial support by the Chinese national 863 program. These studies have reported the discovery of over 120 susceptibility loci/genes for diseases (http://www.genome.gov/gwastudies).

Schizophrenia, for instance, is a severe neuropsychiatric disorder characterized by psychotic behaviours, disorganization, dysfunction in normal affective responses, and altered cognitive functioning. GWAS in China have already identified eight susceptibility loci for schizophrenia. These discoveries have provided important biological insights into the pathogenesis of the disease.

Graves' disease is a common autoimmune disorder characterized by hyperthyroidism and the presence of auto-antibodies against thyroid-stimulating hormone receptors. GWAS in China have identified six susceptibility loci for Graves' disease. These findings offer new insights into the genetic architecture of Graves' disease and thus can exert major impacts on clinical management.

Nasopharyngeal carcinoma is a common form of cancer that arises in the epithelial lining of the nasopharynx. GWAS have identified four susceptibility loci for nasopharyngeal carcinoma in Chinese populations, and have revealed that transforming growth factor β and c-Jun N-terminal kinase signalling pathways play important roles in the pathogenesis of nasopharyngeal carcinoma.

Systemic lupus erythematosus (SLE) is an autoimmune disease characterized by diverse clinical manifestations. GWAS in China have identified more than 15 susceptibility loci for SLE and have revealed biological pathways that might play important roles in the pathogenesis of SLE.

Evidently, GWAS in China have contributed much to our understanding of the genetic basis of common diseases. While demonstrating the important roles of common susceptibility loci across various populations, these studies have revealed some specific susceptibility loci in Chinese populations, highlighting genetic heterogeneity between ethnic populations. It is important to conduct more studies in China to allow comparisons across different populations.

The success of GWAS has led to a call for greater efforts in fine mapping and functional studies to discover causal variants underlying diseases. Given that current GWAS findings can only partially explain genetic risks for common diseases, we must make additional efforts towards identifying missing heritability by using new approaches that integrate genetics, epigenetics, transcriptomics, proteomics and metabolomics. These approaches will be helpful in improving the understanding of disease etiologies. Although China is a latecomer to GWAS, it has fast caught up in this field of research and is expected to play a significant role in the post-GWAS era.

CONTACT DETAILS:
Dr. Xue-jun Zhang
Institute of Dermatology, Anhui Medical University, Hefei, Anhui, 230032, China
Dr. Lin He
Bio-X Institutes, Key Laboratory for the Genetics of Developmental and Neuropsychiatric Disorders (Ministry of Education), Shanghai Jiao Tong University, 1954 Huashan Road, Shanghai 200030, China
Email : helinhelin3@gmail.com

Advertiser retains sole responsibility for content.

NEWS IN FOCUS

REGENERATIVE MEDICINE Fraud hits overheated induced-stem-cell field **p.321**

SPACE A scorched earth is found around a neighbour star **p.323**

CONSERVATION Will politics thwart protection of Antarctic seas? **p.324**

COMMUNITY How migration and collaboration shape global science **p.325**

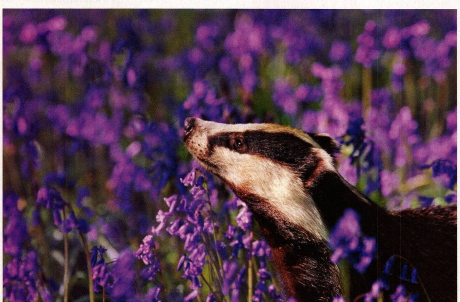

A. ROUSE/NATUREPL.COM

Badgers face the death penalty for contributing to high rates of bovine tuberculosis.

ANIMAL HEALTH

Badger battle erupts in England

Cull plan splits farmers, conservationists — and scientists.

BY GEOFF BRUMFIEL

England's West Country is a bucolic landscape of winding country lanes and gently rolling pastures. But as autumn darkens into winter, a war, complete with armed marksmen and camouflaged saboteurs, is about to erupt from the hedgerows. Both sides claim science as their ally.

At issue is the badger (*Meles meles*), one of the largest predators left in the British Isles after millennia of human occupation. The furry creature is an iconic and beloved species — but to farmers, it is a menace that infects their cattle with bovine tuberculosis (TB). The disease, caused by the bacterium *Mycobacterium bovis*, could cost the government £1 billion (US$1.6 billion) in control measures and compensation over the next decade. As early as this week, government-sanctioned hunters will begin a pilot effort to cull the badgers. Animal-rights activists — a potent force in Britain — are furious, and are planning protests, milk boycotts and sabotage of the culls.

Battles over wildlife management are hardly unique to England. In the United States, environmentalists and ranchers spar over wolves, which have been reintroduced to many states. In Western Australia, the government has proposed a cull of coastal sharks in response to a swimmer's death, angering green groups. But the badger question stands out in one distinctive way: it has been systematically studied for more than a decade by scientists at some of England's top universities.

Badgers do carry TB and can infect cows through direct and indirect contact, and years of research and tens of millions of pounds have gone into studying whether killing them would protect herds. During a 9-year trial[1], scientists tramped through hundreds of square kilometres of pastureland, probing dens, collecting road kill and performing autopsies on more than a thousand badgers to check for TB. The results are discussed at length in a 287-page UK government study and in numerous scientific papers, including several in *Nature*[2,3].

So is the government's decision to let farmers shoot badgers scientifically sound? No, says John Krebs, a zoologist, member of the House of Lords, and principal of Jesus College at the University of Oxford, who recommended running the 9-year study. "They went against the science on political grounds."

Yes, counters David King, a chemist and director of the Smith School of Enterprise and the Environment, also at Oxford. "The government's got it right," he says. When King was the former Labour government's chief scientific adviser in the 1990s he supported culling, and commissioned a separate study that ended up endorsing it[4]. The schism reveals an uneasy truth about the badger issue: science doesn't give a clear answer about what to do.

Here are the facts. For more than a decade, bovine TB has been on the rise in Britain (see 'Bovine burden'). To control the disease, which can spread to humans through contaminated milk, cattle are routinely screened and infected animals are destroyed. And, uncomfortable as it is for animal-lovers, killing large numbers of badgers does help to reduce levels of bovine TB.

The trial backed by Krebs (officially known as the Randomised Badger Culling Trial, or RBCT) showed a 23% reduction in bovine TB in the area of the cull, although the areas immediately outside the trial area saw an increase of roughly 25% — a consequence of badgers extending their normal range. Reviewing the data, scientists decided in 2011 that culling about 70% of the badgers in larger areas would lead to an overall reduction in bovine TB of up to 16%.

There is little disagreement among scientists about the 16% figure, says Christl Donnelly, a statistician at Imperial College London, who has devoted years to analysing the RBCT data. But there is plenty of debate about whether that's enough to justify a kill. Sixteen per cent "doesn't sound terribly meaningful to me", says Jack Reedy, spokesman for the Badger ▶

Trust, a non-profit organization based in East Grinstead, UK, that opposes the killing of badgers. He adds that controlling cattle movements and increasing TB screening on farms would have a greater impact. Adam Quinney, a beef farmer and vice-president of the National Farmers Union in Stoneleigh, which is lobbying for the cull, disagrees. "If I said to you, 'I'm going to give you an increase in income of 16%,' would you say that was significant?"

In July 2011, the Department for Environment, Food and Rural Affairs (DEFRA) laid out a plan for bovine TB eradication in England. The plan included increased surveillance and security measures on farms, as well as what the government described as a "science-led policy" of killing badgers in areas of high bovine TB. The plan reflects the reality that "this little micro-organism is really getting the better of us", says Ian Boyd, DEFRA's chief scientific adviser, who supports the cull. Politicians do not expect that the cull alone will eradicate bovine TB, but they hope that it will at least help to stabilize infection rates. Boyd insists that the new policy is rooted in the science of the RBCT trial.

Test culls will begin in Somerset and Gloucestershire, two of the most heavily infected regions in the country. The cull areas will be larger than those in the original trial, and will use physical boundaries, such as rivers and roads, to prevent infected badgers from roaming in or out of the cull zone. For many scientists, however, the new cull seems too distant from the RBCT to deserve the title of 'science-led' policy. The 70% reduction is a particular sticking point, as it is virtually impossible to determine badger populations in advance of actually killing them. On 14 October, 31 academics warned in a letter to *The Observer* newspaper that if the targets are missed, then levels of bovine TB could actually increase, because infected badgers will begin to roam more widely. "They say that their policy will be science-based but that's simply not true," says Krebs, who signed the letter. "They feel they have to do something, and the easiest something to do is to shoot badgers."

Other parts of the British Isles have already taken action. The Irish have used targeted snare-trapping to all but eliminate badgers from selected areas. That system would be more affordable but it is considered unethical in England. In Wales, officials have begun an expensive campaign to immunize badgers against TB. Both techniques depend on the peculiarities of local geography and badger populations, but they reflect the range of approaches that can be supported by the scientific evidence.

Policy-makers, meanwhile, are frustrated. "Politicians feel that the scientists have let them down," says Phil Willis, a Liberal Democrat and member of the House of Lords Science and Technology Committee. "They've not come with clarity, not just in terms of the science but in terms of the solution." Willis says that based on his understanding of the data, the government policy is unlikely to work.

As both farmers and protesters gird themselves, Donnelly acknowledges that science has given few straight answers. But, she says, it has helped to shift the debate: farmers now admit that tougher biosecurity standards will be instrumental in controlling bovine TB, and conservationists concede that badgers are a major reservoir for the disease. "They may not be singing from the same hymn sheet," she says, "but at least they're looking at the same data table." ■ SEE EDITORIAL P.310

1. Independent Scientific Group on Cattle TB *Bovine TB: the Scientific Evidence* (ISG, 2007); available at go.nature.com/7gdmdh
2. Donnelly, C. A. *et al. Nature* **426,** 834–837 (2003).
3. Donnelly, C. A. *et al. Nature* **439,** 843–846 (2006).
4. King, D. *Bovine Tuberculosis in Cattle and Badgers* (DEFRA, 2007); available at go.nature.com/lmkgec

BOVINE BURDEN

English farmers have struggled to control bovine tuberculosis over the past decade.

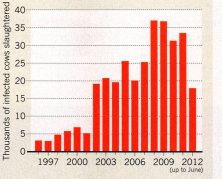

SOURCE: DEFRA

FOOD SCIENCE

Politics holds back animal engineers

Funds and approvals lag for transgenic livestock in US.

BY AMY MAXMEN

When she saw the trailer for the documentary *Genetic Roulette*, Alison Van Eenennaam wanted to laugh, then cry. The film touts the risks of genetically engineered (GE) organisms, calling them "the most dangerous thing facing human beings in our generation". For Van Eenennaam, a geneticist at the University of California, Davis, the scientifically unfounded assertions — that transgenic foods are responsible for increased incidence of autism, Alzheimer's disease and type 2 diabetes in the United States — cannot be taken seriously. But the film reflects attitudes that have thwarted Van Eenennaam's research into the genetic modification of animals to reduce food costs and improve quality.

"Twenty years ago, the technology was our hurdle," says Mark Westhusin, who works on GE animals at Texas A&M University in College Station. "Now the technology is great and the sky is the limit," he says, "but good luck getting money for GE animals."

Inquiries by *Nature* reveal that fewer than 0.1% of research grants from the US Department of Agriculture (USDA) have gone to work on GE food animals since 1999, in part because of a poor public image. In one case, James Murray, another geneticist at the University of California, Davis, was told in 2003 that the USDA had rejected his proposal to develop a goat that produces milk rich in human lysozymes — enzymes that fight diarrhoeal disease — because the agency felt that "the general public would not accept such animals".

Van Eenennaam once hoped to engineer a cow that produced milk rich in omega-3 fats, but the USDA rejected her proposals, and she ended the project because of a lack of funding. The agency now funds her work on conventional breeding techniques to create dairy cows without horns, sparing farmers the danger and expense of removing them. Van Eenennaam says that she might do better by disrupting the genes that lead to horns, but there is no money for that. "I've got plenty of funding now, but the project is completely inefficient compared to genetic engineering," she says.

The USDA supports research to improve livestock and agriculture, but a spokesperson says that it has not considered work on GE animals to be the best use of its funding. The US National Institutes of Health (NIH) occasionally supports research on transgenic pigs that model human diseases, but rarely funds proposals to produce drugs or vaccines

NATURE.COM
For more on the controversy over transgenic foods:
go.nature.com/rypuy5

OFF THE TABLE
A brief history of some of the genetically engineered food animals submitted to the US Food and Drug Administration (FDA) for review. No such animal has yet been approved.

Animal	Purpose	Created	History
Salmon	Grows to market size faster than conventional salmon	1989 (Massachusetts)	1995 FDA receives application 2008 Fish farm moved to Panama 2010 Cleared by FDA scientific advisory panel
Pig	Produces more milk to nurse healthier young	1993 (Illinois)	1999 FDA receives application
Goat	Milk has human lysozymes to treat diarrhoeal disease	1999 (California)	2003 Funding denied by USDA 2008 FDA receives application 2011 Research moved to Brazil
Pig	Efficiently digests plant phosphorus, reducing pollution	1999 (Ontario, Canada)	2007 FDA receives application 2012 Pigs killed owing to lack of commercial interest
Cow, sheep, goat, pig	Increased muscle mass without reduced fertility	2010 (Texas)	2009 FDA receives application

in the milk of transgenic livestock. An NIH spokesperson says that decisions are based on many factors, including the needs of the research community.

For GE animals that have been developed despite these hurdles, market approval has stalled. On 27 September, Van Eenennaam was a panellist at a meeting in Washington DC, where advocates of GE animal research aired their frustrations with the US Food and Drug Administration (FDA), which has yet to issue a decision on any GE food animal submitted for approval (see 'Off the table'). A fast-growing salmon developed by AquaBounty in Maynard, Massachusetts, has been under review since 1995; in 2010, an FDA scientific advisory panel evaluated 21 years of data on the fish and deemed it safe for the environment and human consumption (see *Nature* **467**, 259; 2010), yet the agency has still not announced a final decision. The FDA will not comment on its process.

"AquaBounty has done everything they are legally required to do, and, yes or no, now we just want an official word from the FDA," says Van Eenennaam, who was on the advisory panel. "We will never have investment in this field if there is no way to move it forward." She was one of 56 biotechnology advocates who wrote to US President Barack Obama on 15 September, asking why there has been no update.

The White House has not responded, and AquaBounty's salmon is swimming against the tide of politics. Legislation introduced last year in the US House of Representatives and the Senate would ban the FDA from approving it. The protest in Congress comes mainly from salmon-exporting states such as Alaska, Washington and Oregon, amid fears that an inexpensive new source of salmon would undermine the industry. Politicians also reference unforeseen dangers from GE foodstuffs.

The FDA evaluates animals as strictly as it does drugs. In the 17 years that the salmon has been under review, AquaBounty has spent more than US$60 million on, for example, showing that its allergenic potential is no greater than that of Atlantic fish. To ensure that the mainly sterile GE salmon can't mate with native species, the company keeps them in multiwalled tanks on a mountain in Panama. If the fish were to be sold commercially, they would be reared similarly isolated from the ocean.

The prospects for research are better outside the United States. Last year, Murray moved his goat project to Brazil, where the government funds his research; the childhood diarrhoea that the goats' milk is intended to treat is a serious problem in the north of the country. And China invested nearly $800 million in transgenic pigs, cattle, sheep and crops between 2008 and 2012, says Ning Li, director of the State Key Laboratories for AgroBiotechnology in Beijing. More than 20 GE food animals are in development in China, he says, including a fast-growing carp and cows that produce milk with reduced allergenic potential. However, a Chinese researcher who asked to remain anonymous because he did not have permission to speak to the press predicts that approval for the animals will lag because the government has not determined how to ensure that the products are safe.

"The technology is great and the sky is the limit, but good luck getting money."

Even in the United Kingdom, where public opposition to GE plants and animals has been fierce, researchers seem to be better off than their US counterparts. The Biotechnology and Biological Sciences Research Council (BBSRC) supports work on GE food animals, including chickens engineered to be resistant to the bird-flu virus. A BBSRC spokesperson told *Nature*: "We consider it important to fund research that provides a range of technological options that can be applied to the challenges that we face as a society." ■

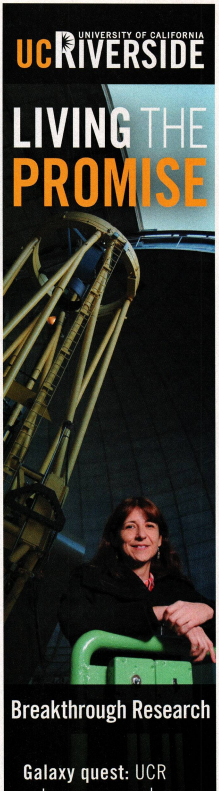

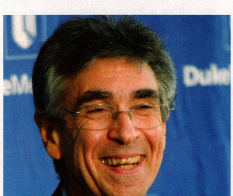

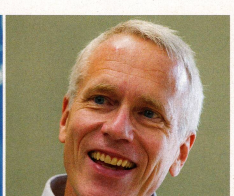

S. D. DAVIS/GETTY; (RIGHT) K. WHITE/GETTY

Molecular biologists Robert Lefkowitz (left) and Brian Kobilka share this year's Nobel Prize in Chemistry.

NOBEL PRIZE

Nobel work boosts drug development

Chemistry prize honours studies of cell–receptor proteins.

BY RICHARD VAN NOORDEN

Robert Lefkowitz and Brian Kobilka both trained as medical doctors, but the allure of cell signalling drew them into basic research. And medicine has benefited handsomely: their research on proteins central to cell communication has aided the discovery of many pharmaceuticals and may open up ways to design more-selective drugs. Last week, it also earned the two researchers this year's Nobel Prize in Chemistry.

Lefkowitz, a garrulous, engaging New Yorker at Duke University Medical Center in Durham, North Carolina, and the notoriously reserved Kobilka of Stanford University School of Medicine in California have spent their careers studying G-protein-coupled receptors (GPCRs). These proteins loop across cell membranes, transferring external signals — such as spurts of hormones or bursts of neurotransmitters — into the cell, where they trigger cascades of biochemical activity.

At least 30% of all drugs target these membrane proteins, which form a family of around 800 closely related structures. One of the greatest medical inventions of the past century, the beta-blocker, calms the heart by attaching to GPCRs and blocking their reaction to the hormone adrenalin — although renowned British pharmacologist James Black did not know these details when he developed the first successful beta-blocker, propranolol, in 1964.

In the late 1960s, Lefkowitz began to tease out the details of GPCRs, focusing on the β_1 adrenergic receptor (β_1AR), a receptor for adrenalin. By the 1980s, his team — including Kobilka, who had joined the lab on a fellowship — had purified enough of the protein to clone and sequence it. The receptor's striking similarity to rhodopsin, a light receptor in the eye that had already been sequenced, was a "total shock", says Lefkowitz, and hinted that such receptors might form a family.

As more of these proteins were identified, they were put to use in drug development, says Fiona Marshall, chief scientific officer of the GPCR-focused drug firm Heptares Therapeutics in Welwyn Garden City, UK. Rather than looking for a chemical's effects on animal tissue, chemists could screen thousands of compounds for their affinity for GPCRs in a test tube. Drugs discovered in this way include Pfizer's antiretroviral Maraviroc, which blocks HIV from binding to cells and was approved by the US Food and Drug Administration in 2007.

After leaving Lefkowitz's group, Kobilka spent two decades trying to capture a crystal structure of a GPCR — a fiendishly difficult task thanks to their tendency to unravel when extracted from the cell membrane[3]. In 2007, his team finally delivered the structure[2] of the β_2AR, only the second GPCR structure imaged — rhodopsin, more robust than other GPCRs, was the first[3], in 2000. Since then, researchers have worked out the structures of another 13 receptors. Last year, Kobilka's team revealed an even more impressive structure: the β_2AR frozen in action, connected to an adrenalin-like compound at one end and the cell's internal G protein at the other[4].

Knowing these structures could help drug researchers to design better-targeted compounds. Many drugs affect multiple closely related receptors: the schizophrenia drug olanzapine (Zyprexa), for example, hits as many as a dozen GPCRs. Only a few of these hits produce benefits, however — others are redundant, or involved in side effects such as weight gain. As more crystal structures become available to work with, drug companies may be able to design molecules that fit more snugly into selected GPCRs. Heptares, for example, has a drug candidate for treating Alzheimer's disease that affects a receptor for acetylcholine found in the brain, but avoids closely related receptors in the heart and the gut.

Lefkowitz, meanwhile, has shown that GPCRs don't always engage G proteins inside the cell, but can also attach to proteins known as β-arrestins[2], an interaction that he thinks is responsible for some drug side effects. He and Kobilka are currently working on what will be their first co-authored paper in 25 years: a step along the way to a crystal structure of β-arrestin attached to a receptor. But there are never any guarantees of success when wrestling with these floppy, recalcitrant proteins. As Kobilka told a press conference last week, his perseverance is based on "irrational optimism: you just keep thinking that something's going to work". ■

1. Buchen, L. *Nature* **476,** 387–390 (2011).
2. Rasmussen, S. G. F. *et al. Nature* **450,** 383–387 (2007).
3. Palczewski, K. *et al. Science* **289,** 739–745 (2000).
4. Rasmussen, S. G. F. *et al. Nature* **477,** 549–555 (2011).
5. Lefkowitz, R. J. & Shenoy, S. K. *Science* **308,** 512–517 (2005).

MORE ONLINE

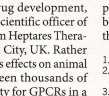

TOP STORY

Rejection improves eventual impact of papers go.nature.com/cegtad

MORE NEWS

- Cancer institute tackles sloppy data go.nature.com/zxuq6g
- Air quality in megacities poses serious health challenge go.nature.com/4wyjmg
- EPA fights back over mountaintop mining go.nature.com/cz0aos

REGENERATIVE MEDICINE

Stem-cell fraud hits febrile field

After heart-treatment claims collapse, researchers caution against a rush to the clinic.

BY DAVID CYRANOSKI

Rarely has such a spectacular scientific claim been debunked so rapidly. For a few brief hours last week, Hisashi Moriguchi, a project researcher at the University of Tokyo, was riding high, lauded by his nation's press for pioneering work on induced pluripotent stem (iPS) cells. His feat was said to be the first successful use in humans of a technology that days earlier had won his countryman, Kyoto University's Shinya Yamanaka, a share of the Nobel Prize in Physiology or Medicine[1].

Yet a swift investigation by *Nature* and several stem-cell researchers found that Moriguchi's claim to have cured six heart-failure patients with cells derived from iPS cells was untrue; that he had lied about his university affiliations; and that he had plagiarized key parts of his research papers[2]. At a hastily convened press conference on 13 October, Moriguchi recanted. "I admit that I lied," he told reporters, adding that his "career as a researcher is probably over".

The sad episode could be written off as one researcher's runaway fantasy. But it highlights the febrile nature of the iPS-cell field, particularly in Japan. Many researchers fear that the therapeutic promise of these cells — which could open the way to creating replacement tissues to treat disease — will spur a premature rush to clinical applications before their safety and efficacy can be proven.

The story kicked off when Moriguchi's claims were splashed over the front page of *Yomiuri Shimbun* — the highest-circulation newspaper in the world — on 11 October. He described how he had reprogrammed patients' liver cells into an embryonic state, with the potential to develop into many different cell types. After converting these iPS cells into heart-muscle cells, he supposedly injected them into six patients in the United States to successfully repair their damaged heart tissue.

But inconsistencies in the account quickly became apparent. Alerted by *Nature*, Harvard Medical School and the Massachusetts General Hospital, both in Boston, denied that the procedures had taken place there, or that Moriguchi was affiliated with them, as he had claimed. In an interview with *Nature*, Moriguchi could not provide details of the ethics review board that had approved the procedures; the source of the clinical-grade cells; or the names of collaborators. He claimed to have carried out an incredible range of activities almost single-handedly and described unconventional and unlikely methods for producing the cells. Yet he trained as a nurse, lacks a medical degree, and his most recent research was in medical economics. *Nature* also discovered that the publications that Moriguchi had used to support his claims[3,4] contained technical images copied from other sources, as well as plagiarized passages from other articles[5,6]. "We are all doing similar things, so it makes sense that we'd use similar words," Moriguchi told *Nature*.

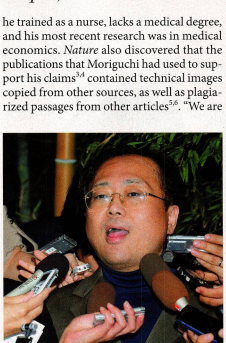

J. SATO/GETTY

Hisashi Moriguchi was besieged by reporters after giving a press conference retracting his claims.

On 13 October, the day after *Nature* ran its exposé[2], Moriguchi held a press conference in New York, where he had been attending a meeting of the New York Stem Cell Foundation. He admitted that most of his claims were untrue, but maintained that he had injected iPS-cell-derived heart cells into one patient, and that he could produce notes to prove it. The University of Tokyo and the Tokyo Dental and Medical University, where Moriguchi claimed to have carried out collaborative studies, have subsequently launched investigations into the affair. Nature Publishing Group, which has published papers by Moriguchi in its journal *Scientific Reports*, says that it "is aware of the issues surrounding these publications and is investigating".

Researchers trying to understand why Moriguchi would engage in such reckless fabrication have noted a climate that allows such claims to gain prominence with little challenge. Since Yamanaka's discovery of iPS cells in 2006, some Japanese media and government officials have taken a highly competitive tone about the technology. In its original article about Moriguchi's claims, *Yomiuri Shimbun* noted that a burdensome regulatory system was holding back Japan's clinical research relative to the United States, and, in a 2009 correspondence published in *Nature*[7], Moriguchi argued that "Japan is in danger of being overtaken in the field of human iPS-cell research".

"Scientists, journalists and regulators here need to be especially careful not to let their pride in Yamanaka's achievement affect their critical faculties, or overwhelm them in national fervour," says Douglas Sipp, who researches stem-cell ethics and regulation at the RIKEN Center for Developmental Biology in Kobe, Japan.

Most stem-cell researchers are convinced that iPS cells have a long way to go before they are ready for the clinic, in part because of concerns that the cells might carry a heightened risk of producing malignant growths. "These kinds of studies should be done many times on hundreds of animals that are then followed long term — a year or more — for safety," says Paul Knoepfler, a stem-cell researcher at the University of California, Davis.

The first clinical trial of cells derived from iPS cells will probably take place in Japan next year. Masayo Takahashi of the RIKEN Center for Developmental Biology plans to use such cells to treat retinal diseases, work that seems to be proceeding cautiously and transparently. Of greater concern is the risk that some clinicians might take advantage of the hype surrounding iPS cells and start to offer untested treatments, in the same way that adult stem cells have become a booming, unregulated business[8]. "In theory, anyone can buy human iPS-cell production kits and starter cells," says Knoepfler. "All it would take is one negative patient outcome to set the field back for years".

"As we have seen from other forms of stem-cell pseudomedicine," adds Sipp, "if there is money to be made, someone will probably begin trying to market them." ■

1. Abbott, A. *Nature* **490,** 151–152 (2012).
2. Cyranoski, D. *Nature* http://dx.doi.org/10.1038/nature.2012.11584 (2012).
3. Moriguchi, H., Mihara, M., Sato, C. & Chung, R. T. in *Embryonic Stem Cells — Recent Advances in Pluripotent Stem Cell-Based Regenerative Medicine* (ed. Atwood, C.) 359–370 (InTech, 2011).
4. Moriguchi, H., Zhang, Y., Mihara, M. & Sato, C. *Sci. Rep.* **2,** 537 (2012).
5. Takahashi, K. *et al. Cell* **131,** 861–872 (2007).
6. Thenappan, A. *et al. Hepatology* **51,** 1373–1382 (2010).
7. Moriguchi, H. & Sato, C. *Nature* **457,** 257 (2009).
8. Cyranoski, D. *Nature* **484,** 149–150 (2012).

N. HALL/REUTERS

GlaxoSmithKline chief executive Andrew Witty, who announced the firm's commitment to openness.

BIOMEDICINE

Drug firm to share raw trial data

Full disclosure could improve health care and restore trust.

BY DECLAN BUTLER

The secrecy that has long surrounded drug-industry trials is crumbling. Scientists are applauding drug giant GlaxoSmithKline (GSK) for its announcement last week that it will make the trove of detailed raw data underlying its clinical trials systematically available to researchers. And GSK's move — the first such commitment for a big player in the industry — is just the beginning. Starting next year, the European Medicines Agency (EMA) intends to open up access to all new clinical-trial data sets it receives from industry for product registration.

The decisions represent a sea change in clinical science. Whereas data sharing is taken for granted in fields from genomics to particle physics, data from clinical trials are rarely shared fully with other scientists, says Joseph Ross, a researcher at Yale School of Medicine in New Haven, Connecticut. This means that doctors, health officials and researchers are forced to make important decisions about patients and health care on the basis of incomplete, and sometimes biased, information. GSK's decision acknowledges the wide value of raw trial data to investigators and public-health officials, says Ross, who says that "the move by GSK is a great public step forward".

Greater openness about clinical-trial data should help to speed up drug development, provide independent assessments of drug safety and efficacy and increase trust in industry science. It could also put an end to the scandals that, over the past few years, have seen almost every major drug company fined hundreds of millions of dollars for putting profits before patient safety and welfare, often through selective data reporting. In July, GSK itself reached a US$3-billion settlement with the US authorities for fraud, including publishing "false and misleading" accounts of trials, and for hiding data on safety concerns (see *Nature* **487,** 139–140; 2012). The settlement covered the antidepressants Paxil (paroxetine) and Wellbutrin (bupropion), and the diabetes drug Avandia (rosiglitazone).

"The move by GSK is a great public step forward."

GSK now intends to make available anonymized patient-level data for all the trials it has carried out since 2007 for both approved and abandoned drugs (the company says that only post-2007 data is in formats suitable for sharing). It will also set up an expert panel at arm's length from the company to review requests to access data for scientific merit, a restriction that some researchers dislike.

James Shannon, chief medical officer of GSK, justifies the restriction as a way to stop people from trawling through the data without a solid scientific question or hypothesis. Such fishing trips could lead to flawed analyses that could alarm the public unnecessarily and damage public health, he says.

WAIT AND SEE

Peter Gøtzsche, director of the Nordic Cochrane Centre in Copenhagen, says that he has "huge problems" with the restrictions, however. He argues that they could lead to arbitrary decisions about data release, which might favour the company rather than the public interest. Any risk of scares is outweighed by having more eyeballs on the data, he says, arguing that the lack of sharing of trial data by industry has been "far more harmful".

Kay Dickersin, director of the Center for Clinical Trials at the Johns Hopkins Bloomberg School of Public Health in Baltimore, Maryland, agrees with GSK that some access restrictions can be helpful. She cautions that the value of GSK's new openness will ultimately depend on how much detail it supplies in the patient-level data and, crucially, on the extent of documentation about how the trials were designed and data were collected, processed and analysed. "Let's wait and see," she says.

Openness will take another step forward next year, when the EMA begins to make public the clinical-trial data sets submitted to it. Although most companies might view the data as confidential, the EMA was empowered by a 2010 ruling by the European Ombudsman that the public-health interest of trial data overrides commercial interests, says Hans-Georg Eichler, a senior medical officer at the EMA.

The EMA's plans are "a phenomenal step in the right direction, a total game changer", adds Ross. The US Food and Drug Administration, by contrast, considers raw data from trials to be commercially confidential, he notes.

Alluding to the scandals that have rocked the drug world, Shannon says that the transparency his company is pioneering is the only way forward for the industry, and that he hopes other companies will follow GSK's lead. To maintain a 'licence to operate' from society, he says, the pharmaceutical industry has to move towards full disclosure. Many within GSK's rank and file have long been gunning for greater sharing of clinical data, he says, and last week's announcement was met with "much internal celebration", and hailed by some GSK scientists as a "dream come true". ■

ASTRONOMY

The exoplanet next door

Earth-sized world discovered in nearby α Centauri star system.

BY ERIC HAND

It is a world so close that E.T. could phone home in just four years. Astronomers have discovered the lowest-mass planet yet orbiting a Sun-like star. It orbits α Centauri B, a member of the stellar system that is our Solar System's nearest neighbour. Although nearly identical to Earth in mass, the planet is much closer to its star than Mercury is to the Sun, meaning that it is a scorched and barren rock. Nevertheless, its astronomical proximity to Earth will undoubtedly stir dreams of interstellar exploration, particularly as astronomers search α Centauri for more hospitable worlds.

Such exoplanets are the closest astronomers can ever find, says Francesco Pepe, an astronomer at the University of Geneva, Switzerland, and a member of the team that reports the discovery online in *Nature* this week (X. Dumusque *et al*. *Nature* http://dx.doi.org/10.1038/nature11572; 2012).

The work is a triumph for a venerable planet-finding technique that monitors a star for a subtle back-and-forth 'wobble' in its motion as seen from Earth, caused by the gravitational tug of an orbiting body. The technique, which formally measures a star's radial velocity, enabled researchers at Geneva to find in 1995 the first exoplanet ever detected orbiting a Sun-like star (M. Mayor and D. Queloz *Nature* **378,** 355–359; 1995).

That planet, a gas giant called 51 Pegasi b, pulled its star at 50 metres per second. The motion of α Centauri B arising from its lightweight planet is 100 times slower, a mere 50 centimetres per second, akin to a slow walk. That the team detected it at all is testimony to the steady refinement of the technique (see 'Lowest of the low').

Pepe and his colleagues found the planet as part of a campaign to monitor ten of the brightest and nearest stars visible from the Southern Hemisphere using the High Accuracy Radial Velocity Planet Searcher (HARPS) spectrograph on the European Southern Observatory's 3.6-metre telescope at La Silla in Chile. Three of the stars have already yielded planets, and the α Centauri system became the fourth after the team measured its velocity three times a night, nearly every night, for just over three years, to tease out the subtle motion measured just above the detection limit.

Finding a true Earth twin, circling a Sun-like star at a distance similar to Earth's orbital radius around the Sun, would require another leap in sensitivity, to motions of just 9 centimetres per second. For now, most astronomers are pinning their hopes of identifying an exo-Earth on a rival planet-finder: the NASA spacecraft Kepler, which watches for a dimming in a star's light as a planet crosses its face. Kepler was launched in 2009, and data from its first two years of operation have revealed about 3,000 candidate exoplanets, says principal investigator William Borucki, who presented fresh results on 15 October at a meeting of the Division of Planetary Sciences of the American Astronomical Society in Reno, Nevada.

Surprisingly, the cumulative data set does not contain a single Earth-sized planet at a habitable distance from its star, according to Borucki, who is based at NASA Ames Research Center in Moffett Field, California. Earth-sized planets may simply be less common than larger ones, perhaps because they are less apt to form, he said, flashing up a slide suggesting that just 10–15% of stars have Earth-sized planets — far fewer than other estimates.

Glumly, Borucki also pointed out that Kepler is now working on borrowed time. One of the spacecraft's four reaction wheels, used to keep the probe pointing at its target, failed in July, and if one of the other wheels follows suit, the mission would be doomed.

Yet an Earth twin could in principle be hiding at α Centauri, which is actually a trio of stars some 1.34 parsecs (4.4 light years) away. Two of the stars in the system, A and B, sometimes pass as near to each other as Saturn is from the Sun. This could disrupt the orbits of planets much farther out than the one discovered by the HARPS team, but a planet orbiting in α Centauri B's habitable zone, about half as far from the star as the distance between Earth and the Sun, would probably still be stable.

Geoff Marcy, an astronomer at the University of California, Berkeley, who leads another ground-based search effort, says that the discovery should bolster calls for a space-based telescope that could image any other planets near α Centauri B, providing they are in orbits large enough to separate them from the glare of the parent star. Such a telescope could also glean clues about a planet's atmospheric composition from its spectrum.

A space-based planet imager is still largely a dream, let alone an interstellar probe that could inspect the α Centauri system close up. Ralph McNutt, a planetary scientist at Johns Hopkins University Applied Physics Laboratory in Laurel, Maryland, has received NASA study funding to design an 'innovative interstellar explorer'. Even when launched by one of the most powerful rockets on Earth, boosted by a gravitational slingshot around Jupiter, and further accelerated by a radioisotope thruster, that probe would take about 28,000 years to reach α Centauri. Quoting British author Douglas Adams, McNutt quips: "Space is big. Really big." ■

➲ NATURE.COM
For a News & Views discussing this discovery see:
go.nature.com/bxtcii

LOWEST OF THE LOW

With improving techniques for measuring exoplanets' mass through their gravitational influence on stars, the lightest exoplanets detected each year (red dots) have reached the range of Earth-mass planets.

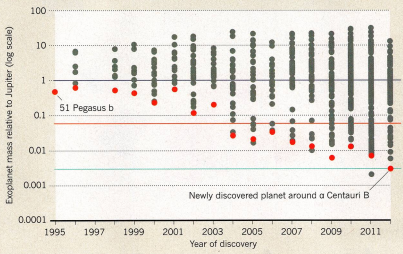

SOURCE: EXOPLANET.EU

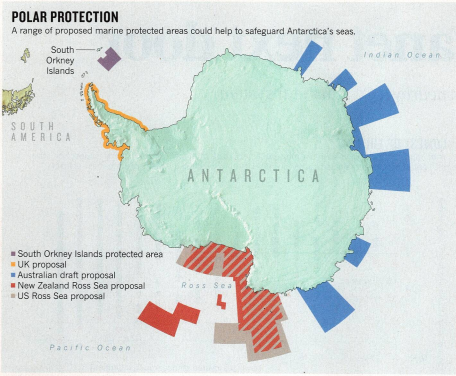

CONSERVATION

Antarctic seas in the balance

Plans to protect swathes of ocean face tough test.

BY DANIEL CRESSEY

Rich in fish, minerals and scientific potential, the seas around Antarctica are among the planet's most pristine waters — but fishing vessels are already moving in. Next week, negotiators at a meeting of the Commission for the Conservation of Antarctic Marine Living Resources (CCAMLR, pronounced 'cam-lar') may try to contain the accelerating rush to access the region's natural resources. At stake is one of the planet's last great wildernesses — as well as the credibility of the international body set up to protect Antarctica's marine life.

CCAMLR will consider four proposals to create vast marine protected areas (MPAs) that would tightly restrict fishing activities in the region. But protection will require unanimous agreement by CCAMLR's members (24 countries and the European Union), and some, including Japan and China, have a record of scepticism about any kind of Antarctic MPA. "This is a particularly important meeting," says Alex Rogers, a conservation biologist at the University of Oxford, UK. "If the proposals were blocked, it would be a very serious situation, and it would set back the whole process probably by a decade or more."

Only one large section of Antarctic waters is currently designated an MPA, a zone of about 94,000 square kilometres near the South Orkney Islands. The United States and New Zealand are now advancing two rival proposals to turn Antarctica's Ross Sea, which is home to seals, whales, fish, penguins and other birds, into one of the world's largest reserves (see 'Polar protection'). Commercial fishing in the Ross Sea, especially for the lucrative Antarctic toothfish (*Dissostichus mawsoni*), has been a sore point for environmentalists (see *Nature* **467,** 15; 2010). The US proposal would protect 1.8 million square kilometres, with 800,000 square kilometres totally off-limits to fishing and set aside as a 'scientific reference area' for studying the effects of climate change. New Zealand's proposal would cover roughly 2.5 million square kilometres, with fishing allowed in some areas. The two countries had once hoped to bring a joint MPA proposal to the table, but could not reach agreement. The Antarctic Ocean Alliance, a coalition of environmental groups, has criticized both plans: New Zealand's for compromising conservation in favour of allowing access for the country's fishing fleets, and the United States' for not covering enough ecologically valuable areas. Having two rival proposals for the same region could also stymie agreement and leave the Ross Sea without an MPA at all, the alliance warns.

Meanwhile, a UK-led effort is seeking protection for areas exposed by collapsing ice shelves around the Antarctic Peninsula. Newly exposed waters can quickly become populated with animals, making them highly attractive to fishing fleets, says Phil Trathan, head of conservation biology at the British Antarctic Survey in Cambridge, UK, who helped to develop the proposal. Protecting these areas would allow researchers to study how the marine ecosystem changes after the ice collapses — something that is expected to happen more frequently as the planet warms. "We understand a lot of the physical issues related to climate change," says Trathan. But "one of the really key issues is, what are the ecological consequences?".

Australia has submitted the fourth proposal, which would create a network of reserves around eastern Antarctica. "All four are very scientifically sound," says Andrew Wright, executive secretary of CCAMLR, based in North Hobart, Australia. But success is far from assured: "It has come down to a political decision now," says Susie Grant, a conservation scientist at the British Antarctic Survey.

If the proposals do not gain consensus by the end of the annual meeting on 1 November, they could in principle be considered at next year's meeting. But the need for all members to agree means that rejection would effectively kill these and any similar plans until there is a major shift in political ideology. Without an agreement this year, says Grant, "CCAMLR will have to consider very carefully what that means for the commitments it has made to conservation". ■

CORRECTIONS

In the Editorial 'Fighting chance' (*Nature* **490,** 144; 2012), we implied that the link between a genetic variant and educational attainment was identified by the Social Science Genetics Association Consortium. In fact, it was identified, and refuted, in earlier work done by Daniel Benjamin.

In the News story 'Economics and genetics meet in uneasy union' (*Nature* **490,** 154–155; 2012), we wrongly attributed to Enrico Spolaore the opinion that using genetic data in economics could help policy-makers to set immigration levels. He actually suggested that the work could reduce barriers to the flows of ideas and innovations across populations.

SCIENCE MAPPED OUT

In a special issue, *Nature* examines the changing global landscape of research.

A fundamental shift is taking place in where, and by whom, science is being done. Once, a succession of science superpowers were dominant: France, Germany, the United Kingdom and the United States. Today, more nations — from China and India to Singapore, Brazil and South Korea — are taking their place at the high table of research. National boundaries are being transcended by networks of collaborators and researchers who are much more mobile than in the past. Academics are moving to where the funding and facilities are. As Rajika Bhandari of the Institute for International Education puts it: "Knowledge generation and research is really a border-less enterprise".

This special issue of *Nature* looks at how this movement of people and ideas will change how science is done, how it is funded and the questions that it addresses. A News Feature explores data on migration and explains that ideas of 'brain drain' and 'brain gain' are being replaced by 'brain circulation', in which scientists move more fluidly around the world (see page 326). Analysing data on co-authorship, a Comment on page 335 charts the rise of collaboration networks — in Asia, Africa, the Middle East and South America — and challenges the traditional science heavyweights to keep up.

But ideas and talent could still circulate more freely, both within and between nations. On page 331, eight leaders of institutes and research programmes worldwide outline the steps that must be taken to raise the scientific bar in their countries. And on page 337, Subra Suresh, head of the US National Science Foundation in Arlington, Virginia, calls for greater cross-border cooperation and the pooling of resources to address global challenges such as climate change, pandemics, earthquakes, nuclear catastrophes, water shortages and malnutrition. Science must go truly global if it is to equip us for life on our changing planet. SEE EDITORIAL P.309

THE NEW MAP OF SCIENCE
The changing global landscape of research. nature.com/global

JASEK KRZYSZTOFIAK

SCIENCE ON THE MOVE

The big picture of global migration shows that scientists usually follow the research money — but culture can skew this pattern.

BY RICHARD VAN NOORDEN

Husband-and-wife neuroscientists Yuh Nung Jan and Lily Jan have run their laboratory at the University of California, San Francisco, for more than three decades: time enough to see the geography of the science world change. When the Jans started hiring employees in the 1980s, they chose home-born scientists. Nine of their first eleven employees were American.

But Yuh Nung and Lily — who themselves arrived in the United States from Taiwan in the 1960s — have increasingly drawn on talent from overseas. Today, researchers originally from China dominate the bench tops, with the lab hosting 16 Chinese scientists, 12 Americans, 2 Koreans and 1 researcher each from Canada, India, Singapore, Taiwan, Turkey and Germany.

The Jans' story is not unusual. "There is a progressively wider geographical variety of graduate students and postdocs in most leading universities," Yuh Nung says. During the 1970s, for example, non-citizens claimed around one-quarter of the doctorates awarded in the United States in physical sciences, engineering, mathematics and computer science; but by 2010, their share had risen to more than half, according to the US National Science Foundation. In life sciences, the foreign share has risen from just under 20% to 30%. The United Kingdom, Germany and Australia have seen similar trends.

By sifting through data, talking to experts and conducting our own survey of 2,300 readers around the world, *Nature* sought to identify underlying trends in scientists' movements, investigate what is driving them and explore how they may change. At stake is the shape of global science and the prospects for individual countries that hope to build up — or preserve — their research strength.

It is plausible — although hard to prove — that highly productive research systems such as those in the United States and the United Kingdom have benefited from their openness to foreign scientists. To the Jans (who together won this year's US$500,000 Gruber prize for their discoveries in molecular neurobiology), the advantages are obvious. They believe that foreign researchers enrich the lab culturally as well as scientifically. Being able to draw on a global talent pool may also help to make up for weaknesses in the US science-education system.

But some countries worry that they are losing their top researchers. Of the world's most highly cited scientists from 1981 to 2003, one in eight were born in developing countries, but 80% of those had since moved to developed countries (mostly the United States), according to a 2010 study by Bruce Weinberg at Ohio State University in Columbus. India, for example, loses out, says Binod Khadria, an economist who studies international mobility at Jawaharlal Nehru University in New Delhi. "The best and brightest are kept in other countries."

All this underscores that science, which has always been a global culture, is now a global marketplace, and one in which countries with well-funded and dynamic research systems come out on top. "Knowledge generation and research is really a borderless enterprise," says Rajika Bhandari, who studies the mobility of international students at the Institute for International Education in New York. "Academics go where the funding is and where the facilities are."

COMINGS AND GOINGS

Yet the global picture of these migrations is blurry. When tracking arrivals and departures, most countries lump scientists with other 'highly skilled migrants', and record-keeping differs from country to country. "What's very frustrating is that there is no consistent tracking of people using the same methodology across countries," says Paula Stephan, who researches economics and science at Georgia State University in Atlanta. "We have lots of little studies on particular groups of scientists, but no world bank of data."

Talk of 'migration' and 'mobility' often confuses permanent long-term relocations with the short-term visits — six-month sabbaticals or fortnight-long trips — that allow scientists to build research networks without actually settling in another country. "There are so many kinds of mobilities, and people rarely specify this," says Grit Laudel, a sociologist at the University of Twente in Enschede, the Netherlands.

> ***"Knowledge generation and research is really a borderless enterprise."***

Stephan is part of one attempt to cut through this confusion: the 'GlobSci' survey, to be published in *Nature Biotechnology* in December. The authors asked around 17,000 researchers in four fields (biology, chemistry, Earth and environmental sciences and materials) in 16 countries about their movements; the result was what they call "the first systematic study of the mobility of scientists in a large number of countries".

The numbers show big disparities from country to country, both in the proportion of scientists with foreign origins (see 'Foreign fractions') and in the proportion of researchers who work outside their countries of origin (see 'The global diaspora'). The United States is indeed open: of the respondents working or studying there when the survey was done in early 2011, 38% were brought up overseas, and it is the number-one destination for expatriate scientists from almost every nation. Proportionally, however, Switzerland, Canada and Australia all housed more foreign researchers than the United States, with Switzerland having the highest foreign share, at 57%. India had the lowest proportion of foreign scientists, followed by Italy and Japan, but also the largest diaspora, with 40% of its home-born researchers working

THE NEW MAP OF SCIENCE
The changing global landscape of research. nature.com/global

THE GLOBAL DIASPORA

Of countries in the GlobSci survey of 17,000 researchers, India sends the largest proportion of its scientists overseas. European countries also have high rates of emigration.

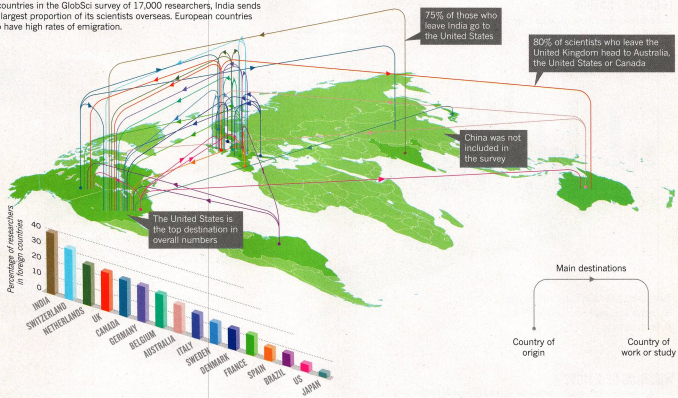

FOREIGN FRACTIONS

Developed countries have the highest proportions of foreign scientists, according to the GlobSci survey, which also identified the major sources of each country's foreign science community (right).

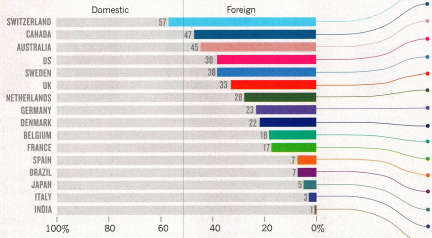

RESTLESS YOUTH

Foreign postdocs outnumber foreign professors in almost all countries included in the GlobSci survey.

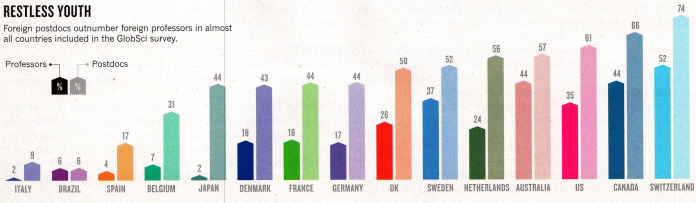

LANDS OF PROMISE

China topped predictions of future impact in a *Nature* survey of 2,300 respondents worldwide. But few of the respondents (who were mostly from the United States and Europe) would move there.

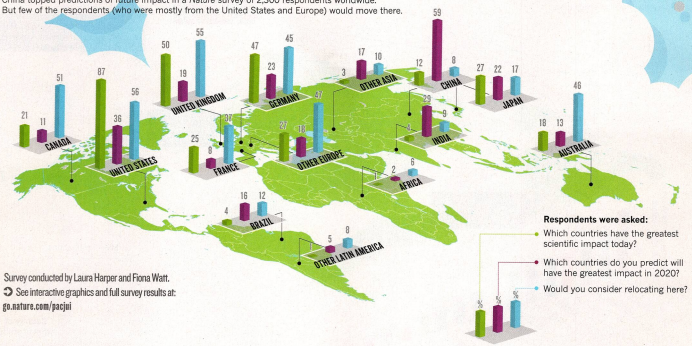

Survey conducted by Laura Harper and Fiona Watt.

➲ See interactive graphics and full survey results at: go.nature.com/pacjwi

WEIGHING UP A MOVE

Nature's survey asked respondents how important various factors would be in making a decision about working abroad.

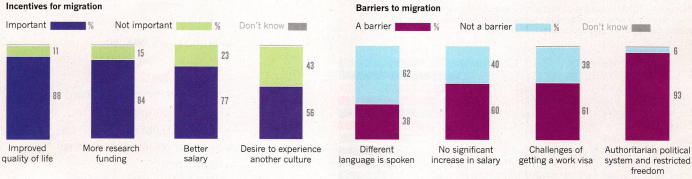

overseas. (The survey did not include China.) Japanese and US researchers were the least likely to be working abroad.

Career stage affects scientists' mobility. Chiara Franzoni, another GlobSci author, who studies science and innovation at Milan Polytechnic in Italy, has done an unpublished analysis of the GlobSci data and shown that a country's postdocs are much more likely to be foreigners than its professors (see 'Restless youth'). In the United States, for example, 61% of postdocs were brought up overseas — but only 35% of assistant, associate or full professors.

Nature found similar patterns when it surveyed readers about their attitudes toward migration, and their own histories. Those who had just obtained their PhDs were much more likely to be living outside their country of upbringing than were more senior scientists — and they were also more open to an international move, presumably because their career paths were not settled and they were less likely to be tied down by relationships and families. The proportion of respondents who said they were "not interested" in international relocation rose from a mere 10% in those who gained their doctorates within the past two years to 40% in those who had done their PhD at least 16 years ago.

"One take-away from a policy perspective is that if you are trying to bring people back who have studied overseas, then you should target the young because they are more likely to move," says Patrick Gaule, an economist who studies science and innovation at Charles University in Prague. He has tracked the movements of almost 2,000 senior-level foreign chemists affiliated with US universities between 1993 and 2007. Only 9% will return home by the end of their professional career, he estimates, and those that do are seven times more likely to return between the ages of 35 and 45 than after 50.

ITCHY FEET

What policy-makers eager to attract foreign scientists — or stem a loss of domestic talent — most want to know is what entices scientists across borders.

In the GlobSci survey, migrants uniformly put the same two factors at the top: opportunities to improve their career prospects and outstanding research teams. The excellence of the foreign institution was also important, with quality of life and other personal reasons coming further down the list. For those who had migrated abroad and subsequently returned to their country of origin, however, personal and family reasons scored highest.

Many economists note that the richer a country becomes, the more researchers tend to flock to it. Gross domestic product and wage levels are convenient metrics, but it is unlikely that they alone are the lure: they almost certainly correlate with career opportunities and top research facilities, for example.

But wealth is not the whole picture: dynamic, flexible and competitive systems for funding and advancement are also crucial, notes Kieron Flanagan, who studies science and technology policy at the University of Manchester, UK. Japan and Italy, for example, are wealthy nations yet attract few foreign scientists because of their relatively rigid bureaucracy. "It's hard to get a job when you go there," Flanagan says, "and when you're in, it's hard to get rid of you."

A rigid system can also discourage native-born researchers from emigrating, Laudel says, noting that in Germany and the Netherlands, young scientists are encouraged to go abroad, but swiftly return. "People tell me: 'I must go back to Germany, or I will never be able to get back into the system,'" she says. "If you return too late you don't fit the career structure any more."

> ***"The key thing is to have a strong-enough science base to interact with a globalized and mobile scientific world."***

Atsushi Sunami, an expert in science and technology policy at Tokyo's National Graduate Institute for Policy Studies, points to another reason for Japan's insularity: culture. "Often when we ask foreign researchers about their daily research activities, they say it's fine but it's hard to adjust to our society outside of the laboratory." In some respects, researchers considering an international move are like all migrants, weighing up factors that include wages and career prospects, but extend to quality of life, schooling for any children and career prospects for spouses, says Louise Ackers, who studies the movement of European scientists at the University of Liverpool, UK.

Governments can try to tip the scales through immigration policies and travel incentives. Europe, for example, has programmes to encourage travel within the multi-country European Research Area; China has a 'One Thousand Talents Scheme' to recruit academics from abroad, as well as to persuade Chinese scientists to return. Recently, says Bhandari, "China and South Korea have done a much better job of deliberately creating well-structured incentives and opportunities for students to return back home, than, say India". And in the United States, both presidential candidates have said that they would like to expand the availability of visas for skilled immigrants.

Yet a dynamic, well-funded science system seems to trump all other incentives. Even the visa crackdown after 9/11 did not dent science students' enthusiasm for migrating to the United States. "Despite all the hand-wringing and the concern that numbers would plummet, statistically there was only a 2% drop in international student enrolment," says Bhandari. "By 2006 the numbers were rebounding."

THE CHINA QUESTION

US science-policy experts are asking how long the nation can retain its grasp on foreign talent. The country's largest contingent of foreign doctoral students in science comes from China, and research by Mike Finn, an economist at the Oak Ridge Institute for Science and Education in Tennessee, shows that for now, most stay on. Studying a cohort of Chinese scientists who had received their PhDs in 2004, Finn found that five years later, 89% were still in the United States.

Higher salaries may be the biggest attraction. Robert Zeithammer, at the Anderson School of Management at the University of California, Los Angeles, has surveyed almost 300 Chinese science students studying for their doctorates in the United States, asking them for their reactions to hypothetical job offers from the two countries. "Chinese doctoral graduates currently tend to remain in the United States because of a large salary disparity between the two countries rather than because of an inherent preference for locating in the United States," he concludes.

But as China continues its economic rise and builds its science infrastructure, that may change. Data from China's Statistical Yearbook show a slight uptick in return rates of Chinese students from abroad over the past few years (although the data do not single out scientists), notes Cong Cao, a sociologist at the School of Contemporary Chinese Studies at the University of Nottingham, UK. But Finn says that there is no sign yet of any overall decline in stay-rates in the United States. The proportion of foreigners who say that they have "plans to stay" after graduation has gone up, not down, over the past decade, he points out.

And the lure of China remains faint for non-Chinese scientists. *Nature*'s survey (which drew responses mainly from the United States and Europe) asked researchers which countries would be producing the best science in their field by 2020, and more than 60% of respondents in both biological and physical sciences picked China as an option. However, only 8% said they would be prepared to relocate to China — instead preferring the United States, Europe, Canada and Australia (see 'Lands of promise'). Responses suggested that China is unappealing for foreign researchers for political and cultural reasons (see 'Weighing up a move', despite high expectations for the future quality of its research.

Such a disparity could be dangerous, says Jonathan Adams, director of research evaluation at Thomson Reuters, which is based in New York. If researchers in Europe and the United States do not spend serious time in China, he says, they will find it hard to understand how research is conducted there, even as the country's influence in science grows.

WIN–WIN?

Those who study scientists' mobility argue that the discussion need not pit nation against nation, as if China's gain is the United States's loss. In place of 'brain drain' and 'brain gain', they prefer to talk about "brain circulation', in which international scientists dip in and out of countries at will, and everyone benefits from the collaboration. "Of course America will decline in relative terms, as the United Kingdom has, but it will do enough leading-edge research to benefit from work done elsewhere," says Flanagan. "The key thing is to have a strong-enough science base to interact with a globalized and mobile scientific world."

Researchers at the Dutch publishing firm Elsevier, who are tracking the movements of scientists by following their publishing addresses, have detected hints of that pattern. Most notable among the early results for each country is a large proportion of 'transitory' scientists, who stay in a country for less than two years at a time. The University of Liverpool's Ackers adds that some evidence, including a survey of researchers in Europe's Marie Curie Fellowship Programme, suggests that shorter, more frequent visits are increasingly supplementing long-term travel to other labs.

With the Internet making it easier to work with international collaborators at a distance, Ackers suggests, repeated week- or month-long visits can yield as much as, if not more than, a half-year stay. "The old idea of researchers moving permanently from one country to another is now quite outdated," she says, adding that it will become increasingly common for people to live in one country but work in two or three. With all this globe-hopping, the question is how long researchers will need to spend in the same place for effective collaboration — an answer that will surely differ between disciplines.

Yet this vision of a globalized, circulating world is still a long way from reality: very few scientists are global citizens, popping in and out of the best research facilities. And in developing countries such as India, "brain circulation" does not accurately reflect the situation, says Khadria. For him, the brain drain is still very real. "It is not the top-of-the-line scientists who come back; rather, they return at a time when most of their productive work is over," he says.

Science may increasingly be a globalized enterprise, but until wouldbe competitors boost their spending on science and facilities, it will simply give scientists even more opportunities to clump inside the countries that are already at the top of the pack. ■

Richard Van Noorden *is a reporter for* Nature *in London.*

Inserm

UNIVERSITÉ JOSEPH FOURIER GRENOBLE

CEA

ESRF

Institut des Neurosciences GRENOBLE

The Grenoble Institute of Neuroscience (GIN) searches for its next Director

The GIN is a Research Centre considered as an Institute of excellence created in 2007 by Inserm, Joseph Fourier University - Grenoble 1 (UJF), CEA (Commissariat of Atomic Energy and Alternative Energies) in partnership with the Hospital of Grenoble (CHU) and the European Synchrotron Radiation Facility (ESRF).

Located in the heart of a dynamic scientific local environment (based on physics, mathematics and computer science, microelectronics, nanoscience, structural biology and chemistry), the GIN gathers teams specialized in the study of normal and pathological processes of the Nervous System and of the nerve-muscle ensemble. The scientific teams of the GIN are characterized by their multidisciplinary and multicultural approach of the questions they address and decipher in an emphasis onto interfaces between disciplines. The GIN provides an excellent scientific environment that allows neuroscientists and physicists to work in close proximity to each other, facilitating the path from bench to bedside. Clinical Neuroscience in Grenoble is at the origin of Deep Brain Stimulation (DBS), which found its pioneer application 25 years ago in the treatment of motor pathologies such as tremor or Parkinsonian akinesia - hypertonia. This very efficient treatment gained widespread use all over the world.

The scientific environment in Grenoble offers a facilitating ground to the development of innovative techniques. The GIN is a key link to the process of innovation with its preclinical and clinical facilities (about 6 different MRI for humans and animals up to 9.4 T, confocal and biphoton microscopy, electron microscopy, optics platform, high-resolution EEG, promotics and transcriptomics, ...) including the presence of large European core facilities (ESRF, Grenoble antenna of EMBL - European Molecular Biology Laboratory, and IBS - Partnership in Structural Biology), the tight relations with CEA, Clinatec and Minatec innovative Centers, and with other research laboratories in Grenoble, where physics, mathematics and computer science are at the forefront.

Located within the health campus of Grenoble, a few meters away from the hospital departments devoted to neuro care, the GIN 6000 m2 building houses about 250 people, researchers, teachers-researchers, physicians, engineers, technicians, post-docs and PhD students along 13 teams (see description at web site http://neurosciences.ujf-grenoble.fr).

The Director will be an eminent scientist, MD, PhD or both, with a track record of excellence in fields relevant to neuroscience and documented leadership credentials in an academic research setting. He/She will serve as Chief Scientific and Executive Officer, with a mandate to expand the Centre's existing strengths, and enhance the international stature of the GIN. He/she will be expected in parallel to carry out his/her own research in the Centre, whose facilities will be made available.

Applicants should send an expression of interest, letter of motivation in support of application, research statement (not exceeding 5 pages), curriculum vitae and three letters of recommendation or names of references to claude.feuerstein@ujf-grenoble.fr at Grenoble Institute of Neuroscience – GIN, Research Centre UJF-Inserm U836-CEA-CHU, Edmond J. Safra Building, Chemin Fortuné Ferrini, Site Santé UJF at La Tronche, BP 170, 38042 Grenoble, FRANCE.

To receive full consideration, applicants should be submitted by **February 25th, 2013.**

W229464R

Institut Pasteur

Head of Proteomics Core Facility

The Institut Pasteur opens a tenured Research Engineer position to recruit the head of its proteomics core facility. This facility is part of the Proteopole and is attached to a recently created Structural Mass Spectrometry and Proteomics Research Unit headed by Dr. Julia Chamot-Rooke.

The candidate will

- Manage an advanced proteomics group
- Develop a wide range of services based on robust procedures
- Oversee instrumentation
- Collaborate with the teams on the Pasteur campus and elsewhere
- Support and train in-house scientists
- Apply for grants for equipment
- Undertake technology development together with the Unit and other groups

Required qualifications, experience and skills

- PhD in mass spectrometry, analytical biochemistry or related areas
- Extensive practical experience in proteomics (ideally on a core facility)
- Experience in the field of quantitative and qualitative mass spectrometry including sample preparation, analytics, data processing and evaluation
- Excellent interpersonal, written and verbal communication skills
- Fluency in reading and speaking English and good level in French
- Successful interdisciplinary collaborations
- Experience in grant acquisition and project management

We offer

- The possibility to work on interesting scientific projects in an international and exciting environment
- Tenured position
- State-of-the-art instrumentation

Deadline for applications: 30 November 2012

Applications should be sent to **proteopositon@pasteur.fr** and should comprise the following (in order) in a single pdf file:

1. A brief introductory letter.
2. A Curriculum Vitae and a full publication list.
3. A description of past and present activities, experience and skills (up to 8 pages with 1.5 spacing).

For more information please contact Julia Chamot-Rooke: **(julia.chamot-rooke@pasteur.fr)**

W228543R

HELSINGIN YLIOPISTO
HELSINGFORS UNIVERSITET
UNIVERSITY OF HELSINKI

UNIVERSITY OF HELSINKI

The University of Helsinki is among the leading multidisciplinary research universities in the world. In addition to its 11 faculties, the University includes several independent institutes, some of which are jointly operated with other universities. Some 36,500 students are currently pursuing an undergraduate or postgraduate degree at the University of Helsinki.

The mission of the Faculty of Medicine, University of Helsinki is to conduct high-quality research and to provide research-based undergraduate and postgraduate education in medicine and dentistry. The faculty's operations are centred on the Meilahti-Ruskeasuo Campus, which offers excellent opportunities for close collaboration with both the University Hospital and government research institutes such as the National Institute of Health and Welfare and the Finnish Institute of Occupational Health.

Research Programs Unit of the Faculty of Medicine is a top-quality research unit. The programs and groups of the Unit are selected through competition every four to six years by an international Scientific Advisory Board. These Research Programs comprise groups that integrate clinical, translational and biomedical research. Current Program Unit contains three Centers of Excellence of the Academy of Finland, and several research groups belong to European Union or Nordic Networks of Excellence. European Research Council currently funds seven research groups in the Unit.

PROFESSOR IN TRANSLATIONAL MEDICINE AND DIRECTOR OF RESEARCH PROGRAMS UNIT

The position will be filled for a period of five years.

The professor's duties include carrying out and supervising scientific research in translational medicine and participating in societal interaction and Finnish and international collaboration in the field.

The professor also performs the duties of the director of the Faculty of Medicine Research Programs Unit. The director leads and monitors the Unit's operations and is responsible for its general operations, financial affairs and personnel administration and its implementation according to the human resources policy of the University. The director's duties are specified in more detail in the administrative model of the Research Programs Unit.

An appointee to a professorship shall hold a doctoral degree and possess top-level scholarly qualifications and experience in the supervision of scientific research, as well as the ability to provide top-level research-based teaching and to supervise theses and dissertations. In addition, the appointee shall present documentation of international cooperation in the field of research he or she represents. Furthermore, the position also calls for academic leadership skills.

Since the appointee will serve as director of the Research Programs Unit with an annual budget close to 20 Mill. €, the candidate needs to be administratively experienced and have demonstrated leadership skills.

The director must have experience in research and doctoral education in a discipline represented in the Research Programs Unit as well as in the management of such research and education.

The position overview as well as instructions and models for drafting the list of publications are available on the Faculty's website at http://www.med.helsinki.fi/hallinto/professorin_tehtava.html, or from the Faculty Office.

Applications addressed to the Faculty of Medicine, together with the required enclosures, must arrive at the following postal address: Registry of the University of Helsinki, P.O. Box 33 (Yliopistonkatu 4), FI-00014 University of Helsinki, Finland.

The deadline for applications is October 26, 2012 at 15.45 local Helsinki time.

For further information, please refer to the university website and if you have any doubts, contact the Vice-Dean of the Faculty, Professor Hannu Sariola, hannu.sariola@helsinki.fi, tel. +358 (0) 9 191 25140.

www.helsinki.fi/university

W228958R

THE SAINSBURY LABORATORY

Head of Proteomics
at The Sainsbury Laboratory, Norwich, UK

The Sainsbury Laboratory (TSL) is seeking a highly motivated individual to lead proteomics activities at the Laboratory. This is an exciting opportunity for the successful talented candidate to contribute to and enhance the world-leading scientific activities of the Laboratory.

The post holder will be responsible for managing a team providing proteomics support to TSL scientists. The key functions of the role will be to deliver proteomics and training to TSL scientists, to work closely with TSL Group Leaders to apply modern proteomic techniques, and to develop cutting-edge methodologies as opportunities arise. The post holder will have direct access to world-class facilities available at TSL and across collaborative institutes within the Norwich Research Park. A joint proteomics platform was established in 2000, which includes: Thermo Scientific LTQ-Orbitrap; Waters Synapt G2; Waters TG-S; Bruker UltraFlex MALDI-ToF/ToF; Bruker MicroFC; and Applied Biosystems QTrap 4000.

The applicant must have extensive hands-on experience of proteomics and must have a PhD degree in any field of research. Previous experience in the analysis of post-translational modifications of proteins is an advantage.

Salary will be within the UEA Research and Analogous Staff Grade 8 scale at between £38,140 and £48,246 pa; the appointment level will reflect qualifications, skills, knowledge and achievements. The position is available for two years in the first instance with possibility of renewal based on performance. Applicants should provide a CV, including the names and contact details of two or more referees, and a covering letter addressing the selection criteria. Please send formal applications, quoting the reference number below, either by e-mail to HR@tsl.ac.uk or by post to Kim Blanchflower, HR Manager, The Sainsbury Laboratory, Norwich Research Park, Colney, Norwich, NR4 7UH, UK.

Applications will be reviewed from 4th November 2012 and the position will remain open until filled.

The Sainsbury Laboratory (TSL) is a world leader in plant and microbial science and is dedicated to making fundamental discoveries in the science of plant-microbe interactions. TSL has expanded its scientific mission not only to continue providing fundamental biological insights into plant-pathogen interactions, but also to deliver novel, genomics-based solutions that will significantly reduce losses from major crop diseases, especially in developing countries.

For more information please visit http://www.tsl.ac.uk

Ref: HoProt/2012

U229352R

To advertise here please contact – US tel. +1 800 989 7718, naturejobs@natureny.com or Europe/ROW tel. +44 20 7843 4961, naturejobs@nature.com

COMMENT

PUBLICATION Regional co-authorship networks are changing research **p.335**

FUNDING Grand challenges require more international collaboration **p.337**

FILM Unsettling documentary probes humans' relationship with caged animals **p.340**

RECESSION New database to help labs to share idle equipment **p.342**

EPA/CORBIS

South Korean President Lee Myung-bak (second from left) talks to young scientists at the Korea Institute of Science and Technology in Seoul.

How to build science capacity

Eight leaders propose ways to boost research in their countries in the next decade.

LIM CHUAN POH

Singapore: Build global networks

Chairman of the Agency for Science, Technology and Research, Singapore

Last year, Singapore celebrated 20 years of government investment in science and technology. From 1991 to 2010, public expenditure on research and development doubled, from 0.4% to 0.8% of the gross domestic product. The number of research scientists in the public sector quadrupled, to nearly 13,000.

One great success is our scholarship programme. Since 2001, it has enabled talented young Singaporeans to pursue education and training — from the undergraduate level to the postdoctoral — in leading universities and labs around the world. These students then return to Singapore to continue their research for up to six years. Working abroad, they see first hand that a rich milieu is crucial to the pursuit of excellent science. They bring back new networks and collaborations.

For the past five years, we have also provided support for students and researchers from beyond Asia to participate in undergraduate research attachments and doctoral and postdoctoral stints in Singapore. So far, we have attracted more than 600 young researchers from more than 50 countries, including the United States, Brazil, the United Kingdom, Russia, Egypt, Sudan and Australia.

Many of these students have told me ▶

THE NEW MAP OF SCIENCE
The changing global landscape of research. nature.com/global

▶ that they are grateful for the opportunity to come to Singapore and to work in a world-class research environment in Asia. They often say that they were surprised by the excellent infrastructure, resource support and quality of science, as well as the presence of leading researchers from around the world. Many see Singapore as a gateway to the region and hope to stay in Asia to further their careers.

These young international students add to the research landscape a richness and diversity not otherwise possible in a country as small as Singapore. Eventually, they will also connect Singapore to research communities around the world.

BERNIE FANAROFF
South Africa: Think big

Director of the Square Kilometre Array, South Africa

Building science capacity might not have seemed a priority after South Africa's transition to democracy in 1994. But in 1996, a government white paper underlined the importance of building competence in "flagship" sciences. Not to do this, it argued, would be to take the view "that we are a second-class nation chained forever to the treadmill of feeding and clothing ourselves".

The large facilities now available in southern Africa have already gone a long way towards creating a major centre for astronomy — the HESS (High Energy Stereoscopic System) γ-ray observatory, the Southern African Large Telescope and the MeerKAT radio telescope. The construction of the largest part of the Square Kilometre Array (SKA) in the region, with 2,700 dishes (the rest will be built in Western Australia), will make southern Africa a world leader in astronomy within a decade.

Mega-projects such as the SKA raise science's profile and draw in young people and resources. Big projects can be won if a country pulls together around a vision, as South Africans have in this case.

The idea of building the world's largest scientific instrument in Africa caught the imagination of people across the continent. The rest of the world was initially sceptical, but the outstanding work done to establish a protected site in South Africa's arid Northern Cape province and to build the MeerKAT precursor telescope won everyone over.

South Africa's bid for the SKA was developed over nine years, with enthusiastic support from government and the public, the media, the business community and the African Union. The site is scientifically excellent and the costs are low. An active radio-astronomy community has grown around the project. Since 2005, more than 400 research, training and study grants have been awarded and five SKA university research chairs funded. Mutual-benefit agreements made with international technology companies recognize the quality of our young scientists and engineers through joint research.

The brain drain is being reversed. Outstanding astronomers from around the world have come to teach and work in South Africa. More than 70 SKA grants have gone to students from other African countries. Many have returned home and started astronomy courses in places such as Madagascar, Mozambique, Kenya, Ghana and Mauritius.

Building the SKA will help to grow a critical mass of young people in Africa who have world-class science and technology skills, and who are committed to innovation.

PATRICK AEBISCHER
Switzerland: Build elite institutions

President of the Swiss Federal Institute of Technology in Lausanne, Switzerland

Europe must reform its academic system. The region needs more world-class universities akin to Harvard University and the Massachusetts Institute of Technology in the United States. Such elite scientific institutions are vital for breeding talent and promoting innovation and economic competitiveness.

The most important step is to give bright junior scientists the independence they need to establish and develop their careers within Europe. They should not have to move to the United States, as my generation had to. A cross-continent tenure-track system should be developed to retain rising stars and build a European market for academics.

More top-tier graduate schools on a par with those at the UK universities of Oxford and Cambridge must be created to select and train the most promising young scientists. Competitive fellowships would attract talent from all over the world. Trans-disciplinary topics such as sustainability or technology management should be included in graduate courses to provide the broad background necessary for tackling society's pressing problems.

Good leadership and funding are crucial in building world-class universities. University governance procedures must be adapted to empower well-respected academics as leaders — it is no coincidence that the best institutions have prominent figureheads. University leaders must see fund-raising as a central task. As much as we Europeans cherish our precious state funding, we must bring in extra resources to achieve excellence.

Lively campuses are important assets to attract the best students. Building dormitories, facilities for sport and culture and technology parks alongside well-equipped research laboratories would reproduce the vibrant campus experience of elite US universities. European institutions should promote their multilingual and cultural heritages to attract the brightest students.

Such improvements are feasible by 2020, as my institution has shown — we implemented many of these reforms in the past decade.

RAFAEL CAMACHO
Spain: Boost translation

Chief executive, Genoma España, Spain

Science, like everything in Spain, must adapt to the economic struggle. Increased investment over the past decade has raised the country to ninth in the global ranking of scientific productivity. The nation's 135,000 researchers generate 70,000 scientific papers a year. Spain must capitalize by translating that research into goods and services.

As chief executive of Genoma España, a public foundation entrusted by the Spanish government to drive biotechnology innovation, I was appointed in 2009 to design and launch InnoCash, a pilot programme for adding value to technologies through market assessment and innovation financing. Three years later, 36 ventures have been funded, half in biotechnology and health, the rest in nanomaterials, information technology and energy.

Any 'accelerator' programme has three drivers: technology, money and talent. Showcasing the first was easy — we promoted patented technologies and results to potential investors through an online marketplace, linking technology-seekers and problem-solvers.

Mobilizing private money for early-stage and high-risk ventures was more difficult. As an incentive, Genoma España offered part-refundable loans of €14 million (US$18.2 million); ultimately, two-thirds (€25 million) of the total funding came from private companies. As InnoCash proves, a modest public investment — just 10% of the total after seed grants are repaid — can accelerate technology business.

The most challenging aspect was finding skilled people to lead the ventures. We need to identify, train and motivate 'innopreneurs' who have technical knowledge, managerial skills and a risk-taking attitude.

S. BALDWIN/CORBIS

Egypt's Library of Alexandria is supervising the spread of online science courses in Africa.

In 2013, a single Research State Agency is due to launch, streamlining funding allocations. We must make scientific careers in Spain more attractive — through better contracts, improved recognition and more provision for researcher mobility. And we must support translational research, so that the benefits of Spanish science flow to society.

ISMAIL SERAGELDIN

Egypt: Share knowledge online

Director, Library of Alexandria, Egypt

Africa produces less science than it could. Its home-grown innovations are not being nurtured by governments. Bottom-up initiatives are needed. We must use new technologies to empower those promoting science in the poorest countries. I am involved in two such projects.

One is the Science Supercourse, a collection of more than 170,000 PowerPoint lectures available for free on the Internet (see go.nature.com/hlksfr). The project is the brainchild of Ron Laporte, an epidemiologist at the University of Pittsburgh in Pennsylvania, in collaboration with the World Health Organization and the Library of Alexandria. It is supervised by Laporte along with Gil Omenn, a biomedical scientist at the University of Michigan in Ann Arbor; Vint Cerf, vice-president at Google in Mountain View, California; and myself.

Our lectures — designed by Nobel laureates as well as young assistant professors — distil the latest knowledge in a field in an accessible way. In epidemiology and public health alone, some 60,000 people have used them to reach 1 million students in more than 170 countries.

The second project — a virtual help desk for researchers using the Supercourse — is still in gestation. Overseen by the same team, it will give researchers in developing countries, particularly in Africa, guidance on research methods and statistics so that they can conduct, evaluate and publish research in international journals. By assisting scientists at the outset and during analysis, such a programme could markedly improve productivity.

Although the private sector has used help desks for decades, the concept has not, to our knowledge, been used to provide external support to individual scientists in their research. Learning from private industry, we intend to begin with a prototype in epidemiology and health, and later expand to other disciplines.

We have already collected and placed in the Supercourse repository many lectures and books as well as software related to research methods and statistics (see go.nature.com/oqfrzg). We invite scientists to add materials and to use what is available.

NIKOLAY SUETIN

Russia: Seed regional science

Director of Science and Technology, IT Cluster, Skolkovo Foundation, Russia

Half of Russia's scientists left after the political crisis of the 1990s. Since then, the country has had no scientific plan. Research resources have been misdirected and productivity has dropped, from about 3% of the total papers published globally in 1995 to less than 2% in 2010.

Changes in the past decade have been more positive. The Russian government has increased the funding of scientific research from 77 billion rubles in 2006 to 323 billion rubles (US$10.4 billion) in 2012. More is needed to overcome the prolonged deterioration of research in Russia and to move to an innovation-led economy.

Russia's share of high-technology products is now only 0.8% of the world market. A gap between pure and applied research is holding innovation back. Entrepreneurs, who turn intellectual property into products, are almost absent in Russia.

The Skolkovo Foundation — a government project that aims to build a Silicon Valley environment in Russia (see go.nature.com/tjzgdi) — bridges the divide between science and industry by supporting the creation of innovative companies.

One of Skolkovo's first success stories is Rock Flow Dynamics (RFD; www.rfdyn.com), a company that develops software for the petroleum industry. Founded in 2005 by three Moscow mathematics and physics graduates, in 2010 RFD attracted an investment of $2 million from technology fund Intel Capital. Today, RFD sells product licences to oil and gas companies around the world.

Regional growth in science is badly needed. Most research is concentrated in the large cities of Moscow, St Petersburg, Tomsk and Novosibirsk. Cooperation between universities and local governments can benefit both, as at the South Ural State University in Chelyabinsk, where a powerful supercomputer centre has been created. Steps to improve researcher mobility, perhaps through competitive programmes such as the 2010 'megagrant' effort to set up a series of elite labs, would boost science across the nation.

With limited money, the Russian Federation must pick priority research areas. Information technology is one. The mathematical sciences have been strong historically, and as local IT companies such as Yandex, Kaspersky Lab and Parallels show, Russia could become a global leader. In the past

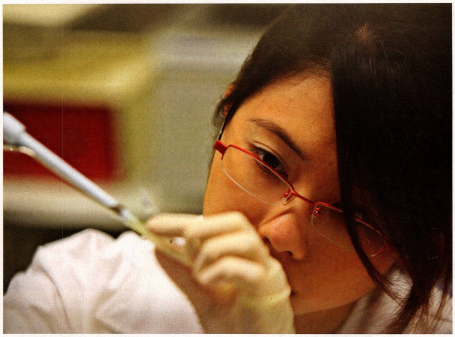

L.E. ASCOY/REUTERS

Singapore's scholarship programme has been building international links since 2001.

ten years, international giants IBM, Boeing and Siemens have created research centres in Russia.

Bureaucratic barriers that raise the cost of research, such as customs tax for imported scientific materials, must also be removed. With these steps, Russia can regain the position in global science that it deserves.

CARLOS HENRIQUE DE BRITO CRUZ

Brazil: Reward quality

Science director, São Paulo Research Foundation (FAPESP), Brazil

In the past 30 years, Brazil has built a broad science base in its universities, research institutes and industry. In 2011, the nation produced more than 12,000 doctoral students and 35,000 articles in international scientific journals. Growth has been impressive. But the system as a whole lags behind in quality and impact. On average, citations of Brazilian authors were the same in 2011 as in 1994: at 65% of the world average.

Boosting Brazilian science requires enhancement of the quality and the social, economic and intellectual impact of research. Reviewers, institutions and agencies still overvalue quantity — of articles or of students. Quality must be better recognized and rewarded in academic careers and in the selection of research-funding proposals.

Brazil's government must develop a plan to support around a dozen universities in executing excellence programmes that would propel institutes to among the 100 best in the world within a decade. Such programmes would improve academic governance, raise standards, encourage globalization of research projects and support worldwide searches for the best faculty members, postdocs and students.

The country already has highly selective universities that could become world class. The three state universities in São Paulo and the Federal University of Rio de Janeiro, for instance, admit on average only 1 in 20 graduate students who apply. In medicine and engineering, it can be 1 in 100. Universities across Brazil should apply more stringent criteria for selecting graduate students and reviewing faculty members.

"Developing international connections is crucial to raising research standards."

Developing international connections is crucial to raising standards. Brazilian scientists should collaborate and publish more with researchers from world-class institutions abroad. Funding agencies should use more international peer reviewers in assessing proposals.

Researchers need greater institutional support — including grant-management offices — as well as better links to government, business and non-governmental organizations. Systems for university governance should promote academic values and merit above petty politics and cronyism. Universities should have effective autonomy.

Improving basic education, stimulating young people to seek scientific careers and better distributing the scientific enterprise across the country are also essential to Brazil's development. Obtaining these goals and expanding the base of the system does not preclude raising academic standards at the top.

JUNE SEUNG LEE

South Korea: Back blue-skies work

President, Korea Institute of Science & Technology Evaluation and Planning (KISTEP), South Korea

From rubble to research, few nations have changed as rapidly as South Korea. Half a century after devastating wars, the country is now a member of the Organisation for Economic Co-operation and Development and hosted the G20 summit in Seoul in 2010. Eagerness for learning and investment in science and technology drove this rise.

Policy-makers recognize that sustaining prosperity will take more than mimicking high-tech products, as in the past. South Korean scientists should contribute to the creation of basic knowledge by investing in blue-skies research.

In the past decade, the South Korean government has doubled its budget for basic research — to about US$5.4 billion in 2012 — and has initiated programmes to build infrastructure and to double the number of researchers. The number of papers published by South Korean scientists has tripled since 2000.

The government is taking a big risk: there is no guarantee that breakthroughs in fundamental research will bring returns. But, having experienced the benefits of science-driven development, South Koreans are ready to return knowledge to others.

The Institute for Basic Science (IBS), headquartered in Daejeon, was launched in May and, among other projects, will construct a heavy-ion accelerator costing about $460 million. With state-of-the-art facilities, and by attracting at least 50 internationally renowned scientists as project leaders (ten are already in place), the IBS will become a world-class research and development complex.

To further strengthen our science base, we must support creativity and reduce bureaucracy. Young, inventive South Korean scientists must be able to secure positions at home, so that those with passion and ambition need not go abroad. ■

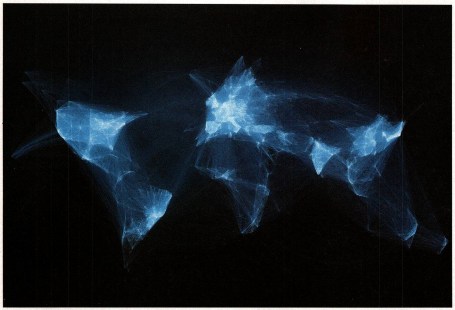

COMPUTED BY O. H. BEAUCHESNE, SCIENCE METRIX, DATA: SCOPUS.

Bright lines in this map of scientific collaborations between 2005 and 2009 show many joint publications.

The rise of research networks

New collaboration patterns are changing the global balance of science. Established superpowers need to keep up or be left behind, says **Jonathan Adams**.

A fundamental shift is taking place in the geography of science. Networks of research collaboration are expanding in every region of the globe. The established science superpowers of the United States and Europe have dominated the research world since 1945. Yet this Atlantic axis is unlikely to be the main focus of research by 2045, or perhaps even by 2020.

New regional networks are reinforcing the competence and capacity of emerging research economies, and changing the global balance of research activity. This may well reveal different ways of approaching challenges, and solutions that are different to those of Western institutions. If the science superpowers are to avoid being left behind, they will need to step out of their comfort zones to keep up with the dynamism of the new players in this shifting landscape.

Collaboration is normally a good thing from a wider public perspective. Knowledge is better transferred and combined by collaboration, and co-authored papers tend to be cited more frequently[1]. But could increased global collaboration mean a blending of objectives that risks leaving bland priorities?

Co-authorship is a valid proxy for collaboration because few scientists surrender credit for their papers lightly, so we can assume that sharing of authorship reflects a tangible engagement. Such publication data are readily available, cover many countries and research disciplines to a good depth, and have reasonable consistency across decades.

Changes in the balance of research done by the lone scientist and that done by teams can be seen in co-authorship data[2]. Co-authorship has been increasing inexorably[3,4]. Recently it has exploded.

An issue of *Nature* today has a similar number of Letters to one from 60 years ago, but at least four times more authors[5]. Similar observations have been documented from clinical science to law. In the early 1980s, papers with more than 100 authors were rare. By 1990, the annual tally with that number exceeded 500 — and it has kept growing. The first paper with 1,000 authors was published in 2004; a paper with 3,000 authors came in 2008. By last year, a total of 120 physics papers had more than 1,000 authors and 44 had more than 3,000 (ref. 6). Many of these are from collaborations at the Large Hadron Collider at CERN, Europe's particle-physics lab near Geneva, Switzerland.

This upwards trend in multi-authorship will continue through shared global priorities in health, energy, climate and social structures, propelled in part by international agencies such as the World Health Organization. Some of this growth will not be true collaboration but will come from independent contributions to joint efforts, usually in the form of data, that involve only weak intellectual interaction.

THE NEW MAP OF SCIENCE
The changing global landscape of research. nature.com/global

BLURRED BORDERS

Papers with hundreds of co-authors contribute to the apparent pervasiveness of collaboration between countries. For example, every country in Europe co-authors with every other country in the region. For the United Kingdom and Germany, this collaboration is relatively intense and represents many individual links. In 2011, the two countries had around 10,000 joint publications in journals indexed on Thomson Reuters' Web of Science — double the total in 2003 and about 10% of each country's total output. Malta, by contrast, shares only 50 papers per year with the United Kingdom, but that represents more than 25% of its total publication output. Consequently, distinguishing Malta's own science performance is already impossible. This blurring of national distinctiveness could be a growing issue.

According to data from Web of Science, the United States currently collaborates on 3–4% of its papers with each of China (now its most frequent partner, with 19,141 papers in 2011), the United Kingdom (19,090) and Germany (16,753). These totals have all roughly doubled in the past decade and have increased by half as a percentage of US total output. No country shared more than 1,000 papers in 1989 with any partner. US collaboration with Asia is rising steeply, as is collaboration between countries in western Europe. There is no reason to suppose that this will not continue.

China's rapid growth since 2000 is leading to closer research collaboration with Japan (up fourfold since 1999), Taiwan (up eightfold), South Korea (up tenfold), Australia (more than tenfold) and with every other research-active country in the Asia-Pacific region.

The rapid growth of each nation's research base and regional links, driven by relatively strong economies investing in innovation, will undoubtedly produce a regional research labour force to be

reckoned with by 2020. Already, cutting-edge technology can be sourced from research developments in South Korea as well as those in Germany.

India has a growing research network with Japan, South Korea and Taiwan, although it is not as frequent a collaborator with China as one might expect[7]. In the Middle East, Egypt and Saudi Arabia have a strong research partnership that is drawing in neighbours including Tunisia and Algeria. The annual tally of joint Egyptian–Saudi Arabian papers has risen tenfold in the past decade and is accelerating. Less than 5% of these papers have a co-author from the United States, the biggest partner outside the region for both countries.

Latin America has an emerging research network focused around Brazil, which — despite language differences — has doubled its collaboration with Argentina, Chile and Mexico in the past five years. By contrast, Africa has three distinct networks: in southern Africa, in French-speaking countries in West Africa and in English-speaking nations in East Africa.

These clusters indicate that proximity is just one of several factors in networks. Nigeria, for example, collaborates not with its neighbours in West Africa but with co-linguists in East Africa. This mirrors a global tendency to use paths of least resistance to partnership, rather than routes that might provide other strategic gains. Such language links have historically benefited the United Kingdom through alliances with Commonwealth countries that speak English and have adopted similar research structures. The United Kingdom cannot rely on this to continue.

This growth of regional collaboration has many implications. It amplifies the development of emergent research economies. Researchers in Asia, for example, do not need recognition from European and US authors if their research is being cited and used by partners within the region. In the short term, students will recognize attractive opportunities closer to home, with fewer alienating cultural challenges than many European campuses have offered.

Singapore, for example, is already reaping the benefits of a 1998 policy change to attract foreign students. Students from China, India and the ten countries in the Association of Southeast Asian Nations (ASEAN) now comprise about 20% of Singapore's university intake — around 11,000 full-time students — with another 20,000 part-time students in other colleges. Students from those countries choose Singapore for its proximity, its lower cost of living compared with Europe and the United States and its generous government scholarships. Job opportunities are excellent: bursary holders sign a bond to work in Singapore for a fixed period after graduation and the government helps them to find a job that fits their skills[8].

All of this means that the significance of Western research economies as preferred partners for research could dwindle. To meet this challenge, these economies need to do much more than just take fees from immigrant postgraduate students.

The United States and the United Kingdom must build new networks by actively exporting students to burgeoning science centres such as China and India. Researchers must stop expecting scientists from the new powerhouses to come to them, and should visit collaborators to experience different approaches — and be ready to learn, not just to teach. Travelling recently in the Pacific basin, I encountered many university leaders trying to increase collaboration with Europe, but finding it difficult to identify responsive contacts, despite having excellent facilities and staff to offer.

"The maverick and the marginal may find a highly collaborative world a difficult place to flourish."

In short, countries in science's old guard must drop their patrician tendencies, open up clear communication channels and join in with new alliances as equal participants before they find themselves the supplicants.

Collaboration between the public and private sectors has become more apparent because of government interest in exploiting research for economic competitiveness. Some data show that industrial investment in research seems to be dropping — perhaps a reaction to the recession, but the trend seems to be long term, at least in the United Kingdom[9]. Governments need to develop an industrial policy that complements science policy. Incentives for collaborative innovation investment that draws directly on the science base would be a good start.

PATRICIAN TO PARTICIPANT

So what are the costs and benefits of collaboration? It provides access to resources, including funding, facilities and ideas. It will be essential for grand challenges in physics, environment and health to have large, international teams supported by major facilities and rich data, which encourage the rapid spread of knowledge.

Collaborative papers tend to get cited more often. For example, those published jointly by UK and US authors are cited on average more often than either nation domestically. It also works at the institutional level, so Harvard University gets a boost from collaborative papers with the University of Cambridge, and even in *Nature* the US–UK co-papers get relatively more citations[1]. And it follows through to industrial collaboration: when the University of Oxford collaborates with GlaxoSmithKline, for example, the papers are cited roughly four times as often as the world average for their field.

Research networks are a tool of international diplomacy. Germany exports excellent research equipment within its partnerships. China expands its cultural influence through the regional programmes it funds.

As for costs, collaboration takes time and travel and means a shared agenda. Of wider concern as teams proliferate is that individuals could end up working only on topics that peer consensus defines as the most interesting. The diversity of choice and opportunity may be diminished. The risk is that international, national and institutional agendas may become driven by the same bland establishment consensus.

This global tendency for convergence became obvious in 1997 when Tony Blair, then UK prime minister, adopted the same technology priorities set out by Bill Clinton and Al Gore in their 1992 presidential campaign, including biotechnology, health and environment. By 2000, the UK regional development agencies had supported the same missions rather than choose those that played to regional university strengths[10]. Leading research universities in North America, Europe and Asia identify strategic missions in similar areas.

It is difficult to go your own way in a village, even one that is global. But the success of science has been the crossing of separate strands of thought and practice that are more innovative at the edges than at the core. The iconoclastic, the maverick and the marginal may find a highly collaborative world a difficult place to flourish. Research-funding agencies should maintain a balance. Collaborative grand challenges seize headlines, but so do Nobel prizes — and only three people can share one of those. ■

Jonathan Adams *is director of research evaluation for Evidence, part of Thomson Reuters, in Leeds, UK.*
e-mail: jonathan.adams@thomsonreuters.com

1. Adams, J. in *International Partnerships of Research Excellence* (ed. Roberts, G.) (2006); available at http://go.nature.com/zzwnBz.
2. Whitfield, J. *Nature* **455**, 720–723 (2008).
3. Leydesdorff, L. & Wagner, C. S. *J. Informetr.* **2**, 317–325 (2008).
4. Adams, J. *Nature* **396**, 615–618 (1998).
5. Greene, M. *Nature* **450**, 1165 (2007).
6. King, C. *ScienceWatch* **23**, 1–2 (2012); available at http://go.nature.com/w3f2jt.
7. Bound, K. & Thornton, I. *Our Frugal Future: Lessons from India's Innovation System* (NESTA, 2012).
8. Ministry of Education, Singapore. *Education Statistics Digest* (2012); available at http://go.nature.com/8dz3ml.
9. Universities UK. *The Future of Research* (Universities UK, 2010).
10. Evidence. *Funding Research Diversity* (Universities UK, 2003).

B. TAFRESHI/ESO

The Atacama Large Millimeter/Submillimeter Array (ALMA) telescope in Chile is a massive collaborative effort between many countries.

Global challenges need global solutions

Subra Suresh sets out the institutional reforms needed for collaborative action among international research-funding agencies to tackle the challenges humanity faces.

The challenges confronting global decision-makers are growing in complexity, intensity and urgency. Environmental change, pandemics, natural disasters, nuclear catastrophes, displaced populations, water shortages, rising ocean levels and widespread malnutrition do not stop at national borders or the water's edge. Addressing such issues requires cross-border cooperation and pooled resources.

Fortunately, the rapid growth in research capability around the world provides a strong foundation for finding science and engineering solutions to global challenges. Convinced that frontier research and technological innovation will spur strong economic growth, more and more countries are committing substantial sums to science and engineering research and education. Collectively, global investment in research and development has doubled within the past 15 years to about US$1.4 trillion annually (amount adjusted for purchasing-power parity)[1,2], even through the turmoil created by the global financial crisis.

I am convinced that greater collaboration will maximize the effectiveness of those investments. Without a coordinated global response, humanity will not overcome the challenges it faces. That is why I have strongly supported the efforts of the US National Science Foundation (NSF) to harmonize global research initiatives among science-funding agencies.

FOUR RECOMMENDATIONS

What are the barriers to cross-border scientific collaboration? One is the current framework for investment in research and development. Funding is governed and constrained largely by national and local policies, processes and priorities. These frequently impede cooperation among different government agencies, institutions and individuals. There are many more. For example, scientific peer review needs to be consistent across borders. Scientists need to be assured that data generated through cross-border collaborations meet certain standards of quality and research integrity, and that they will be preserved and accessible to other researchers — and the public — in the future. There are issues of intellectual-property rights, and constraints on the mobility of scientists.

Removing these barriers will require proactive principles and policies, developed and implemented collectively. To this end, I have four recommendations.

Standardize the principles for merit review and research integrity. Every funding agency needs a transparent, impartial and consistent peer-review process to pick the most scientifically productive ideas and people in the most ethical way. The patchwork of review processes currently in use in different countries is hindering scientific progress. Consequently, there is growing enthusiasm about, and commitment to, coordinating efforts to improve peer review from many science-funding agencies and other organizations in government, education, and the charitable and private sectors, in both developing and developed countries.

To support this, the Global Research Council (GRC; www.globalresearchcouncil.org) was established in May at the NSF, bringing together leaders of key science-funding organizations. At its inaugural meeting, some 50 heads of research councils — mostly from countries within the G20 and the Organisation for Economic Co-operation and Development — collectively

developed a set of principles for effective merit review. These set out six key ingredients: expert assessment, transparency, impartiality, appropriateness, confidentiality, and integrity and ethical considerations. The GRC statement reads: "Rigorous and transparent scientific merit review helps to assure that government funding is appropriately expended on the most worthy projects to advance the progress of science and address societal challenges." The fact that so many of the world's leading science-funding agencies voluntarily and unanimously endorsed such a public statement is a crucial step towards increasing collaborative transnational research agreements.

Share resources to increase the scope and global impact of scientific experimentation. Multi-user facilities enable important scientific discoveries by maximizing resources at a time when many countries face economic constraints. Astronomy offers many examples of how this approach works. In the 1950s, the NSF led an effort to 'democratize' the field by establishing national observatories. Today, radio, optical and solar telescopes around the world serve thousands of scientists and students. Consider the Very Large Array radio telescope built by the NSF in 1980. More than 2,500 scientists from around the world have used this telescope for more than 13,000 projects. Within the past decade, a partnership between funding bodies in North America, Europe and East Asia, in cooperation with Chile, developed and built the Atacama Large Millimeter/Submillimeter Array (ALMA) telescope, which is already a testing ground for theories of star birth and stellar evolution, galaxy formation and evolution, and the evolution of the Universe itself.

Another model for focused global interaction is CERN, Europe's particle-physics laboratory located near Geneva, Switzerland. Discoveries here, such as the potential identification of the elusive Higgs boson, have been made by collaborations among scientists and funding from government agencies in many countries. Two further initiatives deserve mention. The Science Across Virtual Institutes project, launched by the NSF, promotes collaborations in research and education between NSF-supported research communities in the United States and many overseas partners. And the NSF has teamed up with the US Agency for International Development to form the Partnerships for Enhanced Engagement in Research programme, which supports collaboration between scientists in developing countries and in the United States.

A crucial element of international arrangements for scientific collaboration is the need for long-term commitments. Every effort should be made at the outset to support infrastructure and operating expenses, and to develop contingency plans for unexpected shortfalls in funding. Such shortfalls, often caused by economic downturns, have detrimental effects on global science, with a loss of initial investments, loss of momentum in executing the research and the erosion of trust and goodwill among partners.

Explore new ways to share the research output of major scientific infrastructure projects. Given that scientific credit is measured by priority, publications and patents, collaborative research output should be shared among all involved. The Antarctic Treaty is a model here. Under the treaty, the 28 consultative parties provide scientists with logistical support and operational and laboratory facilities in the Antarctic. Research observations and results from scientific work in the Antarctic then have to be made freely available to everyone.

A similar example of international collaboration is being implemented in parallel with the final stages of construction of ALMA. The ALMA Correlator — one of the world's fastest special-purpose supercomputers — is already providing astronomical images for users on several continents. Ultimately, research data acquired from ALMA will be available to all, giving researchers around the world the chance to benefit from this scientific infrastructure.

"Integrating different perspectives will alter, energize and enrich science."

Develop policies and mechanisms to guide the collection, analysis and distribution of 'big data'. Over the past few years, new scientific instrumentation, computational hardware and software, and theoretical analysis have markedly increased the sophistication, resolution, reach and scope of data collection, generating huge data sets. For example, the Large Synoptic Survey Telescope — a partnership involving the NSF, the US Department of Energy and private, educational and international contributors — will probe dark energy and dark matter, inventory the Solar System, explore the transient optical sky and map the Milky Way. It is expected to generate tens of terabytes of data per day.

Such volumes of data have to be organized, manipulated, integrated, distributed and stored — a process that poses major challenges. Together, funding agencies, research institutions and scientists must develop new ways to extract useful knowledge from mountains of information. Funding agencies must support studies of data gathering, access and storage so that information creation does not streak too far ahead of information curation. Policies must be formulated to ensure the privacy and confidentiality of sensitive data, and to safeguard intellectual-property rights and cyber security.

BETTER TOGETHER

These four steps require policies to promote the greater mobility of researchers, especially young scientists and students, across international borders. And there are further questions that the GRC and other international bodies are beginning to address, and which demand well-coordinated international efforts. For example, who will craft policy and ensure compliance for the benefit of the global scientific enterprise? How will the increased interconnectivity of individuals and institutions alter the dynamics of the global enterprise for knowledge generation? And how will institutions and individuals — from nations with very different histories, levels of research experience, financial resources, individual freedoms, priorities and laws — participate in a global enterprise while addressing national and local needs?

The future of science will be influenced by the interconnectivity of governments, research and educational institutions, and individual citizens around the globe. Integrating different perspectives will alter, energize and enrich science.

But policies for new modes of collaboration have implications that go beyond scientific progress. How the science and technology community organizes itself for the global era may determine how effectively humanity can tackle major societal challenges. The increasing integration of social, behavioural and economic sciences with the natural sciences and engineering will be essential in this regard.

I am encouraged by the energy, enthusiasm, commitment and seriousness of the members of the GRC. They represent an expert, interconnected global research enterprise that has decision-making authority, recognizes funding constraints and shows a genuine desire to engage developed and developing nations in the advance of global science. The next meeting of the GRC will be co-hosted by Brazil and Germany in Berlin in May 2013 (go.nature.com/wtgam1). It aims to endorse principles of research integrity and to begin to develop common policies and guidelines for implementing open access to scientific publications and data. Significant progress in these areas will have major implications for government funding agencies, for the researchers they support, and for all the people who will benefit globally from the results of these endeavours. ■

Subra Suresh *is director of the US National Science Foundation, Arlington, Virginia 22230, USA.*
e-mail: ssuresh@nsf.gov

1. National Science Board. *Science and Engineering Indicators 2012* (National Science Foundation, 2012).
2. Grueber, M. & Studt, T. *R&D* (16 December 2011); available at http://go.nature.com/v2vzms.

H. SORENSEN/GETTY

Leaves meet tough physical challenges such as wind and rain with an array of extraordinary coping mechanisms.

BIOPHYSICS

Tales from the canopy

Sandra Knapp considers how the laws of physics influence the function of leaves in myriad ways.

We live highly networked lives at what often seems like warp speed. When you think about how complicated all that commuting, preparing and organizing is, spare a thought for the leaves above. As plant physiologist Steven Vogel reveals in *The Life of a Leaf*, coping with physical variables that humans barely notice — wind, rain, sunshine — makes for a tough existence at leaf level.

Vogel celebrates serendipitous discoveries and ideas, describing his own in detail, and shows the general reader just how exciting science can be. His observations of rhododendron leaves rolling into cigar-shaped tubes led him to experiments showing how leaves keep themselves warm. And his use of down time in a local wind tunnel one Thanksgiving inspired him to discover how leaves handle high winds. Both are great examples of how a seemingly crazy idea can ultimately generate new understanding.

Leaves cover vast stretches of terrestrial Earth's surface, and enable much of life itself through oxygen-producing photosynthesis. Yet we only really notice this multilayered canopy when leaves change colour in the autumn, drop off owing to drought or block the sunlight we crave. The physical environment that leaves experience is like our own, but subtly different, because leaves can't move much. Vogel lucidly outlines the physics and engineering challenges that this presents.

The Life of a Leaf
STEVEN VOGEL
Univ. Chicago Press: 2012. 320 pp. $35, £22.50

His central focus is on a leaf's function, not its structure. He explores the amazing things that physical features do for organisms: how daffodils bloom through the snow without ice crystals bursting their cells; how sap rises to the tops of the tallest trees; how leaves avoid tearing in strong winds. The physics of these phenomena is incredible.

We usually think of physics as informing biology. Vogel shows that in many cases, it is the other way round. Physiologists have discovered basic principles in biological systems that have later been shown to be universal and have become the stuff of fluid dynamics. For example, nineteenth-century French physiologist Jean Louis Marie Poiseuille devised an equation explaining the pressure gradient for liquid upflow in small tubes, such as the conducting tissue of plants. And German physiologist Adolf Eugen Fick formulated the law that describes the central relationship of diffusion across gradients.

Vogel weaves equations and jokes together seamlessly. For the many people who can't 'read' equations, he explains ▶

them verbally, then discusses them in a more conventional way in footnotes. He further enlivens the proceedings by linking the equations with the personalities and lives of the scientists after whom they are named. For instance, the Scholander bomb, a device used to measure pressure in stems, gets its name from the Scandinavian-born physiologist Per Scholander (1905–80), who was renowned for his ingenious experimental-apparatus designs. Vogel's approach certainly worked for me.

As for the jocularity, there is much that is quotable. I love the description of the superhydrophobicity of leaves as "particle pickup predilection", and the idea that ice is "toxic water" from a leaf's perspective. But some of the puns jar — the phrase "to a plant, our water loss problem would be a wet dream" struck me as condescending and crass.

Gags notwithstanding, Vogel does makes the conscientious reader work, although this is more of a challenge than a chore. His focus leaves some issues hanging — forcing us to dig further elsewhere. And he rightly notes that there is still a lot to discover. How, for example, do deciduous trees re-establish unbroken water columns through their trunks to the new leaves in spring?

He even urges readers to do their own demonstrations and experiments at home, to illustrate basic principles in a way that words never can. A loop of thread placed in a glass of water will not form a regular shape, but add a bit of detergent to reduce the surface tension and hey presto: a perfect circle (and party trick). And it is fun to whirl around in the garden holding a stick with leaves attached to the end — especially if you're demonstrating how the leaves behave in the 'wind' you create, which can easily reach 30 kilometres an hour.

The role of phylogeny — the evolutionary relationships between plants — is completely left out of this book. Vogel is a proponent of the adaptationist programme, in which every feature has a function that serves the organism well. He pays lip service to an alternative view by referencing his late friend Stephen Jay Gould, but I think the role of chance in evolution deserves more than just a mention. Features of organisms do not always have a purpose. Sometimes they just are.

Probably the central theme of *The Life of a Leaf* is extracting the extraordinary from the ordinary. In a way, Vogel's view is that science is at its heart simple — and great fun. I couldn't agree more. ■

Sandra Knapp *is a botanist at the Natural History Museum in London.*
e-mail: s.knapp@nhm.ac.uk

PHOTOCASE ADDICTS GMBH/IN ALAMY

Life in a cage disconnects animals from the natural world and breeds apathy.

ZOOLOGY

The animal inside

Josie Glausiusz contemplates a documentary on the human relationship with animals confined and stuffed.

A lion lies asleep atop a glass roof inside a wire enclosure. Beneath the glass, within an enclosed walkway, tourists lift their smartphones and snap photos of the torpid feline. What do they see when they look at it — a magnificent beast, or a cowed one, disconnected from its natural world?

Questions about what we really see when we look at animals run throughout *Bestiaire*, a strange and unsettling documentary directed by Canadian Denis Côté. Awarded a Special Jury Prize at the 2012 Environmental Film Festival at Yale, held in New Haven, Connecticut, *Bestiaire* continually confounds the viewer, undermining our understanding of what it means to be wild, as it reflects our own confined lives.

The film unfolds over four seasons, shot mostly inside Parc Safari, a zoo in Hemmingford in Quebec, Canada. There is no narration and little dialogue, and disparate scenes seem to pop up at random. We move from art students sketching what looks like a stuffed baby deer to snow-filled pens in which woolly bison, llamas and horses lumber back and forth. Zebras stomp frantically. A melancholy monkey cuddles a stuffed teddy bear. In summer, geese waddle through tall grass and children take elephant rides and pat young deer.

People feature too. Guards watch and feed the animals through the mesh of the cages — and are themselves observed on closed-circuit cameras. At one point the film's focus shifts to a taxidermy studio in a Montreal basement, crammed with skulls and stuffed

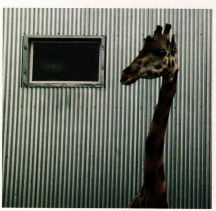

FIDA FILMS

***Bestiaire* raises unsettling questions about humanity's habit of gawking at confined animals.**

Bestiaire
DIRECTED BY
DENIS CÔTÉ
FIGa Films: 2012. Screening at Anthology Film Archives in New York 19–25 October.

deer heads. A man walks up to a rotating metal drum and removes what looks like a handful of dusty feathers. He shakes it, slices out bloody bones with surgical tools, stuffs it, dries it with a hair-dryer and *voilà* — a green-headed duck.

Although Côté insists that *Bestiaire* has no message, it nonetheless depicts perfectly the distorted relationship that zoo-goers and others have with wild animals: no longer free, but dispirited creatures that we incarcerate, ogle, coddle and capture on tiny screens.

That, in turn, raises compelling questions about the role of zoos today. Humans have enjoyed gawking at imprisoned animals since as long ago as 2100 BC, when Mesopotamian kings exhibited lions in cages and pits. The Tower of London was once home to a menagerie that over the centuries featured lions, tigers, alligators and hyenas, whose bodies were dissected in the pursuit of anatomical science. London Zoo took over from it in 1828. Now, an emerging consensus argues that zoos should discard the old 'entertainment' model to devote resources to the conservation of animals that face extinction in the wild. A coordinated zoo-breeding programme of the golden lion tamarin (*Leontopithecus rosalia*), for example, has helped the endangered monkey to thrive once again in its fragmented Brazilian forest habitat.

Life in a cage may protect an animal from habitat destruction, but it also breeds apathy. In one spring-time scene in *Bestiaire*, three bears line up obediently in a pen as a keeper tosses grapes into their open mouths. Denied the opportunity to forage far and wide, they seem to have adapted to a life free from independent exploration.

In an interview, Côté recalled that he wanted his film to be like seeing "through the eyes of a six-year-old who is turning the pages of a bestiary and excited to discover a new picture of an animal at every turn". But the medieval bestiary was also an instructional book, filled with illustrations of animals both real and imaginary — elephants and lions, griffins and unicorns — each of which had a symbolic moral or allegorical value. Like these didactic tomes, Côté's film shows us that we face ethical choices: understand and empathize with the plight of wild animals or treat them as yet more playthings to be photographed, toyed with or stuffed.

Bestiaire prompts viewers to ponder what it really means to be human — or more accurately, humane — in our relationships with wild beasts. Whether or not Côté intended it, the movie has a message — a powerful one. ■

Josie Glausiusz *is a writer based in New York City.*
e-mail: josiegz@gmail.com

Books in brief

One Billion Hungry: Can We Feed the World?
Gordon Conway CORNELL UNIVERSITY PRESS *456 pp. £46.50 (2012)*
Poverty, climate change, booming population, soaring food prices — the obstacles to global food security seem Himalayan. Agricultural ecologist Gordon Conway calls for a "doubly green revolution", with sustainable intensification of production, research and development, and market creation. He ploughs through the crises, discusses methods, delves into the role of farmers as innovators, and faces up to environmental challenges. An impressive marshalling of case studies, new research and long experience from an expert in the field.

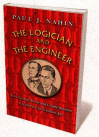

The Logician and the Engineer: How George Boole and Claude Shannon Created the Information Age
Paul J. Nahin PRINCETON UNIVERSITY PRESS *244 pp. £16.95 (2012)*
Meshing logic problems with the stories of two extraordinary men — Victorian philosopher–mathematician George Boole and twentieth-century information theorist Claude Shannon — Paul Nahin fashions a tale of innovation and discovery. Boole's astonishingly advanced ideas seeded Boolean algebra, which underpins the electronic circuits governing today's digitized culture. Alongside a gripping account of how Shannon built on Boole's work, Nahin explores others key to the technological revolution, from Georg Cantor to Alan Turing.

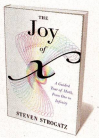

The Joy of X: A Guided Tour of Math, from One to Infinity
Steven Strogatz HOUGHTON MIFFLIN HARCOURT *336 pages £16.87 (2012)*
Is infinity a number? What is the point of quadratic equations? Whither topology? Steven Strogatz, a mathematician in the field of complex networks, steers the 'maths challenged' through his home territory. Beginning with the usefulness of numbers, Strogatz strolls through π, the Pythagorean theorem, probability, solid geometry and more, including the anatomy of that marvellous beast, calculus. The interconnectedness of maths in culture — from art, literature, philosophy and law to medicine — is gracefully unravelled.

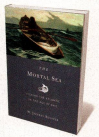

Mortal Sea: Fishing the Atlantic in the Age of Sail
W. Jeffrey Bolster HARVARD UNIVERSITY PRESS *366 pp. £22.95 (2012)*
Historian and seafarer Jeffrey Bolster "writes the ocean into history", tracing the currents leading to today's serious fish-stock depletion. Focusing on the North Atlantic from Cape Cod to Newfoundland's Grand Banks, he shows how one species after another — halibut, lobster, cod — has been exploited for centuries, long before industrialization. Bolster braids marine biology into a narrative driven by courageous chancers, such as fifteenth-century explorer John Cabot and unnamed hordes of fishermen, to argue that the precautionary approach is key to heading off collapse.

Orwell's Cough: Diagnosing the Medical Maladies and Last Gasps of the Great Writers
John Ross ONEWORLD PUBLICATIONS *288 pp. £12.95 (2012)*
Shakespeare may have had syphilis and mercury-vapour poisoning, speculates medical doctor John Ross in this engrossing look at how great writers have grappled with illness and disease. From the satirist Jonathan Swift's putative descent into frontotemporal dementia to Herman Melville's bipolar disorder (and possible ankylosing spondylitis), a book that compels respect for the subjugation of suffering behind so many enduring works of genius.

Correspondence

Citizens add to satellite forest maps

Satellite data are invaluable for mapping India's remaining forests, but their coarse resolution limits the information they can provide for protection purposes (*Nature* **489,** 14–15; 2012).

For example, individual tree species cannot be identified from satellite data. This encourages selective felling of valuable trees, such as teak, while green cover is maintained to avoid satellite detection. Also, remotely sensed data do not reveal areas where local communities have a close relationship with the forests, as in India's Meghalaya hills.

Mobilizing citizens to provide information on the ground ('crowd sourcing') complements remote-sensing data. Using devices such as mobile phones (see www.geo-wiki.org), this approach provides a means to report illegal logging, catalogue trees that need protection because of their cultural, ecological or economic importance, validate spatial forest data and quantify forest degradation. It also raises awareness and informs public debate on sustainable forest management. In Brazil, for example, citizens have used the Globo Amazônia website since September 2008 to log millions of complaints against illegal activities as a cause of deforestation (see www.globoamazonia.com).

The controversy over India's forest resources is worrying, but it points to an emerging transparency in governance that allows people's concerns to be voiced. Crowd sourcing would enhance this transparency while improving the quality of data.

Marijn van der Velde, Linda See, Steffen Fritz *International Institute for Applied Systems Analysis (IIASA), Laxenburg, Austria.*
velde@iiasa.ac.at

Database for sharing costly equipment

To mitigate the effects of the 45% government cuts to capital budgets in 2010, the UK Research Councils promoted the sharing of research equipment within and between institutions.

I published a report on this matter earlier this year for the N8 partnership of eight research-intensive universities in northern England (see go.nature.com/6jvpip), concluding that the overheads of sharing mean that it is mainly confined to expensive items, and that it works best when run within a collaboration. Already the study has catalysed strategic collaborations. Some research-intensive companies are also now exploring the possibility of joining these arrangements.

Logistical and cultural factors can be a problem. Most researchers will help friends and collaborators, but are wary of strangers using their facilities. They may worry about intellectual property or whether visitors will respect the equipment and are adequately trained in using it. It is easiest to set up sharing arrangements at the time of purchasing the equipment.

One challenge is to know what facilities are already available. Researchers might buy an item when there is one with spare capacity nearby. The N8 is developing standardized databases of capital assets built around a taxonomy of equipment types and functions. Availability will need to be checked because state-of-the-art items often operate at near-full capacity or may be configured to a particular experiment. Usage charges are also needed to cover access costs, such as technicians' time.

Luke Georghiou *University of Manchester, UK.*
luke.georghiou@manchester.ac.uk

Cash puts publishing ethics at risk in China

The number of scientific papers published in China in recent years has increased exponentially (see go.nature.com/8fjhdt). There are concerns that these numbers are being inflated by a payment scheme offered by some Chinese institutions to boost publication in journals with high impact factors (J. Shao and H. Shen *Learned Publ.* **24,** 95–97; 2011).

Such monetary incentives could adversely affect scientific publishing behaviour in China. Payments to editors to improve the impact factor of their journal, for example, could encourage them to coerce authors into citing more articles from that journal (see go.nature.com/ye2gae). Or it could result in citation cartels in which journals cite each other for mutual benefit (see, for instance, go.nature.com/p4u8on).

These schemes risk disrupting the drive to reduce ethical issues that undermine Chinese science.

Sarah Huggett *Elsevier, Oxford, UK. s.huggett@elsevier.com*

Rural factories won't fix Chinese pollution

China's green movement is awakening and starting to receive global attention (see, for example, Q. Wang *et al. Nature* **489,** 502; 2012). The municipal governments of Qidong and Shifang should be applauded for suspending two planned industrial plants likely to cause widespread pollution (*Nature* **488,** 261–262; 2012). But there may be plans afoot to relocate these to rural areas.

Moving factories from cities to rural areas is becoming more common. The relocation by local government of a US$1.4-billion paraxylene plant from Xiamen City in Fujian province to the less-developed Gulei Town was not welcomed by residents (T. Ma *China Environ. Ser.* **10,** 33–49; 2008/2009). Their protests received little media attention or help from non-governmental organizations (NGOs), and the new plant is now almost complete.

Shifting pollution from urban to rural areas can only be a short-term fix. For example, rural and semi-rural factories trebled their contribution to the national wastewater discharge between 1990 and 2007 (see go.nature.com/kdgsh3; in Chinese), and there are more than 200 cancer-cluster villages in China where pollution is suspected as the major cause of death.

More local NGOs are needed

to support rural populations in suing polluting industrialists. To ensure sustainability of the country's huge production system, industrialists must embrace the green economy and tackle factory pollution at source.

Hong Yang *University of Southampton, UK.*
hongyanghy@gmail.com
Roger J. Flower, Julian R. Thompson *University College London, UK.*

Metrics: a long-term threat to society

A predictive *h*-index formula for measuring a scientist's potential success (D. E. Acuna *et al. Nature* **489**, 201–202; 2012) might be convenient for decision-making by hiring committees and funding agencies, but such metrics threaten the researcher's wider contribution to society.

Long-term creativity is needed if scientists are to inspire the younger generation. As Albert Einstein said, "creativity is the residue of time wasted" — but researchers are no longer in a position to waste time.

Research pressures also curtail the quality of teaching and supervision, and disadvantage mothers who are trying to build a scientific career (K. R. O'Brien and K. P. Hapgood *Oikos* **121**, 999–1004; 2012). Moreover, early burnout means that some highly trained scientists are being lost to society.

Malgorzata Blicharska, Grzegorz Mikusinski *Swedish University of Agricultural Sciences, Uppsala and Riddarhyttan, Sweden.*
malgorzata.blicharska@slu.se

Metrics: a fetish for high-profile journals

Precise research indicators may be crucial to the field and useful for grant committees, but the failings of the predicted *h*-index proposed by Daniel Acuna *et al.* mean that it is unlikely to be classed among them (*Nature* **489**, 201–202; 2012).

For example, the *h*-index ranking of two co-authors of a research paper can be reversed if they have different individual *h*-indices to start with (L. Waltman and N. J. Van Eck *J. Am. Soc. Inform. Sci. Technol.* **63**, 406–415; 2012). Also, the formula for predicting an *h*-index is probably valid only for neuroscientists, given that different fields have other significant features. The formula's structure does not consider publications in conference proceedings or in books as variables, thereby exacerbating the fetishism surrounding publication in high-profile journals.

Ronald Rousseau *University of Antwerp, Belgium.*
ronald.rousseau@ua.ac.be
Xiaojun Hu *Zhejiang University School of Medicine, Hangzhou, China.*

Metrics: allow more gradual progress

New metrics designed to evaluate a scientist's potential, such as a future *h*-index depending on past trajectories (D. E. Acuna *et al. Nature* **489**, 201–202; 2012), fuel the delusion that only fast results count. Progressive paradigms based on mature ideas, meticulous work, sound ethics, patience and cooperation may be slower, but they still contribute to science in the long term (J.-F. Lutz *Nature Chem.* **4**, 588–589; 2012).

French physicist Louis de Broglie (1892–1987), a pioneer of quantum mechanics, once declared that had Isaac Newton lived in his day and age, Newton might never have become a scientist at all. He would have been bewildered by today's academic rat race and would probably have confined himself to his post as Warden of the Royal Mint instead.

Pedro Cintas *University of Extremadura, Badajoz, Spain.*
pecintas@unex.es

Librarians or science informationists?

As representatives of an international group of library directors, scientists and research administrators, we recognize that science librarians have evolved into 'science informationists' (see go.nature.com/jmvjej). This more accurately reflects their expanded responsibilities, interdisciplinary skills and specialized knowledge.

The increasing volume and complexity of knowledge demands new organizational techniques. Transforming library services calls on technological advances in searching, visualization, data mining and analysis. As technologies and data sources proliferate, there is a growing need to educate students and researchers about these capabilities.

Science informationists collaborate with scientists to enhance their research by helping them to assess its impact, and to curate and manage data. They make knowledge accessible, for example by using their skills in tailoring vocabularies and ontologies. They preserve and showcase their institutions' intellectual output by building networked repositories, and they work with publishers to improve standards, platforms, publication models and search facilities in the interests of better communication.

Science informationists also build sustainable systems through broad collaborations and seek out the best ways to develop these relationships within their institutions. Like researchers, they understand that science needs risk-takers, innovators and visionaries.

Ludmila Pollock* *Cold Spring Harbor Laboratory, Cold Spring Harbor, New York, USA.*
pollock@cshl.edu
**On behalf of 5 co-authors (for a full list, see go.nature.com/88nzz6).*

Clean stoves benefit climate and health

Some 3 billion people worldwide are dependent on rudimentary stoves that burn wood, dung or coal. These account for about 20% of black-carbon emissions globally, as well as 2 million deaths annually from smoke inhalation. More-sophisticated stoves could dramatically reduce these figures, helping to combat climate change and improve public health.

Conventional stoves that burn solid fuels release black and brown carbon particles, along with gases that are implicated in climate warming (including carbon dioxide, ozone-producing gases and methane). As super-efficient absorbers of sunlight, these particles also affect agricultural crop yields.

Modern stoves with natural convection halve solid-fuel use, saving money and collection time. Forced-convection stoves equipped with a fan to increase combustion efficiency cut particulate emissions by 80–90%, black carbon by 60–90% and ozone-producing gases by 50–90% (J. Jetter *et al. Environ. Sci. Technol.* **46**, 10827–10834; 2012; and A. Kar *et al. Environ. Sci. Technol.* **46**, 2993–3000; 2012). Clean fuels, such as liquid petroleum gas, biogas or ethanol, would cut these emissions further.

The Global Alliance for Clean Cookstoves (www.cleancookstoves.org), which has almost 400 partners, including 36 countries, aims to have 100 million homes adopt clean and efficient stoves by 2020. It is developing financing tools for businesses and consumers to ensure that these user-friendly cooking stoves are affordable and available to all.

The Climate and Clean Air Coalition to Reduce Short-lived Climate Pollutants (www.unep.org/ccac) offers a new opportunity to promote energy-efficient stoves that specifically lower black-carbon emissions.

Susan Anenberg* *Department of State and Environmental Protection Agency, Washington DC, USA.*
anenberg.susan@epamail.epa.gov
**On behalf of 4 co-authors (for a full list, see go.nature.com/pmlupe).*

CONTRIBUTIONS

Correspondence may be submitted to **correspondence@nature.com** after consulting the author guidelines at **http://go.nature.com/cmchno**. Alternatively, readers may comment online: **www.nature.com/nature**.

nature OUTLOOK

Published in the 27 September issue of *Nature* and available free online for six months

CHRONIC OBSTRUCTIVE PULMONARY DISEASE

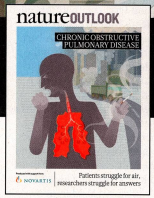

Chronic obstructive pulmonary disease (COPD) robs tens of millions of people of the ability to easily draw in the air they need to live a normal life. Although this incurable, progressive condition is difficult to diagnose, a bevy of new treatment options — including drug combinations, artificial lungs, and dietary supplements — could give COPD patients a breath of fresh air.

Access the Outlook free online for six months.
nature.com/nature/outlook/COPD

Scan this tag to access the Outlook on your smartphone

Produced with support from: NOVARTIS

If you would be interested in partnering with *Nature* on a similar project please contact: sponsorship@nature.com

nature publishing group npg

RESEARCH

NEW ONLINE

Papers published this week at Nature.com/nature

NEWS & VIEWS The extreme choosiness of the chaperone protein HSP90 **p.351**

LETTER Titanium radioisotopes indicate power source of a supernova remnant **p.373**

LETTER VEGF–B antagonists as potential treatment for type 2 diabetes **p.426**

PUBLISHED 14/15 OCTOBER 2012

EVOLUTION

Epistasis in protein evolution

Fyodor Kondrashov and colleagues provide a quantitative estimate of the proportion of amino acid substitutions in evolution that have been influenced by epistasis, instances when substitutions that are accepted in one background genotype are deleterious in another. A comparison of more than a thousand orthologues for selected organellar and nuclear genes reveal a rate of amino acid substitution in recent evolution that is twenty times slower than the rate of neutral evolution — an order of magnitude slower than that expected in the absence of epistasis. These results suggest that the vast majority of amino acids substitutions have different fitness effects in different species, and that epistasis provides the main conceptual framework to describe the mode and tempo of long-term protein evolution.

Epistasis as the primary factor in molecular evolution
M S Breen *et al.*
doi:10.1038/nature11510

PLANT SCIENCES

New resistance gene in soya bean

The soya bean cyst nematode is a constant threat to soya bean crops worldwide. Resistant cultivars are grown, but the mechanisms of resistance are not known. Shiming Liu *et al.* have now identified a gene that confers natural resistance to the nematode. It encodes a serine hydroxymethyltransferase, which is responsible for the interconversion of serine and glycine, and is essential for cellular one-carbon metabolism.

A soybean cyst nematode resistance gene points to a new mechanism of plant resistance to pathogens
S Liu *et al.*
doi:10.1038/nature11651

IMMUNOLOGY

Regulatory B cells control T-cell autoimmunity through IL-21-dependent cognate interactions
A Yoshizaki *et al.*
doi:10.1038/nature11501

STRUCTURAL BIOLOGY

The structural biochemistry of Zucchini implicates it as a nuclease in piRNA biogenesis
J J Ipsaro *et al.*
doi:10.1038/nature11502

Structure and function of Zucchini endoribonuclease in piRNA biogenesis
H Nishimasu *et al.*
doi:10.1038/nature11509

B_{12} cofactors directly stabilize an mRNA regulatory switch
J E Johnson Jr *et al.*
doi:10.1038/nature11607

GENOMICS

Long non-coding antisense RNA controls *Uchl1* translation through an embedded SINEB2 repeat
C Carrieri *et al.*
doi:10.1038/nature11508

NEUROSCIENCE

Input-specific control of reward and aversion in the ventral tegmental area
S Lammel *et al.*
doi:10.1038/nature11527

CELL BIOLOGY

Serine is a natural ligand and allosteric activator of pyruvate kinase M2
B Chaneton *et al.*
doi:10.1038/nature11540

PUBLISHED 17 OCTOBER 2012

EVOLUTION

Cooperativity in an RNA world

In models of early life, characterized by an RNA-only world, it has been suggested that life and evolution would be achieved more easily if RNA molecules interacted, rather than function independently. Niles Lehman and colleagues now show that the molecules can interact using a model system containing RNA fragments that can assemble into a ribozyme. They also show that the cooperative networks formed by these fragments can outcompete self-catalytic RNA fragments. This work indicates that RNA populations have an intrinsic ability to evolve greater complexity through cooperation, and suggests that the benefits of such behaviour were established early in the development of life on Earth.

Spontaneous network formation among cooperative RNA replicators
N Vaidya *et al.*
doi:10.1038/nature11549

The cooperative gene
J Attwater & P Holliger
doi:10.1038/nature11635

PLANETARY SCIENCES

A nearby Earth-mass exoplanet

An exoplanet of Earth-like mass has been found orbiting a nearby star, α Centauri B. The planet is not in the habitable zone; it is much nearer to its star than we are to the Sun. Statistical studies suggest that low-mass planets form preferentially in multi-planet systems, so it is possible that other planets are orbiting α Centauri B, perhaps even in its habitable zone.

An Earth-mass planet orbiting α Centauri B
X Dumusque *et al.*
doi:10.1038/nature11572

Meet our closest neighbour
A P Hatzes
doi:10.1038/nature11636

IMMUNOLOGY

A vaccine strategy that protects against genital herpes by establishing local memory T cells
H Shin & A Iwasaki
doi:10.1038/nature11522

IL-22BP is regulated by the inflammasome and modulates tumorigenesis in the intestine
S Huber *et al.*
doi:10.1038/nature11535

GENOMICS

A physical, genetic and functional sequence assembly of the barley genome
The International Barley Genome Sequencing Consortium
doi:10.1038/nature11543

PALAEONTOLOGY

Development of teeth and jaws in the earliest jawed vertebrates
M Rücklin *et al.*
doi:10.1038/nature11555

STEM CELLS

Progressive degeneration of human neural stem cells caused by pathogenic LRRK2
G-H Liu *et al.*
doi:10.1038/nature11557

STRUCTURAL BIOLOGY

DAXX envelops a histone H3.3–H4 dimer for H3.3-specific recognition
S J Elsässer *et al.*
doi:10.1038/nature11608

PLANETARY SCIENCE

Galvanized lunacy

The finding that magmatic material from the Moon is more enriched in the heavy isotopes of zinc than its terrestrial and Martian analogues prompts fresh thinking about the origin of our natural satellite. SEE LETTER P.376

TIM ELLIOTT

Like the perfect Martini, the Moon has a reputation for being dry. Most obviously, it lacks oceans on its surface, other than those of crystallized magma. Recent evidence suggests, however, that the Moon has a touch of damp. Several studies have found concentrations of water much higher than expected in lunar minerals[1,2] and quenched magma[3,4]. From these observations, it has been suggested that the interior of the Moon may contain similar concentrations of water to those in Earth's mantle. Yet it is difficult to make accurate measurements of water, and rather few samples are amenable to robust analysis. Instead, the abundances of less analytically challenging volatile elements can be studied as proxies for water, allowing investigation of a wider and probably more representative range of lunar materials. In this issue, Paniello and colleagues[5] provide a new perspective on the history of the Moon's volatile elements, based on zinc and, in particular, its isotopic composition. They show that the Moon has a distinctly heavier Zn isotopic composition than Earth, consistent with the satellite having experienced a marked depletion in volatiles.

From our everyday experience, we would not consider Zn to be volatile: there is generally little swooning from its vapours. However, in cosmochemistry, elements that condense at relatively low temperatures (less than about 1,000 °C) from a tenuous gas, as Zn does, are termed volatile. The abundance of these volatile elements varies greatly between planetary bodies — which can be sampled by means of meteorites — but the origin of this variability remains poorly understood. From the first analyses of samples returned by the Apollo missions, it has been clear that the Moon has very low abundances of volatile elements. Yet it is a considerable challenge to translate elemental concentrations measured in the erupted, but now cooled, magmas (melts) at the surface, into a global volatile inventory for the Moon. The power of isotopic measurements, such as those made by Paniello *et al.*, is that isotopes, unlike elements, are not significantly fractionated from each other during magmatic processes, and so erupted melts should faithfully record the composition of their deeper sources.

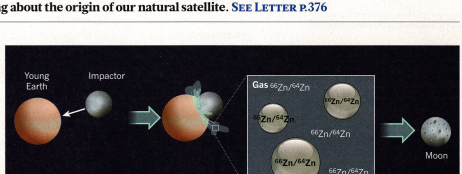

Figure 1 | Zinc isotope enrichment during Moon formation. The diagram illustrates some of the general processes that could have generated a Moon that has a low abundance of volatile elements but is enriched in the heavy isotopes of zinc, as Paniello and colleagues' study indicates[5]. A collision between the young Earth and another planetary body produces the debris from which the Moon formed. The debris consists of silicate melt (spheres) and gas, some of which is lost to the surrounding environment. In chemical equilibrium, the melt phase will invariably have an abundance of the zinc-66 isotope relative to that of zinc-64 ($^{66}Zn/^{64}Zn$) that is higher (black lettering) than that of the gas. Any gas loss from the system will thus result in a Moon both isotopically heavier than the starting composition of the debris and with a lower abundance of Zn. The mechanism of gas loss itself can also contribute to heavy-isotope enrichment of the debris. The lighter isotope ^{64}Zn has a higher mean velocity than the heavier ^{66}Zn, and so can preferentially escape the gravitational bond to the Moon (yellow arrows).

Using this isotopic approach, the authors show that the abundance ratio of Zn isotopes with mass numbers 66 and 64 ($^{66}Zn/^{64}Zn$) is nearly constant for a range of lunar magma types, including those thought to be most representative of the interior. Therefore, the results provide a well-constrained value of this ratio for the Moon as a whole. Most significantly, Paniello *et al.* find that this value is markedly higher — by about 1.5 parts per 1,000 — than that of Earth, Mars and primitive meteorites, which are believed to be the building blocks of the rocky planets. This difference may seem minor, but in terms of isotopic differences between planetary bodies, it is huge.

The exact mechanism by which the Zn isotopic composition of the Moon became heavier than that of Earth is unclear; however, most processes of volatile loss that can be envisaged predict this as an outcome. For example, during condensation of the Moon from a cloud of gas and melt, the heavy isotopes of Zn should have preferentially partitioned into the melt phase (Fig. 1). If the gas phase never fully accreted onto the Moon, the Moon would be left poor in volatiles, but also enriched in the heavy isotopes of volatile elements such as Zn. This diagnostic isotopic signature of volatile depletion has long been sought in lunar samples, and thus its eventual documentation by Paniello *et al.* is notable. Indeed, it was a major surprise that such an effect was not found in a high-precision isotope study[6] of the volatile element potassium almost 20 years ago.

More recently, researchers have reported[7] distinct isotopic differences between lunar and terrestrial chlorine, perhaps a more familiar volatile element. However, the lunar chlorine isotopic composition is not constant, and its trend to heavy values is argued to reflect variable loss of gas from magmas during magma eruption, rather than the interior composition of the Moon[7]. A more complete understanding of planetary volatile evolution requires an explanation of the contrasts in the isotopic signatures of these supposed chemical brethren. Of potential importance in this quest are better estimates of element volatilities under the specific conditions in which the Moon formed. Paniello *et al.* follow a traditional approach of assuming elemental condensation temperatures calculated for a hydrogen-rich, 'nebular' environment[8]. These values are appropriate

for the conditions of the earliest Solar System but not for the accretion of the Moon from a silicate-rich debris disk (Fig. 1).

Paniello and colleagues' new Zn isotope data may also contribute to the reawakened discussion of the very mechanism by which the Moon formed. A theory known as the giant-impact hypothesis — according to which our natural satellite is the outcome of reassembled debris from a collision between the proto-Earth and another planetary body — has dominated recent thinking about lunar genesis. In particular, an oblique-impact scenario was shown[9] to reproduce many of the physical and chemical attributes of the Moon. However, this model predicts that the Moon should be comprised predominantly of material from the colliding impactor rather than the target proto-Earth. Instead, the Moon has proven to be embarrassingly similar to Earth in several isotopic characteristics[10–12], seemingly requiring it to be derived almost wholly from Earth. Models have thus investigated mechanisms by which the isotopic composition of the Earth and Moon could have become homogenized after the impact[13]. The notable differences in Zn isotopic composition between Earth and Moon documented by Paniello *et al.* may be more readily reconciled with an entirely new model for Moon formation, in which the impactor hits a rapidly spinning proto-Earth[14]. This flurry of recent developments emphasizes a waxing interest in our ever-puzzling satellite. ■

Tim Elliott *is in the School of Earth Sciences, University of Bristol, Bristol BS8 1RJ, UK.*
e-mail: tim.elliott@bristol.ac.uk

1. Boyce, J. W. *et al. Nature* **466,** 466–469 (2010).
2. McCubbin, F. M. *et al. Proc. Natl Acad. Sci. USA* **107,** 11223–11228 (2010).
3. Saal, A. E. *et al. Nature* **454,** 192–195 (2008).
4. Hauri, E. H., Weinreich, T., Saal, A. E., Rutherford, M. C. & Van Orman, J. A. *Science* **333,** 213–215 (2011).
5. Paniello, R. C., Day, J. M. D. & Moynier, F. *Nature* **490,** 376–379 (2012).
6. Humayun, M. & Clayton, R. N. *Geochim. Cosmochim. Acta* **59,** 2131–2148 (1995).
7. Sharp, Z. D., Shearer, C. K., McKeegan, K. D., Barnes, J. D. & Wang, Y. Q. *Science* **329,** 1050–1053 (2010).
8. Lodders, K. *Astrophys. J.* **591,** 1220–1247 (2003).
9. Canup, R. M. & Asphaug, E. *Nature* **412,** 708–712 (2001).
10. Wiechert, U. *et al. Science* **294,** 345–348 (2001).
11. Touboul, M., Kleine, T., Bourdon, B., Palme, H. & Wieler, R. *Nature* **450,** 1206–1209 (2007).
12. Zhang, J., Dauphas, N., Davis, A. M., Leya, I. & Fedkin, A. *Nature Geosci.* **5,** 251–255 (2012).
13. Pahlevan, K. & Stevenson, D. J. *Earth Planet. Sci. Lett.* **262,** 438–449 (2007).
14. Čuk, M. & Stewart, S. T. *Early Solar System Impact Bombardment II* Poster 4006 (Lunar & Planetary Inst., 2012).

CANCER THERAPY

Tumours switch to resist

Tumour cells can respond to targeted immune-cell therapies by losing proteins that mark them as being cancerous. Subverting this resistance mechanism may lead to more durable cancer-treatment strategies. SEE LETTER P.412

ANTONI RIBAS & PAUL C. TUMEH

Decades of research have yielded methods for cancer treatment that can be more specifically tailored to a patient's cancer than broader strategies such as radiotherapy or chemotherapy. However, these methods — which include immunotherapy and therapies targeted at cancer-causing genes — are dogged by the problem of acquired resistance, in which many patients initially respond to the treatment but subsequently become unresponsive and experience relapse. Resistance is commonly thought to arise from the proliferation of a small proportion of resistant cells in a mixed tumour-cell population. But on page 412 of this issue, Landsberg *et al.*[1] show, using a mouse model of melanoma, that resistance to a promising form of immunotherapy can develop when cancer cells change their protein-expression profile in response to treatment*.

Cancer immunotherapies are designed to initiate or boost a person's immune response to a tumour. One way of doing this is by adoptive cell transfer (ACT), in which patients receive transfusions of immune cells called T cells that target cancer-specific antigens (an antigen is a substance that elicits responses from the B cells and T cells of the immune system). By contrast, oncogene-targeted therapies work by reducing the function of certain mutated proteins that are overactivated in tumour cells. Although much progress has been made in determining why patients relapse with oncogene-targeted therapies, little is known about the mechanisms underlying acquired resistance in patients receiving ACT. However, there is generally a high initial response rate to ACT, so understanding what then happens to lead to resistance is a challenge worthy of investigation.

The most common sources of tumour-antigen-specific cells for ACT are tumour-infiltrating lymphocytes (TILs) or blood T cells that are isolated from the patient and modified before being reintroduced. In the case of TILs, which already have tumour specificity, this involves expanding the cell population and activating the cells. In therapies using blood T cells, which are initially not tumour specific, the cells' antigen receptors are first genetically engineered to recognize tumour antigens[2]. Tumour responses tend to last longer in TIL-based ACT, probably because each TIL preparation might target several tumour antigens simultaneously[3]. However, TILs can be isolated

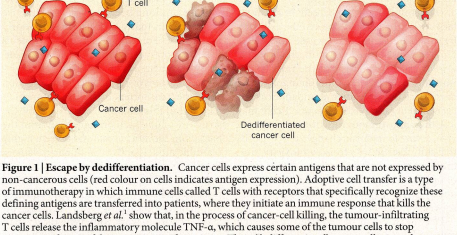

Figure 1 | Escape by dedifferentiation. Cancer cells express certain antigens that are not expressed by non-cancerous cells (red colour on cells indicates antigen expression). Adoptive cell transfer is a type of immunotherapy in which immune cells called T cells with receptors that specifically recognize these defining antigens are transferred into patients, where they initiate an immune response that kills the cancer cells. Landsberg *et al.*[1] show that, in the process of cancer-cell killing, the tumour-infiltrating T cells release the inflammatory molecule TNF-α, which causes some of the tumour cells to stop expressing of some of their cancer-specific antigens. These 'dedifferentiated' cancer cells are no longer recognized by the T cells, resulting in resistance to the therapy and tumour regrowth.

*This article and the paper under discussion[1] were published online on 10 October 2012.

from only a limited number of patients with melanoma, which hinders the application of this approach. Genetically engineered T cells address this problem, because every patient has ample numbers of nonspecific T cells that can be harvested for this purpose. But although ACT based on genetically modified T cells results in a high frequency of positive initial responses, relapse often occurs a few months after the start of treatment[4–6].

To study how this resistance arises, Landsberg *et al.* developed a mouse model of melanoma and an ACT protocol (using genetically modified T cells) that recapitulates the clinical course seen in people. The widely accepted view of how resistance to ACT therapy arises is that tumours contain small numbers of cells (called subclones) with genetic variations that give them a proliferative advantage in the face of the immune-cell attack. However, Landsberg and colleagues observed that the inflammatory response initiated by ACT caused a proportion of the melanoma cells to lose some of the antigens that defined the cells as being cancerous — a change that the authors describe as 'dedifferentiation' (Fig. 1). This is the key to their new hypothesis for tumour resistance: the T cells transferred in ACT are designed to target tumour-specific antigens, but precisely these antigens are lost by the tumour cells during treatment. The authors also identify the pro-inflammatory cell-signalling molecule tumour necrosis factor-α (TNF-α) as a crucial mediator of this cellular change, and show that the change is reversible, meaning that the cancer cells can reacquire expression of the antigens when the treatment is stopped and the inflammation resolves.

Although the cellular dedifferentiation described by Landsberg and colleagues is a new concept in cancer resistance, the idea fits well with previously proposed mechanisms of resistance to tumour-antigen-specific immunotherapy. For example, resistance has been observed after increased proliferation of subclones that did not express a tumour antigen that was being targeted by ACT, and also as a result of some or all cells in a tumour lacking key proteins in the cellular pathway by which antigens are 'presented' to T cells[7]. However, resistance to immunotherapy may also arise from changes in the transferred immune cells, rather than changes to the characteristics or relative abundance of cancer cells. For example, therapeutic T cells may lose their anti-tumour functions over time *in vivo*, owing to intrinsic changes in the T cells that shift their activity from cytotoxicity to an immune-tolerant state[8] or through the effects of immune-suppressive cells in the tumour microenvironment, such as myeloid suppressor cells or regulatory T cells[2].

The mechanism of acquired resistance reported by Landsberg *et al.* has so far been observed only in their mouse model. But if similar effects are seen in patients, then the authors' findings will open up avenues for improving ACT-based therapies. For example, because this resistance mechanism may be restricted to the loss of certain tumour antigens, concurrently targeting several antigens of different classes by transferring a mixed population of T cells might slow or prevent resistance. A similar effect may be achieved by preventing TNF-α expression by the transferred T cells, as this seems to be the key inflammatory molecule that induces antigen loss by the tumour cells. Alternatively, broadening the immune response by combining ACT with other immune-supporting agents, such as anti-CTLA4 or anti-PD-1 antibodies, might minimize the reliance of the therapy on recognizing a single antigen and thereby make it harder for the cancer cells to escape. Thus, by identifying a mechanism by which cancers adapt to evade ACT therapy, Landsberg and colleagues have provided the basis for several testable approaches to overcome this problem in patients. ■

Antoni Ribas *and* **Paul C. Tumeh** *are in the Department of Medicine, Jonsson Comprehensive Cancer Center, University of California, Los Angeles, Los Angeles, California 90095-1782, USA.*
e-mail: aribas@mednet.ucla.edu

1. Landsberg, J. *et al. Nature* **490**, 412–416 (2012).
2. Restifo, N. P., Dudley, M. E. & Rosenberg, S. A. *Nature Rev. Immunol.* **12**, 269–281 (2012).
3. Rosenberg, S. A. *et al. Clin. Cancer Res.* **17**, 4550–4557 (2011).
4. Morgan, R. A. *et al. Science* **314**, 126–129 (2006).
5. Johnson, L. A. *et al. Blood* **114**, 535–546 (2009).
6. Robbins, P. F. *et al. J. Clin. Oncol.* **29**, 917–924 (2011).
7. Ferrone, S. & Marincola, F. M. *Immunol. Today* **16**, 487–494 (1995).
8. Ma, C. *et al. Nature Med.* **17**, 738–743 (2011).

STRUCTURAL BIOLOGY

Bundles of insights into sugar transporters

The structure of a bacterial protein belonging to the 'sugar porter' family guides the building of long-sought molecular models of proteins that transport glucose across cell membranes in humans. SEE ARTICLE P.361

PETER J. F. HENDERSON & STEPHEN A. BALDWIN

Simple carbohydrates, especially glucose, are central to the chemical transformations that maintain life in all organisms[1]. In mammals, including humans, glucose is the major mediator of energy transfer between tissues, and alterations in its blood concentration are intimately involved in conditions such as diabetes and obesity. So glucose uptake by cells has long been the focus of intense research, but many aspects are still poorly understood. For example, cells have proteins that transport sugars across the cell membrane, but we do not have a good grasp of the underlying mechanisms owing to a lack of information about the transporters' molecular features. On page 361 of this issue, Sun *et al.*[2] describe the structure of one such protein, XylE from the bacterium *Escherichia coli*, and present highly plausible models of its evolutionary relatives, the human glucose transporters.

XylE resembles the human glucose transporters (GLUTs) in amino-acid sequence and in biochemical properties[3]. Sun and colleagues chose to work with XylE, rather than with the human proteins, because of its ease of purification and its stability in detergent — two features that facilitated the elucidation of its three-dimensional structure using crystallographic techniques. Although XylE transports, not glucose, but xylose (a similar sugar), the authors showed that glucose can bind to and inhibit the activity of XylE. The researchers' initial attempts to crystallize the protein yielded low-quality crystals, but the addition of a sugar (xylose or glucose) improved crystal quality and enabled the authors to determine the structures of the protein–sugar complexes at a high resolution (2.6–2.9 ångströms). Moreover, on the basis of the XylE data, they proposed structural models for four (GLUT1 to GLUT4) of the 14 human GLUTs (Fig. 1).

XylE and GLUTs belong to the 'sugar porter' family of proteins, which is part of the ubiquitous major facilitator superfamily (MFS) of transporters[4]. Although the structures of several MFS members are known, those of the sugar porters had remained unsolved. Sun *et al.* found that, as expected for an MFS member, XylE has 12 transmembrane α-helices (TM1–TM12) clustered into two structurally related bundles that are arranged around a central sugar-binding site. Bound xylose and glucose interacted with the protein in a similar way, by establishing hydrogen bonds primarily

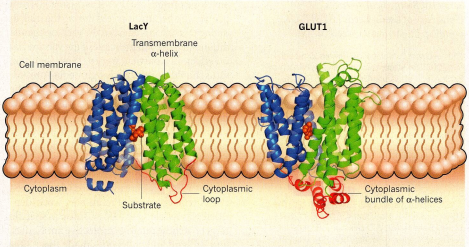

Figure 1 | Relatives but not twins. Proteins belonging to the major facilitator superfamily (MFS) transport vital nutrients such as sugars across cell membranes, and it is thought that their mechanism of action involves alternating inward-facing and outward-facing conformations. MFS proteins typically consist of 12 transmembrane α-helices, organized into two similar bundles (blue and green), as well as cytoplasmic loops. One such protein, LacY, is shown here bound to an analogue of its substrate (the sugar lactose) and in an inward-facing conformation. Sun *et al.*[2] solved the outward-facing structure of another MFS member, the bacterial protein XylE, and used it to construct plausible models of similar human proteins, the glucose transporters GLUT1 to GLUT4. The authors show that, in contrast to other MFS proteins, XylE and GLUTs have a cytoplasmic bundle of four α-helices that might participate in the transport mechanism. (LacY and GLUT1 images courtesy of N. Yan, Tsinghua University, Beijing, China.)

with amino-acid residues in the carboxy-terminal bundle. These residues are largely the same in GLUT1 to GLUT4, which suggests a common mode of sugar binding (Fig. 1).

Surprisingly, the reported structures and models cannot explain a profound difference that exists between XylE and GLUT1–GLUT4: sugar intake is coupled to proton (H^+) translocation in XylE but not in its human counterparts. Proton transport into the bacterial cell drives xylose uptake against its concentration gradient because it is an energetically favourable process (there is a lower concentration of protons inside the cell than outside). By contrast, GLUT1 to GLUT4 facilitate diffusion of glucose only down its concentration gradient. However, comparison of the XylE structure with the GLUT models did not reveal any obvious candidates for proton-binding residues that could account for this functional difference.

Transport of molecules across the membrane is generally thought to occur through a mechanism in which changes in the protein's conformation make the substrate binding site alternately accessible from one or other side of the membrane[5,6]. However, Sun *et al.* report that XylE and the GLUT models have a bundle of four α-helices on the cytoplasmic side of the membrane that are not present in the structures of other MFS proteins (Fig. 1), implying possible mechanistic differences. These additional α-helices participate in an intricate network of hydrogen bonds with residues located near the cytoplasmic ends of some of the transmembrane helices. Interestingly, such residues are found in signature-sequence motifs that are evolutionarily conserved in other members of the sugar-porter family, and the authors observed that mutations affecting these residues had drastic effects on transport.

The precise role of the hydrogen-bond network in substrate translocation remains to be determined. However, it has been shown for GLUT1 that truncation of the carboxy-terminal end of the protein (which would remove some of those interactions) 'locks' the transporter in an inward-facing conformation in which it is able to bind to the sugar but not to transport it[7]. By contrast, the cytoplasmic domain in non-sugar-porter MSF transporters seems to have only a minor role in the proteins' function, as previously shown[8] by mutation of the TM6–TM7 loop in the *E. coli* lactose transporter LacY. Therefore, despite a common evolutionary origin, the precise mechanism of transport might vary in different MFS subfamilies.

The XylE structure and the GLUT models open the way to a greater understanding of the physiological functions, mechanisms and regulation of these proteins. For example, it could be possible to design selective small-molecule inhibitors of these proteins to address the question of why mammals need 14 different GLUT proteins[9]. Similarly, Sun and colleagues' results should help to clarify the molecular basis for the different substrate selectivities displayed by GLUTs; for example, GLUT9 transports urate (a compound resulting from the metabolic breakdown of nucleotides) in addition to sugars[9].

But the significance of the XylE structure extends beyond mammalian metabolism,

50 Years Ago

The distance travelled by grazing sheep and the energy cost of locomotion have been measured … This leaves the energy cost of grazing *per se* and of the animal's reactions to its environment to be accounted for; the first measurements of the former can now be reported. Two sheep were allowed to graze normally for a week. A patch of turf 1.0 × 1.5 m was then dug up and relaid on the floor of a respiration chamber. The sheep, which had both been trained for such work, were then, one at a time, placed in the respiration chamber … The energy expenditure of the sheep always increased during grazing and fell again during the subsequent rest period, but there was no significant change when pre-cut grass was given to the sheep. The grazing increment did not vary significantly from sward to sward, and had a mean value of 0.62 ± 0.04 kcal/h/kg body-weight for a 29-kg Merino ewe and of 0.84 ± 0.12 for a 53-kg Merino wether.

From *Nature* 20 October 1962

100 Years Ago

The accompanying photograph shows a pearl … alleged to have been found in *Nautilus pompilus*, from the Sulu archipelago.

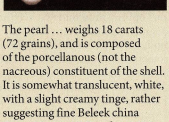

The pearl … weighs 18 carats (72 grains), and is composed of the porcellanous (not the nacreous) constituent of the shell. It is somewhat translucent, white, with a slight creamy tinge, rather suggesting fine Beleek china

From *Nature* 17 October 1912

because other organisms also have panoplies of sugar porters. For example, such proteins are used by plant cells to accumulate sugars into vacuoles (cytoplasmic vesicles)[10], and they regulate sugar fermentation in yeasts during the production of alcohol from grape juice[11]. Moreover, some proteins that transport molecules other than sugars also possess the sugar-porter signature sequences. This is the case for plant PHT1 phosphate transporters[12], which not only take up the vital nutrient phosphate from the soil but also regulate its distribution throughout the plant. Sun and colleagues' paper is therefore likely to have ramifications in fields ranging from medicine to agriculture and the production of food and drink. ■

Peter J. F. Henderson *and* **Stephen A. Baldwin** *are in the Astbury Centre for Structural Molecular Biology, School of Biomedical Sciences, University of Leeds, Leeds LS2 9JT, UK.*
e-mail: p.j.f.henderson@leeds.ac.uk

1. Nicholson, D. *Metabolic Pathways* 22nd edn (2003); www.iubmb-nicholson.org/index.html
2. Sun, L. *et al. Nature* **490**, 361–366 (2012).
3. Maiden, M. C. *et al. Nature* **325**, 641–643 (1987).
4. Pao, S. S., Paulsen, I. T. & Saier, M. H. *Microbiol. Mol. Biol. Rev.* **62**, 1–34 (1998).
5. Jardetzky, O. *Nature* **211**, 969–970 (1966).
6. Boudker, O. & Verdon, G. *Trends Pharmacol. Sci.* **31**, 418–426 (2010).
7. Oka, Y. *et al. Nature* **345**, 550–553 (1990).
8. Weinglass, A. B. & Kaback, H. R. *Proc. Natl Acad. Sci. USA* **97**, 8938–8943 (2000).
9. Thorens, B. & Mueckler, M. *Am. J. Physiol. Endocrinol. Metab.* **298**, E141–E145 (2010).
10. Slewinski, T. L. *Mol. Plant* **4**, 641–662 (2011).
11. Kruckeberg, A. L. & Dickinson, J. R. in *The Metabolism and Molecular Physiology of Saccharomyces cerevisiae* (eds Dickinson, J. R. & Schweizer, M.) 42–103 (2004).
12. Nussaume, L. *et al. Front. Plant Sci.* **2**, 83 (2011).

HIV

Design by trial

A genetic analysis of viruses infecting participants in an HIV vaccine trial indicates that the vaccine is more protective against viruses that have variations at specific sites in the viral envelope. SEE LETTER P.417

DAVID V. GLIDDEN

The past five years have brought stunning progress in the development of biomedical approaches to preventing HIV infection. But despite recent hope for an AIDS-free generation, we still lack a crucial tool needed to reach this goal — an HIV vaccine. However, on page 417 of this issue, Rolland *et al.*[1] present an analysis of a clinical trial that encourages us to believe that this goal is achievable. Furthermore, their work identifies a site on the virus's outer coat as a key target for future vaccine development.

Until a few years ago, the handful of candidate HIV vaccines that had been evaluated in randomized clinical trials had all failed to prevent HIV infections any better than a placebo. But in 2009, researchers conducting a trial in 16,402 volunteers in Thailand reported[2] a 31% reduction in HIV infections in recipients of a vaccine known as RV144. The study's results were met with a range of responses, from cautious optimism to outright scepticism[3]. Although RV144 had some efficiency, this was modest. For example, the credible range for protection from infection elicited by the vaccine ran between 1% and 51% — a very wide range, and negligible at its low end. In addition, sensitivity analyses of the trial results failed to cross the threshold of statistical significance, and some experts openly speculated that the outcome was a statistical fluke.

A recent review[4] that formally combined the trial's findings and expert opinion estimated at least a 22% chance that the reported outcome was a false positive.

In fact, doubts about RV144 had been expressed even before the study started[5]. The concerns stemmed from the fact that RV144 is a 'prime and boost' vaccine composed of two vaccines that had both shown only modest to no efficacy in previous studies. A trial of RV144 had been contemplated but scrubbed by the US-based HIV Vaccine Trials Network, and some informed observers had called for the Thai trial to be cancelled as well[5]. Despite this, it went ahead, and in the intervening three years, follow-up analyses of immune responses[6] and now, from Rolland and colleagues, of HIV infections in the trial participants, are supporting an interpretation that RV144 was indeed successful at stimulating protective immunity in some of the vaccinated individuals.

Several candidate HIV vaccines, including RV144, contain proteins that belong to the outer coat or 'envelope' of HIV, with the intention of inducing protective immune memory against this region of the virus. However, the amino-acid sequence of the envelope varies among different circulating HIV viruses, so that any single vaccine based on this structure may not stimulate immune recognition across all HIV variants.

Rolland *et al.* examined the sequences of the envelope protein of HIV viruses isolated from people who became infected during the trial, to deduce the effectiveness of the vaccine against different viruses. In principle, if the vaccine has no effect on a particular virus type, then that virus should be found in roughly equal proportions in infected people who had received the vaccine and in those given the placebo. The researchers focused their typing on the V1/V2 loop structure of the viral envelope protein, a region previously implicated as being important for immune protection by a study showing that immune responses involving antibodies against V1 and V2 are associated with reduced risk of HIV infection[6]. Preliminary work identified 15 sites along the V1/V2 loop as specific targets of these putative protective antibodies, and Rolland and colleagues made these sites the subject of their sequence analysis.

The authors found two 'genetic signatures' in the V2 region — an amino-acid match between virus and vaccine at position K169 (lysine) and a mismatch at position I181 (isoleucine in the vaccine sequence) — that were proportionally less common in viruses that had infected vaccinated individuals compared with recipients of the placebo. This suggests that the vaccine blocked or 'sieved out' viruses with these sequence features, although this effect was variable: the vaccine had 48% efficacy at preventing infection with viruses matching at K169 and 78% efficacy against viruses with a mismatch at I181. This differential effect of the RV144 vaccine in regard to HIV type is compelling, if indirect, evidence that the vaccine elicited immune responses that protected some people against some variants of HIV. Furthermore, because both sites are on the V2 region, the findings implicate this sequence as a key target for future vaccine development.

In other respects, however, the results defy a simple narrative. First, in the case of the K169 position, the vaccine protects best against viruses with the same sequence as that in the vaccine. Given that a vaccine is expected to 'train' the immune system, this result is unsurprising. However, the opposite is the case for position I181, and the reason for this is unclear. It is not that the vaccine promoted infection with viruses that matched it at I181; the rate of infection with such variants was still lower in vaccine recipients than in people receiving the placebo. It is possible, however, that I181 is merely a proxy for another, unidentified, location on V2 that does indeed match between the vaccine and these viruses.

Second, the results do not square neatly with the recent finding that the presence of antibodies against V1 and V2 was correlated with a reduced risk of HIV infection in those receiving the vaccine[6]. This association seems to be similar for vaccine-matching and non-matching viruses, but if it is the antibodies that provide the 'sieve' effect reported by Rolland and colleagues, one would expect

them to be less protective against strains for which the vaccine was less effective. So although the sieve and correlates-of-protection analyses are both compelling, these two pieces of the story do not fully explain each other.

Although such questions remain open, Rolland and colleagues' study is another demonstration of the indispensable role of randomized trials in the incremental process of HIV vaccine development. The authors' research exemplifies how data from such trials can provide information on strain-specific effects and HIV-protective immune responses, and their analysis has identified an area on the HIV envelope that will be a focus of future vaccine studies. This comes at a time of steady progress in HIV vaccine research[7] and buoys up the hope that an HIV vaccine is possible — and perhaps sooner than later. ■

David V. Glidden *is in the Department of Epidemiology and Biostatistics, University of California, San Francisco, San Francisco, California 94107, USA.*
e-mail: dave@biostat.ucsf.edu

1. Rolland, M. *et al. Nature* **490,** 417–420 (2012).
2. Rerks-Ngarm, S. *et al. N. Engl. J. Med.* **361,** 2209–2220 (2009).
3. Leavy, O. *Nature Rev. Immunol.* **9,** 755 (2009).
4. Gilbert, P. B. *et al. J. Infect. Dis.* **203,** 969–975 (2011).
5. Burton, D. R. *et al. Science* **303,** 316 (2004).
6. Haynes, B. F. *et al. N. Engl. J. Med.* **366,** 1275–1286 (2012).
7. Wu, X. *et al. Science* **329,** 856–861 (2010).

MOLECULAR BIOLOGY

Choose your protein partners

A large-scale study sheds light on the extraordinary molecular-recognition skills of the chaperone HSP90, which allow this protein to interact selectively with hundreds of other proteins of diverse function.

RAHUL S. SAMANT & PAUL WORKMAN

The protein HSP90 plays an essential part in a plethora of cellular processes, in evolution and in disease. It is a molecular chaperone, a type of protein required for the activity and stability of other proteins, which are known as its 'clients'. Many of HSP90's clients are oncogenic protein kinases — when made overactive, they can lead to cancer[1]. That is why 20 small-molecule HSP90 inhibitors are currently in clinical trials for antitumour therapy[2]. Despite all this interest, the fundamental question of how HSP90 chooses its clients remains unanswered. Writing in *Cell*, Taipale *et al.*[3] report that another protein (a co-chaperone) facilitates client-family recognition by HSP90, whereas the thermal stability of the client determines the strength of its interaction with the chaperone itself.

In the absence of functional HSP90, its clients form aggregates or are degraded. So previous large-scale efforts to identify clients were based on either isolation of HSP90-binding proteins[4] or demonstration of client depletion in cells in which HSP90 function had been perturbed (for example, by pharmacological inhibition)[5]. These studies have so far revealed around 350 highly diverse clients for HSP90.

Taipale *et al.* carried out their own large-scale survey of HSP90 clients among selected protein classes, including the protein kinases. They used a modification of the LUMIER assay[6], a luminescence-based measure of association between a 'prey' protein (in this case, HSP90) and 'baits' (putative clients) in mammalian cells. Compared with other techniques used to detect binding, such as mass spectrometry, the modified LUMIER assay is much more sensitive, detects shorter-lived interactions and gives a quantitative rather than a binary (binding/no binding) readout. Of the 314 kinases investigated, 193 (61%) interacted to some extent with HSP90. Strikingly, the strength of these interactions varied across a continuous 100-fold range. This finding supports the growing view that the binary categorization of kinases into clients or non-clients should be replaced by a continuum of HSP90 dependence.

In agreement with an earlier analysis of binary data[7], Taipale and colleagues confirmed and extended previous findings that even very closely related kinases (such as ARAF and BRAF) exhibit extreme differences in the strength of their interactions with HSP90 (refs 1,8). Seeking a structural explanation for this, Taipale *et al.* constructed and analysed variants of ARAF and BRAF containing single-point mutations, and also analysed chimaeric proteins made of different pieces taken from the two kinases. Notably, no single amino-acid change within the catalytic kinase domain (the part of the protein that defines a protein kinase) altered the protein's affinity for HSP90. Rather, the authors found that determinants for HSP90 association were widely distributed across the kinase domain.

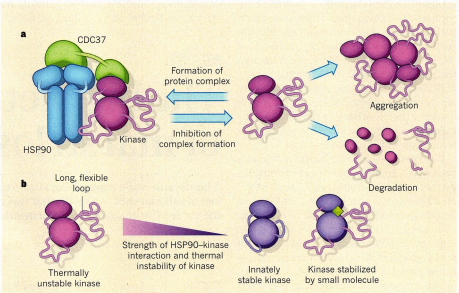

Figure 1 | A helping hand for unstable proteins. a, Many proteins of the protein-kinase family form aggregates or are degraded unless they form a complex with the chaperone protein HSP90. Binding of the kinase to HSP90 can be reversed by the use of HSP90 inhibitors, for example. Taipale *et al.*[3] report that another protein, co-chaperone CDC37, facilitates the recognition of kinase-family features by HSP90. **b**, The authors also show that the strength of the HSP90–kinase interaction is correlated with the thermal instability of the kinase. Some of this instability might be due to the presence of long, highly flexible loops in the kinase domain, because protein-kinase variants possessing certain shorter flexible segments display increased thermal stability and decreased interaction with HSP90. Small molecules stabilized the kinases and led to weaker association with HSP90.

Yet, surprisingly, they also showed that association of a client with HSP90 could be modulated by changes to certain highly localized regions in the kinase domain, regardless of their amino-acid sequences. The changes mimicked those produced by a natural process known as alternative splicing, by which a protein-encoding messenger RNA can be processed in different ways to generate various 'isoforms' of the protein. That finding might explain Taipale and colleagues' observation that isoforms of the same kinase can have distinct affinities for HSP90.

The authors noticed that fewer crystal structures had been reported for the kinase domains of HSP90 clients than for those of non-clients, which suggested that clients might be less soluble and stable than non-clients. On the basis of this and their previous findings, Taipale *et al.* hypothesized that affinity for HSP90 might be related to a client's instability. Indeed, they showed that the strength of the interactions between HSP90 and 56 kinases was correlated with the thermal instability of the kinase domain. The thermal-instability data used had been obtained previously by measuring the progressive unfolding of the proteins at increasing temperatures[9], and probably reflect the presence of flexible, unstructured regions of the kinase domain that HSP90 can identify and bind to.

To delve deeper into their thermal-instability hypothesis, the authors focused on the oncogenic kinase BCR-ABL, because it is known[9] that certain small-molecule inhibitors and activators of this kinase can lock the protein in a stable (active or inactive) conformation — which should increase its thermal stability. Indeed, treatment of cells with such molecules decreased the association of BCR-ABL with HSP90. Moreover, mutations that reduced or enhanced the thermal stability of BCR-ABL resulted in increased or decreased HSP90 affinity, respectively. Several lines of evidence therefore back up the view that the thermal stability of a kinase determines its association with HSP90 (Fig. 1).

But how does HSP90 'know' whether a protein is a kinase? There was previous evidence that the co-chaperone CDC37 mediated the interaction between HSP90 and certain kinases[10]. Taipale *et al.* now provide additional, systematic evidence that HSP90 requires CDC37 to recognize kinases — but not to recognize clients that are transcription-factor proteins. Future large-scale analyses incorporating other co-chaperones may reveal additional recognition determinants specific to various client classes. Such analyses could also be valuable in defining the multi-protein interactions established by HSP90 and how they are affected by small-molecule inhibitors of HSP90 and of client function.

In addition, the researchers report that HSP90 interacted with 117 proteins belonging to the E3 ubiquitin ligase class, which targets proteins for degradation. The recognition rules for choosing clients among these degradation partners must now be determined. Moreover, the mechanisms by which inhibition of HSP90 leads to the destruction of some clients but not others (which then form insoluble aggregates) remain unclear.

Taipale and colleagues' systematic and quantitative study indicates that the co-chaperone CDC37 helps HSP90 to recognize the kinase client class, and that the subsequent HSP90–kinase interaction is determined by an as-yet-unknown feature that can be measured in terms of thermal instability. Exactly how HSP90 recognizes thermally unstable kinase domains is a key question for future research. To answer it, we probably need to solve the three-dimensional structures of HSP90 multi-protein complexes containing clients. However, it is tempting to speculate that thermal instability is related to the flexibility of the kinase 'hinge' — a segment of the protein that connects the amino- and carboxy-terminal parts of a kinase domain — or other mobile regions.

Such emerging recognition mechanisms should eventually provide a molecular explanation for the various roles of HSP90. They are already beginning to reveal precisely how the chaperone acts as a driving force in kinase evolution: by stabilizing potentially advantageous but unstable protein forms, HSP90 buffers the effects of genetic variation that could be detrimental to the organism but that provide improved survival under stress conditions where HSP90 is partially inhibited[11]. In addition, these mechanisms can also explain how HSP90 exhibits its 'dark side': HSP90 protects kinases that are abnormally activated by mutations in cancer cells and that would otherwise be prone to aggregation or degradation[12]. Nevertheless, there is still much to be discovered about how HSP90 chooses its clients, co-chaperones and degradation partners in its highly complex, choreographed dance — knowledge that will have profound implications for evolutionary and cell biology, as well as for the treatment of disease. ■

Rahul S. Samant *and* **Paul Workman** *are in the Cancer Research UK Cancer Therapeutics Unit, The Institute of Cancer Research, London SM2 5NG, UK.*
e-mail: paul.workman@icr.ac.uk

1. Whitesell, L., Mimnaugh, E. G., De Costa, B., Myers, C. E. & Neckers, L. M. *Proc. Natl Acad. Sci. USA* **91,** 8324–8328 (1994).
2. Travers, J., Sharp, S. & Workman, P. *Drug Discov. Today* **17,** 242–252 (2012).
3. Taipale, M. *et al. Cell* **150,** 987–1001 (2012).
4. Hartson, S. D. & Matts, R. L. *Biochim. Biophys. Acta* **1823,** 656–667 (2012).
5. Samant, R. S., Clarke, P. A. & Workman, P. *Cell Cycle* **11,** 1301–1308 (2012).
6. Barrios-Rodiles, M. *et al. Science* **307,** 1621–1625 (2005).
7. Citri, A. *et al. J. Biol. Chem.* **281,** 14361–14369 (2006).
8. da Rocha Dias, S. *et al. Cancer Res.* **65,** 10686–10691 (2005).
9. Federov, O. *et al. Proc. Natl Acad. Sci. USA* **104,** 20523–20528 (2007).
10. Vaughan, C. K. *et al. Mol. Cell* **23,** 697–707 (2006).
11. Rutherford, S. L. & Lindquist, S. *Nature* **396,** 336–342 (1998).
12. Bagatell, R. & Whitesell, L. *Mol. Cancer Ther.* **3,** 1021–1030 (2004).

The authors declare competing financial interests.
See go.nature.com/kiqdeu for details.

ECOLOGY

The big picture of marsh loss

A landscape-scale experiment shows that excessive nutrient levels can cause the loss of salt marshes — a result that was not seen in smaller studies. This illustrates the value of large-scale, long-term studies in ecology. SEE LETTER P.388

STEVEN C. PENNINGS

The widespread use of fertilizers has greatly altered global nitrogen and phosphorus cycles, which are now dominated by anthropogenic rather than natural processes[1,2]. A substantial portion of fertilizers are ultimately transported into rivers and to the sea. One consequence of this increased nutrient supply is the proliferation of 'dead zones' at the mouths of the world's rivers — areas where the decomposition of fertilizer-driven algal blooms has used up most of the oxygen, leading to the death of fish and other large organisms[3]. Wetlands could provide a solution to this problem, because they chemically transform nutrients as they flow from land to sea. In particular, coastal salt marshes transform nitrate, the most abundant form of nitrogen in fresh waters, into nitrogen gas, thereby limiting the amount of nitrogen reaching the ocean[4]. But does providing this 'ecosystem service' to humanity have consequences for wetlands? On page 388 of this

issue, Deegan *et al.*[5] show that the price may be a high rate of global wetland loss.

Coastal wetlands are valuable. In addition to transforming nutrients, they support fisheries, protect coasts from storms and provide habitat for wildlife. To determine how wetlands may be affected by increased nutrient supplies, scientists have experimentally applied nutrients to wetlands in dozens of studies. Almost all of these studies used small plots, rarely larger than 1 square metre, and applied nutrient levels far higher than those that occur in even the most enriched habitats. These experiments have shown that nutrient addition causes a decrease in the mass ratio of plant roots to shoots, an increase in above-ground biomass, a change in plant species composition, and an increased vulnerability of plants to herbivores[6]. Whether these results can be scaled up to entire estuaries, however, has remained an open question.

Deegan *et al.* took a new approach to studying nutrient effects in estuaries. Working at the scale of entire tidal creeks (approximately 30,000 square metres), they added nutrients to the water flowing into a marsh on rising tides, replicating conditions typical of nutrient-enriched estuaries. They then compared the responses of the studied region with those of control creeks over nine years. Because Deegan and colleagues had the resources and time to conduct a large, long-term experiment, they were able to study all the microhabitats that occur in marshes. This broad scope paid off in an unexpected way: the authors observed striking changes to the stability and morphology of creek banks, a microhabitat that is usually not included in plot-based studies. Moreover, the geomorphological changes were not apparent until several years had passed, and so would probably have been overlooked by a standard research project.

Some of the authors' findings were expected on the basis of previous work: plants grew fewer roots because nutrients were easier to find, and the decomposition of organic matter in the soil increased because the added nutrients enabled bacteria to metabolize organic matter more easily. But other results transform our understanding of how nutrients affect coastal wetlands. In particular, Deegan *et al.* observed that the loss of roots and organic matter reduced the stability of creek-bank soils, leading to the collapse of creek banks and the consequent conversion of salt marsh into mudflat (Fig. 1). Although only the area within a few metres of creeks was affected, most salt marshes are highly dissected by a network of tidal creeks; the potentially affected habitat could thus represent a large proportion of overall marsh area.

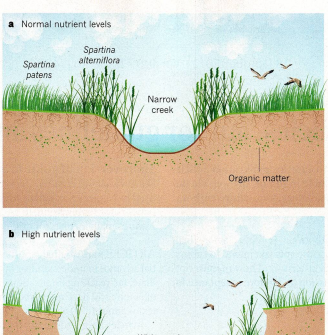

Figure 1 | Nutrients and salt-marsh loss. Over the course of nine years, Deegan *et al.*[5] added nutrients to the water at the mouth of tidal creeks at Plum Island Estuary, Massachusetts, when the tide was rising, so that the nutrients entered the marshes around the creeks. The marshes in this region are dominated by two grasses: *Spartina patens* on the marsh platform and *Spartina alterniflora* along creek banks. **a**, When nutrient supplies to estuaries are normal, marshes are dissected by narrow tidal creeks, the grasses produce substantial root growth and the soil contains lots of organic matter. **b**, By contrast, when nutrients were added, the authors observed that plants produced fewer roots, organic matter decomposed more rapidly and creek banks collapsed, leading to wider creeks and less vegetated marsh, with narrower bands of *S. alterniflora*.

Could increased nutrient availability be contributing to the loss of coastal wetlands worldwide? Deegan *et al.* worked at a relatively high-latitude salt marsh in the northeastern United States. To answer this question, their work needs to be replicated at other sites, particularly at lower-latitude salt marshes, which typically have soils with lower levels of organic matter[7]. Replicating such a large experiment would be a daunting task, but observational studies comparing marshes in high- and low-nutrient environments might also identify effects on creek morphology. Indeed, Deegan *et al.* have taken a first step along these lines, by showing that the history of rapid marsh loss in Long Island Sound and Jamaica Bay (also both in the northeastern United States) is consistent with the timing of nutrient enrichment in these areas.

Because salt marshes are threatened by many factors worldwide[8], including sea-level rise, human development of marshes and adjacent terrestrial habitats, and increased livestock grazing, creek-bank collapse is unlikely to be the only cause of marsh loss. It is likely, however, that nutrient-driven creek-bank collapse will interact with other drivers of marsh loss in unexpected ways. Future studies need to investigate these potential interactions, which may be key to predicting the future health of salt marshes. Moreover, further study is needed to determine whether the process of creek-bank collapse will continue indefinitely, or whether it is self-limiting and will stabilize once creeks equilibrate into a new morphology.

Perhaps the broadest lesson from Deegan and colleagues' work is that ecologists must use caution when extrapolating the results of experiments at modest scales to entire landscapes, because findings from small-scale experiments may be incomplete or even misleading. For example, a typical outcome of plot-based studies is that the composition of plant communities changes in response to increased nutrient levels[3], but Deegan *et al.* found no evidence for such changes. In addition, as Deegan and colleagues discovered, large-scale experiments may uncover processes that have been totally overlooked by small-scale studies. Landscape-level studies are expensive and time-consuming, but they may be indispensable if we are to understand how environmental challenges affect the ecosystems that we depend on. ■

Steven C. Pennings *is in the Department of Biology and Biochemistry, University of Houston, Houston, Texas 77204, USA.*
e-mail: spennings@uh.edu

1. Galloway, J. *et al. Science* **320,** 889–892 (2008).
2. Elser, J. & Bennett, E. *Nature* **478,** 29–31 (2011).
3. Diaz, R. J. & Rosenberg, R. *Science* **321,** 926–929 (2008).
4. Valiela, I. & Cole, M. L. *Ecosystems* **5,** 92–102 (2002).
5. Deegan, L. A. *et al. Nature* **490,** 388–392 (2012).
6. Bertness, M. D., Silliman, B. R. & Holdredge, C. in *Human Impacts on Salt Marshes: A Global Perspective* (eds Silliman, B. R., Bertness, M. D. & Grosholz, E. D.) Ch. 8 (Univ. California Press, 2009).
7. McCall, B. D., & Pennings, S. C. *Oecologia* http://dx.doi.org/10.1007/s00442-012-2352-6 (2012).
8. Silliman, B. R., Bertness, M. D. & Grosholz, E. D. (eds) *Human Impacts on Salt Marshes: A Global Perspective* (Univ. California Press, 2009).
9. Pennings, S. C. *et al. Oikos* **110,** 547–555 (2005).

nature

18 October 2012 / Vol 490 / Issue No. 7420

Publication policies, author guidelines and information

This is a summary of *Nature*'s guide to authors, publication policies and other author information, available in full on the web via our main author information page at www.nature.com/nature/authors.

Getting published in *Nature*

Please read www.nature.com/nature/authors/get_published before finalizing any original scientific research manuscripts you intend to submit. This section explains *Nature*'s editorial criteria, and how manuscripts are handled by the editors after submission and before acceptance for publication.

Formatting guide

Please read www.nature.com/nature/authors/gta before finalizing and submitting your contribution. This section provides instructions for preparing, formatting and writing all types of contribution published by *Nature*.

Publication policies

This section, at www.nature.com/authors, describes *Nature*'s conditions of publication, including policies on authorship; competing financial interests; duplicate publication; prepublicity and embargoes; materials and data availability; research on animal (including human) subjects; referees; corrections, retractions, errata and addenda to published papers; the complaints procedure and refutations; and copyright/licence to publish. All contributions, for whatever section of the journal, are considered for publication and published on the condition that authors agree to these policies.

Submissions

These sections, at www.nature.com/nature/authors/submissions, contain our online service for presubmission enquiries and submission and tracking of Articles, Letters and Review-type manuscripts. Authors should read the formatting guide before using this service. Authors who cannot submit online can submit by post, but *Nature* strongly recommends the online service. **Authors must not submit by both methods.** Authors experiencing operational difficulty in using the online submission service can send an enquiry to mtshelp@nature.com, with a brief explanation of the problem.

Editorial contacts and author services

This section, at www.nature.com/nature/about/contact, provides the addresses of *Nature*'s editorial offices; names of editorial staff; and contact details for advice, reprints, permissions, press office (press@nature.com), and other author-related contact information, including postal addresses for mailed submissions. Short biographies of editors are also available at www.nature.com/nature/about/editors.

Final submissions

This section, at www.nature.com/nature/authors/submissions/final, applies only if an Article or Letter has been accepted in principle for publication and the author has been asked by the editor for a final version. Authors will need to upload electronic files of the text, production-quality figures and supplementary information (if any) to our database. Authors must include a completed manuscript checklist and all relevant signed forms and declarations as requested by the editor.

Short version of guide to authors

See www.nature.com/nature/authors for full version. Contributors not used to *Nature*'s format are advised to read some papers in published issues before submission, to familiarize themselves with *Nature*'s style. *Nature*'s main formats for original research are Articles and Letters.

ARTICLES are original reports whose conclusions represent a substantial advance in understanding of an important problem and have immediate, far-reaching implications. They do not normally exceed **5 pages** of *Nature* and have **no more than 50** references. (One page of undiluted text is about 1,300 words.)

Articles have a summary for readers outside the discipline, separate from the main text and containing no references, of up to 150 words. The summary does not contain numbers, abbreviations, acronyms or measurements unless essential. It contains a brief account of the background and rationale of the work, followed by a statement of the main conclusions, introduced by the phrase 'Here we show' or its equivalent.

The Article itself typically has about 3,000 words of text, beginning with up to 500 words of referenced text expanding on the background to the work, followed by a concise, focused account of the findings, and ending with one or two short paragraphs of discussion. The text can contain a few short subheadings consisting of about 20 but no more than 40 characters (including spaces) each.

LETTERS are short reports of original research focused on an outstanding finding whose importance means that it will be of interest to scientists in other fields. They do not normally exceed **4 pages** of *Nature*, and have **no more than 30** references. They begin with a **fully referenced paragraph** of not more than 300 words, aimed at readers in other disciplines. This paragraph contains a summary of the background and rationale for the work, followed by a one-sentence statement of the main conclusions introduced by the phrase 'Here we show' or its equivalent, and ending with two to three sentences describing the implications in context.

The main text which follows is typically up to 1,500 words long. This text can, if the author requires, start with a further brief paragraph of introductory material. A description of the research then follows. Any discussion at the end of the text should be as succinct as possible.

FIGURES in both Articles and Letters are as small as possible: Articles typically have 5 or 6 figures, Letters typically have 3 or 4 figures. Legends and/or methods are additional to the main text. Methods Summaries (which are published in print only) are no longer than 300 words; Methods sections (which are published online) can be up to 1,000 words; legends should not exceed 100 words each and start with a one-sentence title for the figure, followed by a brief explanation of the parts and symbols.

See www.nature.com/nature/authors/gta/others.html for details of other types of contribution to *Nature*, including Brief Communications Arising; Reviews and Perspectives (presubmission enquiries to reviewsandinsights@nature.com); and Correspondence (submit to corres@nature.com).

See Authors and Referees @ NPG (www.nature.com/authors) for details of Nature journals' publication policies, author and referee services, author benefits and for links to Nautilus and Peer to Peer blogs.

ARTICLE

doi:10.1038/nature11438

The aged niche disrupts muscle stem cell quiescence

Joe V. Chakkalakal[1], Kieran M. Jones[2], M. Albert Basson[2] & Andrew S. Brack[1,3,4]

The niche is a conserved regulator of stem cell quiescence and function. During ageing, stem cell function declines. To what extent and by what means age-related changes within the niche contribute to this phenomenon are unknown. Here we demonstrate that the aged muscle stem cell niche, the muscle fibre, expresses Fgf2 under homeostatic conditions, driving a subset of satellite cells to break quiescence and lose their self-renewing capacity. We show in mice that relatively dormant aged satellite cells robustly express sprouty 1 (*Spry1*), an inhibitor of fibroblast growth factor (FGF) signalling. Increasing FGF signalling in aged satellite cells under homeostatic conditions by removing *Spry1* results in the loss of quiescence, satellite cell depletion and diminished regenerative capacity. Conversely, reducing niche-derived FGF activity through inhibition of Fgfr1 signalling or overexpression of *Spry1* in satellite cells prevents their depletion. These experiments identify an age-dependent change in the stem cell niche that directly influences stem cell quiescence and function.

Pax7-expressing ($Pax7^+$) satellite cells function as an essential stem cell population capable of extensive self-renewal and skeletal muscle repair[1–6]. During ageing, the regenerative capability of muscle is hampered owing in part to impaired satellite cell function[7]. Exposure to a young environment or manipulation of growth factors, which promote proliferative expansion or myogenic progression, can partly restore the proliferation and differentiation of aged satellite cells[8–13]. However, aged skeletal muscle also demonstrates a notable decline in the number of $Pax7^+$ satellite cells under homeostatic conditions[10,13,14]. The signalling cascades responsible for regenerative decline in aged muscle have been intensively investigated[9,11,15]; in contrast, the mechanisms driving satellite cell depletion with age remain unknown.

In invertebrates, age-associated changes in the niche have been shown to cause a decline in stem cell number and function[16,17]. In mammals, the stem cell niche is a critical factor in the maintenance of quiescence, a reversible state of growth arrest crucial to the preservation of adult stem cell number and function[18,19]. Satellite cells are located along the length of the muscle fibre in close contact with the plasma membrane and beneath the basal lamina[20]. The association of adult satellite cells with mature muscle fibre is of vital importance to the maintenance of satellite cell quiescence during homeostasis[21]. Therefore, the muscle fibre is considered to be a component of the satellite cell niche. In this work, we sought to investigate the influence of ageing on the satellite cell niche and its impact on satellite cell homeostasis.

Results

Aged satellite cells cycle more frequently during homeostasis

During ageing, the number of $Pax7^+$ satellite cells declines (Supplementary Fig. 1a–h). Preservation of the quiescent state is a fundamental process that maintains the number and function of self-renewing stem cells[22]. We tested whether muscle stem cell quiescence was disrupted during ageing under homeostatic conditions. The proliferative output of satellite cells throughout life was assessed on the basis of label retention (label retaining cells, LRCs). For this purpose, adult transgenic mice harbouring a histone2B/green fluorescent protein (GFP) reporter driven by a tetracycline (TetO)-inducible transactivator (TetO-H2B-GFP mice) were fed the TetO analogue doxycycline (Dox) for six weeks to transiently activate H2B–GFP and chased for 20 months to monitor proliferative output[23] (Fig. 1a). During the chase period, the satellite cell pool cycled heterogeneously, with at least two distinct populations based on H2B–GFP intensity: an LRC population (~35%; higher intensity) and a non-LRC population (~65%; lower intensity).

We next determined whether the rate of satellite cell cycling differed between adult and aged H2B–GFP mice during a 12-week chase (Fig. 1b). In comparison with adult satellite cells, aged satellite cells demonstrated a more pronounced dilution of the H2B–GFP label, suggesting that aged satellite cells spend less time in a quiescent state. As confirmation of disrupted quiescence, we observed increased numbers of bromodeoxyuridine-expressing ($BrdU^+$) satellite cells (Fig. 1c, e) and an increase in aged cycling ($Ki67^+$; Ki67 also known as Mki67) satellite cells compared with adult (Fig. 1d, f). On the basis of the transcriptional analysis of sorted satellite cells, *MyoD* (*Myod1*), a marker of cycling satellite cells, was higher (Fig. 1g). In contrast, quiescent markers *p27* and *Spry1* (ref. 6) were lower in aged satellite cells relative to adult (Fig. 1h). Therefore, aged satellite cells lose their ability to retain a quiescent state *in vivo*.

Preservation of quiescence protects muscle stem cell function

We next analysed the function of aged satellite cells by transplantation *in vivo* and cell fate assays *in vitro*. TetO-H2B–GFP mice were used to provide a tractable source of nuclear H2B–GFP-expressing satellite cells (Fig. 2a). Thirty days after transplantation into Dox-fed adult wild-type hosts (Fig. 2b, c), in comparison with adult we observed a ~60% decline in the contribution from aged H2B–GFP^+ satellite cells to the myonuclear (Fig. 2d) and $Pax7^+$ (Fig. 2e) compartments. Therefore, aged satellite cells show a cell-autonomous decline in self-renewal and differentiation potential. Moreover, *in vitro* fate analysis of sorted satellite cells (Fig. 2f–i and Supplementary Fig. 2) demonstrates that aged satellite cells tend to lose markers of self-renewal

[1]Center of Regenerative Medicine, Massachusetts General Hospital, Boston, Massachusetts 02114, USA. [2]Department of Craniofacial Development and Stem Cell Biology, King's College London, Guy's Campus, London SE1 9RT, UK. [3]Harvard Stem Cell Institute, 135 Massachusetts Avenue, Boston, Massachusetts 02138, USA. [4]Harvard Medical School, 25 Shattuck Street, Boston, Massachusetts 02115, USA.

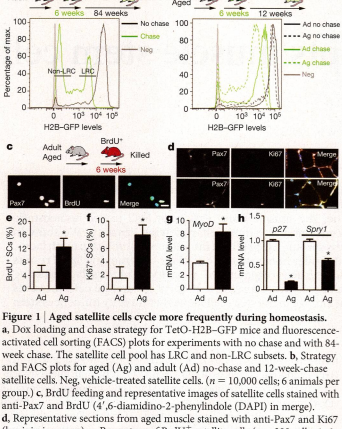

Figure 1 | Aged satellite cells cycle more frequently during homeostasis. **a**, Dox loading and chase strategy for TetO-H2B–GFP mice and fluorescence-activated cell sorting (FACS) plots for experiments with no chase and with 84-week chase. The satellite cell pool has LRC and non-LRC subsets. **b**, Strategy and FACS plots for aged (Ag) and adult (Ad) no-chase and 12-week-chase satellite cells. Neg, vehicle-treated satellite cells. ($n = 10{,}000$ cells; 6 animals per group.) **c**, BrdU feeding and representative images of satellite cells stained with anti-Pax7 and BrdU (4′,6-diamidino-2-phenylindole (DAPI) in merge). **d**, Representative sections from aged muscle stained with anti-Pax7 and Ki67 (laminin in merge). **e**, Percentage of BrdU$^+$ satellite cells ($n = 300$ cells; 4–6 animals per group). **f**, Percentage of Ki67$^+$ and Pax7$^+$ satellite cells (SCs) per section ($n = 4$–6 animals per group). **g**, **h**, Real-time quantitative PCR (RT-qPCR); *Myod* (**g**) *p27* and *Spry1* (**h**) in satellite cells. ($n = 10{,}000$ cells per condition, performed in triplicate; 5 mice per group.) Scale bars, 20 μm; error bars, s.e.m.; *$P < 0.05$.

potential[24–26] (Pax7) and gain markers of differentiation (Myogenin, Myog)[27] and apoptosis (aCasp) (Fig. 2g–i). Thus, fewer satellite cells in aged muscle retain robust self-renewal potential after cell cycle entry.

We next asked whether the relative proliferative output between aged LRC and non-LRC subsets influenced satellite cell phenotypes. Consistent with a more quiescent primitive state, aged LRCs displayed increased expression of *Pax7*, *Spry1* and *p27* and decreased expression of *Myf5* compared with non-LRCs (Fig. 2j). After 4 days *in vitro*, aged non-LRC satellite cells displayed reduced cell growth (Fig. 2k), Pax7 expression (Fig. 2l) and an increase in MyoG expression compared with aged LRC satellite cells (Fig. 2m). Apoptosis was not different between aged LRC and non-LRC satellite cells (Fig. 2n). Next, aged LRC and non-LRC satellite cells were transplanted into adult, pre-injured, Dox-fed recipients and allowed to recover for 30 days (Fig. 2o). LRC satellite cells seeded approximately threefold more satellite cells and differentiated myonuclei than did non-LRC transplant recipients (Fig. 2p, q). Together these data demonstrate that under homeostatic conditions the satellite cell pool is functionally heterogeneous when judged on the basis of proliferative history and that maintenance of quiescence is vital to retain self-renewal potential throughout life.

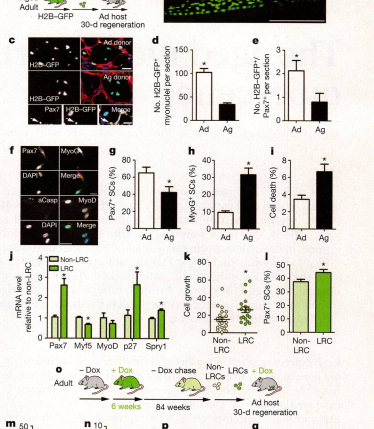

Figure 2 | Preservation of quiescence protects satellite cell function. **a**, Scheme of transplantation assay of 2,000 aged and adult Dox-fed TetO-H2B–GFP satellite cells into pre-injured Dox-fed wild-type hosts. **b**, **c**, Representative images of host whole-mount (**b**) and muscle sections (**c**) of transplant recipients. Lower panels in **c**, Pax7$^+$ and H2B–GFP$^+$ cells. **d**, **e**, Numbers of H2B–GFP$^+$ subluminar myonuclei (**d**) and H2B–GFP$^+$/Pax7$^+$ subluminar satellite cells (**e**), summed over six consecutive 10-μm sections averaged across three regions of muscle ($n = 4$ mice per group). **f**, Representative images of Pax7$^+$, MyoG$^+$, MyoD$^+$ and activated caspase-3$^+$ (aCasp$^+$) satellite cells after 4-day culture. **g**–**i**, Percentage of Pax7$^+$ (**g**), MyoG$^+$ (**h**) and aCasp$^+$ (**i**) satellite cells after 4-day culture ($n = 300$–600 cells, in triplicate). **j**, Myogenic and quiescent marker expression ($n = 3$ mice per condition). **k**–**n**, Number of cells per clone (**k**); percentage of Pax7$^+$ (**l**), MyoG$^+$ (**m**) and aCasp$^+$ (**n**) satellite cells after 4-day culture ($n = 300$–600 cells per condition, performed in triplicate). **o**, Transplant strategy of 2,000 LRC and non-LRCs injected into pre-injured Dox-fed wild-type hosts. **p**, **q**, Numbers of H2B–GFP$^+$ subluminar myonuclei (**p**) and H2B–GFP$^+$/Pax7$^+$ subluminar satellite cells (**q**), summed over six consecutive 10-μm section averaged across three regions of muscle ($n = 4$ mice per group). Scale bars: 25 μm (**b**, **f**), 200 μm (**c**, upper), 10 μm (**c**, lower); error bars, s.e.m.; *$P < 0.05$.

Induction of niche-derived Fgf2 disrupts stem cell quiescence

The stem cell niche is essential for quiescence and maintenance of the stem cell pool[17,19]. We asked whether disrupted quiescence was due to changes in the aged muscle stem cell niche, the muscle fibre[21]. Members of the FGF family of ligands are well-characterized growth factors that are known to possess potent satellite cell mitogenic activity[28,29]. We performed an RT-qPCR array of FGF ligands, in aged and adult purified single muscle fibres. Only five FGF genes were expressed in single muscle fibres and *Fgf2* underwent the greatest fold increase in aged fibres (Fig. 3a and Supplementary Fig. 3a, b). We next used *in situ* hybridization to analyse *Fgf2* expression (Fig. 3b). *Fgf2* was observed in restricted regions along the length of aged muscle fibres,

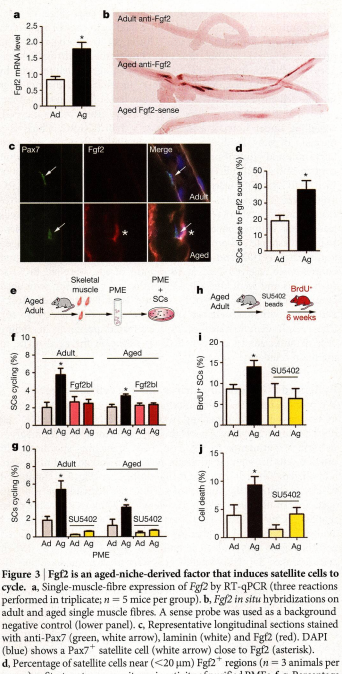

Figure 3 | Fgf2 is an aged-niche-derived factor that induces satellite cells to cycle. **a**, Single-muscle-fibre expression of *Fgf2* by RT-qPCR (three reactions performed in triplicate; $n = 5$ mice per group). **b**, *Fgf2 in situ* hybridizations on adult and aged single muscle fibres. A sense probe was used as a background negative control (lower panel). **c**, Representative longitudinal sections stained with anti-Pax7 (green, white arrow), laminin (white) and Fgf2 (red). DAPI (blue) shows a $Pax7^+$ satellite cell (white arrow) close to Fgf2 (asterisk). **d**, Percentage of satellite cells near (<20 μm) $Fgf2^+$ regions ($n = 3$ animals per group). **e**, Strategy to assess mitogenic activity of purified PMEs. **f**, **g**, Percentage of cycling ($Ki67^+$) adult and aged satellite cells treated with adult or aged PME and Fgf2bl (**f**) or SU5402 (**g**) ($n = 1{,}000$ cells per condition; $n = 5$ animals per group). **h**, Strategy to inhibit FGF activity *in vivo* via implanted SU5402-coated beads. **i**, **j**, Percentage of $BrdU^+$ satellite cells (**i**) and $aCasp^+$ satellite cells (**j**) after 4-day culture from Ad and Ag mice with SU5402 treatment ($n = 300$–600 cells per condition; $n = 4$–6 mice per group). Scale bar, 20 μm; error bars, s.e.m.; $^*P < 0.05$.

some in close proximity to satellite cells (Supplementary Fig. 3c). In addition, we observed a notable increase in Fgf2 protein underneath the basal lamina in aged skeletal muscles relative to adult, whereas Fgf2 was not detected in adult or aged satellite cells (Fig. 3c, d and Supplementary Fig. 2d, e). Moreover, aged muscle had fewer $Fgf2^+$ interstitial cells than did adult muscle (Supplementary Fig. 2f–h). Together these results demonstrate that the aged satellite cell niche, the muscle fibre, is the principal source of Fgf2.

To identify soluble muscle-fibre-derived factors that signal to satellite cells, we isolated purified single muscle fibres, washed them multiple times to minimize interstitial cell contamination and extracted soluble fractions (hereafter termed purified myofibre extract (PME)) (Fig. 3e and Supplementary Fig. 4a–e). PME diluted in basal medium was incubated with quiescent satellite cells (Fig. 3f, g and Supplementary Fig. 4i) and $Pax7^+$ satellite-cell-like reserve cells (RSCs), a model of reversibly quiescent satellite cells[30] (Supplementary Fig. 4i, k), and assayed for cell cycle entry. In comparison with adult PME, aged PME increased the fraction of adult and aged quiescent cells that began to cycle (Fig. 3f and Supplementary Fig. 4i), but did not affect apoptosis (Supplementary Fig. 4f). In contrast to PME, aged serum did not induce cell cycle entry[12] (Supplementary Fig. 4g). Moreover, aged interstitial cell extract did not induce cell proliferation (Supplementary Fig. 4d, e). Collectively, these results demonstrate that the proliferative activity of satellite cells is induced by aged muscle-fibre-derived factors.

To test whether Fgf2 was responsible for the altered biological activity of aged PME, the extract was treated with a blocking antibody against Fgf2 (Fgf2bl) or with Fgf2, before incubation of satellite cells (Fig. 3e, f and Supplementary Fig. 4h) and RSCs (Supplementary Fig. 4j, k). Fgf2 added to adult PME was sufficient to break quiescence, and neutralization of Fgf2 activity prevented aged-PME-induced cell cycle entry (Fig. 3f and Supplementary Fig. 4h, j, k). Therefore, the increased abundance of soluble muscle-fibre-derived Fgf2 in aged muscle leads to a loss of quiescence in aged satellite cells.

To confirm that the active components of the PMEs signal through FGF receptors, we pre-treated quiescent satellite cells and RSC cultures with the Fgfr1 inhibitor SU5402 (Fgfr1i) before PME exposure. Fgfr1i treatment prevented aged-PME-induced cell proliferation (Fig. 3g and Supplementary Fig. 4l). In addition, proliferation of quiescent Cre-adenovirus-treated RSCs cultured from $Fgfr1^{flx/flx}$ satellite cells was abolished in the presence of Fgf2 and aged PME relative to control cultures (Supplementary Fig. 4m). In contrast, Fgfr1i treatment and deletion of *Fgfr1* did not alter proliferation of satellite cells or RSCs cultured with adult PME. Therefore, aged-muscle-fibre-derived Fgf2 signals through Fgfr1 to promote satellite cell loss of quiescence.

To determine whether aged satellite cell quiescence was regulated through FGF signalling *in vivo*, we asked whether long-term administration of Fgfr1i would prevent satellite cell proliferation (Fig. 3h–j). After six weeks of Fgfr1i treatment, the fraction of $BrdU^+$ satellite cells from aged muscle was indistinguishable from that from adult control muscle (Fig. 3i). Moreover, the increased apoptosis observed in aged satellite cells was attenuated (Fig. 3j). These results demonstrate that increased FGF signalling is a major contributor to the loss of stem cell quiescence and possibly stem cell depletion during ageing under homeostatic conditions.

Satellite cell quiescence in the niche is sensitive to FGF signalling

We next asked whether quiescent satellite cells were sensitive to increased levels of FGF signalling from the niche. The genes in the sprouty family function as downstream targets and negative-feedback modulators of the FGF signalling cascade[31,32]. Comparison between sprouty genes revealed that *Spry1* expression, unlike that of other sprouty genes, was decreased by Fgf2 (ref. 33; Supplementary Fig. 5a) and enriched in aged LRCs compared with non-LRCs (Supplementary Fig. 5b). These data are consistent with high levels of *Spry1* expression in quiescent satellite cells and RSCs[19]. To assess whether lower levels of *Spry1* in non-LRC satellite cells was due to an increased number of $Spry1^-$ cycling cells[6], we analysed *Spry1* transcriptional activity at the single-cell level using aged H2B–GFP; $Spry1^{lacZ+/-}$ mice[6,34]. We observed a reduction in β-galactosidase staining intensity in aged quiescent non-LRC relative to LRC satellite cells and a relatively low number of cycling LRC and non-LRC satellite cells (Supplementary Fig. 5c–g). Therefore, aged quiescent satellite cells with a limited proliferative history are enriched for the FGF inhibitor *Spry1*.

To manipulate *Spry1* levels in satellite cells, we used $Pax7\text{-}CreER^{TM}$ crossed with an inducible loss-of-function allele[6] ($Spry1^{flx}$, to create

Spry1null cells) and a gain-of-function allele[35] (*CAG–GFP*^{flx}*Spry1*, to create Spry1OX cells), to increase and decrease FGF signalling, respectively. Tamoxifen (Tmx) was administered to Spry1null and control adult mice, and 10 day later sorted satellite cells were cultured for 24 hours in Fgf2, or PME alone, and in combination with Fgf2bl or Fgfr1i. Consistent with our hypothesis, a larger fraction of Spry1null satellite cells entered the cell cycle in the presence of Fgf2 (Supplementary Fig. 6a) and aged PME (Supplementary Fig. 6b) than did in control satellite cells. Moreover, the loss of quiescence induced by aged PME in Spry1null satellite cells was prevented in the presence of Fgf2bl and Fgfr1i (Supplementary Fig. 6b, c). In contrast, aged-PME-induced proliferation was prevented in Tmx-treated Spry1OX satellite cells compared with controls (Supplementary Fig. 6d). In support of these findings, proliferation of quiescent Cre-adenovirus treated RSCs cultured from *Spry1*$^{flx/flx}$ satellite cells was augmented in the presence of Fgf2 and aged PME relative to control cultures (Supplementary Fig. 6e, f). In contrast, proliferation induced by Fgf2 and aged PME was abrogated in Cre-adenovirus-treated RSC cultures from Spry1OX satellite cells (Supplementary Fig. 6g, h). Together these results demonstrate that *Spry1* levels modulate Fgf2 signalling to maintain muscle stem cell quiescence *in vitro*.

To test the requirement of *Spry1* for maintaining satellite cell quiescence *in vivo*, we administered Tmx to adult and aged control and Spry1null mice to delete *Spry1* (ref. 6; Fig. 4a). This approach efficiently deletes *Spry1* and increases a downstream transcriptional target of FGF signalling, *Erm* (*Etv5*), *in vivo* (Supplementary Fig. 7). After a short-term deletion of *Spry1*, the number of Pax7$^+$ cells (Fig. 4b) and the percentage of cycling Pax7$^+$ cells (Fig. 4c) were significantly increased in Spry1null mice relative to control aged mice, consistent with loss of quiescence. This effect was abrogated in the presence of Fgfr1i (Fig. 4b), thus providing further confirmation that *Spry1* modulates levels of FGF signalling in aged satellite cells. In contrast to aged mice, deletion of *Spry1* in adult mice did not alter satellite cell number, consistent with a low level of Fgf2 in these mice.

To define further the loss of quiescence after increased FGF signalling under homeostasis, we assessed BrdU-LRC, which is a measure of slow-dividing stem cell behaviour[36] in adult and aged Spry1null and control mice (Fig. 4d). Comparison of chased adult control and Spry1null mice revealed no shifts in the fraction of BrdU-LRC satellite cells. In contrast, the fraction of BrdU-LRC satellite cells decreased in aged Spry1null mice relative to aged control mice. Therefore, short-term deletion of *Spry1* in aged satellite cells leads to loss of quiescence. To determine whether *Spry1* was sufficient to inhibit satellite cell proliferation in aged muscle, we analysed aged and adult Spry1OX and control mice (Fig. 4e). Both Spry1OX and control mice received Tmx at 18 months of age, were fed BrdU at 21 months and were killed at 23 months. In comparison with aged control, fewer aged Spry1OX satellite cells incorporated BrdU, consistent with maintenance of satellite cell quiescence (Fig. 4e). These results demonstrate that *Spry1*, expressed specifically in satellite cells, is sufficient to dampen FGF signalling in the aged niche to maintain cellular quiescence.

Prolonged FGF signalling drives satellite cell depletion

We proposed that loss of quiescence driven by an increase in aged-niche-derived Fgf2 signalling was contributing to satellite cell depletion during ageing. To test this, we performed long-term *Spry1*-deletion experiments to increase FGF signalling specifically in satellite cells throughout adult life. Spry1null and control mice were administered Tmx and analysed 18 months later (Fig. 5a). Compared with aged controls, the number of satellite cells decreased by ~50% in aged Spry1null muscle. We next deleted *Spry1* in aged satellite cells, that is, on age-induced Fgf2 increases in the niche (Fig. 5b), and analysed satellite cell number six weeks later. Compared with aged controls, aged Spry1null mice had 50% fewer satellite cells. When cultured, aged Spry1null satellite cells were more prone to differentiation and apoptosis than were aged control cells (Supplementary Fig. 8). Together these data demonstrate that aged-niche-induced FGF signalling leads to an initial loss of quiescence followed by a depletion of the stem cell pool. In contrast, satellite cell number was twofold higher in aged Spry1OX mice than in aged controls (Fig. 5c). Therefore, levels of FGF signalling induced by the aged niche mediate satellite cell pool size in homeostatic conditions.

The observed correlation between diminution of the satellite cell pool[12,13,14] (Supplementary Fig. 1) and regenerative delay during ageing[7] prompted us to ask whether further diminution of the aged satellite cell pool, achieved by *Spry1* disruption in aged satellite cells, impairs muscle regenerative capacity (Fig. 5d). Six weeks after Tmx delivery, aged control and Spry1null muscle were injured and left to recover for 30 days. In aged control mice, muscle regenerative capacity based on myofibre size was reduced by 15% compared with uninjured contralateral muscle. In aged Spry1null mice, the myofibre size of regenerated muscle was 50% smaller than the contralateral control (Fig. 5e). To confirm that the regenerative decline was related to satellite cell loss, we injured aged Spry1null mice 10 days after Tmx administration, when the number of Pax7$^+$ cells had increased owing to the initial loss of quiescence (Supplementary Fig. 9). In contrast to long-term *Spry1* deletion, after short-term *Spry1* deletion muscle fibre size was greater in regenerating aged Spry1null mice than in aged controls (Supplementary Fig. 9). Therefore, the exacerbated loss of the satellite cell pool due to a longer-term increase in FGF signalling in aged uninjured muscle becomes limiting on regeneration.

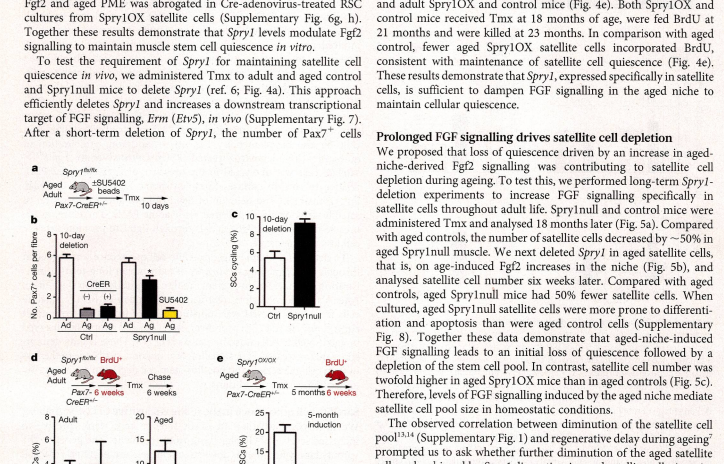

Figure 4 | Aged satellite cells are sensitive to acute changes in FGF signalling. **a**, Strategy to delete Spry1 in satellite cells of adult and aged mice before injection of SU5402-coated beads. **b**, Number of Pax7$^+$ satellite cells per single muscle fibre (20–30 single muscle fibres per animal; $n = 4$–6 mice per group). **c**, Percentage of Ki67$^+$ and Pax7$^+$ satellite cells per 10-μm cross-section 10 days after Tmx injection ($n = 4$–6 animals per group). **d**, Strategy to label and chase BrdU in satellite cells from adult and aged control or Spry1null mice 6 weeks after Tmx injection, and percentage BrdU$^+$ or LRC satellite cells after chase. **e**, Strategy for BrdU incorporation in Tmx-treated control and Spry1OX aged mice, and percentage BrdU$^+$ satellite cells after chase. In **d** and **e**, $n = 1{,}000$ cells per condition ($n = 4$–6 mice per group). Error bars, s.e.m.; *$P < 0.05$.

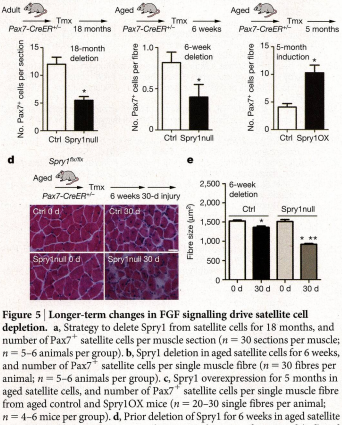

Figure 5 | Longer-term changes in FGF signalling drive satellite cell depletion. a, Strategy to delete Spry1 from satellite cells for 18 months, and number of $Pax7^+$ satellite cells per muscle section ($n = 30$ sections per muscle; $n = 5$–6 animals per group). **b**, Spry1 deletion in aged satellite cells for 6 weeks, and number of $Pax7^+$ satellite cells per single muscle fibre ($n = 30$ fibres per animal; $n = 5$–6 animals per group). **c**, Spry1 overexpression for 5 months in aged satellite cells, and number of $Pax7^+$ satellite cells per single muscle fibre from aged control and Spry1OX mice ($n = 20$–30 single fibres per animal; $n = 4$–6 mice per group). **d**, Prior deletion of Spry1 for 6 weeks in aged satellite cells followed by muscle injury, and HE-stained images of uninjured (0 d) and 30-day regenerated muscles. **e**, Quantification of fibre size 30 days after $BaCl_2$-induced injury, compared with contralateral uninjured muscle (0 d) ($n = 30$ sections per muscle; $n = 4$–6 mice per group). Scale bar, 25 μm; error bars, s.e.m.; $*P < 0.05$ to 0 d, $**P < 0.05$ to control 30 day; analysis of variance with Bonferroni's *post hoc* test.

Finally, to test the impact of long-term inhibition of FGF signalling in response to injury, we injured adult and aged mice after six weeks of Fgfr1i administration (Supplementary Fig. 10). Thirty days after injury, muscle fibre size was 30% smaller in Fgfr1i-treated compared with controls, suggesting that repression of FGF signalling inhibits myofibre repair[37,38]. In contrast, the number of self-renewing satellite cells was greater in aged Fgfr1i mice than in controls. This result demonstrates that repressing Fgfr1 signalling during ageing improves the self-renewal capacity of satellite cells during regeneration.

Discussion

Our data demonstrate that increased levels of FGF signalling directed from the aged satellite cell niche lead to the loss of quiescence and depletion of the resident stem cell population, which eventually diminishes muscle regenerative capacity (Supplementary Fig. 11). The discovery that aged satellite cells break quiescence under homeostatic conditions was surprising considering their proliferative disadvantage in high-mitogen regenerative contexts[39]. In support of our data, aged haematopoietic stem cells are more active in the aged niche[40,41]. It is possible that a consequence of ageing across stem cell niches is their inability to retain stem cells in a quiescent state.

Functional heterogeneity within the adult satellite cell pool is becoming more apparent[26,42,43]. Our results show that the aged satellite cell compartment is composed of highly functioning LRC subsets and non-LRC subsets, that self-renew poorly and tend to differentiate, demonstrating that retention of quiescence is essential for maintenance of stem cell function. Quiescence of adult satellite cells is regulated at multiple levels[44–46]. Satellite cells that retain a more quiescent phenotype and maintain stem cell function express higher levels of the FGF inhibitor *Spry1*. Therefore, feedback inhibition of niche-derived signals may be a means to promote satellite cell maintenance with age.

The systemic environment has a significant role in satellite cell proliferation *in vitro* and during repair. The young systemic environment stimulates satellite cell proliferation; the aged systemic environment inhibits satellite cell proliferation[9,12]. We have showed here that the aged satellite cell niche becomes stimulatory, driving satellite cells out of quiescence, suggesting that the niche is dominant during homeostasis. However, in the context of injury, the relationship between niche and systemic signalling is disrupted, owing to injury-induced niche (muscle fibre) degeneration. Such disruption potentially creates a permissive state for the systemic environment to exert its influence on satellite cells.

To our knowledge, this is the first identification of a ligand that specifically increases within a mammalian aged niche that can promote breaks in quiescence leading to declines in stem cell function and number during homeostasis. The reasons for the increase in Fgf2 are not known. We speculate that Fgf2 induction is a cell-autonomous response as an attempt to repair the aged muscle fibre, akin to the induction of FGFs during development and regeneration to promote myogenic commitment and differentiation[37,38,47–50]. Strategies to prevent chronic Fgf2 production from the aged niche or repress FGF signalling at the level of the aged satellite cell may reduce stem cell loss during ageing.

METHODS SUMMARY

To monitor proliferative history of satellite cells, adult and aged TetO-H2B–GFP mice received Dox (1 mg ml^{-1} supplemented with 5% sucrose in drinking water) for six weeks[23]. Alternatively, mice were fed BrdU (Sigma; 0.5 mg ml^{-1} supplemented with 5% sucrose in drinking water). Some mice were immediately killed whereas others were given normal drinking water to allow chase of BrdU or H2B–GFP labelling before isolation of satellite cells. For satellite cell transplantation studies, after six weeks of Dox feeding 2,000 satellite cell events were purified by fluorescence-activated cell sorting and reconstituted in 50 μl PBS for direct intramuscular delivery into pre-injured (with 1.2% $BaCl_2$) host C57BL/6 tibialis anterior muscle. Host mice were re-fed Dox (1mg ml^{-1} in 5% sucrose in drinking water) to maintain H2B–GFP labelling during the 30-day regeneration period. Subsequently, muscle was prepared for analysis. For immunohistological analysis, 10-μm-thick transverse sections were obtained for every 200 μm region to identify H2B–GFP$^+$ regions. Counts of H2B–GFP$^+$ myonuclei and $Pax7^+$ cells were obtained and summed from six consecutive 10-μm sections per transplant, taken over three regions.

Full Methods and any associated references are available in the online version of the paper.

Received 15 October 2011; accepted 24 July 2012.
Published online 26 September 2012.

1. Sambasivan, R. *et al.* Pax7-expressing satellite cells are indispensable for adult skeletal muscle regeneration. *Development* **138,** 3647–3656 (2011).
2. Collins, C. A. *et al.* Stem cell function, self-renewal, and behavioral heterogeneity of cells from the adult muscle satellite cell niche. *Cell* **122,** 289–301 (2005).
3. Lepper, C., Partridge, T. A. & Fan, C. M. An absolute requirement for Pax7-positive satellite cells in acute injury-induced skeletal muscle regeneration. *Development* **138,** 3639–3646 (2011).
4. Sacco, A., Doyonnas, R., Kraft, P., Vitorovic, S. & Blau, H. M. Self-renewal and expansion of single transplanted muscle stem cells. *Nature* **456,** 502–506 (2008).
5. Murphy, M. M., Lawson, J. A., Mathew, S. J., Hutcheson, D. A. & Kardon, G. Satellite cells, connective tissue fibroblasts and their interactions are crucial for muscle regeneration. *Development* **138,** 3625–3637 (2011).
6. Shea, K. L. *et al.* Sprouty1 regulates reversible quiescence of a self-renewing adult muscle stem cell pool during regeneration. *Cell Stem Cell* **6,** 117–129 (2010).
7. Shavlakadze, T., McGeachie, J. & Grounds, M. D. Delayed but excellent myogenic stem cell response of regenerating geriatric skeletal muscles in mice. *Biogerontology* **11,** 363–376 (2010).
8. Carlson, B. M. & Faulkner, J. A. Muscle transplantation between young and old rats: age of host determines recovery. *Am. J. Physiol.* **256,** C1262–C1266 (1989).
9. Brack, A. S. *et al.* Increased Wnt signaling during aging alters muscle stem cell fate and increases fibrosis. *Science* **317,** 807–810 (2007).
10. Collins, C. A., Zammit, P. S., Ruiz, A. P., Morgan, J. E. & Partridge, T. A. A population of myogenic stem cells that survives skeletal muscle aging. *Stem Cells* **25,** 885–894 (2007).

11. Conboy, I. M., Conboy, M. J., Smythe, G. M. & Rando, T. A. Notch-mediated restoration of regenerative potential to aged muscle. *Science* **302,** 1575–1577 (2003).
12. Conboy, I. M. *et al.* Rejuvenation of aged progenitor cells by exposure to a young systemic environment. *Nature* **433,** 760–764 (2005).
13. Shefer, G., Van de Mark, D. P., Richardson, J. B. & Yablonka-Reuveni, Z. Satellite-cell pool size does matter: defining the myogenic potency of aging skeletal muscle. *Dev. Biol.* **294,** 50–66 (2006).
14. Brack, A. S., Bildsoe, H. & Hughes, S. M. Evidence that satellite cell decrement contributes to preferential decline in nuclear number from large fibres during murine age-related muscle atrophy. *J. Cell Sci.* **118,** 4813–4821 (2005).
15. Carlson, M. E., Hsu, M. & Conboy, I. M. Imbalance between pSmad3 and Notch induces CDK inhibitors in old muscle stem cells. *Nature* **454,** 528–532 (2008).
16. Pan, L. *et al.* Stem cell aging is controlled both intrinsically and extrinsically in the *Drosophila* ovary. *Cell Stem Cell* **1,** 458–469 (2007).
17. Boyle, M., Wong, C., Rocha, M. & Jones, D. L. Decline in self-renewal factors contributes to aging of the stem cell niche in the *Drosophila* testis. *Cell Stem Cell* **1,** 470–478 (2007).
18. Voog, J. & Jones, D. L. Stem cells and the niche: a dynamic duo. *Cell Stem Cell* **6,** 103–115 (2010).
19. Morrison, S. J. & Spradling, A. C. Stem cells and niches: mechanisms that promote stem cell maintenance throughout life. *Cell* **132,** 598–611 (2008).
20. Mauro, A. Satellite cell of skeletal muscle fibers. *J. Biophys. Biochem. Cytol.* **9,** 493–495 (1961).
21. Bischoff, R. Interaction between satellite cells and skeletal muscle fibers. *Development* **109,** 943–952 (1990).
22. Orford, K. W. & Scadden, D. T. Deconstructing stem cell self-renewal: genetic insights into cell-cycle regulation. *Nature Rev. Genet.* **9,** 115–128 (2008).
23. Foudi, A. *et al.* Analysis of histone 2B-GFP retention reveals slowly cycling hematopoietic stem cells. *Nature Biotechnol.* **27,** 84–90 (2009).
24. Zammit, P. S. *et al.* Muscle satellite cells adopt divergent fates: a mechanism for self-renewal? *J. Cell Biol.* **166,** 347–357 (2004).
25. Olguin, H. C. & Olwin, B. B. Pax-7 up-regulation inhibits myogenesis and cell cycle progression in satellite cells: a potential mechanism for self-renewal. *Dev. Biol.* **275,** 375–388 (2004).
26. Rocheteau, P., Gayraud-Morel, B., Siegl-Cachedenier, I., Blasco, M. A. & Tajbakhsh, S. A subpopulation of adult skeletal muscle stem cells retains all template DNA strands after cell division. *Cell* **148,** 112–125 (2012).
27. Yablonka-Reuveni, Z. & Rivera, A. J. Temporal expression of regulatory and structural muscle proteins during myogenesis of satellite cells on isolated adult rat fibers. *Dev. Biol.* **164,** 588–603 (1994).
28. Sheehan, S. M. & Allen, R. E. Skeletal muscle satellite cell proliferation in response to members of the fibroblast growth factor family and hepatocyte growth factor. *J. Cell. Physiol.* **181,** 499–506 (1999).
29. Bischoff, R. A satellite cell mitogen from crushed adult muscle. *Dev. Biol.* **115,** 140–147 (1986).
30. Yoshida, N., Yoshida, S., Koishi, K., Masuda, K. & Nabeshima, Y. Cell heterogeneity upon myogenic differentiation: down-regulation of MyoD and Myf-5 generates 'reserve cells'. *J. Cell Sci.* **111,** 769–779 (1998).
31. Hacohen, N., Kramer, S., Sutherland, D., Hiromi, Y. & Krasnow, M. A. sprouty encodes a novel antagonist of FGF signaling that patterns apical branching of the *Drosophila* airways. *Cell* **92,** 253–263 (1998).
32. Kim, H. J. & Bar-Sagi, D. Modulation of signalling by Sprouty: a developing story. *Nature Rev. Mol. Cell Biol.* **5,** 441–450 (2004).
33. Gross, I., Bassit, B., Benezra, M. & Licht, J. D. Mammalian sprouty proteins inhibit cell growth and differentiation by preventing ras activation. *J. Biol. Chem.* **276,** 46460–46468 (2001).
34. Thum, T. *et al.* MicroRNA-21 contributes to myocardial disease by stimulating MAP kinase signalling in fibroblasts. *Nature* **456,** 980–984 (2008).
35. Yang, X. *et al.* Overexpression of Spry1 in chondrocytes causes attenuated FGFR ubiquitination and sustained ERK activation resulting in chondrodysplasia. *Dev. Biol.* **321,** 64–76 (2008).
36. Wilson, A. *et al.* Hematopoietic stem cells reversibly switch from dormancy to self-renewal during homeostasis and repair. *Cell* **135,** 1118–1129 (2008).
37. Floss, T., Arnold, H. H. & Braun, T. A role for FGF-6 in skeletal muscle regeneration. *Genes Dev.* **11,** 2040–2051 (1997).
38. Lefaucheur, J. P. & Sebille, A. Muscle regeneration following injury can be modified *in vivo* by immune neutralization of basic fibroblast growth factor, transforming growth factor beta 1 or insulin-like growth factor I. *J. Neuroimmunol.* **57,** 85–91 (1995).
39. Conboy, I. M. & Rando, T. A. The regulation of Notch signaling controls satellite cell activation and cell fate determination in postnatal myogenesis. *Dev. Cell* **3,** 397–409 (2002).
40. Morrison, S. J., Wandycz, A. M., Akashi, K., Globerson, A. & Weissman, I. L. The aging of hematopoietic stem cells. *Nature Med.* **2,** 1011–1016 (1996).
41. Sudo, K., Ema, H., Morita, Y. & Nakauchi, H. Age-associated characteristics of murine hematopoietic stem cells. *J. Exp. Med.* **192,** 1273–1280 (2000).
42. Ono, Y. *et al.* Slow-dividing satellite cells retain long-term self-renewal ability in adult muscle. *J. Cell Sci.* **125,** 1309–1319 (2012).
43. Kuang, S., Kuroda, K., Le Grand, F. & Rudnicki, M. A. Asymmetric self-renewal and commitment of satellite stem cells in muscle. *Cell* **129,** 999–1010 (2007).
44. Bjornson, C. R. *et al.* Notch signaling is necessary to maintain quiescence in adult muscle stem cells. *Stem Cells* **30,** 232–242 (2012).
45. Cheung, T. H. *et al.* Maintenance of muscle stem-cell quiescence by microRNA-489. *Nature* **482,** 524–528 (2012).
46. Mourikis, P. *et al.* A critical requirement for Notch signaling in maintenance of the quiescent skeletal muscle stem cell state. *Stem Cells* **30,** 243–252 (2011).
47. Lagha, M. *et al.* Pax3 regulation of FGF signaling affects the progression of embryonic progenitor cells into the myogenic program. *Genes Dev.* **22,** 1828–1837 (2008).
48. Groves, J. A., Hammond, C. L. & Hughes, S. M. Fgf8 drives myogenic progression of a novel lateral fast muscle fibre population in zebrafish. *Development* **132,** 4211–4222 (2005).
49. Flanagan-Steet, H., Hannon, K., McAvoy, M. J., Hullinger, R. & Olwin, B. B. Loss of FGF receptor 1 signaling reduces skeletal muscle mass and disrupts myofiber organization in the developing limb. *Dev. Biol.* **218,** 21–37 (2000).
50. Kudla, A. J. *et al.* The FGF receptor-1 tyrosine kinase domain regulates myogenesis but is not sufficient to stimulate proliferation. *J. Cell Biol.* **142,** 241–250 (1998).

Supplementary Information is available in the online version of the paper.

Acknowledgements We thank H. Hock, K. Hochedlinger and R. Friesel for the generous provision of reagents, and G. Estrada for technical assistance. We are also grateful to L. Prickett-Rice, K. Folz-Donahue and M. Weglarz for cell sorting. This work was supported by MGH start-up funds, Harvard Stem Cell Institute grants and NIH grants (R01 AR060868, R01 AR061002) (A.S.B.); a Wellcome Trust grant (WT091475) (M.A.B.); and an MGH ECOR Postdoctoral Fellow Award (J.V.C.) and a BBSRC Doctoral Training Award (BB/F017626/1) (K.M.J.).

Author Contributions J.V.C. designed and performed experiments, analysed data, interpreted results and wrote the manuscript. K.M.J. performed experiments, analysed data and edited the manuscript. M.A.B. conceived the project, designed experiments, interpreted results, and edited the manuscript. A.S.B. conceived the project, designed experiments, interpreted results, and wrote the manuscript.

Author Information Reprints and permissions information is available at www.nature.com/reprints. The authors declare no competing financial interests. Readers are welcome to comment on the online version of the paper. Correspondence and requests for materials should be addressed to A.S.B. Brack.Andrew@mgh.harvard.edu.

ARTICLE

doi:10.1038/nature11524

Crystal structure of a bacterial homologue of glucose transporters GLUT1–4

Linfeng Sun[1,2,3]*, Xin Zeng[1,2,3]*, Chuangye Yan[1,2,3], Xiuyun Sun[2], Xinqi Gong[1,2,3], Yu Rao[2] & Nieng Yan[1,2,3]

Glucose transporters are essential for metabolism of glucose in cells of diverse organisms from microbes to humans, exemplified by the disease-related human proteins GLUT1, 2, 3 and 4. Despite rigorous efforts, the structural information for GLUT1–4 or their homologues remains largely unknown. Here we report three related crystal structures of XylE, an *Escherichia coli* homologue of GLUT1–4, in complex with D-xylose, D-glucose and 6-bromo-6-deoxy-D-glucose, at resolutions of 2.8, 2.9 and 2.6 Å, respectively. The structure consists of a typical major facilitator superfamily fold of 12 transmembrane segments and a unique intracellular four-helix domain. XylE was captured in an outward-facing, partly occluded conformation. Most of the important amino acids responsible for recognition of D-xylose or D-glucose are invariant in GLUT1–4, suggesting functional and mechanistic conservations. Structure-based modelling of GLUT1–4 allows mapping and interpretation of disease-related mutations. The structural and biochemical information reported here constitutes an important framework for mechanistic understanding of glucose transporters and sugar porters in general.

Glucose is an essential fuel for most living organisms on Earth. Uptake of glucose into mammalian cells is mediated mainly by members of the GLUT (or SLC2A for solute carrier 2A) and SGLT families of transporters[1–3]. GLUTs, which are major facilitator superfamily (MFS)-type passive transporters, catalyse the facilitative diffusion of glucose and other hexoses across the plasma membrane. By contrast, SGLTs are LeuT-type, Na^+-dependent secondary active symporters[4].

Among the 14 human GLUT family members, GLUT1–4 have been rigorously investigated because of their fundamental roles in a multitude of physiological and pathophysiological processes[2,5]. GLUT1, the first glucose transporter cloned[6], is responsible for glucose uptake into erythrocytes and the transport across blood–brain barrier. Mutations of GLUT1 may lead to GLUT1 deficiency syndrome (also known as De Vivo disease), manifested by a broad spectrum of clinical phenotypes including infantile-onset seizure[7–9]. GLUT2 is highly expressed in pancreatic β-cell, intestine, kidney and liver, and is associated with the Fanconi–Bickel syndrome[10,11]. GLUT3 is the main neuronal glucose transporter[12]. The expression levels of GLUT1 and GLUT3 are enhanced in some carcinoma cell lines for increased glucose supply in cancer cells (the Warburg effect)[12–14]. GLUT4 is the main glucose transporter in muscles and adipocytes. Unlike other GLUTs, the cellular localization of GLUT4 is regulated by insulin through a complex mechanism whose aberration contributes to obesity and type 2 diabetes mellitus[15–17].

GLUT1–4 belong to the sugar porter (SP) family (TCDB transporter classification 2.A.1.1)[18], which represents a large and ubiquitous MFS subfamily consisting of members derived from bacteria, archaea, cyanobacteria, fungi, protozoa, plants and animals (Supplementary Figs 1 and 2)[19]. SP subfamily proteins, such as the hexose transporters in yeasts[20] and the sucrose transporters in plants[21,22], have been subject to extensive characterizations for their essential roles in hexose and disaccharide metabolism. GLUT transporters and their homologues have been the targets of rigorous, albeit unsuccessful, structural investigations. Sequence analysis and biochemical characterizations have helped in deducing the boundaries of the transmembrane segments (TMs) for GLUTs[6,23]. The structures of several MFS members have been reported[24–28]. Nevertheless, the lack of sequence similarity between these MFS proteins and GLUT family members has made it a daunting task to generate accurate structure-based models of GLUT1–4.

To elucidate the structure and molecular mechanism of GLUT1–4, we launched a systematic effort to screen for well-behaved GLUT1–4 protein variants as well as their homologues. Among the tested proteins, the *E. coli* D-xylose:H^+ symporter XylE[29–33] showed excellent solution behaviour. XylE, an archetypal member of the SP subfamily[19,32], shares sequence identities of 29%, 30%, 29% and 27%, and similarities of 49%, 51%, 48% and 47%, with GLUT1, GLUT2, GLUT3 and GLUT4, respectively (Supplementary Fig. 1). Here we report the crystal structures of XylE bound separately to three different ligands: D-xylose, D-glucose and 6-bromo-6-deoxy-D-glucose (6-BrGlc). We also performed an extensive, structure-guided, *in vivo* and *in vitro* functional analysis of XylE. These studies reveal significant insights into the structure and function of XylE and its human homologues GLUT1–4.

Structure of D-xylose-bound XylE

The purified, recombinant XylE binds to D-xylose with a dissociation constant (K_d) of about 0.35 ± 0.03 mM (mean ± s.d.) as measured by isothermal titration calorimetry, and transports D-xylose in a pH-dependent manner with a K_m of 0.47 ± 0.05 mM at pH 6.5 as measured by proteoliposome-based counterflow assay (Supplementary Fig. 3). The addition of ligand proved essential for the successful generation of well-diffracting XylE crystals. The structure of XylE bound to D-xylose was determined and refined to 2.8 Å resolution (Fig. 1, Supplementary Fig. 4 and Supplementary Table 1).

XylE contains a typical MFS fold of 12 TMs, with amino and carboxy termini both located on the intracellular side (Fig. 1). The 12 TMs are organized into two distinct domains—the N and C domains—which can be superimposed with a root mean square deviation of 3.11 Å over 153 Cα atoms (Supplementary Fig. 5a). TM7 and TM10 are both discontinuous helices (Supplementary Fig. 5b), which may facilitate conformational changes during substrate transport[34].

[1]State Key Laboratory of Bio-membrane and Membrane Biotechnology, Center for Structural Biology, Tsinghua University, Beijing 100084, China. [2]School of Life Sciences and School of Medicine, Tsinghua University, Beijing 100084, China. [3]Tsinghua-Peking Center for Life Sciences, Tsinghua University, Beijing 100084, China.
*These authors contributed equally to this work.

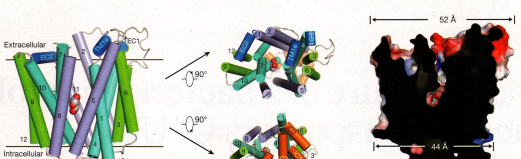

Figure 1 | The structure of XylE bound to D-xylose has an outward-facing, partly occluded conformation. Left: the overall structure of XylE bound to D-xylose. Three perpendicular views are shown. The corresponding TM segments in the four 3-helix bundles, which constitute the typical MFS structural fold, are coloured the same. D-Xylose is shown in space-filling model. The extracellular and intracellular helices are coloured sea-blue and orange, respectively. Right: D-xylose resides in the centre of the structure, occluded from intracellular side and solvent-accessible from the extracellular side. A cut-open view of the surface electrostatic potential is shown here. The surface electrostatic potential was calculated with PyMol[50]. All structure figures were prepared with PyMol.

The overall structure of XylE has an outward-facing conformation. The ligand D-xylose is trapped within the centre of the transmembrane domain, completely occluded from the intracellular side yet solvent-accessible from the extracellular side through a channel, which is too narrow to allow the escape of D-xylose (Fig. 1 and Supplementary Fig. 5c). The structure of XylE was therefore captured in a ligand-bound, outward-facing, partly occluded conformation, which may represent an important expansion to the collection of MFS conformations.

Unlike other MFS transporters of known structure[35], XylE contains an intracellular domain that comprises four helices, three connecting the N and C domains, and one at the C-terminal end (Fig. 1 and Supplementary Fig. 1b). The intracellular helices interact with the cytosolic portion of the TMs through extensive polar interactions (Supplementary Fig. 6). The residues that constitute the intracellular helices are highly conserved in GLUT1–4. In particular, most of the residues that mediate the inter-domain interactions are invariant in XylE and GLUT1–4 (Supplementary Figs 1b and 6). On the basis of this analysis, we predict that a similar cytoplasmic domain is likely to exist in GLUT1–4 and may interact with the TMs of GLUT1–4, as observed in XylE.

Coordination of D-xylose

One molecule of D-xylose is bound between the N and C domains, closer to the latter (Supplementary Fig. 7a). D-Xylose is coordinated by both polar and aromatic residues mainly from the C domain (Fig. 2a, b). Unlike other proton symporters[24,27,36], no charged residue is observed in ligand binding in XylE. The hydroxyl groups of D-xylose are specifically recognized, through a total of eight hydrogen bonds, by polar residues including Gln 168 on TM5, Gln 288/Gln 289/Asn 294 on TM7, Trp 392 on TM10, and Gln 415 on TM11 (Fig. 2b and Supplementary Fig. 7b). Tyr 298 and Gln 415 also contribute to substrate binding through water-mediated hydrogen bonds (Supplementary Fig. 7c).

Several aromatic residues, including Phe 24 on TM1, Tyr 298 on TM7, Trp 392 on TM10, and Trp 416 on TM11, are located in the vicinity of D-xylose (Fig. 2b). The presence of aromatic residues surrounding the substrate is commonly observed in membrane transporters[4,36–40]. Among these aromatic residues, Tyr 298 constitutes the constriction that may prevent the escape of D-xylose to the extracellular side (Figs 1 and 2a, b). Except for Phe 24 and Gln 168, all other ligand-binding residues are from the C domain. In particular, the kinked TM7 is important in substrate coordination by contributing three polar residues, namely Gln 288, Gln 289 and Asn 294, and one aromatic residue, Tyr 298 (Fig. 2b).

To examine the role of these residues in D-xylose transport, we generated several XylE variants, each containing replacement of a specific ligand-binding residue by Ala (Fig. 2c), and examined their transport activities using both a cell-based uptake assay and a proteoliposome-based counterflow experiment. Missense mutation of any of the eight amino acids Gln 168, Gln 288, Gln 289, Asn 294, Tyr 298, Trp 392, Gln 415 and Trp 416 led to nearly complete abrogation of the transport activity in both assays. Mutation of Phe 24 also resulted in significant impairment of the transport activity. By contrast, mutation of Asn 325,

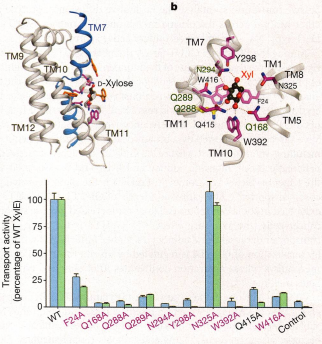

Figure 2 | Recognition of D-xylose by XylE. a, D-Xylose is coordinated mainly by residues from the C domain. The surrounding polar and aromatic residues are shown in magenta and orange sticks, respectively. D-Xylose is shown in black ball-and-sticks. **b**, D-Xylose is coordinated by both polar and aromatic residues. The residues that are invariant in XylE and GLUT1–4 are coloured magenta. **c**, Examination of the role of the ligand-binding residues in the transport of D-xylose in both cell-based uptake (blue bars) and proteoliposome-based counterflow (green bars) assays. Mutations of the invariant residues are labelled in magenta. The transport activities of XylE variants are normalized against those of the WT protein. Control refers to the uptake by *xylE*-deficient *E. coli* cells transformed with empty vector in the whole-cell assay, or liposome without protein in the counterflow assay. Error bars represent s.d.

which is not directly involved in ligand binding, showed slightly increased activity in the cell-based uptake and retained nearly full activity in the counterflow assay. The biochemical analysis is fully consistent with the structural observations.

Specificity of substrate recognition by XylE

D-Xylose is specifically recognized by residues in XylE through hydrogen bonds. Except for Gln 415, all other residues involved in D-xylose recognition are completely invariant in GLUT1–4 (Supplementary Fig. 1b). This analysis suggests that D-glucose, and perhaps other pentoses and hexoses, might be recognized by XylE. We investigated the ability of six distinct sugar molecules to compete with D-xylose for transport by XylE in counterflow experiments (Fig. 3a and Supplementary Fig. 8a). Although five of the sugars had little effect on the transport of D-xylose, D-glucose showed pronounced inhibition, decreasing the transport activity by nearly 90% (Fig. 4a), confirming with the purified protein the specificity originally deduced for XylE from *in vivo* measurements of xylose:H^+ symport[19].

The observed inhibition by D-glucose can be rationalized by the similarity between the chemical structures of D-xylose and D-glucose, the latter having only one extra 6-hydroxylmethyl group (Supplementary Fig. 8a). Furthermore, isothermal titration calorimetry experiments revealed that D-glucose binds to XylE with a K_d of about 0.77 ± 0.01 mM (Supplementary Fig. 8b), similar to that between D-xylose and XylE (Supplementary Fig. 3a). Consistent with *in vivo* observations[19], D-glucose is not a transport substrate for XylE (Fig. 3a, inset), suggesting additional structural elements for the transport activity of XylE towards D-xylose but not towards D-glucose. These results further indicate that, under physiological conditions, abundant D-glucose may serve as an inhibitor of the D-xylose transporter—perhaps as a method of preserving resources[19,41].

Coordination of D-glucose by XylE

Next, we sought to determine the crystal structure of XylE bound to D-glucose. Following generally the same protocols as those for the XylE–D-xylose complex, we succeeded in crystallizing XylE in the presence of 40 mM D-glucose. The structure was refined to 2.9 Å resolution (Supplementary Table 1). The overall protein conformation remains identical to that of XylE bound to D-xylose. To precisely determine the location and orientation of D-glucose in the structure, we chemically synthesized a D-glucose derivative, 6-BrGlc, and crystallized XylE bound to it. The diffraction data were collected at the wavelength for Br anomalous signal and the structure was refined at 2.6 Å resolution with excellent quality (Supplementary Table 1). The position of the Br atom was unambiguously identified by the strong anomalous signal, which not only allowed the determination of the orientation of D-glucose but also confirmed that of D-xylose (Supplementary Fig. 9).

As predicted by our biochemical analysis and sequence conservation, the coordination of D-glucose by XylE is very similar to that of D-xylose (Fig. 3b and Supplementary Fig. 10). In comparison with D-xylose coordination, Gln 168 seems to have a more prominent function in binding to D-glucose, in that it forms three hydrogen bonds with D-glucose. An extra hydrogen bond is found between the carbonyl oxygen of Gly 388 on TM10 and the 1-hydroxyl group of D-glucose. Gln 175, which is not involved in D-xylose binding, is hydrogen-bonded to the 6-hydroxyl group of D-glucose. The extra hydroxylmethyl group of D-glucose is further coordinated through van der Waals contacts by Ile 171 on TM5 and Phe 383 on TM10.

Except for Gln 175 and Gln 415, all other residues that mediate D-glucose recognition are invariant in GLUT1–4. Thus the structural information on XylE provides a molecular framework for understanding the structures and mechanisms of substrate recognition by the physiologically important glucose transporters (Fig. 3b and Supplementary Fig. 1b).

XylE-based structural model of GLUT1

The high degree of sequence conservation between XylE and GLUT1–4, particularly involving the functionally important residues (Supplementary Fig. 1), allowed us to build detailed structural models for GLUT1–4 with the program JACKAL[42]. In these models, the invariant and conserved amino acids in GLUT1–4 are aligned with those in XylE, which underlies functional conservation. We believe that these homology-based models of GLUT1–4 more faithfully represent reality than those derived from sequence analysis or non-homologous LacY-based models.

The XylE-derived homology model of GLUT1 (Fig. 4a, b) reveals several significant findings. First, the new GLUT1 model contains a more accurate demarcation of the secondary structural elements. For example, the TM boundaries in previous models of GLUT1 in textbooks, represented by that on page 392 in the fifth edition of *Lehninger Principles of Biochemistry*, deviate considerably from our model. Second, similarly to XylE, the new GLUT1 model contains four α-helices on the intracellular side (Fig. 4a, b) that were absent from previous models. Amino acids in this intracellular domain and their interacting residues in the TMs are highly conserved between XylE and GLUT1–4 (Supplementary Figs 1b and 6). Third, and most importantly, D-glucose recognition by GLUT1, as well as by GLUT2–4, should be nearly identical to that observed in the structure of D-glucose-bound XylE, because the vast majority of the amino acids involved in substrate

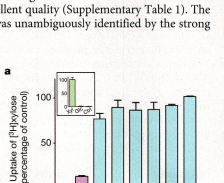

Figure 3 | Coordination of D-glucose by XylE. a, Substrate selectivity of XylE, as determined by liposome-based competition assay. Of the tested pentoses and hexoses, only D-glucose inhibited the transport of D-xylose by XylE, although D-glucose could not be transported by XylE (inset). Control, control experiment without the addition of sugar competitors; the averaged readout of the control experiments is set as 100%. Xyl, D-xylose; Glc, D-glucose; Ctrl, control experiment with XylE-free liposomes. **b**, Coordination of D-glucose by XylE observed in the structure of XylE bound to D-glucose. D-Glucose is shown in black ball-and-sticks. Hydrogen bonds are represented by red dashed lines. The invariant residues in XylE and GLUT1–4 are coloured green. The position and orientation of D-glucose were verified by the bromide anomalous signal for a glucose derivative, 6-BrGlc, whose complex with XylE was determined at 2.6 Å resolution (Supplementary Fig. 9 and Supplementary Table 1).

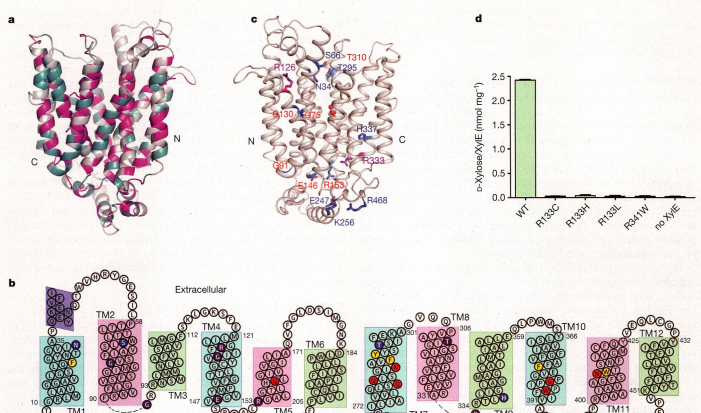

Figure 4 | Homology-based modelling of GLUT1 structure. a, A structural model of GLUT1 is generated on the basis of XylE structure and sequence conservation. Invariant and conserved residues are coloured magenta and dark green, respectively. **b**, Predicted secondary structural elements of GLUT1. Polar and aromatic residues predicted to be involved in D-glucose binding are shaded red and yellow, respectively. The residues whose mutations were found in GLUT1 deficiency syndrome are shaded purple and blue for invariant and variant residues, respectively. **c**, Mapping of the disease-related residues on the structural model of GLUT1. Invariant and variant residues in XylE and GLUT1–4 are labelled red and blue, respectively. **d**, Mutation of Arg 133 or Arg 341 in XylE, which correspond to Arg 126 and Arg 333 of GLUT1 (highlighted in magenta in **c**), led to abrogation of D-xylose transport in a liposome-based counterflow assay.

binding are invariant between XylE and GLUT1–4 (Fig. 3b and Supplementary Figs 1b and 10).

We mapped disease-derived mutations onto the structural model of GLUT1 (Fig. 4c) and speculated on the potential impact of these mutations on GLUT1 transport activity[43,44]. None of these residues is directly involved in glucose binding as observed in the outward-facing, partly occluded conformation of XylE (Fig. 4b, c). Among the mutated residues, Asn 34, Ser 66, Thr 295 and Thr 310 are located on the extracellular side of the putative transport path, suggesting potential involvement in substrate transport. Gly 75 and Gly 130 are positioned in the middle of TM2 and TM4, respectively; their mutations probably lead to a steric clash or impairment of conformational flexibility required for transport activity. Arg 126 and His 337 are away from the transport path and buried within the N and C domains (Fig. 4c), implying a regulatory role for substrate transport. Intriguingly, several residues, including Gly 91, Glu 146, Arg 153, Glu 247, Lys 256, Arg 333 and Arg 468, are clustered on the intracellular side, with some contributing to the interactions between the intracellular α-helices and the TMs (Fig. 4b, c and Supplementary Fig. 6). The fact that the interface involving the intracellular α-helices is targeted for disease-causing mutations suggests functional significance of the intracellular domain.

Several of the disease-related residues in GLUT1 are invariant in XylE. We attempted to examine the effect of some of these mutations on the transport activity of XylE. The XylE variants containing single missense mutations G67W (Gly 75 in GLUT1), G137S (Gly 130 in GLUT1) and R160L (Arg 153 in GLUT1) failed to yield well-behaved recombinant proteins, supporting a structural role for these residues. The variants containing Arg 133 (Arg 126 in GLUT1) mutations or R341W (R333W in GLUT1) gave rise to well-behaved recombinant proteins. These XylE variants, R133C, R133H, R133L and R341W, completely lost the transport activity for D-xylose (Fig. 4d), consistent with the observations that the corresponding mutations in GLUT1 led to a significant decrease in substrate transport, which are thought to be correlated with clinical disorders[43,45,46].

Functional significance of the SP signature motifs

The ligand-bound, outward-facing, partly occluded conformation of XylE is complementary to the other captured conformations for MFS proteins (Fig. 5a). The intramembrane helix domain of XylE is absent from the other MFS members of known structures. In particular, XylE has several distinct features in comparison with LacY and FucP, the other two MFS sugar:H^+ symporters.

XylE lacks charged residues in the vicinity of the substrate-binding site (Figs 2b and 3b), whereas Glu/Asp residues essential for both substrate binding and proton translocation were identified in both LacY[47,48] and FucP[27]. A large number of hydrogen-bond-forming

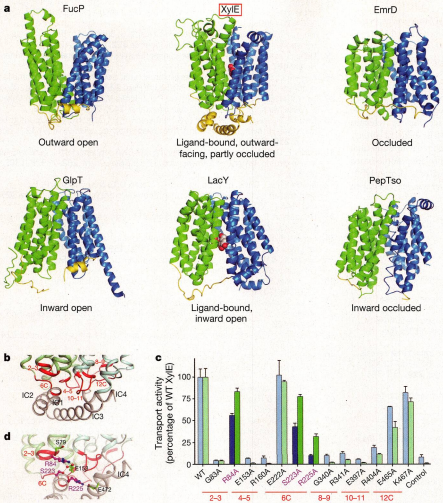

Figure 5 | Functional significance of the conserved SP family signature motifs. **a**, Reported MFS structures display distinct conformations. XylE contains an intracellular helix domain (yellow) that is not seen in the other structures. The distinct N and C domains are coloured green and blue in all the structures. **b**, The SP family signature motifs (coloured red) are located on the intracellular side of XylE. The motifs are labelled according to their locations. For example, '2–3' refers to the one connecting TMs 2 and 3. The N domain is coloured pale green, and the C domain pale cyan. **c**, Functional characterization of the conserved motif residues. The motifs where the indicated residues are located are indicated at the bottom. The presentation scheme is identical to that of Fig. 2c. **d**, Structural analysis of the functionally characterized residues that may be involved in proton-coupled active transport.

residues are distributed on the interface between the TMs and the intracellular domain of XylE (Supplementary Fig. 6), but not in LacY or FucP. Furthermore, common to SP family members, but largely missing in LacY and FucP, conserved signature motifs are found in XylE[19,32], including D(N)RXGRR between TMs 2 and 3 and TMs 8 and 9, E-------R between TMs 4 and 5 and TMs 10 and 11, and PESPR and PETK at the C termini of TM6 and TM12 (hereafter referred to as TM6C and TM12C motifs), respectively (Supplementary Figs 1 and 2). All of these motifs are positioned on the cytoplasmic side of the TMs except a couple of residues in the TM6C motif that are located in intracellular helix α1 (Fig. 5b and Supplementary Figs 1 and 2). Most of these motif residues are charged and polar ones that form an intricate hydrogen-bond network, mediating the interactions between the TMs and the intracellular domain (Supplementary Figs 1, 2 and 6).

To assess the functional importance of these motifs we generated a number of XylE variants each containing an Ala substitution of one conserved motif residue. Both cell-based uptake and proteoliposome-based counterflow experiments were performed for the variants that yielded reasonable protein expression and solution behaviours. More than half of the single point mutations resulted in completely abrogated or seriously impaired activities in both assays, indicating an essential role for the SP signature motifs for transport activity (Fig. 5c). A detailed analysis of the assay results can be found in Supplementary Discussion. Here we focus on three SP motif residues.

Mutation of Arg 84 or Ser 223 had a limited effect on the transport activity of XylE in the counterflow assay, but led to the loss of about half of the activity in the active uptake of D-xylose into the cell. Ala replacement of Arg 225, which is located on intracellular helix α1, completely abolished the active transport but retained more than 30% of the activity in the counterflow assay. The distinct activities of these variants between cell uptake and counterflow experiments suggested that the three residues may be involved in active transport. This speculation seems to be supported by structural observations. Arg 84 and Ser 223 both form hydrogen bonds with Glu 153, whereas Arg 225 is hydrogen-bonded to Glu 472 (Fig. 5d). Protonation and deprotonation may affect hydrogen bond formation between these residues. Nonetheless, further interpretation is complicated by the fact that all three residues are invariant in the proton-gradient-independent uniporters GLUT1–4.

The biochemical characterizations reported here revealed that the SP motifs as well as the intracellular helix domain have a critical role for the function of XylE. Given that extensive hydrogen bonds are formed by these structural elements, some of the residues may contribute to proton symport. Nevertheless, it remains puzzling that all these residues are invariant in GLUT1–4 and XylE (Supplementary Fig. 1b), the former being facilitative uniporters and the latter being a proton symporter. The molecular determinants for the proton coupling in XylE remain to be established.

Here we have reported three related crystal structures of XylE, a bacterial homologue of the human proteins GLUT1–4, in complex with D-xylose, D-glucose and 6-BrGlc. The structural information, together with the biochemical inspections, provides a valuable framework for further deciphering the functional mechanisms of the physiologically important glucose transporters GLUT1–4 and other members of the SP family.

METHODS SUMMARY

Full-length, wild-type (WT) XylE from *E. coli* strain O157:H7 was overexpressed in *E. coli* BL21(DE3) and purified to homogeneity in the presence of 0.2% (w/v) *n*-nonyl-β-D-glucopyranoside and 0.02% (w/v) *n*-dodecyl-*N*,*N*-dimethylamine-*N*-oxide. The identity and structure of the synthesized 6-BrGlc were confirmed by both NMR and high-resolution mass spectrometry analysis. D-Xylose, D-glucose and 6-BrGlc were present at 20, 40 and 40 mM, respectively, for the crystallization of XylE bound to these ligands. Data sets were collected at Shanghai Synchrotron Radiation Facility beamline BL17U and SPring-8 beamline BL41XU. The initial phases were derived from mercury-based and platinum-based single-wavelength anomalous dispersion using the program SheltxC/D/E[39]. The binding affinity between the ligands and purified recombinant XylE was measured with isothermal titration calorimetry. The cell-based uptake assays and proteoliposome-based counterflow experiments were performed by following the published protocols[27,36]. The XylE-based homology model of human GLUT1 structure was generated with the software JACKAL[42].

Full Methods and any associated references are available in the online version of the paper.

Received 12 March; accepted 17 August 2012.

1. Thorens, B. & Mueckler, M. Glucose transporters in the 21st Century. *Am. J. Physiol. Endocrinol. Metab.* **298,** E141–E145 (2010).
2. Pascual, J. M. *et al.* GLUT1 deficiency and other glucose transporter diseases. *Eur. J. Endocrinol.* **150,** 627–633 (2004).
3. Scheepers, A., Joost, H. G. & Schurmann, A. The glucose transporter families SGLT and GLUT: molecular basis of normal and aberrant function. *JPEN J. Parenter. Enteral Nutr.* **28,** 364–371 (2004).
4. Faham, S. *et al.* The crystal structure of a sodium galactose transporter reveals mechanistic insights into Na$^+$/sugar symport. *Science* **321,** 810–814 (2008).
5. Mueckler, M. Facilitative glucose transporters. *Eur. J. Biochem.* **219,** 713–725 (1994).
6. Mueckler, M. *et al.* Sequence and structure of a human glucose transporter. *Science* **229,** 941–945 (1985).
7. Klepper, J. Glucose transporter deficiency syndrome (GLUT1DS) and the ketogenic diet. *Epilepsia* **49** (Suppl 8), 46–49 (2008).
8. Brockmann, K. The expanding phenotype of GLUT1-deficiency syndrome. *Brain Dev.* **31,** 545–552 (2009).
9. Scheffer, I. E. GLUT1 deficiency: a glut of epilepsy phenotypes. *Neurology* **78,** 524–525 (2012).
10. Santer, R. *et al.* Mutations in GLUT2, the gene for the liver-type glucose transporter, in patients with Fanconi–Bickel syndrome. *Nature Genet.* **17,** 324–326 (1997).
11. Leturque, A., Brot-Laroche, E. & Le Gall, M. GLUT2 mutations, translocation, and receptor function in diet sugar managing. *Am. J. Physiol. Endocrinol. Metab.* **296,** E985–E992 (2009).
12. Simpson, I. A. *et al.* The facilitative glucose transporter GLUT3: 20 years of distinction. *Am. J. Physiol. Endocrinol. Metab.* **295,** E242–E253 (2008).
13. Amann, T. & Hellerbrand, C. GLUT1 as a therapeutic target in hepatocellular carcinoma. *Expert Opin. Ther. Targets* **13,** 1411–1427 (2009).
14. Macheda, M. L., Rogers, S. & Best, J. D. Molecular and cellular regulation of glucose transporter (GLUT) proteins in cancer. *J. Cell. Physiol.* **202,** 654–662 (2005).
15. Mueckler, M. The molecular biology of glucose transport: relevance to insulin resistance and non-insulin-dependent diabetes mellitus. *J. Diabetes Complications* **7,** 130–141 (1993).
16. Leney, S. E. & Tavare, J. M. The molecular basis of insulin-stimulated glucose uptake: signalling, trafficking and potential drug targets. *J. Endocrinol.* **203,** 1–18 (2009).
17. Nelson, D. L. & Cox, M. M. *Lehninger Principles of Biochemistry* 1158 (W. H. Freeman, 2008).
18. Pao, S. S., Paulsen, I. T. & Saier, M. H. Jr. Major facilitator superfamily. *Microbiol. Mol. Biol. Rev.* **62,** 1–34 (1998).
19. Henderson, P. J. & Maiden, M. C. Homologous sugar transport proteins in *Escherichia coli* and their relatives in both prokaryotes and eukaryotes. *Phil. Trans. R. Soc. Lond. B* **326,** 391–410 (1990).
20. Ozcan, S. & Johnston, M. Function and regulation of yeast hexose transporters. *Microbiol. Mol. Biol. Rev.* **63,** 554–569 (1999).
21. Buttner, M. The monosaccharide transporter(-like) gene family in *Arabidopsis*. *FEBS Lett.* **581,** 2318–2324 (2007).
22. Li, F. *et al.* Characterization of sucrose transporter alleles and their association with seed yield-related traits in *Brassica napus* L. *BMC Plant Biol.* **11,** 168 (2011).
23. Mueckler, M. & Makepeace, C. Model of the exofacial substrate-binding site and helical folding of the human Glut1 glucose transporter based on scanning mutagenesis. *Biochemistry* **48,** 5934–5942 (2009).
24. Abramson, J. *et al.* Structure and mechanism of the lactose permease of *Escherichia coli*. *Science* **301,** 610–615 (2003).
25. Huang, Y., Lemieux, M. J., Song, J., Auer, M. & Wang, D. N. Structure and mechanism of the glycerol-3-phosphate transporter from *Escherichia coli*. *Science* **301,** 616–620 (2003).
26. Yin, Y., He, X., Szewczyk, P., Nguyen, T. & Chang, G. Structure of the multidrug transporter EmrD from *Escherichia coli*. *Science* **312,** 741–744 (2006).
27. Dang, S. *et al.* Structure of a fucose transporter in an outward-open conformation. *Nature* **467,** 734–738 (2010).
28. Newstead, S. *et al.* Crystal structure of a prokaryotic homologue of the mammalian oligopeptide–proton symporters, PepT1 and PepT2. *EMBO J.* **30,** 417–426 (2011).
29. Lam, V. M., Daruwalla, K. R., Henderson, P. J. & Jones-Mortimer, M. C. Proton-linked D-xylose transport in *Escherichia coli*. *J. Bacteriol.* **143,** 396–402 (1980).
30. Davis, E. O., Jones-Mortimer, M. C. & Henderson, P. J. Location of a structural gene for xylose–H$^+$ symport at 91 min on the linkage map of *Escherichia coli* K12. *J. Biol. Chem.* **259,** 1520–1525 (1984).
31. Davis, E. O. & Henderson, P. J. The cloning and DNA sequence of the gene xylE for xylose–proton symport in *Escherichia coli* K12. *J. Biol. Chem.* **262,** 13928–13932 (1987).
32. Maiden, M. C., Davis, E. O., Baldwin, S. A., Moore, D. C. & Henderson, P. J. Mammalian and bacterial sugar transport proteins are homologous. *Nature* **325,** 641–643 (1987).
33. Henderson, P. J. Proton-linked sugar transport systems in bacteria. *J. Bioenerg. Biomembr.* **22,** 525–569 (1990).
34. Screpanti, E. & Hunte, C. Discontinuous membrane helices in transport proteins and their correlation with function. *J. Struct. Biol.* **159,** 261–267 (2007).
35. Snider, C. & White, S. *Membrane Proteins of Known 3D Structure* (Stephen H. White Lab., Univ. of California Irvine, 2011).
36. Lu, F. *et al.* Structure and mechanism of the uracil transporter UraA. *Nature* **472,** 243–246 (2011).
37. Ressl, S., Terwisscha van Scheltinga, A. C., Vonrhein, C., Ott, V. & Ziegler, C. Molecular basis of transport and regulation in the Na$^+$/betaine symporter BetP. *Nature* **458,** 47–52 (2009).
38. Gao, X. *et al.* Structure and mechanism of an amino acid antiporter. *Science* **324,** 1565–1568 (2009).
39. Fang, Y. *et al.* Structure of a prokaryotic virtual proton pump at 3.2 Å resolution. *Nature* **460,** 1040–1043 (2009).
40. Gao, X. *et al.* Mechanism of substrate recognition and transport by an amino acid antiporter. *Nature* **463,** 828–832 (2010).
41. Desai, T. A. & Rao, D. V. Regulation of arabinose and xylose metabolism in *Escherichia coli*. *Appl. Environ. Microbiol.* **76,** 1524–1532 (2010).
42. Xiang, Z., Steinbach, P. J., Jacobson, M. P., Friesner, R. A. & Honig, B. Prediction of side-chain conformations on protein surfaces. *Proteins* **66,** 814–823 (2007).
43. Wang, D. *et al.* Glut-1 deficiency syndrome: clinical, genetic, and therapeutic aspects. *Ann. Neurol.* **57,** 111–118 (2005).
44. Cunningham, P., Afzal-Ahmed, I. & Naftalin, R. J. Docking studies show that D-glucose and quercetin slide through the transporter GLUT1. *J. Biol. Chem.* **281,** 5797–5803 (2006).
45. Brockmann, K. *et al.* Autosomal dominant Glut-1 deficiency syndrome and familial epilepsy. *Ann. Neurol.* **50,** 476–485 (2001).
46. Ho, Y. Y. *et al.* Glucose transporter type 1 deficiency syndrome (Glut1DS): methylxanthines potentiate GLUT1 haploinsufficiency *in vitro*. *Pediatr. Res.* **50,** 254–260 (2001).
47. Franco, P. J. & Brooker, R. J. Functional roles of Glu-269 and Glu-325 within the lactose permease of *Escherichia coli*. *J. Biol. Chem.* **269,** 7379–7386 (1994).
48. Guan, L. & Kaback, H. R. Lessons from lactose permease. *Annu. Rev. Biophys. Biomol. Struct.* **35,** 67–91 (2006).
49. Schneider, T. R. & Sheldrick, G. M. Substructure solution with SHELXD. *Acta Crystallogr. D* **58,** 1772–1779 (2002).
50. DeLano, W. L. The PyMOL Molecular Graphics System. http://www.pymol.org (2002).

Supplementary Information is available in the online version of the paper.

Acknowledgements We thank J. He, L. Tang, F. Yu and S. Huang at Shanghai Synchrotron Radiation Facility, and K. Hasegawa and T. Kumasaka at the SPring-8 beamline BL41XU, for on-site assistance. This work was supported by funds from the Ministry of Science and Technology (grant numbers 2009CB918802 and 2011CB910501), projects 31125009 and 91017011 of the National Natural Science Foundation of China, and funds from Tsinghua University.

Author Contributions L.S., X.Z. and N.Y. designed all experiments. L.S., X.Z., C.Y., X.G. and N.Y. performed the experiments for structural determination, homology-based structure modelling and biochemical analysis. X.S. and Y.R. synthesized 6-BrGlc. All authors analysed the data and contributed to manuscript preparation. N.Y. wrote the manuscript.

Author Information The atomic coordinates and structure factors of XylE bound to D-xylose, D-glucose and 6-BrGlc are deposited in the Protein Data Bank with accession codes 4GBY, 4GBZ and 4GC0. Reprints and permissions information is available at www.nature.com/reprints. The authors declare no competing financial interests. Readers are welcome to comment on the online version of the paper. Correspondence and requests for materials should be addressed to N.Y. (nyan@tsinghua.edu.cn).

ARTICLE

doi:10.1038/nature11442

Structure of AMP-PNP-bound vitamin B_{12} transporter BtuCD-F

Vladimir M. Korkhov[1], Samantha A. Mireku[1] & Kaspar P. Locher[1]

The ATP-binding cassette (ABC) transporter BtuCD mediates the uptake of vitamin B_{12} across the inner membrane of *Escherichia coli*. Previous structures have shown the conformations of apo states, but the transport mechanism has remained unclear. Here we report the 3.5 Å crystal structure of the transporter-binding protein complex BtuCD–BtuF (BtuCD–F) trapped in an β–γ-imidoadenosine 5′-phosphate (AMP-PNP)-bound intermediate state. Although the ABC domains (BtuD subunits) form the expected closed sandwich dimer, the membrane-spanning BtuC subunits adopt a new conformation, with the central translocation pathway sealed by a previously unrecognized cytoplasmic gate. A fully enclosed cavity is thus formed approximately halfway across the membrane. It is large enough to accommodate a vitamin B_{12} molecule, and radioligand trapping showed that liposome-reconstituted BtuCD–F indeed contains bound B_{12} in the presence of AMP-PNP. In combination with engineered disulphide crosslinking and functional assays, our data suggest an unexpected peristaltic transport mechanism that is distinct from those observed in other ABC transporters.

ABC transporters are membrane proteins that carry out a wide range of physiological functions by coupling the hydrolysis of cellular ATP to the translocation of substrates across biological membranes. They contain a pair of nucleotide-binding domains (NBDs) that hydrolyse ATP, thus controlling the conformation of a single translocation pathway formed by two transmembrane domains (TMDs)[1–3]. Whereas the NBDs are highly conserved in all domains of life, the architectures of the TMDs differ between type I, type II and energy coupling factor ABC-type exporters or importers[4,5]. *E. coli* BtuCD is a type II importer that facilitates vitamin B_{12} uptake[6,7] and is similar in architecture and mechanism to iron-siderophore and haem transporters implicated in the virulence of certain Gram-negative pathogens[8,9]. The structure of BtuCD has been determined in two distinct states, neither of which contained bound ATP. BtuCD by itself has been found to adopt an outward-facing conformation[10], whereas the apo complex with the cognate periplasmic-binding protein BtuF revealed an occluded, asymmetric state[11,12].

To understand the transport reaction, structural information of key intermediate states is essential. Although such information is available for bacterial ABC exporters[13,14] and the type I importer $MalFGK_2$ [15,16], the mechanism of type II importers such as BtuCD has remained enigmatic. Whereas one study demonstrated a strict requirement of ATP hydrolysis for *in vitro* B_{12} translocation[17], another concluded that the binding and hydrolysis of ATP may only be required for the dissociation of BtuF and resetting of the system rather than the actual transport step[18,19]. In addition, the structure of the architecturally related Hi1470/1 protein was reported in an inward-facing conformation without bound nucleotide, indicating distinct conformational coupling[20].

Engineered disulphide locks the ATP-bound state

We previously attempted to determine the key nucleotide-bound state of BtuCD–F by introducing a mutation in the Walker-B motif (E159Q) that reduced ATP hydrolysis by more than 1,000-fold[12]. However, the complex crystallized in a nucleotide-free conformation even in the presence of the non-hydrolysable ATP analogue AMP-PNP[12]. We proposed that, in order to trap BtuCD–F in the nucleotide-bound state for structural studies, not only were non-covalent interactions provided by the nucleotide insufficient, but also residual ATPase activity and conformational dynamics were detrimental. To resolve these issues, we engineered a covalent disulphide bond between the two NBDs. We mutated BtuD to replace N162, a residue located in the D-loop motif, with a cysteine residue. This choice was made because equivalent residues were found in close contact in all high-resolution structures of ATP-bound NBDs reported to date[15,21–25], including that of the soluble DNA repair-related ABC protein Rad50 (ref. 26). All of these structures showed a 'closed sandwich dimer conformation' of NBDs, with the Cα atoms of opposite D-loop residues invariably distanced within 4.6–6.7 Å. By contrast, the equivalent atoms are separated by 8.7 Å in the previously solved structure of apo BtuCD[10] and 9.2 Å in that of BtuCD–F[11]. Our BtuCD(N162C) variant indeed formed a disulphide bond on oxidation by Cu^{2+}, thus covalently crosslinking the two BtuD subunits with quantitative yield, as judged by SDS–polyacrylamide gel electrophoresis (SDS–PAGE) (Supplementary Fig. 1). This considerably decreased the ATPase rate of BtuCD(N162C)–F and consequently also reduced *in vitro* [^{57}Co]cyanocobalamin transport (Fig. 1). However, both effects were largely reversed on reduction of the disulphide bond using dithiothreitol (DTT). In addition, although V_{max} was reduced, neither the $K_{0.5}$ for ATP nor the positive cooperativity (sigmoidal shape of the ATPase curves) was altered by the disulphide bridge (Fig. 1b). In addition, the ATPase activity of BtuCD(N162C)–F was equally as sensitive to the non-hydrolysable ATP analogue AMP-PNP as the wild-type protein, irrespective of whether the disulphide crosslink was formed (Supplementary Fig. 2). This strongly indicated that in the disulphide-stabilized form, the nucleotide-binding sites were intact and the engineered transporter was locked in a conformation that probably reflected the ATP-bound state. The functional characterization of BtuCD(N162C)–F is summarized in Supplementary Table 1.

The engineering of disulphide bonds to trap labile conformations for structural analysis has previously been applied to various membrane proteins[27,28]. We found that even with the disulphide bridge formed, BtuCD(N162C)–F showed a measurable ATPase activity, indicating conformational dynamics that could interfere with crystallization. We

[1]Institute of Molecular Biology and Biophysics, ETH Zürich, CH-8093 Zürich, Switzerland.

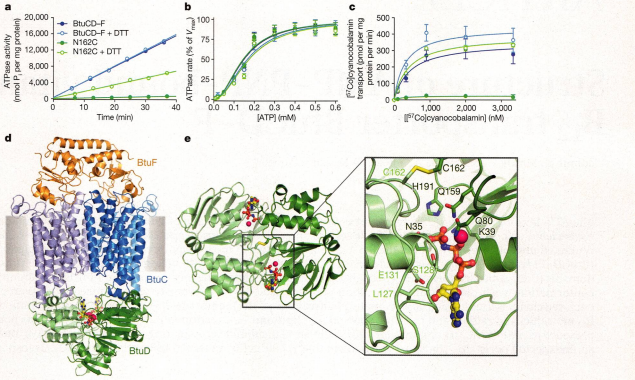

Figure 1 | Functional characterization of BtuCD(N162C)–F and the structure of BtuCD(EQNC)–F. a, ATPase activity of wild-type and mutant (indicated as N162C) BtuCD–F in detergent and in the presence or absence of the reducing agent DTT. **b**, Determination of $K_{0.5}$ for ATP (note the positive cooperativity). Data are mean ± s.d. **c**, Transport of [^{57}Co]cyanocobalamin into BtuCD-containing proteoliposomes. Data are mean ± s.e.m. Curves in **b** and **c** are coloured as in **a** and data statistics are given in Supplementary Table 1. **d**, Ribbon diagram of the BtuCD(EQNC)–F structure, with bound AMP-PNP indicated in ball and stick and Mg^{2+} as pink spheres. BtuF is coloured orange, BtuC subunits are in marine and light blue and BtuD subunits are in light and dark green. **e**, NBD (BtuD) dimer viewed from the interface with BtuC. Residue numbers are indicated, and the engineered, NBD-linking disulphide bond is shown as yellow sticks. AMP-PNP and Mg^{2+} are shown as in **d**.

therefore combined the N162C mutation with the previously characterized E159Q mutation in the Walker-B motif. The resulting construct, BtuCD(EQNC)–F (a complete BtuCD–F complex containing BtuD mutations E159Q and N162C), was capable of binding the nucleotides ATP and AMP-PNP (Supplementary Fig. 2), but was unable to transport substrate despite a very low residual ATP-hydrolysis rate (Supplementary Fig. 3). However, this construct allowed well-diffracting crystals with bound AMP-PNP to be grown, and X-ray data was obtained to 3.5 Å resolution. The structure was determined by molecular replacement (Supplementary Table 2 and Supplementary Figs 1b, 4, 5 and 6).

Conformation of the AMP–PNP–bound state

As expected, the BtuCD(EQNC)–F structure showed a closed sandwich dimer conformation, with the NBDs (BtuD subunits) forming two composite ATP-binding sites at the shared interface (Fig. 1d, e). Clear electron density was visible for the disulphide bridge that covalently linked the BtuD subunits (Supplementary Fig. 6a). Electron density for two bound AMP-PNP molecules was evident, and despite the modest resolution, bound Mg^{2+} ions were also visible (Supplementary Fig. 6b). We found that the residues involved in ATP hydrolysis, including the ABC signature, Walker-A and Walker-B motifs, are arranged as in previously reported ATP-bound NBD dimer structures, ruling out the possibility of a disruptive effect of the engineered disulphide bond and corroborating the physiological relevance of the structure.

Conformational changes in response to ATP binding and hydrolysis are transmitted from the NBDs to the TMDs through the 'coupling helices', an architecturally conserved motif observed in the TMDs of all ABC transporters of known structure[6]. Compared to apo structures of BtuCD[10] and Hi1470/1 (ref. 20), the distance between the coupling helices of AMP-PNP-bound BtuCD(EQNC)–F is decreased by ~7–9 Å (Supplementary Fig. 7). Thus the closure of the BtuD subunits forces the coupling helices together, in agreement with a previously proposed coupling model[29] derived from observed structures of full ABC transporters. However, the concomitant changes in the BtuC subunits are unexpected: as the coupling helices move towards the centre of the transporter, the transmembrane (TM) gating helices of the two BtuC subunits (TM5 and TM5′) are pushed out of the centre and into a conformation reminiscent of the inward-facing state observed in Hi1470/1 (Fig. 2). The loops connecting TM4 and TM5 have previously been described as the 'cytoplasmic gate' (henceforth referred to as cytoplasmic gate I) that opens in response to nucleotide binding, in agreement with electron paramagnetic resonance (EPR) spectroscopic studies[30,31]. However, the BtuCD(EQNC)–F structure showed that the cytoplasmic loops connecting TM2 and TM3 (residues N83–L85) moved into the opening created by the swing-out motion of TM4–TM5, thus sealing the translocation pathway shut (Figs 2a, 3a and Supplementary Figs 6c and 8c). Given its location, we refer to the TM2–TM3 loop as 'cytoplasmic gate II'. Sequence alignments indicate that this newly identified gate may be conserved in type II ABC importers; inspection of the Pfam database[32] showed that N83 and L85 are the most conserved residues in the TM2–TM3 loop of type II ABC importers of the FecCD family, including functionally characterized transporters of haem and iron siderophores (Fig. 3b). The closure of cytoplasmic gate II is reflected by distance changes between the Cα atoms of L85, which are ~7–10 Å closer in AMP-PNP-bound BtuCD(EQNC)–F than in the nucleotide-free structures (Fig. 2).

We corroborated, using independent biochemical evidence, that the orientation and location of transmembrane elements in the BtuCD(EQNC)–F structure indeed reflected a native-like nucleotide-bound state. We first tested whether the cytoplasmic gate II residues

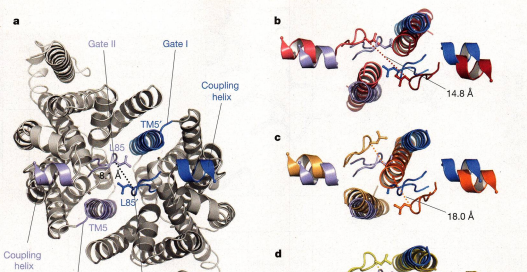

Figure 2 | Rearrangements of cytoplasmic gates and gating helices. **a**, BtuC subunits of BtuCD(EQNC)–F are indicated as light grey ribbons, with coupling helices and gating helices TM5, cytoplasmic gate I and cytoplasmic gate II regions in light blue and marine. The dashed line indicates the distance between the Cα atoms of opposing L85 residues. **b**–**d**, Coupling helices, gating helices TM5 and loop TM2–TM3 (cytoplasmic gate II) of BtuCD(EQNC)–F are shown as in **a**, and the equivalent elements of apo BtuCD (Protein Data Bank (PDB) code 1L7V) (**b**), apo BtuCD–F (PDB code 2QI9) (**c**) and Hi1470/1 (PDB code 2NQ2) (**d**) are shown after superposition with BtuCD(EQNC)–F. Distances between the Cα atoms of juxtaposed L85 residues (L91 in Hi1470/1) are indicated.

approach each other even in the absence of an NBD-stabilizing disulphide bond. We separately substituted BtuC residues N83 and L85 by cysteines in the context of wild-type BtuCD–F and applied oxidative crosslinking to the purified transporter mutants to induce disulphide-bond formation. Whereas the N83C mutant (distance between Cα atoms, 8.3 Å) was only weakly responsive to the treatment (Fig. 3c and Supplementary Fig. 9), a near-complete crosslinking could be observed for L85C (Fig. 3d; distance between Cα atoms, 8.1 Å) in the presence of ATP or AMP-PNP. Notably, a fraction of the L85C mutant was able to form a disulphide bond even in the absence of supplied nucleotide, indicating conformational flexibility in detergent solution. Crosslinked BtuC(L85C)D–F showed a 6.5-fold reduction in ATPase activity compared with the reduced form (Fig. 3e), confirming tight coupling between cytoplasmic gate II movement and ATP hydrolysis in the intact transporter.

Second, to test whether the observed conformation of the transmembrane helices was relevant, we generated the BtuC double mutant L133C/N233C, as the corresponding residues (located in TM4 and TM8, respectively) are in close proximity in our BtuCD(EQNC)–F structure. We indeed observed a complete disulphide crosslink, but only in the presence of ATP (Supplementary Fig. 10). Given that Cu^{2+}-induced disulphide crosslinking is highly dependent on close proximity and proper orientation of the reactive cysteines, these control experiments correlate with the nucleotide-induced conformational changes of the protein in solution with those observed in our BtuCD(EQNC)–F structure.

B_{12} translocation pathway

The closure of cytoplasmic gate II creates a central cavity at the interface of the BtuC subunits (Figs 3a, 4a and Supplementary Fig. 8). The sides of the cavity are lined with residues of TM3, TM5 and helix H5a, and its volume is sufficient to harbour a B_{12} molecule with only minor steric hindrance (Supplementary Fig. 11). However, the cavity interior has no similarity to cofactor-binding pockets of B_{12}-dependent enzymes or to BtuF[33,34], which agrees with the finding that neither BtuCD nor BtuCD–F have a measurable affinity for B_{12}. Transport proteins do not strictly require high-affinity substrate binding, and we conclude that the observed cavity in BtuCD–F has the function of a low-affinity, intermediate translocation chamber. In addition to being closed to the cytoplasm, the cavity is also sealed from the periplasmically attached BtuF by the previously identified 'periplasmic gate' (Supplementary Fig. 8b). This is in contrast to the ATP-bound state of the type I ABC importer $MalFGK_2$, in which a continuous pathway to the binding protein exists[15].

Assigning the observed cavity the function of a substrate-translocation chamber implies that B_{12} is trapped in this pocket when BtuCD–F is in the ATP-bound state. However, no B_{12} was found associated with purified BtuCD or BtuCD–F in detergent solution[7]. We proposed that the increased dynamics of BtuCD–F in a detergent micelle compared to that in a lipid bilayer enabled B_{12} to escape from the translocation pathway. Indeed, EPR spectroscopy indicated a substantial flexibility in the gating regions of BtuCD–F while in detergent solution[20,31]. We therefore reconstituted wild-type BtuCD into liposomes, but instead of adding ATP to the liposome lumen as is required for transport assays, we entrapped AMP-PNP–Mg^{2+}. We then added BtuF-bound [^{57}Co]cyanocobalamin and subsequently collected the liposomes by centrifugation. We found radiolabelled B_{12} specifically bound to BtuCD-containing proteoliposomes, but only if these contained enclosed AMP-PNP (Fig. 4b). We made the same observation with the oxidized BtuCD(N162C) mutant, indicating that the relay between nucleotide binding and vitamin B_{12} translocation is intact even when the designed NBD crosslink is in place. Furthermore, the combination of mutations in BtuCD(EQNC) enabled the transporter to trap [^{57}Co]cyanocobalamin even in the absence of AMP-PNP (Fig. 4b). Compared with wild-type protein, the amount of trapped B_{12} increased twofold on the addition of AMP-PNP to BtuCD(EQNC) (Fig. 4b), confirming the cumulative effect of the BtuD mutations E159Q and N162C for the stabilization of the AMP-PNP-bound state. This is the first experimental trapping of

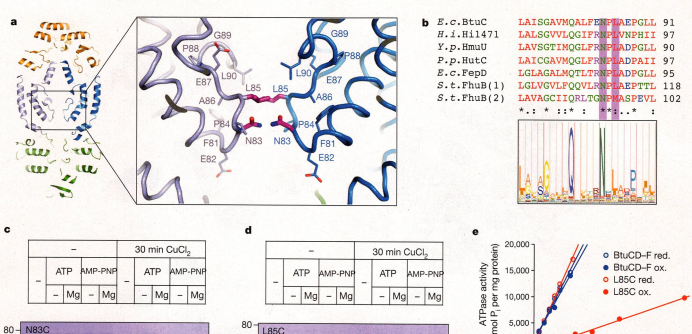

Figure 3 | Structural features of cytoplasmic gate II. a, Slab of ribbon diagram of BtuCD(EQNC)–F, coloured as in Fig. 1a. The boxed region shows a close-up of cytoplasmic gate II. Relevant residues are in ball and stick and labelled, and the conserved N83 and L85 residues are coloured purple. **b**, Top, protein sequence alignment of type II ABC importers with experimentally confirmed function. Residues N83 and L85 of *E. coli* BtuC and equivalent residues in other bacterial species are shaded magenta. Bottom, Pfam logo image depicts the high degree of conservation of BtuC residues N83 and L85 within the FecCD protein family. *E.c.*, *Escherichia coli*; *H.i.*, *Haemophilus influenzae*; *P.p. Photobacterium damselae* subsp. *piscicida*; *S.t.*, *Salmonella enterica* serovar Typhimurium; *Y.p.*, *Yersinia pestis*. Asterisks denote strict conservation, and colons and dots denote a high and low degree of similarity, respectively. **c**, SDS–PAGE of the disulphide-crosslinking reaction in the BtuC(N83C)D–F mutant. Molecular masses are indicated on the left and Btu subunits are indicated on the right. C:C denotes the disulphide-crosslinked BtuC dimer species. Reaction conditions are indicated in the table above the gel. **d**, Similar to **c**, but for the BtuC(L85C)D–F mutant. **e**, ATPase activity of wild-type BtuCD–F and mutant BtuC(L85C)D–F. The labels 'red.' and 'ox.' indicate whether the protein was purified and assayed under reducing conditions (4 mM β-mercaptoethanol) or after oxidative disulphide crosslinking, respectively. ATPase rates (mean ± s.e.m.) for wild-type BtuCD–F ($n = 2$) and the L85C mutant ($n = 3$) were determined as 434 ± 55 (BtuCD–F red.), 410 ± 39 (BtuCD–F ox.), 567 ± 11 (L85C red.) and 87 ± 7 (L85C ox.).

a transport substrate in a type II ABC importer, and we conclude that ATP binding is indeed essential for loading vitamin B_{12} into the translocation cavity in wild-type BtuCD.

Transport mechanism

Since the first structures of ABC transporters were determined, various attempts at formulating a unifying transport mechanism have been made. On the basis of the alternating access model described in ref. 35, we previously proposed a model that linked the ATP-bound state of NBDs to outward-facing conformations of TMDs and the nucleotide-free state of NBDs to inward-facing conformations of TMDs[29,36]. Although this schematic worked well for explaining the functions of ABC exporters and type I ABC importers, it failed with type II ABC importers. It was speculated that this failure was proof of detergent-induced artefacts and that the previous BtuCD structures might be physiologically irrelevant or depict uncoupled states[11,37]. Our AMP-PNP-bound BtuCD(EQNC)–F structure, however, suggests that this interpretation might be incorrect. Indeed, a mechanism can now be formulated for BtuCD-F that accounts for the conserved mechanics of NBDs while putting the observed TMD conformations in the context of a transport cycle.

As illustrated in Fig. 5, the proposed cycle is initiated by the docking of B_{12}-loaded BtuF to the outward-facing conformation of BtuCD (State 1)[10]. EPR spectroscopic studies indicate that, although BtuCD is dynamic in lipid bilayers, the outward-facing conformation is probably predominant, even in the presence of ATP[30,31]. State 2 reflects the ATP-bound conformation as visualized by the BtuCD(EQNC)–F structure, which is reached after (1) binding of two ATP molecules; (2) closure of the NBD sandwich dimer and shortening of the distance between the coupling helices; and (3) the concomitant rearrangements in the TMD that trap B_{12} in the translocation cavity. In the BtuCD–F complex, the high-affinity B_{12} binding pocket of free BtuF is distorted and occupied by periplasmic loops of BtuC[11], abrogating the nanomolar affinity of BtuF for B_{12}. After reaching state 2, B_{12} can only escape if one of the gates (cytoplasmic or periplasmic) opens. Given that ATP hydrolysis invariably proceeds and the hydrolysis products are released, the previously closed NBD sandwich dimer will open and pull the coupling helices (and cytoplasmic gate II) outward. This will generate an inward-facing conformation, much like the one observed in the Hi1470/1 structure, but with BtuF still attached to the periplasmic side of the transporter. Given that B_{12} is in a cavity of very low affinity, such rearrangements

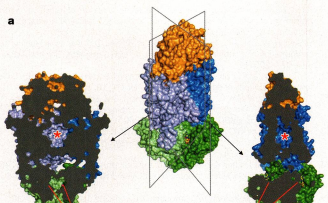

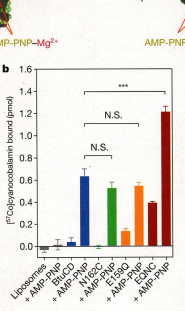

Figure 4 | B_{12} translocation cavity. a, Surface representation of the BtuCD(EQNC)–F structure, with front slabs removed for clarity as indicated by black lines in centre panel. The observed B_{12} translocation cavity is indicated by red asterisks. **b**, Specific trapping of [^{57}Co]cyanocobalamin by reconstituted wild-type BtuCD (blue bars, $n = 5$) and mutants BtuCD(N162C) (green bars, $n = 4$), BtuCD(E159Q) (orange bars, $n = 3$) and BtuCD(EQNC) (red bars, $n = 3$). Grey bars depict a control experiment with empty liposomes ($n = 7$). The bars labelled '+ AMP-PNP' contained 1 mM AMP-PNP preloaded into the liposome lumen. Radiolabelled B_{12} was delivered to the transporter by BtuF (experimental details are provided in Methods). Data are mean ± s.e.m. Measurements with AMP-PNP-bound BtuCD- and mutant-containing proteoliposomes were significantly different from the rest of the conditions (including empty liposomes and in the absence of nucleotide). For $BtuCD_{EQNC}$ + AMP-PNP, the measurement was significantly different from equivalent measurements for other constructs. ***$P < 0.05$. N.S., not significant.

are equivalent to a squeezing out of the substrate, as in peristalsis. A fully inward-facing conformation has not been observed in BtuCD, probably because it is less stable than other conformations. However, it can be trapped using disulphide crosslinking (see above). State 4 corresponds to the apo BtuCD–F complex, which is reached after B_{12} is ejected into the cytoplasm and cytoplasmic gate I is asymmetrically closed. The observed asymmetry is probably functionally irrelevant, because structures of BtuCD–F have been determined with BtuF attached to the asymmetric BtuC dimer in either orientation[11,12]. State 4 is the most stable BtuCD–F complex *in vitro*, with a K_d of $\sim 1 \times 10^{-13}$ M measured for the dissociation of BtuF in the absence of ATP and B_{12} (ref. 3). In the presence of (cytoplasmic) ATP and (periplasmic) B_{12}, the interaction of BtuF and BtuCD was found to be weaker, but other physiological factors, such as the electrochemical membrane potential, may contribute to the release of BtuF, allowing a new transport cycle to be initiated.

The above mechanism implies that, whereas the binding of ATP is coupled to B_{12} transfer into a transient translocation cavity, hydrolysis of ATP is required for the release of the substrate into the cytoplasm. During the cycle, the coupling helices of BtuCD move together and apart as in other ABC transporters, but with distinct consequences for the TMD-provided translocation pathway. The proposed mechanism suggests that state 4 may be required to prevent leakage of small molecules when the transporter reverts to the starting conformation. Despite the large size of the translocation pathway required for B_{12}, we were indeed unable to detect leakage of radiolabelled glycine in BtuCD-containing proteoliposomes, even under conditions of B_{12} transport (not shown). Finally, given that BtuCD has two symmetrical ATPase sites, two ATP molecules are required to fully close the NBD sandwich dimer. We assume that both bound ATP molecules are hydrolysed during a single transport cycle, analogous to the stoichiometry observed in the OpuA transporter[38]. However, given the high level of futile basal ATPase activity in our experimental system, direct determination of the transport stoichiometry was not possible.

Our study shows that BtuCD has an unprecedented, peristalsis-like B_{12} transport mechanism that probably applies to other type II ABC importers, including haem- and siderophore-uptake systems. Although the conserved cytoplasmic motor domains produce a power stroke that is similar to those of type I importers or ABC exporters, the transport mechanism of BtuCD is distinct because its transmembrane architecture is different. Given that new TMD folds may be revealed in as yet uncharacterized ABC transporter subfamilies, it is probable that additional coupling mechanisms will be discovered.

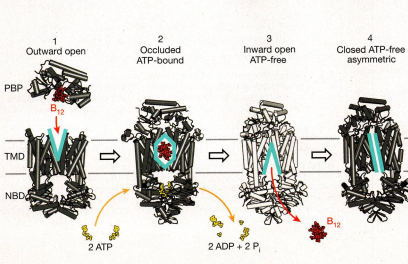

Figure 5 | Schematic of proposed B_{12} transport mechanism. BtuCD and BtuF are depicted as cylinder diagrams, with substrates B_{12} and ATP shown as space-filling models and labelled. The states are ordered to describe a productive translocation cycle. Light blue lines depict the conformation of the translocation pathway in the distinct states. Three out of the four states (1, 2, 4) reflect determined crystal structures: state 1 represents outward-open apo BtuCD (PDB code 1L7V), state 2 represents AMP-PNP-bound BtuCD(EQNC)–F reported here and state 4 represents the closed, asymmetric apo BtuCD–F complex (PDB codes 2Q19 and 4DBL). State 3 is hypothetical and based on the observed structure of Hi1470/1 and on biochemical crosslinking data of BtuCD–F. PBP, periplasmic binding protein.

METHODS SUMMARY

Protein expression and purification was performed as described previously in ref. 11. Wild-type and mutant BtuCD were purified in 0.1% *n*-dodecyl-*N*,*N*-dimethylamine-*N*-oxide (LDAO) and Cu^{2+}-induced disulphide crosslinking was performed after addition of BtuF. ATPase activity of BtuCD–F in 0.01% octaethylene glycol monododecyl ether ($C_{12}E_8$) and in liposomes was determined as described previously in ref. 39. Reconstitution of BtuCD and transport assays were performed as described previously in refs 17 and 40, with minor modifications. The binding of $[^{57}Co]$cyanocobalamin to BtuCD-containing proteoliposomes was assessed using a centrifugation assay. Proteoliposomes containing wild-type or mutant BtuCD were loaded with AMP-PNP by three freeze–thaw cycles and sonication. External nucleotide was removed by centrifugation and re-suspension, and thus produced proteoliposomes were incubated with BtuF-bound $[^{57}Co]$cyanocobalamin on ice for 40 min and pelleted by centrifugation. Supernatants were carefully removed and the radioactivity trapped in the proteoliposomes determined using a gamma counter. Non-specific binding of radiolabelled B_{12} was determined by using an excess of cold B_{12}.

For crystallization, BtuCD(EQNC)–F was purified in LDAO and oxidative crosslinking was performed using 1 mM $CuCl_2$. The detergent was exchanged for $C_{12}E_8$ and the crosslinked BtuCD(EQNC)–F complex was concentrated to 18–25 mg ml^{-1}. Crystals were obtained by vapour diffusion in sitting drops using a reservoir solution containing 20–30% PEG 400, 100 mM *N*-(2-acetamido)-iminodiacetic acid (ADA), pH 6.8, 100 mM sodium potassium citrate. X-ray data were collected at the X06SA beamline of the Swiss Light Source using the microdiffractometer set-up. Data were processed using Denzo/Scalepack (HKL Research). The structure was determined by molecular replacement and model building and refinement were performed using Coot[41] and PHENIX[42].

Full Methods and any associated references are available in the online version of the paper.

Received 26 March; accepted 26 July 2012.
Published online 23 September 2012.

1. Holland, I. B., Cole, S. P. C., Kuchler, K. & Higgins, C. F. *ABC Proteins: From Bacteria to Man* (Academic, 2003).
2. Davidson, A. L., Dassa, E., Orelle, C. & Chen, J. Structure, function, and evolution of bacterial ATP-binding cassette systems. *Microbiol. Mol. Biol. Rev.* **72,** 317–364 (2008).
3. Rees, D. C., Johnson, E. & Lewinson, O. ABC transporters: the power to change. *Nat. Rev. Mol. Cell Biol.* **10,** 218–227 (2009).
4. Hollenstein, K., Dawson, R. J. & Locher, K. P. Structure and mechanism of ABC transporter proteins. *Curr. Opin. Struct. Biol.* **17,** 412–418 (2007).
5. Erkens, G. B. *et al.* The structural basis of modularity in ECF-type ABC transporters. *Nature Struct. Mol. Biol.* **18,** 755–760 (2011).
6. Reynolds, P. R., Mottur, G. P. & Bradbeer, C. Transport of vitamin B12 in *Escherichia coli*. Some observations on the roles of the gene products of BtuC and TonB. *J. Biol. Chem.* **255,** 4313–4319 (1980).
7. DeVeaux, L. C. & Kadner, R. J. Transport of vitamin B12 in *Escherichia coli*: cloning of the btuCD region. *J. Bacteriol.* **162,** 888–896 (1985).
8. Pattey, T., Hernalsteens, J. P. & De Greve, H. Identification and molecular characterization of a novel *Salmonella enteritidis* pathogenicity islet encoding an ABC transporter. *Mol. Microbiol.* **33,** 791–805 (1999).
9. Janakiraman, A. & Slauch, J. M. The putative iron transport system SitABCD encoded on SPI1 is required for full virulence of *Salmonella typhimurium*. *Mol. Microbiol.* **35,** 1146–1155 (2000).
10. Locher, K. P., Lee, A. T. & Rees, D. C. The *E. coli* BtuCD structure: a framework for ABC transporter architecture and mechanism. *Science* **296,** 1091–1098 (2002).
11. Hvorup, R. N. *et al.* Asymmetry in the structure of the ABC transporter-binding protein complex BtuCD-BtuF. *Science* **317,** 1387–1390 (2007).
12. Korkhov, V. M., Mireku, S. A., Hvorup, R. N. & Locher, K. P. Asymmetric states of vitamin B12 transporter BtuCD are not discriminated by its cognate substrate binding protein BtuF. *FEBS Lett.* **586,** 972–976 (2012).
13. Dawson, R. J. & Locher, K. P. Structure of a bacterial multidrug ABC transporter. *Nature* **443,** 180–185 (2006).
14. Ward, A., Reyes, C. L., Yu, J., Roth, C. B. & Chang, G. Flexibility in the ABC transporter MsbA: alternating access with a twist. *Proc. Natl Acad. Sci. USA* **104,** 19005–19010 (2007).
15. Oldham, M. L., Khare, D., Quiocho, F. A., Davidson, A. L. & Chen, J. Crystal structure of a catalytic intermediate of the maltose transporter. *Nature* **450,** 515–521 (2007).
16. Oldham, M. L. & Chen, J. Crystal structure of the maltose transporter in a pretranslocation intermediate state. *Science* **332,** 1202–1205 (2011).
17. Borths, E. L., Poolman, B., Hvorup, R. N., Locher, K. P. & Rees, D. C. *In vitro* functional characterization of BtuCD-F, the *Escherichia coli* ABC transporter for vitamin B_{12} uptake. *Biochemistry* **44,** 16301–16309 (2005).
18. Lewinson, O., Lee, A. T., Locher, K. P. & Rees, D. C. A distinct mechanism for the ABC transporter BtuCD-BtuF revealed by the dynamics of complex formation. *Nature Struct. Mol. Biol.* **17,** 332–338 (2010).
19. Klein, J. S. & Lewinson, O. Bacterial ATP-driven transporters of transition metals: physiological roles, mechanisms of action, and roles in bacterial virulence. *Metallomics* **3,** 1098–1108 (2011).
20. Pinkett, H. W., Lee, A. T., Lum, P., Locher, K. P. & Rees, D. C. An inward-facing conformation of a putative metal-chelate-type ABC transporter. *Science* **315,** 373–377 (2007).
21. Smith, P. C. *et al.* ATP binding to the motor domain from an ABC transporter drives formation of a nucleotide sandwich dimer. *Mol. Cell* **10,** 139–149 (2002).
22. Zaitseva, J., Jenewein, S., Jumpertz, T., Holland, I. B. & Schmitt, L. H662 is the linchpin of ATP hydrolysis in the nucleotide-binding domain of the ABC transporter HlyB. *EMBO J.* **24,** 1901–1910 (2005).
23. Procko, E., Ferrin-O'Connell, I., Ng, S. L. & Gaudet, R. Distinct structural and functional properties of the ATPase sites in an asymmetric ABC transporter. *Mol. Cell* **24,** 51–62 (2006).
24. Dawson, R. J. & Locher, K. P. Structure of the multidrug ABC transporter Sav1866 from *Staphylococcus aureus* in complex with AMP–PNP. *FEBS Lett.* **581,** 935–938 (2007).
25. Newstead, S. *et al.* Insights into how nucleotide-binding domains power ABC transport. *Structure* **17,** 1213–1222 (2009).
26. Hopfner, K. P. *et al.* Structural biology of Rad50 ATPase: ATP-driven conformational control in DNA double-strand break repair and the ABC-ATPase superfamily. *Cell* **101,** 789–800 (2000).
27. Standfuss, J. *et al.* Crystal structure of a thermally stable rhodopsin mutant. *J. Mol. Biol.* **372,** 1179–1188 (2007).
28. Reyes, N., Ginter, C. & Boudker, O. Transport mechanism of a bacterial homologue of glutamate transporters. *Nature* **462,** 880–885 (2009).
29. Dawson, R. J., Hollenstein, K. & Locher, K. P. Uptake or extrusion: crystal structures of full ABC transporters suggest a common mechanism. *Mol. Microbiol.* **65,** 250–257 (2007).
30. Goetz, B. A., Perozo, E. & Locher, K. P. Distinct gate conformations of the ABC transporter BtuCD revealed by electron spin resonance spectroscopy and chemical cross-linking. *FEBS Lett.* **583,** 266–270 (2009).
31. Joseph, B., Jeschke, G., Goetz, B. A., Locher, K. P. & Bordignon, E. Transmembrane gate movements in the type II ATP-binding cassette (ABC) importer BtuCD-F during nucleotide cycle. *J. Biol. Chem.* **286,** 41008–41017 (2011).
32. Sonnhammer, E. L., Eddy, S. R. & Durbin, R. Pfam: a comprehensive database of protein domain families based on seed alignments. *Proteins* **28,** 405–420 (1997).
33. Borths, E. L., Locher, K. P., Lee, A. T. & Rees, D. C. The structure of *Escherichia coli* BtuF and binding to its cognate ATP binding cassette transporter. *Proc. Natl Acad. Sci. USA* **99,** 16642–16647 (2002).
34. Karpowich, N. K., Huang, H. H., Smith, P. C. & Hunt, J. F. Crystal structures of the BtuF periplasmic-binding protein for vitamin B12 suggest a functionally important reduction in protein mobility upon ligand binding. *J. Biol. Chem.* **278,** 8429–8434 (2003).
35. Jardetzky, O. Simple allosteric model for membrane pumps. *Nature* **211,** 969–970 (1966).
36. Hollenstein, K., Frei, D. C. & Locher, K. P. Structure of an ABC transporter in complex with its binding protein. *Nature* **446,** 213–216 (2007).
37. Locher, K. P. Review. Structure and mechanism of ATP-binding cassette transporters. *Phil. Trans. R. Soc. Lond. B* **364,** 239–245 (2009).
38. Patzlaff, J. S., van der Heide, T. & Poolman, B. The ATP/substrate stoichiometry of the ATP-binding cassette (ABC) transporter OpuA. *J. Biol. Chem.* **278,** 29546–29551 (2003).
39. Chifflet, S., Torriglia, A., Chiesa, R. & Tolosa, S. A method for the determination of inorganic phosphate in the presence of labile organic phosphate and high concentrations of protein: application to lens ATPases. *Anal. Biochem.* **168,** 1–4 (1988).
40. Geertsma, E. R., Nik Mahmood, N. A., Schuurman-Wolters, G. K. & Poolman, B. Membrane reconstitution of ABC transporters and assays of translocator function. *Nature Protocols* **3,** 256–266 (2008).
41. Emsley, P., Lohkamp, B., Scott, W. G. & Cowtan, K. Features and development of Coot. *Acta Crystallogr. D* **66,** 486–501 (2010).
42. Adams, P. D. *et al.* PHENIX: a comprehensive Python-based system for macromolecular structure solution. *Acta Crystallogr. D* **66,** 213–221 (2010).

Supplementary Information is available in the online version of the paper.

Acknowledgements We thank the beamline staff at the Swiss Light Source for assistance with data collection. We are grateful to R. Schibli and M. Badertscher for access to the gamma counter. This research was supported by the NCCR Structural Biology Zurich and Swiss National Science Foundation (grant SNF 31003A-131075/1).

Author Contributions V.M.K., S.A.M. and K.P.L. designed the experiments, V.M.K. and S.A.M. performed the experiments, V.M.K. and K.P.L. performed crystallographic calculations and all authors analysed the data. V.M.K. and K.P.L. wrote the manuscript.

Author Information Atomic coordinates and structure factors have been deposited at the Protein Data Bank under accession number 4FI3. The authors declare no competing financial interests. Reprints and permissions information is available at www.nature.com/reprints. Readers are welcome to comment on the online version of the paper. Correspondence and requests for materials should be addressed to K.P.L. (locher@mol.biol.ethz.ch).

LETTER

doi:10.1038/nature11473

Hard-X-ray emission lines from the decay of ^{44}Ti in the remnant of supernova 1987A

S. A. Grebenev[1], A. A. Lutovinov[1], S. S. Tsygankov[1,2,3,4] & C. Winkler[5]

It is assumed[1–3] that the radioactive decay of ^{44}Ti powers the infrared, optical and ultraviolet emission of supernova remnants after the complete decay of ^{56}Co and ^{57}Co (the isotopes that dominated the energy balance during the first three to four years after the explosion) until the beginning of active interaction of the ejecta with the surrounding matter. Simulations[4,5] show that the initial mass of ^{44}Ti synthesized in core-collapse supernovae is $(0.02–2.5)\times10^{-4}$ solar masses ($M_\odot$). Hard X-rays and γ-rays from the decay of this ^{44}Ti have been unambiguously observed from Cassiopeia A only[6–8], leading to the suggestion that values of the initial mass of ^{44}Ti near the upper bound of the predictions occur only in exceptional cases[9]. For the remnant of supernova 1987A[10,11], an upper limit to the initial mass of ^{44}Ti of $<10^{-3}M_\odot$ has been obtained from direct X-ray observations[12], and an estimate of $(1–2)\times10^{-4}M_\odot$ has been made from infrared light curves and ultraviolet spectra by complex and model-dependent computations[13–15]. Here we report observations of hard X-rays from the remnant of supernova 1987A in the narrow band containing two direct-escape lines of ^{44}Ti at 67.9 and 78.4 keV. The measured line fluxes imply that this decay provided sufficient energy to power the remnant at late times. We estimate that the initial mass of ^{44}Ti was $(3.1\pm0.8)\times10^{-4}M_\odot$, which is near the upper bound of theoretical predictions.

The only immediate way to determine the initial mass of ^{44}Ti (denoted M_{44}) in a supernova remnant is through its emission in the direct-escape lines at energies $E_i = 4.1$, 67.9, 78.4, 511 and 1,157 keV. This isotope decays according to the chain $^{44}\mathrm{Ti}\rightarrow{}^{44}\mathrm{Sc}\rightarrow{}^{44}\mathrm{Ca}$, with a characteristic time of $t_{44}\approx85.0\pm0.4$ yr (ref. 16). Photons in the three X-ray lines, namely 4.1, 67.9 and 78.4 keV, are emitted with efficiencies (average numbers of photons per decay) $W_i = 17.4\%$, 87.7% and 94.7% during the first stage of the decay, and photons in the γ-ray lines, namely 511 and 1,157 keV, are produced with $W_i = 188.8\%$ and 99.9% during the second very quick (∼5.7 h) stage. When the ejecta becomes transparent to hard-X-ray and γ-ray lines (typically at $t \gtrsim 20$ years), the corresponding fluxes can be estimated as

$$F_i = \frac{M_{44}W_i}{4\pi d^2 44 m_p t_{44}}\exp(-t/t_{44})$$

where d is the distance to the remnant and m_p is the proton mass. Measurements[6–8] of the 67.9-, 78.4- and 1,157-keV lines from Cas A have yielded the value $M_{44} = 1.6^{+0.6}_{-0.3}\times10^{-4}M_\odot$: tentative detections of the 1,157-keV line from the Vela Junior remnant[17] and the 4.1-keV line from the G1.9+0.3 remnant[18] have been also reported, but they are more uncertain. Assuming a value of M_{44} similar to that in Cas A, we can expect the photon fluxes in these lines from supernova remnant (SNR) 1987A ($d \approx 50$ kpc) about 23 yr after the explosion to be about $F_{68}\approx0.93F_{78}\approx0.48F_{68+78}\approx0.88F_{1,157}\approx0.46F_{511}\approx3.7\times10^{-6}$ photons cm^{-2} s^{-1}. We note that this remnant was the first for which the X-ray and γ-ray emission from the decay of ^{56}Co and ^{57}Co was detected[19–21].

The International Gamma-Ray Astrophysics Laboratory (INTEGRAL)[22] invested considerable observing time in trying to detect these lines from SNR 1987A. The first observation was carried out in 2003 soon after the launch of INTEGRAL. A number of important results have been obtained, including constraints on the luminosity of the stellar remnant[12], but the dedicated exposure (∼1.5 Ms) was insufficient for the detection of the ^{44}Ti lines. The next set of observations was carried out in 2010–11 with a total exposure of ∼4.5 Ms. Figure 1 presents the results of our analysis of all these data. Images of the SNR 1987A field obtained with the IBIS/ISGRI hard-X-ray telescope on board INTEGRAL are shown in three energy bands, 48–65, 65–82 and 82–99 keV, which encompass the ^{44}Ti lines at 67.9 and 78.4 keV. Two known sources, the black-hole binary LMC X-1 and the 50-ms Crab-like pulsar PSR B0540−69, are seen in all images. Remarkably, there is an obvious excess at the position of SNR 1987A, but only in the energy band that includes the ^{44}Ti lines. The location of the excess coincides within 4′ with that of SNR 1987A—a typical uncertainty for moderately bright sources (the angular resolution of IBIS is ∼12′ full-width at half-maximum (FWHM)).

The signal-to-noise ratio for this excess, $S/N \approx 4.1$ (related to the flux measured in both lines at once), corresponds to a rather small probability of detecting such an excess by chance, $P_0 \approx 2\times10^{-5}$. The probability of detecting a random excess with the same S/N ratio at an arbitrary position in the whole 29° × 29° IBIS field of view is much higher (it can be estimated as $mP_0 \approx 0.43$ where $m \approx (29°/12')^2 \approx 2.1\times10^4$ is the number of uncorrelated spots within the IBIS field of view; a 'spot' is the area of the sky image that can be occupied by a single source). In reality, the probability of detecting the ^{44}Ti lines by chance is even smaller than P_0, because significant excesses were simultaneously detected at the position of SNR 1987A in the images accumulated in the narrow energy bands 62.7–73.2 and 73.2–83.7 keV. Each of these bands contains one of the ^{44}Ti lines and they are nearly independent in terms of the energy resolution of IBIS/ISGRI, which is 8% at ∼70 keV (FWHM). The S/N ratios measured for SNR 1987A in these images are respectively 3.0 and 3.1, and the corresponding chance probabilities are $P_1 = 1.3\times10^{-3}$ and $P_2 = 9.7\times10^{-4}$. The combined probability of detecting the ^{44}Ti emission by chance is then equal to $P_1\times P_2 \approx 1.3\times10^{-6}$ (∼4.7σ).

The hard-X-ray spectrum obtained with IBIS/ISGRI from SNR 1987A is presented in Fig. 2. We fitted it using two lines of Gaussian shape with fixed centroid energies, equal widths and self-consistent (according to the ^{44}Ti emission efficiencies) normalizations. The flux measured in both lines at once, $F_{68+78}\approx(1.7\pm0.4)\times10^{-5}$ photons cm^{-2} s^{-1}, corresponds to a value for initial amount of synthesized ^{44}Ti of $M_{44}\approx(3.5\pm0.8)\times10^{-4}M_\odot$ (the uncertainty is purely statistical). This estimate can be slightly decreased if we assume the presence of some underlying continuum in the SNR 1987A spectrum—for example, in the form of a power law with a photon index of 2.1 (a Crab-like spectrum), which should describe the hard-X-ray emission well up to ∼80 keV (ref. 23). Its possible

[1]Space Research Institute, RAS, Profsoyuznaya 84/32, 117997 Moscow, Russia. [2]Max-Planck-Institut für Astrophysik, Karl-Schwarzschild-Strasse 1, D-85741 Garching, Germany. [3]FINCA, University of Turku, Vätsäläntie 20, FI-21500 Piikkiö, Finland. [4]Astronomy Division, Department of Physics, University of Oulu, FI-90014 Oulu, Finland. [5]European Space Agency, ESTEC, Keplerlaan 1, 2200 AG Noordwijk, The Netherlands.

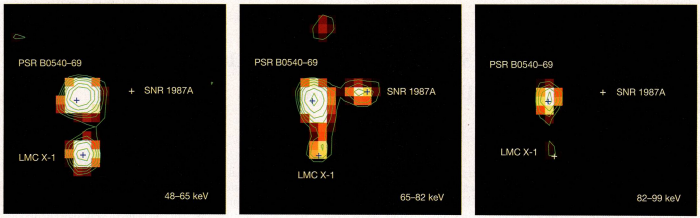

Figure 1 | Hard-X-ray images indicating the detection of ^{44}Ti emission lines from SNR 1987A. a–c, Maps of the signal-to-noise ratio (S/N) of the $1.5^\circ \times 1.5^\circ$ sky region around SNR 1987A accumulated in three energy bands with the IBIS/ISGRI telescope on board INTEGRAL during observations in 2003–2011 (~6.0 Ms of real exposure or ~4.2 Ms of dead-time-corrected exposure): 48–65 keV (**a**); 65–82 keV (**b**); 82–99 keV (**c**). The maps were reconstructed using standard techniques[27] with contours given at S/N levels of 2.7, 3.3, 3.9, 4.5, 5.4 and 6.3. Two well-known sources, PSR B0540–69 and LMC X-1, are seen bright in all three images, but SNR 1987A is confidently detected only in **b**, in the band that contains the 67.9- and 78.4-keV direct-escape lines of radioactive ^{44}Ti decaying inside the ejecta.

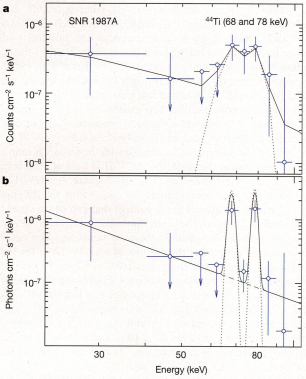

Figure 2 | Hard-X-ray spectra of SNR 1987A measured with IBIS/ISGRI in 2003–2011. a, The observed (count) spectrum together with the simulated response curves; **b**, the unfolded (photon) spectrum. In each panel, open circles show the spectra, dotted curves show the fit with two Gaussian lines at 67.9 and 78.4 keV of the radioactive decay of ^{44}Ti and solid curves show a similar fit which includes an additional power-law continuum with photon index $\alpha = 2.1$. Each data point (open circles) represents the result of flux measurement at the position of SNR 1987A in the image corresponding to the given energy band. It is expected that ^{44}Ti is produced inside the supernova core, which is expanding with velocity $v_{44} \leq 1{,}700\ \mathrm{km\ s^{-1}}$; thus, the internal width of the lines (that is, their width before smoothing due to the finite energy resolution of the instrument) is unlikely to exceed $\Delta E \approx 0.4$ keV. We kept the width of the line used for fitting fixed at 2.8 keV FWHM, which is half of the energy resolution of ISGRI (such a choice does not affect flux measurements in the internally narrow lines, thereby making it possible to work with the discrete response matrix of ISGRI). Upper limits are 1.7σ (90% confidence); error bars on the other points are 1σ.

contribution at 1 keV, $(8.5 \pm 3.2) \times 10^{-4}$ photons cm^{-2} s^{-1} keV^{-1}, coincides with the normalization of the non-thermal X-ray component in the SNR 1987A spectrum following the XMM-Newton observations in 2009[24]. With such a component (shown in Fig. 2 by a solid curve) the flux in the lines decreases to $F_{68+78} = (1.5 \pm 0.4) \times 10^{-5}$ photons cm^{-2} s^{-1}, which may be translated to $M_{44} \approx (3.1 \pm 0.8) \times 10^{-4} M_\odot$.

The SPI γ-ray spectrometer on board INTEGRAL observed SNR 1987A simultaneously with IBIS/ISGRI in the 511- and 1,157-keV lines of ^{44}Ti; however, the smaller effective area and presence of strong background features at 511 and ~1,100 keV preclude their confident detection. The photon spectrum measured in the 1,106–1,205-keV band is presented in Fig. 3. The solid curve shows the 1.7σ upper limit (90% confidence) for the flux in the 1,157-keV Gaussian line, namely $F_{1,157} \leq 2.6 \times 10^{-5}$ photons cm^{-2} s^{-1}. It can be converted to the limit

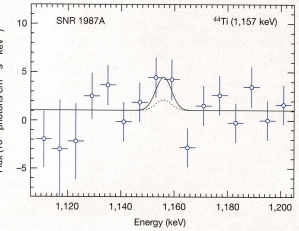

Figure 3 | γ-ray spectrum of SNR 1987A measured with SPI in 2003–2011. The spectrum (open circles) was reconstructed using standard techniques[28] near the highest-energy (1,157 keV) direct-escape line of ^{44}Ti. The solid curve shows the Gaussian line with the flux at its 1.7σ upper limit. Its centroid energy was redshifted by 1.1 keV to take into account the heliocentric velocity of SNR 1987A (285 km s^{-1}; ref. 29); its FWHM was taken to be 7.0 keV (internal width ~1,157 keV $\times$ $v_{44}/c \approx 6.5$ keV, corrected for the energy resolution of SPI, namely ~3 keV FWHM at 1.2 MeV; here $v_{44} \leq 1{,}700\ \mathrm{km\ s^{-1}}$ is the expansion velocity of the ejecta layer containing ^{44}Ti, and c is the velocity of light). The similar Gaussian line with total flux corresponding to the ^{44}Ti mass measured by IBIS/ISGRI in the hard-X-ray lines is shown by a dotted curve. Error bars, 1σ.

for the amount of ^{44}Ti, $M_{44} \lesssim 9 \times 10^{-4} M_{\odot}$. For comparison, the dotted curve in Fig. 3 shows the Gaussian line corresponding to the value of M_{44} measured with IBIS/ISGRI.

The detection of emission in the 67.9- and 78.4-keV lines allows us to measure directly the amount of radioactive ^{44}Ti synthesized during the explosion, that is, $M_{44} \approx (3.1 \pm 0.8) \times 10^{-4} M_{\odot}$. This amount formally exceeds by a factor of 1.5 to 2 the estimates based on theoretical simulations of explosive nucleosynthesis in supernova 1987A and on the infrared and ultraviolet data (although the discrepancy represents only one standard deviation). We note that ^{44}Ti may be produced either as a result of strong deviation from nuclear statistical equilibrium during the explosion (so-called α-rich freeze-out)[5] or as a result of incomplete Si-burning in a thin shell surrounding the region of main energy release[5,25]. In both cases, the simulations are not straightforward and many poorly known parameters (for example, the mass of the collapsed core, the maximum temperature and density behind the shock wave, the neutron excess and the composition of the pre-supernova interior) could affect the results. In this sense, the value of M_{44} that we report here may be useful for studying explosive nucleosynthesis and physical conditions reached during the shock-wave passage in the ejecta.

We note finally that the shock interaction of the ejecta and the surrounding matter is responsible for the synchrotron emission observed at present from SNR 1987A in the radio and soft-X-ray bands[26]. The reprocessing of this emission in the ejecta is contributing to the late-time optical–infrared emission of SNR 1987A[15]. Our estimate of the power-law component in the spectrum of SNR 1987A may be translated to a 2σ upper limit for the luminosity of synchrotron emission of $\sim 3 \times 10^{35}$ erg s^{-1} in the 20–60 keV band. This value can be also considered as the limit for the luminosity of the stellar remnant (pulsar or black hole) harboured inside the ejecta.

Received 23 November 2011; accepted 13 August 2012.

1. Suntzeff, N. B. The energy sources powering the late-time bolometric evolution of SN 1987A. *Astrophys. J.* **384,** L33–L36 (1992).
2. Clayton, D. D. *et al.* The ^{57}Co abundance in SN 1987A. *Astrophys. J.* **399,** L141–L144 (1992).
3. Fransson, C. & Kozma, C. The phase of SN 1987A: implication for the light curve. *Astrophys. J.* **408,** L25–L28 (1993).
4. Thielemann, F.-K., Hashimoto, M. & Nomoto, K. Explosive nucleosynthesis in SN 1987A. II. Composition, radioactivities, and the neutron star mass. *Astrophys. J.* **349,** 222–240 (1990).
5. Woosley, S. E. & Hoffman, R. D. ^{57}Co and ^{44}Ti production in SN 1987A. *Astrophys. J.* **368,** L31–L34 (1991).
6. Iyudin, A. F. *et al.* COMPTEL observations of ^{44}Ti gamma-ray line emission from Cas A. *Astron. Astrophys.* **284,** L1–L4 (1994).
7. Vink, J. *et al.* Detection of the 67.9 and 78.4 keV lines associated with the radioactive decay of ^{44}Ti in Cassiopeia A. *Astrophys. J.* **560,** L79–L82 (2001).
8. Renaud, M. *et al.* The signature of ^{44}Ti in Cassiopeia A revealed by IBIS/ISGRI on INTEGRAL. *Astrophys. J.* **647,** L41–L44 (2006).
9. The, L.-S. *et al.* Are ^{44}Ti-producing supernovae exceptional? *Astron. Astrophys.* **450,** 1037–1050 (2006).
10. Arnett, W. D., Bahcall, J. N., Kirshner, R. P. & Woosley, S. E. Supernova 1987A. *Annu. Rev. Astron. Astrophys.* **27,** 629–700 (1989).
11. Imshennik, V. S. & Nadezhin, D. K. Supernova 1987A in the Large Magellanic Cloud: observations and theory. *Sov. Sci. Rev. E* **8,** 1–147 (1989).
12. Shtykovskiy, P. E., Lutovinov, A. A., Gilfanov, M. R. & Sunyaev, R. A. Constraints on the luminosity of the central source in the SNR 1987A. *Astron. Lett.* **31,** 258–262 (2005).
13. Chugai, N. N., Chevalier, R. A., Kirshner, R. P. & Challis, P. M. Hubble Space Telescope spectrum of SN 1987A at an age of 8 years: radioactive luminescence of cool gas. *Astrophys. J.* **483,** 925–940 (1997).
14. Jerkstrand, A., Fransson, C. & Kozma, C. The ^{44}Ti-powered spectrum of SN 1987A. *Astron. Astrophys.* **530,** A45 (2011).
15. Larsson, J. *et al.* X-ray illumination of the ejecta of supernova 1987A. *Nature* **474,** 484–486 (2011).
16. Ahmad, I. *et al.* Improved measurement of the ^{44}Ti half-life from a 14-year long study. *Phys. Rev. C* **74,** 065803 (2006).
17. Iyudin, A. F. *et al.* Emission from ^{44}Ti associated with a previously unknown Galactic supernova. *Nature* **396,** 142–144 (1998).
18. Borkowski, K. J. *et al.* Radioactive scandium in the youngest Galactic supernova remnant G1.9+0.3. *Astrophys. J.* **724,** L161–L165 (2010).
19. Sunyaev, R. A. *et al.* Discovery of hard X-ray emission from supernova 1987A. *Nature* **330,** 227–229 (1987).
20. Matz, S. M. *et al.* Gamma-ray line emission from SN1987A. *Nature* **331,** 416–418 (1988).
21. Sunyaev, R. A. *et al.* Hard X-ray radiation from SN 1987A. Roentgen observatory observations from 1987 to 1989. *Sov. Astron. Lett.* **16,** 171–176 (1990).
22. Winkler, C. *et al.* The INTEGRAL mission. *Astron. Astrophys.* **411,** L1–L6 (2003).
23. Berezhko, E. G., Ksenofontov, L. T. & Völk, H. J. Expected gamma-ray emission of supernova remnant SN 1987A. *Astrophys. J.* **732,** 58 (2011).
24. Sturm, R., Haberl, F., Aschenbach, B. & Hasinger, G. High resolution X-ray spectroscopy of SN 1987A: monitoring with XMM-Newton. *Astron. Astrophys.* **515,** A5 (2010).
25. Thielemann, F.-K., Nomoto, K. & Hashimoto, M. Core-collapse supernovae and their ejecta. *Astrophys. J.* **460,** 408–436 (1996).
26. Park, S., Zhekov, S. A., Burrows, D. N. & McCray, R. SNR 1987A: opening the future by reaching the past. *Astrophys. J.* **634,** L73–L76 (2005).
27. Krivonos, R. *et al.* INTEGRAL/IBIS 7-year all-sky hard X-ray survey. I. Image reconstruction. *Astron. Astrophys.* **519,** A107 (2010).
28. Churazov, E. *et al.* Positron annihilation spectrum from the Galactic Centre region observed by SPI/INTEGRAL revisited: annihilation in a cooling ISM? *Mon. Not. R. Astron. Soc.* **411,** 1727–1743 (2011).
29. Measburn, J., Bryce, M. & Holloway, A. J. The kinematics of the rings around SN 1987A. *Astron. Astrophys.* **299,** L1–L4 (1995).

Acknowledgements We thank R. A. Sunyaev for reading the manuscript and for comments; V. S. Imshennik, D. K. Nadezhin and N. N. Chugai for discussions about aspects of the physics of the supernova 1987A explosion; R. A. Krivonos for information regarding the analysis of INTEGRAL/IBIS data; and M. Coe for allowing us access to his INTEGRAL data of the LMC observations (~1 Ms) before the end of the proprietary period. This work is based on data obtained through the Russian and European INTEGRAL science data centres, and was supported by grants RFBR-11-02-12285ofi-m-2011 and RAS-P20 'The origin, structure and evolution of objects of the Universe'.

Author Contributions S.A.G. was Principal Investigator of the proposal requesting INTEGRAL time (~3.5 Ms) to observe SNR 1987A; made a preliminary analysis of the IBIS/ISGRI data and detected an excess at the SNR 1987A position; and wrote a draft of the text. A.A.L. was Co-investigator of the proposal, and participated in the analysis of IBIS/SIGRI data and the verification of the result. S.S.T. carried out the analysis of SPI data. C.W. provided general support for this project and participated in its different aspects, and C.W. and A.A.L. contributed substantially to the final text. All authors discussed the results and their presentation.

Author Information Reprints and permissions information is available at www.nature.com/reprints. The authors declare no competing financial interests. Readers are welcome to comment on the online version of the paper. Correspondence and requests for materials should be addressed to S.A.G. (sergei@hea.iki.rssi.ru).

LETTER

doi:10.1038/nature11507

Zinc isotopic evidence for the origin of the Moon

Randal C. Paniello[1]*, James M. D. Day[2]* & Frédéric Moynier[1]

Volatile elements have a fundamental role in the evolution of planets. But how budgets of volatiles were set in planets, and the nature and extent of volatile-depletion of planetary bodies during the earliest stages of Solar System formation remain poorly understood[1,2]. The Moon is considered to be volatile-depleted and so it has been predicted that volatile loss should have fractionated stable isotopes of moderately volatile elements[3]. One such element, zinc, exhibits strong isotopic fractionation during volatilization in planetary rocks[4,5], but is hardly fractionated during terrestrial igneous processes[6], making it a powerful tracer of the volatile histories of planets. Here we present high-precision zinc isotopic and abundance data which show that lunar magmatic rocks are enriched in the heavy isotopes of zinc and have lower zinc concentrations than terrestrial or Martian igneous rocks. Conversely, Earth and Mars have broadly chondritic zinc isotopic compositions. We show that these variations represent large-scale evaporation of zinc, most probably in the aftermath of the Moon-forming event, rather than small-scale evaporation processes during volcanism. Our results therefore represent evidence for volatile depletion of the Moon through evaporation, and are consistent with a giant impact origin for the Earth and Moon.

The mode of origin of the Earth–Moon system that is most consistent with both physical and chemical constraints is through a giant impact between the proto-Earth and a Mars-sized body[7,8]. Depending on the Hf/W ratios of the bulk silicate Earth and Moon, this event is calculated to have occurred some 10–150 Myr after the formation of the first Solar System solids[9,10]. This highly energetic collision is predicted to have melted the impactor, with much of its core material being sequestered into Earth, while silicate material spun into an Earth-orbiting disk that later accreted to form the Moon[11,12]. Despite this cataclysmic mode of origin, and silicate vapour-phase models proposed to explain non-volatile stable isotope fractionation[13], to date there have been no collateral heavy isotope enrichments found for moderately volatile elements (for example, K) in lunar or terrestrial rocks[3].

Zinc is more volatile than both K and Cl (ref. 14) under solar nebula conditions and exhibits limited isotopic fractionation during igneous processes[6,15]. On Earth, and in primitive meteorites such as chondrites, variations of δ^{66}Zn (see Fig. 1 legend for definition) larger than 1‰ have only been observed in association with evaporation events[4,16]. Therefore any Zn isotopic fractionation, combined with differences in Zn concentrations between planetary igneous rocks from differentiated bodies such as Earth, the Moon and Mars, can reveal important differences in volatile depletion and replenishment events for these bodies.

Here we report high-precision Zn isotopic data for lunar basalts, Martian meteorites and terrestrial igneous rocks (see Methods, Supplementary Table 1 and Supplementary Information). Combined with previously published data for lunar rocks, terrestrial basalts, and carbonaceous, ordinary and enstatite chondrites, these new data allow us to establish the nature and extent of volatile depletion in Earth, the Moon and Mars. Fractionation between δ^{66}Zn and δ^{68}Zn is mass-dependent (Fig. 1), conforming to the expected mass-dependent mass-fractionation slope of two, hence only δ^{66}Zn is discussed here although ^{64}Zn, ^{66}Zn and ^{68}Zn intensities were precisely measured. Because terrestrial, Martian and lunar rocks all lie on the same mass-dependent mass-fractionation line, along with all classes of chondritic meteorites[16,17], this implies that Zn from all of the analysed samples evolved from a single, isotopically homogeneous reservoir. This relationship presumably reflects Zn isotope homogeneity in the solar nebula before terrestrial planet formation and, thus, that all reported isotopic variations are due to mass-dependent fractionations. Spallogenic effects or secondary neutron capture would lead to non-mass-dependent behaviour.

Low-Ti lunar mare basalts, including the mare basalt meteorite LaPaz Icefield (LAP) 02205, span a range in δ^{66}Zn of -3.13‰ to $+1.56$‰ (Fig. 2). Sample 12018 is isotopically light (δ^{66}Zn = -3.10 ± 0.03‰, $n = 2$) when compared with the other 11 low-Ti mare basalt samples measured. If sample 12018 is excluded from the comparison, we find a limited range in δ^{66}Zn for low-Ti mare basalts of $+0.84$‰ to $+1.56$‰, with a mean of $+1.31 \pm 0.13$‰. The mean δ^{66}Zn for low-Ti mare basalts is identical, within the uncertainties, to that derived for high-Ti mare basalts (δ^{66}Zn = $+1.39 \pm 0.31$‰; $n = 8$), and excluding the isotopically light sample 10017 (δ^{66}Zn = -5.42‰; ref. 18). Zinc concentrations in mare basalts range from 0.6 to 12 p.p.m., and are lower than concentrations of Zn measured in lunar soils (average = 25 p.p.m.), or in lunar pyroclastic glass beads (129 to 231 p.p.m.).

Martian SNC (Shergotty–Nakhla–Chassigny) meteorites span a limited range in δ^{66}Zn ($+0.13$‰ to $+0.35$‰), with an average δ^{66}Zn of $+0.25 \pm 0.03$‰ ($n = 10$) (Fig. 2). Measured values of δ^{66}Zn are slightly higher in Mg-rich shergottites (for example, Elephant Moraine 79001, Allan Hills (ALHA) 77005), than in more evolved shergottites, nakhlites and ALH 84001, which has the lowest δ^{66}Zn composition of Martian meteorites. The average Zn isotopic composition of Martian meteorites ($+0.25 \pm 0.03$‰) is identical to the

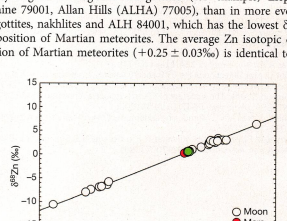

Figure 1 | δ^{68}Zn versus δ^{66}Zn for lunar, terrestrial and Martian samples. All of the samples fall on the mass-dependent mass-fractionation line of slope 2. Analytical uncertainties (2σ) are smaller than the data marker size. δ^{X}Zn = $[(^{X}\mathrm{Zn}/^{64}\mathrm{Zn})_{\mathrm{sample}}/(^{X}\mathrm{Zn}/^{64}\mathrm{Zn})_{\mathrm{JMC\ Lyon\ standard}} - 1] \times 1{,}000$, where $X = 66$ or 68.

[1]Department of Earth and Planetary Sciences and McDonnell Center for Space Sciences, Washington University, St Louis, Missouri 63130, USA. [2]Geosciences Research Division, Scripps Institution of Oceanography, La Jolla, California 92093-0244, USA.
*These authors contributed equally to this work.

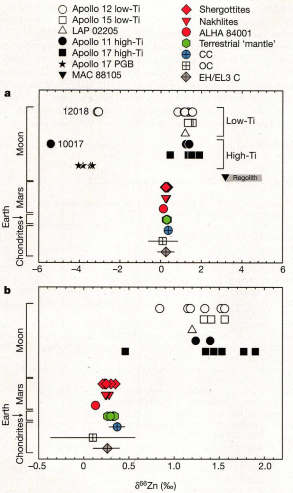

Figure 2 | Zinc isotopic composition of terrestrial, lunar, Martian and chondritic samples. CC, carbonaceous chondrite; OC, ordinary chondrite; EH/EL3 C, enstatite chondrite; PGB, pyroclastic glass beads. Data for chondrites and Earth represent an average of the different samples measured so far (refs 4, 6, 16, 17 and Methods); error bars, 2σ. For Martian meteorites and lunar samples, each data point represents one sample; 2σ on the δ^{66}Zn is 0.05‰.

average measured δ^{66}Zn composition of terrestrial igneous rocks (+0.27 ± 0.10‰). Zinc concentrations in shergottite meteorites are higher than for lunar mare basalts at between 41 and 130 p.p.m., and Zn concentrations in nakhlite meteorites lie within the range of shergottite meteorites at between 61.5 and 89 p.p.m. (Supplementary Information); Martian igneous rock Zn concentrations are therefore similar to terrestrial basaltic lavas (typically 70 to 100 p.p.m.; see the GERM database at http://earthref.org/GERM/).

The range of δ^{66}Zn values measured for lunar rocks are bracketed by the low δ^{66}Zn values of 12018 (−3.10 ± 0.03‰), 10017 (−5.42‰) and pyroclastic glass beads (−2.9‰ to −4.2‰), and by the high δ^{66}Zn values of MacAlpine Hills (MAC) 88105 (δ^{66}Zn +3.18‰) that we have measured. MAC 88105 is a lunar anorthositic regolith breccia meteorite[19], and has a δ^{66}Zn value similar to lunar regolith and soil samples from the Apollo 14, 15, 16 and 17 sites (+2.6‰ to +5.6‰) (Fig. 2). The high δ^{66}Zn of the regolith and soil samples reflect both sputtering effects and impact gardening of the lunar regolith[4,18], and donot represent primary magmatic compositions, so will not be considered further.

The isotopically light Zn values measured for 10017, 12018 and pyroclastic glass beads are not associated with petrology, mineralogy or cosmic ray exposure ages (see Supplementary Information). Previously, light Zn isotope enrichment in pyroclastic glass beads has been attributed to Zn evaporation during fire-fountaining, with condensation of isotopically light Zn on the surfaces of the ejected beads[4], as also proposed for ^{32}S enrichments[20]. These observations appear to be supported by increased Zn concentrations on the exterior portions of the pyroclastic glass beads, relative to interior portions (see, for example, refs 18, 21). Vapour loss should increase the δ^{66}Zn value of the residual magma and this process can be modelled assuming exhalative evaporation of Zn as $ZnCl_2$ on the Moon (for example, ref. 21); in contrast, Zn is evaporated as Zn^{2+} on Earth (see, for example, ref. 22) with essentially no fractionation between vapour and melt (that is, $\alpha = 1$; see below).

For volatilization of a liquid into a vacuum, fractionation between vapour and melt during Rayleigh distillation (differential distillation) leads to: $\delta_{final} = \delta_{initial} + [(1{,}000 + \delta_{initial})(F^{(\alpha-1)} - 1)]$, where F is the fraction of Zn remaining in the melt, and $\delta_{initial}$ and δ_{final} are the δ^{66}Zn of the initial and final liquid, respectively. The value of α can be approximated as the square-root of the mass number of the light isotopologue over that of the mass number of the heavy isotopologue of the vaporizing species; for $ZnCl_2$, the α value is 0.993. Extreme fractionations of Zn isotopes in the melt and associated vapour phase are computed for low remaining Zn in the melt fraction, and fractionations greater than those measured for lunar rocks can be calculated; such fractionations could possibly reflect incomplete evaporation to low melt fractions, or the competing effect of diffusion rates being insufficient to maintain isotopic homogeneity in melts on the Moon (this latter effect is exemplified as a lower α value of 0.999; Fig. 3). These calculations demonstrate that isotopically light vapour conforming to those measured in 12018, 10017 and pyroclastic glass beads can also be achieved by evaporation and re-deposition of $ZnCl_2$ from lunar melts. We therefore exclude these isotopically light samples from the planetary comparisons made between Earth, the Moon and Mars.

As demonstrated above, Zn isotopes can be strongly fractionated during high-temperature evaporative processes, and an important distinction to be made is how and when Zn isotopic fractionation occurred between different planetary basalts. For example, there is a clear difference in the Zn isotopic composition of lunar mare basalts relative to Martian and terrestrial rocks, but with no corresponding differences between terrestrial and Martian rocks. Zinc isotopic compositions for the majority of mare basalts (0.7–1.9‰) can be attained from between 10% to >90% evaporative loss of Zn using the different α values shown in Fig. 3, whereas terrestrial and Martian samples do not require significant evaporative loss. Therefore, the conditions responsible for Zn isotopic fractionation in lunar rocks do not appear to have existed, or have been overprinted, for terrestrial and Martian igneous rocks.

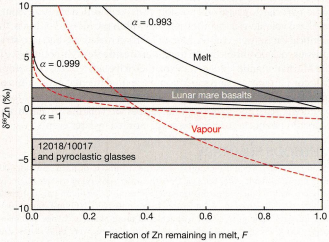

Figure 3 | Zinc isotopic fractionation as a function of the fraction of Zn remaining during open-system Rayleigh distillation. Results are shown for three different fractionation factors (α) between vapour and melt versus the range of Zn isotopic compositions measured for lunar samples. The two grey areas represent the δ^{66}Zn ranges of lunar mare basalts and the 12018/10017/ pyroclastic glasses.

There is strong evidence that 'planet-scale' evaporation of Zn during the Moon-forming event, rather than 'localized-scale' evaporation processes during volcanic eruption into hard vacuum (as suggested for Cl isotopes[23]), is responsible for the Zn isotopic character of mare basalts. The limited range in Zn isotopic compositions and systematically low Zn abundances for 19 of the 21 studied mare basalts, combined with the identical δ^{66}Zn values for low- and high-Ti mare basalts, support a large-scale planetary volatile depletion process. Low-Ti mare basalts are the predominant form of basalt exposed on the lunar surface (~90%; ref. 24), and their prevalence over high-Ti mare basalts is consistent with magma ocean crystallization models that indicate >78% of the lunar mantle would be dominated by olivine and orthopyroxene, whereas ilmenite-rich cumulates formed after 95% crystallization[25]. Thus, low-Ti mare basalts are often considered more representative of lunar mantle composition than high-Ti mare basalts (for example, ref. 26) and so the identical Zn isotopic composition of low- and high-Ti mare basalts points towards identical processes acting on both basalt types, despite conspicuously differing modes of origin and lunar mantle sources.

The evidence for extreme volatile depletion of the Moon from Zn isotopes and Zn abundance contrasts with the greater Zn abundance and broadly chondritic Zn isotopic compositions of Earth and Mars. The simplest explanation for these differences is that conditions during or after formation of the Moon may have led to more extensive volatile loss and Zn isotopic fractionation than experienced by Earth or Mars. The Zn isotopic homogeneity in lunar materials suggests that this would have to result from a large-scale process rather than from small-scale processes, or from hydrodynamic escape[15]. Given these lines of evidence, the most likely large-scale event to explain evaporative Zn isotopic fractionation would be a wholesale melting event associated with the formation of the Moon. The Zn isotope data therefore support existing dynamical models that argue for a giant impact event as the origin of the Earth–Moon system[11,12,27].

Whereas Zn abundances and isotopic compositions for Earth, the Moon and Mars provide compelling evidence for evaporative loss of volatile elements during lunar formation, they also provide important insights into planetary volatile inventories. In the case of the Moon, studies have shown that pyroclastic glass beads have elevated volatile contents, and contain water[28], suggesting a volatile-rich reservoir in the lunar interior. However, a study of Cl isotopes[23] suggests a volatile-depleted Moon, and our results for Zn isotopes suggest that the source regions of mare basalts are strongly volatile-depleted. In contrast with mare basalts, the elevated Zn abundances and light δ^{66}Zn values of lunar pyroclastic glasses are possibly consistent with derivation from a localized volatile-rich mantle reservoir within the Moon. For Mars, the identical Zn isotopic composition of Martian meteorites and terrestrial igneous rocks, combined with the elevated estimate of Zn abundance in the Martian mantle[29], suggests a volatile-rich planet. Thus, Zn isotopic data for Earth, Mars and the Moon place fundamental constraints on planetary accretion, pointing to evaporative loss during the Moon-forming event but that evaporative loss of volatiles in Earth and Mars did not occur, or has been over-printed by later events.

METHODS SUMMARY

Fragments (each of 500–1,000 mg) were leached in double-distilled water for 300 s in an ultrasonic bath. After removal from the water and drying, sample fragments were crushed to a homogeneous fine powder using an agate mortar and pestle. Samples were dissolved in a 4:1 mixture of ultra-pure HF/HNO_3 in Teflon beakers for four days. Zinc purification was achieved using anion-exchange chromatography using procedures described previously[4], with recovery of 99 ± 1%. Zinc was purified by anion-exchange chromatography. The samples were loaded in 1.5 M HBr on 0.25-ml AG-1X8 (200–400 mesh) ion-exchange columns and Zn was collected in 0.5 M HNO_3. The Zn fraction was further purified by eluting the samples twice on a 100-μl column with the same eluting solutions. Blanks were <10 ng and represent less than 1% of total measured Zn. Zinc isotopic compositions were measured on the ThermoElectron Neptune Plus multi collector-inductively coupled plasma-mass spectrometer housed at the Isotope Geochemistry Laboratory, Washington University, St Louis. The Faraday cups were positioned to collect masses 62, 63, 64, 65, 66, 67 and 68. Possible ^{64}Ni isobaric interferences were controlled and corrected by measuring the intensity of the ^{62}Ni peak. A solution containing 500 p.p.b. Zn in 0.1 M HNO_3 was prepared for isotopic analysis. Isotopic ratios of Zn in all samples were analysed using a spray chamber combined with a 100 μl min^{-1} PFA nebulizer. One block of 30 ratios, in which the integration time of one scan was 10 s, was measured for each sample. The background was corrected by subtracting the on-peak zero intensities from a blank solution. The instrumental mass bias was corrected by bracketing each of the samples with standards. External precision based on the JMC Lyon Zn standard was 0.05‰ per a.m.u. (2σ).

Full Methods and any associated references are available in the online version of the paper.

Received 1 September 2011; accepted 8 August 2012.

1. Albarède, F. Volatile accretion history of the terrestrial planets and dynamic implications. *Nature* **461,** 1227–1233 (2009).
2. Wood, B. J., Halliday, A. N., & Rehkämper, M. Volatile accretion of the Earth. *Nature* **467,** E6–E7 (2010).
3. Humayun, M. & Clayton, R. N. Potassium isotope cosmochemistry: genetic implications of volatile element depletion. *Geochim. Cosmochim. Acta* **59,** 2131–2148 (1995).
4. Moynier, F., Albarède, F. & Herzog, G. Isotopic composition of zinc, copper, and iron in lunar samples. *Geochim. Cosmochim. Acta* **70,** 6103–6117 (2006).
5. Moynier, F. et al. Isotopic fractionation of zinc in tektites. *Earth Planet. Sci. Lett.* **277,** 482–489 (2009).
6. Ben Othman, D., Luck, J. M., Bodinier, J. L., Arndt, N. & Albarede, F. Cu–Zn isotopic variations in the Earth's mantle. *Geochim. Cosmochim. Acta* **70,** A46 (2006).
7. Hartmann, W. & Davis, D. Satellite-sized planetesimals and lunar origin. *Icarus* **24,** 504–515 (1975).
8. Cameron, A. The origin of the Moon and the single impact hypothesis V. *Icarus* **126,** 126–137 (1997).
9. Yin, Q. et al. A short timescale for terrestrial planet formation from Hf-W chronometry of meteorites. *Nature* **418,** 949–952 (2002).
10. Touboul, M., Kleine, T., Bourdon, B., Palme, H. & Wieler, R. Late formation and prolonged differentiation of the Moon inferred from W isotopes in lunar metals. *Nature* **450,** 1206–1209 (2007).
11. Canup, R. Origin of the Moon in a giant impact near the end of the Earth's formation. *Nature* **412,** 708–712 (2001).
12. Ida, S., Canup, R. & Stewart, G. Lunar accretion from an impact-generated disk. *Nature* **389,** 353–357 (1997).
13. Pahlevan, K. & Stevenson, D. J. Equilibration in the aftermath of the lunar-forming giant impact. *Earth Planet. Sci. Lett.* **262,** 438–449 (2007).
14. Lodders, K. Solar System abundances and condensation temperatures of the elements. *Astrophys. J.* **591,** 1220–1247 (2003).
15. Albarède, F. The stable isotope geochemistry of copper and zinc. *Rev. Mineral. Geochem.* **55,** 409–427 (2004).
16. Moynier, F. et al. Nature of volatile depletion and genetic relations in enstatite chondrites and aubrites inferred from Zn isotopes. *Geochim. Cosmochim. Acta* **75,** 297–307 (2011).
17. Luck, J. M., Othman, D. B. & Albarède, F. Zn and Cu isotopic variations in chondrites and iron meteorites: early solar nebula reservoirs and parent-body processes. *Geochim. Cosmochim. Acta* **69,** 5351–5363 (2005).
18. Herzog, G. F., Moynier, F., Albarède, F. & Berezhnoy, A. A. Isotopic and elemental abundances of copper and zinc in lunar samples, Zagami, Pele's hairs, and a terrestrial basalt. *Geochim. Cosmochim. Acta* **73,** 5884–5904 (2009).
19. Neal, C. R., Taylor, L. A. & Schmitt, R. A. Paired lunar meteorites MAC88104 and MAC88105: a new "FAN" of lunar petrology. *Geochim. Cosmochim. Acta* **55,** 3037–3049 (1991).
20. Ding, T. P., Thode, H. G. & Rees, C. E. Sulphur content and sulphur isotope composition of orange and black glasses in Apollo 17 drive tube 74002/1. *Geochim. Cosmochim. Acta* **47,** 491–496 (1983).
21. Chou, C. L., Boynton, W. V., Sundberg, L. L. & Wasson, J. T. Volatiles on the surface of Apollo 15 green glass and trace-element distributions among Apollo 15 soils. *Lunar. Planet. Sci. Conf.* **6,** 1701–1727 (1975).
22. Symonds, R. B., Rose, W. I., Reed, M. H., Lichte, F. E. & Finnegan, D. L. Volatilization, transport and sublimation of metallic and non-metallic elements in high temperature gases at Merapi Volcano, Indonesia. *Geochim. Cosmochim. Acta* **51,** 2083–2101 (1987).
23. Sharp, Z., Shearer, C., McKeegan, K., Barnes, J. & Wand, Y. The chlorine isotope composition of the moon and implications for an anhydrous mantle. *Science* **329,** 1050–1053 (2010).
24. Giguere, T., Taylor, G. J., Hawke, B. & Lucey, P. G. The titanium contents of lunar mare basalts. *Meteorit. Planet. Sci.* **35,** 193–200 (2000).
25. Snyder, G. A., Taylor, L. A. & Neal, C. R. A chemical model for generating the sources of mare basalts: combined equilibrium and fractional crystallization of the lunar magmasphere. *Geochim. Cosmochim. Acta* **56,** 3809–3823 (1992).
26. Spicuzza, M. J., Day, J. M. D., Taylor, L. A. & Valley, J. W. Oxygen isotope constraints on the origin and differentiation of the Moon. *Earth Planet. Sci. Lett.* **253,** 254–265 (2007).
27. Reufer, A., Meier, M. M. M., Benz, W. & Wieler, R. A hit-and-run giant impact scenario. *Icarus* **221,** 296–299 (2012).

28. Hauri, E. H., Weinreich, T., Saal, A., Rutherford, M. & Van Orman, J. A. High pre-eruptive water contents preserved in lunar melt inclusions. *Science* **333**, 213–215 (2011).
29. Lodders, K. & Fegley, B. An oxygen isotope model for the composition of Mars. *Icarus* **126**, 373–394 (1997).

Supplementary Information is available in the online version of the paper.

Acknowledgements We thank the NASA curation staff, CAPTEM and the meteorite working group for samples. This work was supported by grants from the NASA LASER and Cosmochemistry programmes to F.M. (NNX09AM64G, NNX12AH70G) and J.M.D.D. (NNX11AG34G; NNX12AH75G) and from the Exobiology programme (NNX12AD88G) to F.M.

Author Contributions R.C.P. and F.M. performed zinc isotope and abundance measurements. All authors wrote the Letter and contributed to discussion and interpretation of results in the manuscript.

Author Information Reprints and permissions information is available at www.nature.com/reprints. The authors declare no competing financial interests. Readers are welcome to comment on the online version of the paper. Correspondence and requests for materials should be addressed to F.M. (moynier@levee.wustl.edu).

LETTER

doi:10.1038/nature11559

Circuit quantum electrodynamics with a spin qubit

K. D. Petersson[1], L. W. McFaul[1], M. D. Schroer[1], M. Jung[1], J. M. Taylor[2], A. A. Houck[3] & J. R. Petta[1,4]

Electron spins trapped in quantum dots have been proposed as basic building blocks of a future quantum processor[1–3]. Although fast, 180-picosecond, two-quantum-bit (two-qubit) operations can be realized using nearest-neighbour exchange coupling[4], a scalable, spin-based quantum computing architecture will almost certainly require long-range qubit interactions. Circuit quantum electrodynamics (cQED) allows spatially separated superconducting qubits to interact via a superconducting microwave cavity that acts as a 'quantum bus', making possible two-qubit entanglement and the implementation of simple quantum algorithms[5–7]. Here we combine the cQED architecture with spin qubits by coupling an indium arsenide nanowire double quantum dot to a superconducting cavity[8,9]. The architecture allows us to achieve a charge–cavity coupling rate of about 30 megahertz, consistent with coupling rates obtained in gallium arsenide quantum dots[10]. Furthermore, the strong spin–orbit interaction of indium arsenide allows us to drive spin rotations electrically with a local gate electrode, and the charge–cavity interaction provides a measurement of the resulting spin dynamics. Our results demonstrate how the cQED architecture can be used as a sensitive probe of single-spin physics and that a spin–cavity coupling rate of about one megahertz is feasible, presenting the possibility of long-range spin coupling via superconducting microwave cavities.

The weak magnetic moment of the electron makes it difficult to couple spin qubits that are separated by a large distance. Approaches to transferring spin information include physically shuttling electrons with surface acoustic waves or using exchange-coupled spin chains, both of which are experimentally challenging to realize[11–13]. An attractive alternative for realizing long-distance spin-qubit interactions is to interface spins with a superconducting microwave cavity in the cQED architecture. Unfortunately, direct coupling between a single spin magnetic dipole and the magnetic field of the cavity results in a spin–cavity coupling rate of $g_{s1}/2\pi \approx 10$ Hz, which is much too weak to be useful for quantum information processing[14]. Recent experiments have explored coupling ensembles of spins to superconducting resonators, with the large number of spins, $N_S \approx 10^{12}$, giving a $\sim N_S^{1/2}$ enhancement in the spin–cavity coupling rate[15–17].

Another approach to spin–cavity coupling relies on the spin–orbit interaction[18]. Spin–orbit coupling mixes spin and orbital degrees of freedom, resulting in spin states that have some orbital character, the spin–orbit doublets, $|\Uparrow\rangle$ and $|\Downarrow\rangle$. Although electron spin states cannot be coupled directly to an electric field, the spin–orbit interaction enables electrical control by perturbing the orbital component of the electron wavefunction. Fast, coherent electrical control of spin states in quantum dots has been demonstrated in InAs nanowires where the spin–orbit interaction strength is large[8,9,19]. The cQED architecture could be used to couple two distant InAs nanowire quantum dot spin qubits with the spin–orbit interaction enabling a significantly increased spin–cavity coupling rate, g_S (ref. 18). In this Letter, we take the first steps towards realizing this approach and couple the electric field of a high-quality-factor superconducting cavity to an InAs nanowire double quantum dot (DQD) device. We determine the charge–cavity coupling rate, g_C, for the molecular orbital states of a single excess charge in the DQD. Then, with each of the two quantum dots acting as a spin qubit, we perform fast electrical spin-state control followed by single spin read-out using the microwave cavity. Our results demonstrate that spin qubits, which require substantial magnetic fields for their operation, can be readily integrated into the superconducting cQED architecture and pave the way for long-range coupling of spin qubits via microwave cavities.

Our hybrid spin-qubit/superconducting device is shown in Fig. 1. We fabricate a half-wavelength superconducting Nb resonator (the cavity) with a resonance frequency of $f_0 = \omega_0/2\pi \approx 6.2$ GHz and quality factor of $Q \approx 2000$ (Supplementary Information, section 2). The amplitude and phase responses of the cavity are detected using a homodyne measurement with a microwave probe frequency f_R (ref. 5). We couple a single InAs nanowire spin qubit to the electric field generated by the cavity[18]. The qubit consists of a DQD defined in an InAs nanowire[8,9]. A series of Ti/Au depletion gates create a simple double-well confinement potential containing (N_L, N_R) electrons, where N_L and N_R are the numbers of electrons in

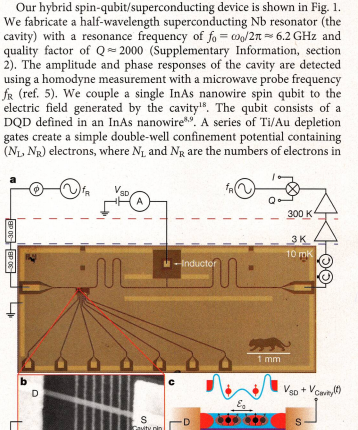

Figure 1 | Hybrid DQD/superconducting resonator device. a, Circuit schematic and micrograph of the hybrid device design. Transmission through the half-wavelength superconducting Nb resonator is measured using homodyne detection at a frequency f_R. Standard d.c. transport measurements are made possible by applying a source–drain bias, V_{SD}, to the DQD using a ~4-nH spiral inductor that is connected to the voltage node of the resonator[23]. See Supplementary Information, section 1, for further details. **b**, **c**, Scanning electron micrograph (**b**) and cross-sectional schematic view (**c**) of a typical nanowire DQD. The left and right barrier gates (B_L and B_R), left and right plunger gates (L and R), and middle gate (M) are biased to create a double-well potential within the nanowire. The drain contact of the nanowire, D, is grounded, and the source contact, S, is connected to an antinode of the resonator, oscillating at a voltage $V_{Cavity}(t)$. An a.c. voltage at a frequency f_G is applied to gate M to generate an oscillating electric field, $\mathcal{E}_0$.

[1]Department of Physics, Princeton University, Princeton, New Jersey 08544, USA. [2]Joint Quantum Institute/NIST, College Park, Maryland 20742, USA. [3]Department of Electrical Engineering, Princeton University, Princeton, New Jersey 08544, USA. [4]Princeton Institute for the Science and Technology of Materials (PRISM), Princeton University, Princeton, New Jersey 08544, USA.

the left- and right-hand dots, respectively. We tune the tunnel coupling, t_C, of the DQD by adjusting the voltage, V_M, on the middle barrier gate (M in Fig. 1b). A trapped electron in the DQD has an electric dipole moment of $d \approx 1{,}000ea_0$, where a_0 is the Bohr radius and e is the electronic charge.

For a spin in a single quantum dot, the calculation in ref. 18 predicts a spin–cavity coupling rate of $g_S = g_C(E_Z/\Delta E_0)(l/\lambda_{SO})$, where E_Z is the Zeeman splitting of the spin states, ΔE_0 is the orbital level spacing, l is the quantum dot size and λ_{SO} is the spin–orbit length, which characterizes the strength of the spin–orbit interaction[18]. Therefore, strong spin–cavity coupling requires two key components: a large charge–cavity coupling rate and a strong spin–orbit interaction. Charge–cavity coupling is achieved through the electric dipole interaction, as in experiments with superconducting qubits. An oscillating electric field, with amplitude $\mathcal{E}_0$, periodically displaces the electron quantum dot potential by a distance $r_0 = e\mathcal{E}_0 l^2/\Delta E_0$ (Fig. 1c), which is dependent on the quantum dot confinement as determined by ΔE_0 and l (ref. 19). To enhance the cavity electric field at the position of the DQD—and maximize the charge–cavity coupling rate—the source and drain contacts of the nanowire are connected directly to the voltage antinode and the ground of the resonator. In the presence of a strong spin–orbit interaction, the displacement of the electron can induce spin-state rotations at a rate $E_Z/\hbar \times r_0/\lambda_{SO}$, where $\hbar$ denotes Planck's constant divided by 2π, with the linear dependence in E_Z due to the Van Vleck zero-field cancellation of the spin–orbit term. Strong spin–orbit coupling is achieved using InAs, which has a short spin-orbit length, $\lambda_{SO} \approx 100$ nm (ref. 20).

We first characterize the interaction between an electron trapped in a DQD and the electric field of the cavity, demonstrating a 30-MHz charge–cavity coupling rate with this device architecture. We focus on the cavity response near the $(M, N+1) \leftrightarrow (M+1, N)$ interdot charge transition in the many-electron regime ($M \approx 20$, $N \approx 20$; Supplementary Information, section 3). The DQD forms a two-level 'artificial molecule' with an energy splitting of $\Omega = \sqrt{\varepsilon^2 + 4t_C^2}$, where ε is the detuning (Fig. 2a, top). Interdot tunnel coupling hybridizes the charge states around $\varepsilon = 0$, resulting in a tunnel splitting of $2t_C$. The detuning-dependent dipole moment of the DQD has an admittance that loads the cavity. We characterize the strength of the interaction by the a.c. susceptibility, χ (ref. 21; Fig. 2a, bottom).

A qualitative understanding of the coupling between the quantum dot and the cavity can be obtained by considering the relevant energy scales in the system. The single-dot charging energy, $E_C \approx 12$ meV, is much larger than the relevant photon energy, $hf_R \approx 25\,\mu$eV, and the cavity is largely unaffected by the DQD in Coulomb blockade. However, near interdot charge transitions (for example $(M, N+1) \leftrightarrow (M+1, N)$) or transitions with the source and drain electrodes (for example $(M, N) \leftrightarrow (M, N+1)$), the energy scales associated with the DQD are close to the cavity energy, and the cavity is damped, resulting in a phase shift in microwave transmission at the bare cavity frequency. In Fig. 2b, the DQD charge stability diagram is measured around the $(M, N+1) \leftrightarrow (M+1, N)$ transition by probing the phase response of the microwave cavity as a function of the gate voltages V_L and V_R (refs 10, 22).

Quantitative analysis of the cavity response requires a fully quantum mechanical model that accounts for photon exchange between the microwave field and the DQD[18,23]. In cavity QED, the pertinent interactions are those between an atom with transition frequency $\omega_a = \Omega/\hbar$ and the photon field of the cavity, characterized by the resonance frequency ω_0. The atom and cavity energy levels hybridize when the atom–cavity detuning, $\Delta = \omega_a - \omega_0$, is less than g_C, leading to the Jaynes–Cummings ladder of quantum states[24]. When the atom and cavity are detuned in the dispersive limit ($\Delta > g_C$), the cavity field exhibits a phase shift in microwave transmission at the bare cavity frequency that is given by $\phi = -\arctan(2g_C^2/\kappa\Delta)$, where κ is the cavity decay rate. In Fig. 2d, we plot the phase response of the cavity for several values of the interdot tunnel coupling (see Supplementary Information, section 4 for the magnitude response). We observe a sign change in the phase as the atom–cavity detuning, Δ, is varied from positive to negative values[5]. We fit the phase and magnitude data to a master equation model (Supplementary Information, section 6.1) using a best-fit value of $g_C/2\pi = 30$ MHz; an inhomogeneous broadening parameter, $\sigma_\varepsilon/h = 5.1$ GHz, to account for low-frequency charge noise; and a V_M-dependent tunnel coupling that ranges from $2t_C/h = 1.8$ to 7.0 GHz (Fig. 2c). The charge–cavity coupling rate extracted here compares favourably to values obtained using Cooper pair box qubits[3] ($g_C/2\pi \approx 6$ MHz), transmon qubits[25] ($g_C/2\pi \approx 100$ MHz) and many-electron GaAs quantum dots[10] ($g_C/2\pi \approx 50$ MHz).

We characterize the strength of the spin–orbit interaction by operating the device as a spin qubit (Fig. 3). For simplicity, we label the charge states (1, 1) and (0, 2) (ref. 4). The ground state with two electrons in the right quantum dot is the singlet $S(0, 2)$. At negative detuning, the electrons are separated in a (1, 1) charge state, and the four relevant spin states are $|\uparrow\uparrow\rangle$, $|\downarrow\downarrow\rangle$, $|\uparrow\downarrow\rangle$ and $|\downarrow\uparrow\rangle$ (ref. 8). The level diagram is similar to a GaAs singlet–triplet spin qubit, with a key difference being that the g-factors for the two spins can vary significantly[4] (Supplementary Information, section 6.2). Interdot tunnel coupling hybridizes the states with singlet character near $\varepsilon = 0$, and an external field results in Zeeman splitting, $E_Z = \tilde{g}\mu_B B$, of the spin states, where $\tilde{g}$ is the electronic g-factor, μ_B is the Bohr magneton and B is the magnetic field.

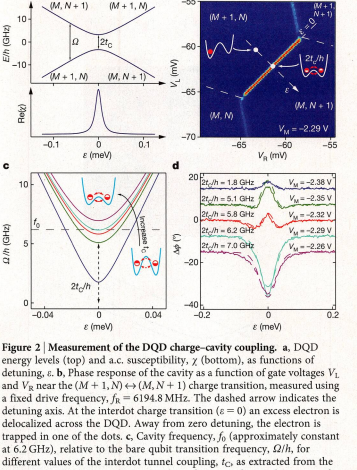

Figure 2 | Measurement of the DQD charge–cavity coupling. a, DQD energy levels (top) and a.c. susceptibility, χ (bottom), as functions of detuning, ε. **b**, Phase response of the cavity as a function of gate voltages V_L and V_R near the $(M+1, N) \leftrightarrow (M, N+1)$ charge transition, measured using a fixed drive frequency, $f_R = 6194.8$ MHz. The dashed arrow indicates the detuning axis. At the interdot charge transition ($\varepsilon = 0$) an excess electron is delocalized across the DQD. Away from zero detuning, the electron is trapped in one of the dots. **c**, Cavity frequency, f_0 (approximately constant at 6.2 GHz), relative to the bare qubit transition frequency, Ω/h, for different values of the interdot tunnel coupling, t_C, as extracted from the data in **d**. **d**, Phase response measured as a function of DQD detuning, ε, for a range of tunnel couplings, t_C, as set by V_M. The detuning is varied by sweeping V_R. Phase data are offset by 7.5° for clarity. Dashed lines are fits to the data, allowing the determination of the charge–cavity coupling rate, $g_C/2\pi \approx 30$ MHz (see main text).

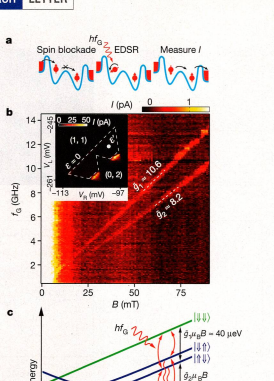

Figure 3 | Spin-qubit spectroscopy. a, The measurement cycle for spin-qubit spectroscopy. The DQD is put in either the $|\uparrow\uparrow\rangle$ or the $|\downarrow\downarrow\rangle$ spin configuration as a result of Pauli spin blockade. EDSR transitions lift this blockade, resulting in current flow through the device. **b**, Spin-qubit spectroscopy as a function of magnetic field, B, measured under Pauli blockade. Pauli blockade is lifted by EDSR driving when the microwave frequency is $f_G = \tilde{g}_i \mu_B B/h$, where $\tilde{g}_i$ ($i = 1, 2$) is the electronic g-factor of dot i. Inset, current through the DQD as a function of gate voltages V_L and V_R, with $V_{SD} = 2.5$ mV. Current is suppressed inside the dashed region owing to Pauli spin blockade. **c**, Energy levels of the spin–orbit qubit plotted as a function of ε. The data in **b** are acquired with $\varepsilon = \varepsilon' \approx 1$ meV.

Spin selection rules result in Pauli blockade at the two-electron transition, a key ingredient for spin preparation and measurement[8,8,26] (Fig. 3b, inset). For example, state $|\uparrow\uparrow\rangle$ cannot tunnel to S(0, 2) due to Pauli exclusion. Modulation of the confinement potential with a gate voltage results in spin–orbit-driven electric dipole spin resonance (EDSR) transitions that lift the Pauli blockade[8,19]. In Fig. 3b, we plot the current, I, through the DQD with $V_{SD} = 2.5$ meV and the gates tuned in Pauli blockade (Fig. 3b, white dot in inset). Hyperfine fields rapidly mix spin states when $E_Z = g\mu_B B < B_N$, where $B_N \approx 2$ mT is the hyperfine field[9]. At finite fields, the leakage current is non-zero when the a.c. driving frequency on the gate, f_G, satisfies the electron spin resonance condition $E_Z = hf_G$. We observe two resonance conditions corresponding to single spin rotations in the left- and right-hand quantum dots, with g-factors of 8.2 and 10.6 (ref. 8).

In cQED with superconducting qubits, measurements of the cavity response can be used for qubit read-out. For spin qubits, around $\varepsilon = 0$, the DQD has a spin-state-dependent dipole moment due to Pauli blockade that allows spin-state read-out via the superconducting cavity[27]. We combine quantum control of the spins using EDSR and cavity detection of single-spin dynamics using the pulse sequence shown in Fig. 4a, b. Starting with the spin qubit in state $|\uparrow\uparrow\rangle$, we pulse to negative detuning ($\varepsilon = \varepsilon' \approx -2$ meV) and apply a microwave burst of length τ_B to drive EDSR transitions. For example, an EDSR π-pulse will drive a spin transition from $|\uparrow\uparrow\rangle$ to $|\uparrow\downarrow\rangle$. The resulting spin state is probed by pulsing back to $\varepsilon = 0$ for a measurement time T_M. The cavity is most sensitive to charge dynamics near $\varepsilon = 0$ owing to the different a.c. susceptibilities of spin states $|\uparrow\downarrow\rangle$ and $|\uparrow\uparrow\rangle$ (Supplementary Information, section 6.3). In Fig. 4c, we plot the cavity phase shift as a function of f_G and B. We again observe two features that follow the standard spin resonance condition, consistent with the d.c. transport data in Fig. 4b. By varying T_M, we fit the measured phase response to theory and estimate a spin lifetime of $T_1 \approx 1$ μs (Fig. 4d). We anticipate that the relaxation time is detuning dependent, with longer spin relaxation times away from $\varepsilon = 0$ (ref. 28; Supplementary Information, section 5).

We demonstrate coherent control of the spin qubit and read-out via the cavity by varying the EDSR microwave burst length, τ_B. Figure 4e

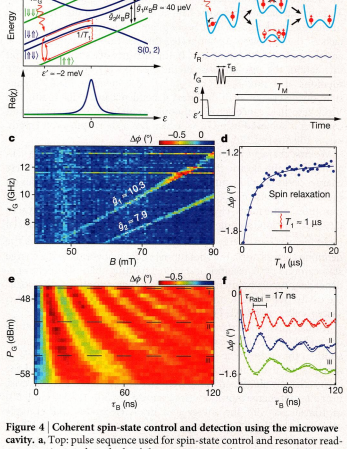

Figure 4 | Coherent spin-state control and detection using the microwave cavity. a, Top: pulse sequence used for spin-state control and resonator read-out, superimposed on the level diagram. Bottom: the a.c. susceptibility, χ, is dependent on the spin state of the DQD and allows for sensitive spin read-out via the microwave cavity. **b**, Pulse sequence used for spin-state control and resonator read-out. Starting in state $|\uparrow\uparrow\rangle$, an EDSR burst is applied at far detuning ($\varepsilon = \varepsilon' \approx -2$ meV). The resultant spin state is then measured at $\varepsilon = 0$ by probing the cavity transmission using a weak continuous tone of frequency f_R. **c**, Phase response of the cavity measured as a function of EDSR drive frequency, f_G, and external field, B, with $\tau_B = 100$ ns and $T_M = 850$ ns. EDSR transitions are observed in the phase response, in agreement with the d.c. transport data, with small differences in $\tilde{g}_1$ and $\tilde{g}_2$ attributable to the difference in sample tuning necessary to optimize the response. **d**, Measured phase shift as a function of T_M, with $\tau_B = 100$ ns, $B = 90$ mT and $f_G = 13.1$ GHz. A fit to theory yields a spin relaxation time of $T_1 \approx 1$ μs. **e**, Phase response of the cavity as a function of EDSR burst length, τ_B, and approximate driving power at the sample, P_G, for $B \approx 86$ mT, $f_G = 9.5$ GHz and $T_M = 1.75$ μs. Data were taken at a different sample tuning from data in **c**–**d**. **f**, Rabi oscillations at different powers, indicated by the dashed lines in **e**. The data are shifted in phase by 0.45° for clarity. The solid curves are fits to a power-law decay. We obtain a minimum Rabi period of $\tau_{Rabi} = 17$ ns (Supplementary Information, section 5).

shows the measured phase as a function of τ_B and the gate drive power, P_G. We observe Rabi oscillations with a minimum period of 17 ns (Fig. 4f), consistent with an EDSR driving mechanism[8]. These data show how the microwave field of the cavity is sensitive to the spin state of a single electron and that by using the cQED architecture quantum dot spin states may be coherently controlled and measured using microwave electric fields.

Long-distance coupling of spin qubits via a cavity will require a spin–cavity coupling rate that is larger than the cavity decay rate and the qubit decoherence rate. Although the method of spin-state readout that we have demonstrated does not imply spin–cavity coupling, on the basis of our results we can estimate the effective spin–cavity coupling strength. From our measurements, we find that $g_c/2\pi = 30\,\mathrm{MHz}$, $E_Z = 25\,\mu\mathrm{eV}$ and $\Delta E_0 = 1.7\,\mathrm{meV}$, which gives $l = \hbar/\sqrt{m^* \Delta E_0} \approx 40\,\mathrm{nm}$, where m^*, the effective electron mass in InAs, is 0.023 times the bare electron mass. Assuming a spin–orbit length of $\lambda_{SO} \approx 100\,\mathrm{nm}$ (ref. 20), we find a spin–cavity coupling rate of $g_s/2\pi \approx 0.2\,\mathrm{MHz}$, which is four orders of magnitude larger than the coupling rate g_{sk} that would be obtained by coupling a single spin to the magnetic field of a microwave cavity. This spin–cavity coupling rate could be readily increased to ~1 MHz by increasing the cavity resonance frequency to $f_0 = 15\,\mathrm{GHz}$ (which would proportionally increase both g_C and E_Z). Recent theoretical work also predicts an enhanced spin–cavity coupling for a single spin in a DQD biased at $\varepsilon = 0$ (ref. 29).

In addition to increasing the spin–cavity coupling rate, there is significant scope for improving the cavity decay rate and the qubit decoherence rate. Optimization of the resonator design will reduce the cavity decay rate to well below 1 MHz (Supplementary Information, section 2). There are several options for decreasing the qubit decoherence rate, which is at present limited by coupling to the nuclear spin bath. Dynamical decoupling has already been used to reduce the qubit decay rate to ~1 MHz in the InAs system[8]. InAs could also be replaced by nuclear-spin-free Ge/Si core–shell nanowires where hole spin–orbit coupling is predicted to be large[30]. On the basis of our results, we anticipate that the strong-coupling regime for single spins can be reached, eventually allowing spin qubits to be interconnected in a quantum bus architecture.

METHODS SUMMARY

Samples were fabricated on high-resistivity, (100)-orientation silicon wafers with 250 nm of dry thermal oxide. Superconducting resonators were formed by first sputter-depositing a 100-nm-thick Nb layer followed by a 30-nm Au film without breaking vacuum. The Au film was removed, except in regions that were later contacted by either wire bonds or electron-beam lithography (EBL), by a chemical wet etch in a solution of hydrochloric acid and nitric acid. A half-wavelength resonator was defined using photolithography followed by etching in a solution of hydrofluoric acid and nitric acid. Bottom gate electrode arrays were then patterned using EBL as described in further detail elsewhere[8,9]. A ~26-nm-thick layer of SiNx was deposited on top of the gate electrodes using plasma-enhanced chemical vapour deposition with the Nb film protected with photoresist, followed by lift-off and then further patterning using EBL and reactive ion etching. InAs nanowires were then dispersed from an ethanol solution, located using optical microscopy, and contacted using EBL.

The microwave response was measured using homodyne detection. A resonator tone with frequency f_R was applied through heavily attenuated, semi-rigid coaxial cables. The transmitted signal was first passed through two stages of isolators and then amplified using a ~3 K cryogenic amplifier. Room-temperature (~300 K) amplifiers provided additional gain of 55 dB, before the signal was demodulated using an *IQ* mixer. Following further amplification and filtering, we recorded the in-phase (*I*) and quadrature (*Q*) components to extract the amplitude and phase of the transmitted microwave signal. The EDSR microwave drive was provided by a vector microwave source, and detuning pulses were generated by an arbitrary-waveform generator. These were combined and coupled to gate M through an attenuated semi-rigid coaxial cable and a bias tee at the sample holder. The waveform generator also controlled the timing of the EDSR microwave bursts.

Received 4 June; accepted 24 August 2012.

1. Loss, D. & DiVincenzo, D. P. Quantum computation with quantum dots. *Phys. Rev. A* **57,** 120–126 (1998).
2. Koppens, F. H. L. *et al.* Driven coherent oscillations of a single electron spin in a quantum dot. *Nature* **442,** 766–771 (2006).
3. Hanson, R., Kouwenhoven, L. P., Petta, J. R., Tarucha, S. & Vandersypen, L. M. K. Spins in few-electron quantum dots. *Rev. Mod. Phys.* **79,** 1217–1265 (2007).
4. Petta, J. R. *et al.* Coherent manipulation of coupled electron spins in semiconductor quantum dots. *Science* **309,** 2180–2184 (2005).
5. Wallraff, A. *et al.* Strong coupling of a single photon to a superconducting qubit using circuit quantum electrodynamics. *Nature* **431,** 162–167 (2004).
6. Reed, M. D. *et al.* Realization of three-qubit quantum error correction with superconducting circuits. *Nature* **482,** 382–385 (2012).
7. Sillanpää, M. A., Park, J. I. & Simmonds, R. W. Coherent quantum state storage and transfer between two phase qubits via a resonant cavity. *Nature* **449,** 438–442 (2007).
8. Nadj-Perge, S., Frolov, S. M., Bakkers, E. & Kouwenhoven, L. P. Spin-orbit qubit in a semiconductor nanowire. *Nature* **468,** 1084–1087 (2010).
9. Schroer, M. D., Petersson, K. D., Jung, M. & Petta, J. R. Field tuning the g factor in InAs nanowire double quantum dots. *Phys. Rev. Lett.* **107,** 176811 (2011).
10. Frey, T. *et al.* Dipole coupling of a double quantum dot to a microwave resonator. *Phys. Rev. Lett.* **108,** 046807 (2012).
11. Hermelin, S. *et al.* Electrons surfing on a sound wave as a platform for quantum optics with flying electrons. *Nature* **477,** 435–438 (2011).
12. McNeil, R. P. G. *et al.* On-demand single-electron transfer between distant quantum dots. *Nature* **477,** 439–442 (2011).
13. Friesen, M., Biswas, A., Hu, X. & Lidar, D. Efficient multiqubit entanglement via a spin bus. *Phys. Rev. Lett.* **98,** 230503 (2007).
14. Imamoğlu, A. Cavity QED based on collective magnetic dipole coupling: spin ensembles as hybrid two-level systems. *Phys. Rev. Lett.* **102,** 083602 (2009).
15. Schuster, D. I. *et al.* High-cooperativity coupling of electron-spin ensembles to superconducting cavities. *Phys. Rev. Lett.* **105,** 140501 (2010).
16. Kubo, Y. *et al.* Hybrid quantum circuit with a superconducting qubit coupled to a spin ensemble. *Phys. Rev. Lett.* **107,** 220501 (2011).
17. Amsüss, R. *et al.* Cavity QED with magnetically coupled collective spin states. *Phys. Rev. Lett.* **107,** 060502 (2011).
18. Trif, M., Golovach, V. N. & Loss, D. Spin dynamics in InAs nanowire quantum dots coupled to a transmission line. *Phys. Rev. B* **77,** 045434 (2008).
19. Golovach, V. N., Borhani, M. & Loss, D. Electric-dipole-induced spin resonance in quantum dots. *Phys. Rev. B* **74,** 165319 (2006).
20. Fasth, C., Fuhrer, A., Samuelson, L. G., Vitaly, N. & Loss, D. Direct measurement of the spin-orbit interaction in a two-electron InAs nanowire quantum dot. *Phys. Rev. Lett.* **98,** 266801 (2007).
21. Blais, A., Huang, R. S., Wallraff, A., Girvin, S. M. & Schoelkopf, R. J. Cavity quantum electrodynamics for superconducting electrical circuits: an architecture for quantum computation. *Phys. Rev. A* **69,** 062320 (2004).
22. Delbecq, M. R. *et al.* Coupling a quantum dot, fermionic leads, and a microwave cavity on a chip. *Phys. Rev. Lett.* **107,** 256804 (2011).
23. Chen, F., Sirois, A. J., Simmonds, R. W. & Rimberg, A. J. Introduction of a dc bias into a high-Q superconducting microwave cavity. *Appl. Phys. Lett.* **98,** 132509 (2011).
24. Jaynes, E. T. & Cummings, F. W. Comparison of quantum and semiclassical radiation theories with application to the beam maser. *Proc. IEEE* **51,** 89–109 (1963).
25. Schuster, D. I. *et al.* Resolving photon number states in a superconducting circuit. *Nature* **445,** 515–518 (2007).
26. Ono, K., Austing, D. G., Tokura, Y. & Tarucha, S. Current rectification by Pauli exclusion in a weakly coupled double quantum dot system. *Science* **297,** 1313–1317 (2002).
27. Petersson, K. D. *et al.* Charge and spin state readout of a double quantum dot coupled to a resonator. *Nano Lett.* **10,** 2789–2793 (2010).
28. Johnson, A. C. *et al.* Triplet-singlet spin relaxation via nuclei in a double quantum dot. *Nature* **435,** 925–928 (2005).
29. Hu, X., Lu, Y. & Nori, F. Strong coupling of a spin qubit to a superconducting stripline cavity. *Phys. Rev. B* **86,** 035314 (2012).
30. Kloeffel, C., Trif, M. & Loss, D. Strong spin-orbit interaction and helical hole states in Ge/Si nanowires. *Phys. Rev. B* **84,** 195314 (2011).

Supplementary Information is available in the online version of the paper.

Acknowledgements Research at Princeton University was supported by the Alfred P. Sloan Foundation, the David and Lucile Packard Foundation, US Army Research Office grant W911NF-08-1-0189, DARPA QuEST award HR0011-09-1-0007 and the US National Science Foundation through the Princeton Center for Complex Materials (DMR-0819860) and CAREER award DMR-0846341. J.M.T. acknowledges support from ARO MURI award W911NF-09-1-0406.

Author Contributions K.D.P. fabricated the sample and performed the measurements. K.D.P., L.W.M. and A.A.H. developed the resonator fabrication and measurement processes. K.D.P., M.D.S. and M.J. developed the nanowire device fabrication processes. M.D.S. grew the nanowires. J.M.T. developed the theory for the experiment. K.D.P. and J.R.P. wrote the paper with input from the other authors. J.R.P. planned the experiment.

Author Information Reprints and permissions information is available at www.nature.com/reprints. The authors declare no competing financial interests. Readers are welcome to comment on the online version of the paper. Correspondence and requests for materials should be addressed to J.R.P. (petta@princeton.edu).

LETTER

doi:10.1038/nature11563

Bonding and structure of a reconstructed (001) surface of $SrTiO_3$ from TEM

Guo-zhen Zhu[1], Guillaume Radtke[2]† & Gianluigi A. Botton[1]

The determination of the atomic structure and the retrieval of information about reconstruction and bonding of metal oxide surfaces is challenging owing to the highly defective structure and insulating properties of these surfaces. Transmission electron microscopy (TEM) offers extremely high spatial resolution (less than one ångström) and the ability to provide systematic information from both real and reciprocal space. However, very few TEM studies[1–3] have been carried out on surfaces because the information from the bulk dominates the very weak signals originating from surfaces. Here we report an experimental approach to extract surface information effectively from a thickness series of electron energy-loss spectra containing different weights of surface signals, using a wedge-shaped sample. Using the (001) surface of the technologically important compound strontium titanate, $SrTiO_3$ (refs 4–6), as a model system for validation, our method shows that surface spectra are sensitive to the atomic reconstruction and indicate bonding and crystal-field changes surrounding the surface Ti cations. Very good agreement can be achieved between the experimental surface spectra and crystal-field multiplet calculations based on the proposed atomic surface structure optimized by density functional calculations[3]. The distorted TiO_{6-x} units indicated by the proposed model can be viewed directly in our high-resolution scanning TEM images. We suggest that this approach be used as a general method to extract valuable spectroscopic information from surface atoms in parallel with high-resolution images in TEM.

Crystals of $SrTiO_3$ attract continuing interest owing to the novel structure and properties exhibited at their surfaces, which have led to their widespread application as standard substrates for the epitaxial growth of functional thin films and nanostructures[4,5] and as the preferred photocatalyst to split water for solar hydrogen generation[6]. In spite of the technological and scientific importance of $SrTiO_3$ crystal surfaces, the understanding of their atomic and electronic structure is still incomplete owing to the limitation of high-resolution characterization[7]. The use of TEM to provide high-resolution information on oxide surfaces is rather limited, as the key pioneering studies have been carried out mainly through diffraction techniques, which only provide the projected information of the reconstructed surfaces in reciprocal space[2,3]. A set of plausible atomic models can be matched to observed quantitative diffraction measurements; however, the ubiquitous 'phase problem'—that is, the difficulty of measuring the crystallographic phase from a diffraction pattern and hence determining the atomic structure—remains a fundamental hurdle for this approach. Additionally, quantitative interpretation of diffraction patterns requires precisely calibrated detectors and consideration of any nonlinearity in measurements of intensities; it also requires either strict control of the thickness of specimens in order to minimize dynamical effects of diffraction, or full consideration of such effects with a precise knowledge of the thickness. Alternatively, direct imaging of reconstructed surface patterns with atomic-level resolution can be achieved through profile imaging[8] and plan-view imaging techniques[1]. The former requires the reconstructed surface to be parallel to the electron beam, but has an obvious limitation in that only a projection of the structure is observed. In the latter, when the reconstructed surface is normal to the electron beam, both surface and bulk information are integrated and recorded as plan-view images or spectra. However, correctly extracting the relatively weak surface signal from images or spectra containing dominant bulk information has been a major restriction of the technique.

Although extracting the surface signal from a single plan-view acquisition (image or spectrum) may thus seem unconventional, a series of plan-view acquisitions can in principle be used to retrieve the missing surface information. Our approach requires each acquisition to contain a different contributing weight of surface signal; we achieve this by using a wedge-shaped sample, with each acquisition from a region of different thickness. In order to separate 'blind' (that is, unknown and difficult to detect directly) surface signals from bulk signals, many algorithms, such as principal component analysis (PCA) and independent component analysis (ICA)[9], can be used. Even so, the representative 'signals' output by these methods are linear combinations of the real components—in our case, the blind surface and bulk signals. The direct separation of blind signals is not trivial because of the indeterminate equations, in which both the sources and their mixing weights are unknown. However, if the mixing weights of surface and bulk signals can be precisely estimated from quantitative local thickness measurements, the extraction of blind surface signals becomes potentially straightforward, more reliable and relatively simple. In this Letter, we demonstrate the application of high-resolution electron energy-loss spectroscopy (EELS) and TEM, with in-plane and edge view imaging modes, to extract both experimental structural and spectroscopic information on the valence state and local crystal field of atoms on the surface of a $SrTiO_3$ crystal. The results show that valuable spectroscopic information can be deduced about surface atoms even in TEM.

A TEM wedge specimen with an air-stable surface, exhibiting a $c(4 \times 2)$ reconstruction, was prepared using the approach described in ref. 3. The extra reflections in the diffraction pattern (primitive cells are marked in Fig. 1) reveal the existence of a rearrangement of surface atoms with 4×2 unit cells consistent with the literature[3]. Using scanning TEM high-angle annular dark-field (STEM-HAADF) imaging, uniform contrast from individual approximately rectangular domains is visible. These uniform-intensity domains correspond to terraces of constant thickness separated by steps. The lateral dimensions of the terraces vary from 30 to 100 nm in length along <100> directions, and imply that the local thickness is constant within these regions. Samples prepared by the same approach have been shown to exhibit terraces of uniform thickness, as demonstrated from secondary electron images[10].

Acquisition of EEL spectra in transmission mode from these terraces, over areas of different sample thickness, provides a series of measurements where the surface and bulk components can be varied

[1]Canadian Centre for Electron Microscopy and Department of Materials Science and Engineering, McMaster University, 1280 Main Street West, Ontario L8S 4M1, Canada. [2]IM2NP UMR 7334 CNRS, Faculté des Sciences de Saint-Jérôme, case 262, Aix-Marseille University, F-13397 Marseille Cedex 20, France. †Present address: Université Pierre et Marie Curie – Paris 6, IMPMC-CNRS UMR 7590 Campus Jussieu, 4 place Jussieu, F-75252 Paris Cedex 05, France.

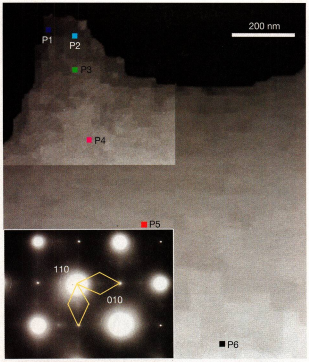

Figure 1 | STEM-HAADF image and diffraction pattern of a ~[001] oriented $SrTiO_3$ sample. Main figure, STEM-HAADF image showing locations P1–P6 where EEL spectra were taken. Inset, diffraction pattern of the c(4 × 2) surface reconstruction. Yellow lines in the diffraction pattern highlight the extra reflections arising from the surface reconstruction. The pattern was intentionally overexposed to reveal the weak surface reconstruction reflections.

in a controlled fashion. Spectra from regions labelled P1–P6 in the HAADF image (Fig. 1) thus provide a constant contribution of the surface signal at each thickness while the bulk component varies systematically. The Ti $L_{2,3}$-edge and O K-edge EEL spectra were acquired and used to probe the surface electronic structure, for the following two reasons. First, their major peaks are sensitive to local physical and chemical environments, including oxidation state and crystal-field effects[11]. Second, EEL signal intensity is linearly related to the local thickness of the specimen under the single inelastic electron scattering condition in the samples studied in our work. In fact, the thickness in the thickest area (point P6), 60 nm, is considerably smaller than the total inelastic mean free path (>100 nm). As a consequence, multiple inelastic scattering is negligible in this region of the spectrum, as also demonstrated by the very similar shape of all spectra in the series for the energy window corresponding to the continuum past the edge threshold (Fig. 2a).

To optimize background subtraction and thus obtain the ionization edge alone, a Matlab code, based on maximum likelihood estimation[12], was developed and applied to original data sets, providing unbiased and minimum mean-square error estimates of all parameters for the power-law background model. Furthermore, extraction of the surface signal from the EEL spectra demands accurate alignment of all recorded spectra along the energy-loss axis and re-normalization of the signal on account of changing thickness and the variation in incident electron beam intensity over time. Under the reasonable assumption of dominating bulk signals, EEL spectra were precisely aligned in relation to major features of the bulk EEL spectra. Additionally, EEL spectra were normalized to the continuum past the edge (about 15 eV above the threshold), which is largely insensitive to bonding variations but proportional only to the number of atoms excited by the electron beam and to the electron beam current within the single inelastic scattering regime.

As shown in Fig. 2a, the Ti $L_{2,3}$-edge spectra show a decrease in intensity with decreasing thickness, particularly of the e_g peaks. This could indicate that, based on the Pearson ratio[13], the bonding configuration of Ti gradually changes as the sample thickness decreases (and the surface component increases relative to the bulk). (The Pearson ratio quantitatively describes the intensity ratio between the white-line intensity (the sum of e_g and t_{2g} intensities over the L_3 and L_2 lines) and the continuum past the edge as a monitor of 3*d*-orbital occupancy.) This is accompanied by a slight broadening of the spectral features, as evidenced by the broader tails of the e_g and t_{2g} features. This broadening is associated with an increase of the surface signal weight. Additionally, the position of the e_g peaks exhibits a red-shift with decreasing thickness, probably owing to the surface re-organization of ionic positions. These changes in the edge shape, so close to the edge

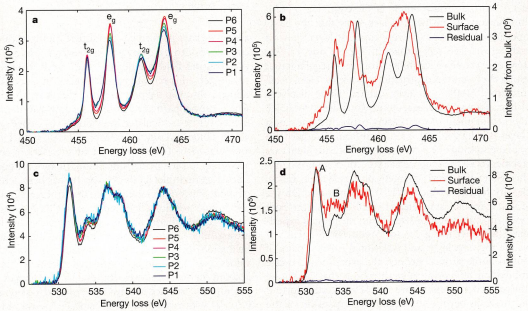

Figure 2 | Experimental spectra. a, **c**, Ti $L_{2,3}$-edge (**a**) and O K-edge (**c**) EEL spectra at the positions P1–P6 marked in Fig. 1. Panels **b** and **d** show fits to **a** and **c** respectively; surface and bulk EELS spectra were fitted using the linear least-squares method, and coefficients for the surface spectra were deduced in line with the thickness measurements.

threshold, cannot be attributed to multiple inelastic scattering effects. As shown below, all these spectral changes are due to the surface reorganization of the atoms.

The experimental Ti $L_{2,3}$-edge spectra were treated as linear combinations of surface and bulk signals as a result of an effective single inelastic electron scattering condition. Precise evaluation of the local thickness associated with individual EEL spectra was achieved through two complementary techniques: low-loss EEL spectra for thick regions (~>40 nm) and position-averaged convergent beam electron diffraction (PACBED)[14] images for very thin samples. A linear least-squares fitting method was used to extract the surface and bulk signals for individual energy intervals where the coefficients were deduced from the thickness measurements. As shown in Fig. 2b, the isolated bulk signal fits the standard $SrTiO_3$ Ti $L_{2,3}$-edge spectrum perfectly, whereas the isolated surface component has significantly broader features that could either be attributed to a reduction of Ti (ref. 15; that is, Ti^{3+}) or/and changes in the coordination[16] of the Ti^{4+} cations located at the surface. Similar conclusions can be drawn when applying this numerical decomposition to the O K-edge spectra. As expected, the isolated bulk component completely matches the standard $SrTiO_3$ O K-edge spectrum. The isolated surface signal is consistent with the bonding of titanium and strontium cations with oxygen anions (Fig. 2d). The titanium–oxygen hybridization, reflected by the broadening of peak A (corresponding to the unoccupied Ti 3*d* (t_{2g})–O 2*p* bands) and peak B (representing the unoccupied Ti 3*d* (e_g)–O 2*p* bands), suggests strong distortions of the Ti coordination octahedra. These distortions are possibly due to a reduction of the local coordination, or to more prominent O–O interaction[17], or both. It should be noted that the shape of the surface spectra shows features also consistent with the appearance of oxygen vacancies, as demonstrated in ref. 18.

To gain insight into the origin of these spectral changes, we investigated the local atomic arrangement of the reconstructed surface using atomic-resolution HAADF (*Z*-contrast) images at the edge of the thin foil; we made the reasonable assumption that the pattern formed at the edge of the TEM foil should be exactly the same as the pattern on the surface (these would be exactly the same {001} crystallographic planes). Surface steps with heights corresponding to one unit cell are visible at the edge of the foil (Fig. 3a, b). Although the length of these steps appears to be inconsistent with the dimension of the terraces seen from the plan-view image, this length and the step height of terraces vary as a result of different inclination angles with respect to the {100} planes, which is 1.4° on the surface but 9° at the edge. The STEM-HAADF and simultaneous bright-field images show that the Ti–O columns are unperturbed, whereas the very topmost layer shows a significant rearrangement (see red arrows in Fig. 3a and b). We observed that a few (edge) atoms have shifted from their regular lattice positions, suggesting that some reconstruction, up to few atoms high above the reconstructed (100) monolayer, occurs. These displaced atoms are also visible as rows (individual atoms would not be visible). The experimental measurement of the spacing between the topmost and subsurface layer is roughly 2.4 ± 0.1 Å, significantly larger than the normal (100) plane spacing of 1.9 Å. The above measurements are in fairly good agreement with the proposed atomic model of Erdman *et al.* (type B)[3], this being the more energetically favourable model deduced from density functional theory (DFT) calculations. On the basis of the same atomic model[3], simulated HAADF images from both [010] and [001] view directions are consistent with the present experimental profile image (as shown in Fig. 3c), which shows a row of tightly spaced atoms on the topmost layer and occasional isolated pairs of atoms sticking out from the surface. Because the experimental image represents a combination of viewing edge directions that cannot be identified from the projection alone, we are unable to ascertain further information from imaging beyond extracting the expansion of the subsurface layer.

To elucidate the origin of the peculiar Ti $L_{2,3}$ spectral features observed at the surface on the basis of the structural model proposed

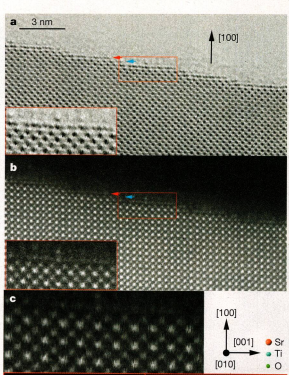

Figure 3 | High-resolution images. a–c, Bright-field (**a**) and HAADF (**b** and **c**) images of the typical edge of the surface-reconstructed sample. Red and blue arrows identify the topmost atomic layer and the subsurface Ti–O atomic layer, respectively. Inset, higher-magnification view of the edge of the sample. **d**, **e**, Simulated HAADF images using the multi-slice method[21] with view directions of [010] (**d**) and [001] (**e**); simulations were performed using data from a detailed atomic model[3]. The simulation box contains 11,520 atoms within a supercell of 31 Å × 31 Å × 312 Å. Fairly good agreement is achieved between the simulation (**d** and **e**) and the experimental HAADF image after applying singular value decomposition (**c**) to reduce the noise and highlight the surface features.

above, we have performed crystal-field multiplet calculations using the code developed by Uldry and co-workers[19]. In contrast with conventional ligand-field multiplets[20] with freely controllable crystal-field parameters, this recent approach relies on a crystal field constructed numerically from the positions and charges of the surrounding atoms, which proves particularly useful for low-symmetry surface environments. We have calculated individual Ti $L_{2,3}$-edge spectra of all inequivalent Ti ions present in the topmost (two such Ti inequivalent sites) and subsurface (three inequivalent sites) layers, and summed them according to their actual stoichiometric ratio. A good convergence of calculated multiplet levels and spectra has been achieved with clusters of about 500 ions generated from the structural model, including both the atomic positions deduced from DFT[3] and the related empirical bond valence charge also deduced from this model[3]. Scaling of the intra-atomic Coulomb interactions, spin–orbit coupling and crystal-field strength have been kept constant and equal to the $SrTiO_3$ bulk values[19], so these can be considered parameter-free calculations. To account for the core-level shift due to the changes in coordination[16], the topmost surface spectra were shifted down in energy (around 0.65 eV) with respect to the subsurface spectra. As shown in Fig. 4a, Ti $L_{2,3}$-edge spectra keep their bulk spectroscopic signature, even from the monolayer closest to the reconstructed surface, which confirms the origin of the experimental surface EELS. It is also worth noticing that

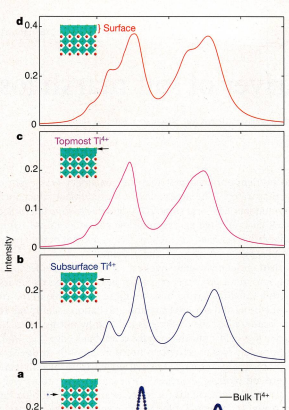

Figure 4 | Crystal-field multiplet calculations of Ti $L_{2,3}$-edge EEL spectra. The structural model used to generate the crystal field is the same as that used in Fig. 3. **a**, Calculated EEL spectrum for the ideal bulk and the closest monolayer to the reconstructed surfaces. **b**–**d**, Calculated EEL spectra for the subsurface layer (**b**), the topmost layer (**c**), and surfaces (**d**) containing all non-equivalent Ti surface ions.

the separate topmost spectra (Fig. 4c) show strong similarities with experimental signatures of five-fold-coordinated Ti^{4+} (ref. 16). Very good agreement is achieved between the simulated surface spectrum (Fig. 4d) based on a $c(4\times2)$ recontruction[3] and the numerically extracted experimental surface component. This suggests that the experimental surface signature can be interpreted as that of Ti^{4+} in both five-fold and six-fold coordination polyhedra, taking account of local distortions and changes in bond ionicities, and is not due to a simple reduction of this cation.

We have provided an experimental spectroscopic signature of the change of crystal field and bonding of titanium cations located in the subsurface and topmost layer of the reconstructed (001) $SrTiO_3$ surface, together with a high-resolution profile image of the reconstructed surfaces; these surfaces consist of distorted TiO_6 octahedra and distorted square-pyramidal TiO_5, which are generally consistent with the most stable atomic structure reported from DFT simulations[3]. More importantly, we have reported here an experimental approach to accessing the surface electronic structure of insulating oxides, by combining structural information on displacements as provided by atomic resolution images, which together provide a comprehensive and complementary picture of the bonding and reconstruction of the surface.

Received 10 December 2011; accepted 4 September 2012.
Published online 10 October 2012.

1. Erdman, N. *et al.* The structure and chemistry of the TiO_2-rich surface of $SrTiO_3$(001). *Nature* **419,** 55–58 (2002).
2. Enterkin, J. A. *et al.* A homologous series of structures on the surface of $SrTiO_3$(110). *Nature Mater.* **9,** 245–248 (2010).
3. Erdman, N. *et al.* Surface structures of $SrTiO_3$ (001): a TiO_2-rich reconstruction with a c(4 x 2) unit cell. *J. Am. Chem. Soc.* **125,** 10050–10056 (2003).
4. Jiang, Q. D. & Zegenhagen, J. $SrTiO_3$(001) surfaces and growth of ultra-thin $GdBa_2Cu_3O_{7-\delta}$ films studied by LEED/AES and UHV-STM. *Surf. Sci.* **338,** L882–L888 (1995).
5. Silly, F. & Castell, M. R. Growth of Ag icosahedral nanocrystals on a $SrTiO_3$(001) support. *Appl. Phys. Lett.* **87,** 213107 (2005).
6. Domen, K., Kudo, A. & Onishi, T. Mechanism of photocatalytic decomposition of water into H_2 and O_2 over NiO-$SrTiO_3$. *J. Catal.* **102,** 92–98 (1986).
7. Castell, M. R. Scanning tunneling microscopy of reconstructions on the $SrTiO_3$(001) surface. *Surf. Sci.* **505,** 1–13 (2002).
8. Cowley, J. M. Electron microscopy of surface structure. *Prog. Surf. Sci.* **21,** 209–250 (1986).
9. Comon, P. & Jutten, C. (eds) *Handbook of Blind Source Separation* (Academic, 2010).
10. Inada, H. *et al.* Atomic imaging using secondary electrons in a scanning transmission electron microscope: experimental observations and possible mechanisms. *Ultramicroscopy* **111,** 865–876 (2011).
11. Radtke, G. & Botton, G. A. in *Scanning Transmission Electron Microscopy* (eds Pennycook, S. J. & Nellist, P. D.) 207–245 (Springer, 2011).
12. Unser, M., Ellis, J. R., Pun, T. & Eden, M. Optimal background estimation in EELS. *J. Microsc.* **145,** 245–256 (1987).
13. Pearson, D. H., Ahn, C. C. & Fultz, B. White lines and d-electron occupancies for the 3d and 4d transition metals. *Phys. Rev. B* **47,** 8471–8478 (1993).
14. LeBeau, J. M., Findlay, S. D., Allen, L. J. & Stemmer, S. Position averaged convergent beam electron diffraction: theory and applications. *Ultramicroscopy* **110,** 118–125 (2010).
15. Sefat, A. S., Amow, G., Wu, M.-Y., Botton, G. A. & Greedan, J. E. High-resolution EELS study of the vacancy-doped metal/insulator system, $Nd_{1-x}TiO_{3-}$, $x = 0$ to 0.33. *J. Solid State Chem.* **178,** 1008–1016 (2005).
16. Höche, T., Grodzicki, M., Heyroth, F. & van Aken, P. A. Assessment of transition-metal coordination in glasses by electron energy-loss spectroscopy. *Phys. Rev. B* **72,** 205111 (2005).
17. de Groot, F. M. F. *et al.* Oxygen 1s X-ray absorption of tetravalent titanium oxides: a comparison with single-particle calculations. *Phys. Rev. B* **48,** 2074–2080 (1993).
18. Muller, D. A., Nakagawa, N., Ohtomo, A., Grazul, J. L. & Hwang, H. Y. Atomic-scale imaging of nanoengineered oxygen vacancy profiles in $SrTiO_3$. *Nature* **430,** 657–661 (2004).
19. Uldry, A., Vernay, F. & Delley, B. Systematic computation of crystal-field multiplets for X-ray core spectroscopies. *Phys. Rev. B* **85,** 125133 (2012).
20. Cowan, R. D. *The Theory of Atomic Structure and Spectra* (Univ. California Press, 1981).
21. Kirkland, E. J. *Advanced Computing in Electron Microscopy* Illustrated edn, 289 (Springer, 2010).

Supplementary Information is available in the online version of the paper.

Acknowledgements We are grateful to NSERC for Discovery and Strategic Grants supporting this work. The microscopy was carried out at the Canadian Centre for Electron Microscopy, a National Facility supported by NSERC and McMaster University. G.-z.Z. thanks J. LeBeau for help and advice on the simulations of the PACBEDs.

Author Contributions G.-z.Z. and G.A.B. conceived and are responsible for the experiments, performed the simulations and jointly wrote the paper. G.R. contributed to the analysis of crystal-field multiplet simulations and the final version of this manuscript.

Author Information Reprints and permissions information is available at www.nature.com/reprints. The authors declare no competing financial interests. Readers are welcome to comment on the online version of the paper. Correspondence and requests for materials should be addressed to G.A.B. (gbotton@mcmaster.ca).

LETTER

doi:10.1038/nature11533

Coastal eutrophication as a driver of salt marsh loss

Linda A. Deegan[1], David Samuel Johnson[1,2], R. Scott Warren[3], Bruce J. Peterson[1], John W. Fleeger[4], Sergio Fagherazzi[5] & Wilfred M. Wollheim[6]

Salt marshes are highly productive coastal wetlands that provide important ecosystem services such as storm protection for coastal cities, nutrient removal and carbon sequestration. Despite protective measures, however, worldwide losses of these ecosystems have accelerated in recent decades[1]. Here we present data from a nine-year whole-ecosystem nutrient-enrichment experiment. Our study demonstrates that nutrient enrichment, a global problem for coastal ecosystems[2–4], can be a driver of salt marsh loss. We show that nutrient levels commonly associated with coastal eutrophication increased above-ground leaf biomass, decreased the dense, below-ground biomass of bank-stabilizing roots, and increased microbial decomposition of organic matter. Alterations in these key ecosystem properties reduced geomorphic stability, resulting in creek-bank collapse with significant areas of creek-bank marsh converted to unvegetated mud. This pattern of marsh loss parallels observations for anthropogenically nutrient-enriched marshes worldwide, with creek-edge and bay-edge marsh evolving into mudflats and wider creeks[5–7]. Our work suggests that current nutrient loading rates to many coastal ecosystems have overwhelmed the capacity of marshes to remove nitrogen without deleterious effects. Projected increases in nitrogen flux to the coast, related to increased fertilizer use required to feed an expanding human population, may rapidly result in a coastal landscape with less marsh, which would reduce the capacity of coastal regions to provide important ecological and economic services.

An accelerated global nitrogen cycle[1–3] has greatly increased the flow of reactive nitrogen (primarily as NO_3^-) from land to coastal marine ecosystems, causing harmful algal blooms, hypoxia and fisheries losses[5,8]. Salt marshes occupy a critical interface between the land and the sea, where they provide important ecological and economic services, such as nutrient removal, storm protection for coastal cities and carbon sequestration, and habitats for numerous species of fish, birds and invertebrates. It is thought that salt marshes can protect coastal bays by removing land-derived nutrients[9,10], a conclusion based on measures of whole-system nutrient budgets[11,12] and plot-level experiments in which added nutrients were transformed into greater above-ground plant production (primarily cordgrass *Spartina* spp.) or denitrified[4]. Globally between a quarter and half of the area of the world's tidal marshes has been lost, and although multiple factors (sea-level rise, development, loss of sediment supply) are known to contribute to marsh loss[1], in some locations the drivers remain unexplained. Understanding the mechanisms underlying the continued loss of this ecologically and economically important ecosystem is a global priority.

Here we present an ecosystem-level experimental approach to understanding how the intertwined responses of plant biomass allocation, microbial decomposition, and geomorphic stability to coastal nutrient enrichment may drive salt marsh loss. For nine years (2004–2012) we have enriched multiple whole-ecosystem marsh landscapes to nutrient levels that correspond to moderately-to-highly eutrophic waters by adding dissolved nutrients to flooding tidal water[13]. Approximately 50%–60% of the added NO_3^- was processed (assimilated or denitrified) in the nutrient-enriched systems; the remainder was exported in ebbing tidal water[12]. The large scale of this experiment, which included creeks, mudflats, tall-form smooth cordgrass (*Spartina alterniflora*) at the creek-channel edge and saltmeadow cordgrass (*S. patens*) in the high marsh, has revealed interactions that would not be apparent from plot-level experiments in individual habitats.

Nutrient enrichment may invoke a series of positive feedbacks by altering ecosystem processes that affect below-ground dynamics and creek-bank stability, leaving marshes more susceptible to the erosive forces of storms and sea-level rise and gravitational slumping. In less than a decade, a cascade of changes induced by nutrient enrichment resulted in loss of low marsh along the creek-bank edge (Fig. 1a–f) and a corresponding loss of ecosystem function. Smooth cordgrass along the creek-bank edge responded to nutrient enrichment with increased above-ground biomass expressed as heavier, taller shoots (Fig. 2a), lower structural compounds (decrease of about half in foliar lignin), and increased N content (Table 1), with response ratios comparable to plot-level nutrient-enrichment experiments[4,14]. Increased plant height coupled with less structural tissue caused more extensive areas of smooth cordgrass to fall over (lodge)—a well-known response to over-fertilizing grasses[15]. Using permanent transects and high-precision global positioning system (GPS) mapping across the elevation gradient, we found no evidence (D.S.J., R.S.W. and L.A.D., manuscript in preparation) for the hypothesized shift in the up-elevation boundary between *S. alterniflora* and *S. patens* in response to nutrients[15]. In nutrient-enriched marshes, smooth cordgrass allocated less photosyntate to nutrient-gathering roots and storage rhizomes, resulting in a third less total below-ground biomass and a lower root:shoot ratio (Fig. 2b, c). Two smooth cordgrass growth attributes, a highly plastic above-ground/below-ground allocation[16] and foliar uptake of NO_3^- (ref. 17), contribute to the reductions in total below-ground biomass observed in nutrient-enriched marshes.

The continuous availability of high NO_3^- in the water and more decomposable marsh grass detritus (due to higher N content and lower lignin) increased decomposition rates (Table 1). Whole-ecosystem nitrate removal was 40 times higher in the nutrient-enriched marsh and was primarily attributable to microbial use of the added NO_3^- to decompose organic matter[12]. Potential denitrification—an indicator of anaerobic microbial decomposition using nitrate as an electron acceptor with the end product being N_2 gas—increased 1.7-fold in creek bank sediments, while litter respiration—a measure of aerobic microbial decomposition—almost doubled (1.9-fold). Denitrification is the highest energy-yielding decomposition process in anoxic marsh sediments and is favoured in the presence of high nitrate[5]. Accelerated decomposition increased the fraction of fine detrital organic matter, with 65% of the cores from nutrient-enriched creeks having a higher percentage of fine organic matter. As a result, the fine-grained, less-consolidated creek banks retained more water at low tide (Fig. 2d).

The combination of fewer roots and rhizomes, drag by tidal currents on lodged plants, more decomposed organic matter and higher water content undermines the structural integrity of the creek bank such that the effects of standard physical forces become enhanced. Loss of roots

[1]The Ecosystems Center, Marine Biological Laboratory, 7 MBL Street, Woods Hole, Massachusetts 02543, USA. [2]Department of Biology, Sewanee University of the South, 735 University Avenue, Sewanee, Tennessee 37383, USA. [3]Department of Botany, Connecticut College, 270 Mohegan Avenue, New London, Connecticut 06320, USA. [4]Department of Biological Sciences, Louisiana State University, Baton Rouge, Louisiana 70803, USA. [5]Department of Earth and Environment, Boston University, 675 Commonwealth Avenue, Boston, Massachusetts 02215, USA. [6]Department of Natural Resources and the Environment, University of New Hampshire, 8 College Road, Durham, New Hampshire 03824, USA.

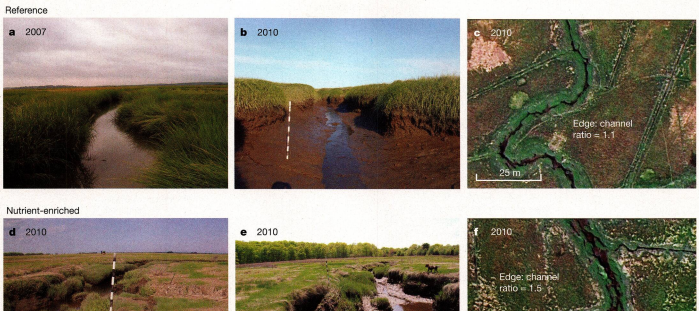

Figure 1 | Comparison photos of the marshes from the ecosystem nutrient-enrichment experiment. **a**–**c**, Reference. **d**–**f**, Nutrient-enriched. Photo credits: **a**, **b**, **d** and **e**, L.A.D.; **c** and **f**, Google Earth (19 June 2010 image, copyright 2012 Google).

and rhizomes (which bind sediments and provide drainage macropores) and loss of large organic matter particles (which form air pockets that can help drain creek banks) both contribute to increased creek-bank water content[18]. The higher pore water pressure in the bank reduces the frictional shear strength of the soil and increases the sliding force by adding weight to the creek bank[19]. At low water, the weight of the saturated bank exceeds the cohesive forces holding it together, the top of the bank cracks and creek-bank sections slide downward by gravitational slumping[18]. The structural failure of the creek edge implies that tidal forces, which under non-eutrophic conditions can be withstood, overcome the lowered cohesive strength of the nutrient-enriched bank habitat. Cracks developed over time with nutrient enrichment (Fig. 2d), and after seven years of enrichment, there were more (threefold) and longer (4.5-fold) fractures at the top of the bank parallel to the creek (Table 1) and large blocks of low marsh slumped into the creek (Fig. 2e). Without the buttressing edge of low marsh, high-marsh turf sheared from the sediment at the base of the active rooting layer creating 'toupees' that slid down slope into creek channels (Supplementary Fig. 1), tripling the area of bare mud over time (Table 1). The average width of the band of tall *S. alterniflora* along the creek edge decreased from approximately 3 m to approximately 2 m wide and became highly reticulated (Fig. 1c versus Fig. 1f; Fig. 2e) in nutrient-enriched systems. High-resolution measurements of channel cross-sections between the fifth and eighth years of enrichment indicate that the maximum erosion rate of creek banks was 0.2 m^3 per year per metre of channel length. Loss of marsh along creek channel edges contrasts sharply with models that suggest that higher above-ground plant biomass in response to nutrients would in turn trap more sediment and stabilize marsh edges relative to sea-level rise[20]. Slumping and cracking leads to a positive feedback, with increased infiltration by nutrient-rich water into sediments, which stimulate microbial decomposition of peat and further weakens sediments. As nutrient-enriched creek banks collapse and retreat, channels widen, increasing the unvegetated intertidal area at the expense of vegetated marsh.

The generality of our whole-ecosystem experiment is supported by extensive process work in small marsh fertilization plots and in anthropogenically nutrient-enriched estuaries. From Louisiana to Nova Scotia, nutrient enrichment has been shown consistently to increase above-ground plant biomass[14,16], mainly to decrease but sometimes not to change below-ground biomass[16,21–24] and to increase decomposition[22,25]. The decomposition response might be expected to be stronger in Northern marshes with a high percentage of organic matter, but because the organic content of our creek-bank marsh is in the middle of the range for Atlantic coast marshes (Methods), we expect our decomposition response is typical. The combination of root loss and increased decomposition can decrease soil strength[26]. The development of cracks that lead to marsh loss has been approximately linear over the initial nine-years; however, this is a process that will play out over decades. Much uncertainty remains about whether this process of marsh loss is self-limiting, because creek banks may eventually be stabilized by the decrease in slope steepness from slumps, or self-reinforcing owing to fractures facilitating the seepage of nutrient-enriched water into the bank and stimulating decomposition. Other local environmental factors (such as tidal range, temperature and sediment deposition) may modify the effects of nutrients on ecosystem processes. Therefore, understanding the whole-ecosystem response to nutrient loading across broad environmental gradients and longer timescales requires more experimental ecosystem-level studies.

Many salt marshes may be at risk, because nutrient fluxes to the coast have increased worldwide, with the largest increases in N flux occurring at coastlines with large areas of intertidal marshland in the temperate zones of eastern North America, Europe and eastern China (Fig. 3a). A recent survey[27] documented 415 eutrophic coastal systems of concern worldwide, and found that only 13 systems were in recovery. There is evidence that salt-marsh loss in Europe[5] and along the Atlantic coast of the United States [6,7] may be driven, in part, by anthropogenic nutrient enrichment. Along Long Island Sound, Connecticut, USA, coincident with increased total N in runoff, several marshes lost 27%–54% of their low marsh (Fig. 3b), but very little high marsh, resulting

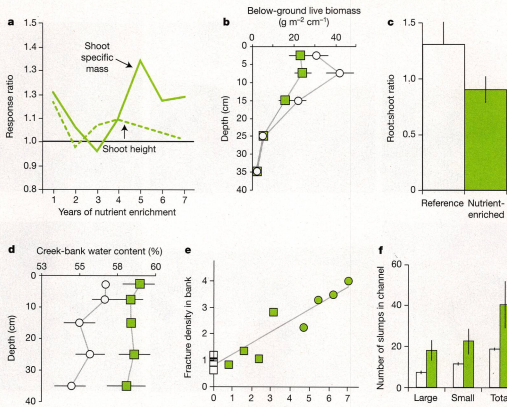

Figure 2 | Ecosystem attributes of reference and nutrient-enriched salt marshes after up to 7 years of nutrient enrichment. **a**–**c**, Plant attributes. **a**, Annual response ratio (nutrient-enriched/reference) for above-ground shoot attributes. Responses were comparable to other marsh nutrient-enrichment studies along the North American Atlantic coast and, as is typical in marshes, the strength was variable from year to year (green indicates average values of fertilized marshes greater than reference marshes, $n = 6$ per year; solid green line is shoot specific mass; dashed green line is shoot height; points above the response-ratio of 1.0 (horizontal black line) indicate increased growth in response to fertilization in that year). **b**, Below-ground root and rhizome biomass in reference (open circles) and nutrient-enriched (solid green squares) marshes (2010; $n = 20$ per treatment). **c**, The above-ground to below-ground plant biomass ratio ($n = 20$ per treatment). **d**–**f**, Creek-bank geotechnical and geomorphic attributes. **d**, Vertical profile of percentage water content in reference (open circles) and nutrient-enriched (solid green squares) marsh creek-bank sediments with depth (2010; $n = 20$ per treatment). **e**, Fracture density in high marsh plotted against years of nutrient enrichment. Annual means are shown for reference (open squares), the start of enrichment in 2009 (solid squares) and the start of enrichment in 2004 (solid circles). **f**, Number of low-marsh creek-bank slumps in the channel in reference (open bars) and nutrient-enriched (solid green bars) marshes (2010; $n = 2$). Values are all mean ± standard error.

Table 1 | Response of salt marsh ecosystem properties to chronic nutrient enrichment

Ecosystem properties	Response ratio	Mean (standard error)		*P*-value
		Reference	Nutrient	
Vascular plants				
Shoot height (cm)*	1.1	146 (3)	154 (2)	0.04
Shoot mass (g)*	1.2	6.18 (0.28)	7.18 (0.18)	0.01
Shoot specific mass (g cm^{-1})*	1.1	0.042 (0.002)	0.046 (0.001)	0.02
Lodging (%)		0 (0)	41 (2)	<0.001
Foliar N (%)*	1.1	1.43 (0.08)	1.54 (0.09)	<0.001
Lignin (%)***	0.6	30 (7.5)	17 (1.6)	0.07
Below-ground biomass (g m^{-2})	0.7	579 (60)	387 (64)	0.08
Creek geomorphology and sediment geotechnical properties				
Fracture density (number per 50 m of creek edge)**	3	1.1 (0.2)	3.3 (0.7)	<0.001
Amount of creek bank with fractures (%)**	4.5	6.6 (0.7)	29.5 (2.6)	<0.001
Fracture length (m)**	4.5	3.3 (0.4)	14.7 (1.7)	0.002
Exposed mud area (%)**	3	7.5 (1.7)	22.8 (4.6)	0.004
Total number of slumps in channel per creek	2.1	19.0 (1.0)	40.5 (11.5)	0.07
Fine organic matter (%)	1.7	16.1 (1.9)	26.7 (4.5)	0.17
Water content (%)	1.04	56.2 (0.4)	58.5 (0.1)	0.02
Channel width/depth ratio	1.3	3.02 (0.11)	3.86 (0.02)	<0.001
Microbial decomposition processes				
Plant litter respiration (CO_2 g^{-1} d^{-1})	1.9	1.29 (0.12)	2.49 (0.33)	0.04
Potential denitrification in creekbank sediment (nmol g^{-1} h^{-1})***	1.7	40.7 (7.9)	70.8 (6.3)	0.01

A response ratio (nutrient-enrichment/reference) greater than one indicates a positive response to nutrient enrichment. *P*-values indicate the effect of nutrient enrichment on response variables; see 'Statistical summary' in Methods. Means (±s.e.m., standard error of the mean) were calculated from the data averaged by creek each year ($N = 2$ for nutrient-enriched and $N = 2$ for reference, except where noted). *Means (±s.e.m.) calculated from data averaged by creek and pooled across seven years of data. **Means (±s.e.m.) calculated from long-term nutrient-enriched and reference data averaged by creek and pooled across two years (2009 and 2010) of data. ***Data averaged across subplots within creeks ($N = 1$ per treatment).

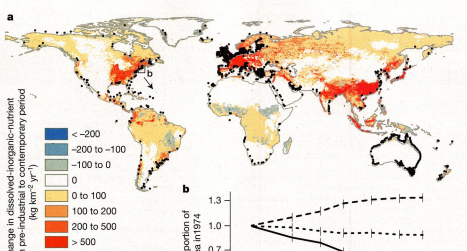

Figure 3 | The global relationship between nutrient loading and salt-marsh distribution and loss. a, The spatial distribution of the ramping up of anthropogenic nitrogen loading (dissolved inorganic nutrient (DIN) fluxes) from continents to coastal oceans from the pre-industrial period (1800s) to the contemporary period compared to global locations of salt marshes. **b**, Conversion of low marsh to mudflat in six nutrient-enriched Long Island Sound estuaries[10] (see box in **a** indicating location of **b**). Substantial loss of low marsh (solid line), smaller loss of high marsh (dotted line) and increase in mudflat (dashed line) area over time correlates with increased nutrients from sewage treatment plants and runoff from land. Values are mean ± standard error.

in wider creeks and increased mudflat area over the last three decades[7]. In Jamaica Bay, New York, USA, the rate of creek and open-bay-edge marsh loss in the 1990s was almost double that of the previous four decades (134 km^2 yr^{-1} versus 72 km^2 yr^{-1}) and the timing corresponds to an increase in total nitrogen loading (up to 80 μM open-bay total dissolved N) from sewage inputs[6]. Jamaica Bay marshes also have reduced root and rhizome mass and more degraded sediment[24], similar to our experimentally nutrient-enriched marshes.

The loss of creek-channel marsh banks is particularly significant because it is the most productive marsh zone and a critical area for regulating (C storage and N removal) and provisioning (fisheries) ecosystem services. Below-ground plant productivity disproportionately contributes to detrital organic matter in a wide variety of ecosystems[28], suggesting that the measured reduction in below-ground allocation may decrease the C storage potential of marshes. Marshes along creek channel edges are hotspots for denitrification with rates of N removal fivefold to tenfold higher than mudflats[29], suggesting that marsh conversion to mudflat decreases the ability of the coastal landscape to remove N from tidal waters. Considerable research shows the importance of the creek marsh edges in providing shelter and food to juvenile fish and shrimp[30,31], so the loss of marsh-edge habitat may ultimately negatively affect fisheries production.

Simultaneous increases in nutrient loading and in sea-level rise may result in synergistic marsh loss greater than the effects of either stressor alone. For example, the higher wave energy and flow velocities associated with sea level rise[32] when combined with decreased creek-bank stability induced by nutrient enrichment may accelerate erosion and creek-bank loss. The drowning of high marsh due to sea-level rise and loss of creek-edge marsh due to eutrophication, especially when exacerbated by upland development that limits the ability of marshes to move inland, may lead to a coastal landscape with a dramatically reduced capacity to provide important ecological and economic services. N flux to the coastal zone has already increased at least tenfold over pre-industrial levels and is projected to continue to increase as we ramp up fertilizer use to produce food for the expanding human population over the next few decades[1,27]. The potential deterioration of coastal marshes due to eutrophication adds an unanticipated dimension to the challenge of managing nitrogen while meeting food production in the twenty-first century.

METHODS SUMMARY

We enriched primary tidal creeks in Plum Island Estuary, Massachusetts, USA, to nutrient levels corresponding to moderately-to-highly eutrophic coastal waters by adding N and P to the twice-daily flooding tides for nine years (2004–2012) during the growing season (about 120 days, 15 May–15 September), enriching about 30,000 m^2 of marsh per experimental primary creek system ($N = 2$ enrichment started in 2004, $N = 1$ started in 2009, reference $N = 2$–6)[13]. Initial measurements (1998–2003) found few differences among tidal creeks[13], and other potential drivers did not differ among treatment marshes or do not occur in the Plum Island Estuary (Supplementary Information).

To detect changes in plant biomass allocation, the height, dry weight, and quality (percentage N, lignin content) of *Spartina alterniflora* above-ground shoots were measured and below-ground cores were analysed for live roots and rhizome biomass. Cores were also analysed for sediment geotechnical properties (water content, percentage organic matter and particle size). To determine changes in creek geomorphology, fractures in the vegetated marsh platform were enumerated along 250–300 m of creek banks and point-intercept transects indicated the presence or absence of vegetation in the creek bank. Creek-bank blocks that had slumped into tidal creeks were enumerated and creek width, depth and erosion measured over time using a 'total station' and high-precision GPS surveys. Microbial decomposition was measured as potential denitrification in the creek bank and microbial respiration of surface litter.

Full Methods and any associated references are available in the online version of the paper.

Received 16 April; accepted 20 August 2012.

1. Millennium Ecosystem Assessment. *Ecosystems and Human Well-Being—Synthesis Report* (World Resources Institute, 2005).
2. Galloway, J. *et al.* Transformation of the nitrogen cycle: recent trends, questions and potential solutions. *Science* **320,** 889–892 (2008).
3. Canfield, D. E., Glazer, A. N. & Falkowski, P. G. The evolution and future of Earth's nitrogen cycle. *Science* **330,** 192–196 (2010).
4. Verhoeven, J. T. *et al.* Regional and global concerns over wetlands and water quality. *Trends Ecol. Evol.* **21,** 96–103 (2006).
5. MacGarvin, M. *Out of Sight, Out of Mind: Marine Eutrophication in the United Kingdom* (WWF-UK, 2001).
6. Hartig, E. K., Gornitz, V., Kolker, A., Mushacke, F. & Fallon, D. Anthropogenic and climate-change impacts on salt marshes of Jamaica Bay, New York City. *Wetlands* **22,** 71–89 (2002).
7. Tiner, R. W., Huber, I. J., Nuerminger, T. & Marshall, E. *Salt Marsh Trends in Selected Estuaries of Southwestern Connecticut.* NWI Cooperative Report (US Fish and Wildlife Service, Long Island Studies Program, Connecticut Department of Environmental Protection, 2006).

8. Diaz, R. J. & Rosenberg, R. Spreading dead zones and consequences for marine ecosystems. *Science* **321,** 926–929 (2008).
9. Valiela, I. & Cole, M. L. Comparative evidence that salt marshes and mangroves may protect seagrass meadows from land-derived nitrogen loads. *Ecosystems* **5,** 92–102 (2002).
10. Sousa, A., Lillebø, A. I., Caçador, I. & Pardal, M. Contribution of *Spartina maritima* to the reduction of eutrophication in estuarine systems. *Environ. Pollut.* **156,** 628–635 (2008).
11. Childer, D., Day, J. W. Jr & Mckeller, H. H. Jr. in *Concepts and Controversies in Tidal Marsh Ecology* (eds Weinstein, M. & Kreeger, D.) 391–424 (Kluwer Academic, 2000).
12. Drake, D. *et al.* Salt marsh ecosystem biogeochemical responses to nutrient enrichment: a paired ^{15}N tracer study. *Ecology* **90,** 2535–2546 (2009).
13. Deegan, L. A. *et al.* Susceptibility of salt marshes to nutrient enrichment and predator removal. *Ecol. Appl.* **17,** S42–S63 (2007).
14. Bertness, M. D. & Pennings, S. in *Concepts and Controversies in Tidal Marsh Ecology* (eds Weinstein, M. & Kreeger, D.) 39–58 (Kluwer Academic, 2000).
15. Pinthus, M. J. Lodging in wheat, barley and oats: the phenomenon, its causes and preventative measures. *Adv. Agron.* **25,** 209–263 (1974).
16. Darby, F. A. & Turner, R. E. Effects of eutrophication on salt marsh root and rhizome biomass accumulation. *Mar. Ecol. Prog. Ser.* **363,** 63–70 (2008).
17. Mozdzer, T. *et al.* Nitrogen uptake by the shoots of smooth cordgrass *Spartina alterniflora*. *Mar. Ecol. Prog. Ser.* **433,** 43–52 (2011).
18. Terzaghi, K., Peck, R. B. & Mesri, G. *Soil Mechanics in Engineering Practice* 3rd edn (Wiley-Interscience, 1996).
19. Rinaldi, M., Casagli, N., Dapporto, S. & Gargini, A. Monitoring and modelling of pore water pressure changes and riverbank stability during flow events. *Earth Surf. Processes Landf.* **29,** 237–254 (2004).
20. Fagherazzi, S. *et al.* Numerical models of salt marsh evolution: ecological, geomorphic, and climatic factors. *Rev. Geophys.* **50,** RG1002 (2012).
21. Valiela, I., Teal, J. M. & Persson, N. Y. Production and dynamics of experimentally enriched salt marsh vegetation: belowground biomass. *Limnol. Oceanogr.* **21,** 245–252 (1976).
22. Wigand, C., Brennan, P., Stolt, M., Holt, M. & Ryba, S. Soil respiration rates in coastal marshes subject to increased watershed nitrogen loads in southern New England, USA. *Wetlands* **29,** 952–963 (2009).
23. Turner, R. E. *et al.* Salt marshes and eutrophication: an unsustainable outcome. *Limnol. Oceanogr.* **54,** 1634–1642 (2009).
24. Davey, E. *et al.* Use of computed tomography imaging for quantifying coarse roots, rhizomes, peat, and particle densities in marsh soils. *Ecol. Appl.* **21,** 2156–2171 (2011).
25. Morris, J. T. & Bradley, P. M. Effects of nutrient loading on the carbon balance of coastal wetland sediments. *Limnol. Oceanogr.* **44,** 699–702 (1999).
26. Turner, R. E. Beneath the salt marsh canopy: loss of soil strength with increasing nutrient loads. *Estuaries Coasts* **34,** 1084–1093 (2011).
27. Selman, M., Greenhalgh, S., Diaz, R. & Sugg, Z. Eutrophication and hypoxia in coastal areas: a global assessment of the state of knowledge. http://www.wri.org/publication/eutrophication-and-hypoxia-in-coastal-areas (World Resources Institute, 2008).
28. Schmidt, M. W. *et al.* Persistence of soil organic matter as an ecosystem property. *Nature* **478,** 49–56 (2011).
29. Piehler, M. F. & Smyth, A. R. Habitat-specific distinctions in estuarine denitrification affect both ecosystem function and services. *Ecosphere* **2,** art12 (2011).
30. Deegan, L. A. Lessons learned: the effects of nutrient enrichment on the support of nekton by seagrass and saltmarsh ecosystems. *Estuaries* **25,** 727–742 (2002).
31. Minello, T. J., Able, K. W., Weinstein, M. P. & Hays, C. G. Salt marshes as nurseries for nekton: testing hypotheses on density, growth and survival through meta-analysis. *Mar. Ecol. Prog. Ser.* **246,** 39–59 (2003).
32. Mariotti, G. *et al.* Influence of storm surges and sea level on shallow tidal basin erosive processes. *J. Geophys. Res.* **115,** C11012 (2010).

Supplementary Information is available in the online version of the paper.

Acknowledgements We thank our TIDE (Trophic cascades and Interacting control processes in a Detritus-based Ecosystem), LENS (Landscape Evolution in a Nutrient enriched Saltmarsh) and PIE-LTER (Plum Island Ecosystems Long-term Ecological Research) colleagues for field assistance and comments. We thank the many research assistants, graduate and undergraduate students who maintained the nutrient enrichment and analysed samples. This work is supported by grants from the NSF (DEB0816963, DEB0213767, OCE0923689, OCE 0423565, OCE0924287), the NOAA and The Mellon Foundation.

Author Contributions L.A.D., D.S.J., R.S.W., B.J.P. & J.W.F. designed the experiment and participated in sampling and data analysis. S.F. participated in geomorphic and geotechnical evaluation. W.M.W. estimated global N loading to coastal saltmarshes. L.A.D. and D.S.J. wrote the initial manuscript. All authors contributed to and approved the manuscript.

Author Information The data reported in this paper are archived in the Plum Island PIE-LTER database. Reprints and permissions information is available at www.nature.com/reprints. The authors declare no competing financial interests. Readers are welcome to comment on the online version of the paper. Correspondence and requests for materials should be addressed to L.A.D. (ldeegan@mbl.edu).

LETTER

doi:10.1038/nature11493

Delayed build-up of Arctic ice sheets during 400,000-year minima in insolation variability

Qingzhen Hao[1], Luo Wang[1], Frank Oldfield[2], Shuzhen Peng[3], Li Qin[4], Yang Song[1,5], Bing Xu[1], Yansong Qiao[6], Jan Bloemendal[2] & Zhengtang Guo[1]

Knowledge of the past variability of climate at high northern latitudes during astronomical analogues of the present interglacial[1] may help to inform our understanding of future climate change. Unfortunately, long-term continuous records of ice-sheet variability in the Northern Hemisphere only are scarce because records of benthic ^{18}O content represent an integrated signal of changes in ice volume in both polar regions[2]. However, variations in Northern Hemisphere ice sheets influence the Siberian High[3] (an atmospheric pressure system), so variations in the East Asian winter monsoon (EAWM)—as recorded in the aeolian dust deposits on the Chinese Loess Plateau—can serve as a useful proxy of Arctic climate variability before the ice-core record begins. Here we present an EAWM proxy record using grain-size variations in two parallel loess sections representative of sequences across the whole of the Chinese Loess Plateau over the past 900,000 years. The results show that during periods of low eccentricity and precessional variability at approximately 400,000-year intervals, the grain-size-inferred intensity of the EAWM remains weak for up to 20,000 years after the end of the interglacial episode of high summer monsoon activity and strong pedogenesis. In contrast, there is a rapid increase in the EAWM after the end of most other interglacials. We conclude that, for both the 400,000-year interglacials, the weak EAWM winds maintain a mild, non-glacial climate at high northern latitudes for much longer than expected from the conventional loess and marine oxygen isotope records. During these times, the less-severe summer insolation minima at 65° N (ref. 4) would have suppressed ice and snow accumulation, leading to a weak Siberian High and, consequently, weak EAWM winds.

Knowledge of natural climate variability at high northern latitudes is crucial for understanding the future development of the Northern Hemisphere ice sheets, the melting or growth of which would lead to major changes in sea level[3]. Key proxies for past glacial variability include ice-rafted debris and $\delta^{18}O$ in foraminifera preserved in marine sediments. The $\delta^{18}O$ records, frequently used as a measure of changes in ice volume, actually reflect variability in both polar regions[2], and may also be overprinted by deep-water temperature variability[6]. Direct sedimentary records of Northern Hemisphere polar ice sheets exist only for the late Quaternary period, and longer-term records are scarce[7].

EAWM variability is tightly linked to variations in high-northern-latitude climate via the Siberian High[3] (Fig. 1, Supplementary Fig. 1 and Supplementary Information). This allows the use of the loess record of the last 900,000 years (900 kyr) from the Chinese Loess Plateau (CLP) to show the timing of build-up of Northern Hemisphere ice sheets around the 413-kyr minima in eccentricity and precessional variability. This time frame falls within the current period of dominantly eccentricity-paced glacial–interglacial cycles and has also provided the most comprehensive records of climate change over the CLP in terms of both temporal resolution and spatial coverage (Supplementary Figs 2–4).

Orbital changes in summer insolation at high northern latitudes drive the sequence of glacial–interglacial alternations that have characterized the Quaternary Epoch. We live in a time of low-amplitude precessional insolation variability modulated by the 413-kyr eccentricity cycle. The closest, relatively recent, analogues for the present interglacial occur around marine oxygen isotope stages 11 and 19 (MIS 11 and MIS 19; ref. 1). Despite recent efforts to reconcile them, there remain significant discrepancies in estimates of the length of MIS 11 (for example), both between model-based inferences[1,8] and reconstructions from geological records[9–11] and among the geologically based estimates themselves[9–13]. This work adds independent, empirically based data from Northern Hemisphere terrestrial archives not previously used to estimate MIS lengths.

The loess–palaeosol sequences in the CLP comprise high-resolution archives of East Asian monsoon climate variability[3,14–16]. The climate in this region is mainly controlled by two seasonally alternating monsoon circulations, the warm/humid southerly East Asian summer monsoon (EASM) and the dry/cold northerly EAWM. The EAWM refers to the movement of cold air over Asia coming from the Siberian High mainly in response to strong and continuous radiative cooling in the lower troposphere over snow-covered surfaces[17]. The predominance of low-altitude EAWM winds in transporting the dust deposited on the CLP is

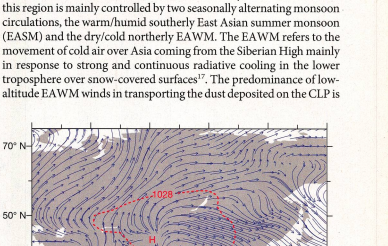

Figure 1 | Location map with the surface circulation over Eurasia in winter. Dec–Jan–Feb mean surface vector winds (blue arrows) based on the NCEP-DOE Reanalysis 2 data during 1979–2011 at http://www.esrl.noaa.gov/psd/data/gridded/reanalysis/. The grey area indicates land. 'H' indicates the centre of the Siberian High, and the area enclosed by the red-dashed line shows the region with mean sea level pressure exceeding 1,028 hPa. 'YMG' and 'LC' refer to the Yimaguan and Luochuan loess sections in this work.

[1]Key Laboratory of Cenozoic Geology and Environment, Institute of Geology and Geophysics, Chinese Academy of Sciences, PO Box 9825, Beijing 100029, China. [2]School of Environmental Sciences, University of Liverpool, Liverpool L69 7ZT, UK. [3]Key Laboratory of Tourism and Resources Environment in Universities of Shandong, Taishan University, Taian 271021, China. [4]Chongqing Three Gorges Institute of Paleoanthropology, China Three Gorges Museum, Chongqing 400015, China. [5]Graduate University of Chinese Academy of Sciences, Beijing 100049, China. [6]Institute of Geomechanics, Chinese Academy of Geological Sciences, Beijing 100081, China.

clearly indicated by an approximately north–south gradient of decreasing loess grain size[18].

The two loess–palaeosol sections used here, Yimaguan (35° 55′ N, 107° 37′ E) and Luochuan (35° 43′ N, 109° 25′ E), preserve a relatively complete suite of mineral dust deposits and can be well correlated by distinctive stratigraphic markers[19,20]. The chronology of the Yimaguan and Luochuan loess sections was generated by correlation of the studied sequences with the benthic $\delta^{18}O$ stack LR04 (ref. 10) (see Methods Summary).

Magnetic susceptibility and grain size are two well accepted proxies for summer and winter monsoon climates, respectively[3,14,15,21]. Justification for their use and their close correlation with other, independent proxies is provided in the Supplementary Figs 1 and 5, and related discussion. Here, the time series of the EAWM and EASM was reconstructed using the content of particles over 32 μm in size (GT32) and frequency-dependent magnetic susceptibility (χ_{fd}) of bulk samples from the two sections. The samples were usually analysed at 5-cm intervals for both sections, with 2.5-cm intervals for palaeosols S1 (12.875–16.100 m depth) and S5 (53.075–59.825 m depth) from Yimaguan. The 5-cm interval represents an average time resolution for loess and palaeosol layers of 0.36 kyr and 0.89 kyr for Yimaguan, and 0.56 kyr and 1.24 kyr for Luochuan.

The temporal changes in GT32 and χ_{fd} can be closely correlated between the two sections (Fig. 2d–g). During glacial times, high GT32 and minimum χ_{fd} values indicate that the climate on the CLP was characterized by overall strong EAWM winds and weakened EASM winds. Here, as reported in previous studies[21,22], the climate during interglacial times was characterized by much weaker EAWM winds and strengthened EASM winds. The GT32 time series shows orbital periodicities of 41 kyr and 23 kyr; the χ_{fd} time series shows orbital periodicities of 100 kyr, 41 kyr and 23 kyr (Supplementary Fig. 9), confirming the pacing of the changes by variations in the Earth's orbit.

Comparison between the EAWM and EASM proxy records (Fig. 2d–g) reveals major differences in the amplitude of fluctuation in glacial periods between the two monsoon climate components. The summer monsoon is very weak overall in the glacial periods, with the χ_{fd} curves in Fig. 2e and g nearly parallel to the marine $\delta^{18}O$ record (Fig. 2c). However, as found in previous studies[21,22], the winter monsoon has strong precessional cycles in several glacial loess units, such as L2, L5 and L6. These precession cycles match well with those predicted by the theoretical model of ice volume in the Northern Hemisphere[23] (Fig. 2b). The contrast in precessional cycles between summer and winter monsoon proxies highlights the fact that they have evolved in a relatively independent manner and are controlled by different driving factors. The grain-size records in loess lack the 'saw-tooth' shape typical of the marine $\delta^{18}O$ curve, implying that factors other than Northern Hemisphere ice volume have affected grain-size variations during glacial intervals. However, on orbital timescales, the extent of Northern Hemisphere ice sheets plays the leading role in controlling changes in loess grain size, hence our use here of these changes to indicate the large-scale growth of Northern Hemisphere ice sheets.

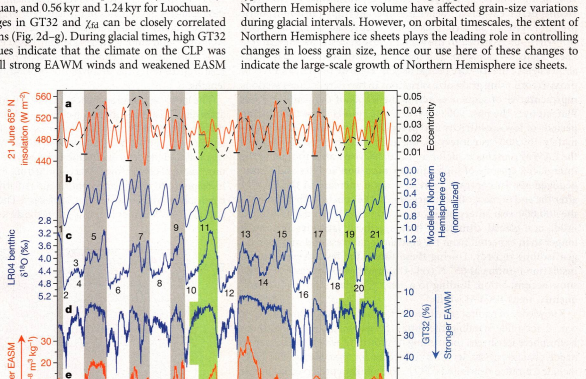

Figure 2 | Comparison of the East Asian winter monsoon (EAWM) and summer monsoon (EASM) proxy records in loess with other palaeoclimatic data of the past 880 kyr. **a**, 21 June insolation 65° N (orange trace)and long-term variations of eccentricity[4] (black trace). Short black (or grey) horizontal bars mark the strong (or weak) insolation minima coincident with each glacial inception. **b**, Northern Hemisphere modelled ice volume[23]. **c**, Benthic $\delta^{18}O$ stack LR04 (ref. 10). Numbers indicate MIS. **d**, Grain-size data expressed as GT32 (>32-μm particle content) in the Yimaguan loess section. **e**, Frequency-dependent magnetic susceptibility (χ_{fd}) in the Yimaguan loess section. **f** and **g**, GT32 and χ_{fd} data in the Luochuan loess section, respectively. The major loess and palaeosol units are labelled. The shaded areas indicate the major palaeosol units and their correlation with other palaeoclimatic records, with the green shading highlighting the delayed changes in loess grain size.

The most striking feature in the proxy records is that there are two types of coupling between EAWM and EASM at interglacial–glacial transitions (Fig. 2d–g and Supplementary Fig. 11). For most interglacial-to-glacial transitions (palaeosol S1 to loess unit L1, S2–L2, S3–L3, S5–L5 and S6–L6), the increase in GT32 values coincides closely with the decrease in the χ_{fd} values, indicating that the increased wind strength of the EAWM and weakening of the EASM were synchronous. However, at the transition of MIS 11 to MIS 10 (S4–L4), there is a period of around 20 kyr during which fine-grained loess persists after χ_{fd} values have decreased to levels typical of glacial loess. Such decoupled changes can also be found at the boundaries of S7–L7 and S8–L8. The decoupling is independent of the chronology model (Supplementary Fig. 6 for loess proxies plotted against depth). Comparison with the record of summer insolation at 65° N (ref. 4 and Fig. 2a) indicates that these three exceptions occur around minima in insolation variability modulated by the 413-kyr eccentricity cycle.

The EAWM proxy records in this study reveal different histories of Northern Hemisphere ice-volume growth at the conclusion of different interglacial periods. The reduction in boreal summer insolation is thought to be the primary trigger for glaciation[24,25]. The alignment of obliquity and precession insolation minima is important because low obliquity plays a significant part in reinforcing the processes driving glacial inception[25,26]. The amplitude of summer insolation variability in the precessional band is modulated at the eccentricity periods of 100 kyr and 413 kyr. At times of high eccentricity, each glacial inception (MIS 16, MIS 12, MIS 8, MIS 6 and MIS 4) was triggered by a very low precessional minimum of summer insolation (Fig. 2a), favouring the rapid accumulation of snow/ice at high northern latitudes. When the high-northern-latitude climate began to experience glacial conditions, the presence of the ice sheets and lowered CO_2 would have made the northern continents persistent sources for cold air surges[27]. The consequently strong EAWM winds would have led to a cold and arid climate over the Eurasian region[27], and carried coarser aeolian dust to the CLP, reflecting both increased wind strength and a southward expansion of the zone of extreme aridity. Therefore, the rapidly strengthening EAWM in these glacial periods indicates rapid build-up of ice-sheets at high northern latitudes, consistent with the benthic $\delta^{18}O$ records (Fig. 2c).

At times of low eccentricity in the 413-kyr cycles, all three glacials after each of MIS 21, MIS 19 and MIS 11 (corresponding to palaeosols S8, S7 and S4) were triggered by a very weak precessional insolation minimum leading to warm summer conditions unfavourable to Northern Hemisphere ice-sheet build-up at the inception of each of MIS 20, MIS 18 and MIS 10 (Fig. 2a). The interval lacking coarse-grained loess in early MIS 10 (L4) appears to span a precessional cycle and this is in sharp contrast to the records during high eccentricity periods in the 413-kyr cycle (Fig. 3). The continuing fine-grained loess deposition spanning nearly 20 kyr indicates a weak EAWM comparable to that during the MIS 11 interglacial (Figs 2 and 3). Owing to their inherent link with Northern Hemisphere ice extent, the weak EAWM and Siberian High during early MIS 10 strongly suggest that the high-northern-latitude climate was still experiencing non-glacial conditions with limited ice-sheet extent. This is strongly supported by independent pollen records off southwest Greenland that indicate a nearly ice-free Greenland during the MIS 11 optimum and a prolonged temperate climate for around 360 kyr (ref. 7). There are similar indications for the early glacial period recorded above palaeosols S7 (MIS 19) and S8 (MIS 21) (Fig. 2 and Supplementary Fig. 12).

Although the EAWM proxy records indicate a prolonged non-glacial climate at high northern latitudes, the χ_{fd} indicates that the summer monsoon significantly weakened after the end of the three exceptional interglacials: MIS 21, MIS 19 and MIS 11. The CLP is located on the fringe of the EASM, which becomes displaced over hundreds of kilometres in a north–south direction during glacial–interglacial cycles[16]. The displacement of the summer monsoon climate regime reflects, among other factors, distance from the sea. The sea level history extending to 500 kyr BP (before present) shows that sea level decreased gradually

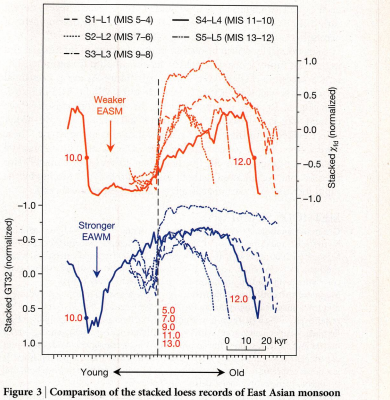

Figure 3 | Comparison of the stacked loess records of East Asian monsoon climate around the last five interglacial–glacial transitions. The grain size, GT32, and frequency-dependent magnetic susceptibility, χ_{fd}, data in different interglacial–glacial transitions are aligned (vertical dashed line) using the termination age of each interglacial defined by the benthic $\delta^{18}O$ stack LR04 (ref. 10), and are plotted against the uniform time-length unit. Numbers indicate MIS boundaries (red text). The stacked records are generated by averaging normalized GT32 and χ_{fd}, respectively. The normalized data were first interpolated linearly at 1-kyr intervals before stacking.

during early MIS 10 (ref. 28). This would have placed the CLP beyond the control of the EASM by increasing the distance from the source of moisture[16]. We suggest that the changes in sea level and $\delta^{18}O$ may have

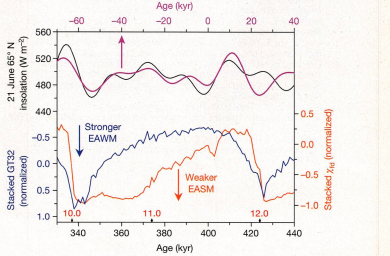

Figure 4 | Summer insolation during MIS 11–10 compared with present and future summer insolation. MIS 11 is selected as an astronomical analogue based on the high linear correlation of 65° N insolation in June between periods of 405–340 kyr BP and of 5 kyr BP to 60 kyr after present (AP)[3]. Only the insolation of 40 kyr BP–70 kyr AP, shown as a purple line, is plotted against the upper x axis (negative age refers to the future). MIS numbering (in red) is given along the bottom x axis.

been caused by a build-up of ice volume in the Antarctic region during early MIS 10 (Supplementary Fig. 13). Asymmetrical development of hemispheric ice sheets has been suggested by climate models[29].

Astronomically driven insolation during the present interglacial and in the near future is characterized by its low-amplitude variability. The best analogue is MIS 11 (ref. 1), though future 23-kyr precessional variability is even weaker than it was across the MIS 11–MIS 10 transition (Fig. 4). In terms of orbital forcing, the closest comparison for the present day is with conditions around 400 kyr BP, some 40–45 kyr before evidence for the onset of glacial conditions in the Arctic. These observations lead us to speculate that the future Arctic climate may still remain in non-glacial mode for more than 40 kyr (approximately two precessional cycles), even without taking into account forcing by the rapid increase in anthropogenically generated greenhouse gases.

METHODS SUMMARY

Grain-size analysis. After removal of organic matter by 10% H_2O_2, of carbonate by 10% HCl, and dispersal using 0.05 N $(NaPO_3)_6$, samples were measured using a Mastersizer 2000 analyser with size range of 0.02–2,000 μm in diameter and with a precision of ±1%. The GT32 (>32-μm particle content) used here shows good correlation with median grain-size changes (Supplementary Fig. 6).

Magnetic susceptibility. Low-frequency magnetic susceptibility (χ_{lf}) and high-frequency magnetic susceptibility (χ_{hf}) were measured at 0.47 kHz and 4.7 kHz, respectively, using a Bartington Instruments MS 2B magnetic susceptibility meter. Frequency-dependent susceptibility, χ_{fd}—the difference between χ_{lf} and χ_{hf}—is an indicator of the formation of fine-grained secondary ferrimagnetic oxides as a result of pedogenesis[30], and is closely linked with the strength of the summer monsoon. It is a better indicator of pedogenesis than χ_{lf}, which includes signals from both fine pedogenic particles and coarse detrital aeolian input.

Establishment of the chronology. The chronology of the Yimaguan and Luochuan loess sections was established using the accepted correlation scheme between Chinese loess and deep-sea sediments[21,22] (Supplementary Figs 7–10). The absolute age control points are transferred from MIS boundaries[10] by correlating them with interglacial palaeosol boundaries[18,20]. Between control points, interpolation, weighted by grain-size[15], was used to generate the timescale. The age uncertainties arising from choice of age control points and interpolation methods are averaged to within a few thousand years (Supplementary Fig. 7). Therefore, the duration of delayed changes in grain size is much greater than age uncertainties. The cross-spectral analysis with the theoretical orbital record[4] of the Earth confirms the validity of the present chronology (Supplementary Fig. 9).

Received 7 April; accepted 7 August 2012.
Published online 3 October 2012.

1. Loutre, M. F. & Berger, A. Marine Isotope Stage 11 as an analogue for the present interglacial. *Global Planet. Change* **36,** 209–217 (2003).
2. Raymo, M. E., Lisiecki, L. E. & Nisancioglu, K. H. Plio-Pleistocene ice volume, Antarctic climate, and the global $\delta^{18}O$ record. *Science* **313,** 492–495 (2006).
3. Ding, Z., Liu, T., Yu, Z., Guo, Z. & Zhu, R. Ice-volume forcing of East Asian winter monsoon variations in the past 800,000 years. *Quat. Res.* **44,** 149–159 (1995).
4. Laskar, J., Joutel, F. & Boudin, F. Orbital, precessional, and insolation quantities for the Earth from -20 Myr to +10 Myr. *Astron. Astrophys.* **270,** 522–533 (1993).
5. Alley, R. B., Clark, P. U., Huybrechts, P. & Joughin, I. Ice-sheet and sea-level changes. *Science* **310,** 456–460 (2005).
6. Shackleton, N. J. The 100,000-year ice-age cycle identified and found to lag temperature, carbon dioxide, and orbital eccentricity. *Science* **289,** 1897–1902 (2000).
7. de Vernal, A. & Hillaire-Marcel, C. Natural variability of Greenland climate, vegetation, and ice volume during the past million years. *Science* **320,** 1622–1625 (2008).
8. Berger, A. & Loutre, M. F. An exceptionally long interglacial ahead? *Science* **297,** 1287–1288 (2002).
9. McManus, J. F., Oppo, D. W. & Cullen, J. L. A 0.5-million-year record of millennial-scale climate variability in the North Atlantic. *Science* **283,** 971–975 (1999).
10. Lisiecki, L. & Raymo, M. A Pliocene-Pleistocene stack of 57 globally distributed benthic $\delta^{18}O$ records. *Paleoceanography* **20,** PA1003 (2005).
11. Jouzel, J. *et al.* Orbital and millennial Antarctic climate variability over the past 800,000 years. *Science* **317,** 793–796 (2007).
12. Howard, W. R. A warm future in the past. *Nature* **388,** 418–419 (1997).
13. Droxler, A. W., Alley, R. B., Howard, W. R., Poore, R. Z. & Burckle, L. H. in *Earth's Climate and Orbital Eccentricity: The Marine Isotope Stage 11 Question* (eds Droxler, A. W., Poore, R. Z. & Burckle, L. H.) 1–14 (AGU Geophys. Monogr. Ser. 137, 2003).
14. An, Z. *et al.* The long-term paleomonsoon variation recorded by the loess-paleosol sequence in central China. *Quat. Int.* **7–8,** 91–95 (1990).
15. Porter, S. C. & An, Z. S. Correlation between climate events in the North Atlantic and China during last glaciation. *Nature* **375,** 305–308 (1995).
16. Liu, T. & Ding, Z. Chinese loess and the paleomonsoon. *Annu. Rev. Earth Planet. Sci.* **26,** 111–145 (1998).
17. Panagiotopoulos, F., Shahgedanova, M., Hannachi, A. & Stephenson, D. B. Observed trends and teleconnections of the Siberian high: a recently declining center of action. *J. Clim.* **18,** 1411–1422 (2005).
18. Nugteren, G. & Vandenberghe, J. Spatial climatic variability on the Central Loess Plateau (China) as recorded by grain size for the last 250 kyr. *Global Planet. Change* **41,** 185–206 (2004).
19. Liu, T. *Loess and the Environment* (China Ocean, 1985).
20. Kukla, G. & An, Z. S. Loess stratigraphy in central China. *Palaeogeogr. Palaeoclimatol. Palaeoecol.* **72,** 203–225 (1989).
21. Sun, Y., Clemens, S. C., An, Z. & Yu, Z. Astronomical timescale and palaeoclimatic implication of stacked 3.6-Myr monsoon records from the Chinese Loess Plateau. *Quat. Sci. Rev.* **25,** 33–48 (2006).
22. Ding, Z. L. *et al.* Stacked 2.6-Ma grain size record from the Chinese loess based on five sections and correlation with the deep-sea $\delta^{18}O$ record. *Paleoceanography* **17,** 1033 (2002).
23. Imbrie, J. & Imbrie, J. Z. Modeling the climatic response to orbital variations. *Science* **207,** 943–953 (1980).
24. Milankovitch, M. *Kanon der Erdebestrahlung und seine Anwendung auf das Eiszeitenproblem* (Stamparija Mihaila Curcica, 1941); *Canon of Insolation and the Ice-age Problem* [English transl.] (Israel Program for Scientific Translations, US Department of Commerce and the National Science Foundation, 1969).
25. Vettoretti, G. & Peltier, W. Sensitivity of glacial inception to orbital and greenhouse gas climate forcing. *Quat. Sci. Rev.* **23,** 499–519 (2004).
26. Ruddiman, W. F. Orbital insolation, ice volume, and greenhouse gases. *Quat. Sci. Rev.* **22,** 1597–1629 (2003).
27. Kutzbach, J. *et al.* Climate and biome simulations for the past 21,000 years. *Quat. Sci. Rev.* **17,** 473–506 (1998).
28. Rohling, E. *et al.* Antarctic temperature and global sea level closely coupled over the past five glacial cycles. *Nature Geosci.* **2,** 500–504 (2009).
29. Huybrechts, P. & de Wolde, J. The dynamic response of the Greenland and Antarctic ice sheets to multiple-century climatic warming. *J. Clim.* **12,** 2169–2188 (1999).
30. Zhou, L. P., Oldfield, F., Wintle, A. G., Robinson, S. G. & Wang, J. T. Partly pedogenic origin of magnetic variations in Chinese loess. *Nature* **346,** 737–739 (1990).

Supplementary Information is available in the online version of the paper.

Acknowledgements This work was supported by the National Natural Science Foundation of China (grant 41172323), Ministry of Science and Technology (grant 2010CB950204), Ministry of Land and Resources (grant 201211077), and the Chinese Academy of Sciences.

Author Contributions Q.H. and L.W. designed the study. Q.H. and Y.S. undertook the field work. S.P. and Q.H. organized and supervised the grain-size measurement. Y.S. and Q.H. performed the magnetic susceptibility measurements. Q.H. and F.O. wrote the manuscript. All the authors contributed to the interpretation of the data and provided significant input to the final manuscript.

Author Information Reprints and permissions information is available at www.nature.com/reprints. The authors declare no competing financial interests. Readers are welcome to comment on the online version of the paper. Correspondence and requests for materials should be addressed to Q.H. (haoqz@mail.iggcas.ac.cn) or F.O. (oldfield.f@gmail.com).

LETTER

doi:10.1038/nature11451

Nonlinear dendritic processing determines angular tuning of barrel cortex neurons *in vivo*

Maria Lavzin[1]*, Sophia Rapoport[1]*, Alon Polsky[2], Liora Garion[1] & Jackie Schiller[1]

Layer 4 neurons in primary sensory cortices receive direct sensory information from the external world[1,2]. A general feature of these neurons is their selectivity to specific features of the sensory stimulation[3–5]. Various theories try to explain the manner in which these neurons are driven by their incoming sensory information[6–11]. In all of these theories neurons are regarded as simple elements summing small biased inputs to create tuned output through the axosomatic amplification mechanism[12]. However, the possible role of active dendritic integration[13–15] in further amplifying the sensory responses and sharpening the tuning curves of neurons[16–19] is disregarded. Our findings show that dendrites of layer 4 spiny stellate neurons in the barrel cortex can generate local and global multi-branch *N*-methyl-D-aspartate (NMDA) spikes, which are the main regenerative events in these dendrites. In turn, these NMDA receptor (NMDAR) regenerative mechanisms can sum supralinearly the coactivated thalamocortical and corticocortical inputs. Using *in vivo* whole-cell recordings combined with an intracellular NMDAR blocker and membrane hyperpolarization, we show that dendritic NMDAR-dependent regenerative responses contribute substantially to the angular tuning of layer 4 neurons by preferentially amplifying the preferred angular directions over non-preferred angles. Taken together, these findings indicate that dendritic NMDAR regenerative amplification mechanisms contribute markedly to sensory responses and critically determine the tuning of cortical neurons.

To examine the active properties of layer 4 spiny stellate dendrites in the rodent barrel cortex and their role in synaptic integration, we first characterized layer 4 dendrites *in vitro* and then studied the contribution of active dendritic processing to sensory responses of these neurons *in vivo*.

The excitable properties of layer 4 spiny stellate dendrites *in vitro* were studied using focal synaptic stimulation of fluorescently identified dendrites while recording the somatic voltage[18,20] (Fig. 1a). Linearly increasing the stimulus intensity resulted in an S-shaped input–output curve, with an abrupt amplitude jump, suggesting initiation of a dendritic spike (Fig. 1b–c). The average amplitude of dendritic spikes as recorded at the soma was 20.3 ± 2.7 mV and their average voltage threshold was 6.2 ± 1.1 mV ($n = 8$, 129 ± 33 μm from soma). Blocking NMDAR channels by extracellular APV (2-amino 5-phosphonovalerate; 50 μM) or intracellular MK801 through the recording pipette (see Methods for controls) completely abolished the spike, linearized the S-shaped input–output curve and significantly reduced the duration of the response (the half width was reduced by 50.3 ± 5.8%, $P < 0.01$) (Fig. 1b–e). The extracellular APV had a larger average effect compared to intracellular MK801 (Fig. 1e), possibly owing to the fact that concentrations of MK801 did not fully equilibrate in distal dendrites where the focal stimulation occurred.

Unlike layer 5 pyramidal neurons, where dendritic NMDA spikes were mediated mostly by the NR2A subunit of the NMDAR channel[21], in layer 4 spiny stellate neurons both the NR2A (NVP-AAM077, 0.4 μM) and NR2B (ifenprodil, 3 μM) blockers did not significantly change the amplitude and threshold of the dendritic NMDA spikes (Fig. 1f–h; $P > 0.2$). These findings are consistent with a previous study that reported that NR2C subunits mediate the NMDA component of corticocortical excitatory postsynaptic potentials (EPSPs) in spiny stellate neurons[22].

Next we used glutamate uncaging combined with specific blockers for voltage-gated calcium, sodium and NMDAR channels to further investigate the ionic mechanism mediating these dendritic spikes. Glutamate uncaging onto a single dendrite evoked a local spike that resembled the synaptically evoked dendritic spikes (Fig. 1i–j). Consecutive application of the specific voltage-gated sodium and calcium-channel blockers (1 μM tetrodotoxin (TTX), 100 μM Cd^{2+} and 100 μM Ni^{2+}) did not change significantly the spike amplitude and threshold (Fig. 1i–k, $P = 0.2$). In contrast, consecutive application of APV blocked the spike completely (Fig. 1i–k; $n = 11$, $P < 0.01$). Taken together, our findings indicate that, similar to thin dendrites of layer 5 pyramidal neurons[20,23,24], NMDA spikes are the main regenerative events in dendrites of layer 4 spiny stellate neurons.

Our focal synaptic stimulation mostly activates corticocortical synaptic inputs as they constitute the majority of inputs to layer 4 spiny stellate dendrites[25]. A second important source of inputs to these neurons (approximately 10% of all synapses) is the thalamocortical pathway, which carries the sensory input from the external world[1,11,26]. Under physiological conditions the thalamocortical response is followed by a powerful feed-forward excitatory corticocortical activation originating from neighbouring layer 4 neurons[25]. Thus, we next set out to examine the contribution of NMDAR-dependent dendritic regenerative mechanisms to the interaction between these two main excitatory inputs converging on layer 4 neurons. Thalamocortical responses were evoked by stimulating ventrobasal thalamic neurons while recording from somatotopically aligned layer 4 spiny stellate neurons (see Methods and Supplementary Figs. 1 and 2). Coactivation of a single predominantly corticocortical EPSP (average amplitude of 3.1 ± 0.6 mV), evoked by focal synaptic activation, with a train of thalamocortical EPSPs[5] (5 pulses at 50 Hz) yielded an S-shaped curve. At the lower stimulus intensities, the two inputs summated sublinearly. As we gradually increased the thalamocortical stimulus intensity, an abrupt jump in the voltage response was observed, and the two inputs summated supralinearly (Fig. 2a–c, f). At just above threshold thalamocortical stimulus intensities, the paired response was 228.7 ± 32.5% greater than that expected from the linear summation of the thalamocortical and corticocortical EPSPs (Fig. 2b, c, f; $n = 12$). Extracellular APV or intracellular MK801 completely abolished this coincident amplification (Fig. 2a, f; the paired response was 86.8 ± 18.2% and 102.6 ± 9.7% of the expected arithmetic sum of the two individual responses for APV and MK801, respectively) and decreased the duration of the response (half width decreased by 49.0 ± 4.3%; $n = 10$, $P < 0.01$). Similar results were obtained with

[1]Department of Physiology, the Rappaport Faculty of Medicine & Research Institute, Technion-Israel Institute of Technology, Bat-Galim, Haifa 31096, Israel. [2]Synaptic Physiology Section, National Institute of Neurological Disorders & Stroke. National Institutes of Health, Bethesda, Maryland 20892-3701 USA.
*These authors contributed equally to this work.

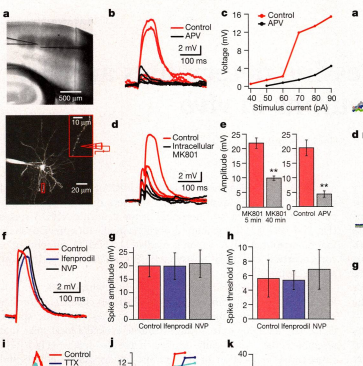

Figure 1 | NMDA spikes in layer 4 spiny stellate neurons. **a**, Experimental setup. Top panel, thalamocortical slice with two schematic electrodes (left, recording; right, stimulating). Bottom panel, layer 4 spiny stellate neuron loaded with alexa 633 (50 μM). Inset, the stimulated dendritic branch (position indicated by a red rectangle) and a schematic drawing of the stimulating theta electrode. **b**, Somatic voltage recordings in response to gradual increase of the stimulus current at the dendrite, in control conditions and after NMDAR channels blockade with APV (50 μM). **c**, Stimulus current–voltage relationship of the experiment shown in **b**. **d**, Same as **b**, except that the electrode contained MK801 (2 mM). Recordings were taken after 5 min (red) and 40 min (black). **e**, Average somatic amplitudes of the dendritic spike in control conditions and after NMDAR blockade with extracellular APV ($n = 8$) or intracellular MK801 ($n = 7$, after 40 min; $^{**}P < 0.01$). **f**, Traces of NMDA spikes in control conditions, with ifenprodil (3 μM) and followed by addition of NVP-AM077 (0.4 μM). NVP, specific blocker of the NR2A subunit of the NMDAR. **g**, **h**, Averaged spike amplitude (**g**) and threshold (**h**). Colours are the same as in **f** ($n = 8$). **i**, Effect of voltage-gated sodium- and calcium-channel blockers on local spikes evoked by glutamate uncaging at a dendrite (160 μm from soma). Spike in control conditions, with TTX (1 μM), with consecutive addition of Ni^{2+} (100 μM) and Cd^{2+} (100 μM), and consecutive application of APV (50 μM). **j**, Peak somatic voltage as a function of stimulus laser intensity (colours are the same as in i). **k**, The average amplitudes of the dendritic spike as recorded at the soma (colours are the same as in **i** and **j**) ($n = 11$, $^{**}P < 0.01$ compared with control). Error bars, mean ± s.e.m.

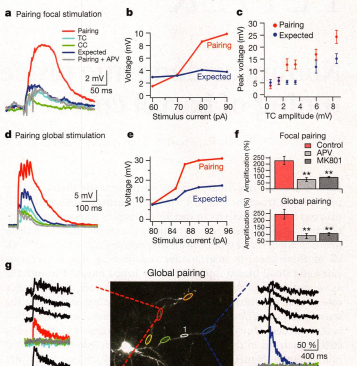

Figure 2 | Corticocortical and thalamocortical pairing of activity evokes local and multi-branch global dendritic NMDA spikes. **a**, Simultaneous activation of thalamocortical (TC) axons (100 Hz, 5 pulses) and corticocortical (CC) axons (1 pulse, focal stimulation) caused a large supralinear response (red) that was blocked by APV (grey). The expected arithmetic sum of the two individual responses is shown in blue. **b**, Voltage amplitude in response to pairing of corticocortical input (constant intensity) and thalamocortical input (increasing intensities) (red). Blue, expected arithmetic summed response. **c**, Peak average (mean ± s.e.m.) paired and expected summed voltage responses as a function of the thalamocortical peak voltage amplitude ($n = 7$). **d**, **e**, Same as **a** and **b** but for global corticocortical stimulation (electrode was located approximately 200 μm from the soma of the recorded neuron). **f**, Amplification (as a percentage of expected arithmetic summed response) in control conditions, with APV and with MK801. Data are presented for focal (top panel, $n = 12$) or global (bottom panel, $n = 10$) corticocortical activation ($^{**}P < 0.01$ compared with control). Error bars, mean ± s.e.m. **g**, Image of a spiny stellate neuron filled with OGB-1 (100 μM) showing the location of five calcium hot spots (coloured ovals) during global pairing (red/blue) of thalamocortical (cyan) and corticocortical (green) activation. Spatial profiles of the red (left panel) and blue (right panel) hot spots are shown. The blue and red traces were recorded at the peak locations of the spots, and the black traces were recorded at adjacent sites with distance steps of 3 to 5 μm between consecutive traces. **h**–**j**, Spatial profiles of two 'cold spots' (white ovals in **g**) and the corresponding somatic voltage recordings during the pairing protocol (**i**).

20-Hz and 100-Hz thalamocortical stimulation frequencies ($n = 6$; data not shown).

To mimic a distributed corticocortical activation pattern we activated the corticocortical inputs using a large extracellular stimulating electrode placed within the barrel that we recorded from. Similar to our previous results, pairing of a distributed corticocortical EPSP (average amplitude of 5.3 ± 0.89 mV) with thalamocortical EPSPs, evoked at gradually increasing stimulation intensities, resulted in a steep S-shaped input-output curve with supralinear summation of these two inputs above a threshold value (Fig. 2d–f). At just above threshold thalamocortical stimulus intensities, the response was 213.2 ± 25.5% greater than the calculated arithmetic sum of the two individual responses (Fig. 2e–f, $n = 10$). This amplification was blocked by extracellular APV or intracellular MK801 (Fig. 2d, f; $n = 8$, the amplitude of the paired response decreased to 68.8 ± 18.2% relative to the calculated arithmetic sum of the individual responses, and half width decreased to 48.8 ± 6.5%, $P < 0.01$).

The intracellular block of NMDAR channels indicated mainly a postsynaptic effect in the recorded neuron rather than a recurrent

network effect (see controls in Methods and Supplementary Figs. 3 and 4).

To understand better the dendritic events underlying the supralinear summation in the focal and global pairing protocols, we carried out simultaneous calcium imaging recordings in dendrites of the activated layer 4 neurons. During the global and focal pairing, calcium imaging revealed intense dendritic 'hot spots' (Fig. 2g–j and Supplementary Fig. 5). During the focal pairing, calcium transients were localized to the activated sites and reached an average amplitude of 170 ± 30.5% ($\Delta F/F$) which was significantly larger than the corticocortical-evoked calcium transients (30 ± 7%, $P < 0.01$) and thalamocortical-evoked transients alone (undetectable, below the noise level) ($n = 4$ neurons; Supplementary Fig. 5). Similar results were obtained when the focal synaptic stimulation was replaced with focal glutamate uncaging ($n = 6$; Supplementary Fig. 6).

In the case of global pairing we observed multiple calcium hot spots in several dendrites (Fig. 2g, i). On average we observed 3.8 ± 0.6 calcium hot spots per neuron when scanning approximately 30% of the dendritic tree. The average size of the maximal calcium hot zone ranged between 9 and 30 μm (average 15 ± 1.4 μm) and their average peak amplitude during the pairing was 135 ± 14% ($n = 18$ spots). During thalamocortical activation alone, calcium transients were undetectable, as was the case in most instances of corticocortical activation (Fig. 2g; 14 out of the 18 cases). In the 4 cases in which we observed calcium transients during corticocortical activation, the average peak calcium transient was 34 ± 11.5%. The calcium transients evoked by the pairing protocol were abolished altogether by APV (Fig. 2g; $n = 15$ spots). Similar multi-branch NMDA spikes were also observed in layer 4 pyramidal neurons (Supplementary Fig. 7). Interestingly, in contrast to previously reported data in layer 2 neurons of the visual cortex[27] where calcium hot spots originated from activation of single inputs, in this study the calcium hotspots were found to extend over larger dendritic segments, indicating supralinear interactions between neighbouring synapses.

Computer simulations succeeded in reproducing the experimental results of NMDA spike generation and their accompanying calcium profiles during both focal and global activation patterns (Supplementary Figs 8 and 9). Simulations show that during global multi-branch NMDA spikes, the voltage profile was relatively homogenous across the neuron, whereas the calcium profile was highly non-homogenous, showing calcium hot spots in different dendritic segments (Supplementary Fig. 9a, d). Our simulation indicated that the global multi-branch NMDA spike resulted from regenerative interactions between closely spaced synapses as well as from long-range inter-branch interactions between more distant synapses.

To investigate directly the contribution of NMDAR-dependent dendritic regenerative mechanisms to tuning of sensory responses, we turned to *in vivo* experiments. More specifically, we examined the hypothesis that NMDAR-dependent dendritic regenerative mechanisms can serve to sharpen the angular tuning curves[5,28] of barrel cortex layer 4 neurons by comparing the whisker-evoked responses to deflection in 8 cardinal angular directions (in 45° increments) in control conditions and after blockade of the postsynaptic NMDAR in the recorded neuron with either intracellular MK801 or membrane hyperpolarization. Whole-cell patch-clamp recordings from layer 4 neurons were carried out *in vivo* from an a priori mapped principal barrel (mapped by intrinsic optical imaging) (Fig. 3a and Supplementary Fig. 10). The recorded neurons and their relationship to the barrel boundaries were identified histologically at the end of each experiment (see Methods and Supplementary Fig. 10).

Consistent with previous studies[5], we found that responses of layer 4 neurons were tuned to the angular direction of the whisker deflection in the sub- and suprathreshold range (Figs 3 and 4). The average selectivity index was 0.64 ± 0.03 for subthreshold responses. The angular tuning maps remained stable throughout the length of the recording when the recording electrode contained control solution

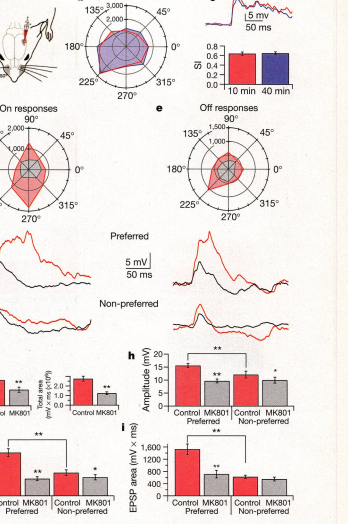

Figure 3 | The role of NMDAR-dependent dendritic regenerative responses in angular tuning of layer 4 neurons *in vivo*. **a**, Whole-cell patch-clamp recordings were carried out from layer 4 cells *in vivo* while deflecting the principal whisker in eight cardinal directions (see Methods). **b**, Polar plot showing average EPSP area (in mV × ms) of the 'on' responses to whisker deflection in 8 directions (every 45°) obtained 2 to 12 min (red) and 30 to 40 min (blue) after whole-cell break with control pipette solution. **c**, Top, response to the preferred direction (225°) in the first 10 min and after 40 min. Bottom, average selectivity index (SI) calculated 10 and 40 min after whole-cell break ($n = 6$). **d**, Top, polar plot showing average on responses obtained 2 to 8 min (red) and 30 to 36 min (grey) after whole-cell break with an electrode containing MK801 (4 mM). Bottom, example traces of on responses to the preferred (upper traces) and non-preferred (lower traces) directions, during control recordings (red) and after 32 min with MK801 (black). **e**, Same as **d** but for the off responses (same neuron as in **d**). **f**, Average SI (left panel) of neurons in control conditions (first 10 min of recording) and with intracellular MK801 (after 40 min). Average area (right panel) of the angular tuning maps in control conditions (first 10 min of recording) and with intracellular MK801 (after 40 min). **g**–**i**, Average EPSP half width, amplitude and area of the subthreshold responses to preferred and non-preferred directions in control conditions (first 10 min of recording) and with intracellular MK801 (after 40 min). In all measurements the preferred and non-preferred directions were the directions of whisker deflection with the largest and smallest responses, respectively. $n = 13$, $^*P < 0.05$; $^{**}P < 0.01$. Error bars, mean ± s.e.m.

(102 ± 7% after 40 min of recordings, $n = 6$; Fig. 3b, c). In contrast, angular tuning was significantly affected when MK801 (2–4 mM) was present in the recording electrode. Following intracellular NMDAR blockade, the selectivity index dropped significantly from 0.71 ± 0.06 in the first 10 min of the recording to 0.44 ± 0.07 after 30 to 40 min from the break to the whole-cell configuration ($P < 0.01$, $n = 13$;

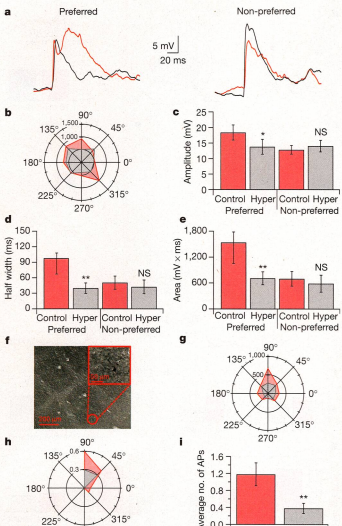

Figure 4 | Effect of hyperpolarization on the angular tuning responses of layer 4 neurons *in vivo* and the effect of MK801 on angular tuning of suprathreshold responses. **a**, Examples of traces of on responses to whisker deflection in the preferred (left panel) and non-preferred (right panel) directions in control (red) and after membrane potential hyperpolarization by 15 mV (black). **b**, Angular tuning maps (area measured in mV × ms) of the on subthreshold responses to whisker deflection in eight different directions in resting membrane potential (control, red) and after membrane potential hyperpolarization by 15 mV (grey). **c**–**e**, The average (mean ± s.e.m.; $n = 6$) EPSP amplitude (**c**) half width (**d**) and area (**e**) of the preferred and non-preferred responses in resting membrane potential (control), and after membrane potential hyperpolarization (Hyper) by 15 mV. **f**, Tangential view of the biocytin-stained spiny stellate neuron and its location according to the cytochrome-oxidase-dense regions typical to layer 4 barrels. **g**, **h**, Angular tuning maps of the on subthreshold responses (**g**) and the on suprathreshold action-potential firing responses (**h**) to whisker deflection in eight different directions in the presence of intracellular MK801 in the first 10 min (control, red) and after 40 min (grey). **i**, The average number (± s.e.m; $n = 6$) of action potentials fired during the preferred angular direction in the presence of intracellular MK801 in the first 10 min (control) and after 40 min. The subthreshold maps depict the average EPSP area, and the suprathreshold map depicts the average number of action potentials during the on responses. *$P < 0.05$; **$P < 0.01$. APs, action potentials; NS, not significant.

Fig. 3d–f and Supplementary Fig. 11). The sharp drop in angular tuning selectivity was caused by the fact that the NMDAR preferentially contributed to the area, half width and amplitude of the responses to the preferred angular deflection compared with the non-preferred angles, which were affected as expected from *in vitro* data[8] (Fig. 3d–i). The large contribution of NMDAR (59.8% and 49.6% of the EPSP half width and area, respectively) indicated the participation of NMDAR dendritic regenerative mechanism in amplifying the preferred responses. Consistent with participation of regenerative dendritic NMDAR responses, hyperpolarization of the membrane potential by approximately 15 mV caused a significant decrease in the responses to the preferred direction (Fig. 4a–e).

For the suprathreshold range, we observed a sharp reduction in the average number of action potentials in the preferred angular direction with intracellular blockade of NMDAR channels. The average number of action potentials in the preferred direction dropped from 1.18 ± 0.27 per stimulus in the first 10 min of recording to 0.38 ± 0.13 after 30 to 40 min of recording with intracellular MK801 (67.8%, $n = 6$, $P < 0.01$, Fig. 4f–i). Analysis of suprathreshold responses was limited to the preferred angles owing to the small number of action potentials evoked by non-preferred angles already under control conditions.

Similar to its contribution in angular tuning responses, NMDAR dendritic regenerative activation also significantly contributed to sensory responses in layer 4 neurons evoked by artificial whisking (see Supplementary Fig. 12).

To understand further the contribution of NMDAR-dependent dendritic mechanisms to shaping the angular tuning responses of layer 4 neurons, we simulated thalamocortical and feed-forward excitatory and inhibitory responses in a multi-compartmental spiny stellate cell model (Supplementary Fig. 13a). Our simulations show that dendritic NMDAR regenerative properties crucially contributed to angular tuning. The preferred selectivity was determined by the input bias, which is amplified further by regenerative dendritic NMDAR responses (Supplementary Fig. 13). Indeed, the selectivity index dropped to the level represented by the presynaptic excitatory bias across a wide range of stimulation intensities when the NMDAR channels were excluded (Supplementary Fig. 13d, f, g).

In conclusion, our data indicate that dendritic NMDARs in layer 4 neurons can facilitate a spectrum of dendritic regenerative events ranging from graded amplification to full-blown local and global dendritic NMDA spikes[29]. This dendritic regenerative mechanism has a role in shaping the responses to whisker sensing, and is crucial for the formation of angular tuning responses in layer 4 neurons.

Dendritic NMDAR regenerative amplification can carry several 'physiological benefits', including the ability to drive the neuron by a smaller number of thalamocortical inputs and a reduction in the number of biased thalamic inputs[5] required to generate sharp and stable tuning curves. We propose that the axonal amplification mechanism of biased inputs[30] suggested previously is combined with dendritic amplification mechanisms to efficiently translate small biases in the input profile to sharply tuned output responses.

METHODS SUMMARY

For the *in vitro* experiments, thalamocortical slices were prepared from CD-1 mice. Whole-cell patch-clamp recordings, focal and global synaptic stimulation calcium imaging and glutamate uncaging were carried out with visually identified layer 4 spiny stellate neurons using standard techniques[21,23].

For *in vivo* experiments, whole-cell patch-clamp recordings were performed using urethane-anaesthetized Wistar rats. The principal whisker was identified using intrinsic optical imaging and activated using either artificial whisking evoked by stimulating the buccal branch of the facial motor nerve or by passive whisker deflection in eight cardinal directions using a pair of crossed piezoelectric bimorphs[5].

Simulations were conducted on a multi-compartmental spiny stellate neuron with realistic morphology, voltage-gated channel distribution and parameters of synaptic activation.

Received 20 May; accepted 27 July 2012.
Published online 2 September 2012.

1. Benshalom, G. & White, E. L. Quantification of thalamocortical synapses with spiny stellate neurons in layer IV of mouse somatosensory cortex. *J. Comp. Neurol.* **253,** 303–314 (1986).

2. Binzegger, T., Douglas, R. J. & Martin, K. A. A quantitative map of the circuit of cat primary visual cortex. *J. Neurosci.* **24,** 8441–8453 (2004).
3. Hubel, D. H. & Wiesel, T. N. Receptive fields, binocular interaction and functional architecture in the cat's visual cortex. *J. Physiol.* **160,** 106–154 (1962).
4. Woolsey, T. A. & Van der Loos, H. The structural organization of layer IV in the somatosensory region (SI) of mouse cerebral cortex. The description of a cortical field composed of discrete cytoarchitectonic units. *Brain Res.* **17,** 205–242 (1970).
5. Bruno, R. M., Khatri, V., Land, P. W. & Simons, D. J. Thalamocortical angular tuning domains within individual barrels of rat somatosensory cortex. *J. Neurosci.* **23,** 9565–9574 (2003).
6. Wang, H. P., Spencer, D., Fellous, J. M. & Sejnowski, T. J. Synchrony of thalamocortical inputs maximizes cortical reliability. *Science* **328,** 106–109 (2010).
7. Bruno, R. M. & Sakmann, B. Cortex is driven by weak but synchronously active thalamocortical synapses. *Science* **312,** 1622–1627 (2006).
8. Gil, Z., Connors, B. W. & Amitai, Y. Efficacy of thalamocortical and intracortical synaptic connections: quanta, innervation, and reliability. *Neuron* **23,** 385–397 (1999).
9. Stratford, K. J., TarczyHornoch, K., Martin, K. A. C., Bannister, N. J. & Jack, J. J. B. Excitatory synaptic inputs to spiny stellate cells in cat visual cortex. *Nature* **382,** 258–261 (1996).
10. Sarid, L., Bruno, R., Sakmann, B., Segev, I. & Feldmeyer, D. Modeling a layer 4-to-layer 2/3 module of a single column in rat neocortex: interweaving *in vitro* and *in vivo* experimental observations. *Proc. Natl Acad. Sci. USA* **104,** 16353–16358 (2007).
11. Alonso, J. M., Usrey, W. M. & Reid, R. C. Precisely correlated firing in cells of the lateral geniculate nucleus. *Nature* **383,** 815–819 (1996).
12. Priebe, N. J. & Ferster, D. Inhibition, spike threshold, and stimulus selectivity in primary visual cortex. *Neuron* **57,** 482–497 (2008).
13. Johnston, D., Magee, J. C., Colbert, C. M. & Cristie, B. R. Active properties of neuronal dendrites. *Annu. Rev. Neurosci.* **19,** 165–186 (1996).
14. Magee, J., Hoffman, D., Colbert, C. & Johnston, D. Electrical and calcium signaling in dendrites of hippocampal pyramidal neurons. *Annu. Rev. Physiol.* **60,** 327–346 (1998).
15. Häusser, M., Spruston, N. & Stuart, G. J. Diversity and dynamics of dendritic signaling. *Science* **290,** 739–744 (2000).
16. Poirazi, P. & Mel, B. W. Impact of active dendrites and structural plasticity on the memory capacity of neural tissue. *Neuron* **29,** 779–796 (2001).
17. Branco, T. & Hausser, M. The single dendritic branch as a fundamental functional unit in the nervous system. *Curr. Opin. Neurobiol.* **20,** 494–502 (2010).
18. Polsky, A., Mel, B. W. & Schiller, J. Computational subunits in thin dendrites of pyramidal cells. *Nature Neurosci.* **7,** 621–627 (2004).
19. Archie, K. A. & Mel, B. W. A model for intradendritic computation of binocular disparity. *Nature Neurosci.* **3,** 54–63 (2000).
20. Schiller, J., Major, G., Koester, H. J. & Schiller, Y. NMDA spikes in basal dendrites of cortical pyramidal neurons. *Nature* **404,** 285–289 (2000).
21. Polsky, A., Mel, B. & Schiller, J. Encoding and decoding bursts by NMDA spikes in basal dendrites of layer 5 pyramidal neurons. *J. Neurosci.* **29,** 11891–11903 (2009).
22. Fleidervish, I. A., Binshtok, A. M. & Gutnick, M. J. Functionally distinct NMDA receptors mediate horizontal connectivity within layer 4 of mouse barrel cortex. *Neuron* **21,** 1055–1065 (1998).
23. Larkum, M. E., Nevian, T., Sandler, M., Polsky, A. & Schiller, J. Synaptic integration in tuft dendrites of layer 5 pyramidal neurons: a new unifying principle. *Science* **325,** 756–760 (2009).
24. Major, G., Polsky, A., Denk, W., Schiller, J. & Tank, D. W. Spatiotemporally graded NMDA spike/plateau potentials in basal dendrites of neocortical pyramidal neurons. *J. Neurophysiol.* **99,** 2584–2601 (2008).
25. Stratford, K. J., Tarczy-Hornoch, K., Martin, K. A., Bannister, N. J. & Jack, J. J. Excitatory synaptic inputs to spiny stellate cells in cat visual cortex. *Nature* **382,** 258–261 (1996).
26. White, E. L. & Rock, M. P. Three-dimensional aspects and synaptic relationships of a Golgi-impregnated spiny stellate cell reconstructed from serial thin sections. *J. Neurocytol.* **9,** 615–636 (1980).
27. Jia, H., Rochefort, N. L., Chen, X. & Konnerth, A. Dendritic organization of sensory input to cortical neurons *in vivo*. *Nature* **464,** 1307–1312 (2010).
28. Kremer, Y., Leger, J. F., Goodman, D., Brette, R. & Bourdieu, L. Late emergence of the vibrissa direction selectivity map in the rat barrel cortex. *J. Neurosci.* **31,** 10689–10700 (2011).
29. Schiller, J. & Schiller, Y. NMDA receptor-mediated dendritic spikes and coincident signal amplification. *Curr. Opin. Neurobiol.* **11,** 343–348 (2001).
30. Priebe, N. J. & Ferster, D. Direction selectivity of excitation and inhibition in simple cells of the cat primary visual cortex. *Neuron* **45,** 133–145 (2005).

Supplementary Information is available in the online version of the paper.

Acknowledgements We thank Y. Schiller and G. Major for their helpful comments and discussions on the manuscript. We thank A. Korngreen and C. de Kock for help with Neurolucida reconstructions, U. Dubin for help in programming the stimulus and analysis programs, O. Schiff for help with Igor software and R. Azouz for help with the passive stimulus. We thank I. Reiter for her technical help, particularly with histology. We also thank R. Bruno for sharing his knowledge of *in vivo* patch clamp recordings. This study was supported by the Israel Science Foundation (ISF) and the Rappaport Foundation (J.S.).

Author Contributions M.L. and L.G. performed the *in vivo* experiments and S.R. carried out the *in vitro* slice experiments and helped with analysis. A.P. performed the computer simulations. J.S. designed the study, assisted in the experiments, carried out the analysis and prepared the manuscript. M.L. also participated in the manuscript preparation.

Author Information Reprints and permissions information is available at www.nature.com/reprints. The authors declare no competing financial interests. Readers are welcome to comment on the online version of the paper. Correspondence and requests for materials should be addressed to J.S. (Jackie@tx.technion.ac.il).

LETTER

doi:10.1038/nature11436

Severe stress switches CRF action in the nucleus accumbens from appetitive to aversive

Julia C. Lemos[1,2,3], Matthew J. Wanat[1,2], Jeffrey S. Smith[2], Beverly A. S. Reyes[4], Nick G. Hollon[1,2,3], Elisabeth J. Van Bockstaele[4], Charles Chavkin[2,3] & Paul E. M. Phillips[1,2,3]

Stressors motivate an array of adaptive responses ranging from 'fight or flight' to an internal urgency signal facilitating long-term goals[1]. However, traumatic or chronic uncontrollable stress promotes the onset of major depressive disorder, in which acute stressors lose their motivational properties and are perceived as insurmountable impediments[2]. Consequently, stress-induced depression is a debilitating human condition characterized by an affective shift from engagement of the environment to withdrawal[3]. An emerging neurobiological substrate of depression and associated pathology is the nucleus accumbens, a region with the capacity to mediate a diverse range of stress responses by interfacing limbic, cognitive and motor circuitry[4]. Here we report that corticotropin-releasing factor (CRF), a neuropeptide released in response to acute stressors[5] and other arousing environmental stimuli[6], acts in the nucleus accumbens of naive mice to increase dopamine release through coactivation of the receptors CRFR1 and CRFR2. Remarkably, severe-stress exposure completely abolished this effect without recovery for at least 90 days. This loss of CRF's capacity to regulate dopamine release in the nucleus accumbens is accompanied by a switch in the reaction to CRF from appetitive to aversive, indicating a diametric change in the emotional response to acute stressors. Thus, the current findings offer a biological substrate for the switch in affect which is central to stress-induced depressive disorders.

CRF initiates neuroendocrine signalling in the hypothalamic–pituitary–adrenal axis and also regulates neurotransmission directly through two receptor subtypes, CRF receptor 1 (CRFR1) and CRFR2, which are distributed widely throughout the brain[7,8]. In the nucleus accumbens, CRF facilitates cue-elicited motivation[9] and social bonding[10], behaviours that are thought to be mediated by dopamine transmission[11,12]. Therefore, we sought evidence for CRF–dopamine interactions in the nucleus accumbens, first using fluorescent immunohistochemistry. Dense CRF immunoreactivity was present throughout the rostro-caudal axis of the nucleus accumbens core and lateral shell, and in the most rostral portion of the medial shell in sparsely located large cell bodies (cholinergic interneurons, see Supplementary Fig. 1) and fibre terminals that were interdigitated with tyrosine-hydroxylase-immunoreactive fibres that are indicative of dopamine-containing axons (Fig. 1a). Immunoreactivity for the CRFR1 receptor displayed punctate staining with co-localization of tyrosine-hydroxylase immunoreactivity on fibre segments in addition to localization on cell bodies within the nucleus accumbens (Fig. 1b and Supplementary Fig. 2). CRFR2 immunoreactivity had a more diffuse but still punctate pattern of staining, similar to that in other regions[8,13], with some co-localization with tyrosine-hydroxylase immunoreactivity (Fig. 1c and Supplementary Fig. 3). Expression of CRF receptors on subcellular profiles in the nucleus accumbens, including tyrosine-hydroxylase-positive terminals, was confirmed at higher spatial resolution using transmission electron microscopy (Fig. 1d; quantified in Supplementary Table 1). Together, these data indicate that the localization of CRF and its receptors in the nucleus accumbens is well-suited for modulation of dopamine release.

To directly test the functional effects of CRF on dopamine release in the nucleus accumbens, we selectively monitored dopamine release evoked by a single biphasic electrical pulse (2 ms per phase, 100–500 μA delivered once per minute) in acute coronal brain slices using fast-scan cyclic voltammetry at carbon-fibre microelectrodes (Fig. 2a and Supplementary Fig. 4). Vehicle or CRF (10, 100 or 1,000 nM) was applied to the slice for 15 min after 5 min of stable baseline, and the resultant effect was quantified by averaging the evoked dopamine current in the last 10 minutes. After application of vehicle, there was a modest (~7%) decrease in dopamine release (Fig. 2b), whereas CRF increased dopamine release in a concentration-dependent manner eliciting effects significantly greater than vehicle at 100 and 1,000 nM (27.8 ± 6.7 and 30.0 ± 8.4%, respectively, mean ± s.e.m.; $F_{3,49} = 5.026$, $P < 0.01$, one-way analysis of variance (ANOVA) with Dunnett's post-hoc *t*-tests; Fig. 2b and Supplementary Fig. 5). Interestingly, this effect could be blocked by application of either the selective CRFR1 antagonist, antalarmin (1 μM), or the selective CRFR2 antagonist, anti-sauvagine 30 (ASVG 30; 250 nM), to the slice beginning 20 min before CRF application ($F_{2,50} = 5.142$, $P < 0.01$, one-way ANOVA with Dunnett's post-hoc *t*-tests; Fig. 2c) indicating that coactivation of both receptors is required. Consistently, CRF (10,

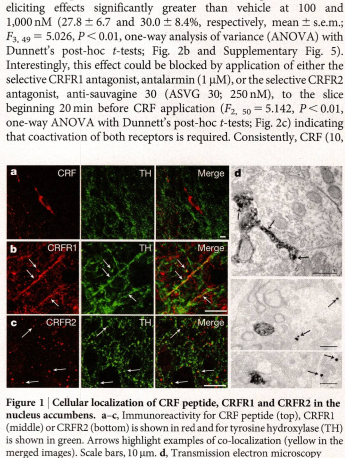

Figure 1 | Cellular localization of CRF peptide, CRFR1 and CRFR2 in the nucleus accumbens. a–c, Immunoreactivity for CRF peptide (top), CRFR1 (middle) or CRFR2 (bottom) is shown in red and for tyrosine hydroxylase (TH) is shown in green. Arrows highlight examples of co-localization (yellow in the merged images). Scale bars, 10 μm. **d**, Transmission electron microscopy photomicrographs showing CRF receptors (labelled with immunogold particles; arrows) present on both TH-positive (immunoperoxidase labelled) and TH-negative profiles. Scale bars, 0.5 μm (top panel) and 1 μm (bottom panels).

[1]Department of Psychiatry and Behavioral Sciences, University of Washington, Seattle, Washington 98195, USA. [2]Department of Pharmacology, University of Washington, Seattle, Washington 98195, USA. [3]Program in Neurobiology and Behavior, University of Washington, Seattle, Washington 98195, USA. [4]Department of Neuroscience, Farber Institute for Neurosciences, Thomas Jefferson University, Philadelphia, Pennsylvania 19107, USA.

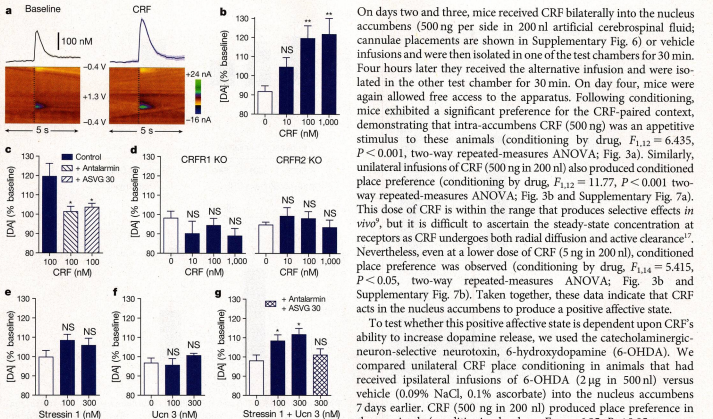

Figure 2 | CRF increases dopamine release in the nucleus accumbens through coactivation of CRFR1 and CRFR2. a, Representative dopamine release evoked by electrical stimulation (dashed lines) before (left) and after (right) application of 100 nM CRF (mean ± s.e.m. for 5 consecutive stimulations, top) and corresponding two-dimensional plots depicting changes in faradaic current (pseudocolour) with time as the abscissa and applied potential as the ordinate (bottom). **b**, Concentration response to CRF, $n = 11–18$. **c**, Effect of antagonists for CRFR1 (antalarmin, 1000 nM) or CRFR2 (anti-sauvagine 30 (ASVG 30), 250 nM), $n = 18–20$. **d**, CRF in mice lacking the gene encoding the CRFR1 (left) or CRFR2 (right) receptors, $n = 7–13$. **e**–**g**, Effect of the CRFR1 agonist, stressin 1, $n = 9–15$ (**e**), the CRFR2 agonist, urocortin 3 (100 or 300 nM), $n = 5–8$ (**f**) or their co-application, $n = 8–15$ (**g**). Error bars, s.e.m. DA, dopamine; NS, not significant (with $P > 0.05$); $^*P < 0.05$; $^{**}P < 0.01$ versus vehicle.

100, 1,000 nM) failed to increase dopamine release in the nucleus accumbens of mice with deletion of either the *Crfr1* (ref. 14) or *Crfr2* (ref. 15) gene (Fig. 2d). Application of the selective CRFR1 agonist stressin 1 (100 or 300 nM) or the selective CRFR2 agonist urocortin 3 (100 or 300 nM) failed to significantly increase dopamine release when applied individually ($P > 0.05$ compared to respective vehicles; Fig. 2e, f), but significantly increased dopamine release when applied together ($F_{3,36} = 3.528$, $P < 0.05$ versus vehicle, one-way ANOVA with Dunnett's post-hoc *t*-tests). The effect of the agonists together could be blocked by pre-treatment with antalarmin and ASVG 30 (unpaired *t*-test, $P > 0.05$; Fig. 2g). Together these data provide convergent evidence that CRF increases dopamine release in the nucleus accumbens through coactivation of CRFR1 and CRFR2.

If this ability for CRF to positively regulate dopamine in the nucleus accumbens has specific motivational relevance to the behaving animal, we would predict that it would cause conditioned place preference when restricted to the nucleus accumbens, even though centrally administered CRF elicits robust conditioned place aversion[16]. Therefore, we used a balanced place-conditioning apparatus consisting of two visually distinct test chambers separated by a smaller neutral compartment. On day one, mice were allowed to freely roam the apparatus, and the time they spent in each chamber was recorded. On days two and three, mice received CRF bilaterally into the nucleus accumbens (500 ng per side in 200 nl artificial cerebrospinal fluid; cannulae placements are shown in Supplementary Fig. 6) or vehicle infusions and were then isolated in one of the test chambers for 30 min. Four hours later they received the alternative infusion and were isolated in the other test chamber for 30 min. On day four, mice were again allowed free access to the apparatus. Following conditioning, mice exhibited a significant preference for the CRF-paired context, demonstrating that intra-accumbens CRF (500 ng) was an appetitive stimulus to these animals (conditioning by drug, $F_{1,12} = 6.435$, $P < 0.001$, two-way repeated-measures ANOVA; Fig. 3a). Similarly, unilateral infusions of CRF (500 ng in 200 nl) also produced conditioned place preference (conditioning by drug, $F_{1,12} = 11.77$, $P < 0.001$ two-way repeated-measures ANOVA; Fig. 3b and Supplementary Fig. 7a). This dose of CRF is within the range that produces selective effects *in vivo*[9], but it is difficult to ascertain the steady-state concentration at receptors as CRF undergoes both radial diffusion and active clearance[17]. Nevertheless, even at a lower dose of CRF (5 ng in 200 nl), conditioned place preference was observed (conditioning by drug, $F_{1,14} = 5.415$, $P < 0.05$, two-way repeated-measures ANOVA; Fig. 3b and Supplementary Fig. 7b). Taken together, these data indicate that CRF acts in the nucleus accumbens to produce a positive affective state.

To test whether this positive affective state is dependent upon CRF's ability to increase dopamine release, we used the catecholaminergic-neuron-selective neurotoxin, 6-hydroxydopamine (6-OHDA). We compared unilateral CRF place conditioning in animals that had received ipsilateral infusions of 6-OHDA (2 µg in 500 nl) versus vehicle (0.09% NaCl, 0.1% ascorbate) into the nucleus accumbens 7 days earlier. CRF (500 ng in 200 nl) produced place preference in sham animals (conditioning by drug, $F_{1,18} = 6.95$, $P < 0.05$ two-way repeated-measures ANOVA; Supplementary Fig. 8a), of similar magnitude to controls (treatment by drug, $F_{1,30} = 0.35$, $P > 0.05$, two-way ANOVA). However, place preference to intra-accumbens CRF was absent in animals that received 6-OHDA (conditioning by drug, $F_{1,18} = 0.00$, $P > 0.05$, two-way repeated-measures ANOVA; Supplementary Fig. 8b) showing a significant change in the subjective effects of CRF ($P < 0.05$, unpaired *t*-test; Fig. 3b). This 6-OHDA treatment produced a significant dopamine depletion on the side of the injection ($P < 0.001$; Supplementary Fig. 8c), but did not alter locomotor activity ($P > 0.05$, unpaired *t*-test; Supplementary Fig. 8d), demonstrating that the unilateral lesions did not produce a general deficit in motor function. These data demonstrate that the positive affective state produced by CRF in the nucleus accumbens is dependent on its ability to increase dopamine release.

To ascertain the role of endogenously released CRF in the nucleus accumbens in mediating appetitive behaviours, we tested the effect of CRF antagonism on the response to an arousing stimulus by assaying novel object exploration, a behaviour that requires intact dopamine transmission[18]. We bilaterally infused the CRF antagonist, α-helical CRF (500 ng in 200 nl per side) or vehicle (lactated ringer's with 1% acetic acid), into the nucleus accumbens, placed animals into an arena, and then 15 min later introduced a novel object into the centre. Although α-helical CRF had no effect on baseline exploration of the centre of the arena compared to vehicle, it significantly attenuated the appetitive effects (that is, eliciting of approach and exploration) of the novel object (treatment by stimulus, $F_{1,18} = 4.62$, $P < 0.05$, two-way repeated-measures ANOVA; Fig. 3c). These data demonstrate that endogenous CRF in the nucleus accumbens is used under physiological conditions to mediate appetitive responses to arousing environmental stimuli.

Exposure to severe or chronic stress can produce profound alterations in normal stress signalling that can be detrimental to physical and mental health, predisposing individuals to depression[19]. To model this phenomenon, we used a modified Porsolt paradigm in which mice are exposed to 2 days of repeated swim stress. Animals were placed in a vessel of water (29–31 °C) for 15 min followed by four additional

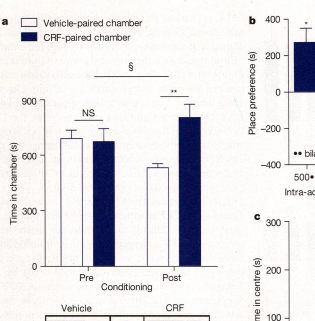

Figure 3 | CRF in the nucleus accumbens promotes appetitive behaviour. **a**, Mean difference in times spent in the CRF-paired chamber compared to the vehicle-paired chamber before and after conditioning (top panel; $n = 7$) and representative post-conditioning activity trace (bottom panel). **b**, Place preference (time in CRF-paired chamber minus the time spent in the vehicle-paired chamber post conditioning) for intra-nucleus accumbens injections of 500 ng CRF bilateral, 500 ng unilateral or 5 ng bilateral (left panel; $n = 7$–10). Place preference for 500 ng CRF (unilateral) in sham or 6-OHDA-treated mice (right; $n = 10$). **c**, Time spent in the centre of an open field before and during presentation of a novel object (placed in the centre of the field) after bilateral intra-accumbens infusion of the CRF-receptor antagonist α-helical CRF (500 ng) or its vehicle ($n = 10$). Error bars, s.e.m. NS, $P > 0.05$; *$P < 0.05$; **$P < 0.01$; ***$P < 0.001$; §$P < 0.05$ for interaction.

6-min swim sessions (separated by 6-min recovery periods) 24 h later. This protocol has been shown to produce escalating immobility across sessions, indicating a depression-like phenotype[20]. We prepared coronal slices of the nucleus accumbens from these animals 30 minutes after the final stress exposure and found that the ability for CRF to potentiate dopamine release was completely abolished (stress exposure by drug, $F_{4,116} = 12.61$, $P < 0.001$ two-way ANOVA; Fig. 4a). Notably, we established that this change in the ability of CRF to regulate dopamine release was not a generalized change in stress-related peptide signalling as the effect of a κ-opioid agonist to reduce dopamine release was unaffected by the 2-day stress-exposure paradigm (Supplementary Fig. 9). Therefore, these data show that severe stress selectively abolishes CRF's ability to modulate dopamine release in the nucleus accumbens. Surprisingly, there was no recovery of the action of CRF on dopamine release in the nucleus accumbens 7, 30 or even 90 days after stress exposure (stress exposure by drug, $F_{4,116} = 4.852$, $P < 0.01$, two-way ANOVA; Fig. 4a). This time period is consistent with the protracted course of stress-induced depressive disorders[21], and indeed, a depression-like phenotype was maintained across this 90-day post-stress period, as assessed by swim immobility (Supplementary Fig. 10). Importantly, the loss of the CRF response was not due to a baseline change in evoked dopamine release (Supplementary Fig. 11) and it was not simply an age-related phenomenon (Supplementary Fig. 12). Therefore, we have shown that severe stress produces a persistent dysregulation of CRF-dopamine interactions that normally produce a positive affective state.

Stress-induced depressive disorders are associated with altered levels of several neurochemicals that interact with the CRF system, including serotonin[22], dynorphin[23] and glucocorticoids[4,24]. Therefore, we targeted these systems to gain mechanistic insight into the stress-induced loss of CRF's regulation of dopamine release. We pretreated animals (10 ml kg^{-1} intraperitoneal) with vehicle, fluoxetine (selective serotonin-reuptake inhibitor; 10 mg kg^{-1}), norBNI (κ-opioid-receptor antagonist; 10 mg kg^{-1}) or RU486 (glucocorticoid-receptor antagonist; 30 mg kg^{-1}) before stress exposure on each of the swim-stress days. The animals were allowed to recover for 7 days, then slices were prepared and the CRF response was tested. Although acute regimens of fluoxetine do not alleviate pre-existing depression-related symptoms in patients or animal models, they have been shown to prevent the induction of some depression-like responses to stress[25]. Nevertheless, this treatment did not affect the abolition of CRF modulation of dopamine release by stress ($P > 0.05$; Supplementary Fig. 13). Similarly, this stress-induced perturbation was not significantly affected by norBNI ($P > 0.05$; Supplementary Fig. 13); however, it was prevented by RU486 (30 mg kg^{-1}; $P < 0.001$; Fig. 4a and Supplementary Fig. 13), even at a lower dose (10 mg kg^{-1}; $P < 0.01$; Supplementary Fig. 13). These data show that glucocorticoid signalling is a critical component of the profound stress-induced dysregulation of CRF–dopamine interactions in the nucleus accumbens.

This robust loss of the neurochemical response to CRF in the nucleus accumbens after severe stress suggests a long-lasting alteration in its subjective qualities. To test this idea, we used the place-conditioning paradigm in animals that had been exposed to the 2-day swim-stress regimen. Mice that underwent repeated swim stress 7 days before conditioning spent significantly less time in the CRF-paired chamber than in the vehicle-paired chamber after conditioning, establishing that CRF in the nucleus accumbens is now aversive to these animals (conditioning by drug, $F_{1,\ 10} = 5.824$, $P < 0.01$, two-way ANOVA, Supplementary Fig. 14a). Therefore, severe stress produces a diametric shift in the subjective qualities of CRF in the nucleus accumbens from positive to negative (Fig. 4b). Consistent with the enduring loss of CRF regulation of dopamine observed *in vitro*, the

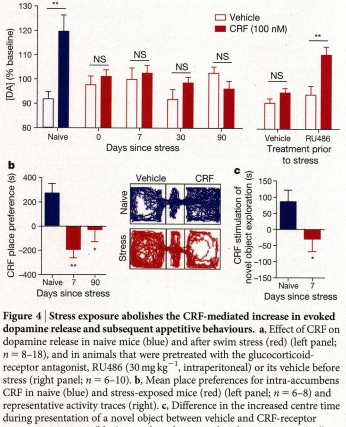

Figure 4 | Stress exposure abolishes the CRF-mediated increase in evoked dopamine release and subsequent appetitive behaviours. a, Effect of CRF on dopamine release in naive mice (blue) and after swim stress (red) (left panel; $n = 8–18$), and in animals that were pretreated with the glucocorticoid-receptor antagonist, RU486 (30 mg kg^{-1}, intraperitoneal) or its vehicle before stress (right panel; $n = 6–10$). **b**, Mean place preferences for intra-accumbens CRF in naive (blue) and stress-exposed mice (red) (left panel; $n = 6–8$) and representative activity traces (right). **c**, Difference in the increased centre time during presentation of a novel object between vehicle and CRF-receptor antagonism in naive (blue) animals and in animals 7 days post stress (red) ($n = 9–10$). Error bars, s.e.m. NS, $P > 0.05$, *$P < 0.05$, **$P < 0.01$; §$P < 0.05$; §§$P < 0.01$ for interaction.

absence of CRF conditioned place preference persisted for at least 90 days after repeated stress exposure ($F_{2,20} = 6.870$, $P < 0.05$, one-way ANOVA with Dunnett's post hoc; Fig. 4b and Supplementary Fig. 14b). Similarly, endogenously released CRF no longer stimulated exploration of a novel object when tested 7 days after stress exposure (stimulus by drug, $F_{1,16} = 0.004$, $P > 0.05$, two-way repeated-measures ANOVA; Supplementary Fig. 15) showing that severe stress abolished the function of CRF in the nucleus accumbens to stimulate appetitive responses to arousing stimuli (unpaired t-test, $P < 0.05$, Fig. 4c). Therefore, these findings demonstrate the long-term loss of a regulatory mechanism of motivated behaviour after severe stress.

Major depressive disorder has a lifetime prevalence of 17%, making it one the world's greatest public-health concerns[26]; however, its molecular foundation has been elusive. Patients suffering from this disorder present with constellations of symptoms that include loss of affect, cognitive impairment and homeostatic imbalance[27]; symptoms that are presumably precipitated by dysregulation of several brain regions[4]. It is established that glucocorticoid-dependent hippocampal atrophy is a critical mediator of cognitive impairment in depression such as memory loss[4]. More recently, disruption of nucleus accumbens function has been implicated in the affective symptoms of depression[4]. In the current work, we studied the actions of CRF on neurotransmission within this brain region in an attempt to connect pathological stress-related neuroadaptation with the shift in affect observed in depressed patients.

CRF receptors are distributed widely throughout the brain[6] and mediate disparate effects (see Supplementary Discussion). Our data highlight the specificity of the local action of both exogenously applied and endogenously released CRF in the nucleus accumbens in producing a positive, rather than negative, subjective state by increasing dopamine release. Importantly, we show that severe stress disables this capacity of CRF to positively regulate dopamine, removing CRF's appetitive qualities, leaving a negative perceptual bias. This dysregulation is mediated by glucocorticoid, but not κ-opioid, receptors and is not ameliorated by acute prophylactic administration of a selective serotonin-reuptake inhibitor. Glucocorticoid signalling has been shown to have genomic repressive effects on the CRF system, in particular the downregulation of CRFR1[24]. Genetic deletion of the CRFR1 gene selectively from dopamine neurons increases anxiety-like behaviour[28], demonstrating further that disruption of CRF-dopamine interactions alone is sufficient to produce a negative affective state similar to that following severe stress[29].

Collectively, our data show a specific defect in the regulation of dopamine transmission in the nucleus accumbens as a consequence of exposure to stress that induces depression-like behaviour. Depressive disorders produce a profound change in the perception of, and behavioural response to, acute stressors and other arousing environmental stimuli that elicit CRF signalling. Taken together, our findings provide a neurobiological mechanism for the affective shift from engagement of the environment to withdrawal following severe stress, central to the manifestation of major depressive disorder.

METHODS SUMMARY

Subjects. Male C57BL/6 mice aged >50 days had *ad libitum* access to food and water. Mice housed together (two to four per cage) were subjected to the same behavioural treatments. All animal procedures were approved by the University of Washington Institutional Animal Care and Use Committee.

Neuroanatomy. Immunohistochemistry was carried out as described previously[26]. Sections were incubated for 24 h with a mixture of mouse anti-tyrosine hydroxylase 1:1,000 and rabbit anti-CRF (peptide) 1:150, and chicken anti-ChAT antibody 1:150 or rabbit anti-CRFR1 or goat anti-CRFR2 (1:100 to 1:500), then incubated in the appropriate fluorescently tagged secondary antibodies (1:500), and were imaged using epifluorescent and confocal microscopes. Transmission electron microscopy was carried out as previously described[10].

Fast-scan cyclic voltammetry. 250-μm coronal slices containing the nucleus accumbens were continuously perfused (1.5–2.0 ml min^{-1}) with oxygenated artifical cerebrospinal fluid (aCSF) maintained at 31–33 °C. The potential at a carbon-fibre electrode was held at −0.4 V versus Ag/AgCl, ramped to +1.3 V and back to −0.4 V (400 V s^{-1}) every 100 ms. A single biphasic electrical pulse (2 ms per phase, 100–500 μA) was applied to the slice to evoke dopamine release.

Conditioned place preference. A three-compartment place-conditioning apparatus was used to measure preference as described previously[26]. On days 2 and 3, mice received two intra-accumbens microinjections per day: one injection of aCSF and one injection of CRF (500 ng in 200 nl per side) paired with different chambers. On day 4, mice were allowed free access to the apparatus for 30 min. At the end of behavioural testing, cannulae placements were assessed.

Novel-object exploration. The novel object exploration assay was similar to an assay that has been described previously[28]. Animals received bilateral intra-accumbens microinfusions of vehicle or α-helical CRF (500 ng in 200 nl) counterbalanced across 2 days of testing. On each testing day, the animal was exposed to a new novel object.

Full Methods and any associated references are available in the online version of the paper.

Received 13 May 2011; accepted 23 July 2012.
Published online 19 September; corrected online 17 October 2012 (see full-text HTML for details).

1. Korte, S. M., Koolhaas, J. M., Wingfield, J. C. & McEwen, B. S. The Darwinian concept of stress: benefits of allostasis and costs of allostatic load and the trade-offs in health and disease. *Neurosci. Biobehav. Rev.* **29,** 3–38 (2005).
2. Beck, A. T. The evolution of the cognitive model of depression and its neurobiological correlates. *Am. J. Psychiatry* **165,** 969–977 (2008).
3. Clark, D. A. & Beck, A. T. Cognitive theory and therapy of anxiety and depression: convergence with neurobiological findings. *Trends Cogn. Sci.* **14,** 418–424 (2010).
4. Nestler, E. J. *et al.* Neurobiology of depression. *Neuron* **34,** 13–25 (2002).
5. Wang, B. *et al.* Cocaine experience establishes control of midbrain glutamate and dopamine by corticotropin-releasing factor: a role in stress-induced relapse to drug seeking. *J. Neurosci.* **25,** 5389–5396 (2005).
6. Merali, Z., McIntosh, J. & Anisman, H. Anticipatory cues differentially provoke *in vivo* peptidergic and monoaminergic release at the medial prefrontal cortex. *Neuropsychopharmacology* **29,** 1409–1418 (2004).
7. Gallagher, J. P., Orozco-Cabal, L. F., Liu, J. & Shinnick-Gallagher, P. Synaptic physiology of central CRH system. *Eur. J. Pharmacol.* **583,** 215–225 (2008).

8. Steckler, T. & Holsboer, F. Corticotropin-releasing hormone receptor subtypes and emotion. *Biol. Psychiatry* **46,** 1480–1508 (1999).
9. Peciña, S., Schulkin, J. & Berridge, K. C. Nucleus accumbens corticotropin-releasing factor increases cue-triggered motivation for sucrose reward: paradoxical positive incentive effects in stress? *BMC Biol.* **4,** 8 (2006).
10. Lim, M. M. *et al.* CRF receptors in the nucleus accumbens modulate partner preference in prairie voles. *Horm. Behav.* **51,** 508–515 (2007).
11. Aragona, B. J. *et al.* Nucleus accumbens dopamine differentially mediates the formation and maintenance of monogamous pair bonds. *Nature Neurosci.* **9,** 133–139 (2006).
12. Lex, A. & Hauber, W. Dopamine D1 and D2 receptors in the nucleus accumbens core and shell mediate Pavlovian-instrumental transfer. *Learn. Mem.* **15,** 483–491 (2008).
13. Waselus, M., Nazzaro, C., Valentino, R. J. & Van Bockstaele, E. J. Stress-induced redistribution of corticotropin-releasing factor receptor subtypes in the dorsal raphe nucleus. *Biol. Psychiatry* **66,** 76–83 (2009).
14. Timpl, P. *et al.* Impaired stress response and reduced anxiety in mice lacking a functional corticotropin-releasing hormone receptor 1. *Nature Genet.* **19,** 162–166 (1998).
15. Bale, T. L. *et al.* Mice deficient for corticotropin-releasing hormone receptor-2 display anxiety-like behaviour and are hypersensitive to stress. *Nature Genet.* **24,** 410–414 (2000).
16. Cador, M., Ahmed, S. H., Koob, G. F., Le Moal, M. & Stinus, L. Corticotropin-releasing factor induces a place aversion independent of its neuroendocrine role. *Brain Res.* **597,** 304–309 (1992).
17. Oldfield, E. H. *et al.* Active clearance of corticotropin-releasing factor from the cerebrospinal fluid. *Neuroendocrinology* **40,** 84–87 (1985).
18. Fink, J. S. & Smith, G. P. Mesolimbic and mesocortical dopaminergic neurons are necessary for normal exploratory behavior in rats. *Neurosci. Lett.* **17,** 61–65 (1980).
19. Bale, T. L. Stress sensitivity and the development of affective disorders. *Horm. Behav.* **50,** 529–533 (2006).
20. Bruchas, M. R. *et al.* Stress-induced p38 mitogen-activated protein kinase activation mediates κ-opioid-dependent dysphoria. *J. Neurosci.* **27,** 11614–11623 (2007).
21. Coryell, W. *et al.* The time course of nonchronic major depressive disorder. Uniformity across episodes and samples. National Institute of Mental Health Collaborative Program on the Psychobiology of Depression–Clinical Studies. *Arch. Gen. Psychiatry* **51,** 405–410 (1994).
22. Torres, G., Horowitz, J. M., Laflamme, N. & Rivest, S. Fluoxetine induces the transcription of genes encoding *c-fos*, corticotropin-releasing factor and its type 1 receptor in rat brain. *Neuroscience* **87,** 463–477 (1998).
23. Bruchas, M. R. & Chavkin, C. Kinase cascades and ligand-directed signaling at the kappa opioid receptor. *Psychopharmacology (Berl.)* **210,** 137–147 (2010).
24. Iredale, P. A. & Duman, R. S. Glucocorticoid regulation of corticotropin-releasing factor1 receptor expression in pituitary-derived AtT-20 cells. *Mol. Pharmacol.* **51,** 794–799 (1997).
25. Cryan, J. F. & Mombereau, C. In search of a depressed mouse: utility of models for studying depression-related behavior in genetically modified mice. *Mol. Psychiatry* **9,** 326–357 (2004).
26. Kessler, R. C. *et al.* Lifetime prevalence and age-of-onset distributions of DSM-IV disorders in the National Comorbidity Survey Replication. *Arch. Gen. Psychiatry* 62**,** 593–602 (2005); erratum **62,** 768 (2005).
27. Gelernberg, A. J. Depression symptomatology and neurobiology. *J. Clin. Psychiatry* **71,** e02 (2010).
28. Refojo, D. *et al.* Glutamatergic and dopaminergic neurons mediate anxiogenic and anxiolytic effects of CRHR1. *Science* **333,** 1903–1907 (2011).
29. Chaki, S. *et al.* Anxiolytic- and antidepressant-like profile of a new CRF1 receptor antagonist, R278995/CRA0450. *Eur. J. Pharmacol.* **485,** 145–158 (2004).
30. Reyes, B. A., Valentino, R. J. & Van Bockstaele, E. J. Stress-induced intracellular trafficking of corticotropin-releasing factor receptors in rat locus coeruleus neurons. *Endocrinology* **149,** 122–130 (2008).

Supplementary Information is available in the online version of the paper.

Acknowledgements This work was supported by National Institutes of Health grants F31-MH086269 (J.C.L.), F32-DA026273 (M.J.W.), R01-DA009082 (E.J.V.B.), R01-DA030074 (C.C.), R01-MH079292 and R01-DA016782 (P.E.M.P.), the National Science Foundation (N.G.H.) and NARSAD (P.E.M.P.). We thank C. Zietz, M. Miyatake and P. Groblewski for assisting with histological verification of cannula placement, H. Gill for help with data analysis, D. Messinger for breeding and genotyping mice and N. Stella for use of a microscope. We thank M. Darvas and R. Palmiter for providing $Th^{Tv/Tv}$;$Dbh^{Tv/+}$ mice. We thank R. Sapolsky, J. Day, S. Sesack, M. Soden, C. Walker and E. Horne for useful suggestions and insights.

Author Contributions J.C.L. performed immunohistochemistry. J.C.L. and N.G.H. carried out fast-scan cyclic-voltammetry experiments. J.C.L., M.J.W. and J.S.S. performed the behavioural experiments. B.A.S.R. and E.J.V.B. provided transmission electron microscopy data. J.C.L., M.J.W., C.C. and P.E.M.P. developed the conceptual and experimental framework, and J.C.L. and P.E.M.P. wrote the paper.

Author Information Reprints and permissions information is available at www.nature.com/reprints. The authors declare no competing financial interests. Readers are welcome to comment on the online version of the paper. Correspondence and requests for materials should be addressed to P.E.M.P. (pemp@uw.edu).

LETTER

doi:10.1038/nature11435

Androgenetic haploid embryonic stem cells produce live transgenic mice

Wei Li[1,2]*, Ling Shuai[1,3]*, Haifeng Wan[1,2]*, Mingzhu Dong[1,2]*, Meng Wang[4], Lisi Sang[1,2], Chunjing Feng[1,2], Guan-Zheng Luo[4], Tianda Li[1,3], Xin Li[1,3], Libin Wang[1,2], Qin-Yuan Zheng[1,2], Chao Sheng[1,3], Hua-Jun Wu[2,4], Zhonghua Liu[3], Lei Liu[1], Liu Wang[1], Xiu-Jie Wang[4], Xiao-Yang Zhao[1] & Qi Zhou[1]

Haploids and double haploids are important resources for studying recessive traits and have large impacts on crop breeding[1], but natural haploids are rare in animals. Mammalian haploids are restricted to germline cells and are occasionally found in tumours with massive chromosome loss[2,3]. Recent success in establishing haploid embryonic stem (ES) cells in medaka fish[4] and mice[5,6] raised the possibility of using engineered mammalian haploid cells in genetic studies. However, the availability and functional characterization of mammalian haploid ES cells are still limited. Here we show that mouse androgenetic haploid ES (ahES) cell lines can be established by transferring sperm into an enucleated oocyte. The ahES cells maintain haploidy and stable growth over 30 passages, express pluripotent markers, possess the ability to differentiate into all three germ layers *in vitro* and *in vivo*, and contribute to germlines of chimaeras when injected into blastocysts. Although epigenetically distinct from sperm cells, the ahES cells can produce viable and fertile progenies after intracytoplasmic injection into mature oocytes. The oocyte-injection procedure can also produce viable transgenic mice from genetically engineered ahES cells. Our findings show the developmental pluripotency of androgenentic haploids and provide a new tool to quickly produce genetic models for recessive traits. They may also shed new light on assisted reproduction.

Haploid stem cells offer an easy-to-manipulate genetic system and therefore hold great value for studies of recessive phenotypes. Recently, haploid ES cells have been successfully derived from medaka fish[4] and mice[5,6], and this has provided opportunities for genetic manipulations at the cellular level in a haploid but pluripotent system. However, the feasibility of using mammalian haploid ES cells for animal-level assays is untested. In addition, several basic questions regarding mammalian haploid ES cells are still unsolved and deserve more investigations, including: first, whether the haploid nature of ES cells can be steadily maintained in further-differentiated cells; second, whether the haploid ES cells can function as haploid gametes to support fertilization and development; and third, whether genetic modifications in the haploid ES cells can bypass the germline barrier to be transmitted properly to offspring.

In an attempt to address the above questions, we established a protocol to generate mouse androgenetic haploid embryos by injecting sperm into enucleated MII phase oocytes[7,8] (Supplementary Fig. 1 and Supplementary Table 1). Using the 2i medium[9] with leukaemia inhibitory factor (LIF) and feeder cells, we generated a total of 27 androgenetic haploid embryonic stem cell (ahES) lines from 262 reconstructed embryos (Supplementary Table 2). The addition of commonly used additives for ES culture had no obvious effect on the ahES-cell-derivation efficiency (Supplementary Table 2). The transgenic chicken β-actin promoter-driven enhanced green fluorescent protein (eGFP) from the donor sperms was successfully inherited and expressed in the derived ahES-cell lines (Fig. 1a). We also established ahES-cell lines carrying an Oct4 (also known as Pou5f1) promoter-driven eGFP (Oct4–eGFP) reporter, by which eGFP expression was primarily restricted in pluripotent cells and germ cells[10].

Most of the originally obtained ahES-cell lines contained approximately 10–30% haploid cells. After three or more rounds of purification by separating Hoechst 33342-stained cells using fluorescence-activated cell sorting (FACS), haploid ahES cells with nearly 90% purity were obtained (Fig. 1b). The established ahES-cell lines all had a single X chromosome (Fig. 1c, d). They retained the haploid genome (19 autosomes and the X chromosome (19 + X)) after being passaged more than 25 times. Continuous haploid purification by FACS (more than 6 rounds) slowed down (with over 50% decrease) the autodiploidization rate of ahES cells (Supplementary Fig. 2). The lack of ahES cells containing the Y chromosome is in accordance with previous reports of the poor developmental ability of androgenetic embryos of YY chromosomes[11,12]. Comparative genomic hybridization (CGH) analysis revealed no consistent copy-number variation among the examined ahES-cell lines (AH129-5, AH129-N1 and AH129-NC1), except for a common deletion on the X chromosome (Fig. 1e and Supplementary Table 3). This deletion is a CGH artefact attributed to the probe design around the 1.75-Mb highly repetitive region (Supplementary Fig. 3). The same artefact was observed in previous reports of haploid ES cells[5,13] using the same NimbleGen whole-genome tiling array.

The ahES cells expressed typical pluripotent marker genes[14], including Oct4, Nanog and Sox2 (Supplementary Fig. 4). Global gene-expression analysis among 3 independently generated ahES-cell lines (AH129-5, AH129-NC1 and AH129-N1), 2 diploid ES-cell lines (R1 and CS 1-1), mouse round spermatids and embryonic fibroblast (MEF) cells revealed a very high correlation ($r = 0.98$) between ahES cells and ES cells, both with distinct gene-expression profiles from mouse round spermatids (Supplementary Fig. 4).

The ahES cells could form embryoid bodies and differentiate further into neural-lineage cells *in vitro*, but the majority of the differentiated cells had already undergone diploidization (Supplementary Fig. 5). Teratomas containing all 3 germ layers could be detected after subcutaneously injecting ahES cells (with nearly 90% purity) into severe-combined-immune-deficiency mice (Fig. 2a). We then injected freshly FACS-sorted G0- or G1-phase eGFP-positive ahES cells (from mice with black-coloured coats) into CD-1 blastocysts (from mice with white-coloured coats) to test their ability to form chimaeras. Chicken β-actin-driven eGFP and Oct4-eGFP expression were detected in both somatic and germline cells of the dissected chimaeric embryos at embryonic day 12.5 (E12.5), respectively (Fig. 2b, c, Supplementary Fig. 6 and Supplementary Table 4). Evidence for the

[1]State Key Laboratory of Reproductive Biology, Institute of Zoology, Chinese Academy of Sciences, Beijing 100101, China. [2]Graduate University of Chinese Academy of Sciences, Beijing 100049, China. [3]College of Life Science, Northeast Agricultural University of China, Harbin 150030, China. [4]Center for Molecular Systems Biology, Institute of Genetics and Developmental Biology, Chinese Academy of Sciences, Beijing 100101, China.
*These authors contributed equally to this work.

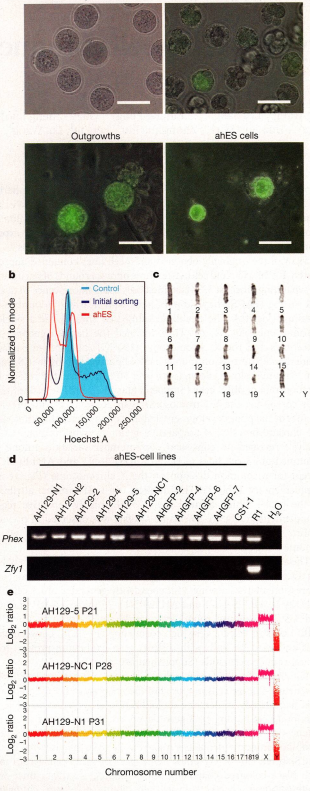

Figure 1 | Generation of androgenetic haploid ES cells. **a**, Schematic overview of the derivation process of ahES-cell lines carrying an eGFP marker. Scale bar, 100 μm. PN, pronuclear. **b**, FACS analysis of the DNA content of ahES-cell lines. Diploid ES-cell line with 2*n* chromosome sets is chosen as control (bright blue). The initial FACS sorting of the AHGFP-4 ahES-cell line at passage 5 resulted in 33.7% of haploid cells (dark blue). After purifying the G0- or G1-phase haploid cells for 3 times and followed by culturing the cells for 2 passages, 89.9% of haploid cells (passage 16) were obtained (red). **c**, Standard G-banding karyotype of an ahES cell line (passage 16), with 19 + X chromosomal set. **d**, Determination of the sex chromosome of ahES-cell lines by polymerase-chain-reaction (PCR) amplification of an X-chromosome-specific (*Phex*) or a Y-chromosome-specific (*Zfy1*) gene. ES-cell lines R1 (male) and CS 1-1 (female mouse ES-cell line.) were used as controls. **e**, CGH analysis of 3 ahES cell lines: AH129-5 (P21), AH129-NC1 (P28) and AH129-N1 (P31). Comparison of results between the genomic DNA of ahES cells and control 129Sv male mouse kidney is shown as the *y* axis, on a $\log_2$ base scale.

contribution of the ahES cells to adult chimaeric mice was provided by their coat-colour chimaerism (Fig. 2d) and by the presence of eGFP-positive cells within various tissues of dissected adult chimaeric mice, with eGFP$^+$ cells constituting 5.9%, 27.5%, 67.1% and 9.7% of the total number of cells analysed in the spleen, liver, kidney and heart, respectively (Supplementary Fig. 7). No haploid cells were detected among eGFP-positive cells (Supplementary Fig. 7), as they may have already undergone diploidization like observed in other studies[5]. Collectively, these results provide evidence of the pluripotent nature of the ahES cells.

We explored the feasibility of generating differentiated haploid cells from the ahES cells both *in vivo* and *in vitro*. Haploid G0- or G1-phase ahES cells freshly sorted by FACS were injected into diploid blastocysts to produce chimaeric embryos. In the E6.5 chimaeric embryos, approximately 6% of eGFP-positive cells were haploid by flow-cytometry analysis (Fig. 2e). However, no eGFP-positive haploid cells were identified from E12.5 embryos (Supplementary Fig. 6). After four or more rounds of FACS selection, we successfully established haploid epiblast-stem-cell-like cell lines with 87.8% of haploid cells (Fig. 2f, g and Supplementary Fig. 8), showing the feasibility of establishing haploid non-ES-cell lines in mammals. The cells expressed marker genes of epiblast stem cells (Oct4, Nanog, Gata4 and Fgf5), lost alkaline phosphatase activity and had a similar gene-expression profile to that of the diploid epiblast stem cells, but were distinct from the parental ahES cells (Fig. 2h and Supplementary Fig. 8c–e)[15–17]. The haploid epiblast-stem-cell-like cells maintained the haploid karyotype (19 + X) after being passaged for up to 15 generations. They had the ability to form embryoid bodies when being cultured without growth factors in low-attachment dishes (Supplementary Fig. 8f), and to differentiate further into haploid neural progenitor cells (with 42.3% haploid cells; Supplementary Fig. 9). These results show that the ahES cells could differentiate under the haploid state.

To test the genetic transmissibility of the ahES cells, we injected the FACS-selected G0- or G1-phase haploid ahES cells into pre-activated oocytes (intracytoplasmic ahES-cell injection (ICAI); Supplementary Fig. 10)[18,19]. The obtained embryos formed 'paternal' pseudo-pronuclei with a dynamic demethylation pattern typical of embryos produced by intracytoplasmic sperm injection[20,21] (Supplementary Fig. 11). A total of 599 2-cell embryos and 171 blastocysts reconstructed from 6 randomly selected ahES-cell lines were transplanted into 38 pseudopregnant mice. The derived embryos were normal at E13.5 with correctly inherited eGFP (Fig. 3a). Twenty-four female full-term pups were successfully obtained from four independent ahES cell lines, of which ten survived to adulthood (Table 1 and Supplementary Fig. 12a). The 14 pups that did not survive died within 30 min after birth, probably owing to developmental retardation, indicated by their abnormally small body size (Fig. 3b, c and Supplementary Fig. 12b).

Among the 10 surviving mice, 9 looked normal at adulthood and delivered healthy progeny with litter sizes of 8–11 pups when mated with CD-1 males at 8 weeks of age. The ICAI-produced mice were validated by the simple sequence-length polymorphism (SSLP) (Supplementary Fig. 12c), and their offspring showed Mendelian segregation of coat colour (Fig. 3d) and the inherited expression of β-actin eGFP (Supplementary Fig. 12d). The other mouse has a smaller body and has been unable to become pregnant so far. These results showed the ability of ahES cells to 'fertilize' oocytes and produce healthy and fertile animals, and thereby to transmit their genetic material to offspring.

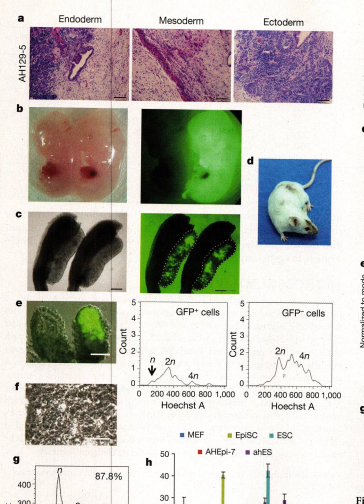

Figure 2 | The pluripotency of the ahES cells. **a**, Teratoma formation of ahES cells (from ahES-cell line AH129-5). Shown are the teratoma dissection slices representing all three germ layers identified by staining with haematoxylin and eosin in teratomas. Scale bar, 500 μm. **b**, E12.5 chimaeric embryos formed by blastocyst injection of G0- or G1-phase haploid AHGFP-4 cells into CD-1 diploid blastocysts. eGFP fluorescence indicated the chimaeric contribution of AHGFP-4 (right panel) and its non-chimaeric littermate without eGFP (left panel). **c**, Fluorescence detection of the gonads (female) of an E12.5 Oct4–GFP ahES cell derived chimaeric embryo. Scale bar, 2 mm. **d**, Adult chimaeric mouse produced by microinjection of G0- or G1-phase haploid AHGFP-4 cells into diploid blastocysts. **e**, Flow-cytometry analysis of DNA content of both the eGFP-positive and eGFP-negative cells in E6.5 chimaeric embryos. An E6.5 chimaeric embryo generated from ahES cells (AHGFP-4) is shown on the right of the image (left panel), and on the left of the image is a non-chimaeric embryo at the same stage as the control for eGFP detection. Scale bar, 100 μm. The arrow (middle panel) shows the peak of the haploid chromosome set among $eGFP^+$ cells. **f**, Brightfield of haploid epiblast-stem-cell-like cells (EpiSC-like cells; diploid EpiSCs derived from post-implantation embryos[17]). Shown is the AHEpi-7-cell line (haploid EpiSC-like cell line 7) at passage 8. **g**, Flow-cytometry analysis of DNA content of a haploid EpiSC-like cell line, AHEpi-7 (passage 6). **h**, Real-time PCR analysis of EpiSC-marker gene expression in different cell lines. Error bars, s.d. of triplicate reactions.

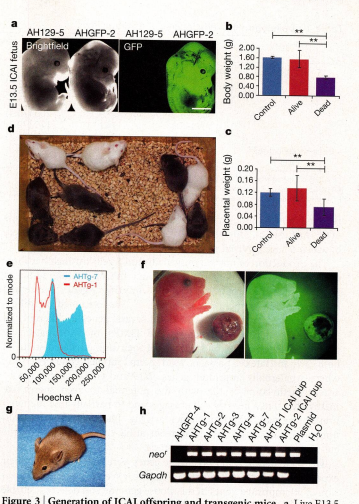

Figure 3 | Generation of ICAI offspring and transgenic mice. **a**, Live E13.5 ICAI embryos produced by 2 androgenetic haploid ahES-cell lines AH129-5 (left panel, eGFP negative) and AHGFP-2 (right panel, eGFP positive). Scale bar, 50 μm. **b**, **c**, Comparison of the body weights (**b**) and placenta weights (**c**) of the alive (1.56 ± 0.36 g; $n = 12$ (mean $\pm$ s.e.m.)) and dead (0.78 ± 0.07 g; $n = 17$) ICAI pups with the control group (wide-type mice, 1.63 ± 0.05 g; $n = 12$). $^{**}P < 0.001$ (student t-test). **d**, Coat-colour separation among the F2 generation of an ICAI-produced adult mouse (129/Sv X CD-1 background) after mating with a CD-1 male mouse. **e**, FACS analysis of the DNA content of 2 established genetically modified ahES-cell lines. AHTg-1 (red) maintained high proportions of haploid cells, whereas AHTg-7 (light blue) had no haploid cells. **f**, Live normal newborn mice produced from the transgenic ahES-cell line AHTg-1 through ICAI, with the expression of the eGFP transgene detected throughout the pup body and the placenta. **g**, A PGK–neo^r transgenic ICAI mouse that survived to adulthood. **h**, PCR analysis of the integration of the transgene neo^r in 5 transgenic cell lines, and the offspring of the AHTg-1 and AHTg-2 cell lines. Non-transgenic cell line AHGFP-4 is used as a negative control.

To demonstrate the feasibility of using ahES cells in transgenic manipulations, vectors carrying a neomycin-resistant gene (neo^r) were electroporated into 5×10^6 ahES cells (passage 12, FACS-sorted AHGFP-4 cells with the β-actin eGFP transgene). A total of 187 neomycin-resistant colonies appeared after 1 week of antibiotic (geneticin, G418) selection. We randomly picked and expanded 12 G418-resistant colonies into sub-lines (Supplementary Fig. 13a). Six lines (named AHTg-1 to AHTg-6) maintained the haploid chromosome set even after 17 passages (Fig. 3e and Supplementary Fig. 13b), whereas the other 6 cell lines (AHTg-7 to AHTg-12) were mostly converted to diploid cells (Fig. 3e and Supplementary Fig. 13c). After injecting these transgenic ahES cells (collected immediately after FACS sorting) from two sub-lines into pre-activated MII phase oocytes, we successfully obtained 143 2-cell embryos and transplanted them into pseudopregnant mice. Five full-term live pups derived from two transgenic cell lines were obtained from three foster mothers (Table 1) carrying the neo^r transgene and also inherited the eGFP transgene (Fig. 3f and Fig. 3h). Two pups were healthy and survived to adulthood (Fig. 3g). The others had lower body weights and died quickly after birth, probably owing to

Table 1 | Developmental efficiencies of ICAI embryos

Cell type	Donor cells	No. of injected oocytes	No. of cleavages (% injected)	No. of transferred embryos	No. of implantations (% ET)	No. of full-term pups (% ET)	No. of survived (% ET)
Control ahES cells	Round spermatids	104	84 (80.8)	84	ND	7 (8.3)	7 (8.3)
	AH129-NC1	257	200 (77.8)	48	21 (10.5)	0*†	0
	AH129-4	496	399 (80.4)	72	63 (15.8)	4 (1.0)*†	1 (0.3)
	AH129-5	337	240 (71.2)	51	24 (10.0)	2 (0.8)*†	1 (0.4)
	AHGFP-2	289	205 (70.9)	205	36 (17.6)	0*†	0
	AHGFP-4	241	170 (70.5)	170	ND	9 (5.3)	6 (3.5)
	AHGFP-6	317	224 (70.7)	224	51 (22.8)	9 (4.0)	2 (0.9)
Gene-modified ahES cells	AHTg-1	65	50 (76.9)	50	18 (36.0)	2 (4.0)	2 (4.0)
	AHTg-2	125	93 (74.4)	93	37 (39.8)	3 (3.2)	0

* $P < 0.05$ compared with control (two-tailed Fisher's exact test).
† $P < 0.05$ compared with the best ahES-cell AHGFP-4 (two-tailed Fisher's exact test).
ET, embryonic transfer. ND, not determined.

retarded growth (Supplementary Fig. 13d). During the revision process of this manuscript, a further 23 full-term transgenic pups were obtained, of which 6 have survived so far (Supplementary Table 5).

The production of normal progeny by ahES cells through 'fertilization' raises an intriguing question about the imprinting status of ahES cells, as the proper regulation of imprinted genes is essential for normal development of mammals[22–24]. We examined the differentially methylated regions (DMRs) of several genes in different cell lines by bisulphite sequencing. The DMRs of two maternally imprinted genes, *Snrpn* and *Airn*, kept their unmethylated status at both early and late cell passages, as in sperm (Supplementary Fig. 14a), whereas paternally imprinted genes (*H19* and *Gtl2*) showed inconsistent methylation status, with the potential to keep sperm-like methylated status in early cell passages and to partially lose methylation during passaging (Supplementary Fig. 14a). Whether this phenomenon was an intrinsic feature of ahES cells or caused by the culturing process requires further study.

The methylation changes of these genes were reflected well in their expression levels (Supplementary Fig. 14b). We analysed the expression of 90 imprinted genes in the mouse genome and detected reliable signals for 54 genes. Unexpectedly, the expression of these genes did not exhibit consistent parent-of-origin effects (Supplementary Fig. 14c). Four cell lines that produced live ICAI animals and two cell lines that failed to generate full-term ICAI pups were included in the study, and no group difference was found between them (Supplementary Fig. 14c).

We tested further the correlation of abnormal development of ICAI pups and the aberrant regulation of imprinted genes in the alive and early-dead (died within 30 minutes after birth) ICAI mice. The expression profiles of imprinted genes showed high concordance between healthy adult ICAI mice and age-matched wild-type controls, whereas there was more variation between the expression profiles of early-dead ICAI pups and controls (Supplementary Fig. 15a). The methylation level of *Gnas* was maintained well in all transgenic mice, but both early-dead mice lost imprinting at the *H19* DMR, and one of them showed slight hyper-methylation at the *Snrpn* DMR (Supplementary Fig. 15b), suggesting a potential link between the abnormal development of ICAI embryos and the altered regulation of imprinted genes[25,26].

Our data shows that laboratory-produced haploid pluripotent stem cells, although epigenetically distinct from germ cells, could function like gametes to form zygotes and produce viable progenies, which may provide an invaluable resource for assisted reproduction. The production of fertile adult mice from ahES cells shows that the genetic information in haploid ES cells is functionally complete and stable, thus enhances the merits of haploid ES cells in genetic studies. During the revision process of this work, an independent study[13] also reported the production of androgenic haploid ES cells and the feasibility of using them to produce healthy progenies, which confirmed part of our findings. The establishment of stable haploid epiblast-stem-cell-like cell lines proved that the haploid status of ahES cells can be transmitted and stably maintained in other cell types under certain circumstances. The work also provides a new approach for genetic manipulation in animal models without available germline-competent ES cells, including non-human primates[27], as modifications in such haploid stem cells could be transmitted to offspring through intracytoplasmic injection into mature oocytes, which may serve as a more efficient and simple strategy for gene-targeting studies.

METHODS SUMMARY

Androgenetic haploid embryos were reconstructed as described previously[7]. A total of 262 morula-stage embryos were plated in 4-well plates coated with mitomycin-C-treated mouse embryonic fibroblast (MEFs) as feeder cells and cultured with 2i medium[8], from which 27 ahES cell lines were successfully derived. ahES cells were purified and examined for their haploid and pluripotent characteristics using standard methods. Approximately 1×10^7 ahES cells were subcutaneously injected into the hind limbs of severe-combined-immune-deficient mice to generate teratomas. Approximately 12–15 G0- or G1-phase ahES cells collected immediately after FACS sorting were microinjected into each blastocysts to produce chimaeric embryos. ICAI was carried out as described[18], by injecting ahES cells into oocytes. The embryo development was examined at E13.5 and at full term. PGK-*neo*^{r} vectors were transfected into the ahES cells by electroporation and ICAI was carried out to generate transgenic animals.

Full Methods and any associated references are available in the online version of the paper.

Received 1 April; accepted 23 July 2012.
Published online 30 September 2012.

1. Germanà, M. A. Gametic embryogenesis and haploid technology as valuable support to plant breeding. *Plant Cell Rep.* **30,** 839–857 (2011).
2. Carette, J. E. *et al.* Haploid genetic screens in human cells identify host factors used by pathogens. *Science* **326,** 1231–1235 (2009).
3. Kaufman, M. H., Robertson, E. J., Handyside, A. H. & Evans, M. J. Establishment of pluripotential cell lines from haploid mouse embryos. *J. Embryol. Exp. Morphol.* **73,** 249–261 (1983).
4. Yi, M., Hong, N. & Hong, Y. Generation of medaka fish haploid embryonic stem cells. *Science* **326,** 430–433 (2009).
5. Leeb, M. & Wutz, A. Derivation of haploid embryonic stem cells from mouse embryos. *Nature* **479,** 131–134 (2011).
6. Elling, U. *et al.* Forward and reverse genetics through derivation of haploid mouse embryonic stem cells. *Cell Stem Cell* **9,** 563–574 (2011).
7. Zhou, Q. *et al.* Generation of fertile cloned rats by regulating oocyte activation. *Science* **302,** 1179 (2003).
8. Yanagimachi, R., Wakayama, T., Perry, A. C. F., Zuccotti, M. & Johnson, K. R. Full-term development of mice from enucleated oocytes injected with cumulus cell nuclei. *Nature* **394,** 369–374 (1998).
9. Ying, Q. L. *et al.* The ground state of embryonic stem cell self-renewal. *Nature* **453,** 519–523 (2008).
10. Yoshimizu, T. *et al.* Germline-specific expression of the Oct-4/green fluorescent protein (GFP) transgene in mice. *Dev. Growth Differ.* **41,** 675–684 (1999).
11. Tarkowski, A. K. *In vitro* development of haploid mouse embryos produced by bisection of one-cell fertilized eggs. *J. Embryol. Exp. Morphol.* **38,** 187–202 (1977).
12. Latham, K. E., Patel, B., Bautista, F. D. & Hawes, S. M. Effects of X chromosome number and parental origin on X-linked gene expression in preimplantation mouse embryos. *Biol. Reprod.* **63,** 64–73 (2000).
13. Yang, H. *et al.* Generation of genetically modified mice by oocyte injection of androgenetic haploid embryonic stem cells. *Cell* **149,** 605–617 (2012).
14. Nichols, J. & Smith, A. Naive and primed pluripotent states. *Cell Stem Cell* **4,** 487–492 (2009).
15. Brons, I. G. *et al.* Derivation of pluripotent epiblast stem cells from mammalian embryos. *Nature* **448,** 191–195 (2007).
16. Tesar, P. J. *et al.* New cell lines from mouse epiblast share defining features with human embryonic stem cells. *Nature* **448,** 196–199 (2007).
17. Maruotti, J. *et al.* Nuclear transfer-derived epiblast stem cells are transcriptionally and epigenetically distinguishable from their fertilized-derived counterparts. *Stem Cells* **28,** 743–752 (2010).

18. Kimura, Y. & Yanagimachi, R. Mouse oocytes injected with testicular spermatozoa or round spermatids can develop into normal offspring. *Development* **121,** 2397–2405 (1995).
19. Loren, J. & Lacham-Kaplan, O. The employment of strontium to activate mouse oocytes: effects on spermatid-injection outcome. *Reproduction* **131,** 259–267 (2006).
20. Mayer, W., Niveleau, A., Walter, J., Fundele, R. & Haaf, T. Demethylation of the zygotic paternal genome. *Nature* **403,** 501–502 (2000).
21. Santos, F., Hendrich, B., Reik, W. & Dean, W. Dynamic reprogramming of DNA methylation in the early mouse embryo. *Dev. Biol.* **241,** 172–182 (2002).
22. Surani, M. A., Barton, S. C. & Norris, M. L. Development of reconstituted mouse eggs suggests imprinting of the genome during gametogenesis. *Nature* **308,** 548–550 (1984).
23. Surani, M. A. *et al.* Genome imprinting and development in the mouse. *Dev.* (Suppl.) 89–98 (1990).
24. McGrath, J. & Solter, D. Completion of mouse embryogenesis requires both the maternal and paternal genomes. *Cell* **37,** 179–183 (1984).
25. Tsai, T. F., Jiang, Y. H., Bressler, J., Armstrong, D. & Beaudet, A. L. Paternal deletion from *Snrpn* to *Ube3a* in the mouse causes hypotonia, growth retardation and partial lethality and provides evidence for a gene contributing to Prader-Willi syndrome. *Hum. Mol. Genet.* **8,** 1357–1364 (1999).
26. Kono, T. *et al.* Birth of parthenogenetic mice that can develop to adulthood. *Nature* **428,** 860–864 (2004).
27. Tachibana, M. *et al.* Generation of chimeric rhesus monkeys. *Cell* **148,** 285–295 (2012).

Supplementary Information is available in the online version of the paper.

Acknowledgements We thank all members of the Group of Reproductive Engineering for discussion and help. This study was supported by a grant from the National Science Foundation of China 90919060 (to Q.Z.) and the China National Basic Research Program 2012CBA01300 (to Q.Z.), and a grant from the Strategic Priority Research Program of the Chinese Academy of Sciences XDA01020100 (to Q.Z.). We thank Fluidigm Corporation for their support in the utilization of BioMark HD system. We thank Eppendorf and Leica for supporting the facility.

Author Contributions Q.Z. and X.-Y.Z. designed the experiments;; W.L., L.S., H.W., M.D., M.W., L.S., C.F., T.L., X.L., L.W., Q.-Y.Z. and C.S. performed experiments; Q.Z, X.-Y.Z, X.-J.W., G.-Z.L., W.L., H.-J.W. and L.L. analysed data; Q.Z., X.-Y.Z., Z.L., and L.W. supervised experiments; W.L., L.S., H.W. and M.D. contributed to part of the Methods. Q.Z., X.-Y.Z., X.-J.W. and W.L. wrote the paper.

Author Information CGH data and gene-expression data are deposited at the Gene Expression Omnibus under accession numbers GSE39390 and GSE39391, respectively. Reprints and permissions information is available at www.nature.com/reprints. The authors declare no competing financial interests. Readers are welcome to comment on the online version of the paper. Correspondence and requests for materials should be addressed to Q.Z. (qzhou@ioz.ac.cn) or X.-Y.Z. (xyzhao@ioz.ac.cn).

LETTER

doi:10.1038/nature11538

Melanomas resist T-cell therapy through inflammation-induced reversible dedifferentiation

Jennifer Landsberg[1]*, Judith Kohlmeyer[1]*, Marcel Renn[1]*, Tobias Bald[1], Meri Rogava[1], Mira Cron[1], Martina Fatho[2], Volker Lennerz[2], Thomas Wölfel[2], Michael Hölzel[3] & Thomas Tüting[1]

Adoptive cell transfer therapies (ACTs) with cytotoxic T cells that target melanocytic antigens can achieve remissions in patients with metastatic melanomas, but tumours frequently relapse[1,2]. Hypotheses explaining the acquired resistance to ACTs include the selection of antigen-deficient tumour cell variants[3–5] and the induction of T-cell tolerance[6]. However, the lack of appropriate experimental melanoma models has so far impeded clear insights into the underlying mechanisms. Here we establish an effective ACT protocol in a genetically engineered mouse melanoma model that recapitulates tumour regression, remission and relapse as seen in patients. We report the unexpected observation that melanomas acquire ACT resistance through an inflammation-induced reversible loss of melanocytic antigens. In serial transplantation experiments, melanoma cells switch between a differentiated and a dedifferentiated phenotype in response to T-cell-driven inflammatory stimuli. We identified the proinflammatory cytokine tumour necrosis factor (TNF)-α as a crucial factor that directly caused reversible dedifferentiation of mouse and human melanoma cells. Tumour cells exposed to TNF-α were poorly recognized by T cells specific for melanocytic antigens, whereas recognition by T cells specific for non-melanocytic antigens was unaffected or even increased. Our results demonstrate that the phenotypic plasticity of melanoma cells in an inflammatory microenvironment contributes to tumour relapse after initially successful T-cell immunotherapy. On the basis of our work, we propose that future ACT protocols should simultaneously target melanocytic and non-melanocytic antigens to ensure broad recognition of both differentiated and dedifferentiated melanoma cells, and include strategies to sustain T-cell effector functions by blocking immune-inhibitory mechanisms in the tumour microenvironment.

Primary melanomas frequently show lymphoid infiltrates with local regression, suggesting that the immune system can restrain tumour growth. The identification of target antigens recognized by melanoma-infiltrating cytotoxic T cells (CTLs) enabled the development of therapeutic approaches to reinforce cellular anti-tumour immunity[7,8]. ACTs with *in vitro* expanded $CD8^+$ CTLs specific for the melanocytic differentiation antigens Melan-A (also known as MART-1) or gp100 (also known as Pmel17) effectively induce regression of melanoma metastases in the clinic[9,10]. However, tumours often relapse after a period of remission, suggesting that they acquire resistance to T-cell therapy[2]. To study the mechanisms of ACT resistance, we generated an appropriate preclinical *in vivo* model that recapitulates the regression, remission and relapse of melanoma as observed in patients. First, we established genetically engineered mice in which melanocyte transformation and tumour progression is driven by deregulated receptor tyrosine kinase signalling due to transgenic overexpression of hepatocyte growth factor (HGF) and impaired $p16^{Ink4a}$-dependent cell cycle regulation due to an oncogenic CDK4(R24C) germline mutation[11–13]. Second, we developed an effective ACT protocol similar to treatment regimens used in the clinic, consisting of chemotherapeutic preconditioning with cyclophosphamide, an adoptive transfer of gp100-specific $CD8^+$ CTLs derived from Pmel-1 T-cell receptor (TCR)-transgenic mice that are activated *in vivo* with a recombinant adenoviral vector vaccine expressing gp100 (Ad-gp100), and three injections with the immunostimulatory nucleic acids CpG and polyriboinosinic:polyribocytidylic acid (poly(I:C))[14]. This ACT protocol can induce regression of macroscopically visible melanomas in most HGF–CDK4(R24C) mice. However, after two months of remission, tumours frequently resume progressive growth[12,14].

A booster vaccination with Ad-gp100 expands persisting gp100-specific Pmel-1 memory CTLs in HGF–CDK4(R24C) mice with melanoma relapse[14]. Investigations in larger cohorts of HGF–CDK4(R24C) mice showed that CTL reactivation delayed melanoma progression and significantly increased survival compared with mice that were not revaccinated (351 ± 34 (mean ± s.e.m.) versus 257 ± 31 days, $P < 0.01$; Fig. 1a and Supplementary Fig. 1). Thus, one reason for melanoma relapses in our experimental system is the gradual loss of T-cell effector functions. However, we also noted that some melanomas with late relapse after long-term remission showed hypomelanotic tumour areas with partial loss of gp100 expression and significantly increased $CD45^+$ immune cell infiltration, a pattern never seen in control tumours (Fig. 1b–d and Supplementary Fig. 2a–c). Although some gp100-specific $CD8^+$ CTLs were still present in relapsed tumours, most infiltrating immune cells consisted of $CD11b^+$ myeloid cells (Fig. 1d and Supplementary Fig. 2d). Accordingly, the gene expression levels of key proinflammatory cytokines were significantly enhanced in relapsed tumours compared with controls (Fig. 1e).

On the basis of these findings, we proposed that the loss of antigen expression in melanoma cells and diminished T-cell effector functions in an inflammatory tumour microenvironment may be co-existing or even functionally connected resistance mechanisms that together contribute to acquired ACT resistance. However, our results obtained in HGF–CDK4(R24C) mice, in which carcinogen-induced autochthonous melanomas show regression, remission and relapse after successful ACT, require careful interpretation. In this model it can not be ruled out that delayed but independently arising melanomas could be erroneously considered as relapsed melanomas. We therefore established a more controlled experimental setting using the melanoma cell line HCmel3 derived from a primary HGF–CDK4(R24C) melanoma. HCmel3 cells show a typical melanocytic appearance *in vitro* and closely recapitulate the growth kinetics and histomorphology of parental primary melanomas after transplantation into syngeneic and immunocompetent C57/BL6 mice *in vivo* (Supplementary Fig. 3).

Using this cell line we could now treat groups of mice bearing single tumours of defined origin. As expected, established HCmel3 melanomas regressed in most C57BL/6 mice treated with our ACT protocol.

[1]Laboratory of Experimental Dermatology, Department of Dermatology and Allergy, University of Bonn, D-53105 Bonn, Germany. [2]Third Department of Medicine, Haematology/Oncology/Pneumology, University Medical Centre of the Johannes Gutenberg University, D-55101 Mainz, Germany. [3]Department of Clinical Chemistry and Clinical Pharmacology, Unit for RNA Biology, University of Bonn, D-53105 Bonn, Germany.

*These authors contributed equally to this work.

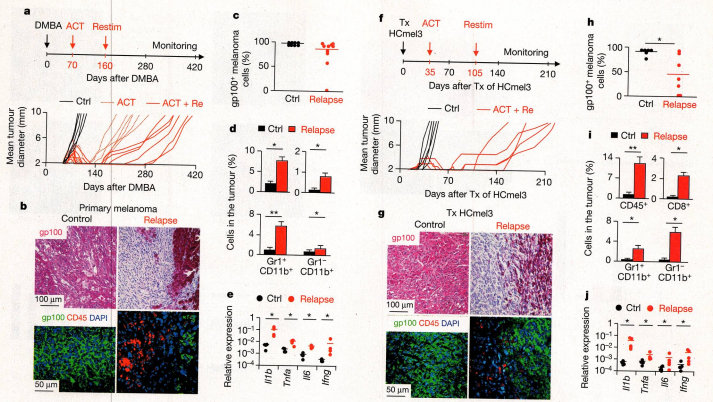

Figure 1 | HGF–CDK4(R24C) melanomas resisting ACT with gp100-specific CTLs show partial loss of antigen expression in an inflammatory tumour microenvironment. **a**–**j**, The primary (**a**–**e**) and transplanted HGF–CDK4(R24C) (**f**–**j**) melanoma model. **a**, **f**, Experimental protocols (top) and tumour growth kinetics in individual mice treated as indicated (bottom, $n = 5$–6). DMBA, 7,12-dimethylbenz(a)anthracene; Re, restim; Tx, transplant. **b**, **g**, Immunohistochemical stain for gp100 (top) and corresponding immunofluorescence analysis for gp100 and CD45 (bottom) of a control and a relapse melanoma. DAPI, 4′,6-diamidino-2-phenylindole. **c**, **h**, Quantification of gp100 expression ($n = 10$). **d**, **i**, Flow cytometric analysis of tumour-infiltrating immune cells (mean percentage ± s.e.m., $n = 8$). **e**, **j**, Real-time PCR analysis of tumours ($n = 5$). *$P < 0.05$; **$P < 0.01$.

In a subset of these mice, tumours also relapsed after a prolonged period of remission (Fig. 1f and Supplementary Fig. 3b). Relapsed HCmel3 melanomas showed a macroscopically visible morphological heterogeneity (Supplementary Fig. 3c, d) and prominent loss of gp100 expression in association with increased immune cell infiltration, again consisting of some $CD8^+$ CTLs and many $CD11b^+$ myeloid cells (Fig. 1g–i). Accordingly, relapsed tumours expressed enhanced messenger RNA levels of proinflammatory cytokines compared with controls (Fig. 1j). These results recapitulate our findings with the carcinogen-induced spontaneous melanomas (Fig. 1a–e) and unambiguously demonstrate the development of true acquired resistance to gp100-specific T-cell immunotherapy associated with focal loss of target antigen expression in an inflammatory microenvironment.

The HCmel3 model allowed us to analyse the mechanism of acquired therapy resistance on a cellular level further by comparing parental HCmel3 melanoma cells with those derived from relapsed melanomas, designated as HCmel3-R. Six such relapse cell lines uniformly showed an amelanotic phenotype *in vitro*, and they neither expressed the T-cell target antigen gp100 nor the melanocytic protein TRP2, suggesting that HCmel3-R cells may have acquired a dedifferentiated phenotype (Fig. 2a). Accordingly, HCmel3-R3 cells showed strongly reduced recognition by gp100-specific Pmel-1 CTLs (Fig. 2b). After re-transplantation into new recipient C57BL/6 mice, HCmel3-R3 cells grew with similar kinetics to parental HCmel3 cells. Surprisingly, we found that these HCmel3-R3 tumours were again susceptible to ACT with Pmel-1 CTLs owing to near complete restoration of gp100 expression *in vivo*, which was again considerably reduced in an inflammatory microenvironment of melanomas that resisted ACT a second time (Fig. 2c–f). These findings indicated that acquired therapy resistance in relapsed tumours involves a reversible downregulation of antigen expression associated with T-cell driven inflammation rather than the expected selection of stably antigen-deficient tumour cell variants with persistent genetic loss of the antigen.

To get a more complete picture of the inflammation-induced changes, we performed whole genome mRNA expression analyses of control, relapsed and re-transplanted HCmel3 melanomas. Consistent with our results so far, we found a reversible downregulation of 25 pigmentation genes in relapsed tumours accompanied by a broad upregulation of immune-response genes (Supplementary Fig. 4 and Supplementary Tables 1 and 2). A Gene Ontology (GO) analysis suggested that infiltrating myeloid immune cells suppress CTL effector functions through the production of interleukin (IL)-10 and nitric oxide, consistent with a large body of literature[15]. Next, we integrated gene expression data from *in vitro* cultures of dedifferentiated HCmel3 relapse lines to subtract immune-cell-associated profiles, and identified a set of cell adhesion, migration and extracellular matrix genes that is reversibly upregulated in relapsed HCmel3 melanomas *in vivo* (Supplementary Fig. 5 and Supplementary Tables 3 and 4). These results strongly suggest a mesenchymal-like phenotype switch of melanoma cells in the context of an inflammatory microenvironment.

Relapsed HCmel3 melanomas showed an increased proportion of spindle-shaped tumour cells. In areas with intense immune cell infiltration these spindle-shaped cells strongly expressed nerve growth factor receptor (NGFR, also known as CD271), a neural crest marker that discriminates human desmoplastic melanomas lacking melanocytic antigens from other neoplasms in clinical histopathology[16] (Fig. 3a). Approximately 25% of HCmel3 cells also expressed NGFR along with low levels of gp100 *in vitro* (Fig. 3b). On the basis of these findings, we proposed that the melanocytic differentiation status may be dynamically regulated in the tumour microenvironment by immune cell-derived proinflammatory mediators as seen at relapse to ACT. Consistent with this notion, we observed upregulation of NGFR

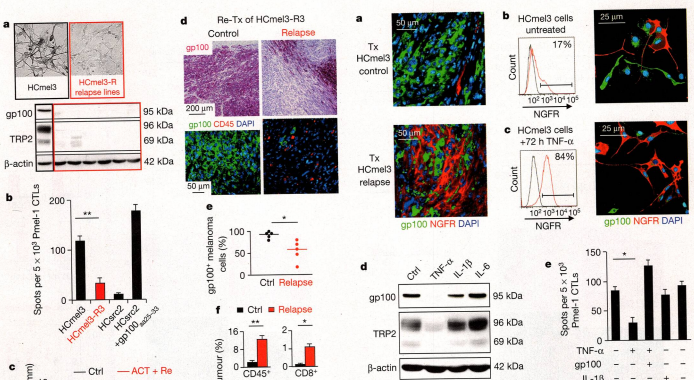

Figure 2 | Loss of gp100 antigen expression in relapsed HGF–CDK4(R24C) melanoma lines is reversible after re-transplantation. a, *In vitro* morphology (top) and immunoblot analysis (bottom) of parental and relapse HCmel3 (termed HCmel3-R) cells. **b**, Recognition by gp100-specific CTLs in IFN-γ ELISpot assays (mean spot number ± s.e.m. of triplicates). $gp100_{aa25–33}$ denotes a synthetic peptide corresponding to amino acids 25–33 of gp100. **c**, Growth kinetics of re-transplanted HCmel3-R3 tumours in individual mice treated as indicated ($n = 7$). **d**, Immunohistochemical stain for gp100 (top) and corresponding immunofluorescence analysis for gp100 and CD45 (bottom). **e**, Quantification of gp100 expression ($n = 5$). **f**, Flow cytometric analysis of tumour-infiltrating immune cells (mean percentage ± s.e.m., $n = 5$). $*P < 0.05$; $**P < 0.01$.

Figure 3 | Proinflammatory mediators directly promote HGF–CDK4(R24C) melanoma cell dedifferentiation leading to impaired recognition by gp100-specific CTLs. a, Immunofluorescence analysis for gp100 and NGFR of a control and a relapse HCmel3 melanoma. **b**, NGFR surface expression on HCmel3 cells (left) and corresponding immunofluorescence analysis for gp100 and NGFR (right). **c**, Corresponding analyses after 72 h exposure to TNF-α. **d**, **f**, Immunoblot analyses of HCmel3 cells treated for 72 h as indicated. CM, conditioned media; MPH, macrophages; TC, T cells. **e**, **g**, Recognition of HCmel3 cells treated as indicated by gp100-specific CTLs in IFN-γ ELISpot assays (mean spot number ± s.e.m. of triplicates). $*P < 0.05$.

expression and downregulation of gp100 expression 72 h after incubation of HCmel3 cells with conditioned medium from activated T cells or macrophages (Supplementary Fig. 6). Among the cytokines secreted by these immune cells we identified TNF-α as a potent stimulator of NGFR expression (Supplementary Fig. 7). TNF-α, but not IL-1β or IL-6, also decreased gp100 expression leading to poor recognition by gp100-specific Pmel-1 CTLs (Fig. 3c–e). Blockade of TNF-α by the TNFR2–IgG fusion protein partially restored gp100 expression and T-cell recognition that was downregulated by conditioned medium from activated T cells or macrophages (Fig. 3f, g). Finally, gene expression profiling showed that the transcriptional response to TNF-α includes the downregulation of 25 pigmentation genes and resembles the changes observed in HCmel3 relapse cell lines compared with parental HCmel3 cells (Supplementary Fig. 8 and Supplementary Tables 5 and 6). These observations demonstrate that immune cell-derived TNF-α is an important inflammatory mediator that promotes dedifferentiation of melanoma cells resulting in impaired recognition by melanocyte-specific T cells.

TNF-α-mediated dedifferentiation of HCmel3 cells proceeded within 72 h and did not require selective proliferation or apoptosis of subpopulations as evidenced by experiments with the cell cycle inhibitor aphidicolin (Supplementary Fig. 9). Furthermore, highly pure fluorescence-activated cell sorting (FACS)-sorted $NGFR^{low}$ $gp100^{+}$ melanoma cells also completely converted to an $NGFR^{+}$ $gp100^{low}$ phenotype after TNF-α exposure (Supplementary Fig. 10). Within 12 days, both $NGFR^{low}$ $gp100^{+}$ and $NGFR^{+}$ $gp100^{low}$ FACS-sorted HCmel3 cells spontaneously returned to their equilibrium between differentiated and dedifferentiated cells, as seen before sorting. The plasticity of HCmel3 cells was also observed *in vivo*, as TNF-α-treated and -untreated HCmel3 cells showed similar growth kinetics, histomorphology and gp100 expression when transplanted into C57BL/6 mice (Supplementary Fig. 11). These data support a model in which differentiated and dedifferentiated melanoma cell subpopulations exist in a dynamic, interconvertible equilibrium state that rapidly adapts to inflammatory signals in the environment.

In subsequent experiments we addressed whether the observations in our mouse model could be extended to the human system. We

found that TNF-α upregulated NGFR expression and downregulated gp100 and Melan-A expression in several human melanoma cell lines, including the highly differentiated MZ7-MEL and the poorly differentiated SK-MEL-29 cells (Fig. 4a–d). In agreement with our findings using mouse HCmel3 cells, we observed that the TNF-α-mediated conversion of $NGFR^{low}$ $gp100^{+}$ differentiated MZ7-MEL cells to an $NGFR^{+}$ $gp100^{low}$ phenotype also did not require cell proliferation (Supplementary Figs 12 and 13). Finally, cutaneous metastases from patients with melanoma showed selective expression of NGFR on melanoma cell subpopulations in close association with infiltrating immune cells, further supporting the clinical relevance of our findings (Supplementary Fig. 14).

The availability of several autologous tumour-specific CTL clones recognizing both shared melanocytic antigens and individual mutated antigens expressed by MZ7-MEL and the SK-MEL-29 cells allowed us to study the effect of TNF-α on T-cell recognition carefully[13,17]. Interferon (IFN)-γ enzyme-linked immunosorbent spot (ELISpot) assays showed a selectively impaired recognition of TNF-α-treated MZ7-MEL cells by CTLs specific for gp100, whereas the recognition by CTLs specific for the mutated SNRPD1 protein was not affected (Fig. 4e). Furthermore, we found a selectively impaired recognition of TNF-α-treated SK-MEL-29 cells by CTLs specific for Melan-A, and notably the recognition by CTLs specific for the mutated CDK4 protein was increased (Fig. 4f). Similar data were obtained with two other melanoma cell lines and matched autologous CTL clones specific for melanocytic and non-melanocytic antigens (not shown). Thus, we conclude that inflammation-induced dedifferentiation of melanoma cells is a clinically relevant mechanism of acquired resistance to T-cell therapy directed against melanocytic antigens.

On the basis of our work we propose that future ACT protocols should simultaneously target melanocytic and non-melanocytic antigens to ensure broad recognition of both differentiated and dedifferentiated melanoma cells. This seems especially important for TCR gene transfer strategies, which have so far been primarily directed against melanocytic antigens[18–21]. We expect that the therapeutic success of ACT also depends on the functional reactivation and proliferation of other T cells that already pre-exist in tumour tissue, as has been demonstrated in melanoma vaccination studies[22]. These T cells can recognize truly tumour-specific mutated antigens that are not affected by inflammation-driven plasticity.

Given that our ACT model recapitulates clinically relevant aspects of progressive impairment of T-cell effector functions, we also explored the expression of PD-L1 (also known as CD274) on melanoma cells because targeted disruption of its interaction with the co-inhibitory receptor PD-1 on activated T cells potentiates ACT in mice[23] and can induce melanoma regression in some patients[24,25]. In line with a recent report[26] we found that conditioned medium from activated T cells, and in particular IFN-γ but not TNF-α, strongly upregulated the expression of PD-L1 and major histocompatibility complex (MHC) class I on melanoma cells (Supplementary Fig. 15). Thus, IFN-γ-dependent PD-L1 upregulation and TNF-α-dependent dedifferentiation represent two functionally connected inflammation-induced adaptive mechanisms that together contribute to acquired ACT resistance. These findings provide a foundation for future work to optimize ACT with clinically relevant combination therapies in our experimental model.

In summary, our study demonstrates that the immunoselection of tumour cell variants that escape CTL recognition owing to persistent genetic alterations, as predicted by the immunoediting theory[4,5,27,28], is not a prerequisite for melanoma cells to acquire resistance to ACT targeting melanocytic lineage antigens. Instead, we found that melanoma cells can resist ACT by a reversible process of dedifferentiation in response to the T-cell induced inflammatory microenvironment. We propose that this inflammation-induced phenotypic plasticity observed both in the mouse and human models represents a previously unrecognized dynamic form of immunoediting, in which proinflammatory factors such as TNF-α secreted by macrophages and T cells in the microenvironment reversibly alter the dynamic equilibrium between differentiated and dedifferentiated melanoma cells. We assume that this cell-extrinsic adaptive mechanism of immune escape predominates in cases of extensive local inflammation, as observed in our experimental setting, in which ACT targets and destructs large established tumours. Studies addressing the tumorigenic potential of human melanoma cell subpopulations in immunodeficient mice led to the suggestion that the emergence of $NGFR^{+}$, dedifferentiated melanoma cells allows tumours to escape immune cell control[29]. Our results now provide the first experimental proof for this hypothesis. The microenvironment-dependent regulation of NGFR and melanocytic lineage markers established by our study may also help to characterize the cellular heterogeneity of individual melanomas and the spectrum of histological variants that probably reflect the plasticity of the neural crest lineage. Finally, our results provide new insights into the important role of dynamic changes in the microenvironment as a mechanism of therapy resistance that is at present also emerging for targeted inhibitors of signal transduction pathways in BRAF(V600E) mutant melanomas[30].

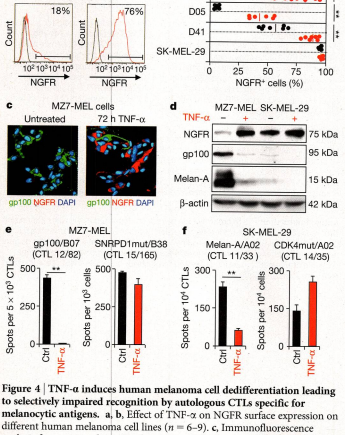

Figure 4 | TNF-α induces human melanoma cell dedifferentiation leading to selectively impaired recognition by autologous CTLs specific for melanocytic antigens. **a**, **b**, Effect of TNF-α on NGFR surface expression on different human melanoma cell lines ($n = 6$–9). **c**, Immunofluorescence analysis for gp100 and NGFR of control and TNF-α-exposed human MZ7-MEL cells. **d**, Immunoblot analyses of control and TNF-α-exposed human MZ7-MEL and SK-MEL-29 cells. **e**, **f**, Effect of TNF-α on the recognition of MZ7-MEL and SK-MEL-29 cells by the indicated autologous CTL clones in IFN-γ ELISpot assays (mean spot number ± s.e.m. of triplicates). $^{**}P < 0.01$.

METHODS SUMMARY

Animal experiments. Wild-type, melanoma-prone HGF–CDK4(R24C) and TCR-transgenic Pmel-1 C57BL/6 mice were bred as described previously[14]. Mice bearing palpable primary carcinogen-induced or transplanted HGF–CDK4(R24C) melanomas received the 'CLVT' adoptive cell therapy protocol[14]. Tumour sizes were recorded weekly and mice killed when progressively growing melanomas exceeded 10 mm or when signs of illness were observed. All animal experiments were approved by the local government authorities (LANUV, NRW, Germany) and

were performed according to the institutional and national guidelines for the care and use of laboratory animals.

Tumour analyses. Haematoxylin and eosin (H&E) staining and immunohistology were performed with antibodies against gp100, NGFR and CD45. Tumour-infiltrating immune cells were analysed by flow cytometry with antibodies against CD45, CD8a, CD90 (also known as Thy1.1), Gr-1 and CD11b. Gene expression was determined by real-time PCR analysis and by complementary DNA microarrays.

Cell culture, cytokine treatment and analyses. Mouse melanoma cell lines established from primary or transplanted HGF–CDK4(R24C) melanomas and human melanoma cell lines were maintained in RPMI with 10% FCS and supplements. Responses to conditioned media or recombinant cytokines were analysed by FACS, immunofluorescence and immunoblots with antibodies against mouse or human gp100, TRP2, Melan-A, NGFR, PD-L1 and MHC class I.

Recognition of melanoma cell lines by CTLs. Antigen-specific secretion of IFN-γ by mouse Pmel-1 CTLs or by human autologous CTL clones derived from mixed tumour lymphocyte cultures with MZ7-MEL or SK-MEL-29 (refs 13, 18) was assayed using the ELISpot technique.

Statistics. Statistical analyses were performed using the unpaired two-tailed Student's *t*-test and GraphPad Prism 4 software ($*P < 0.05$; $**P < 0.01$; and $***P < 0.001$).

Full Methods and any associated references are available in the online version of the paper.

Received 1 June; accepted 24 August 2012.
Published online 10 October 2012.

1. Restifo, N. P., Dudley, M. E. & Rosenberg, S. A. Adoptive immunotherapy for cancer: harnessing the T cell response. *Nature Rev. Immunol.* **12,** 269–281 (2012).
2. Rosenberg, S. A. *et al.* Durable complete responses in heavily pretreated patients with metastatic melanoma using T-cell transfer immunotherapy. *Clin. Cancer Res.* **17,** 4550–4557 (2011).
3. Khong, H. T. & Restifo, N. P. Natural selection of tumor variants in the generation of "tumor escape" phenotypes. *Nature Immunol.* **3,** 999–1005 (2002).
4. Matsushita, H. *et al.* Cancer exome analysis reveals a T-cell-dependent mechanism of cancer immunoediting. *Nature* **482,** 400–404 (2012).
5. DuPage, M., Mazumdar, C., Schmidt, L. M., Cheung, A. F. & Jacks, T. Expression of tumour-specific antigens underlies cancer immunoediting. *Nature* **482,** 405–409 (2012).
6. Willimsky, G. & Blankenstein, T. Sporadic immunogenic tumours avoid destruction by inducing T-cell tolerance. *Nature* **437,** 141–146 (2005).
7. Boon, T., Coulie, P. G., Van den Eynde, B. J. & van der Bruggen, B. Human T cell responses against melanoma. *Annu. Rev. Immunol.* **24,** 175–208 (2006).
8. Mellman, I., Coukos, G. & Dranoff, G. Cancer immunotherapy comes of age. *Nature* **480,** 480–489 (2011).
9. Yee, C. *et al.* Adoptive T cell therapy using antigen-specific $CD8^+$ T cell clones for the treatment of patients with metastatic melanoma: *in vivo* persistence, migration, and antitumor effect of transferred T cells. *Proc. Natl Acad. Sci. USA* **99,** 16168–16173 (2002).
10. Dudley, M. E. *et al.* Cancer regression and autoimmunity in patients after clonal repopulation with antitumor lymphocytes. *Science* **298,** 850–854 (2002).
11. Tormo, D. *et al.* Therapeutic efficacy of antigen-specific vaccination and toll-like receptor stimulation against established transplanted and autochthonous melanoma in mice. *Cancer Res.* **66,** 5427–5435 (2006).
12. Landsberg, J. *et al.* Autochthonous primary and metastatic melanomas in Hgf-$Cdk4^{R24C}$ mice evade T-cell-mediated immune surveillance. *Pigment Cell Melanoma Res.* **23,** 649–660 (2010).
13. Wölfel, T. *et al.* A $p16^{INK4a}$-insensitive CDK4 mutant targeted by cytolytic T lymphocytes in a human melanoma. *Science* **269,** 1281–1284 (1995).
14. Kohlmeyer, J. *et al.* Complete regression of advanced primary and metastatic mouse melanomas following combination chemoimmunotherapy. *Cancer Res.* **69,** 6265–6274 (2009).
15. Gabrilovich, D. I., Ostrand-Rosenberg, S. & Bronte, V. Coordinated regulation of myeloid cells by tumours. *Nature Rev. Immunol.* **12,** 253–268 (2012).
16. Kanik, A. B., Yaar, M. & Bhawan, J. p75 nerve growth factor receptor staining helps identify desmoplastic and neurotropic melanoma. *J. Cutan. Pathol.* **23,** 205–210 (1996).
17. Lennerz, V. *et al.* The response of autologous T cells to a human melanoma is dominated by mutated neoantigens. *Proc. Natl Acad. Sci. USA* **102,** 16013–16018 (2005).
18. Morgan, R. A. *et al.* Cancer regression in patients after transfer of genetically engineered lymphocytes. *Science* **314,** 126–129 (2006).
19. Johnson, L. A. *et al.* Gene therapy with human and mouse T-cell receptors mediates cancer regression and targets normal tissues expressing cognate antigen. *Blood* **114,** 535–546 (2009).
20. Robbins, P. F. *et al.* Tumor regression in patients with metastatic synovial cell sarcoma and melanoma using genetically engineered lymphocytes reactive with NY-ESO-1. *J. Clin. Oncol.* **29,** 917–924 (2011).
21. Vatakis, D. N. *et al.* Antitumor activity from antigen-specific CD8 T cells generated *in vivo* from genetically engineered human hematopoietic stem cells. *Proc. Natl Acad. Sci. USA* **108,** E1408–E1416 (2011).
22. Corbière, V. *et al.* Antigen spreading contributes to MAGE vaccination-induced regression of melanoma metastases. *Cancer Res.* **71,** 1253–1262 (2011).
23. Pilon-Thomas, S., Mackay, A., Vohra, N. & Mule., J. J. Blockade of programmed death ligand 1 enhances the therapeutic efficacy of combination immunotherapy against melanoma. *J. Immunol.* **184,** 3442–3449 (2010).
24. Topalian, S. L. *et al.* Safety, activity, and immune correlates of anti-PD-1 antibody in cancer. *N. Engl. J. Med.* **366,** 2443–2454 (2012).
25. Brahmer, J. R. *et al.* Safety and activity of anti-PD-L1 antibody in patients with advanced cancer. *N. Engl. J. Med.* **366,** 2455–2465 (2012).
26. Taube, J. M. *et al.* Colocalization of inflammatory response with B7-H1 expression in human melanocytic lesions supports an adaptive resistance mechanism of immune escape. *Sci. Transl. Med.* **4,** 127ra37 (2012).
27. Koebel, C. M. *et al.* Adaptive immunity maintains occult cancer in an equilibrium state. *Nature* **450,** 903–907 (2007).
28. Schreiber, R. D., Old, L. J. & Smyth, M. J. Cancer immunoediting: integrating immunity's roles in cancer suppression and promotion. *Science* **331,** 1565–1570 (2011).
29. Boiko, A. D. *et al.* Human melanoma-initiating cells express neural crest nerve growth factor receptor CD271. *Nature* **466,** 133–137 (2010).
30. Straussman, R. *et al.* Tumour micro-environment elicits innate resistance to RAF inhibitors through HGF secretion. *Nature* **487,** 500–504 (2012).

Supplementary Information is available in the online version of the paper.

Acknowledgements We would like to thank G. Merlino and M. Barbacid for providing genetically engineered mice; E. Endl for help with FACS sorting; S. Herms and P. Hoffmann for the cDNA microarrays; S. Mikus, A. Sporleder and C. Lemke for managing the mouse colony and performing histopathology, immunohistopathology, immunoblotting and real-time PCR. This research was supported in part by grants from the DFG (A12 in the SFB832 and A22 in the SFB704) and the Deutsche Krebshilfe (P9 in the Melanoma Research Network) to T.T., by grants from BONFOR to J.L. and J.K., and by a DFG grant (A1 in the SFB 432) to T.W. T.T. and M.H. are members of the Excellence Cluster ImmunoSensation.

Author Contributions J.L., J.K., M.Re., T.B. and M.C. performed all experiments with mouse melanomas, analysed the data and reviewed the manuscript. J.K., M.Ro. and M.F. performed experiments with human melanoma cells and analysed the data. V.L. and T.W. designed and supervised experiments with human melanoma cells, interpreted the data and reviewed the manuscript. M.H. designed experiments, performed the bioinformatic analyses, interpreted data and helped to write the manuscript. T.T. conceived and supervised all aspects of the project, designed experiments, interpreted the data and wrote the manuscript.

Author Information The microarray data have been deposited in the Gene Expression Omnibus (GEO) database under the accession number GSE40213. Reprints and permissions information is available at www.nature.com/reprints. The authors declare no competing financial interests. Readers are welcome to comment on the online version of the paper. Correspondence and requests for materials should be addressed to T.T. (thomas.tueting@ukb.uni-bonn.de).

LETTER

doi:10.1038/nature11519

Increased HIV-1 vaccine efficacy against viruses with genetic signatures in Env V2

Morgane Rolland[1]*, Paul T. Edlefsen[2]*, Brendan B. Larsen[3], Sodsai Tovanabutra[1], Eric Sanders-Buell[1], Tomer Hertz[2], Allan C. deCamp[2], Chris Carrico[4,5], Sergey Menis[4,5], Craig A. Magaret[2], Hasan Ahmed[2], Michal Juraska[2], Lennie Chen[3], Philip Konopa[3], Snehal Nariya[3], Julia N. Stoddard[3], Kim Wong[3], Hong Zhao[3], Wenjie Deng[3], Brandon S. Maust[3], Meera Bose[1], Shana Howell[1], Adam Bates[1], Michelle Lazzaro[1], Annemarie O'Sullivan[1], Esther Lei[1], Andrea Bradfield[1], Grace Ibitamuno[1], Vatcharain Assawadarachai[6], Robert J. O'Connell[1], Mark S. deSouza[6], Sorachai Nitayaphan[6], Supachai Rerks-Ngarm[7], Merlin L. Robb[1], Jason S. McLellan[8], Ivelin Georgiev[8], Peter D. Kwong[8], Jonathan M. Carlson[9], Nelson L. Michael[1], William R. Schief[4,5], Peter B. Gilbert[2]*, James I. Mullins[3]* & Jerome H. Kim[1]*

The RV144 trial demonstrated 31% vaccine efficacy at preventing human immunodeficiency virus (HIV)-1 infection[1]. Antibodies against the HIV-1 envelope variable loops 1 and 2 (Env V1 and V2) correlated inversely with infection risk[2]. We proposed that vaccine-induced immune responses against V1/V2 would have a selective effect against, or sieve, HIV-1 breakthrough viruses. A total of 936 HIV-1 genome sequences from 44 vaccine and 66 placebo recipients were examined. We show that vaccine-induced immune responses were associated with two signatures in V2 at amino acid positions 169 and 181. Vaccine efficacy against viruses matching the vaccine at position 169 was 48% (confidence interval 18% to 66%; $P = 0.0036$), whereas vaccine efficacy against viruses mismatching the vaccine at position 181 was 78% (confidence interval 35% to 93%; $P = 0.0028$). Residue 169 is in a cationic glycosylated region recognized by broadly neutralizing and RV144-derived antibodies. The predicted distance between the two signature sites (21 ± 7 Å) and their match/mismatch dichotomy indicate that multiple factors may be involved in the protection observed in RV144. Genetic signatures of RV144 vaccination in V2 complement the finding of an association between high V1/V2-binding antibodies and reduced risk of HIV-1 acquisition, and provide evidence that vaccine-induced V2 responses plausibly had a role in the partial protection conferred by the RV144 regimen.

Vaccination with the RV144 regimen (ALVAC-HIV and AIDSVAX B/E gp120) afforded an estimated 31% protection against HIV-1 acquisition[1]. Two immune correlates of infection risk were identified: plasma IgA antibodies to Env were associated with increased risk, and IgG binding to Env V1/V2 with decreased risk[2]. These analyses compared HIV-1-infected and uninfected vaccine recipients and established correlates of risk[3,4], which are not necessarily predictive of protection as immune responses are not randomized among vaccinees. In contrast, sieve analyses[5–7] compare breakthrough viruses in vaccine and placebo recipients, leveraging the randomization to causally attribute observed differences between HIV-1 sequences to the vaccine. Sieve analyses look for evidence that vaccine-induced immune responses selectively block certain viruses and/or drive escape mutations post-infection, and interrogate treatment differences in HIV-1 sequences derived at the time of HIV-1 diagnosis as evidence for this effect.

We proposed that RV144 vaccine-induced antibodies to Env V1/V2 could selectively prevent HIV-1 infections by certain variants, and that this effect would be evident in the V1/V2 region of breakthrough viruses. To test this hypothesis, we examined the relationship between vaccine status and V1/V2 sequence characteristics using 936 HIV-1 sequences from 110 breakthrough infections: 44 vaccine and 66 placebo recipients (focusing on subjects infected with HIV-1 CRF01_AE, that is, 110 of the 121 characterized infections that occurred after the first immunization). One epidemiologically known transmission pair was confirmed by phylogenetic reconstructions; thus, sensitivity analyses were performed after removing sequences from the individual who was the second to become HIV-1 infected to preserve independence of infection events.

Our analysis focused on HIV-1 sequences corresponding to the glycoprotein 70 gp70-V1/V2 clade B reagent used to identify the correlate of risk (amino acids 120 to 204 of the reference sequence HXB2). Supplementary Methods 1 summarize the pre-filtering of sites that was performed as pre-specified to increase statistical power. First, sites that were invariant or where there was little confidence in the alignment were excluded. Then, sites were selected following two approaches. The first approach, termed 'contact residues', required that sites were both (1) known contact residues for monoclonal antibodies or had been implicated as such in neutralization sensitivity assays[8–11], and (2) 'hotspots' of vaccine-induced binding antibody reactivity from a linear peptide binding microarray analysis of uninfected RV144 vaccine recipients. The 'contact residues' approach yielded eight sites for analysis: HXB2 positions 120, 124, 165, 166, 168, 169, 171 and 181. The second approach, called EPIMAP (epitope prediction by interrogating conformational ensembles of glycosylated antigens with a multi-oriented antibody probe), was based on structural predictions of antibody epitopes: thousands of potential antibody epitopes (centred on gp120 surface residues for the three Env in the vaccine) were predicted and used to rank V1/V2 sites by their likelihood of being antibody targets. The EPIMAP approach yielded 12 high-ranking sites: HXB2 positions 160, 166, 168–173, 178, 179, 181 and 197.

To test if vaccination (through vaccine-induced antibodies to Env V1/V2) protected against acquisition of certain HIV-1 variants, we adapted the primary analysis method used previously[5] to assess vaccine efficacy against HIV-1 genotypes differing at the 15 selected sites identified by either the 'contact residues' or EPIMAP approaches (Supplementary Table 1 and Supplementary Fig. 2; note that vaccine efficacy is estimated based on all RV144 participants, that is, 8,197 vaccine and 8,198 placebo recipients). We found that vaccine efficacy significantly differed for HIV-1 genotypes defined by whether they presented a residue matching the vaccine insert (or not) at position

[1]US Military HIV Research Program, Silver Spring, Maryland 20910, USA. [2]Statistical Center for HIV/AIDS Research and Prevention, Vaccine and Infectious Disease Division, Fred Hutchinson Cancer Research Center, Seattle, Washington 98109, USA. [3]Department of Microbiology, University of Washington, Seattle, Washington 98195, USA. [4]Department of Biochemistry, University of Washington, Seattle, Washington 98195, USA. [5]IAVI Neutralizing Antibody Center and Department of Immunology and Microbial Sciences, The Scripps Research Institute, La Jolla, California 92037, USA. [6]Royal Thai Army Component, AFRIMS, Bangkok 10400, Thailand. [7]Thai Ministry of Public Health, Nonthaburi 11000, Thailand. [8]Vaccine Research Center, NIAID, NIH, Bethesda, Maryland 20892, USA. [9]Microsoft Research, Redmond, Washington 98052, USA.
*These authors contributed equally to this work.

169 ($P = 0.034$) and 181 ($P = 0.024$) (Table 1). The estimated cumulative HIV-1 incidence curves in the vaccine and placebo groups illustrate vaccine efficacy for two genotypes (K169 and I181X) and no efficacy for the opposite residues (Supplementary Fig. 2) (diagnostic tests did not show significant evidence of violation of the proportional hazards assumption), and the cumulative HIV-1 incidence curves showed a trend towards waning vaccine effect on genotype over time, analogous to the temporal effect on efficacy seen in RV144[1,12]. The estimated vaccine efficacy against viruses matching the vaccine at position 169 (K169) was 48% ($P = 0.0036$; 95% confidence interval (CI): 18%, 66%), whereas vaccine efficacy versus position-169-mismatched viruses was not significant. Vaccine efficacy against viruses differing from the vaccine insert at 181 (181X) was 78% ($P = 0.0028$; 95% CI: 35%, 93%), whereas vaccine efficacy versus vaccine-matched viruses at that site was not significant. Furthermore, vaccine efficacy against viruses that were both 169-matched and 181-mismatched was 80% ($P = 0.0046$; CI: 31%, 94%). These results indicate that vaccine-induced immune responses to the Env V2 may have blocked infections with viruses matching the vaccine at K169 and differing from the vaccine at I181. We applied the statistical method from ref. 2 to test whether gp70-V1/V2 antibodies and V2 'hotspot' antibodies were correlates of risk of infection for specific HIV-1 genotypes. The estimated association of these antibodies with genotype-specific infection risk was similar across the genotypes, such that the sieve effects are not explained by these antibody correlates. However, there is low power to detect differences by genotype because only 34 infected vaccinees could be included in the analysis (see Supplementary Table 2).

To further evaluate site-specific differences between viruses from vaccine and placebo recipients, we applied three additional site-scanning methods to both the 'contact residues' and 'EPIMAP' sets of sites: the nonparametric weighted distance comparison test (GWJ)[13], the mismatch bootstrap method (MMBootstrap)[7], and a model-based method that is more sensitive to differences in non-insert amino acid frequencies[14]. Based on both the 'contact residues' and 'EPIMAP'-derived sets of sites, the most general method GWJ identified positions 169 and 181 as significantly distinguishing HIV-1 sequences from vaccine and placebo recipients (Figs 1 and 2). These two sites showed significant or borderline significant results with the additional site-scanning methods (MMBootstrap and model-based) (Supplementary Table 3). These results were corroborated after excluding a subject from the transmission pair: results were consistent although with weaker statistical support. As pre-specified, corrections for multiple testing were performed separately for each analysis method and for each of the three vaccine insert sequences; no correction for multiple tests was applied across the tests because these are considered sensitivity analyses meant to evaluate congruence.

The fact that our sequence data were obtained through an effectively implemented randomized trial[15] reduces the need for phylogenetic corrections as performed in observational studies (Supplementary Note 1). Nonetheless, to potentially assess mechanisms behind sieve effects, we tested the impact of shared ancestry among viruses in our data set with phylogenetic dependency networks[16] and independent contrasts[17]. Both approaches found that the sieve effect at site 181 was independent of the tree topology, whereas that of site 169 was not (Supplementary Tables 4 and 5); these results must be interpreted with caution because the sequence data were used both to infer the phylogenetic tree and to evaluate sieve effects[17].

In agreement with the vaccine efficacy results, the consensus amino acid K169 was more frequently different from the CRF01_AE vaccine sequence among viruses from vaccinees, whereas site 181, the third position of the putative tri-peptide $\alpha_4\beta_7$ integrin binding motif, was more likely to be similar to the vaccine sequence in vaccinees. When we tested whether sites in the two groups were evolving under different selective pressures along internal tree branches, likelihood ratio test results[18] provided evidence that site 169 was under differential pressure across treatment arms ($P = 0.043$ based on data set with 110 subjects; $P = 0.064$ based on 109 subjects) (Supplementary Table 6).

HIV-1 variants with K169X might have had longer V2 loops (mean = 43.2 (interquartile range (IQR): 40–46) versus 41.9 (IQR: 39–44), $P = 0.11$) and more potential N-linked glycosylation sites (PNGS) (mean = 2.44 (IQR: 2–3) versus 2.12 (IQR: 2–3), $P = 0.08$) than K169 viruses (Supplementary Table 7). Although the latter P values were not significant, longer loops and increased PNGS have been associated with reduced sensitivity to neutralization[19]. The trend towards longer V2 and more PNGS in individuals with K169X was apparently not explained by a longer duration of HIV-1 infection (no difference in the time since the last HIV-1-negative visit used as a proxy for the duration of HIV-1 infection (K169X versus K169: median = 181 versus 179, mean = 250 versus 207, $P = 0.41$)) (Supplementary Table 7). Furthermore, studies with quaternary-structure-preferring (QSP) antibodies (for example, PG9, PG16, CH01-04 and PGT141-145) showed that mutations at positions 169 and 181 were associated with significant alterations in neutralization[10,20]. Some strains became sensitive to QSP antibodies by mutating residue 169 to K[21]. These results indicate that K169X mutations could be a mechanism for avoidance of QSP antibodies and potentially other V2-specific antibodies. Indeed, the epitope of CH58, an anti-V2 monoclonal antibody isolated from an RV144 vaccine recipient, spanned amino acids 167–180 and position 169 was critical for binding (Liao, H.-X. *et al.*, personal communication).

To explore whether the sieve effects at sites 169 and 181 were linked, we looked at structural data and covariability. We found no conclusive evidence suggesting that the two sites were contained within the same epitope. The Cα–Cα distance between residues 169 and 181 was 21 ± 7 Å (mean ± s.d.) on the basis of the 3,000 low-energy all-atom models computed for the three vaccine inserts (Supplementary Table 8), whereas sites 169 and 181 were more than 30 Å apart in the crystal structure of J08-scaffolded HIV-1 gp120 V1/V2 bound to the broadly neutralizing monoclonal antibody PG9 (ref. 22; Supplementary Fig. 3). The two sites could lie in a single antibody epitope because the average diameter of antibody-bound epitopes was predicted to be 30.5 Å (on

Table 1 | Estimated vaccine efficacies to prevent infection with specific HIV-1 genotypes, and estimated ratios of hazard ratios

Genotype	Number of infections		Vaccine efficacy (95% CI)	*P* value
	Vaccine	Placebo		
Overall	44	66	34% (7.8%, 54.7%)	0.034
K169	**30**	**57**	**48% (18%, 66%)**	**0.0036**
K169X	14	9	−55% (−258%, 33%)	0.3
I181	40	48	17% (−26%, 45%)	0.38
I181X	**4**	**18**	**78% (35%, 93%)**	**0.0028**
K169-I181	27	42	36% (−4%, 61%)	0.071
K169-I181X	**3**	**15**	**80% (31%, 94%)**	**0.0046**
K169X-I181	13	6	−116% (−467%, 19%)	0.11
K169X-I181X	1	3	67% (−219%, 97%)	0.32
			Estimated HR/HR* (95% CI)	***P* value**
K169X/K169			**2.73 (1.08, 6.92)**	**0.034**
I181/I181X			**3.77 (1.19, 11.92)**	**0.024**
Else/K169-I181			1.04 (0.49, 2.22)	0.92
Else/K169-I181X			1.85 (0.79, 4.32)	0.16
K169X-I181/Else			**2.76 (1.23, 6.20)**	**0.014**
Else/K169X-I181X			1.06 (0.40, 2.86)	0.9

Shown are estimated vaccine efficacies (vaccine efficacies = 1 − hazard ratios (HRs)) to prevent infection with specific HIV-1 genotypes, and estimated ratios of HRs measuring the relative protection against given pairs of HIV-1 genotypes.
* Each HR is the hazard ratio (vaccine versus placebo) of HIV-1 infections with a particular genotype. For example, for the K169X/K169 entry, the numerator HR measures the vaccine effect to prevent HIV-1 infections with K169X-variants and the denominator HR measures the vaccine effect to prevent HIV-1 infections with K169-variants, and the result 2.73 means that the vaccine lowers the rate of infection 2.73-times more against K169-matched HIV-1 viruses than against K169-mismatched HIV-1 infections, that is, the level of protection is 2.73 greater against K169-matched than against K169-mismatched HIV-1 viruses (that is against all viruses with a residue differing from K at site 169). Else: all genotypes other than the joint genotype under consideration.

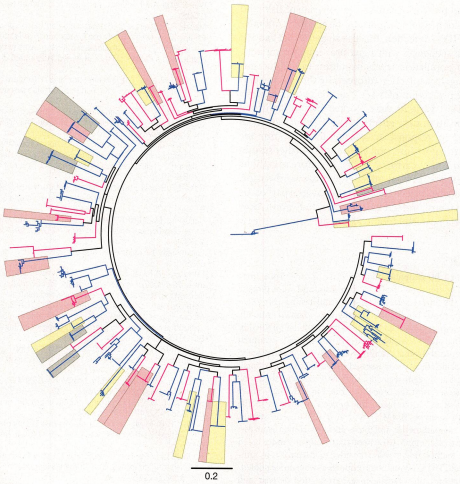

Figure 1 | Phylogenetic tree of *env-V1/V2* nucleotide sequences. Highlights are used for sequences presenting mutations at either site 169 (in pink) or 181 (in yellow) or at both sites (in grey). Sequences from vaccine recipients are figured in red, those from placebo recipients are in blue.

the basis of 32 pairs of bound antigen structures[23]). Furthermore, we found no evidence that the sieve effect at site 181 was linked to site 169 by analysing covariation on pre-selected V1/V2 sites[24,25]. We noted covariability in the mid-V2 loop, which corresponds to the binding site of the V1/V2-specific mAb from RV144 (ref. 2 and personal communication, Liao H.-X. *et al.*, Supplementary Table 9).

The unexpected sieve effect at site 181 showing greater vaccine efficacy against mismatched HIV-1 indicates a vaccine-induced constraint that either hindered the establishment of infection with I181X variants or promoted infections with I181 variants. Although it is plausible that vaccine-induced antibodies enhanced HIV-1 infections with I181 variants, there was no statistical support for such enhancement because there was no evidence of negative vaccine efficacy against I181 viruses: estimated vaccine efficacy = 17%, 95% CI = −26% to 45%, $P = 0.38$ (Table 1). Other hypotheses include: (1) the stricter conservation at site 181 may be a marker of a non-identified sequence characteristic (possibly linked to the variable loop that starts a few amino acids downstream of 181), (2) specific variants may be unable to establish infection due to steric/quaternary structure constraints with vaccine-induced antibodies, and (3) I181X viruses may be preferentially targeted by vaccine-induced antibodies.

Sieve analysis is an important component of assessing immune correlates of protection because it compares vaccine to placebo recipients and could identify selective pressures below the level of detection of standard immune assays[7]. Our V1/V2-focused analysis leveraged randomized treatment assignments to establish a causal connection between vaccination and a selective filtering of V1/V2 variants. The identification of signatures in V2 provides a corroborative

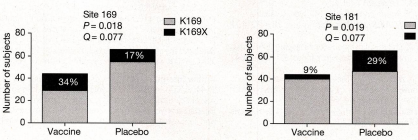

Figure 2 | Bar graphs representing the mutations at positions 169 and 181 based on sequences from 44 vaccine and 66 placebo recipients. The *P* and *Q* values correspond to the site-scanning sieve analysis method GWJ. The values correspond to comparisons against the 92TH023 vaccine insert based on the selected sites identified through the 'contact residues' approach. Pre-specified *P* value and *Q* value significance thresholds of 0.05 and 0.2, respectively. Full results in Supplementary Table 3.

virological determinant to the V1/V2 antibodies correlate of risk[2] and highlights the mid-V2 loop as an important target for antibody-mediated prevention of HIV-1 infection, but also suggests that vaccine efficacy is ablated by viral sequences with signature sequence variants, raising the possibility of population-level adaptation to the vaccine. Given the 31% efficacy against infection afforded by the vaccine and the suspected mechanism of action of V1/V2 antibody, our analysis suggests that specific HIV-1 variants were blocked from establishing HIV-1 infection (an acquisition sieve effect); however, viral sequences may also have mutated in response to vaccine-induced immune pressure, corresponding to a post-infection sieve effect. Further studies with infectious molecular clones carrying V1/V2 signature mutations are needed to clarify their role in viral infectivity, fitness and escape. Together, these results vouch for sieve analysis as an integral part of the search for immune correlates of protection in vaccine studies and show that sieve analysis can be a powerful tool to assess the efficacy of new vaccine candidates.

METHODS SUMMARY

Viral genomes were amplified by endpoint-dilution PCR of viral RNA from plasma specimens collected at the time of HIV-1 diagnosis, and were directly sequenced[7]. Sites in Env V1/V2 were selected for statistical testing using two approaches: one based on a peptide binding microarray assay, known antibody contact sites and literature, the other based on a computational prediction algorithm of antibody binding sites. Each site was tested with four site-scanning sieve analysis methods to identify those that discriminated the vaccine and placebo group. Genotype-specific vaccine efficacy was assessed with the Cox proportional hazards model and score test as described previously[23], and differential vaccine efficacy by genotype was assessed with the model described in refs 26,27. Three additional methods were designed to compare the subjects' sequences to the vaccine insert sequences (a subtype B (MN) and two CRF01_AE strains, 92TH023 and CM244): a nonparametric weighted distance comparison test (GWJ)[12], a mismatch bootstrap method (MMBootstrap)[7] and a model-based Bayesian-frequentist hybrid method that is more sensitive to differences in non-insert amino acid frequencies[13]. The GWJ method computes a two-sample pooled-variance *t*-statistic and compares this statistic to a permutation-derived null distribution. The MMBootstrap method computes the difference in the fraction of mismatches to the insert amino acids using all available sequences, and compares this to a bootstrap-derived null distribution. The model-based method compares the posterior probability of a sieve effect to a null distribution for a Bayesian multinomial model. A *Q*-value multiplicity adjustment procedure was pre-specified to limit the false discovery rate to 20% (ref. 28). Covariation was detected using the Kullback–Leibler divergence and differential tests[23], and a Bayesian graphical method[24]. A schematic description of the study is found in Supplementary Fig. 1.

Full Methods and any associated references are available in the online version of the paper.

Received 25 April; accepted 24 August 2012.
Published online 10 September 2012.

1. Rerks-Ngarm, S. *et al.* Vaccination with ALVAC and AIDSVAX to prevent HIV-1 infection in Thailand. *N. Engl. J. Med.* **361,** 2209–2220 (2009).
2. Haynes, B. F. *et al.* Immune-correlates analysis of an HIV-1 vaccine efficacy trial. *N. Engl. J. Med.* **366,** 1275–1286 (2012).
3. Plotkin, S. A. & Gilbert, P. B. Nomenclature for immune correlates of protection after vaccination. *Clin. Infect. Dis.* **54,** 1615–1617 (2012).
4. Rolland, M. & Gilbert, P. Evaluating immune correlates in HIV type 1 vaccine efficacy trials: what RV144 may provide. *AIDS Res. Hum. Retroviruses* **28,** 400–404 (2012).
5. Gilbert, P. B., Self, S. G. & Ashby, M. A. Statistical methods for assessing differential vaccine protection against human immunodeficiency virus types. *Biometrics* **54,** 799–814 (1998).
6. Gilbert, P., Self, S., Rao, M., Naficy, A. & Clemens, J. Sieve analysis: methods for assessing from vaccine trial data how vaccine efficacy varies with genotypic and phenotypic pathogen variation. *J. Clin. Epidemiol.* **54,** 68–85 (2001).
7. Rolland, M. *et al.* Genetic impact of vaccination on breakthrough HIV-1 sequences from the STEP trial. *Nature Med.* **17,** 366–371 (2011).
8. Wei, X. *et al.* Antibody neutralization and escape by HIV-1. *Nature* **422,** 307–312 (2003).
9. Moore, P. L. *et al.* Limited neutralizing antibody specificities drive neutralization escape in early HIV-1 subtype C infection. *PLoS Pathog.* **5,** e1000598 (2009).
10. Tomaras, G. D. *et al.* Polyclonal B cell responses to conserved neutralization epitopes in a subset of HIV-1-infected individuals. *J. Virol.* **85,** 11502–11519 (2011).
11. Lynch, R. M. *et al.* The B cell response is redundant and highly focused on V1V2 during early subtype C infection in a Zambian seroconverter. *J. Virol.* **85,** 905–915 (2011).
12. Robb, M. L. *et al.* Risk behaviour and time as covariates for efficacy of the HIV vaccine regimen ALVAC-HIV (vCP1521) and AIDSVAX B/E: a post-hoc analysis of the Thai phase 3 efficacy trial RV 144. *Lancet Infect. Dis.* **12,** 531–537 (2012).
13. Gilbert, P. B., Wu, C. & Jobes, D. V. Genome scanning tests for comparing amino acid sequences between groups. *Biometrics* **64,** 198–207 (2008).
14. Edlefsen, P. T. Model-based sieve analysis. Preprint at http://arxiv.org/abs/1206.6701 (2012).
15. Gilbert, P. B. *et al.* Statistical interpretation of the RV144 HIV vaccine efficacy trial in Thailand: a case study for statistical issues in efficacy trials. *J. Infect. Dis.* **203,** 969–975 (2011).
16. Carlson, J. M. *et al.* Phylogenetic dependency networks: inferring patterns of CTL escape and codon covariation in HIV-1 Gag. *PLoS Comput. Biol.* **4,** e1000225 (2008).
17. Felsenstein, J. Phylogenies and the comparative method. *Am. Nat.* **125,** 1–15 (1985).
18. Pond, S. L. & Frost, S. D. Datamonkey: rapid detection of selective pressure on individual sites of codon alignments. *Bioinformatics* **21,** 2531–2533 (2005).
19. Derdeyn, C. A. *et al.* Envelope-constrained neutralization-sensitive HIV-1 after heterosexual transmission. *Science* **303,** 2019–2022 (2004).
20. Moore, P. L. *et al.* Potent and broad neutralization of HIV-1 subtype C by plasma antibodies targeting a quaternary epitope including residues in the V2 loop. *J. Virol.* **85,** 3128–3141 (2011).
21. Doria-Rose, N. A. *et al.* A short segment of the HIV-1 gp120 V1/V2 region is a major determinant of resistance to V1/V2 neutralizing antibodies. *J. Virol.* **86,** 8319–8323 (2012).
22. McLellan, J. S. *et al.* Structure of HIV-1 gp120 V1/V2 domain with broadly neutralizing antibody PG9. *Nature* **480,** 336–343 (2011).
23. Rubinstein, N. D. *et al.* Computational characterization of B-cell epitopes. *Mol. Immunol.* **45,** 3477–3489 (2008).
24. Gilbert, P. B., Novitsky, V. & Essex, M. Covariability of selected amino acid positions for HIV type 1 subtypes C and B. *AIDS Res. Hum. Retroviruses* **21,** 1016–1030 (2005).
25. Poon, A. F., Lewis, F. I., Pond, S. L. & Frost, S. D. An evolutionary-network model reveals stratified interactions in the V3 loop of the HIV-1 envelope. *PLoS Comput. Biol.* **3,** e231 (2007).
26. Prentice, R. L. *et al.* The analysis of failure times in the presence of competing risks. *Biometrics* **34,** 541–554 (1978).
27. Lunn, M. & McNeil, D. Applying Cox regression to competing risks. *Biometrics* **51,** 524–532 (1995).
28. Grambsch, P. & Therneau, T. M. Proportional hazards tests and diagnostics based on weighted residuals. *Biometrika* **81,** 515–526 (1994).

Supplementary Information is available in the online version of the paper.

Acknowledgements We thank B. F. Haynes and F. A. Matsen for advice and comments, and I. A. Wilson and R. L. Stanfield for assistance. This study was supported in part by an Interagency Agreement Y1-AI-2642-12 between US Army Medical Research and Material Command (USAMRMC) and the National Institutes of Allergy and Infectious Diseases. This work was also supported by a cooperative agreement (W81XWH-07-2-0067) between the Henry M. Jackson Foundation for the Advancement of Military Medicine, Inc., and the US Department of Defense (DOD). Additional support was provided to P.B.G. through the NIH grant 2R37AI05465-10. The opinions herein are those of the authors and should not be construed as official or representing the views of the US Department of Defense or the Department of the Army.

Author Contributions M.R. conducted the sequence analysis with contributions from B.B.L., W.D. and B.S.M.; P.T.E. and P.B.G. conducted the site-scanning sieve analyses. M.R., S.T., E.S.-B. and J.I.M. designed the sequencing experiments. B.B.L., L.C., P.K., S.N., J.N.S., K.W., H.Z., M.B., S.H., A. Bates, M.L., A.O'S., E.L., A. Bradfield, G.J. and V.A. performed viral sequencing. T.H., A.C.deC., C.A.M., H.A. and M.J. contributed statistical analyses. C.C., S.M. and W.R.S. developed the EPIMAP approach. J.S.M., I.G. and P.D.K. identified antibody contact residues and performed V2 structural analyses. J.M.C. performed phylogenetic dependency network analyses. R.J.O'C., M.S.deS., S.N., S.R.-N., M.L.R., N.L.M. and J.H.K. conducted the RV144 trial. M.R., P.T.E., P.B.G., J.I.M. and J.H.K. designed the studies, analysed data, prepared the manuscript (with contributions from J.M.C., P.D.K. and W.R.S.) and supervised the project.

Author Information Sequences are available under GenBank accession numbers JX446645–JX448316. Reprints and permissions information is available at www.nature.com/reprints. The authors declare no competing financial interests. Readers are welcome to comment on the online version of the paper. Correspondence and requests for materials should be addressed to M.R. (mrolland@hivresearch.org).

LETTER

doi:10.1038/nature11428

A FOXO3–IRF7 gene regulatory circuit limits inflammatory sequelae of antiviral responses

Vladimir Litvak[1], Alexander V. Ratushny[1,2], Aaron E. Lampano[1], Frank Schmitz[1], Albert C. Huang[2], Ayush Raman[2], Alistair G. Rust[3], Andreas Bergthaler[4], John D. Aitchison[1,2] & Alan Aderem[1]

Antiviral responses must be tightly regulated to defend rapidly against infection while minimizing inflammatory damage. Type 1 interferons (IFN-I) are crucial mediators of antiviral responses[1] and their transcription is regulated by a variety of transcription factors[2]; principal among these is the family of interferon regulatory factors (IRFs)[3]. The IRF gene regulatory networks are complex and contain multiple feedback loops. The tools of systems biology are well suited to elucidate the complex interactions that give rise to precise coordination of the interferon response. Here we have used an unbiased systems approach to predict that a member of the forkhead family of transcription factors, FOXO3, is a negative regulator of a subset of antiviral genes. This prediction was validated using macrophages isolated from *Foxo3*-null mice. Genome-wide location analysis combined with gene deletion studies identified the *Irf7* gene as a critical target of FOXO3. FOXO3 was identified as a negative regulator of *Irf7* transcription and we have further demonstrated that FOXO3, IRF7 and IFN-I form a coherent feed-forward regulatory circuit. Our data suggest that the FOXO3–IRF7 regulatory circuit represents a novel mechanism for establishing the requisite set points in the interferon pathway that balances the beneficial effects and deleterious sequelae of the antiviral response.

Systems biology approaches were used to identify the gene regulatory circuits that control the anti-viral response. We combined gene expression analysis with transcription factor binding site motif scanning algorithms to infer a network of associations between transcription factors and target genes that were activated in macrophages by polyinosinic-polycytidylic acid (PIC), a widely used surrogate for double-stranded RNA (dsRNA) viruses that stimulates the interferon response[4] (Supplementary Fig. 1 and Supplementary Table 1). Transcription factor binding site (TFBS) motifs for IRF, STAT and FOXO transcription factors were significantly over-represented within cluster 2, which includes antiviral genes such as *Gbp2*, *Ccl5*, *Ifit1*, *Irf7* and *Oasl1* (Supplementary Fig. 2 and Supplementary Tables 1 and 2). Although all FOXO transcription factors bind a common DNA element[5], we decided to focus on FOXO3 because it was the sole member of the family that was significantly repressed after PIC stimulation of macrophages (Supplementary Table 3). Interestingly, the repression of *Foxo3* transcription was mirrored by increased transcription of *Irf5*, *Irf7*, *Irf8*, *Stat1*, *Stat2*, *Stat3* and *Stat5a* genes (Supplementary Fig. 3). This result indicated that FOXO3 might act as a repressor of the IRF and STAT transcription factors, master regulators of the IFN-I pathways.

To investigate the role of FOXO3 in the regulation of the IFN-I pathway we examined the global gene expression profile in macrophages derived from *Foxo3*-null mice (Fig. 1). We detected significantly increased transcription of a subset of interferon-stimulated genes (ISGs) under basal conditions in *Foxo3*-null macrophages when compared to their wild-type counterparts, indicating that FOXO3 functions as a repressor of these genes (Fig. 1a, b and Supplementary Table 4). Stimulation of *Foxo3*-null macrophages with PIC further increased the levels of this subset of ISGs (Fig. 1c, d and Supplementary Table 5), and also revealed the transcription of additional ISGs (Fig. 1c, d and Supplementary Tables 4 and 5). The induction of these ISGs was validated by quantitative PCR with reverse transcription (RT–PCR; Fig. 1e). Importantly, *Ifnb1* itself was super-induced in PIC-stimulated macrophages from *Foxo3*-null mice (Fig. 1c, e and Supplementary Fig. 4b), indicating the possibility that the additional subset of ISGs were regulated by autocrine feedback. To distinguish whether the enhanced expression of ISGs in *Foxo3*-null macrophages was due to direct effects of the transcription factor or due to autocrine effects of the cytokine, we performed genome-wide chromatin immunoprecipitation/DNA sequencing (ChIP–Seq) analysis in unstimulated macrophages as well as in macrophages stimulated by PIC. Direct FOXO3 target genes included *Cmpk2*, *Ddx58*, *Ifih1*, *Irf7*, *Mx2* and *Rsad2*, all of which have antiviral functions[1,6] (Fig. 2a, b, Supplementary Fig. 5 and Supplementary Table 6).

The *Irf7* gene was of particular interest because of its critical role in the establishment of the antiviral response[7], and we therefore examined the relationship between it and FOXO3 in more detail. Quantitative RT–PCR demonstrated that basal levels of *Irf7* messenger RNA from *Foxo3*-null macrophages were 5.5-fold higher than those in wild-type cells, whereas PIC-induced *Irf7* mRNA levels were similar in wild-type and *Foxo3*-null cells (Fig. 1e). These results were validated by western blot analysis (Supplementary Fig. 4a). Furthermore, deletion of FOXO3 TFBS in the *Irf7* gene promoter resulted in an increased basal *Irf7* promoter activity, and thus recapitulated the phenotype of *Foxo3*-null macrophages (Supplementary Fig. 6). These results indicate that FOXO3 functions as a negative regulator of basal *Irf7* transcription.

In order to identify the mechanism by which FOXO3 suppresses the transcription of *Irf7*, we quantified histone acetylation, ubiquitination and methylation at the *Irf7* gene promoter in wild-type and *Foxo3*-null macrophages (Fig. 2c). Histone acetylation was significantly increased in *Foxo3*-null macrophages, suggesting an epigenetic mechanism for FOXO3-mediated repression of the *Irf7* gene (Fig. 2c, d). It is worth noting that enhanced histone acetylation correlates with increased transcription of the *Irf7* gene in activated macrophages (Supplementary Fig. 7). Histone acetylation is associated with an open chromatin structure that allows access of transcription factors to the DNA[8]; decreased acetylation results in the chromatin closing thereby impeding the binding of transcription factors to the promoter. A protein–protein interaction map[9] predicted 8 histone deacetylases that might mediate this effect (data not shown), and direct biochemical approaches including co-immunoprecipitation and ChIP–ReChIP demonstrated the existence of a ternary complex consisting of FOXO3, nuclear co-repressor 2 (NCOR2) and histone deacetylase 3 (HDAC3) on the *Irf7* promoter (Fig. 2e and Supplementary Fig. 8). A functional role for this complex is supported by the observation that treatment of macrophages with HDAC inhibitors, valproic acid (VPA) and apicidin[10], results in increased levels of *Irf7* mRNA (Supplementary Fig. 9). Most importantly, the binding of NCOR2 and HDAC3 to

[1]Seattle Biomedical Research Institute, Seattle, Washington 98109, USA. [2]Institute for Systems Biology, Seattle, Washington 98109, USA. [3]Experimental Cancer Genetics, Welcome Trust Sanger Institute, Hinxton, Cambridge CB10 1HH, UK. [4]Research Center for Molecular Medicine, Austrian Academy of Sciences, Lazarettgasse 14 AKH BT 25.3, 1090 Vienna, Austria.

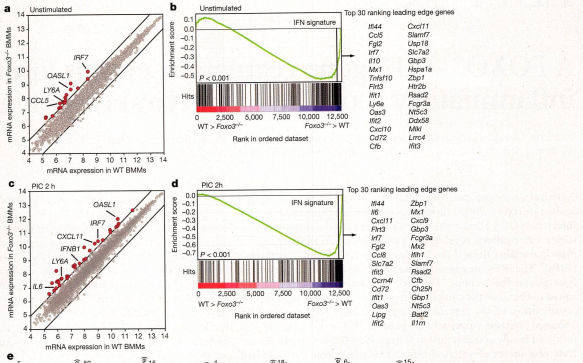

Figure 1 | FOXO3 is a negative regulator of the antiviral response. a, Scatter plot comparing global gene expression profiles between unstimulated wild-type (WT) and *Foxo3*-null bone marrow macrophages (BMMs). The black lines indicate a twofold cut-off for the difference in gene expression levels. Data represent the average of three independent experiments. mRNA expression levels are on a $\log_2$ scale. **b**, Gene-set enrichment analysis (GSEA) reveals the over-representation of IFN transcriptional signature genes in unstimulated *Foxo3*-null BMMs. Genes are ranked into an ordered list on the basis of relative expression in wild-type and *Foxo3*-null BMMs. The middle part of the plot shows the distribution of the genes in the IFN transcriptional signature gene set ('Hits') against the ranked list of genes. The list on the right shows the top 30 genes in the leading edge subset. Data represent the average of three independent experiments. **c**, Global gene expression in PIC-stimulated wild-type and *Foxo3*-null BMMs was analysed as in **a**. **d**, Gene-set enrichment analysis demonstrates upregulation of IFN transcriptional signature genes in PIC-stimulated *Foxo3*-null BMMs. Data represent the average of three independent experiments. **e**, mRNA levels of *Cmpk2*, *Ddx58*, *Irf7*, *Isg20*, *Mx2*, *Rsad2* and *Ifnb1* in wild-type and *Foxo3*-null macrophages in the presence or absence of PIC stimulation. Data are representative of three experiments (average of three values ± standard error).

the *Irf7* promoter was significantly reduced in *Foxo3*-null macrophages (Fig. 2f).

To ascertain the transcriptional circuitry underlying the regulation of the *Irf7* gene we needed to identify all of the participating transcription factors. Motif scanning of the *Irf7* gene promoter predicted STAT, IRF and FOXO binding sites (Supplementary Table 7). The potential presence of the IRF site raised the possibility of auto-regulation of the *Irf7* gene by IRF7 itself, a contention supported by previous overexpression studies[11]. ChIP analysis validated the prediction that IRF7 binds to its own promoter (Fig. 2f), and importantly, FOXO3 restrained this interaction (Fig. 2g). Taken together, these results suggest a model in which a ternary complex of FOXO3, NCOR2 and HDAC3 facilitates a closed chromatin structure and limits IRF7 auto-regulation in macrophages under basal conditions (Fig. 2h).

If the FOXO3, NCOR2 and HDAC3 ternary complex keeps basal transcription of *Irf7* in check, how then does PIC-stimulation overcome this inhibition? We have observed that PIC-stimulation of macrophages results in the clearance of FOXO3, NCOR2 and HDAC3 from the *Irf7* promoter, and that this clearance is temporally associated with PIC-induced *Ifnb1* production (Fig. 2b and Supplementary Figs 8b and 10). The most plausible hypothesis is that PIC-stimulated IFN production regulates the association of FOXO3 with the *Irf7* promoter. This hypothesis was confirmed by the observation that stimulation of macrophages with IFN-β induced the phosphorylation of FOXO3, and this was accompanied by a decrease in *Foxo3* mRNA and protein levels (Fig. 3a, b and Supplementary Fig. 10a). Furthermore, PIC-dependent repression of *Foxo3* mRNA and protein levels did not occur in macrophages isolated from IFN-I receptor (IFNAR1)-null mice (Fig. 3a and Supplementary Fig. 10b). The decrease in mRNA levels is explained by the observation that FOXO3 is required for its own transcription (Supplementary Fig. 11). The decrease in protein levels can be explained as follows. It has been shown previously that the serine–threonine kinase AKT phosphorylates FOXO3, leading to its translocation from the nucleus and its degradation in the cytosol[12,13]. We show here that stimulation of macrophages with IFN-β induced the phosphorylation of AKT that was accompanied by phosphorylation of FOXO3 at the Thr 32 residue, a known AKT phosphorylation site (Fig. 3b). Furthermore, treatment of the cells with AKT inhibitor IV abrogated IFN-I-dependent AKT and FOXO3 phosphorylation and prevented IFN-I-mediated decrease in *Foxo3* mRNA and protein levels (Fig. 3b, c and Supplementary Fig. 10c). Taken together, these results indicate that IFN-I activates the PI3K/AKT pathway, which in turn leads to FOXO3 degradation and to the cessation of *Foxo3* transcription.

FOXO3 has been shown to control CTLA-4-mediated regulation of IL-6, TNF-α, MCP-1 and IFN-γ in dendritic cells[14–16], and this was proposed to occur via increased transcription of superoxide dismutase (SOD2)[15]. This mechanism does not seem to function in FOXO3-mediated repression of antiviral responses in macrophages because no differences in *Sod2* mRNA levels in *Foxo3*-null macrophages were

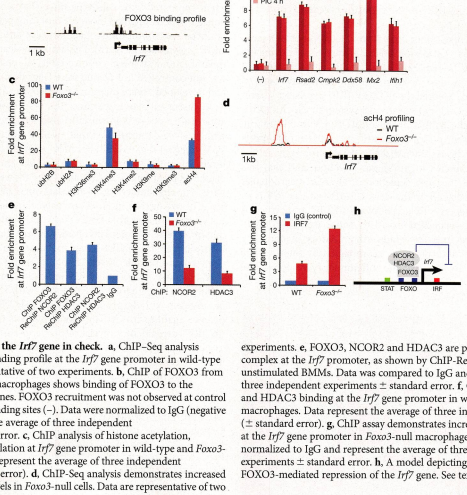

Figure 2 | FOXO3 keeps the *Irf7* gene in check. **a**, ChIP–Seq analysis demonstrates FOXO3 binding profile at the *Irf7* gene promoter in wild-type BMMs. Data are representative of two experiments. **b**, ChIP of FOXO3 from unstimulated wild-type macrophages shows binding of FOXO3 to the promoters of the target genes. FOXO3 recruitment was not observed at control regions lacking FOXO binding sites (–). Data were normalized to IgG (negative control) and represent the average of three independent experiments ± standard error. **c**, ChIP analysis of histone acetylation, ubiquitination and methylation at *Irf7* gene promoter in wild-type and *Foxo3*-null macrophages. Data represent the average of three independent experiments (± standard error). **d**, ChIP-Seq analysis demonstrates increased histone H4 acetylation levels in *Foxo3*-null cells. Data are representative of two experiments. **e**, FOXO3, NCOR2 and HDAC3 are present in the ternary complex at the *Irf7* promoter, as shown by ChIP-ReChIP assays in unstimulated BMMs. Data was compared to IgG and represent the average of three independent experiments ± standard error. **f**, ChIP analysis of NCOR2 and HDAC3 binding at the *Irf7* gene promoter in wild-type and *Foxo3*-null macrophages. Data represent the average of three independent experiments (± standard error). **g**, ChIP assay demonstrates increased recruitment of IRF7 at the *Irf7* gene promoter in *Foxo3*-null macrophages relative. Data was normalized to IgG and represent the average of three independent experiments ± standard error. **h**, A model depicting the mechanism of FOXO3-mediated repression of the *Irf7* gene. See text for details.

detected (data not shown). Taken together, the data indicate that FOXO3 acts in a coherent feed-forward loop, thereby modulating the antiviral response (Fig. 3d). Under basal conditions FOXO3 activity serves to limit *Irf7* expression (1). IFN-I induces the transcription of *Irf7* (ref. 17); this represents the direct, rapid, arm of the feed-forward motif (2). Concomitantly, IFN-I inhibits the transcription of *Foxo3* (3), which leads to the depletion of FOXO3 and alleviates the repression of *Irf7*. This represents the indirect, slow, arm of the feed-forward motif. Thus, activation of both arms of the feed-forward motif is required to achieve the high level of IRF7 that is essential for the maximal antiviral response. In addition, this feed-forward pathway is aided by positive feedback regulation of IRF7 on IFN-I (4) (Supplementary Fig. 12), and by positive auto-regulation of IRF7 (5). By limiting the transcription of *Irf7*, FOXO3 prevents leakiness

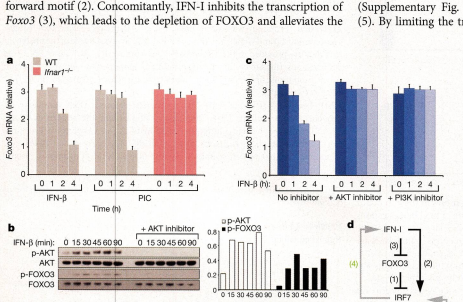

Figure 3 | IFN-β represses FOXO3. **a**, IFN-β- or PIC-stimulation of wild-type macrophages was associated with a significant decrease in *Foxo3* mRNA levels. PIC-induced decrease of *Foxo3* mRNA levels was not observed in *Ifnar1*-null cells. Data are representative of three experiments (average of three values ± standard error). **b**, IFN-β induces activation of AKT in macrophages. Bar graph demonstrates densitometric quantification of phosphorylated AKT and FOXO3 protein levels. **c**, IFN-β-induced repression of *Foxo3* mRNA levels in wild-type BMMs was measured in the presence and absence of PI3K and AKT inhibitors. Data are representative of three experiments (average of three values ± standard error). **d**, A model depicting the FOXO3/IRF7/IFN-I regulatory circuit. See text for details.

of IRF7-induced genes in the absence of a viral infection. In addition, FOXO3 prevents spurious noise in the activity of IFN-I because it is capable of dampening the IRF7-induced positive feedback on IFN-I production.

A fine balance exists between optimal immune clearance of a virus and the collateral damage that is inflicted on infected tissue during the host response. The FOXO3–IRF7 regulatory circuit represents an ideal mechanism for balancing host defence with inflammatory damage. Since we discovered and explored the FOXO3–IRF7 regulatory circuit in macrophages we needed an *in vivo* model system in which macrophages are the principal cells that produce IFN-I in a viral infection. The vesicular stomatitis virus (VSV) lung infection model fully meets this criterion since it has been shown that alveolar macrophages are the primary interferon producers to intranasal infection, and that this response is cell-intrinsic because depletion of alveolar macrophages completely ablates host defence to the virus[18]. Furthermore, VSV is an RNA virus[19] which triggers similar pathways to PIC and which is controlled in an IRF7-dependent manner[7]. Intranasal infection of wild-type mice resulted in a low-grade inflammatory response by day two following infection that was accompanied by intermediate viral load (Fig. 4a–c). By day five the inflammatory response had resolved and viral titres were at basal levels (Fig. 4a–c). By contrast, *Foxo3*-null mice had significantly decreased viral loads at day two when compared with wild-type mice (Fig. 4b, c); however, this response was accompanied by significant lung pathology, including pronounced neutrophil influx, haemorrhage and tissue damage (Fig. 4a and Supplementary Fig. 13). The virus was cleared by day five and lung inflammation was mostly resolved (Fig. 4a–c). Finally, viral replication was not controlled in *Irf7*-null mice (Fig. 4b, c). By day five these mice had developed severe pulmonary oedema and were killed (Fig. 4a).

As discussed above, we chose the VSV model system because the anti-viral response is intrinsic to alveolar macrophages[18]. Consistent with this, we demonstrated that alveolar macrophages, isolated from VSV-infected *Foxo3*-null animals, expressed considerably greater levels of mRNA encoding *Irf7*, *Ifnb1* and other inflammatory cytokines including *Ccl5*, *Ccl7* and *Ccl12* than their wild-type counterparts (Supplementary Fig. 14 and data not shown). The increased basal levels of *Irf7* mRNA in *Foxo3*-null alveolar macrophages further support a cell-intrinsic role for FOXO3, although it is formally possible that other targets are also involved. A recent study demonstrated a cell-intrinsic increase in CD8 T-cell expansion in *Foxo3*-null mice[20]. We detected comparable T-cell numbers in the lungs of VSV-infected wild-type and *Foxo3*-null mice, indicating that T cells are not contributing to the phenotype (data not shown). The data presented above is consistent with the proposed role of the FOXO3–IRF7 circuit in host defence against viruses. The model predicts that FOXO3 suppresses the IRF7-dependent antiviral response to curb the collateral damage associated with host defence. We argue that the dynamic interplay between FOXO3, IRF7 and IFN-I optimizes the antiviral response to achieve the appropriate balance between host defence and rampant inflammation.

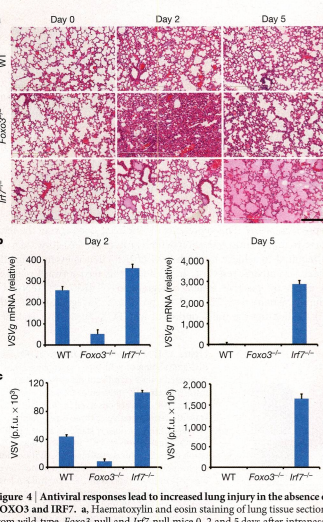

Figure 4 | Antiviral responses lead to increased lung injury in the absence of FOXO3 and IRF7. a, Haematoxylin and eosin staining of lung tissue sections from wild-type, *Foxo3*-null and *Irf7*-null mice 0, 2 and 5 days after intranasal infection with VSV serotype Indiana 10^5 plaque-forming units (p.f.u.). Data are from one experiment that is representative of three independent experiments ($n = 6$ mice per group). Scale bar, 200 μm. **b**, **c**, The viral burden in lungs was determined by measurement of *VSVg* mRNA levels in lung samples using quantitative real-time PCR assay (**b**) and by standard plaque assays in Vero cells (**c**). Data are representative of three experiments (average of three values ± standard error).

METHODS SUMMARY

Cell culture. Bone marrow macrophages (BMMs) were isolated from C57BL/6, *Foxo3*$^{-/-}$, *Irf7*$^{-/-}$ and *Ifnar1*$^{-/-}$ mice, essentially as described[21]. BMMs collected from femurs were plated on non-tissue-culture-treated plastic in complete RPMI medium containing 10% (v/v) FBS (Hyclone Laboratories), 2 mM L-glutamine, 100 IU ml^{-1} of penicillin and 100 g ml^{-1} of streptomycin (all from Cellgro, Mediatech) and supplemented with recombinant human macrophage colony-stimulating factor (50 ng ml^{-1}; Peprotech). BMMs were treated for various length of time with high-purity LPS (10 ng ml^{-1}; *Salmonella minnesota*; List Biologicals), Pam_3CSK_4 (300 ng ml^{-1}; EMC Microcollections), PIC (6 μg ml^{-1}; Amersham), purified murine IFN-β (1.45×10^{-8} U ml^{-1}; PBL-interferon source), VPA (5 mM; Sigma), Apicidin (2.5 μM; Sigma), Ly294002 (50 μM; Sigma) and AKT inhibitor IV (20 μM; EMD Chemicals).

Microarrays and quantitative RT–PCR. RNA isolation for transcriptome analysis of BMMs was performed using TRIzol reagent (Invitrogen). Gene expression profiling was performed using Affymetrix GeneChip Mouse Genome 430 2.0 and GeneChip Mouse Exon 1.0 ST arrays. Details of the analytical methods are provided in the Methods. For quantitative RT–PCR, total RNA was reverse-transcribed to complementary DNA and amplified using primers specific for murine transcripts. Expression values were calculated relative to the *Eef1a1* mRNA transcripts.

ChIP–Seq and ChIP. For ChIP-Seq, immunoprecipitated DNA samples were sequenced on a Illumina HiSeq 2000 sequencing system and aligned using the ELAND software package (Illumina). Peaks identification was performed according to standard methods and is described in full in Methods. For quantitative ChIP, immunoprecipitated DNA samples were amplified with target promoter-specific primers.

Full Methods and any associated references are available in the online version of the paper.

Received 13 May 2012; accepted 20 July 2012.
Published online 16 September 2012.

1. Liu, S. Y., Sanchez, D. J. & Cheng, G. New developments in the induction and antiviral effectors of type I interferon. *Curr. Opin. Immunol.* **23**, 57–64 (2011).
2. Panne, D., Maniatis, T. & Harrison, S. C. An atomic model of the interferon-beta enhanceosome. *Cell* **129**, 1111–1123 (2007).
3. Tamura, T., Yanai, H., Savitsky, D. & Taniguchi, T. The IRF family transcription factors in immunity and oncogenesis. *Annu. Rev. Immunol.* **26**, 535–584 (2008).

4. Barbalat, R., Ewald, S. E., Mouchess, M. L. & Barton, G. M. Nucleic acid recognition by the innate immune system. *Annu. Rev. Immunol.* **29,** 185–214 (2011).
5. Benayoun, B. A., Caburet, S. & Veitia, R. A. Forkhead transcription factors: key players in health and disease. *Trends Genet.* **27,** 224–232 (2011).
6. Schoggins, J. W. *et al.* A diverse range of gene products are effectors of the type I interferon antiviral response. *Nature* **472,** 481–485 (2011).
7. Honda, K. *et al.* IRF-7 is the master regulator of type-I interferon-dependent immune responses. *Nature* **434,** 772–777 (2005).
8. Shahbazian, M. D. & Grunstein, M. Functions of site-specific histone acetylation and deacetylation. *Annu. Rev. Biochem.* **76,** 75–100 (2007).
9. Szklarczyk, D. *et al.* The STRING database in 2011: functional interaction networks of proteins, globally integrated and scored. *Nucleic Acids Res.* **39,** D561–D568 (2011).
10. Khan, N. *et al.* Determination of the class and isoform selectivity of small-molecule histone deacetylase inhibitors. *Biochem. J.* **409,** 581–589 (2008).
11. Ning, S., Huye, L. E. & Pagano, J. S. Regulation of the transcriptional activity of the IRF7 promoter by a pathway independent of interferon signaling. *J. Biol. Chem.* **280,** 12262–12270 (2005).
12. Brunet, A. *et al.* Akt promotes cell survival by phosphorylating and inhibiting a Forkhead transcription factor. *Cell* **96,** 857–868 (1999).
13. Plas, D. R. & Thompson, C. B. Akt activation promotes degradation of tuberin and FOXO3a via the proteasome. *J. Biol. Chem.* **278,** 12361–12366 (2003).
14. Dejean, A. S. *et al.* Transcription factor Foxo3 controls the magnitude of T cell immune responses by modulating the function of dendritic cells. *Nature Immunol.* **10,** 504–513 (2009).
15. Fallarino, F. *et al.* CTLA-4–Ig activates Forkhead transcription factors and protects dendritic cells from oxidative stress in nonobese diabetic mice. *J. Exp. Med.* **200,** 1051–1062 (2004).
16. Wang, S. T. *et al.* RNA interference-mediated silencing of Foxo3 in antigen-presenting cells as a strategy for the enhancement of DNA vaccine potency. *Gene Ther.* **18,** 372–383 (2011).
17. Ning, S., Pagano, J. S. & Barber, G. N. IRF7: activation, regulation, modification and function. *Genes Immun.* 10.1038/gene.2011.21.
18. Kumagai, Y. *et al.* Alveolar macrophages are the primary interferon-α producer in pulmonary infection with RNA viruses. *Immunity* **27,** 240–252 (2007).
19. Lyles, D. S. & Rupprecht, C. E. in *Fields Virology* 5th edn, Vol. 1 (eds Howley, P. M. & Knipe, D. M.) 1363–1408 (2007).
20. Sullivan, J. A., Kim, E. H., Plisch, E. H., Peng, S. L. & Suresh, M. FOXO3 regulates CD8 T cell memory by T cell-intrinsic mechanisms. *PLoS Pathog.* **8,** e1002533 (2012).
21. Gilchrist, M. *et al.* Systems biology approaches identify ATF3 as a negative regulator of Toll-like receptor 4. *Nature* **441,** 173–178 (2006).

Supplementary Information is available in the online version of the paper.

Acknowledgements We thank K. A. Kennedy and J. J. Peschon for discussions and critical reading of the manuscript; and S. A. Danziger, T. Stolyar and E. van Gaver for technical assistance. This work was supported by grants and contracts from the National Institutes of Health (R01AI025032, R01AI032972, HHSN272200700038C, HHSN272200800058C and U54GM103511).

Author Contributions V.L. designed experiments, carried out all experimental studies and drafted the manuscript; A.V.R. performed data mining and microarray data analysis; A.E.L. provided technical assistance for experiments, including quantitative real-time PCR, ChIP and *in vivo* studies; F.S. carried out western blots; A.C.H. and A.R. performed ChIP-Seq data analysis; A.G.R. did genome-wide motif scanning analysis; A.B. did *in vivo* studies; J.D.A. supervised the computational analysis and A.A. supervised the study and wrote the manuscript.

Author Information Microarray and ChIP–Seq raw data have been submitted to the Gene Expression Omnibus under accession number GSE37052. Reprints and permissions information is available at www.nature.com/reprints. The authors declare no competing financial interests. Readers are welcome to comment on the online version of the paper. Correspondence and requests for materials should be addressed to A.A. (alan.aderem@seattlebiomed.org).

LETTER

doi:10.1038/nature11464

Targeting VEGF-B as a novel treatment for insulin resistance and type 2 diabetes

Carolina E. Hagberg[1,2]*, Annika Mehlem[1]*, Annelie Falkevall[1,2], Lars Muhl[1,2], Barbara C. Fam[3], Henrik Ortsäter[4], Pierre Scotney[5], Daniel Nyqvist[1], Erik Samén[6,7], Li Lu[6], Sharon Stone-Elander[6,7], Joseph Proietto[3], Sofianos Andrikopoulos[3], Åke Sjöholm[4], Andrew Nash[5] & Ulf Eriksson[1]

The prevalence of type 2 diabetes is rapidly increasing, with severe socioeconomic impacts[1,2]. Excess lipid deposition in peripheral tissues impairs insulin sensitivity and glucose uptake, and has been proposed to contribute to the pathology of type 2 diabetes[3–5]. However, few treatment options exist that directly target ectopic lipid accumulation[6]. Recently it was found that vascular endothelial growth factor B (VEGF-B) controls endothelial uptake and transport of fatty acids in heart and skeletal muscle[7]. Here we show that decreased VEGF-B signalling in rodent models of type 2 diabetes restores insulin sensitivity and improves glucose tolerance. Genetic deletion of *Vegfb* in diabetic *db/db* mice prevented ectopic lipid deposition, increased muscle glucose uptake and maintained normoglycaemia. Pharmacological inhibition of VEGF-B signalling by antibody administration to *db/db* mice enhanced glucose tolerance, preserved pancreatic islet architecture, improved β-cell function and ameliorated dyslipidaemia, key elements of type 2 diabetes and the metabolic syndrome. The potential use of VEGF-B neutralization in type 2 diabetes was further elucidated in rats fed a high-fat diet, in which it normalized insulin sensitivity and increased glucose uptake in skeletal muscle and heart. Our results demonstrate that the vascular endothelium can function as an efficient barrier to excess muscle lipid uptake even under conditions of severe obesity and type 2 diabetes, and that this barrier can be maintained by inhibition of VEGF-B signalling. We propose VEGF-B antagonism as a novel pharmacological approach for type 2 diabetes, targeting the lipid-transport properties of the endothelium to improve muscle insulin sensitivity and glucose disposal.

Type 2 diabetes affects approximately 310 million individuals worldwide[1], and its prevalence is expected to increase in the future[2,8]. The disease is strongly associated with obesity and pathological lipid deposition within extra-adipose tissues[6], and lipid-induced insulin resistance in muscles has been suggested to contribute to the development of type 2 diabetes[3,4]. Several mechanisms for the deleterious effect of ectopic lipids have been suggested, including the accumulation of diacylglycerols or ceramides that disrupt insulin signalling[9,10], and intracellular redistribution of key components of the molecular machinery required for glucose uptake[11,12]. Of the therapies currently available for the treatment of type 2 diabetes very few specifically target lipid deposition in peripheral tissues[6].

We recently reported that VEGF-B acts on the vascular endothelium to regulate trans-endothelial transport of circulating fatty acids into cardiac and skeletal muscle[7,13,14]. VEGF-B is expressed by tissue cells with high metabolic activity, such as cardiac and skeletal myocytes, brown adipocytes and pancreatic β-cells, from where it signals to the endothelium[7,15,16]. The interaction of VEGF-B with the endothelial receptor VEGF receptor 1 (VEGFR1, also known as FLT1; ref. 17) and the co-receptor neuropilin 1 (ref. 18) induces transcriptional upregulation of the vascular-specific fatty acid transport protein 3 (*Fatp3*, also known as *Slc27a3*) and the more ubiquitously expressed *Fatp4* (also known as *Slc27a4*; ref. 7). Mice lacking VEGF-B ($Vegfb^{-/-}$)[19] are healthy and fertile, but exhibit decreased fatty-acid uptake and lipid deposition in muscles. Instead, lipids are shunted to the white adipose tissue, and therefore $Vegfb^{-/-}$ mice gain more weight[7]. Conversely, cardiac overexpression of VEGF-B causes ceramide accumulation in the heart, and ultimately leads to mitochondrial dysfunction[20]. Taken together, these observations suggest that targeting VEGF-B could be a novel approach to preventing pathological lipid deposition, with the accumulation of lipids halted at the level of the endothelium.

To address this possibility, we examined the effect of *Vegfb* deletion in mice fed a high-fat diet (HFD mice) and in diabetic *db/db* mice[21]. Both mouse models are characterized by obesity, hyperglycaemia and ectopic lipid deposition (Supplementary Fig. 1a–c). In contrast to our previous observations[7], mitochondrial gene expression was decoupled from the expression of *Vegfb* and its downstream target *Fatp3* in obese mice. Expression of mitochondrial genes was reduced in HFD and *db/db* mice[22,23], whereas skeletal and cardiac muscle expression of *Vegfb* and *Fatp3* were increased (Supplementary Fig. 1d–g). This suggested that targeting VEGF-B-mediated fatty-acid uptake could have beneficial effects on intramuscular lipid accumulation, and thus the diabetic phenotypes. We observed that although $Vegfb^{-/-}$ mice fed a HFD (HFD $Vegfb^{-/-}$ mice) gained more weight and had larger fat pads than HFD wild-type mice, they showed lower blood glucose levels (Supplementary Fig. 2). These effects were even more prominent in $Vegfb^{-/-}$ mice crossed with *db/db* mice (*db/db* $Vegfb^{-/-}$ mice). *db/db* $Vegfb^{-/-}$ mice had normal blood glucose levels in both the fasted and postprandial state, in contrast to the severely hyperglycaemic *db/db* control animals (Fig. 1a, b). There appeared to be a gene dosage effect in males, with heterozygous *db/db* $Vegfb^{+/-}$ mice showing slightly elevated blood glucose levels compared with homozygous *db/db* $Vegfb^{-/-}$ mice. In contrast, the deletion of a single copy of *Vegfb* was sufficient for female *db/db* $Vegfb^{+/-}$ mice to remain normoglycaemic (Supplementary Fig. 3a, b). The *db/db* $Vegfb^{+/-}$ and *db/db* $Vegfb^{-/-}$ mice had equal or lower plasma insulin levels compared to *db/db* controls, indicating that their normalized blood glucose was not due to compensatory hyperinsulinaemia (data not shown). All three genotypes had similar body weight and weight gain until 20 weeks of age, when the *db/db* control animals became catabolic, that is, they stopped gaining weight and developed glucosuria (Fig. 1c, d and Supplementary Fig. 3c–f). In contrast, *db/db* mice lacking one or both *Vegfb* alleles did not become catabolic (Fig. 1c, d and Supplementary Fig. 3c–f). Deletion of *Vegfb* did not affect food intake in mice on either a normal diet or HFD, or in diabetic mice (Supplementary Fig. 4).

Deletion of *Vegfb* in *db/db* mice reduced *Fatp3* messenger RNA expression (Supplementary Fig. 5), and significantly decreased lipid

[1]Tissue Biology Group, Division of Vascular Biology, Department of Medical Biochemistry and Biophysics, Karolinska Institutet, SE-171 77 Stockholm, Sweden. [2]Ludwig Institute for Cancer Research Ltd, Stockholm Branch, Karolinska Institutet, Box 240, SE-171 77 Stockholm, Sweden. [3]Department of Medicine (AH), University of Melbourne, Heidelberg, Victoria 3091, Australia. [4]Diabetes Research Unit, Department of Clinical Science and Education, Södersjukhuset, Karolinska Institutet, SE-118 83 Stockholm, Sweden. [5]CSL Limited, Parkville, Victoria 3052, Australia. [6]Karolinska University Hospital, Neuroradiology Department and Karolinska Experimental Research and Imaging Center, Solna, SE-17176 Stockholm, Sweden. [7]Clinical Neurosciences, Karolinska Institutet, SE-171 76, Stockholm, Sweden.
*These authors contributed equally to this work.

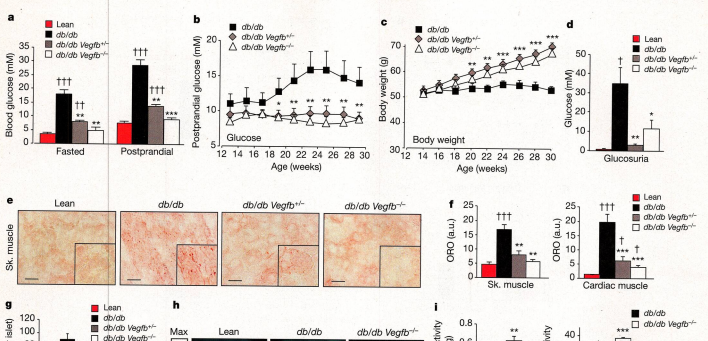

Figure 1 | *Vegfb* deficiency protects *db/db* mice against the onset of type 2 diabetes. **a**, Endpoint blood glucose levels for fasted lean ($n = 34$), *db/db* ($n = 5$), *db/db Vegfb*$^{+/-}$ ($n = 7$) and *db/db Vegfb*$^{-/-}$ ($n = 5$) mice, and for fed lean ($n = 22$), *db/db* ($n = 7$), *db/db Vegfb*$^{+/-}$ ($n = 6$) and *db/db Vegfb*$^{-/-}$ ($n = 8$) mice. **b**, **c**, Bi-weekly measurements of blood glucose and body weight of *db/db* ($n = 15$), *db/db Vegfb*$^{+/-}$ ($n = 32$) and *db/db Vegfb*$^{-/-}$ ($n = 20$) mice. **d**, Endpoint glucosuria in lean ($n = 5$), *db/db* ($n = 18$), *db/db Vegfb*$^{+/-}$ ($n = 20$) and *db/db Vegfb*$^{-/-}$ ($n = 17$) mice. **e**, **f**, Staining (**e**; scale bars, 50 μm) and quantification (**f**) of oil-red-O (ORO)-stained neutral lipids in skeletal (sk.) and cardiac muscles from lean ($n = 4$), *db/db* ($n = 6$), *db/db Vegfb*$^{+/-}$ ($n = 4$ skeletal, $n = 10$ cardiac) and *db/db Vegfb*$^{-/-}$ ($n = 5$) mice. a.u., arbitrary units. **g**, Quantification of triglycerides (TGs) in isolated pancreatic islets from lean, *db/db*, *db/db Vegfb*$^{+/-}$ and *db/db Vegfb*$^{-/-}$ mice ($n = 5$ per group). **h**, [^{18}F]FDG accumulation in hearts during PET. **i**, Post-PET measurement of radioactivity in skeletal muscles and hearts ($n = 4$ per group). % ID per g, percentage of injected tracer dose per gram tissue. †/*$P < 0.05$, ††/**$P < 0.01$, †††/***$P < 0.001$ compared to lean and to *db/db* mice, respectively. Values are means ± s.e.m.

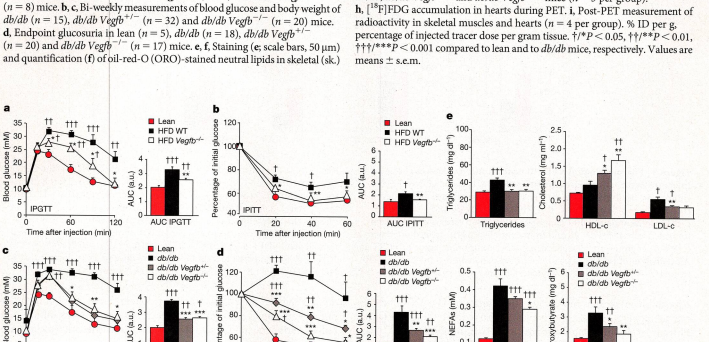

Figure 2 | *Vegfb* deficiency ameliorates the metabolic syndrome. **a**–**d**, Intraperitoneal glucose and insulin tolerance tests (IPGTTs and IPITTs) and area under curve (AUC) analysis of lean, HFD wild-type (WT) and HFD *Vegfb*$^{-/-}$ mice (**a**, **b**, $n = 7$ per group), and of lean (**c**, **d**, $n = 7$), *db/db* ($n = 12$ in **c**, $n = 7$ in **d**), *db/db Vegfb*$^{+/-}$ ($n = 19$) and *db/db Vegfb*$^{-/-}$ mice ($n = 9$ in **c**, $n = 12$ in **d**). **e**, Plasma levels of triglycerides ($n = 12$ lean, $n = 6$ *db/db*, $n = 15$ *db/db Vegfb*$^{+/-}$, $n = 6$ *db/db Vegfb*$^{-/-}$), HDL-c and LDL-c ($n = 3$ lean, $n = 7$ *db/db*, $n = 13$ *db/db Vegfb*$^{+/-}$, $n = 7$ *db/db Vegfb*$^{-/-}$), NEFAs ($n = 27$ lean, $n = 10$ *db/db*, $n = 14$ *db/db Vegfb*$^{+/-}$, $n = 11$ *db/db Vegfb*$^{-/-}$) and ketones ($n = 13$ lean, $n = 8$ *db/db*, $n = 13$ *db/db Vegfb*$^{+/-}$, $n = 13$ *db/db Vegfb*$^{-/-}$). †/*$P < 0.05$, ††/**$P < 0.01$, †††/***$P < 0.001$ compared to lean and to HFD wild-type mice (**a**, **b**), or lean and *db/db* mice (**c**–**e**), respectively. Values are means ± s.e.m.

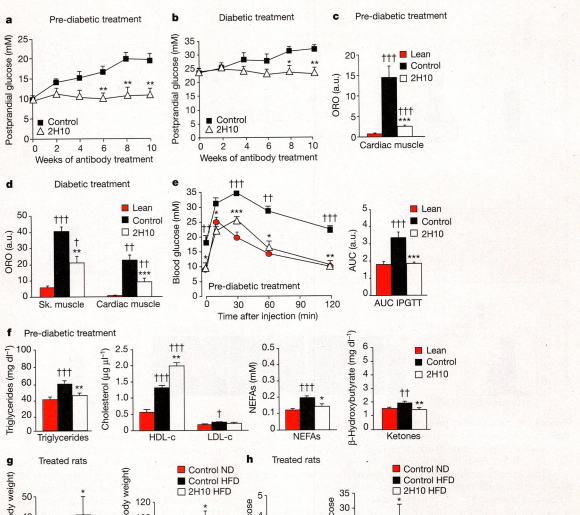

Figure 3 | Pharmacological VEGF-B neutralization enhances glucose tolerance in diabetic mouse and rat models. **a**, **b**, Blood glucose levels of control- or 2H10-treated pre-diabetic (**a**, $n = 10$ per group) and diabetic (**b**, $n = 12$ control-treated, $n = 16$ 2H10-treated) *db/db* mice. **c**, **d**, Quantification of ORO staining in skeletal and cardiac muscles from untreated lean mice ($n = 4$), and from control- or 2H10-treated pre-diabetic (**c**, $n = 6$ per group) and diabetic (**d**, $n = 4$ per group) *db/db* mice. **e**, IPGTT and AUC analysis of untreated lean mice ($n = 6$), and control- ($n = 5$) or 2H10-treated ($n = 5$) pre-diabetic *db/db* mice. **f**, Plasma levels of triglycerides ($n = 17$ lean, $n = 12$ control-treated, $n = 13$ 2H10-treated mice), HDL-c and LDL-c ($n = 3$ per group), NEFAs ($n = 27$ lean, $n = 6$ control-treated, $n = 8$ 2H10-treated mice) and ketones ($n = 16$ lean, $n = 9$ control-treated, $n = 11$ 2H10-treated mice). **g**, **h**, GIR and GDR (**g**), and [^{14}C]-deoxyglucose uptake into muscles (**h**), after a hyperinsulinaemic/euglycaemic clamp in control- and 2H10-treated HFD-fed rats ($n = 6$ per group), compared to control-treated normal diet (ND)-fed ($n = 5$) rats. †/*$P < 0.05$, ††/**$P < 0.01$, †††/***$P < 0.001$ compared to lean/*db/db* control mice (**a**–**f**), or control-treated ND-fed/HFD-fed rats (**g**, **h**). Values are means ± s.e.m.

deposition in skeletal muscle and myocardium (Fig. 1e, f and Supplementary Fig. 6a). VEGF-B depletion also reduced the accumulation of triglycerides in isolated pancreatic islets from *db/db Vegfb*$^{+/-}$ and *db/db Vegfb*$^{-/-}$ mice (Fig. 1g), but did not affect lipid accumulation in liver (data not shown). Reduced intramuscular lipid levels have been proposed to shift metabolism towards glucose usage[24]. Therefore, *in vivo* uptake and accumulation of the glucose analogue [2-^{18}F]-2-fluoro-2-deoxy-D-glucose ([^{18}F]FDG) was assessed in *db/db* and *db/db Vegfb*$^{-/-}$ mice using positron emission tomography (PET). Analyses of the *db/db Vegfb*$^{-/-}$ mice showed a 29% increase in cardiac [^{18}F]FDG uptake as compared to *db/db* controls (Fig. 1h and Supplementary Fig. 6b). Post-PET measurement of radioactivity in dissected tissues confirmed increased glucose uptake in both skeletal and cardiac muscles in *db/db Vegfb*$^{-/-}$ mice (Fig. 1i). Taken together, the deletion of either one or both copies of *Vegfb* in diabetic mouse models was sufficient to reduce peripheral lipid deposition in muscular tissues, increase glucose uptake and maintain normoglycaemia.

Type 2 diabetes and the metabolic syndrome are characterized by glucose intolerance, insulin resistance and dyslipidaemia[25]. HFD *Vegfb*$^{-/-}$ mice demonstrated improved glucose tolerance compared to HFD wild-type mice, and were comparable to lean mice in their response to insulin injections (Fig. 2a, b). Similarly, *db/db Vegfb*$^{-/-}$ and *db/db Vegfb*$^{+/-}$ mice were more glucose tolerant and insulin sensitive than *db/db* controls (Fig. 2c, d). The expression of gluconeogenic and lipogenic genes was increased in the livers of control *db/db* mice, probably owing to hepatic insulin resistance[6], but the *db/db Vegfb*$^{-/-}$ mice

showed a normal hepatic expression pattern of such genes (Supplementary Fig. 6c). Furthermore, dyslipidaemia was ameliorated in *db/db Vegfb*$^{-/-}$ mice (Fig. 2e). The *db/db Vegfb*$^{-/-}$ mice had reduced plasma triglyceride levels and low-density lipoprotein (LDL)/very-low-density lipoprotein (VLDL)-bound cholesterol (LDL-c) levels, and higher levels of high-density lipoprotein (HDL)-bound cholesterol (HDL-c) than the *db/db* controls (Fig. 2e). The *db/db Vegfb*$^{-/-}$ mice also had a normal HDL-c to LDL-c ratio (lean mice, 4.3 ± 0.5; *db/db*, 1.8 ± 0.3; *db/db Vegfb*$^{+/-}$, 4.0 ± 0.4; *db/db Vegfb*$^{-/-}$, 4.2 ± 0.6), indicating a lower risk for cardiovascular disease, although total plasma cholesterol was higher in *db/db Vegfb*$^{-/-}$ mice compared to lean mice. Moreover, the levels of circulating non-esterified fatty acids (NEFAs) and ketones were reduced in *db/db Vegfb*$^{-/-}$ mice (Fig. 2e). Genetic deletion of *Vegfb* thus targeted several hallmarks of type 2 diabetes, and improved the metabolic balance.

To investigate whether pharmacological inhibition of VEGF-B signalling could ameliorate type 2 diabetes and the metabolic syndrome, *db/db* mice were injected with a specific neutralizing anti-VEGF-B antibody (2H10, mouse version[26]) or a control antibody for 10 weeks. Two treatment strategies were applied, one preventative using pre-diabetic *db/db* mice, and one therapeutic using diabetic *db/db* mice (Supplementary Fig. 7a). Both strategies lowered cardiac *Fatp3* messenger RNA levels at the end of the study, whereas no effect on *Vegfb* expression was detected (Supplementary Fig. 7b, c). Treatment of pre-diabetic *db/db* mice with 2H10 prevented the development of hyperglycaemia (Fig. 3a), and the progression of hyperglycaemia was halted in diabetic *db/db* mice receiving 2H10 (Fig. 3b). At the end of the study, *db/db* mice receiving 2H10 showed reduced lipid deposition in skeletal muscle and heart (Fig. 3c, d and Supplementary Fig. 8), and improved glucose tolerance compared to control-treated *db/db* mice (Fig. 3e and Supplementary Fig. 9a), although no effect on weight gain was observed (data not shown). Administration of 2H10 protected the pre-diabetic *db/db* mice against elevated levels of circulating triglycerides, LDL-c, NEFAs and ketones, and increased plasma HDL-c levels (Fig. 3f). 2H10 treatment of diabetic *db/db* mice had no effect on plasma triglyceride levels, and increased the levels of both HDL-c and LDL-c as compared to controls (Supplementary Fig. 9b). However, 2H10 treatment did lower both circulating NEFAs and ketones in diabetic *db/db* mice (Supplementary Fig. 9b). In summary, anti-VEGF-B treatment over a 10-week period, in either a preventative or a therapeutic context, was able to considerably limit disease progression.

To determine further the therapeutic potential of an anti-VEGF-B antibody in insulin resistance and type 2 diabetes, rats were fed a HFD (HFD rats) for 8 weeks, and in parallel given 2H10 (chimaeric mouse/rat antibody), or a control antibody. Treatment with 2H10 normalized glucose tolerance and glucose-stimulated insulin secretion in the HFD rats (Supplementary Fig. 10a–c). A hyperinsulinaemic/euglycaemic clamp study demonstrated that control-treated HFD rats exhibited reduced glucose infusion rates (GIRs) and glucose disposal rates (GDRs) compared to lean control-treated animals, indicative of insulin resistance (Fig. 3g). In contrast, 2H10 treatment of HFD rats increased both GIR and GDR, and significantly promoted glucose uptake in skeletal muscle and heart (Fig. 3g, h). Food consumption and endogenous glucose production remained unchanged in the 2H10-treated HFD rats compared to HFD controls (Supplementary Fig. 10d, and data not shown). Anti-VEGF-B treatment thus restored insulin sensitivity, increased muscle glucose usage, and reversed type 2 diabetes pathology in these rodent models.

The improved glucose tolerance after VEGF-B neutralization in mice and rats suggested that inhibition of VEGF-B might preserve islet function in addition to ameliorating insulin resistance. Histochemical analysis showed that 2H10 treatment of pre-diabetic and diabetic mice did not prevent pancreatic islet hyperplasia (Fig. 4a, b) or influence islet density (Supplementary Fig. 11a). However, 2H10-treated diabetic mice had large islets with few signs of degeneration, whereas the diabetic control mice had small islets with grossly disrupted architecture (Fig. 4a, b). The 2H10-treated *db/db* mice had normalized expression of insulin and glucagon within their islets as compared to control-treated mice

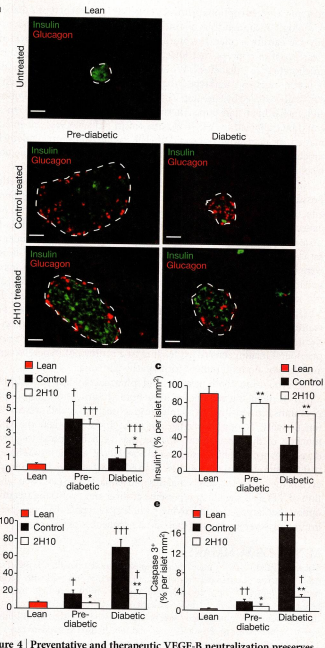

Figure 4 | Preventative and therapeutic VEGF-B neutralization preserves insulin production and pancreatic islet morphology in *db/db* mice. **a**–**e**, Analysis of control-treated or 2H10-treated pre-diabetic ($n = 3$ control-treated, $n = 4$ 2H10-treated) or diabetic ($n = 3$ per group) *db/db* mice, as compared to untreated lean mice ($n = 6$). **a**, Pancreatic islets stained for insulin and glucagon. Scale bars, 100 μm. **b**–**d**, Quantification of mean islet size (**b**), percentage of insulin-stained area per islet (**c**) and stained glucagon to insulin ratio (**d**). **e**, Quantification of cleaved caspase 3 stained area per islet. Plus signs denote positively stained area. †/*$P < 0.05$, ††/**$P < 0.01$, †††/***$P < 0.001$ as compared to lean and *db/db* controls, respectively. Values are means ± s.e.m.

(Fig. 4a, c and Supplementary Fig. 11b). Furthermore, 2H10-treated animals had a normalized ratio between glucagon and insulin staining (Fig. 4d), and fewer centrally located α-cells within the islets (Supplementary Fig. 11c), indications of preserved islet integrity. Staining for the apoptosis marker cleaved caspase 3 confirmed that the *db/db* mice treated with 2H10 showed significantly reduced β-cell apoptosis (Fig. 4e and Supplementary Fig. 12). Thus, therapeutic inhibition of VEGF-B signalling preserved insulin production and islet functionality by protecting islet architecture and preventing β-cell apoptosis.

Insulin resistance characterizes >90% of type 2 diabetes patients[27]. However, with the exception of the thiazolidinediones, none of the

current treatment options primarily targets this aspect of type 2 diabetes pathology. Although thiazolidinediones have recently been linked to adverse cardiovascular outcomes, the use of these drugs provided a clear proof of concept that lowering peripheral lipid deposition can ameliorate type 2 diabetes[28]. We show, in four different rodent models of insulin resistance and type 2 diabetes, that glucose intolerance can be efficiently reduced by targeting VEGF-B-regulated FATP expression and endothelial lipid transport. Alternatively, the observed improvements could be explained by VEGF-B antagonism reducing vascular inflammation or increasing trans-endothelial insulin transport, endothelial functions that have both been shown to be important for whole body insulin sensitivity[29,30].

Anti-VEGF-B treatment also improved pancreatic β-cell function, possibly by reducing triglyceride accumulation within the islets. Direct effects of VEGF-B signalling on β-cells are unlikely, as VEGFR1 is only expressed by endothelial cells in the pancreas[16]. We analysed HFD-fed mice overexpressing VEGF-B selectively in pancreatic β-cells under the rat insulin promoter (RIP VEGF-B mice). HFD-fed RIP VEGF-B mice were indistinguishable from wild-type mice in glucose tolerance, insulin sensitivity, islet morphology and circulating levels of insulin (data not shown). Furthermore, no alterations were detected in lean RIP VEGF-B mice in pancreatic islet physiology, lipid staining or *Fatp* expression[16]. Hence, systemic 2H10 treatment could be protecting the islets through a combination of reduced lipotoxicity and improved peripheral insulin sensitivity, leading to a reversal of hyperglycaemia and thereby no requirement for hyperinsulinemia.

In conclusion, both genetic and pharmacological inhibition of VEGF-B signalling can limit ectopic lipid accumulation, restore peripheral insulin sensitivity and muscle glucose uptake, and preserve islet functionality. To our knowledge, this is the first study where the barrier function of the vascular endothelium has been harnessed to prevent development of insulin resistance and type 2 diabetes. The results indicate that the endothelium can function as an effective barrier to lipid transport even in the context of obesity and dyslipidaemia. We propose that inhibition of VEGF-B signalling represents a novel and promising treatment option that targets the underlying pathology of type 2 diabetes, thereby improving several adverse metabolic consequences of the disease.

METHODS SUMMARY

Mice. C57BL/6 *Vegfb*$^{-/-}$ mice have previously been described[19]. C57BKS/Lepr^{db} (*db/db*) mice were purchased from Jackson Laboratory, and bred with *Vegfb*$^{-/-}$ mice. *db/db Vegfb*$^{-/-}$ and control *db/db Vegfb*$^{+/+}$ mice were bred by mating heterozygous *db/+ Vegfb*$^{+/-}$ mice with each other. Wild-type C57/BL6 mice from the *Vegfb*-knockout mouse colony were used as lean wild-type controls. All animals had *ad libitum* access to chow and water, and were housed in standard cages with 12 h light–12 h dark cycles. All mouse work was conducted in accordance with protocols approved by Swedish Animal Welfare Board in Stockholm, Sweden.

Full Methods and any associated references are available in the online version of the paper.

Received 11 January; accepted 31 July 2012.
Published online 26 September 2012.

1. World Health Organization. World Health Organization Diabetes Fact sheet no. 312. http://www.who.int/mediacentre/factsheets/fs312/en/ (2011).
2. Diabetes Prevention Program (DPP) Research Group. The Diabetes Prevention Program (DPP): description of lifestyle intervention. *Diabetes Care* **25,** 2165–2171 (2002).
3. Perseghin, G. *et al.* Intramyocellular triglyceride content is a determinant of *in vivo* insulin resistance in humans: a 1H-13C nuclear magnetic resonance spectroscopy assessment in offspring of type 2 diabetic parents. *Diabetes* **48,** 1600–1606 (1999).
4. Samuel, V. T., Petersen, K. F. & Shulman, G. I. Lipid-induced insulin resistance: unravelling the mechanism. *Lancet* **375,** 2267–2277 (2010).
5. Unger, R. H. Lipotoxic diseases. *Annu. Rev. Med.* **53,** 319–336 (2002).
6. Stumvoll, M., Goldstein, B. J. & van Haeften, T. W. Type 2 diabetes: principles of pathogenesis and therapy. *Lancet* **365,** 1333–1346 (2005).
7. Hagberg, C. E. *et al.* Vascular endothelial growth factor B controls endothelial fatty acid uptake. *Nature* **464,** 917–921 (2010).
8. Zimmet, P., Alberti, K. G. & Shaw, J. Global and societal implications of the diabetes epidemic. *Nature* **414,** 782–787 (2001).
9. Schmitz-Peiffer, C. *et al.* Alterations in the expression and cellular localization of protein kinase C isozymes epsilon and theta are associated with insulin resistance in skeletal muscle of the high-fat-fed rat. *Diabetes* **46,** 169–178 (1997).
10. Schmitz-Peiffer, C. Targeting ceramide synthesis to reverse insulin resistance. *Diabetes* **59,** 2351–2353 (2010).
11. Boström, P. *et al.* SNARE proteins mediate fusion between cytosolic lipid droplets and are implicated in insulin sensitivity. *Nature Cell Biol.* **9,** 1286–1293 (2007).
12. Bostrom, P. *et al.* The SNARE protein SNAP23 and the SNARE-interacting protein Munc18c in human skeletal muscle are implicated in insulin resistance/type 2 diabetes. *Diabetes* **59,** 1870–1878 (2010).
13. Muoio, D. M. Metabolism and vascular fatty acid transport. *N. Engl. J. Med.* **363,** 291–293 (2010).
14. Lahteenvuo, J. E. *et al.* Vascular endothelial growth factor-B induces myocardium-specific angiogenesis and arteriogenesis via vascular endothelial growth factor receptor-1- and neuropilin receptor-1-dependent mechanisms. *Circulation* **119,** 845–856 (2009).
15. Olofsson, B. *et al.* Vascular endothelial growth factor B, a novel growth factor for endothelial cells. *Proc. Natl Acad. Sci. USA* **93,** 2576–2581 (1996).
16. Albrecht, I. *et al.* Suppressive effects of vascular endothelial growth factor-B on tumor growth in a mouse model of pancreatic neuroendocrine tumorigenesis. *PLoS ONE* **5,** e14109 (2010).
17. Olofsson, B. *et al.* Vascular endothelial growth factor B (VEGF-B) binds to VEGF receptor-1 and regulates plasminogen activator activity in endothelial cells. *Proc. Natl Acad. Sci. USA* **95,** 11709–11714 (1998).
18. Makinen, T. *et al.* Differential binding of vascular endothelial growth factor B splice and proteolytic isoforms to neuropilin-1. *J. Biol. Chem.* **274,** 21217–21222 (1999).
19. Aase, K. *et al.* Vascular endothelial growth factor-B-deficient mice display an atrial conduction defect. *Circulation* **104,** 358–364 (2001).
20. Karpanen, T. *et al.* Overexpression of vascular endothelial growth factor-B in mouse heart alters cardiac lipid metabolism and induces myocardial hypertrophy. *Circ. Res.* **103,** 1018–1026 (2008).
21. Genuth, S. M., Przybylski, R. J. & Rosenberg, D. M. Insulin resistance in genetically obese, hyperglycemic mice. *Endocrinology* **88,** 1230–1238 (1971).
22. Sparks, L. M. *et al.* A high-fat diet coordinately downregulates genes required for mitochondrial oxidative phosphorylation in skeletal muscle. *Diabetes* **54,** 1926–1933 (2005).
23. Mootha, V. K. *et al.* PGC-1α-responsive genes involved in oxidative phosphorylation are coordinately downregulated in human diabetes. *Nature Genet.* **34,** 267–273 (2003).
24. Randle, P. J. Regulatory interactions between lipids and carbohydrates: the glucose fatty acid cycle after 35 years. *Diabetes Metab. Rev.* **14,** 263–283 (1998).
25. Eckel, R. H., Grundy, S. M. & Zimmet, P. Z. The metabolic syndrome. *Lancet* **365,** 1415–1428 (2005).
26. Scotney, P. D. *et al.* Human vascular endothelial growth factor B: characterization of recombinant isoforms and generation of neutralizing monoclonal antibodies. *Clin. Exp. Pharmacol. Physiol.* **29,** 1024–1029 (2002).
27. Fujimoto, W. Y. The importance of insulin resistance in the pathogenesis of type 2 diabetes mellitus. *Am. J. Med.* **108** (suppl. 6a), 9–14 (2000).
28. Chaggar, P. S., Shaw, S. M. & Williams, S. G. Review article: thiazolidinediones and heart failure. *Diab. Vasc. Dis. Res.* **6,** 146–152 (2009).
29. Kim, F. *et al.* Vascular inflammation, insulin resistance, and reduced nitric oxide production precede the onset of peripheral insulin resistance. *Arterioscler. Thromb. Vasc. Biol.* **28,** 1982–1988 (2008).
30. Kubota, T. *et al.* Impaired insulin signaling in endothelial cells reduces insulin-induced glucose uptake by skeletal muscle. *Cell Metab.* **13,** 294–307 (2011).

Supplementary Information is available in the online version of the paper.

Acknowledgements We thank S. Wittgren and A. Gustafsson for technical assistance, and G. Christofori for the RIP VEGF-B mice. C.E.H. was supported by the Frans Wilhelm och Waldemar von Frenckells Fond and Wilhelm och Else Stockmanns Stiftelse. D.N. was supported by the Swedish Society for Medical Research. This study was supported by the Ludwig Institute for Cancer Research, the Novo Nordisk Foundation, the Swedish Cancer Foundation, the Swedish Research Council, Torsten och Ragnar Söderbergs Stiftelser, Dr Peter Wallenbergs Foundation for Economics and Technology, the Swedish Heart and Lung Foundation, the Diabetes Foundation and Karolinska Institutet.

Author Contributions C.E.H. designed and performed *in vivo* mouse experiments, collected the material, performed transcriptional analysis and wrote the paper; A.M. performed *in vivo* mouse experiments, transcriptional analyses, ORO analyses, plasma analyses, triglyceride content measurements, all histological analyses of the pancreas and helped write the paper; A.F. performed ORO analyses, assisted with *in vivo* mouse studies and helped write the paper; L.M. assisted with *in vivo* studies; B.C.F. performed the rat study; P.S. helped design and interpret the rat study, helped write the paper and developed and supplied the 2H10, rat/mouse chimaeric 2H10 and 6H6 antibodies; D.N. performed the islet isolation and triglyceride content measurements; E.S., L.L. and S.S.-E. performed and analysed the FA scan data; J.P. and S.A. designed, supervised and analysed the rat study; H.O. and Å.S. provided expertise in diabetes, advised on islet analysis, interpreted results and commented on the manuscript; A.N. helped design and interpret the rat study, and helped write the paper; U.E. designed and supervised the study, analysed and interpreted the data and helped write the paper. All authors discussed the results and commented on the manuscript.

Author Information Reprints and permissions information is available at www.nature.com/reprints. The authors declare competing financial interests: details accompany the full-text HTML version of the paper at www.nature.com/nature. Readers are welcome to comment on the online version of the paper. Correspondence and requests for materials should be addressed to U.E (ulf.pe.eriksson@ki.se).

LETTER

doi:10.1038/nature11430

Initiation of transcription-coupled repair characterized at single-molecule resolution

Kévin Howan[1]†, Abigail J. Smith[2], Lars F. Westblade[3]†, Nicolas Joly[1], Wilfried Grange[1], Sylvain Zorman[1]†, Seth A. Darst[3], Nigel J. Savery[2] & Terence R. Strick[1]

Transcription-coupled DNA repair uses components of the transcription machinery to identify DNA lesions and initiate their repair. These repair pathways are complex, so their mechanistic features remain poorly understood. Bacterial transcription-coupled repair is initiated when RNA polymerase stalled at a DNA lesion is removed by Mfd, an ATP-dependent DNA translocase[1–3]. Here we use single-molecule DNA nanomanipulation to observe the dynamic interactions of *Escherichia coli* Mfd with RNA polymerase elongation complexes stalled by a cyclopyrimidine dimer or by nucleotide starvation. We show that Mfd acts by catalysing two irreversible, ATP-dependent transitions with different structural, kinetic and mechanistic features. Mfd remains bound to the DNA in a long-lived complex that could act as a marker for sites of DNA damage, directing assembly of subsequent DNA repair factors. These results provide a framework for considering the kinetics of transcription-coupled repair *in vivo*, and open the way to reconstruction of complete DNA repair pathways at single-molecule resolution.

In bacteria, the Mfd protein couples transcription and nucleotide excision repair (NER). Mfd is a superfamily 2 ATP-dependent DNA translocase[1,2] (Supplementary Fig. 1) with two distinct functions: first, it recognizes a stalled RNA polymerase (RNAP) and uses the energy of ATP hydrolysis to dissociate the RNAP–DNA elongation complex (RD_e). Second, Mfd recruits UvrA, a component of the Uvr(A)BC excinuclease machinery. As a consequence of Mfd action, bulky lesions that stall RNAP are repaired more efficiently than similar lesions repaired by the transcription-independent global NER pathway[3]. Transcription-coupled repair (TCR) in eukaryotes is more complex, but the functional homologue of Mfd in humans (CSB, also known as ERCC6) is also a superfamily 2 DNA translocase[4].

Although the role of Mfd in the recognition and dissociation of a stalled RD_e has been well-studied genetically[2,5,6], biochemically[1,7–10] and structurally[11–14], the mechanism by which Mfd promotes RD_e dissociation has not been determined. Because Mfd can rescue back-tracked RD_e, it is thought that it acts by pushing RNAP downstream, in what is termed the forward-translocation mechanism[7]. Furthermore, identification of a specific interaction between Mfd and RNAP that is required for Mfd function led to the proposal that Mfd simultaneously interacts with RNAP (by means of its RNAP-interacting domain) and with DNA (by means of its ATPase domains)[7,11], allowing its translocase activity to generate positive torque on the DNA, wrenching shut the transcription bubble and thus destabilizing RD_e[13,16].

To investigate the mechanism of action of Mfd on stalled RD_e, we developed a single-molecule assay allowing us to monitor Mfd interactions with single stalled *E. coli* RNAP molecules in real time[17] (Fig. 1a and Supplementary Fig. 2). Here the mechanical properties of a nanomanipulated DNA are used to detect a single RNAP initiating transcription, progressing to form RD_e, and dissociating after reaching a terminator[17] (Fig. 1b). By omitting cytidine triphosphate (CTP), we can stall RNAP at position +20 of the template for an indefinite amount of time[7,20] (Fig. 1c and Supplementary Fig. 3).

A single-molecule time-trace obtained when Mfd is present during the RNAP stall indicates that Mfd forms a remarkably long-lived intermediate, denoted I (Fig. 1d). Analysis of changes in DNA extension during formation and resolution of I provides information on its structural properties (Supplementary Fig. 4 and refs 18, 19), revealing that, in the intermediate, at least two-thirds of the transcription bubble

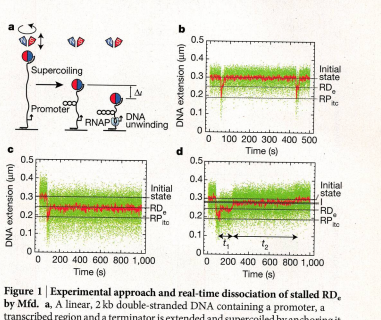

Figure 1 | Experimental approach and real-time dissociation of stalled RD_e by Mfd. a, A linear, 2 kb double-stranded DNA containing a promoter, a transcribed region and a terminator is extended and supercoiled by anchoring it to a glass surface at one end and a 1-μm magnetic bead at the other, and manipulating the bead using a magnetic field. RNAP–DNA interactions are observed in real-time using videomicroscopy-based bead tracking to measure changes in DNA conformation (see Supplementary Fig. 2 and ref. 17). **b**, Single-molecule time-trace showing two complete transcription events. Green points, raw DNA extension data (31 Hz); red points, data averaged over approximately 1 s. Black lines indicate the DNA extension for the initial state, the RNAP-promoter initial transcribing complex (RP_{itc}) during which DNA scrunching occurs, and the ternary elongation complex (RD_e). The increase in extension from RP_{itc} to RD_e corresponds to promoter escape, and the increase in extension from RD_e back to the initial state corresponds to termination. **c**, Representative time-trace obtained when CTP is omitted. RNAP stalls ~5 base pairs (~0.5 s; ref. 17) after promoter escape. Termination is not observed. **d**, Representative time-trace obtained as in **c**, but in the presence of 100 nM Mfd. Return to the initial state takes place by two distinct increases in DNA extension that occur, respectively, t_1 and $t_1 + t_2$ seconds after promoter escape. In the intervening time a stable, long-lived intermediate is formed, here labelled I.

[1]Institut Jacques Monod, CNRS, UMR 7592, University Paris Diderot, Sorbonne Paris Cité F-75205 Paris, France. [2]DNA-Protein Interactions Unit, School of Biochemistry, University of Bristol, Bristol BS8 1TD, UK. [3]The Rockefeller University, 1230 York Avenue, New York, New York 10065, USA. †Present addresses: Statistical Physics Laboratory, Ecole Normale Superieure, 24 rue Lhomond 75005 Paris (K.H.); Department of Pathology and Laboratory Medicine, Division of Infectious Disease Diagnostics, North Shore LIJ Health System Laboratories, 10 Nevada Drive, Lake Success, New York 11718, USA (L.F.W.); Department of Cell Biology, Yale University School of Medicine, 333 Cedar Street, New Haven, Connecticut 06520, USA (S.Z.).

is rewound and the DNA is bent by approximately 90°. As permanganate footprinting suggests that the transcription bubble is rapidly and fully rewound by Mfd action (Supplementary Fig. 5), the DNA deformation observed in the intermediate is probably due to bending/wrapping interactions between proteins and DNA rather than residual unwinding in a partially collapsed transcription bubble.

Pulse-chase experiments show that both formation and resolution of the intermediate require ATP binding (Fig. 2a, b) and hydrolysis (Supplementary Figs 6 and 7). Moreover, when we trap the intermediate with a wash step that removes both ATP and free Mfd from solution we find that adding back only ATP is sufficient to allow resolution of the trapped intermediate (Fig. 2b). Thus, the same molecule of Mfd is responsible for formation and resolution of the intermediate. Finally, we occasionally observe that after formation of the intermediate, a second RNAP can bind to the promoter, initiate transcription, stall, and become a target for a second molecule of Mfd (Fig. 2c). No such reloading events are observed when RNAP is stalled in the absence of Mfd (Supplementary Fig. 3). Thus, as Mfd modifies the structure of RD_e it also clears the transcription start site for a new RNAP to initiate[7,15].

Surprisingly, single-molecule experiments with Mfd alone show that in the nucleotide-bound state (that is, in the presence of ATP-γ-S but not in the presence of ATP), the protein distorts the DNA in a pattern characteristic of unwinding or wrapping (Supplementary Figs 6 and 8). In the presence of ATP, Mfd distorts the DNA provided that core RNAP is present at high concentration in solution (Supplementary Fig. 8). Because permanganate attack of DNA in the presence of Mfd and ATP-γ-S detects no unwinding (Supplementary Fig. 6), this distortion is most likely due to partial, left-handed wrapping of DNA about Mfd. However, in contrast to the remarkably stable nature of the Mfd-containing TCR intermediate in all nucleotide conditions tested, the Mfd–DNA complexes in Supplementary Figs 6 and 8 are unstable as they do not persist after free Mfd is washed out.

Real-time monitoring of the formation and resolution of the repair intermediate allows for its precise kinetic description. Although the mean lifetime $\bar{t}_1$ of the stalled RD_e decreases as the Mfd concentration increases (Fig. 3a), the mean lifetime $\bar{t}_2$ of the intermediate complex is unchanged (Supplementary Table), confirming that the same molecule of Mfd is present throughout the reaction (Fig. 2b). Thus, formation of the intermediate is expected to obey Michaelian kinetics according to:

$$\mathrm{Mfd} + \mathrm{RD_e} \underset{k_2}{\overset{k_1}{\rightleftharpoons}} \mathrm{Mfd \cdot RD_e} \xrightarrow{k_3} \mathrm{I}$$

(in which k_1, k_2 and k_3 denote rate constants; I denotes intermediate), whereas disassembly of the intermediate is expected to depend on simple rate constants (see below). Fitting the mean lifetime data

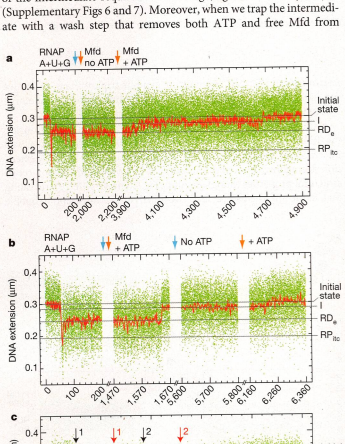

Figure 2 | Mfd ATP usage and displacement of stalled RNAP. Arrows indicate wash steps for trapping and release of the intermediate. For clarity, we present 200-s snapshots of the states thus obtained. **a**, ATP is required for formation of the intermediate. Stalled RD_e is formed, then trapped by washing out (blue arrow) free RNAP and nucleoside 5′-triphosphates (NTPs). After addition of Mfd (200 nM), DNA extension is unchanged. When supplemented with ATP (2 mM) (orange arrow), the intermediate forms. **b**, ATP is required for release of the intermediate. Stalled RD_e is formed and trapped as above. After addition of both Mfd and ATP (first orange arrow) the intermediate forms. After washing out free Mfd and ATP (second blue arrow) the intermediate is stable for thousands of seconds. After adding back ATP (second orange arrow) the intermediate is resolved. **c**, After intermediate formation, stalled RNAP is displaced from its promoter-proximal stall site. Black arrows indicate transcription initiation events; red arrows indicate intermediate formation. The first initiation event (first black arrow) is followed by intermediate formation (first red arrow), a second RNAP can then initiate transcription (second black arrow) and become stalled, forming a new substrate for another Mfd to displace (second red arrow). No reloading by a second RNAP occurs in the absence of Mfd (Supplementary Fig. 3).

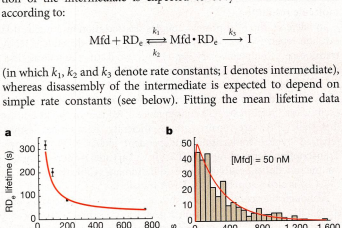

Figure 3 | Kinetic characterization of the action of Mfd on RD_e. a, Mean of RD_e lifetime $\bar{t}_1$ versus Mfd concentration, and fit to the Michaelis–Menten model. Error bars denote s.e.m. **b**, Full distributions of t_1 for [Mfd] = 50 nM (n = 273 events) and [Mfd] = 750 nM (n = 281 events). Red curves denote global fits with a difference-of-two-exponentials according to the single-molecule Michaelis–Menten model (see Supplementary Materials and Supplementary Fig. 9). **c**, Distribution of reaction intermediate lifetime t_2 (n = 146 events). Red curve, fit with a normal distribution model with a mean of 335 ± 15 s and a standard deviation of 181 s. Experiments were performed on DNA supercoiled by +4 turns.

for t_1 (Fig. 3a) yields Michaelis constant (K_m) = 760 ± 350 nM and $1/k_3$ = 19 ± 7 s. Thus, formation of the intermediate is characterized by weak binding of Mfd to RD_e followed by a remarkably slow catalytic step.

The statistical distributions of dwell-times t_1 preceding formation of the intermediate (Fig. 3b) allow further resolution of K_m into the diffusion-controlled on-rate and the thermodynamically controlled off-rate of Mfd from RD_e. The shape of the distribution—an exponential rise followed by an exponential decay—is characteristic of a reaction with at least two intermediates, namely diffusion/docking of Mfd to RD_e and a forward-catalytic event (see Supplementary Materials and ref. 21). Taking $k_3 = 0.05\ s^{-1}$ from our previous analysis of t_1, we obtain $k_1 \approx 1.9 \times 10^5\ M^{-1}\ s^{-1}$ and $k_2 \approx 0.11\ s^{-1}$. By performing a global fit to the distributions obtained at four different Mfd concentrations (Supplementary Fig. 9), the constraint on k_3 can be relaxed, yielding $k_1 = 1.6 \times 10^5 \pm 0.6 \times 10^5\ M^{-1}\ s^{-1}$, $k_2 = 0.08 \pm 0.04\ s^{-1}$, and $k_3 = 0.059 \pm 0.01\ s^{-1}$, with a reduced $\chi^2 = 0.88$, supporting the internal consistency of the data and the validity of the kinetic model.

Surprisingly, the statistical distribution of intermediate lifetimes, t_2 (corresponding to resolution of the intermediate), is non-exponential (Fig. 3c). It tends instead to a normal distribution characteristic of a reaction consisting of several irreversible steps with equivalent rate constants. The data thus give $\bar{t}_2 = 335 \pm 15$ s and a standard deviation of 181 s. Variance analysis of this distribution suggests that a minimum of three irreversible events takes place during this time, each thus having a rate constant $k_4 = 3/\bar{t}_2$. Pulse-chase analysis of ATP usage in this reaction indicates that at least one of these steps requires ATP hydrolysis.

The data analysed here were collected using a substrate bearing five successive C residues on the non-template strand at the stall site, but the process leading to disassembly of the intermediate is not sequence-dependent as similar results were obtained when only one C residue was present (Supplementary Figs 10 and 11). Similarly, disassembly of the intermediate is only weakly torque-dependent, as a long-lived complex was observed using negatively supercoiled DNA: $\bar{t}_2 = 180 \pm 40$ s ($n = 16$; data collected as described in Supplementary Fig. 4). Finally, we analysed the interactions between Mfd and RNAP stalled on a cyclopyrimidine dimer located on the template strand (Supplementary Fig. 12). The kinetics of the entire pathway are essentially identical to those observed when RNAP is stalled by withholding a nucleotide. Indeed, a crystal structure of RNAP II stalled on a cyclopyrimidine dimer showed no conformational changes compared with elongation complexes stalled by nucleotide deprivation[22].

On the basis of these data, we propose a model to describe RD_e displacement during TCR (Fig. 4). From a structural standpoint, the mechanism by which Mfd initiates displacement of the stalled RNAP involves sufficient collapse of the transcription bubble to destabilize the stalled RD_e[23]. Concurrently, promoter-proximal DNA is cleared for another RNAP to initiate (Fig. 2c), indicating either forward translocation of RNAP or full dissociation of RNAP. Mfd remains associated with the DNA long after the bubble collapse. The structure of the DNA deformation observed in the intermediate cannot be fully ascribed from our current data. On the basis of the observation that free Mfd is capable of distorting DNA, we favour a model in which the transcription bubble is fully collapsed after formation of the intermediate, and the residual DNA deformation observed in the long-lived intermediate is caused by Mfd (Fig. 4). Because Mfd alone does not form long-lived complexes on DNA, we propose that the intermediate is stabilized by a combination of Mfd–DNA interactions, Mfd–RNAP interactions (mediated by the RNAP-interacting domain) and, potentially, interaction of the Mfd-tethered core RNAP with DNA (Fig. 4). Binding of Mfd to RNAP derepresses the DNA translocation domains of the helicase, and so the Mfd–DNA interactions in this activated ternary complex probably differ from those made by the isolated protein[8,13,24].

From a kinetic standpoint, the rate constants k_1, k_2 and k_3 indicate that Mfd attempts binding to RD_e several times before engaging productively, and the rate-limiting step itself is slow. This suggests that Mfd kinetically discriminates stalled RD_e from paused RD_e[25], as only stalled RD_e is sufficiently long-lived to act as an Mfd target. This model is supported by our observation that the kinetics of displacement are the same for RNAP stalled at a CPD lesion or by nucleotide starvation. The slow catalytic event could be related to derepression of Mfd, which probably involves large conformational changes[8,24]. The intermediate I is formed in an ATP hydrolysis-dependent step, and Mfd then performs at least three irreversible steps before releasing the DNA. As ATP hydrolysis is required to proceed out of this intermediate state, we propose that Mfd hydrolyses a second ATP molecule, and possibly more, before dissociating.

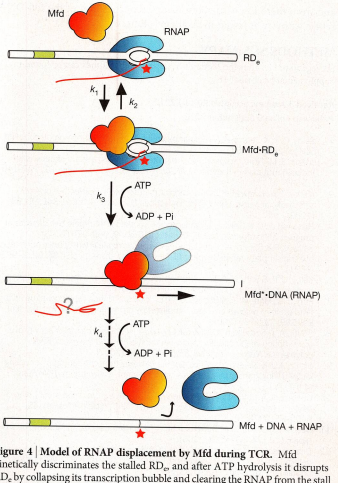

Figure 4 | Model of RNAP displacement by Mfd during TCR. Mfd kinetically discriminates the stalled RD_e, and after ATP hydrolysis it disrupts RD_e by collapsing its transcription bubble and clearing the RNAP from the stall site. Subsequently, further ATP hydrolysis events are required for activated Mfd (denoted Mfd*) to dissociate from DNA. RNA presumably dissociates after the transcription bubble collapse, but the moment of RNAP disassembly from DNA and Mfd is unclear.

The lifetime of the intermediate is surprisingly long for an organism that repairs its DNA in much shorter times and which can divide every 20 min; *in vivo*, downstream repair proteins may capture and process the intermediate, reducing this period. Nevertheless, the fact that the intermediate is reliably long-lived could ensure that repair components have ample opportunity to assemble.

The recruitment of UvrA by Mfd to the damage site is not well understood. The interaction between UvrA and Mfd is inhibited by inter-domain contacts within free Mfd, and the interaction between Mfd and RNAP probably overcomes this inhibition by domain repositioning (Supplementary Fig. 1 and refs 8, 11, 24 and 26–28). As Mfd has a central role in the recruitment of the NER machinery, it will be interesting to see how the addition of subsequent players (such as UvrA, UvrB and UvrC) affects the temporal properties of the system,

and from there to pursue bottom-up reconstruction of the full DNA repair pathway at single-molecule resolution.

METHODS SUMMARY

See legend to Fig. 1 for the Methods Summary; full Methods can be found in the Supplementary Information.

Received 3 January; accepted 20 July 2012.
Published online 9 September 2012.

1. Selby, C. P. & Sancar, A. Molecular mechanism of transcription-repair coupling. *Science* **260,** 53–58 (1993).
2. Witkin, E. M. Time, temperature, and protein synthesis: a study of ultraviolet-induced mutation in bacteria. *Cold Spring Harb. Symp. Quant. Biol.* **21,** 123–140 (1956).
3. Mellon, I. & Hanawalt, P. C. Induction of the *Escherichia coli* lactose operon selectively increases repair of its transcribed DNA strand. *Nature* **342,** 95–98 (1989).
4. Hanawalt, P. C. & Spivak, G. Transcription-coupled DNA repair: two decades of progress and surprises. *Nature Rev. Mol. Cell Biol.* **9,** 958–970 (2008).
5. Selby, C. P. & Sancar, A. Gene- and strand-specific repair *in vitro*: partial purification of a transcription-repair coupling factor. *Proc. Natl Acad. Sci. USA* **88,** 8232–8236 (1991).
6. Selby, C. P. & Sancar, A. Transcription-repair coupling and mutation frequency decline. *J. Bacteriol.* **175,** 7509–7514 (1993).
7. Park, J. S., Marr, M. T. & Roberts, J. W. *E. coli* transcription repair coupling factor (Mfd protein) rescues arrested complexes by promoting forward translocation. *Cell* **109,** 757–767 (2002).
8. Smith, A. J., Szczelkun, M. D. & Savery, N. J. Controlling the motor activity of a transcription-repair coupling factor: autoinhibition and the role of RNA polymerase. *Nucleic Acids Res.* **35,** 1802–1811 (2007).
9. Smith, A. J. & Savery, N. J. Effects of the bacterial transcription-repair coupling factor during transcription of DNA containing non-bulky lesions. *DNA Repair (Amst.)* **7,** 1670–1679 (2008).
10. Chambers, A. L., Smith, A. J. & Savery, N. J. A DNA translocation motif in the bacterial transcription–repair coupling factor, Mfd. *Nucleic Acids Res.* **31,** 6409–6418 (2003).
11. Deaconescu, A. M. *et al.* Structural basis for bacterial transcription-coupled DNA repair. *Cell* **124,** 507–520 (2006).
12. Deaconescu, A. M. & Darst, S. A. Crystallization and preliminary structure determination of *Escherichia coli* Mfd, the transcription-repair coupling factor. *Acta Crystallogr. F* **61,** 1062–1064 (2005).
13. Westblade, L. F. *et al.* Structural basis for the bacterial transcription-repair coupling factor/RNA polymerase interaction. *Nucleic Acids Res.* **38,** 8357–8369 (2010).
14. Deaconescu, A. M., Savery, N. J. & Darst, S. A. The bacterial transcription repair coupling factor. *Curr. Opin. Struct. Biol.* **17,** 96–102 (2007).
15. Park, J. S. & Roberts, J. W. Role of DNA bubble rewinding in enzymatic transcription termination. *Proc. Natl Acad. Sci. USA* **103,** 4870–4875 (2006).
16. Savery, N. J. The molecular mechanism of transcription-coupled DNA repair. *Trends Microbiol.* **15,** 326–333 (2007).
17. Revyakin, A., Liu, C. Y., Ebright, R. H. & Strick, T. R. Abortive initiation and productive initiation by RNA polymerase involve DNA scrunching. *Science* **314,** 1139–1143 (2006).
18. Revyakin, A., Ebright, R. H. & Strick, T. R. Promoter unwinding and promoter clearance by RNA polymerase: detection by single-molecule DNA nanomanipulation. *Proc. Natl Acad. Sci. USA* **101,** 4776–4780 (2004).
19. Revyakin, A. *et al.* Single-molecule DNA nanomanipulation: detection of promoter-unwinding events by RNA polymerase. *Methods Enzymol.* **370,** 577–598 (2003).
20. Smith, A. J. & Savery, N. J. RNA polymerase mutants defective in the initiation of transcription-coupled DNA repair. *Nucleic Acids Res.* **33,** 755–764 (2005).
21. Kou, S. C. *et al.* Single-molecule Michaelis–Menten equations. *J. Phys. Chem. B* **109,** 19068–19081 (2005).
22. Brueckner, F., Hennecke, U., Carell, T. & Cramer, P. CPD damage recognition by transcribing RNA polymerase II. *Science* **315,** 859–862 (2007).
23. Komissarova, N. *et al.* Shortening of RNA:DNA hybrid in the elongation complex of RNA polymerase is a prerequisite for transcription termination. *Mol. Cell* **10,** 1151–1162 (2002).
24. Srivastava, D. B. & Darst, S. A. Derepression of bacterial transcription-repair coupling factor is associated with a profound conformational change. *J. Mol. Biol.* **406,** 275–284 (2011).
25. Landick, R. The regulatory roles and mechanism of transcriptional pausing. *Biochem. Soc. Trans.* **34,** 1062–1066 (2006).
26. Manelyte, L. *et al.* Regulation and rate enhancement during transcription-coupled DNA repair. *Mol. Cell* **40,** 714–724 (2010).
27. Selby, C. P. & Sancar, A. Structure and function of transcription-repair coupling factor. I. Structural domains and binding properties. *J. Biol. Chem.* **270,** 4882–4889 (1995).
28. Deaconescu, A. M., Sevostyanova, A., Artsimovitch, I. & Grigorieff, N. Nucleotide excision repair (NER) machinery recruitment by the transcription-repair coupling factor involves unmasking of a conserved intramolecular interface. *Proc. Natl Acad. Sci. USA* **109,** 3353–3358 (2012).

Supplementary Information is available in the online version of the paper.

Acknowledgements We thank K. Neumann for showing us how to perform global fitting with the Igor software package. K.H. was supported by a PhD scholarship from the Frontieres Interdisciplinaires du Vivant Doctoral Program and the Fondation pour la Recherche Médicale. Work in the laboratory of N.J.S. was supported by BBSRC grant BB/I003142/1, and work in the laboratory of S.A.D. was supported by National Institutes of Health grant GM073829. This work was also made possible by a EURYI grant, in addition to CNRS and University of Paris Diderot core funding, to T.R.S.

Author Contributions K.H., N.J.S. and T.R.S. devised and carried out experiments; S.A.D., K.H., N.J., N.J.S., A.J.S., T.R.S. and L.F.W. provided unique reagents and A.J.S. carried out further control experiments; K.H., W.G., N.J.S., T.R.S. and S.Z. analysed data; and S.A.D., N.J.S. and T.R.S. wrote the paper.

Author Information Reprints and permissions information is available at www.nature.com/reprints. The authors declare no competing financial interests. Readers are welcome to comment on the online version of the paper. Correspondence and requests for materials should be addressed to T.R.S. (strick.terence@ijm.univ-paris-diderot.fr).

World-leading drug discovery and development

The Academy of Military Medical Sciences (AMMS) is a leading centre of life science research in China, and one of the country's powerhouses of drug development. Over the past 60 years, the AMMS has discovered, developed, and engineered a series of groundbreaking new drugs, more than a few of which have had a profound impact on global medicine.

Part four of the AMMS supplementary feature covers the academy's impressive achievements in drug innovation — achievements such as the multi-drug resistance malaria treatment Coartem, which has already saved the lives of millions worldwide, and even a potential malaria vaccine. The academy's comprehensive and integrated platform for drug discovery and development employs the latest in computational and microbiological technology supported by an unrivalled pharmaceutical engineering system that makes it possible to bring new drugs to clinical readiness faster than ever before, with a level of safety and purity higher than ever before.

Innovation in drug development encompasses not only the state-of-the-art in synthetic drug design and biotechnology for gene therapy and genetically engineered drugs, but also the vast potential resources of traditional Chinese medicine and other natural products. The AMMS' grand success with Coartem owes its origins to traditional medicine, and the academy has embarked on an ambitious screening program to identify other potentially revolutionary ingredients in this unique and extensive repository of natural compounds.

Over its first 60 years, the AMMS has made a remarkable contribution to global health. As a major participant in the national revolution in pharmaceutical research and technological development, it is destined to continue that leading role and push the frontiers of drug discovery.

SPONSOR FEATURE

AMMS RESEARCH

An integrated drug development system

Over the past six decades, the AMMS has remained firmly at the forefront of drug discovery and development in China through a disciplined focus on technological development and process integration. The result is a comprehensive drug research and development system, backed by over 4,000 years of medical tradition.

Clinical medicine today is all but unrecognizable from that of 60 years ago, a time when penicillin had only just become available for civilian use in but a handful of countries around the world. The process of drug discovery and development, too, has undergone many revolutions of change, from the accidental discovery of mould in a Petri dish to a computer-aided, genome-guided search for complementary molecules using some of the most advanced technology available to science. The AMMS was established at the dawn of this rapid evolution and with military determination has forged itself into one of the world's giants of drug development, responsible for such medicine-changing drugs as Coartem — a multidrug-resistant malaria treatment that has already saved the lives of millions of people since its introduction in 2001.

Coartem is an example of how the AMMS used some of the most advanced technologies of the time to study the active compounds of a traditional Chinese treatment for malaria and then synthesise and develop a series of compounds for use in a commercial drug. That process continues, but the range of technologies available to the AMMS today and the close integration of those technologies in the drug development system has greatly expanded the process's scope and efficiency. The AMMS has also invested heavily in developing its capacity for the mass-production of high-quality, structurally complex drugs.

The Institute of Pharmacology and Toxicology is one of the core institutes of the AMMS and the unit responsible for much of the research and development that goes into new drugs. "In order to succeed in drug development," says Professor Hua Li, a leading scientist at the institute, "you need expertise covering a wide range of fields, from drug design to synthesis, screening, and isolation of active ingredients, which is the first phase for discovering active compounds, and then evaluation of efficacy, safety and controllability, or toxicology research. We cover most if not all subjects in both fields."

Integration of technologies

The Institute of Pharmacology and Toxicology continues to develop better ways of conducting its research. The introduction of computer-based molecular simulation and drug design, for example, enables rapid search of the active agents in traditional remedies and the efficient scanning of multitudes of intricate protein–ligand crystal complexes. Nuclear magnetic resonance (NMR) technologies allow AMMS scientists to investigate how drugs interact with biological targets, opening up a world of detail that makes it possible to understand the mechanisms of drugs action and to make improvements at the molecular level.

Another analytical technique that has become indispensable for drug design is mass spectrometry — a highly sensitive method that allows the chemical composition of massive arrays of samples to be determined in a rapid succession. By integrating mass spectrometry with biological studies, AMMS scientists are developing systems for the rapid screening of compounds and the determination of their mechanisms of action in order to multiply the number of candidate compounds entering the drug development pipeline.

"Prior to the 1990s," says Li, "drug discovery was all about finding lots of synthetic compounds, and then through screening, identifying compounds that are more active than others and conducting research on those active compounds. The time it took for this process was typically very long — a new drug, from discovery to commercialisation, would involve at least 10 years of development."

Drug discovery took a further step forward with the invention of combinatorial chemistry in which a number of chemical variants of a basic molecular scaffold — often identified by computer simulation of potentially active compounds — are created rapidly and efficiently in a small number of reaction steps. "Through computer-based drug molecular design and

rapid synthesis, we obtain these structurally related molecules and use high-throughput screening methods to filter out the active compounds," continues Li. "Unlike the conventional method, there is no need to synthesise many compounds, which dramatically shortens development time." If the structure of a particular target is known, such as a target on an enzyme, computer simulations can be used to investigate which compounds could bind to this target and the affinity of each binding. "We can even use computer simulation to predict the toxicity of the compound, its solubility in water, and how the compound is metabolised in the human body."

Identifying compounds suitable for development is an important step, but it is only the first in a long and rigorous process. AMMS recognises the importance of establishing a comprehensive development pathway, from discovery through to clinical testing and the patient. To this end, the academy has developed a molecular drug discovery system called Multi-Objective Simultaneous Optimization, or MOSO.

Computer-based drug molecular design and high-efficient synthesis are the core techniques utilised by MOSO. With early evaluation of drug-like properties of new compounds, this system is able to enhance the efficiency of drug discovery and reduce risk in later processes. MOSO has been fundamental to the success of a series of important research projects that have led to the rapid discovery of drugs that target new mechanisms to treat critical illness. In one instance, the AMMS secured intellectual property rights over a new medicine within a mere two years of initiating its development, highlighting the remarkable efficiency improvements MOSO offers in the research and development of new drugs.

Using the MOSO system, the AMMS has made significant advances in targeting several important clinical conditions. For example, researchers of obesity and obesity-related disorders have discovered that the cannabinoid receptor — a protein-coupled receptor on the cell membrane — could provide an effective means of mitigating the effects of the disease. Initial work by the AMMS in this area has been encouraging, and already one particular candidate drug targeting the inhibition of the cannabinoid receptor has passed pre-clinical evaluations and is soon to be trialled in full clinical evaluations. AMMS researchers are also focusing on the activation of peroxisome proliferator-activated receptors (PPARs) as means of controlling blood glucose and lipid levels in patients with type-II diabetes — one of the world's largest public health issues.

The MOSO system is also being applied in numerous other research programs, including work on the common cold-causing rhinovirus, leukaemia, stroke and autoimmune disease.

A systematic approach

Research into drugs to prevent stroke is a good example of how MOSO benefits molecular drug discovery. The family of FK506-binding proteins, known as FKBPs, are promising targets for the treatment of many types of neurodegenerative disease, including stroke. The first step in the MOSO process is the virtual synthesis of candidate compounds using sophisticated computer methods and screening of those compounds through simulations to identify those that interact in a suitable way with the target receptors. Virtual synthesis in this case resulted in a library of more than 80 million candidate compounds, from which just 200 were identified as having suitable receptor interactions. These 200 were then synthesised as real compounds and subjected to numerous rounds of analysis for physicochemistry, pharmaceutical effects, metabolic properties and toxicological effects. The final molecular drug candidate obtained at the end of this process provides significant therapeutic benefits for ischemic stroke and has progressed to pre-clinical evaluation.

FKBP-based stroke treatment is just one example of the MOSO process. AMMS researchers are also investigating other treatments for stroke using similar methods. The primary cause of heart attacks and strokes is the progressive occlusion of arteries with fatty compounds such as cholesterol — a disease called atherosclerosis. Researchers at the AMMS are targeting the phospholipid transfer protein (PLTP) amongst others for the treatment of atherosclerosis, and are well into the process of virtual synthesis and screening for possible candidate compounds.

The AMMS' integrated approach to developing innovative new drugs has resulted in an impressive pipeline of drug candidates that has kept the academy at the national forefront of drug development. The development of new drugs is a complex and systematic process involving many different technologies. While no single technological breakthrough can bring revolutionary change, the AMMS' continuous and disciplined integration of core technologies and progressive testing of technological limits will ensure that it retains its leading position well into the future.

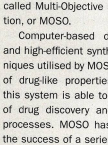

Hua Li

"We design and synthesise structurally related molecules and use high-throughput screening to filter out the active compounds...this dramatically shortens development time."

SPONSOR FEATURE

AMMS RESEARCH

Drug development for safety and efficacy

The discovery of a drug candidate and its possible therapeutic activity is just the start of a long and rigorous process of pharmaceutical engineering. Before a drug reaches the clinic it must surmount many obstacles such as drug safety, stability and minimisation of side-effects as well as issues of targeted delivery, optimised efficacy and efficient, high-quality mass-production. The AMMS has established a stringent preclinical drug development regime to ensure that such problems are recognised and overcome, providing safer and more effective medicines.

Possibly the most critical aspect of drug development is how to deliver a therapeutic agent safely to its site of action without unwanted side-effects. The AMMS has developed state-of-the-art methods for evaluation of drug efficacy and safety and exploits the very latest in drug delivery technology.

Among its numerous strengths, the AMMS gains a particularly powerful competitive advantage in drug development through its sophisticated system for the evaluation of new candidate drug compounds. This highly integrated system includes analyses for micro impurities, quality control procedures for the optical purity of chiral drugs and analyses of drug polymorphism, as well as a complete system for the identification of active compounds in traditional Chinese medicines.

The AMMS has developed many new drugs in recent years, and all of these have passed stringent pharmaceutical standards. Notable examples include penehyclidine hydrochloride and phencynonate hydrochloride, two new anticholinerigic drugs with promising potential for the treatment of a range of conditions, from gastrointestinal disorders to dizziness and insomnia. The Institute of Pharmacology and Toxicology, where these new anticholinerigic drugs are synthesised, performs pharmaceutical analysis research and also regularly provides testing and quality control services for new drugs. The institute has provided well over 1,000 such services to date and published over 100 research papers on the outcomes in leading international journals.

"The three most important factors for the success of a drug are efficacy, safety and controllability," says Professor Hua Li, a leading scientist at the Institute of Pharmacology and Toxicology.

"What do I mean by controllability? It means that after synthesis, it is necessary to find out if there are impurities in the synthesised compound, how much is there, and whether the impurities are toxic."

Quality control

The identification and control of impurities is one of the most important components of overall drug quality assurance in the drug development process, as any contamination could compromise how a drug works or even jeopardise its safety. The Institute of Pharmacology and Toxicology performs a thorough analysis of its drugs to ensure that they are produced with trace impurities under control, using an integrated series of cutting-edge techniques.

More than half of all drugs are chiral compounds — molecules that have the same chemical structure but occur in mirror-image structural versions known as enantiomers. Importantly, the two enantiomers of a given chemical compound could have remarkable differences in biological activity and toxicity, and it is usually only one of the enantiomers that is the true drug candidate. Ensuring the enantiomeric purity of a synthesised chiral compound is therefore a crucial aspect of drug production. The AMMS has developed new chiral recognition systems specifically for this task, and have been successful in producing over ten new chiral drugs with extremely high enantiomeric purity.

"In this area we are at the forefront in China," says Li. "Our institute is one of the

national leaders in chiral drug research, and was the first in the country to undertake this research. We have techniques for chiral structural analyses, the ability to disassemble a chiral molecule into its two enantiomers, and also the ability to assemble any enantiomer we wish — all as part of an integrated process."

Drug metabolism and pharmacokinetics

The AMMS' Drug Metabolism and Pharmacokinetics Laboratory provides another crucial part of the drug discovery and development process. The early absorption, distribution, metabolism and excretion (ADME) evaluations are performed for lead compounds during the drug discovery phase. These evaluations are mainly performed *in silico*, or *in vitro* using cell based models and liver microsomes from different species. "The advantage of using computers or *in vitro* models is that we minimise the need to use animals in testing and improve throughput of the processes," says Li. "When we have identified the candidate compound, we start performing pre-clinical animal testing and then clinical evaluation. This greatly reduces both risk and capital at this close-to-final stage of experiments, and also shortens the time needed to advance the drug and improves the final quality of the drug."

After a promising drug compound has been selected from a few of the candidates, it is subjected to comprehensive and systematic pre-clinical pharmacokinetic studies to determine the absorption, distribution, excretion, elimination rate, and biotransformation pathway of the compounds in animals. The optimisation of dose and formulation are also studied. The research conducted by the laboratory, including whole-of-system metabolic processes — known as pharmacometabolomics — and toxicokinetics, contributes to the complete set of data and material that is needed to submit a new drug for regulatory approval.

Pharmacometabolomics research also benefits significantly from new computational methods. "Pharmacometabolomics requires a suite of simulation technologies in order to predict how drugs are metabolised in the body," says Li. "We do this research because many drugs behave differently in animals and in the human body. Pharmacometabolomics helps us minimise the risk of side effects of new drugs in clinical use."

Pharmaceutical engineering

The development of the drug preparation itself — its form and mode of delivery of the active compound — is often as critical to the success of a drug as all of the research that has come before it. "For those drugs that are eliminated rapidly in the body through biotransformation, or 'first-pass metabolism', we might want them to transform slowly, in which case we would inhibit metabolic enzymes by co-administration of an enzyme inhibitor with drugs to reduce metabolic rate, and consequently enhance plasma concentration and lengthen duration of its action," says Li. "Other times we might want a compound to break up rapidly in the body, for which its binding affinity with enzymes becomes very important. We can now test all these types of interactions *in vitro* and *in vivo*."

The AMMS has invested heavily in the best technology for pharmaceutical engineering, providing its scientists with state-of-the-art software and hardware for computer-based drug engineering. Through these simulations, pharmaceutical engineers figure out how to deliver a drug to its target in the body, and how best to control the release of the active agent at the site using the latest in macro-, micro- and molecular-scale drug delivery technology. The advanced drug delivery systems now being applied by the AMMS in the development of new drugs include highly specific microcarrier drug delivery systems, self-administered drug delivery devices including automatic microinjection systems and dry powder inhalations, and mucous membrane and percutaneous drug delivery systems. New technologies under development include nanoliposomes, lipid microbubbles, nano drug delivery systems and slow-release microspheres.

Osmotic pump technology for the controlled release of drugs administered orally is another major area of research at the AMMS and a field in which the academy leads nationally. Using this system, it is possible to modulate the release characteristic for a drug in a way that is largely independent of pH and other physiological parameters.

"We are a leader in controlled release," says Li. "Normal tablets break up quickly in the human body. The idea of controlled release is that we can design drugs that release in specific manners (for example, immediate-release, controlled release, pulse release), or at specific sites within the body. Such technology has the unique advantage of leading to many treatments."

A pipeline of breakthroughs

The major advancements the AMMS has achieved in overcoming critical technological problems have helped clear the bottleneck between drug development and clinical practice, and accelerated the commercialisation of new drugs.

The AMMS' success is not limited to China, however. A new pharmaceutical technology of thermo-sensitive liposome developed by the AMMS has also been used for developing the thermo-sensitive liposome preparation of doxorubicin, an important anticancer drug that is the first nanoliposome pharmaceutical to be approved by the US Food and Drug Administration, and the first to enter phase-III clinical trials in the United States.

"The Institute of Pharmacology and Toxicology is a leading institute for drug design and drug target research in China. We have several candidates in the pipeline at the moment, and some could be advanced to the clinical trial stage in as little as five years," says Li.

SPONSOR FEATURE

AMMS RESEARCH

A biotechnology revolution

Biotechnology has unlocked the vast potential of microbiology to address clinical needs. The AMMS was the first research organization in China to harness biotechnology for medical applications, and today boasts high-tech biotechnology systems producing advanced biotech therapies and diagnostics.

Gene therapy, engineered microorganisms and recombinant DNA vaccines are all products of the bourgeoning field of biotechnology. The AMMS is unrivalled in China in its application of biotechnology in developing clinical therapies and diagnostics, and has developed a world-class program of biotechnology research.

Recombinant vaccines

Vaccines form a key pillar of modern medicines, and are used to prevent a range of diseases that claim millions of lives every year. With the introduction of genetic engineering technologies in the 1980s, a new tool became available for vaccine developers. By inserting antigen genes from a target virus such as influenza or hepatitis into a conventional vector vaccine for another virus, it became possible to produce vaccines for a much wider range of viral targets. However, there remain many viruses for which vaccines, even recombinant vaccines, are still not available.

The AMMS has developed advanced research capabilities for genetically engineered subunit vaccines, genetically engineered bacteria carrier vaccines and recombinant DNA vaccines. The academy has also applied reverse vaccinology, in which the genomes of pathogenic agents are screened to identify genes that could be targeted by vaccines.

Using these technologies, the academy has developed genetically engineered vaccines for cholera, dysentery, pandemic influenza and *Escherichia coli* infection and is actively researching vaccines for many other major diseases, including therapeutic vaccines for certain cancers and HIV. For example, researchers at the AMMS have developed a genetically engineered vaccine for *Helicobacter pylori*, a bacteria responsible for gastritis, stomach ulcers and even stomach cancer. This vaccine is now undergoing clinical approval. Another promising oral vaccine for diarrhoea is also currently in clinical trials.

Another vital vaccine that has been developed by the AMMS is a recombinant DNA vaccine for malaria. Malaria is one of the top priorities for disease prevention globally, and while the AMMS has had major success in the development of the anti-malaria drug Coartem, a vaccine for the disease remains elusive. The 'cocktail' malaria DNA vaccine developed by the AMMS, now in the process of regulatory approvals in China, has the potential to change the lives of billions of people living with the daily threat of infection around the world.

Genetically engineered drugs

The range of possible applications of biotechnology is not limited to vaccines. The AMMS has also established a complete drug discovery system for genetically engineered therapeutics that encompasses all aspects of the drug development process, from protein design and expression, to mass culturing of genetically engineered bacteria, large-scale protein purification and drug analysis.

This development system for genetically engineered drugs has yielded some major therapeutic breakthroughs. In collaboration with the Institute of Biochemistry and Cell Biology at the Shanghai Institute for Biological Sciences, part of the Chinese Academy of Sciences, the AMMS developed recombinant human Interleukin-2 — an important immunotherapy drug in the treatment of cancers and chronic viral infections. The AMMS also developed a hormone called granulocyte colony stimulating factor that stimulates the production of white blood cells and which is an effective therapeutic for patients recovering from chemotherapy.

Other successes include a drug based on genetically engineered erythrogenin protein that stimulates the production of red blood cells in patients with anaemia related to HIV or kidney failure, and a recombinant human

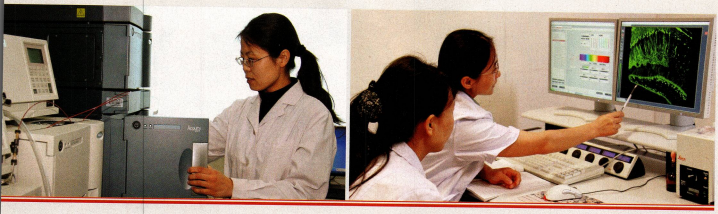

epidermal growth factor therapy that promotes cellular proliferation, differentiation and survival with a range of uses including the repair of eye damage.

An exciting and long-anticipated line of drug research at the AMMS has been the development of a therapy for heart attack. For the past 20 years, AMMS researchers have been trying to genetically engineer human pro-urokinase (pro-UK), a plasminogen activator protein that can break down blood clots in the arteries of the heart. The researchers recently succeeded in the mass-production of pro-UK using recombinant methods from a Chinese hamster ovary cell line, resulting in the first pro-UK therapy in acute ST-elevation myocardial infarction to be approved anywhere in the world.

Ongoing clinical research includes the development therapies based on recombinant human interferon-omega, a promising antiviral agent with potential uses in treating chronic viral diseases such as hepatitis C; a thrombolytic agent known as staphylokinase that could be used in treating blood clots associated with heart attack; and recombinant bone morphogenetic protein-2, a molecule that can promote cartilage formation and potentially accelerate bone repair following injury.

Antibody engineering

Antibodies play an important role in the research, diagnosis and therapy of diseases, and it is one of the fastest-growing fields in biotech-based therapeutics. The AMMS began research on monoclonal antibodies over 40 years ago and more than ten monoclonal antibodies against human leukocyte differentiation antigen (HLDA) have been developed since then. HLDAs are important targets of therapeutic antibody, due to their significant effects on the function of leucocytes and even the whole immune system. Since the 1990s, the AMMS has been engaged in the study of engineering antibodies and perfecting platforms of antibody humanization, and a fully human synthetic antibody library has been established, which could be used for novel therapeutic antibody production.

Through close collaboration with several drug companies, the AMMS has produced numerous monoclonal antibodies for a range of important cell markers, some of which have displayed satisfactory developing potency. The academy has many antibody drugs in the early stage of development, including an engineered antibody-like molecule ATF-Fc, which targets the urokinase receptor and has promising antitumour activity. Other active research includes TEM8-Fc, another antibody-like molecule with anti-tumour activity, which works by inhibiting the vascularisation of abnormal tissue in tumours, and CMG2-Fc, a recombinant fusion protein with the activity to neutralise anthrax toxin.

Diagnostic reagents

Using recombinant antibody technology coupled with the latest real-time PCR detection techniques and biochip devices, the AMMS has the capability to develop advanced immune diagnostic kits, and is developing immunoassays for the detection of immunity to various contagious diseases, toxins and tumours. The AMMS developed tests for antigens of hepatitis B and the anti-HBe enzyme more than 20 years ago using the latest state-of-the-art gene engineering technology of the time, and soon after developed a diagnostic test for hepatitis C viral antibodies. A more advanced protein chip diagnostic kit for antibodies to hepatitis C was approved for clinical use in 2002. Antibody-based diagnostic kits have also been developed by the academy for O6-methylguanine DNA methyltransferase levels in cancer patients, for the *Mycobacterium tuberculosis* pathogen responsible for tuberculosis, and for multiple subtypes of leukaemia antibodies with a combined diagnostic accuracy of up to 95%.

Biochip technology is a key strength of the AMMS, which secured the first drug certification for silica-based biochips anywhere in the world. It was also the first to develop a hepatitis B drug-resistant gene chip and human leukocyte antigen genotyping chip. A new composite real-time fluorescent probe inspection technology for PCR molecules developed by AMMS researchers for the inspection of pathogenic microorganisms is another significant development of real-time PCR technology.

Gene therapy

First discovered in the 1970s but only just starting to fulfill its promise in the last few years, gene therapy is being heralded as a revolutionary frontier in medicine with the potential to treat a range of intractable diseases and degenerative conditions. The AMMS has devoted significant research resources to the development of gene therapies over the past decade, and has now progressed three gene-based therapeutics to the clinical trial stage: a treatment for ischemic heart disease using adenoviral hepatocyte growth factor, a treatment for peripheral arterial occlusive disease using a recombinant plasmid with human hepatocyte growth factor gene, and a treatment for cephalocervical tumours using recombinant adenovirus BB-102. With these latest achievements, the AMMS has emerged as a major participant in the gene therapy revolution.

The AMMS is unrivalled in China in its application of biotechnology in developing clinical therapies and diagnostics, and has developed a world-class program of biotechnology research.

SPONSOR FEATURE

AMMS RESEARCH

Modern medicine, traditional roots

While being one of the most progressive and innovative medical research organizations in China, the AMMS places great importance on the value of traditional Chinese medicine (TCM) and its potential therapeutic applications in modern medicine. The AMMS is carrying out an extensive research program to identify and exploit pharmacologically active compounds from medicinal flora and fauna used in TCM. This approach is bearing fruit in the shape of new and highly effective drugs that are already benefitting patients around the world.

The Chinese theory of medicine is rooted in its traditional philosophy of the human body in balance with the natural environment. This holistic concept of deficiency and excess, equilibrium and imbalance, has guided TCM for over 4,000 years. Modern Western medicine, by comparison, has a very short history and is founded instead on evidence-based scientific research focusing on the treatment of specific disease targets. Although both approaches to medicine aim to cure disease, they represent very different clinical and pharmaceutical systems.

The enormous wealth of medical knowledge locked up in the treatments and philosophies of TCM represents a potent medical resource for researchers with the desire and ability to tap into it. The rapid evolution of modern Western medicine has understandably wrested the focus of most medical research institutes in China. The AMMS, however, is one of the few research organizations with a well-established traditional medicine development platform and a commitment to expanding its exploration in this area. And the rewards have been breathtaking — huperzine A, for example, is a novel acetylcholinesterase inhibitor discovered and isolated by AMMS, which has been shown to be effective in improving cognitive performance, enhancing memory and preventing brain damage. This integration of Chinese and Western medical theories and methods is a key characteristic of the AMMS drug discovery program.

"These new drugs are more potent, but have fewer side effects and better biocompatibility than the natural compounds," says Professor Hua Li, a leading scientist at the AMMS Institute of Pharmacology and Toxicology. "Following pharmacological evaluation of the active ingredient artemisinin, scientists at the AMMS further discovered and developed a novel compound, benflumetol, and then the compound drug Coartem, containing both artemether and benflumentol. Coartem is now recognised by the World Health Organization as the official drug for fighting multi-drug resistant malaria — it is one of our greatest achievements."

Rediscovering tradition

The AMMS began its life 60 years ago as a military-focused medical research organization with the sole aim of protecting the health of the nation's military personnel. It is the search for a treatment for malaria for the country's soldiers that turned the attention of the AMMS to the common traditional remedy of wormwood tea. Years of painstaking work by more than 500 researchers from 60 research institutes in the country in identifying and isolating the active principle and then refining it for clinical use resulted in a drug that now saves the lives of tens of millions of people around the world every year.

The translation of traditional medicine into modern therapeutics is now a core strength of the AMMS and the Institute of Pharmacology and Toxicology in particular. "Another great example is our work on *liuwei dihuang* decoction, which I think is a revolution," says Li. *Liuwei dihuang* decoction is one of the mainstays of Chinese medicine and the basis for remedies to a wide range of ailments. "The conventional prescription for *liuwei dihuang* decoction requires the patient to drink the medicine from a bowl. Through research, we have identified the active ingredients and formulated a standard prescription that is safe and controllable, so the patient knows how much of the active ingredients they are taking. The preparation is already undergoing clinical trials in China."

On the back of the success of the AMMS with drugs such as Coartem and the increasing popularity of TCM in the US and Europe,

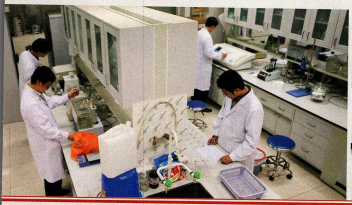

the central Chinese government has invested over US$700 million into building the capacity of research institutes in China to employ the very latest technologies and modern scientific practice to investigate the active ingredients in traditional remedies, with the goal of developing pharmaceuticals that treat a range of ailments and diseases.

Two paths, one destination

Research and development into TCM at the AMMS has taken two paths — one involving scientific study of traditional medicines to discover the intrinsic nature of the medicine through identification of the active ingredients with clinical values, and the search for bioactive natural products from a wider range of natural sources, from terrestrial plants to marine flora and fauna and their metabolic products.

The path of TCM research makes use of the latest technologies to explore the pharmacological and chemical properties of the active components. At the AMMS, researchers employ biological activity evaluation models at different levels of investigation, from whole animals and tissues down to cells, genes, proteins and the proteome, as well as testing and evaluating technologies relevant to the effectiveness of Chinese medicine. Systematic chemical research is supported by advanced modern separation and analysis equipmentation and related techniques and methodologies.

As well as researching natural products that are commonly used in TCM, the AMMS is also exploring microorganisms that live in extreme and/or unique environments, the discovery of bioactive secondary metabolites, the regulation of gene expression, heterologous expression and the activation of silenced genes.

"The Institute of Pharmacology and Toxicology was the first to identify huperzine A, a drug derived from the firmoss *Huperzia serrata*, which can be used to fight Alzheimer's disease and memory loss," says Li. "At that time, we used various solvents to extract many compounds from the plants and through evaluation of these compounds, we identified the active components and developed a drug based on it. That was the old way — now with the aid of computer modeling, we can use microbes to produce compounds with structural variations and we can now modify the compounds into new potential leads."

The power of plants

AMMS scientists have an ongoing screening program involving thousands of medicinal plants to search for active compounds as potential therapeutics. In addition to *Huperzia serrata*, the hanging firmoss *Phlegmariurus fordii* was also found by the screening process to contain metabolites of interest, and a follow-up study confirmed the presence of active agents that may hold promise in treating Alzheimer's disease.

Another medicinal plant found to contain potentially useful compounds is the Indian mulberry, or *Morinda officinalis*. The root is used in TCM to treat a range of conditions including back pain, infertility and muscular atrophy. During the screening program, the extract of this root was found to have potential to be developed further as an antidepressant — an activity not referred to in the traditional use of the remedy. It was then selected for advanced study and found to contain the active components that are responsible for this property. The *M. officinalis* oligosaccharide has minimal side effects or toxicity, and has completed all three phases of clinical trials. The antidepressant is now approved by Chinese regulatory officials as a new drug.

The early days of research in finding bioactive microbial natural products often resulted in enormous waste of inactive microbes and therefore inefficiency in the process. When screening bacterial and fungal strains for active agents, for example, most of the strains were discarded because they did not produce any bioactive secondary metabolites that might have potential as a pharmaceutical agent.

However, researchers at the AMMS have now established a series of new techniques to make further use of inactive strains by modifying their metabolic functions. Many of these mutated strains have produced active compounds with novel molecular structures, representing a valuable new resource for drug discovery.

"This is what drug discovery is all about," says Li. "We find a new compound or chemical entity — from different sources, such as synthetic, biotech, as well as natural products — then, step by step, develop various new products based on this new compound." From the very beginning, the academy's drug research has been demand-driven, and it is the pressing need to combat malaria that first turned its researchers to traditional medicine. "Malaria was extremely severe in China during the early days of the AMMS, and we were deeply involved in the national anti-malaria project, which brought us back to traditional medicine and led to great success in developing antimalarial drugs. As we went on to build the new drug R&D capability, we started doing more research and development on civilian drugs, and traditional and natural medicines became one of our strengths. We are very proud of our achievements."

AMMS' involvement in the national anti-malaria project led to the successful development of Coartem, now recognised by the World Health Organization as the official drug for fighting multi-drug resistant malaria.

Principles of **Biology**

by nature EDUCATION

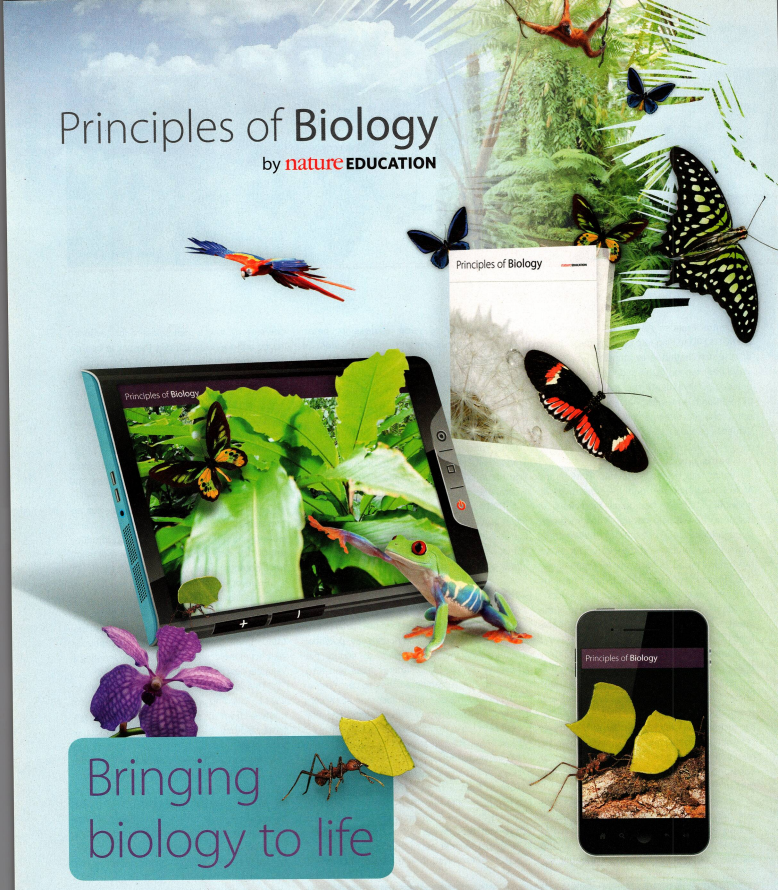

Bringing biology to life

To learn more about *Principles of Biology*, the first interactive textbook from Nature Education, visit **www.nature.com/principles**

nature publishing group npg

TURNING POINT Neuroscientist's fishy finding helps to improve data interpretation **p.437**

@NATUREJOBS Follow us on Twitter for the latest news and features **go.nature.com/e492gf**

NATUREJOBS For the latest career listings and advice **www.naturejobs.com**

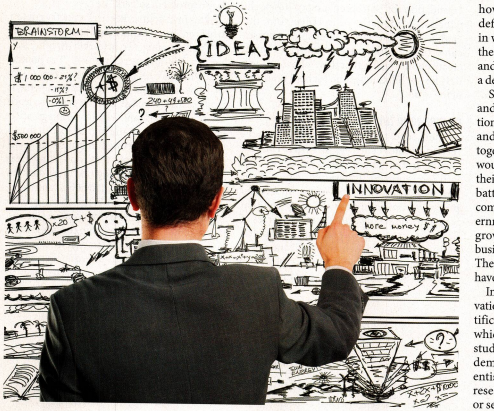

SHUTTERSTOCK/LEEDSN

INNOVATION

Brushing up on business

Entrepreneurship training can open up new avenues for scientists. And it doesn't take a business degree.

BY NEIL SAVAGE

After 15 years as a practising cardiologist, Catherine McGorrian enrolled in a PhD programme at University College Dublin (UCD), studying family risk factors for sudden cardiac death. To fulfil her credit requirements, she chose to undertake an optional course in entrepreneurship for scientists. "It just struck me as something really different," she says, "something that wasn't a skill you would pick up just anywhere."

Her class attended a presentation from the Irish Marine Institute, based in Oranmore, about SmartBay — a network of sensors and communications technology attached to buoys and undersea cables that gathers oceanographic data and transmits them to researchers. McGorrian wondered whether similar technology could be applied to one of her own interests: the portable defibrillators that are used widely to deliver regulating electric shocks to people having heart attacks.

In an emergency, McGorrian wondered, how would someone know where to find a defibrillator, or whether it was charged and in working order? "I just thought, 'There are these buoys in the ocean talking to each other and here I am on land, and I can't tell if there's a defibrillator in the next room.'"

So, taking what she had learned in the course and drawing on the resources of the Innovation Academy, a joint programme of the UCD and Trinity College Dublin, McGorrian put together a business plan for defibrillators that would transmit information on their location, their maintenance schedule and whether their batteries were charged. She entered it into a competition held by Enterprise Ireland, a government organization that promotes business growth. She didn't win, but is still talking to business people about implementing her idea. The experience has convinced her that she will have other marketable ideas in future.

In addition to McGorrian's course, the Innovation Academy has launched a graduate certificate in innovation and entrepreneurship, which takes the equivalent of seven weeks of study. It is one of a growing number of academic programmes aimed at teaching scientists and engineers how the fruits of their research can become commercial products or seed companies. The development of such programmes has been promoted by governments, which see the creation of businesses — especially technology-focused ones — as an economic driver.

BREADTH NOT DEPTH

Scientists who want to learn about entrepreneurship can spend one or two years of full-time education earning a master's degree in business administration (MBA). But many institutions offer more focused options, with programmes that teach enough finance, marketing and management for scientists and engineers to learn how to apply their strengths to the commercial world. "We're not going to make them into financiers. We're not going to make them into marketers," says Jeanne Simmons, associate dean of the Graduate School of Management at Marquette University in Milwaukee, Wisconsin. "We're not trying to give them this full-blown MBA. We want to give them the knowledge to ask the right questions." Such focused options range from a course or two during or after a normal degree programme to a certificate in entrepreneurship (see 'Training top-up').

Business courses are often geared towards bioengineers, biomedical researchers and ▶

computer scientists. But good ideas can come from anywhere, and entrepreneurship classes can be useful for people from any discipline. More important than background, say educators, is a willingness to take risks, to think in new ways and to put up with the lack of security and support that comes from being self-employed. Entrepreneurship is hard for most faculty members, says Alistair Fee, who teaches business in the School of Mechanical and Aerospace Engineering at Queen's University Belfast in Northern Ireland. "It is different from research and publishing. It moves at a fast pace," he says.

"We want to give them the knowledge to ask the right questions."
Jeanne Simmons

A business degree costs a lot of time and money. An MBA in the United States, for example, can require 45–50 course credits — four semesters of work or more. Marquette offers a more accessible option: a Certificate in Entrepreneurship that takes only 16 credits. The first set of students graduated in May. Simmons says that the course provides a grounding in the basic principles of entrepreneurship, helping scientists to decide, for instance, whether a product actually fills a need in the marketplace or can be sold at a reasonable price. It also helps researchers to hire the right business people, should they build a company that grows.

Courses and certificates of this type often offer more breadth of knowledge than depth, focusing on skills such as forming market strategies, finding venture money, creating teams and managing cash flow. "I'm not an expert in any of these things," says John Melas-Kyriazi, a graduate student in materials science and engineering at Stanford University in California and an alumnus of the Mayfield Fellows Program, a nine-month work–study course run by the Stanford Technology Ventures Program. "I know a little bit about a lot of things," he adds. Melas-Kyriazi, who wants to develop better storage systems for wind and solar power, appreciates what the programme taught him about founding and running a business. "If you're looking to change the world and make a positive impact," he says, "one of the ways of doing it is commercializing your technology."

Entrepreneurial education need not lead to a start-up, says Tim Keane, entrepreneur in residence at Marquette, who helped to develop the university's entrepreneurship programme. Business skills and knowledge make scientists more attractive to venture-capital firms looking for advice about promising technologies. "Helping people understand what the game is, even if all they do is go work for an entrepreneurial company, I think that is a big deal," says Keane, who has founded and sold a web-analytics company, Retail Target Marketing Systems, and launched a venture-capital fund called the Golden Angels Network.

"It's also about being more entrepreneurial no matter what they do," says Karen Wilson, an adviser and board member of the European Foundation for Entrepreneurship Research, which is headquartered in Hilversum, the Netherlands. She adds that business courses can promote willingness to take risks, think creatively and lead rather than follow. "It's not only for the Bill Gateses and Richard Bransons of the world."

CHANGE YOUR THINKING

At their core, these courses teach science-related problem solving, says Matt Harvey, content and communications editor for Stanford's entrepreneurship courses, which cover how to choose an idea and license intellectual property from a university. Harvey says that Stanford doesn't measure success in terms of how many start-ups its graduates found, but how well they learn to identify, fill and profit from an unmet need in the marketplace. He mentions Stanford graduates Kevin Systrom and Mike Krieger, both of whom were Mayfield fellows. They founded the online photo-sharing service Instagram, which they sold to Facebook this year for US$1 billion. But Harvey insists that the value of their education doesn't lie in that one sale, however lucrative: "The story is not about Kevin and Mike founding Instagram. The story is what are they going to do for the next 10, 20, 30 years, because they're problem solvers," he says.

In his own course, Fee uses a poetry contest to help engineers think in ways they're not used to. "I've had young men in tears in my office saying 'I can't write poetry,'" he says. "The point is to get the students to explore their emotional soul, if you like." He feels that poetry heightens awareness of language, helping people to learn when to be precise and when to be imaginative. Fee also emphasizes the importance of drawing connections between disparate subjects. He argues, for example, that connecting ideas from origami and cardiology led to the creation of stents that can be folded to fit into an artery.

Learning creative problem-solving often requires hands-on classes, not passive lectures. Accordingly, entrepreneurship courses seldom run on the model of the large lecture courses that are common in undergraduate science. Students "don't sit in a classroom listening to us

COURSE OPTIONS

Training top-up

There are plenty of programmes and other resources for scientists and engineers who want to sample entrepreneurship without pursuing a business master's degree.

In the United States:

- Rensselaer Polytechnic Institute's Lally School of Management and Technology in Troy, New York, runs a one-year master of science in technology commercialization and entrepreneurship.
- The Child Family Institute for Innovation and Entrepreneurship at the University of California, Davis, has a one-year business development certificate for graduate students and postdocs in science and engineering.
- The Maryland Technology Enterprise Institute at the University of Maryland, College Park, runs courses and online programmes including a degree minor in technology entrepreneurship.
- The Marshall School of Business at the University of Southern California in Los Angeles offers a graduate certificate in technology commercialization.

In Europe:

- The Innovation Academy at University College Dublin and Trinity College Dublin offers PhD students a graduate certificate in innovation and entrepreneurship.
- The Management of Technology and Entrepreneurship Institute at the Swiss Federal Institute of Technology in Lausanne lets master's students from other university departments minor in management, technology and entrepreneurship.
- The Strascheg Center for Entrepreneurship in Munich, Germany, together with Munich University of Applied Sciences, provides entrepreneurship courses including a two-semester certification programme in innovation and entrepreneurial spirit.
- The Centre for Entrepreneurship at Delft University of Technology in the Netherlands offers courses in finance, product development and marketing.

Available globally:

- The Kauffman Foundation in Kansas City, Missouri, runs the Global Scholars Program, which allows graduates in science, engineering and technology from around the world to study with successful entrepreneurs in the United States for six months.
- The Stanford Technology Ventures Program at Stanford University in California offers free videos of talks by entrepreneurs at http://ecorner.stanford.edu. N.S.

tell them what we think. They're out experiencing things," says Suzi Jarvis, a UCD biophysicist and co-director of the Innovation Academy.

Keane divides students into teams with different disciplinary backgrounds, and describes real-life financial and personnel issues that have faced the founders of Zipcar, a car-sharing service based in Cambridge, Massachusetts. The students have to come up with ideas about how to address those issues — first individually, then as a team. It is often hardest for them to grasp that there is no one correct solution, says Keane.

To learn how creativity translates into business success, students often hear talks from accomplished entrepreneurs. Not only do such talks provide important networking opportunities, but they can also give students a different perspective on entrepreneurship. "If people in engineering and science don't have any exposure to entrepreneurs, they may think 'That's only for business people. That's only for people with MBAs. That's only for people who aren't like me,'" says Wilson.

IDEAL APPROACH

For scientists interested in entrepreneurship, Wilson recommends dipping a toe in with a single course, or searching the web for one of the many conferences held on the subject every year. The website TechCrunch, for instance, runs the biannual Disrupt conference, at which start-ups can demonstrate their technology and compete for a monetary prize. The Kauffman Foundation, based in Kansas City, Missouri, joined with Enterprise UK in London to create Global Entrepreneurship Week, which covers a variety of events around the world. O'Reilly Media in Sebastopol, California, a publisher of computer-related books, holds regular Ignite events, at which people give 5-minute talks about their passions, which could include start-up ideas.

Wilson strongly suggests getting some work experience before trying to start a company. Although famous successes such as Facebook give the impression that graduates can immediately build a billion-dollar company, most successful entrepreneurs actually have a decade or more of business experience. Wilson herself studied applied mathematics as an undergraduate, and after working for a couple of years, went to Harvard Business School in Boston, Massachusetts. Her only regret is that she didn't work for longer, perhaps gaining experience at a second company. "Go and make all your mistakes at somebody else's expense," agrees Fee. "Learn how difficult it is to get projects off the ground." ■

Neil Savage *is a freelance writer based in Lowell, Massachusetts.*

TURNING POINT
Craig Bennett

Craig Bennett, a postdoc in cognitive neuroscience at the University of California, Santa Barbara, has highlighted the prevalence of statistical errors in interpretations of functional magnetic resonance imaging (fMRI) data. He showed that such errors can lead to ambiguous and sometimes absurd results, such as registering brain activity in a dead salmon (C. M. Bennett et al. J. Serendipitous Unexpected Results *1, 1–5; 2010). On 20 September, Bennett accepted an Ig Nobel Prize — a riff on the Nobel prize that recognizes unusual research — for his work. He describes how the fishy findings have affected the field and his career.*

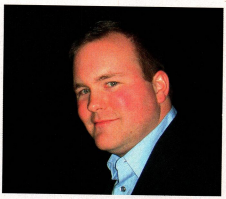

Did you conduct a 'dead salmon' experiment?

No. We do a lot of calibration and testing before undertaking fMRI studies, to make sure that the scanner is working before we put a human into it to measure their brain activity. One of my PhD advisers and I made a game out of finding all kinds of things to scan, from a pumpkin to a game hen to a salmon. But there was no reason to dig into the results until about five years ago, when my other adviser was lecturing on false positives and asked me to find some good data. It was pure luck that we found them in the salmon's brain.

How did the story evolve from there?

False positives in fMRI studies had caused increasing concern in neuroscience. The dead salmon was a good example of how an improperly corrected threshold value — which separates the signal from noise — could compromise results. We submitted our findings as a poster to the 2009 Human Brain Mapping conference in San Francisco, California, and at first colleagues thought it was a joke. Ultimately they included it, but we realized that we would face challenges in trying to publish.

What sort of challenges?

We knew that the article could mean that our statistics would receive closer scrutiny. We have experienced some of that, but it keeps us on our toes. Our work has improved — we are meticulous about analyses.

What happened when you submitted the dead-salmon paper?

We tried to get it published in two major neuroimaging journals. One rejected it and the other sent it out for review. One reviewer said it was fantastic; the other gave us a hateful, livid review that sunk it. But less-mainstream journals were clamouring for the paper. We went with the *Journal of Serendipitous and Unexpected Results*, which led to other publications and fostered a debate on statistical errors.

Has the field changed?

In the salmon paper, we did a meta-analysis of major journal articles and found that 25–40% of neuroimaging papers that we studied were not properly correcting for threshold values. We surveyed a couple of journals last year as a follow-up, and found that fewer than 10% of people are now using incorrect statistics. The decline is not all attributable to the salmon paper, but it is all progress. We gave the field a kick in the pants — and I've heard that a lot of groups reviewed the paper in lab meetings.

Are you concerned that being an Ig Nobel winner might harm your career prospects?

We were a tad worried, given that the Ig Nobel's original criterion was to recognize research that "cannot or should not be replicated". We didn't feel that the salmon fell into that category. But when we got a call from Marc Abrahams, founder of the awards, he described their new context: recognizing science that "first makes people laugh, then makes them think". That seemed appropriate, and we worried less.

What is next for you?

I am keeping track of job openings while I complete some research. I'm convinced that a big part of a successful job search is shaping your personal story. You need a coherent thread of research. I study how teens and adults make decisions, and I am interested in how best to analyse fMRI data to answer these questions. I just co-authored a big review on fMRI reliability, and I will make clear in interviews that all my work tells a coherent story — otherwise I would just be the 'dead fish' guy. ■

INTERVIEW BY VIRGINIA GEWIN

Germany – Partner for Medical Technology

Leading-edge imaging for the bigger picture

German cutting-edge research, focused support and efficient networking are helping to create the healthcare technologies of tomorrow.

Ever since Wilhelm Conrad Röntgen's discovery of X-rays in 1895, Germany has been a hotbed of innovation in medical imaging. Now the German Federal Ministry of Education and Research (BMBF) has made medical technology the focus of the most recent campaign under its "Research in Germany – Land of Ideas" initiative.

Launched at Medica 2011 in Düsseldorf, the "Germany – Partner for Medical Technology" campaign aims to raise the country's profile as a world-class location for research and development in this sector. This year the campaign will bring some of the most innovative researchers and institutions to the Radiological Society of North America (RSNA) annual meeting in Chicago, with a strong emphasis on medical imaging.

Germany is already at the centre of the global research landscape in medical technology. Scientific publications originating from Germany account for between 5 and 20 percent of the worldwide total in this area, in its various fields. Almost 9 percent of the 20 billion euros in turnover generated by the country's medical technology industry is spent on research and development. Each year around 2,300 students graduate from courses dedicated to medical technology, offered by some 20 German universities and 35 universities of applied sciences, while almost 75,000 students obtain a degree in one of the science, technology, engineering and medicine (STEM) subjects. Many of them go on to enter careers in the medical technology sector.

One of the keys to Germany's success in this sector is its network of medical technology clusters, made up of universities, research institutes, clinics, small to medium enterprises (SMEs) and large companies. Strengthening and extending these clusters

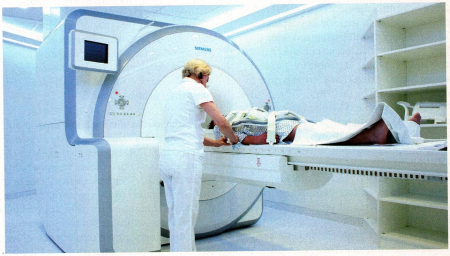

Biograph mMR, the first clinically approved MR-PET scanner.

is vital in order to promote and expand the country's leading role. To this end, the German Federal Government is supporting the most productive clusters in their rise to pre-eminence, with initiatives such as the leading-edge cluster competition – a flagship of Germany's High-Tech Strategy 2020.

Medical imaging – a central focus

Advances in medical imaging are a central part of the progress of medical technology, delivering images with ever higher spatial and temporal resolution, and enabling ever faster and more precise diagnoses. One indicator of Germany's current strong position in this field is the fact that 50 percent of the world's magnetic resonance imaging (MRI) scanners originate here. Imaging techniques including ultrasonography, computed tomography (CT) and positron emission tomography (PET), as well as magnetic resonance tomography (MRT), continue to be developed further, and are being applied in such diverse areas as oncology, cardiovascular diseases and neurology, to name but a few.

One outstanding example is the powerful hybrid device, combining the advantages of MRI and PET, developed by scientists at the Jülich Research Centre – a member of the Helmholtz Association – in close co-operation with their colleagues at Siemens. The MR-PET scanner, applying a magnetic field of 9.4 Tesla (about 190,000 times that of the Earth), is the first instrument capable of simultaneously analysing the structure and function as well as the metabolism of the brain down to the molecular level at ultra-high field strength. In order to combine the tissue-imaging properties of MRI with PET's ability to elucidate the brain's physiological and biochemical activities, the Jülich and Siemens researchers had to overcome significant challenges, among them the incompatibility of conventional, photomultiplier-based PET detectors with magnetic fields. Instead, they employed newly developed avalanche photodiodes. Like conventional PET detectors, these measure a flow of electrons generated by photons, but in their case this flow takes place in a semiconductor layer system over distances too short to be affected

UNIVERSITY HOSPITAL ERLANGEN, GERMANY

by the device's powerful magnetic fields. Eventually, these technical developments enabled Siemens to build the Biograph™ mMR, the first clinically approved MR-PET scanner for simultaneous MR and PET acquisition.

While MRI measurements rely on the magnetic properties of hydrogen nuclei in tissues, magnetic particle imaging (MPI) exploits the distribution of a magnetic tracer substance in the organism. Usually, this tracer substance consists of superparamagnetic iron oxide nanoparticles. A crucial improvement of this technology – a single-sided detector – is being developed by scientists at the Institute of Medical Engineering at Lübeck University, in co-operation with their partners at Phillips Research. Whereas a conventional MPI scanner's field of view lies within a symmetric coil configuration, thereby limiting the size of specimens that can be investigated, this limit would be eliminated by using a single-sided scanner geometry. So far, resolutions of down to one millimetre in one dimension have already been achieved.

A completely new range of optical imaging methods is opened up by the multispectral opto-acoustic tomography (MSOT) technique invented by leading researchers at Helmholtz Center Munich and developed and marketed by the start-up company iThera Medical. While fluorescence imaging methods are well established in the analysis of cells in culture or of isolated tissues, their use in whole organisms had been subject to severe limitations. MSOT overcomes these limitations by using the photoacoustic effect. Tissues are irradiated with laser pulses in the near infrared part of the spectrum. The absorbed photons cause ultrasound shockwaves that can be detected and used for a reconstruction of the object being investigated. Currently this method is proving very useful for pre-clinical studies in animals. For example, the continuous monitoring of the development of a tumour in a mouse can help both to reduce the number of animals being used in research, and to improve the reproducibility of the results that are obtained. The range of possible future clinical applications is quite wide, from diagnosing deep-lying tissues, to high-resolution vascular diagnosis, to endoscopic applications.

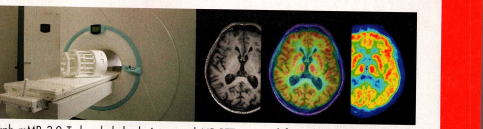

Biograph mMR 3.0 Tesla whole-body integrated MR-PET system (left) and clinical examples for simultaneously acquired MR-PET hybrid images. The Biograph mMR system combines the excellent soft tissue contrast and high spatial resolution of MR imaging with the high sensitivity of PET.

Future trends

These three examples out of many already shed some light on two of the most important trends in medical imaging today: the ever-closer convergence of classical imaging techniques like CT and MRI, and the development of optical methods with modern molecular and cell biology, which together move towards the goal of molecular imaging. These new approaches will, for example, enable physicians to reach a diagnosis earlier and to launch more focused therapies, as well as allowing them to better monitor applications such as chemotherapy. They will also help researchers gain new insights into the cause as well as the progression of diseases. The molecular imaging innovation alliance, "Innovationsallianz Molekulare Bildgebung", brings together the leading German research clusters in this field, such as the cluster MOIN CC (Molecular Imaging network), with numerous partners in the scientific community and commercial companies.

A further overarching trend is the continuous improvement and development of new software systems and algorithms for data processing and image analysis, with the goal of expanding diagnostic possibilities and enhancing the safety of therapies.

Leading BMBF-funded German clusters in this area are "Quantitative Imaging in Oncology (QUINO)", "3D Imaging in Medicine", and "German Medical Imaging in Motion (GMIM)". QUINO, which is developing new procedures in medical image analysis, is a competence network consisting of the German Cancer Research Center (Deutsches Krebsforschungszentrum; DKFZ), the University Hospital of Heidelberg and the medium-sized companies CHILI Radiology GmbH and Mint Medical GmbH.

Health technology is one of the main research and teaching topics of the Friedrich-Alexander University (FAU) in Erlangen, with its numerous spin-offs forming part of the "3D Imaging in Medicine" cluster. FAU scientists have made substantial contributions to medical imaging, telemedicine, biomaterials, and therapeutic systems. Strong links to Siemens Healthcare, Fraunhofer IIS and about 50 companies in the surrounding Nuremberg Metropolitan Region contribute to the excellent FAU research environment.

The GMIM consortium reflects the medical technology strengths of southern Germany and particularly the Munich area. It focuses both on innovative topics from different fields of preclinical, research oriented imaging, such as multimodal imaging, and on innovations in clinical imaging and image processing.

Federal Ministry
of Education
and Research

Research in
Germany
Land of Ideas

www.research-in-germany.de

ADVERTISER RETAINS SOLE RESPONSIBILITY FOR CONTENT

W229539RL

naturejobs

European Head Office, London naturejobs@nature.com
The Macmillan Building, 4 Crinan Street, London N1 9XW, UK
Tel: +44 (0) 20 7843 4961 Fax: +44 (0) 20 7843 4996

Global Head:
Nils Moeller; +44 (0) 20 7843 4953 n.moeller@nature.com

Southwest UK/RoW:
Emma Hare, +44 (0) 20 7843 4944 e.hare@nature.com

Northeast UK/Ireland:
Matthew Ward, +44 (0) 20 7014 4059 m.ward@nature.com

France/Switzerland/Belgium:
Julie Aramburu, +44 (0) 20 7843 4994 j.aramburu@nature.com

Scandinavia/Spain/Portugal/Italy:
Megan Ball, +44 (0) 20 7843 4973 m.ball@nature.com

North Germany/The Netherlands/Eastern Europe:
Kristin Doelling; +44 (0) 20 7843 4970 k.doelling@nature.com

South Germany/Austria:
Maria Kubalova, +44 (0) 20 7014 4084 m.kubalova@nature.com

Natureevents:
Matthew Clare, +44 (0) 20 7014 4015 m.clare@nature.com

Business Development Manager, Middle East:
Jon Giuliani, +44 (0) 20 7843 4922 j.giuliani@nature.com

USA Head Office, New York naturejobs@us.nature.com
75 Varick Street, 9th Floor, New York, NY 10013-1917
Tel: +1 800 989 7718 Fax: +1 800 989 7103

US Sales Manager:
Ken Finnegan, +1 212 726 9248 k.finnegan@us.nature.com

Japan Head Office, Tokyo
Chiyoda Building, 2–37 Ichigayatamachi, Shinjuku-ku, Tokyo 162-0843
Tel: +81 3 3267 8751, Fax: +81 3 3267 8746

Asia-Pacific Sales & Business Development Manager:
Yuki Fujiwara, +81-3-3267-8765 y.fujiwara@natureasia.com

Business Development Manager, Greater China/Singapore:
Gloria To, +852 2811 7191 g.to@natureasia.com

India
3a, 4th Floor, DLF Corporate Park, Gurgaon, I22 002, India

Advertisement Sales:
Vikas Chawla, +91 I242881057 v.chawla@nature.com

the Beatson
institute for cancer research

Staff Scientist

Starting salary £33,300 - £57,100 (depending on experience)

Pre-clinical Imaging of Genetic Cancer Models

The Beatson Institute in Glasgow is one of Europe's leading cancer research institutes. It is core funded by Cancer Research UK and supports cutting edge research into the molecular mechanisms of cancer development. The Institute provides an outstanding research environment underpinned by state-of-the-art core services and advanced technologies and together with Carestream Molecular Imaging we have established a centre of excellence to develop pre-clinical imaging of transgenic cancer models using the Carestream Albira. The Institute also benefits from close interactions with the University of Glasgow through the Institute of Cancer Sciences.

Applications are being accepted for a staff scientist position to facilitate the use of PET, SPECT, and CT for investigation of murine cancer models. You will lead a small team (which can include students and post-docs) having a dual research and service function based around use of PET, SPECT, and CT for preclinical imaging using transgenic cancer models. The main responsibility will be to promote the use of preclinical imaging among Beatson Research Groups by demonstrating the potential of these methods through your own research. Also you will assist Beatson Research Groups with project design and the acquisition and interpretation of data. This post will involve close interaction with Carestream.

You will have a relevant PhD and post-doctoral experience. Good communication and team-working skills are essential. Previous experience of managing a small team would be advantageous.

Applications with CV and names of two referees should be sent to Dr Kurt Anderson, Beatson Institute for Cancer Research, Garscube Estate, Switchback Road, Bearsden, Glasgow, G61 1BD or by e-mail to k.anderson@beatson.gla.ac.uk

Closing date: 16 November 2012

CANCER RESEARCH UK

Scottish charity no SC006106

U229758R

INFN
Istituto Nazionale di Fisica Nucleare

POST-DOCTORAL FELLOWSHIPS IN EXPERIMENTAL PHYSICS

The INFN Fellowship Programme 2012/2013 offers 16 (sixteen) positions for research activity in Experimental Physics.

Eligible candidates are non-Italian citizens. Applicants should have a Ph.D. degree or an equivalent qualification. Candidates who are preparing their doctoral thesis are eligible to apply, however they will have to obtain their Ph.D. degree before taking up their appointment with INFN.

Applicants with a Ph.D. of eight years or over eight are not eligible.

The annual gross salary is €40.000,00. Each fellowship is initially granted for one year and may be extended to a second year. Travel tickets to and from INFN sites will be reimbursed at the beginning and at the end of the fellowship; also lunch tickets will be provided for working days.

Online applications are to be sent to INFN not later than **November 20th, 2012** applying at the website http://www.ac.infn.it/personale/exp_fellowships/. The applications should include the research topic(s) of interest, the preferred INFN site(s) - two at the most, chosen among those listed in Annex 1 - and:

- a statement of research interests;
- a curriculum vitae;
- a publication list;
- at least three reference letters (specifying name, last name and e-mail of each referee).

At the end of the selection process the candidates will be informed by e-mail about the result of their application. Successful candidates will then receive an official communication from the INFN administration offices. The appointed fellows should start their fellowships not later than November 1st, 2013; special requests to defer the starting date can be considered.

ISTITUTO NAZIONALE DI FISICA NUCLEARE
Il PRESIDENTE
(Prof. Fernando Ferroni)

ANNEX 1

INFN SITES

INFN Laboratories: Laboratori Nazionali di Frascati (Roma), Laboratori Nazionali del Gran Sasso (L'Aquila), Laboratori Nazionali di Legnaro (Padova), Laboratori Nazionali del Sud (Catania);

INFN Sections in the Universities of: Bari, Bologna, Cagliari, Catania, Ferrara, Firenze, Genova, Lecce, Milano, Milano Bicocca, Napoli, Padova, Pavia, Perugia, Pisa, Roma La Sapienza, Roma Tor Vergata, Roma Tre, Torino, Trieste.

RESEARCH PROGRAMS

The research programs of the candidates must be focused on the research fields of the INFN Sections and Laboratories selected. The INFN research fields are listed below:

- PARTICLE PHYSICS
- ASTROPARTICLE PHYSICS
- NUCLEAR PHYSICS
- TECHNOLOGY RESEARCH

W229669R

ASSISTANT PROFESSOR OF PARTICLE THEORY

Department of Physics
Arts and Science

The Physics Department of New York University anticipates filling a tenure-track Assistant Professor position in particle theory, as part of an ongoing program to develop this area to begin September 1, 2013, pending administrative and budgetary approval. Duties will include undergraduate and graduate teaching. Exceptional candidates at higher levels will also be considered.

Applicants must apply online at the Center for Cosmology and Particle physics website (**http://cosmo.nyu.edu/opportunities.html**) and upload a CV, publication list, research interests and list of names of at least three people who will be submitting letters of recommendation. All application materials and supporting documents should be received by ***December 1, 2012***, if possible.

NEW YORK UNIVERSITY

NYU is an Equal Opportunity/Affirmative Action Employer.

NW229716R

ROTHAMSTED RESEARCH

WHERE KNOWLEDGE GROWS: SENIOR OPPORTUNITIES IN SOIL SCIENCES AND AGROECOLOGY

With an enviable international reputation as a centre for excellence and innovation for science in support of agricultural productivity, crop production and soil science and an annual operating budget of circa £30 million, we are one of the best-funded centres for agricultural research nationally and internationally. Our science is used by policymakers, agri-businesses, food manufacturers, energy companies and the farming community enabling us to make a significant contribution to the Global Challenges of food security and finding viable sources of bioenergy.

We are now seeking to make three senior appointments of key strategic importance to our future development. Successful candidates will be expected to build and lead strong research programmes either in an existing area of excellence or in a new area consistent with our focus and mission.

Senior Scientist & Head of Department of Sustainable Soils and Grassland Systems

You will combine personal scientific standing, as demonstrated by your outstanding research and publication record in soil science and success in competing for grants and other research support, with the strategic leadership acumen that will enable you to be an inspirational head of department. It is likely that you are already operating at professorial/principal scientist level.

The post will be based at Harpenden, Hertfordshire.

Senior Scientist – Soil Sciences

You will have a track record of publishing in international journals, experience in winning support from and interaction with different funding sources and the ability to build a strong research programme. Preferred candidates will have the leadership and interpersonal skills that would allow them to play a key role in the further development of the Department of Sustainable Soils and Grassland Systems.

The post will be based at North Wyke, near Okehampton, Devon.

Senior Scientist & Head of Department of AgroEcology

With a significant record of research achievement, the ability to build a strong research programme, track record of publishing in international journals and success in winning funding, you will have the energy and vision and personal standing to lead and further develop the Department of AgroEcology.

The post will be based at Harpenden, Hertfordshire.

The posts are tenured and will be well supported by internal resources to provide a long-term research foundation for the post-holders.

An attractive salary is available, reflecting the level of experience and achievement.

Further information, including instructions on how to apply, may be obtained from Rothamsted Research's recruitment consultants, Carbon-NfP, who would be happy to have an informal and confidential telephone discussion with potential candidates. Please contact Sharon Taylor by email sharon.taylor@carbon-nfp.com in the first instance.

The closing date for applications is Friday, 23rd November 2012.

Carbon-NfP Ltd, 17 Russell Court, Woburn Place, London WC1H 0LL.

Rothamsted Research is a registered charity (no. 802038) limited by guarantee and is an Equal Opportunities Employer

U229764R

www.carbon-nfp.com

CARBON-NfP

NANYANG TECHNOLOGICAL UNIVERSITY

RISE TO THE OPPORTUNITY

with one of the world's fastest-rising universities. **NTU.**

Faculty Positions at School of Chemical and Biomedical Engineering (SCBE)

Nanyang Technological University (NTU) in Singapore is ranked 47th in the 2012 QS World University Rankings and is the fastest-rising university in the world's top 50.

SCBE at NTU invites applications for Assistant, Associate or Full Professors. For more information, visit www.scbe.ntu.edu.sg/About_Us/Pages/Open_Positions.aspx

Research Areas

Chemical and Biomolecular Engineering Division

- Process systems engineering
- Product and process design
- Pharmaceutical engineering
- Food engineering
- Separation technology

Bioengineering Division

- Cardiovascular biomechanics
- Bioinstrumentation
- Biosignal processing and imaging
- Biofluid
- Neuro bioengineering
- Nature inspired bioengineering

Application Details

Guidelines: www.ntu.edu.sg/ohr/Career/SubmitApplications/Pages/Faculty.aspx

Email: scbe_recruit@ntu.edu.sg

www.ntu.edu.sg

JP229616R

MAX PLANCK INSTITUTE FOR **BIOLOGY OF AGEING**

Since its founding in 2008, the Max Planck Institute for Biology of Ageing in Cologne, Germany, has become a hub within a network of research institutes constituting a unique cluster in the field of ageing research worldwide.

The institute will move into a new building with state-of-the-art laboratories and facilities, located on the Campus of the University of Cologne and the Cologne Medical Center.

Fundamental questions on the nature of ageing and longevity are being investigated in various model organisms: Why do organisms age? What biological processes determine lifespan? And what are the roles of genes and environment? Researchers at the institute currently represent almost 30 different countries. The MPI is expected to grow to a size of 350 employees. There will be four directors with corresponding departments and four Max Planck Research Groups ready to welcome junior scientists of exceptional talent.

IMPRS-Age Graduate School Investigating the nature of ageing and longevity

In close collaboration with the graduate school of the CECAD Cluster of Excellence, also based in Cologne, the International Max Planck Research School IMPRS-Age provides a first-class education in the field of ageing and age-related diseases. Outstanding PhD students will receive training in biological and medical disciplines, gain experience in the use of diverse model organisms as well as state-of-the-art technologies, and develop communication skills essential for a successful scientific career.

For a list of current vacancies, please visit **www.age.mpg.de**

W229074R

THE UNIVERSITY OF
WARWICK

Academic posts in the new School of Life Sciences

Salary negotiable

The new School of Life Sciences is following an exciting new vision for developing its research and teaching activities, progressing towards relocation into the planned **Warwick Interdisciplinary Biocentre** building, which will house interdisciplinary science that focuses on the principles of system organisation that underpin function and diversity in the biosphere. We study systems from animals (including man), plants, fungi, protozoa and bacteria. In the fourth phase of growth of the academic faculty of the School of Life Sciences, we seek outstanding candidates for appointment to two new professorial posts. A central theme of all of the new appointments will be that of advancing fundamental understanding of the complex behaviour of biological systems using an integrated combination of state-of-the-art experimental and computational methods.

Candidates can be active in either of the following fields, and will be selected primarily on the basis of their research track record and potential. Outstanding publications in top-tier journals and an internationally recognised leadership role in a research area are prerequisites. These are positions for ambitious Scientists who wish to contribute to the leadership of a highly dynamic and forward-looking community that is supported by excellent facilities in key technologies, including imaging, 'omics methods, structural biology and computation.

Professor of Developmental Biology

Ref: 71204-102

Candidates can be working on any of a wide range of developmental questions but should be committed to the integration of quantitative experimental data (particularly molecular and cellular) into new types of conceptual model as a strategy to advance understanding of developmental biology at the system level. This integrated approach can be achieved through collaboration. Candidates can be studying any question that has broader relevance in terms of the principles of development, and should be motivated by a commitment to elucidating fundamental system properties.

Professor of Integrative Cellular Systems Biology

Ref: 71205-102

Candidates will work in any area of eukaryotic cell biology, including gene expression, cell signalling, intracellular and trans-membrane transport mechanisms, epigenetics and differentiation. The organism under study can be of any type, including human pathogens. As with the first post, candidates should be motivated by a commitment to elucidating fundamental system properties. There will be exciting opportunities for collaboration with other members of the sizeable community of researchers in our School.

In addition to the above posts, we also invite applications from outstanding Scientists who either already hold ***Research Fellowships*** or are seeking a top-class institution that will host an application for such a Fellowship. The new School of Life Sciences will provide an exciting and highly supportive environment in which researchers can develop highly productive careers.

The above appointees will play major roles in driving forward an ambitious, forward-looking and coherent research vision for the new School that will offer a diversity of opportunities for Scientists at all levels. They will be able to work in a highly supportive and well-equipped research environment as well as contribute to innovative training programmes at the undergraduate and graduate levels.

If you would like to obtain more information on these and other aspects of our plans for the new School, feel free to contact John McCarthy, Head of School (Tel: (44) 24 7652 8380; Email: john.mccarthy@warwick.ac.uk).

For more information and to apply, please visit our website.
Closing date: 16 November 2012

U229761R

The University Values Diversity **www.warwick.ac.uk/jobs**

UNIVERSITY OF COPENHAGEN

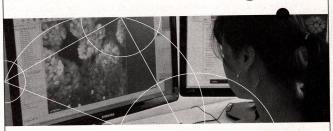

Group leader positions at The Danish Stem Cell Center

Faculty of Health and Medical Sciences

The University seeks to appoint Associate Professors as Group Leaders to the The Danish Stem Cell Center (Danstem) to commence as soon as possible.

The Danish Stem Cell Center (Danstem) is a research center of excellence at the University of Copenhagen. The overall scientific goal is to develop new stem cell-based therapeutic approaches, currently in the area of diabetes and cancer, addressing basic questions in stem cell and developmental biology and seeking to identify the factors that govern the development of different cell types in the body. Read about Danstem at www.danstem.ku.dk

Danstem is recruiting outstanding and ambitious candidates with important and original research contributions as well as the ability to develop a strong research program. Investigators with particular interests in basic and disease-oriented stem cell and developmental biology are encouraged to apply.

Danstem offers newly established lab and core facilities for stem cell research as well as a competitive start-up package in a young, dynamic, and international environment. The positions are tenure-track, and the first appointment will be for six years. The group leaders are expected to develop a strong research program and must be willing to interact with other scientists and contribute to common activities at Danstem such as seminars and PhD courses.

For further information about the positions and Danstem please contact the Director of Danstem, Professor Henrik Semb, semb@sund.ku.dk

Application
The application must be submitted electronically including the required attachments. For further instruction of how to apply for these positions please go to www.danstem.ku.dk/jobs/vacancies. Only online applications are accepted.

The closing date for applications is Friday 7 December 2012.

www.ku.dk/english

W229663R

wellcome trust

A world where the brightest minds in science get the support they need.

Opportunities in Science Funding

The Science Funding division is the main scientific interface between the Wellcome Trust and our global biomedical and public health research community. The division, a stimulating group of 40 professional scientific administrators, is responsible for funding and supporting a large part of the biomedical science community in the UK and overseas. In 2010, we spent almost £500m supporting thousands of scientists in dozens of countries, to implement the challenges and foci of our Strategic Plan. We seek people who'll be uncompromising in pursuit of our mission, willing to question authority, and confident with their peers and the external community.

Head of Department, Science Funding
Cellular, Developmental and Physiological Sciences
£75 000+ per annum

In this key role, reporting to the Director of Science Funding, you'll manage a departmental staff to develop our portfolio in cellular, developmental and physiological sciences – seeking out excellence, catalysing opportunities and supporting our grant holders in these scientific areas. The role is based at our landmark Gibbs Building headquarters in central London, but will involve some UK travel. To meet the challenge, you'll need a doctoral degree and significant research experience, as well as experience in science administration – possibly leading your own research group.

Science Portfolio Manager, Science Funding
Deputy Head of Department, Basic Science Careers
£50 000+ per annum

Working closely with our Head of Basic Science Careers, you'll develop and support our portfolio of training and early career schemes in the basic sciences, including PhD, post doctoral and intermediate fellowship programmes. You'll need a doctoral degree and significant research experience, in addition to excellent interdisciplinary knowledge. You'll also need outstanding interpersonal, organisational and analytical skills and judgement, and direct experience of supervising research students and/or post docs.

Find out more and apply online at **www.wellcome.ac.uk/jobs**.

Alternatively, send a CV and covering letter, stating clearly the role for which you'd like to be considered and explaining how you meet the criteria, to HR, Wellcome Trust, 215 Euston Road, London NW1 2BE or to **HR@wellcome.ac.uk**.

Closing date: **Friday 16 November 2012**

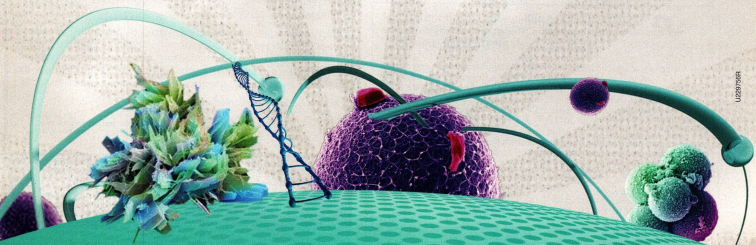

INFN
Istituto Nazionale di Fisica Nucleare

POST-DOCTORAL FELLOWSHIPS IN THEORETICAL PHYSICS

The INFN Fellowship Programme 2012/2013 offers 12 (twelve) positions for research activity in Theoretical Physics.

Eligible candidates may be non-Italian citizens, or Italian citizens who, at the time of the applications, are abroad for at least three years.

Applicants must have a Ph.D degree or an equivalent qualification. Candidates who are preparing their doctoral thesis are eligible to apply; however they must have obtained their Ph.D degree before taking up their appointment with INFN.

Applicants with eight or more years of post-doctoral experience are not eligible.

The research topics of the twelve fellowships and the corresponding INFN sites are listed in Annex 1. Each candidate may apply up to a maximum of three fellowships.

The annual gross salary is €40.000,00. Each fellowship is initially granted for one year and may be extended for a second year. Travel tickets to and from INFN sites will be reimbursed at the beginning and at the end of the fellowship; also lunch tickets will be provided for working days.

Applications, in electronic form, must be sent to INFN no later than **November 20, 2012** through the website http://www.ac.infn.it/personale/theo_fellowships/. The applications must specify the research topic(s) and the corresponding INFN site(s) (up to a maximum of three) among those listed in Annex 1, and must include:

- a curriculum vitae;
- a publication list;
- at least three reference letters (specifying name, surname and e-mail of each referee).

For each fellowship primary consideration will be given to candidates working in the corresponding specific research topic; however candidates working in other subjects may be also considered.

At the end of the selection process the candidates will be informed by e-mail about the result of their application. Successful candidates will then receive an official communication from the INFN Administation Offices. The appointed fellows should start their fellowships no later than November 1, 2013; special requests to defer the starting date can be considered.

ISTITUTO NAZIONALE DI FISICA NUCLEARE
IL PRESIDENTE
(Prof. Fernando Ferroni)

Annex 1
Research field INFN site (Section, Laboratory, Gruppo Collegato)

BARI	Foundations of quantum mechanics, entanglement and complexity
CATANIA	Nuclear astrophysics and compact stellar matter
LABORATORI NAZIONALI DI FRASCATI	Phenomenology of elementary particle interactions at colliders
LABORATORI NAZIONALI DI FRASCATI	Strongly correlated electron systems and nanostructures
MILANO	Nuclear physics and finite many body systems
PADOVA	Phenomenology of fundamental interactions
PISA	Non-perturbative dynamics in gauge and string theories
ROMA	Phenomenology of fundamental interactions and lattice gauge theories
ROMA	Astroparticle physics and cosmological applications
TORINO	String theory, supergravity and applications
GRUPPO COLLEGATO DI TRENTO	Nuclear physics and strongly interacting many-body systems
TRIESTE	String theory and applications

W229670R

INSTITUTE for PROTEIN RESEARCH
OSAKA UNIVERSITY

Call for Applications for International Collaborative Research at Institute for Protein Research (IPR), Osaka University

The research should be conducted in the form of a collaboration including at least one of the Principal Investigators (PIs) at IPR, or it should use particular experimental facilities of IPR, including solution- and solid-state-NMR spectrometers with ultra-high magnetic fields, and a synchrotron beam line for biological macromolecular assemblies at SPring-8. The research period is from **April 1st, 2013 to March 31st, 2014**. IPR will support each project for visiting IPR. Each applicant should submit an application form for the collaborative research along with a recommendation letter from the PI in IPR. **The dead-line for submission is December 10th, 2012**. The application form and the precise information can be given at our web page:
http://www.protein.osaka-u.ac.jp/eng/applications/applications/

Contact person: Yuji Goto, Prof., IPR, Osaka University,
3-2 Yamadaoka, Suita, Osaka 565-0871, Japan.
FAX: +81-6-6879-8616, **E-MAIL**: yogo@protein.osaka-u.ac.jp

JP228580R

nature

Chief News Editor, London

Nature, the international weekly journal of science, seeks a Chief News Editor to head its global news operation. With 15 staff reporters and a network of freelance correspondents, *Nature* produces daily online coverage and weekly print stories about all fields of research, the scientific community, policy, funding, and science and society.

The Chief News Editor plans coverage, commissions and edits stories, and works with art, production, and other *Nature* editors to deliver unique, high-impact journalism aimed at an audience of working scientists.

We seek a science journalist with extensive reporting and editing experience and a demonstrated interest in science policy and funding as well as in research findings. Management skills are essential, as is the ability to thrive under pressure.

This position is offered on a full-time, permanent basis and is based in our London office.

Applicants should submit a CV and a covering letter explaining their interest in the post to vacancy **NPG/112/12** on http://jobs.macmillan.com.

Closing Date: 5th November 2012

nature publishing group npg

IN229584R

Assistant Professor

Department of Biological Chemistry and Molecular Pharmacology
Harvard Medical School

The Department of Biological Chemistry and Molecular Pharmacology at Harvard Medical School invites applicants for a tenure-track faculty position at the rank of Assistant Professor. We are seeking individuals with a demonstrated potential for imaginative research and who propose to work on exciting problems in any area of chemical, structural, and/or mechanistic biology. The successful candidate will be expected to direct innovative and independent research and participate in the teaching of graduate and/or medical students. Our highly interactive environment provides the opportunity to engage and collaborate with other dedicated researchers both within the Department and throughout the diverse Harvard research community. Significant scholarly and scientific resources will be made available for this appointment. For further information about our Department, please see our Web Page: http://bcmp.med.harvard.edu.

Applicants should submit electronic copies of their curriculum vitae, a description of research accomplishments and future research interests (three pages maximum), and ask at least three references to provide letters of recommendation. These materials should be submitted using the following link: https://academicpositions.harvard.edu/postings/4340.

Applications will be considered starting December 1, 2012.

Harvard Medical School is an Equal Opportunity/Affirmative Action employer. We are actively committed to increasing the diversity of our faculty. Women and members of underrepresented minority groups are therefore strongly encouraged to apply.

HARVARD MEDICAL SCHOOL

NW229481R

UT SOUTHWESTERN MEDICAL CENTER AT DALLAS

ENDOWED SCHOLARS PROGRAM IN MEDICAL SCIENCE

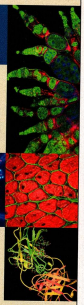

Unique and highly competitive, **THE ENDOWED SCHOLARS PROGRAM IN MEDICAL SCIENCE** is designed to launch the next generation's scientific leaders on their biomedical research careers by providing seed money, research space and startup support for groundbreaking projects. The Endowed Scholars Program gives early-career investigators the chance to take risks, supported by the mentoring of experienced and highly distinguished established researchers at **The University of Texas Southwestern Medical Center at Dallas.**

As one of the foremost research institutions in the world, UT Southwestern, with four Nobel Prizes awarded to its faculty since 1985 and 18 members of the National Academy of Sciences, is poised to lead the way in a new era of scientific discovery in the 21st century. We conduct more than 3,500 research projects annually totaling more than $400 million. Endowed Scholars have access to exceptional core facilities, which include DNA microarray services; electron microscopy; live-cell imaging; mouse gene knockouts, transgenesis and metabolic phenotyping; high-throughput chemical screening; and structural biology. UT Southwestern also is home to one of the nation's first 7-Tesla magnetic resonance imaging devices for human studies. UT Southwestern has a vibrant graduate school and nearly 4,400 medical, graduate and health professions students, residents and postdoctoral fellows.

The Endowed Scholars Program, which is fully funded from private endowment, provides more than $1,000,000 over four years to support the independent research activities, salary and benefits of each scholar. Up to five new scholars are selected each year from top universities, institutions and laboratories around the world. Each scholar is appointed as a tenure-track assistant professor in a UT Southwestern academic department or research center. Positions in both basic science and clinical departments are available.

Potential scholars submit nomination materials to a chair or director of one of UT Southwestern's basic or clinical academic departments or research centers. Those chairs or directors then forward finalists' materials for consideration to the medical center's Endowed Scholars Committee.

For detailed information about nomination materials and currently available positions, please visit our Web page: **utsouthwestern.edu/utsw/home/scholars**

Applications from women and underrepresented minority candidates are strongly encouraged. UT Southwestern is an equal opportunity institution.

UT SOUTHWESTERN MEDICAL CENTER

NW226634R

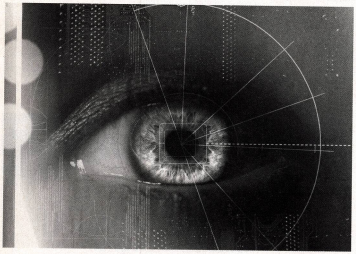

Creative Thinkers! Bold Ideas! Accelerate Research!

Submit a one-page concept for your chance to win $3,000
Learn more at www.nei.nih.gov/challenge

NIH...Turning Discovery into Health®

National Eye Institute

NW227665R

National Taiwan University

National Taiwan University Presidential Search

National Taiwan University (NTU) is a full-fledged comprehensive university with outstanding achievements. As the current presidency ends in June, 2013, Presidential Search Committee now invites nominations and applications for the position of President.

President candidates should meet the following requirements: Academician at Academia Sinica, or professor, or professional with prior teaching and academic research experience equivalent to that required of a professor, and at least three years of experience, accumulative, as a director in schools, government agencies, or in other state-owned or private business entities. The ideal President should be a leader of integrity with excellent academic achievement and administrative skills in education. The new leader should also be able to administer matters impartially and beyond the interests of any political groups.

For those who would like to nominate a candidate, please fill in all required forms and send it to the address below via registered mail or express mail delivered before 5pm on December 3, 2012. Application dossier will not be returned.

NTU Presidential Search Committee
No.1, Sec. 4, Roosevelt Road
Taipei
Taiwan 10617

If you have any inquiries, please call (886)-2-33662035, or fax (886)-2-23629997. The nomination form can be downloaded from the NTU Website: http://www.ntu.edu.tw/president/eng.html

JP229471R

南方科技大学
SOUTH UNIVERSITY OF SCIENCE AND TECHNOLOGY OF CHINA

Faculty Positions at South University of Science and Technology of China(SUSTC)

SUSTC is a public institution funded by the municipality of Shenzhen, a special economic zone city in southern China. The University receives full financial support from the municipality. Set on five hundred acres of wooded landscape in the picturesque Nanshan (South Mountain) area, SUSTC offers an idyllic environment suitable for learning and scholarship. SUSTC promotes academic freedom, engages in basic and problem-solving research of lasting impact to benefit society and mankind, and strives to become one of the best research universities in the world.

Academic Disciplines:
SUSTC has a broad range of academic disciplines, covering natural science, engineering and some newly emerging inter-disciplines. All disciplines are open to applicants. The university especially encourages research that requires a multi-disciplinary and non-traditional approach. Successful applicants are expected to lead or establish new research directions at SUSTC.

Positions:
SUSTC invites applications and nominations from outstanding scholars of all nationalities for faculty positions at all ranks with full-time arrangements. Full-time positions include leading professor, chair professor, professor, associate professor, assistant professor, and PostDoc.

Qualifications & Responsibilities:
Applicants should have a doctoral degree in a relevant research field with outstanding communication skills and a proven record of research excellence.

Responsibilities include teaching undergraduate and graduate courses, developing and sustaining externally funded research programs, graduate student supervision, and professional/institutional services.

Recruiting Positions at:
- Leading Professor
  Applicants should have a Ph.D. degree with extensive research and teaching experience. Applicants should be internationally recognized as holding a leading position in important areas of research.
- Chair Professor
  Applicants should have a Ph.D. degree with extensive research and teaching experience. Applicants should possess a large number of internationally recognized research accomplishments.
- Professor
  Applicants should have a Ph.D. degree with extensive research and teaching experience. Applicants should have made a number of important contributions in research.
- Associate Professor
  Applicants should have a Ph.D. degree. Applicants should have made a few important contributions in research.
- Assistant Professor
  Applicants should have a Ph.D. degree. Applicants should possess evidence that demonstrates the ability in performing high quality research.

Salaries and Benefits:
The University offers competitive salaries and start-up packages. Benefits include housing, medical insurances, pensions, etc.

Contact Us:
Qualified applicants are invited to send a job intention letter and a curriculum vitae to: **hiring@sustc.edu.cn.**

Mailing Address:
Human Resources Department,
South University of Science and Technology of China
No.1088, Xueyuan Blvd, Xili, Nanshan, Shenzhen, China Zip Code: 518055

Telephone: +86-755- 86249985, 86249969

Relevant Links:
South University of Science and Technology of China: http://www.sustc.edu.cn/

JP221489R

UNIVERSITÄTSMEDIZIN GÖTTINGEN UMG

The Department of Pharmacology, Center of Pharmacology and Toxicology, Medical Center of the Georg-August-University Goettingen and the Section Organismic Primate Biology at the German Primate Center (Deutsches Primatenzentrum, DPZ) GmbH jointly invite applications for the position of a

University Professor of "Stem Cell Biology of Primates" (W2)

to fill this position at the earliest possible date.

The successful candidate is expected to head a department at the German Primate Center and to take part in teaching at the Faculty of Medicine. Candidates are expected to be experienced in interdisciplinary research on non-human primates (preferably rhesus macaques and mantled tamarins) in the field of stem cell biology with focus on pluripotent stem cells. The appointment procedure is jointly implemented by representatives of the Faculty of Medicine and of the German Primate Center. Applications will also be accessible to the committees of the German Primate Center.

Further information: http://www.med.uni-goettingen.de/de/content/ueberuns/4548.html

Applications are to be sent within three weeks after the appearance of this advertisement online following the link: http://www.med.uni-goettingen.de/de/content/ueberuns/berufungen_onlinebewerbung.html

If you have any further queries, please do not hesitate to contact us: Berufungen@med.uni-goettingen.de

W229760R

PRIFYSGOL ABERYSTWYTH UNIVERSITY www.aber.ac.uk/hr

Chair/Reader in Rumen Systems Biology Institute of Biological, Environmental and Rural Sciences (IBERS)

Salary will be made on the Professorial Scale
Ref: IBERS.12.46
Closing Date: 9 November 2012
Interview Date : 29 November 2012

For information and application forms please go to www.aber.ac.uk/hr
Email: vacancies@aber.ac.uk
Hotline: (01970) 628555

Aberystwyth University is a registered charity. No 1145141.
Bilingual Institution which operates a Welsh Language Scheme. Committed to Equal Opportunities.

L222/SSR

CHINA RETURNEES
我想你 (I MISS YOU)
Head back to China now with Life Technologies.
A lot has happened since you've been away. Your mother turned 70. Your sister graduated from college. Your nephew took his first steps. Your China has transformed from a third-world country to a world-class economy. And Life Technologies, the world's most innovative biotechnology company, formed from the merger of Applied Biosystems and Invitrogen, is growing fast in China. So now there's no reason to keep missing out on the chance to be closer to your family and to be part of a team that makes science easier and life better everyday.
For more information, go to lifetechnologies.com/careers

We want to hear from you. Email us at **cn.recruit@lifetech.com**

life technologies™

Life Technologies is an Equal Employment Opportunity/Affirmative Action employer. ©2012 Life Technologies Corporation. All rights reserved.
The trademarks mentioned herein are the property of Life Technologies Corporation or their respective owners. CO03060 0712

NW2297793R

Invitrogen™ Applied Biosystems® Gibco® Molecular Probes® Novex® TaqMan® Ambion® Ion Torrent™

Massachusetts Institute of Technology

Come work with us!

Faculty Position in Biological Engineering Department of Biological Engineering

The MIT Department of Biological Engineering (BE) invites applications for a tenure-track faculty position at the assistant professor level, to begin July 2013 or thereafter. Applicants should hold a Ph.D. in a science or engineering discipline related to biological engineering. A more senior faculty appointment may be considered in special cases. Candidates should aspire to direct a leading research program that fuses molecular/cellular bioscience with quantitative engineering analysis/synthesis approaches. Faculty duties include teaching at the graduate and undergraduate levels as well as supervision of research, and candidates should be capable of instructing in our core biological engineering educational curricula. Current research in BE spans a broad application range of biotechnology from medicine and infectious disease to energy and the environment, along with fundamental studies of biological processes (see http://web.mit.edu/be/research/).

Candidates must register with the BE search website at http://be-fac-search.mit.edu, and must submit application materials electronically to this website. Candidate applications should include a description of professional interests and goals in both teaching and research. Each application should include a curriculum vitae and the names and addresses of three or more references who will provide recommendation letters. References should submit their letters directly to MIT at the http://be-fac-search.mit.edu website. Applications received by 1 December 2012 will be given priority.

Questions may be directed to: Prof. Douglas Lauffenburger, Head, Department of Biological Engineering, MIT 16-343, Cambridge, MA 02139, lauffen@mit.edu

MIT is an Equal Opportunity/Affirmative Action employer.

http://web.mit.edu

WWW2954198

Geisel School of Medicine at Dartmouth

FACULTY POSITION IN GENOMICS

The Geisel School of Medicine at Dartmouth has launched a major initiative in genomics and informatics that includes sustained growth in the **Department of Genetics.** We seek an outstanding individual with a vigorous and innovative genomics research program focused on using the biology of genes and genomes to understand complex genetic problems related to primary biological functions and/or human diseases, including but not limited to cancer, immunity, inflammation, and/or neuroscience. Applicants must have a PhD and/or MD degree and a strong publication record in the field. Evidence of extramural funding is essential. The position carries a faculty appointment in the Geisel School of Medicine at the rank of Assistant, Associate or Full Professor, commensurate with experience.

Applicants should submit a PDF file of their curriculum vitae and 2-3 page description of their research interests and future research plans, as well as have 3 letters of reference sent directly to the search committee. Review of applications will begin immediately. All materials should be sent to Genomics.Faculty.Search@Dartmouth.edu, and addressed to:

Search Committee
Department of Genetics, HB 7400
Hanover, NH 03755-7400, USA

Geisel School of Medicine is an Affirmative Action/Equal Opportunity Employer. We will extend equal opportunity to all individuals without regard for gender, race, religion, color, national origin, sexual orientation, age, disability, handicap or veteran status.

http://geiselmed.dartmouth.edu/genetics/

WWW2952200

ETH

Eidgenössische Technische Hochschule Zürich
Swiss Federal Institute of Technology Zurich

The **Department of Biosystems Science and Engineering** (D-BSSE) is the first truly interdisciplinary research unit of the ETH Zurich where theory, engineering and experimental biology groups team up to foster advances in Systems Biology, Biotechnology and Synthetic Biology. With its headquarters in Basel, the D-BSSE is situated in the heart of the Biovalley, a tri-national region hosting 40% of the global life science industry including several pharma giants, which provides a unique environment for high-leverage translational research. The D-BSSE is looking for several highly qualified and motivated

PhD Students/Postdocs/Senior Scientists

As member of the D-BSSE, you will foster novel research initiatives in the field of gene therapy, drug discovery, host-pathogen crosstalk, tissue engineering and biopharmaceutical manufacturing. Using synthetic biology principles, these research activities should converge to enable the design of prosthetic gene networks that prevent or treat metabolic disorders.

You are highly skilled in standard molecular cell biology and in vivo techniques. Furthermore, you have a good command of state-of-the-art transduction technologies and advanced skills in cultivating primary cells. From postdocs we expect an outstanding publication record; the handling of stem cells and confidence in animal experimentation will be a plus. A high degree of ambition to pursue an academic career or to initiate spin-off activities completes your profile.

For further information visit our website www.bsse.ethz.ch.

Applications (two hardcopies) with a CV, a publication list, a one-page three-year research plan and two letters of recommendation should be sent to Prof. Dr. Martin Fussenegger, c/o Swantje Pless, ETH Zurich, D-BSSE, Mattenstrasse 26, CH-4058 Basel.

W228967R

Visit

www.naturejobs.com

to seriously improve your career prospects.

naturejobs making science work

UNIVERSITY OF CAMBRIDGE

A world of opportunities
www.cam.ac.uk/jobs/

University Lecturer: The cellular basis for organismal function

Department of Zoology
£37,012 - £46,846 pa

The Department of Zoology is seeking to appoint as a University Lecturer, an outstanding scientist whose research focuses on the cellular mechanisms that underlie organismal form or physiological function. We are particularly keen to recruit applicants with interests in the mechanistic underpinning of diversity and adaptation. The successful candidate will combine excellence in research with a commitment to teaching at both undergraduate and graduate levels, and will have demonstrated the ability to fund and lead an effective research group. Appointment will be from 1 October 2013.

The University has a responsibility to ensure that all employees are eligible to live and work in the UK. For further details and to apply, please see Job Opportunities in the Department at: http://www.zoo.cam.ac.uk/zooone/administration/vacancy.html

Quote reference: PF00471. Closing date: 12 November 2012.

The University values diversity and is committed to Equality of Opportunity.

U259765R

a nature conference

University of Miami, International Union of Biochemistry and Molecular Biology, Nature Publishing Group and Scripps Florida present:

Miami 2013 Winter Symposium: The Molecular Basis of Metabolism and Nutrition

Join leaders in the field to discuss advances in our molecular understanding of obesity, calorie restriction, diabetes, ageing and the microbiome as they relate to human nutrition.

February 10-13, 2013
JW Marriott Marquis Miami
Miami, FL, USA

SYMPOSIUM AWARDEES

Feodor Lynen Lectures
Ana Maria Cuervo (Albert Einstein College of Medicine, USA)
Leonard Guarente (Massachusetts Institute of Technology, USA)
David Sabatini (Whitehead Institute for Biomedical Research, USA)

Distinguished Service Award
Bruce Spiegelman (Harvard University, USA)

Special Achievement Awards
Lewis Cantley (Harvard University, USA)

IUBMB Jubilee Lecture
Michael Karin (University of California, San Diego, USA)

CONFIRMED SPEAKERS:

Arthur Agatston
Fredrik Bäckhed
Anne Brunet
Tom Burris
John Cleveland
Miguel Constância
Ronald DePinho
Richard Flavell
Stanley Hazen
Jules Hirsch
Randal Kaufman
Salvador Moncada
Deborah Muoio
Chris Newgard
Jared Rutter
Reuben Shaw
Matthew Vander Heiden
Douglas Wallace
Robert Waterland

For more information and to register visit:
www.nature.com/natureconferences/miami/mws2013

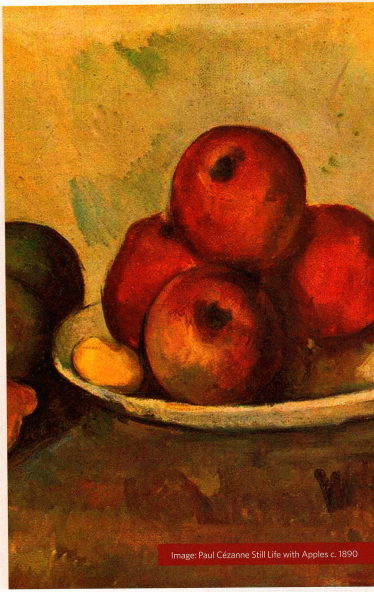

Image: Paul Cézanne Still Life with Apples c. 1890

UNIVERSITY OF MIAMI
MILLER SCHOOL of MEDICINE

SCRIPPS FLORIDA
THE SCRIPPS RESEARCH INSTITUTE

IUBMB

IN228654E

HIGHER & HIRE!

Post all your vacancies for FREE on the largest dedicated job board for the scientific community:

naturejobs.com

nature publishing group npg

哈爾濱工業大學

HARBIN INSTITUTE OF TECHNOLOGY

Faculty and SRF Positions in School of Life Science and Technology of Harbin Institute of Technology, China

The University: Harbin Institute of Technology (en.hit.edu.cn) is one of the top nine universities in China. It is located in the northeast of China, hosts 48,000 Students, with an annual research income of 291M USD. HIT was established in 1920 and is known for its achievement in Engineering and Technology. HIT offers competitive packages for its employees.

The School: The School of Life Science and Technology (SLST) was founded in 2011 as a new strategic development of the university. The School currently offers two Degree Programs, Life Science and Biomedical Engineering at Bachelor and Master Levels, and admits about 30 PhD students a year. SLST currently has 8 Professors, 17 Associate Professors, 14 Lecturers. The School occupies nearly 7000 sqm purpose built space, and has established several platform facilities. These include:

(1) Image Analysis System: SEM (Quanta 200), TEM (Tecnai G2 spirit TWIN), AFM (Agilent 5500 ILM SPM), LSCM (Zeiss-Meta 510, Leica DM5500), Live Cell Station and Small Animal in Vivo Imaging System, etc.
(2) Mass Spectrometric Analysis System: MALDI TOF/TOF (AUTOFLEXIII), LCMS Q-TOF (Agilent 1200-6520), UPLC MS/MS (Xevo TQMS Tandem) and Bruker FTMS
(3) NMR System: 400MHz and 600MHz (Bruker AVANCEIII)
(4) Protein Structure and Molecules Interaction Analysis System: AKTA Purifier, 2D Gel Electrophoresis System, Super Nova X-ray, Bruker X8, CD (Applied Photophysics), ITC and DSC, etc.
(5) Nucleic Acid Analysis System: ABI-3130, ABI-3500, ABI-7500 and AB ViiA7, etc.
(6) Clean rooms for Nanobiotechnology and biosensor
(7) Cell culture facilities, Flow Cytometry
(8) Animal facilities

It is our ambition to build SLST to a world class school of Life Science and Technology. A significant fraction of our courses will be delivered in English. We are expanding and establishing cutting-edge basic and applied research programmes. As the next phase of strategic development, SLST is now recruiting Faculty members and Senior Research Fellows to lead the following research programmes:

A Nano-biotechnology
B Synthetic biology
C Bioinformatics
D Neurobiology
E Regenerative biotechnology

The positions are open to all applicants worldwide. Candidates should have a PhD in the relevant fields and established research track records. Faculty position applicants should be able to teach relevant subjects in English or Chinese.

Applications, including a cover letter, a detailed resume, publication list, names of three referees, and a research plan, should be sent to Ms Ding Yuqing, Secretary of Faculty Search Committee, via email: dyqlyb@yahoo.com.cn, before the deadline of 31 Dec 2012. The start date of the appointment is flexible but no later than 1 Sept 2013. For informal inquiry, please contact Prof Yu Li, Head of the SLST, email: liyugene@hit.edu.cn.

JP229655R

SAO PAULO SCHOOL OF ADVANCED SCIENCE FOR PREVENTION OF MENTAL DISORDERS

Y-MIND

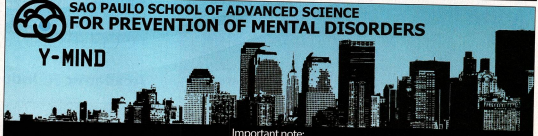

Important note:
For every approved student/participant the organization will cover all travelling costs for one week stay in Sao Paulo.

March 25th to 29th 2013 • Sao Paulo/Brazil

"Call for action: a vanguard school of multidisciplinary studies on prevention of mental, emotional and behavioral disorders"

Selection of students/participants:
100 positions will be offered for graduate students and post-doctoral fellows working in the field of prevention of mental, emotional and behavioral disorders. Half (50) of these positions are reserved for applicants coming from outside of Brazil. The other half will be distributed among applicants from Sao Paulo state (25 positions) and students from other Brazilian states (25).

The applications have to be made from the 15th of October to the 15th of November in the website:
http://www.ymind.com.br
Additional information can be obtained in the e-mail:
ymind@ymind.com.br

UNIFESP
FAPESP

NW229485E

www.naturejobs.com

MAX-PLANCK-GESELLSCHAFT

Alexander von Humboldt
Stiftung/Foundation

Call for Nominations

Max Planck Research Award 2013

The International Research Award of the Alexander von Humboldt Foundation and the Max Planck Society

The Alexander von Humboldt Foundation and the Max Planck Society jointly confer the Max Planck Research Award, which is funded by the German Federal Ministry for Education and Research, on exceptionally highly-qualified German and foreign scientists. The researchers are expected to have already achieved international recognition and to continue to produce outstanding academic results in international collaboration – not least with the assistance of this award.

Every year, two research awards are conferred on internationally renowned scientific researchers. One of the awards should be given to a researcher working in Germany and the other to a researcher working abroad. As a rule, each Max Planck Research Award is endowed with 750,000 euros. Nominations of qualified female scientific researchers are especially welcome.

On an annually-alternating basis, the call for nominations addresses areas within the natural and engineering sciences, the life sciences, and the human and social sciences.

The Max Planck Research Award 2013 will be awarded in the area of life sciences in the subject

The Impact of Climate Change on Ecosystems

The long-term effects of climate change are expected to have a major impact on global ecosystems. Such impacts may initially only gradually manifest themselves in the composition of soil organisms or freshwater communities, while other effects on flora and fauna will become more immediately apparent.

The exact consequences, for example, on human food sources, cannot be foreseen. The Max Planck Research Award is to be given in recognition to individuals who, both in the lab and in the field, conduct research into the potential effects of climate change on our ecosystem, both in terms of their function and anticipated dynamics.

The Rectors/Presidents of German universities or research organisations and the scientific heads of institutes of these organisations are eligible to nominate candidates. Nominations must be submitted to the Alexander von Humboldt Foundation. Applications by prospective candidates themselves are not possible. The deadline for nominations is **31 January 2013**.

Further information can be obtained from the

Alexander von Humboldt-Stiftung, Bonn (Germany)
www.humboldt-foundation.de/web/max-planck-award.html
e-mail: michaela.kreilos@avh.de

SPONSORED BY THE
Federal Ministry of Education and Research

W229617AM

Bringing jobseekers and recruiters together.

Academic • Industry • Government

Search now at **naturejobs.com**

naturejobs
making science work

"I believe, this was the first ever advert that was placed into Naturejobs by our University and was convincingly successful."

Dr. Judit Erzsebet Pongracz, University of Pecs, Hungary

naturejobs

REPROGRAPHICS: CC Media Group, London EC1V 8AR UK and **The Charlesworth Group,** Wakefield, UK.
PRINTED BY: William Gibbons & Sons Ltd, UK; **Publishers Press,** Lebanon Junction, Ky, USA and **Obun Printing Co. Inc,** Tokyo, Japan

Skolkovo Tech

Skolkovo Institute of Science and Technology

Call for International Research Center Proposals

Skolkovo Tech invites collaborative proposals from research and educational institutions around the world in the following areas:

- Biomedicine
- Energy
- Information Technology
- Nuclear
- Space

Skolkovo Tech is a private graduate research university located outside Moscow, Russia. Established in 2011 in collaboration with MIT and the Skolkovo Foundation, the university is founding 15 multidisciplinary Centers for Research, Education and Innovation (CREI) to address critical scientific and technology challenges.

With three centers in negotiations, the Second Round Call for Proposals offers an opportunity to partner with Russian investigators in a world-class research program.

Visit **www.skolkovotech.ru/research** for details.

SkTech/MIT INITIATIVE

30 November 2012 deadline

$6-12M USD annually, up to five years

Scientific impact

Education

World-class research in Russia

THE TELL-TALE EAR

A sound investment.

BY ALEX SHVARTSMAN

From: *ceo@telltalemarketing.com*
To: *Telltale Marketing Employees mailing list*
Subject: *Misdirected broadcast*
We seem to be having an equipment malfunction. I can hear bits broadcast from the Grand Cayman Casino and Erectile Dysfunction marketing campaigns while at the office. Somebody get on top of this.
James Finch
PS It's a little annoying on repeat. At least now we know how the recipients feel. Haha.

From: *ceo@telltalemarketing.com*
To: *IT@telltalemarketing.com*
Subject: *Leak?*
Apparently only I can hear the ads, not the whole company. They're playing on a loop and driving me up the wall. Whose bright idea was this? The stuff is supposed to be broadcast in the streets, not in my office. Get it fixed. Pronto.

From: *ceo@telltalemarketing.com*
To: *IT@telltalemarketing.com*
Subject: *RE: Leak?*
What do you mean you can't figure it out? I'm telling you, I hear our commercials. ALL THE TIME. I even hear them at home now; can't get a good night's rest. Somebody must be doing this maliciously, and when I figure out who, heads are going to roll.

Do whatever it is you do to make this stop. Come on people, what am I paying you for?

From: *ceo@telltalemarketing.com*
To: *drseanngnguyen@ntkmetical.com*
Subject: *Appointment*
Dear Dr Nguyen,
I run Telltale Marketing, the company that produces the hypersonic sound commercials. Over the past several days I've been hearing our ads, at increasing frequency and volume.

At first I resisted the suggestion that this might be a psychological issue, but my IT people are swearing up and down that the problem isn't technical in nature, so I'm beginning to worry. May I come in for an evaluation at your earliest convenience?

Sincerely,
James Finch

From: *ceo@telltalemarketing.com*
To: *drseanngnguyen@ntkmetical.com*
Subject: *RE: Appointment*
I'm sorry to hear that you aren't able to fit me in. Also, I appreciate your feedback about the hypersonic ads, but I assure you that your assertion about us breaking the law is entirely false. We broadcast them only in public spaces and only between the hours of 8 a.m. and 11 p.m., in accordance with FCC regulations. It's just like playing an advertisement on a radio or posting up a billboard.

JACEY

This is absolutely not an invasion of privacy. We get a bum rap in all the other media, but only because they're jealous. A technology that beams sound directly into people's ears is far more effective than their outdated methods. It's much easier to tune out ads on TV and radio than to ignore our product, and the advertisers know it.

Also, I completely agree, broadcasting the pornographic website commercials where young children can hear them is completely inappropriate. We don't do that. It's those upstarts at Electronic EAR. They have no class.

From: *ceo@telltalemarketing.com*
To: *SandraFinch@ufopub.com*
Subject: *Tonight*
Finally found a shrink who'll see me. Going to her office after work, so don't wait with dinner.

I can't believe it was so hard to find a doctor. As soon as they learn who I am, they want nothing to do with me. One even went as far as to call me a spammer and say that I deserve this. Didn't they take some sort of an oath to help people? Geez.

➲ **NATURE.COM**
Follow Futures on Facebook at:
go.nature.com/mtoodm

From: *ceo@telltalemarketing.com*
To: *legal@telltalemarketing.com*
Subject: *Exposure*
I've been seeing a psychologist twice a week about my hearing-the-ads problem, but it's only getting worse. The noise is loud and incessant. I haven't had a decent night of sleep in weeks. Dr Harris says that it's all in my head, my guilty subconscious torturing me over "forcing your ads on people who don't want to hear them". According to Dr Harris I might only get better if I admit to some of the shadier stuff that the company has done, to get it off my chest. It's nuts, I know. I dismissed the idea initially, but I may literally be losing my mind. I can't stand it any more and am willing to try anything.

If I go through with this, how bad is it going to be, for me or for the company?

From: *ceo@telltalemarketing.com*
To: *SandraFinch@ufopub.com.com*
Subject: *Update*
The minimum security facility they're holding me in isn't so bad. Food is tolerable, and the other inmates are white-collar types, mostly from the financial sector. I even get to use the computer for 15 minutes a day.

But the most important thing is: it worked. I told them about beaming ads into people's homes, advertising knock-off pills that weren't approved by the FDA, and the bribes we paid to make the regulators look the other way. And once I admitted these things, the cursed noise in my head finally stopped.

I may be in here for a couple of years, but I tell you, it was worth it.

From: *AgentWellsley@fbi.gov*
To: *Director.ConsumerFraudDivision@fbi.gov*
Subject: *Finch*
It worked like a charm.

After getting blasted with a taste of his own medicine for a couple of weeks straight, Finch sang like a canary (pardon the pun). He confessed to some stuff we didn't even know about. My team is disassembling the broadcast equipment as we speak. We're going to be moving Operation Poe on to our next target tomorrow.

Tell agent Harris to expect a call from the president of Electronic EAR some time soon. ■

Alex Shvartsman *is a writer and game designer from Brooklyn, New York. Read more of his fiction at www.alexshvartsman.com.*

nature | ENCODE

ENCODE, the Encyclopedia of DNA Elements, is a project funded by the National Human Genome Research Institute and focuses on identifying all regions of transcription, transcription factor association, chromatin structure and histone modification in the human genome sequence. The main findings of ENCODE are now presented in 30 papers published simultaneously in *Nature*, *Genome Research* and *Genome Biology*.

Access videos, Features and the collected research papers, and explore the thematic threads that run through them via the *Nature* ENCODE explorer or the *Nature* ENCODE app.

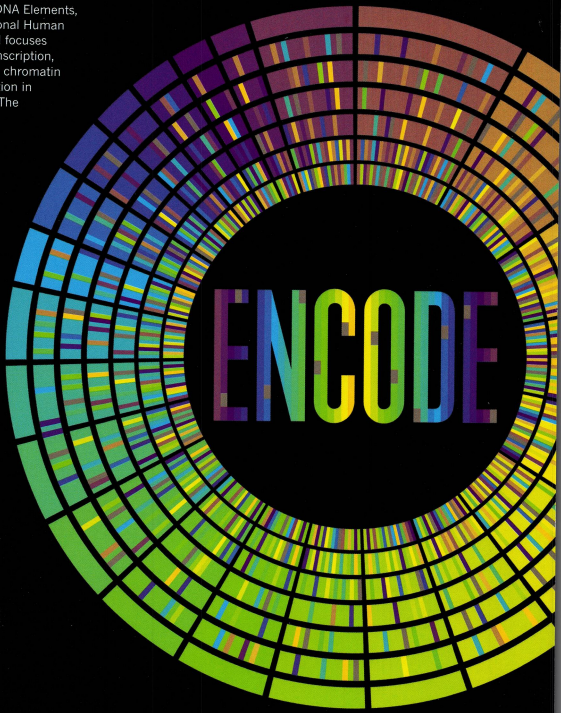

Produced with support from

illumina®

Available on the App Store

nature.com/ENCODE

nature publishing group npg

R&D Systems Tools for Cell Biology Research™

NEW Interactive Pathways & Processes

✓ Designed by scientists for scientists

✓ One click to access the widest collection of products

✓ Request a printed copy, which includes additional resources

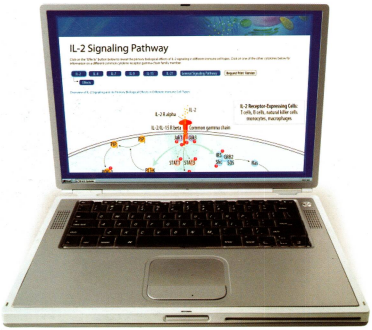

R&D Systems is excited to announce the addition of Interactive Pathways & Processes to the growing list of reference tools available on our website. These new fully-interactive pathways allow you to explore a variety of biological processes, including Apoptosis, Wnt Signaling, and Th1 Differentiation.

Start exploring today
www.RnDSystems.com/**Pathways**

R&D SYSTEMS®